The Design and Synthesis of Transition Metal Complexes Supported by Non-innocent Ligand Scaffolds for Small Molecule Activation

Thesis by
Kyle Tadashi Horak

In Partial Fulfillment of the Requirements
for the Degree of Doctor of Philosophy

CALIFORNIA INSTITUTE OF TECHNOLOGY
Division of Chemistry and Chemical Engineering
Pasadena, California
2016
(Defended on February 4th, 2016)

To Mom and Dad,
and my younger brother Erik

"All's well that ends better."

-J.R.R. Tolkien, *The Lord of the Rings*

"Ah yes… I was wondering what would break first… your spirit, or your body?"

-Bane*, The Dark Knight Rises*

ACKNOWLEDGMENTS

Much like the concluding remarks of a presentation, it appears that all that remains for me to do is acknowledge the numerous people that have mentored, supported, and inspired me to arrive at where I am today. Looking back at the past six years, I feel that I have come a long way as a scientist and I believe this to be largely attributable to the invaluable interactions and experiences that I have accumulated over my time here. My time in graduate school has certainly had its ups and downs as projects started and ended (sometimes crashing and burning in a spectacular fashion), and as friends were found and then would graduate. However, if you were to add up all those moments and interactions, both good and bad, the result would be a net positive and rewarding experience. I am grateful for the opportunity to study at the truly unique scientific environment that is the California Institute of Technology.

The first person whose acknowledgement should not go unmentioned would have to be without a doubt my principle advisor Prof. Theodor Agapie. At this point it sounds like a cliché thing to say to me, but I sincerely thank you for taking a chance by accepting me into your group as a person from a strictly biochemistry background who had never even used a Schlenk line or done a vacuum transfer. Perhaps more importantly, thank you for giving me an excellent good graduate student mentor to teach me the ropes, a practice which both strengthens the group dynamic and is also instrumental in preserving the group's standards of chemical rigor. Under your supervision in the group, both in the lab and in meetings, I have learned an incredible amount the discipline of synthetic inorganic chemistry. Thank you for also giving me the intellectual freedom to manage my projects (and even come up with some of my own) and be creative from day one, something I feel is central to being a scientific researcher rather than a laboratory technician. You have trained me to be a hard worker and a problem solver, qualities that I am sure will serve me well in the future. I wish you the best of luck in the future, and look forward to thumbing through the group's publications for years to come so I can watch how the research of the group continues to evolve and diversify.

I must also thank the members of my thesis committee, Prof. Jonas Peters, Prof. Dennis Dougherty, and most recently Prof. Harry Gray, who have provided crucial insight into my research and various scientific proposals over the years. Collectively, all

of you have always challenged me to think about the bigger picture with my science and ideas, reminding me that while it is easier to keep one's head down and tinker and tweak systems it is important to look up and explore the concepts in a broader context and ask their relevance to fundamental challenge at hand. I thank Prof. John Bercaw for giving me the free reign to run many Toepler pump experiments on his awesome high-vacuum line. I must also extend a special thanks to Prof. Jonas Peters for allowing me to use his group's Mössbauer and ATIR instruments.

A substantial acknowledgement must be given to my family as they have provided unconditional support throughout my entire time here at Caltech. Whenever graduate school would get me down my family was there to cheer me up. I could always rely on them to welcome me back to Vermont for the holidays with my winter jacket (yes California weather has made me soft!) and hug at the airport. They have always encouraged me to excel and pursue the study of subjects I find interesting. My grandfather and dad were both chemists, and were highly instrumental in inspiring me to pursue a Ph. D. in chemistry. Thank you for teaching me to never stop asking questions and seek out those individuals with the answers or insight required to tackle life's challenges. Thanks mom for always keeping my spirits up and maintaining a heated Words with Friends competition going whenever I need a distraction from work. Erik, I wish you best of luck your own graduate studies and I expect to hear about your research in the future. It's always good to see you again (usually) for the holidays, although sometimes our chemistry talk can get on Kayla's nerves (Kayla, thanks for dealing with the two of us brothers together!). I also need to thank my LA aunts, Denise and Alice, who have always helped make California feel like a home away from home. Thanks for inviting me over for holiday feasts, and making sure that I left with plenty of leftovers (soooo much turkey!).

During my time here I have overlapped with many students. I can only hope that I haven't missed too many of you here. I first want to thank Sandy Suseno, my graduate student mentor and my best friend. Thank you so much for training me, and turning me into the synthetic inorganic chemist that I am today. You kept me sane throughout my time at Caltech, and definitely taught me to be more patient with my chemistry and coworkers. Thank you for always being supportive and understanding of me despite my numerous quirks and strange sense of humor. I am looking forward to continuing

to spend time with you up at Intel in the future, even though I didn't quite graduate as soon as you wanted me to.

I have had the privilege to overlap with a large number of talented graduate students during my time in the Agapie group. Thank you for generally being a helpful and hardworking group of individuals that collectively have taught me a lot about laboratory techniques and box etiquette. Emily Tsui, thanks for asking tough questions and not letting people's (myself included) crazy theories get out of hand. I learned a lot about how to present and think about science from you, and your suggestions for my chemistry have always proved insightful. Madalyn Radlauer, thanks for being our group's first and best safety officer. You were always willing to take the time teach me and your seemingly endless positivity around the lab was awesome. Sibo Lin, thanks for helping me wrap my head around the whole concept of DFT calculations, and also putting up with my general entropy in the box. Paul Kelley, I am not sure I ever quite understood you, but I am actually thankful I didn't since your antics brought a little much needed randomness to my daily routine which certainly kept things interesting. Thanks Davide Lionetti and Joshua Buss for accommodating my need to frequently get drinks at the Athenaeum, Lucky Baldwin's, the Blind Donkey, or wherever to decompress after a hard day's work, bad experiment, or just because it was Tuesday. Davide, I am glad I met someone with such a compatible sense of humor, music, and interests as myself. I have learned an academic ton scientifically-speaking from conversations with you and we got to have a lot fun going to the U2 concert and playing soccer together. I hope that you enjoy your new postdoc goes well, and you are able to inspire and teach new group of graduate students. Jacob Kanady, thanks for keeping me in line and stopping me from complaining too much about things. Which brings me to Mr. Guy Edouard and Justin "The Bear" Henthorn. As the two people in the Agapie group also graduating my year, it is safe to say that I have overlapped with these individuals more than anyone else in the group. Thanks Guy for your impressions and jokes. Your positivity and sense of humor definitely kept the group morale up more than you know in dark times. I look forward to seeing you up in Hillsboro when we both start working at Intel. Justin, well you always were a force for anarchy and managed to surprise me at every turn with what Caltech was willing to let you do. However, you have also proved to be one of the most generally knowledgeable people

in the group, and have often provided synthetic advice for making both my ligands and metal complexes. I think we shared many ideas and approaches as both of our hydroquinone/catechol-based ligand platforms shared many similarities. I wish you the best of luck in Germany (you lucky dog!), and hope to hear about your great scientific accomplishments in the future. Joshua Buss, thanks for organizing soccer and being synthetic force to be reckoned with the group. Like Davide, I have learned a lot through conversations with you, and I wish you best of luck with your chemistry in the future. Keep the group's *original* standards alive and never stop asking the tough questions (or making compounds with obscure chemical shifts by NMR)! Marcus, HB, and Jessica, soon all you will be the senior graduate students in the group, and I hope you will teach the newer students how we do things in the Agapie group. Marcus. One job: keep Buss in line (and on his toes). That is all. HB, I hope you get the dangler in a rational *and* reproducible manner hopefully without self-assembly. Jessica, try not to work too late and good luck with your continued efforts on team polymerization. To Chris Reed (you work with Marcus to keep Buss in line), Nate Hirscher, and Ryan Ribson (may he return with a bionic knee), I didn't overlap with all of you that much but I wish all of you the best luck with your projects and candidacy moving forward. To Charlie Arnett and Jeremy Tran (the heir apparent of Chapter 5), the newest members of the cluster subgroup, good luck with your respective projects. Aim high and work hard.

I have also worked with a number of postdocs throughout my time here. Prof. Dave Herbert, thanks for being a source of great insight into my projects while I was on team phosphine. You always had references handy regardless of what my question was. Prof. Po-heng Lin, thanks for good times and laughs we had together, and that super helpful crash course in SQUID. To the more recent post-docs, Graham de Ruiter, Zhiji Han, Siti Riduan, Aimee Bryan, Gyeongshin Choi, and Alejo Lifshitz, I wish you the best of luck in your continued research, future jobs, and job searches.

I also want to thank people from outside of the Agapie group who have served as an invaluable scientific resource (as well as stolen chemicals) for me during my time here at Caltech. I would like to thank Jon Rittle and Matthew Chalkley for useful discussion about chemistry and for helping me collect all of my Mössbauer data. I learned a lot through many discussion with the both and you, and wish you the best of luck in the future with your research and academic careers. Josh Wiensch, as the fourth

member of the four graduate students that joined Theo's group my year, I wish you all the best to you in the upcoming year and beyond. To the Sattlers (Wes and Aaron) from the Gray and Bercaw groups, respectively, thanks for all the good times and laughs over drinks and on the softball field, which brings me to Oliver Shafaat in the Gray group. Thanks for running the Cp All-Stars during my time here. I had a blast playing softball with the combined Gray/Bercaw/Agapie group team for multiple years. Speaking of sports teams, thanks to the pickup soccer crew as a whole. Thanks for giving me a great way to get cardio exercise and decompress outside of work.

One more group of people who need to be acknowledged, since they really keep things working around here, are a various facilities staff members I have crossed paths throughout my years here. In particular, I would like to thank Larry Henling and Mike Takase for usually managing to find the one good crystal in a sea of twinned and, to quote Larry here, "ugly" crystals. X-ray crystallography was a huge component of every single one of my thesis chapters, so thanks to both of you for running an excellent facility and making my thesis possible. I also need to thank David VanderVelde for running an amazing NMR facility during my time here at Caltech. While I only recently started coming to you for advice and help with assigning some NMRs of my nickel complexes, I have realized that I should have been coming to you with my NMR questions a lot sooner. Thank you Mona Shahgholi for keeping the Mass Spec facility running smoothly despite all of cluster samples the Agapie group has to run. My thanks to Rick Gerhart for fixing my glassware (especially J-young tubes and the Schlenk line occasionally) quickly, and being willing to try Davide and my homebrewed beer. Thank you to Agnes Tong for keeping me on schedule. Joe Drew,thanks for always being helpful with pretty much whatever questions of repairs I needed to get done around the lab. And finally thanks to our floor's custodian, José, who has never failed to be friendly and say good morning to me every day.

Thanks again to everyone who has helped me complete the body of work contained within my thesis. I am glad to have been part of the Caltech community. And with that, on to the science.

Published Content

Parts of this thesis have been adapted from published articles co-written by the author and articles that are currently in preparation.

The following article was reproduced in part with permission from the Royal Society of Chemistry:

"Arene non-innocence in dinuclear complexes of Fe, Co, and Ni supported by a *para*-terphenyl diphosphine" Horak, K. T.; Velian, A.; Day, M. W.; Agapie, T. *Chem. Commun.*, **2014**, *50*, 4427-4429. URL: http://pubs.rsc.org/en/Content /ArticleLanding/2014/CC/c4cc00838c#!divAbstract

The following article was reproduced in part with permission from the American Chemical Society:

"Trinuclear Nickel Complexes with Metal–Arene Interactions Supported by Tris- and Bis(phosphinoaryl)benzene Frameworks" Suseno, S.; Horak, K. T.; Day, M. W.; Agapie, T. *Organometallics*, **2013**, *32*, 6883-6886. URL: http://pubs.acs.org/doi/abs/10.1021 /om400976x

"Heterometallic Effects in Trinuclear Complexes Supported by *p*-Terphenyl Diphosphine Ligands" Horak, K. T.; Lin, S.; Rittle, J.; Agapie, T. *Organometallics*, **2015**, *34*, 4429-4432. URL: http://pubs.acs.org/doi/abs/10.1021/acs.organomet.5b00579

"Tuning of Metal Complex Electronics and Reactivity by Remote Lewis Acid Binding to π-Coordinated Pyridine Diphosphine Ligands" Horak, K. T.; VanderVelde, D. G.; Agapie, T. *Organometallics*, **2015**, *34*, 4753-4765. URL: http://pubs.acs.org/doi/abs/10.1021/acs.organomet.5b00562

RESPECTIVE CONTRIBUTIONS

Parts of the work described in this thesis are the result of collaborative efforts, without which these studies would not have been possible. Specific notes are included for compounds synthesized by other researchers and spectroscopic characterization carried out by our collaborators.

In Chapter 2, the initial synthesis and characterization of complex **11** was carried out by Dr. Alexandra Velian. The late Dr. Michael W. Day was responsible for refining the solid-state structure of complex **11**. Density functional theory calculations were run by Dr. Sibo Lin. Mössbauer data were collected and simulated in collaboration with Dr. Jonathan Rittle from the Peters group.

In Chapter 4, the 2D NMR assignments for complex **6Ni**, **7Ni**, and **8Ni** were completed with the assistance of Dr. David VanderVelde.

In Chapter 5, Mössbauer data were collected and simulated in collaboration with Matthew Chalkley from the Peters group with additional help provided by Niklas Thompson (Peters Group) and Chris Reed (Agapie Group).

ABSTRACT

This dissertation focuses on the incorporation of non-innocent or multifunctional moieties into different ligand scaffolds to support one or multiple metal centers in close proximity. Chapter 2 focuses on the initial efforts to synthesize hetero- or homometallic tri- or dinuclear metal carbonyl complexes supported by *para*-terphenyl diphosphine ligands. A series of $[M_2M'(CO)_4]$-type clusters (M = Ni, Pd; M' = Fe, Co) could be accessed and used to relate the metal composition to the properties of the complexes. During these studies it was also found that non-innocent behavior was observed in dinuclear Fe complexes that result from changes in oxidation state of the cluster. These studies led to efforts to rationally incorporate central arene moieties capable managing both protons and electrons during small molecule activation.

Chapter 3 discusses the synthesis of metal complexes supported by a novel *para*-terphenyl diphosphine ligand containing a non-innocent 1,4-hydroquinone moiety as the central arene. A Pd^0-hydroquinone complex was found to mediate the activation of a variety of small molecules to form the corresponding Pd^0-quinone complexes in a formal two proton / two electron transformation. Mechanistic investigations of dioxygen activation revealed a metal-first activation process followed by subsequent proton and electron transfer from the ligand. These studies revealed the capacity of the central arene substituent to serve as a reservoir for a formal equivalent of dihydrogen, although the stability of the M-quinone compounds prevented access to the Pd^{II}-quinone oxidation state, thus hindering of small molecule transformations requiring more than two electrons per equivalent of metal complex.

Chapter 4 discusses the synthesis of metal complexes supported by a ligand containing a 3,5-substituted pyridine moiety as the linker separating the phenylene

phosphine donors. Nickel and palladium complexes supported by this ligand were found to tolerate a wide variety of pyridine nitrogen-coordinated electrophiles which were found to alter central pyridine electronics, and therefore metal-pyridine π-system interactions, substantially. Furthermore, nickel complexes supported by this ligand were found to activate H–B and H–Si bonds and formally hydroborate and hydrosilylate the central pyridine ring. These systems highlight the potential use of pyridine π-system-coordinated metal complexes to reversibly store reducing equivalents within the ligand framework in a manner akin to the previously discussed 1,4-hydroquinone diphosphine ligand scaffold.

Chapter 5 departs from the phosphine-based chemistry and instead focuses on the incorporation of hydrogen bonding networks into the secondary coordination sphere of [$Fe_4(\mu_4\text{-}O)$]-type clusters supported by various pyrazolate ligands. The aim of this project is to stabilize reactive oxygenic species, such as oxos, to study their spectroscopy and reactivity in the context of complicated multimetallic clusters. Herein is reported this synthesis and electrochemical and Mössbauer characterization of a series of chloride clusters have been synthesized using parent pyrazolate and a 3-aminophenyl substituted pyrazolate ligand. Efforts to rationally access hydroxo and oxo clusters from these chloride precursors represents ongoing work that will continue in the group.

Appendix A discusses attempts to access [Fe_3Ni]-type clusters as models of the enzymatic active site of [NiFe] carbon monoxide dehydrogenase. Efforts to construct tetranuclear clusters with an interstitial sulfide proved unsuccessful, although a (μ_3-S) ligand could be installed through non-oxidative routes into triiron clusters. While [$Fe_3Ni(\mu_4\text{-}O)$]-type clusters could be assembled, accessing an open heterobimetallic edge site proved challenging, thus prohibiting efforts to study chemical

transformations, such as hydroxide attack onto carbon monoxide or carbon dioxide coordination, relevant to the native enzyme. Appendix B discusses the attempts to synthesize models of the full H-cluster of [FeFe]-hydrogenase using a bioinorganic approach. A synthetic peptide containing three cysteine donors was successfully synthesized and found to chelate a preformed synthetic [Fe_4S_4] cluster. However, efforts to incorporate the diiron subsite model complex proved challenging as the planned thioester exchange reaction was found to non-selectively acetylate the peptide backbone, thus preventing the construction of the full six-iron cluster.

TABLE OF CONTENTS

Dedication **iii**
Acknowledgements **iv**
Published Content **ix**
Respective Contributions **x**
Abstract **xi**
Table of Contents **xiv**

Chapter 1 **1**
General Introduction

Chapter 2 **6**
Synthesis of Multinuclear Carbonyl Complexes Supported by a *Para*-Terphenyl Diphosphine Ligand
Abstract 7
Introduction 8
Results and Discussion 9
Conclusions 34
Experimental Section 36
References 69

Chapter 3 **73**
Synthesis and Reactivity of Metal Complexes Supported by a Non-Innocent Hydroquinone *Para*-Terphenyl Diphosphine Ligand
Abstract 75
Introduction 76
Results and Discussion 77
Conclusions 106
Experimental Section 108
References 136

Chapter 4 **139**
Synthesis and Reactivity of Metal Complexes Supported by a Pyridine Diphosphine Ligand with Tunable Electronics Utilizing Remote Lewis Acid Binding
Abstract 141
Introduction 143
Results and Discussion 144
Conclusions 169
Experimental Section 171
References 198

Chapter 5 **200**
Synthesis of Site-Differentiated [$Fe_4(\mu_4\text{-}O)$] Complexes Supported by Pyrazolate Ligands Possessing Pendant Hydrogen Bond Donors
Abstract 202
Introduction 203

Results and Discussion 205
Conclusions 223
Experimental Section 225
References 232

Appendix A **233**
Towards the Synthesis of Heterometallic Multinuclear Complexes as Models of [NiFe]-Carbon Monoxide Dehydrogenase
Abstract 235
Introduction 236
Results and Discussion 239
Conclusions 249
Experimental Section 252
References 258

Appendix B **258**
Modeling the [FeFe]-Hydrogenase H-Cluster: Combining a Peptide-Supported [Fe_4S_4] Cluster and a Synthetic Diiron Subsite Mimic
Abstract 260
Introduction 261
Results and Discussion 262
Conclusions 270
Experimental Section 271
References 275

Appendix C **275**
NMR Spectra
Chapter 2 277
Chapter 3 292
Chapter 4 306
Chapter 5 336
Appendix A 342

About the Author **345**

Chapter 1

GENERAL INTRODUCTION

INTRODUCTION

This dissertation focuses on the study of multifunctional and non-innocent ligands in the context of small molecule activation in a variety of mono- and multinuclear complexes. This general concept was explored in two distinct types of systems: 1) multiple diphosphine ligands containing non-innocent central arene, 1,4-hydroquinone, or pyridine-based moieties poised to interact with supported transition metals, and 2) the incorporation of hydrogen bonding moieties into the secondary coordination sphere of site-differentiated [$Fe_4(\mu_4$-O)]-type clusters as a way to stabilize terminal oxido ligands in multinuclear complexes. In recent decades the use of redox or acid / base non-innocent ligands as well as secondary coordination sphere hydrogen bonding networks to promote novel reactivity, facilitate catalysis, or stabilize otherwise reactive intermediates has grown into an area of substantial research effort. However, the development of ligand scaffolds capable of storing / delivering both protons and electrons to small molecule substrates in transition metal-mediated processes and the study of hydrogen bonding networks in multinuclear complexes are comparatively less so. The work reported herein seeks to address these two concepts with appropriate background and references incorporated into each individual chapter. This chapter aims to discuss the interest in these avenues of research in more general terms and describe the motivations and development of each of the related projects.

For the purposes of this dissertation multiple classes of ligand non-innocence can be defined. The term redox non-innocence will be used to describe systems in which the ligand serves as an electron reservoir. These systems typically have low-lying unpopulated ligand-based orbitals that are more easily reduced than the coordinated metal center. From the discovery of the redox non-innocence 1,2-dithiolene ligands by

Eisenberg and Gray in the 1960s to more recent examples such as bis(imino)pyridine ligands studied extensively by Weighart and Chirik as well as others (Bart, Berben), the use of redox non-innocence has resulted in the ability to mediate a range of challenging chemical transformations, including some more commonly associated with noble metal catalysis, in Earth-abundant first-row transition metals. Work from the Heyduk group has also applied this strategy to achieve a variety of redox transformations at formally d^0 metal centers by taking advantage of redox-active aminophenolate ligand scaffolds.

A second class of non-innocent ligand can be described as acid / base non-innocent whereby the ligand is capable of facilitating the transfer of protons or other electrophiles by serving as a local Lewis basic or acidic site. Inspiration for these systems can be partially attributed to enzymatic systems such as [FeFe]-hydrogenase which takes advantage of an aza dithiolate ligand to facilitate dihydrogen evolution or oxidation by serving as a base during catalysis. A recent example of this type of strategy are the PNN pincers reported by Milstein, which utilize the reversible deprotonation of a benzylic position in the ligand framework to mediate chemical transformation. Work by Mayer and Savéant has demonstrated electrocatalytic systems can take advantage of pendant protic or basic functionalities that alter the product selectivity in dioxygen and carbon dioxide reduction in porphyrin-based systems.

Conceptually, these systems are related to ligand scaffolds which utilize secondary coordination sphere tuning with hydrogen bond donating or accepting moieties to stabilize reactive species. The Borovik group has employed a variety of mono- and multinucleating scaffolds employing hydrogen bonding networks to isolate and study a variety of high-valent metal centers coordinated to terminal oxygenic fragments to spectroscopically characterize and study their reactivity. More recently, others such as

the Fout and Szymczak group have also begun to incorporate hydrogen bonding functionalities into novel ligand scaffolds as well. While most effort has focused on monometallic systems, examples of dinuclear complexes featuring hydrogen bond networks have also been reported to a much lesser extent. These ligands do not facilitate or mediate proton transfer to or from metal-bound species; however, they provide a unique secondary coordination sphere environment whose influence on small molecule reactivity can be studied in its own right.

Finally, there is one last class of non-innocent ligands that can be defined are both redox and acid / base non-innocent, meaning they are capable of storing and delivering both electrons and electrophiles during metal-mediated small molecule activation. Systems capable of this are considerably less common though not unprecedented. Again, Nature can serve as a source of inspiration with NAD^+ whose core pyridinium moiety is capable of serving as an organic hydride acceptor, formally two electrons and a proton. This concept has been recently applied and reviewed by the Colbran group. Another notable example comes from the Heyduk group in the reduction of dioxygen using an amine bis(phenolate) supported Zr complex. Our own group has recently published the use of π-bound Mo-catechol complexes demonstrating the capacity to transfer a variety of electrophiles and electrons to dioxygen. With the reduction of many small molecules including carbon dioxide, dioxygen, and dinitrogen requiring the input of multiple protons and electrons, the exploration of ligand scaffolds capable of facilitating the transfer of multiple electron and electrophile equivalents could serve as a strategy to achieve these challenging reductions and impart selectivity on the types of products produced. Overall, the interest in multifunctional and non-innocent ligands stems from the desire to develop novel strategies to accomplish challenging chemical

transformations. By emphasizing metal-ligand cooperativity, the reactivity observed by these complexes can often be described as greater than the sum of its parts as individually neither component can accomplish the targeted chemical behavior.

Building off the initial reports of non-innocent *para*-terphenyl diphosphine ligands in our group, efforts turned to rationally incorporating multifunctional moieties into both mono- and multinuclear complexes. While a variety of hetero- and homometallic tri- and dinuclear complexes were synthesized (Chapter 2), with evidence for central arene redox non-innocence arising from strong metal-arene interactions that were observed in dinuclear Co_2 and Fe_2 complexes (Chapter 2). Efforts to rationally incorporate non-innocent aromatic linkers were then expanded to two new ligand scaffolds: a *para*-terphenyl diphosphine containing a 1,4-hydroquinone fragment as the central arene moiety (Chapter 3), and a 3,5-substituted pyridine diphosphine ligand (Chapter 4). Metal complexes supported by both ligand scaffold showed differing small molecule with the hydroquinone system being capable of rapidly delivering reducing equivalents to substrates, while the pyridine diphosphine system could efficiently add B-H, Si-H, and hydride equivalents into the ligand scaffolds. Most recently, efforts to incorporate hydrogen bonding networks into the secondary coordination sphere of $[Fe_4(\mu_4\text{-}O)]$-type complexes have also been attempted (Chapter 5). Overall, this body of work aims to expand the range of ligand scaffolds capable of reversibly storing both protons and electrons during small molecule activation and gain insight into how hydrogen bonding network play into reactivity in multinuclear clusters.

CHAPTER 2

SYNTHESIS OF MULTINUCLEAR CARBONYL COMPLEXES SUPPORTED BY A PARA-TERPHENYL DIPHOSPHINE LIGAND

The text for this chapter was reproduced in part from:

Suseno, S.; Horak, K. T.; Day, M. W.; Agapie, T. *Organometallics*, **2013**, *32*, 6883-6886.

Horak, K. T.; Velian, A.; Day, M. W.; Agapie, T. *Chem. Commun.*, **2014**, *50*, 4427-4429.

Horak, K. T.; Lin, S.; Rittle, J.; Agapie, T. *Organometallics*, **2015**, *34*, 4429-4432.

Abstract

Multinuclear hetero- and homometallic clusters supported by *para*-terphenyl diphosphine ligands were targeted with the goal of studying cooperative small molecule activation across multiple metal centers. A series of isostructural trinuclear complexes of metal composition Pd_2Fe, Pd_2Co, and Ni_2Fe, were synthesized in a stepwise fashion. Using dinuclear precursors (Pd^{I}_2 and Ni^{I}_2) supported by *para*-terphenyl diphosphine ligands allowed for the selective incorporation of a single additional metal center. The effects of both metal composition and ligand electronics on cluster properties were studied. These results highlight the importance of metal-metal interactions in mixed-metal sites of structurally analogous clusters. Additionally, cofacial Fe_2, Co_2, Ni_2, and Ni_3 complexes supported by a *para*-terphenyl diphosphine ligand were prepared. Central arene deplanarization and a μ_2:(η^3,η^3) coordination mode suggest partial bis-allyl character in the Fe_2 and Co_2 complexes. An oxidation induced shift in Fe_2-arene binding highlights the non-innocent nature of the arene ligand.

INTRODUCTION

Discrete mixed-metal complexes have been studied for molecular-level insight into the structural and electronic factors that influence cluster properties.[1] As the performance of heterogenous catalysts, in terms of activity, durability, selectivity, or cost, can be improved upon inclusion of cometals, an understanding of the underlying metal-metal interactions is needed.[2] To gain insight into such interactions, the study of well-defined, homogeneous, multinuclear heterometallic complexes has been pursued. Heterometallic dinuclear complexes are an active area of current research.[3] Additionally, heterometallic trinuclear complexes in triangular geometries are particularly appealing as one of the simplest model clusters displaying major and minor metal components and direct interactions between all metals, similar to heterogeneous catalysts. Although many advances have been made on the synthesis of multinuclear complexes containing isolated triangular heterometallic motifs,[2, 4] systematic access to related isostructural clusters suitable for structure-property studies is limited. Triangular trinuclear motifs are common in multinuclear heterometallic complexes, but differences in nuclearity, supporting ligands, or cluster oxidation states make systematic comparisons challenging.[2]

Another advantage of multinuclear systems is their potential to facilitate multi-electron transformations by distributing the redox load across several metal centers. Dinuclear metal complexes also have the potential to act in a cooperative fashion in small molecule activation and multi-electron processes.[5] In particular, low-valent Fe_2, Co_2, and Ni_2 complexes have been shown to participate in a variety of transformations, including proton reduction,[5a-c] dihydrogen activation,[5d] Pauson-Khand-type cycloadditions,[5e] C–C coupling,[5f-h] group transfer,[5i, 5j] and carbon dioxide activation.[5k-n]

The development of novel dinucleating ligand scaffolds and complexes capable of both undergoing redox processes and facilitating novel chemical transformations is currently a topic of active research.[6] Our group has recently utilized bis- and tris(phosphinoaryl)benzene ligands as multinucleating scaffolds for Ni and Pd complexes, where the central arene participates as a flexible donor ligand.[5g, 7]

The following chapter summarizes two distinct projects targeting multinuclear hetero- and homometallic complexes. Herein we report the rational synthesis of a series of isostructural, low oxidation state heterometallic complexes of the M_2M'-type, supported by two *para*-terphenyl diphosphine ligands with differing central arene electronics. We also describe a series of homometallic, dinuclear, first-row transition metal complexes supported by a *para*-terphenyl diphosphine and study the flexible Fe_2-arene coordination observed upon one-electron redox chemistry.

RESULTS AND DISCUSSION

2.1 Ligand Synthesis

Scheme 1. Synthesis of ligand *para*-terphenyl diphosphine ligands

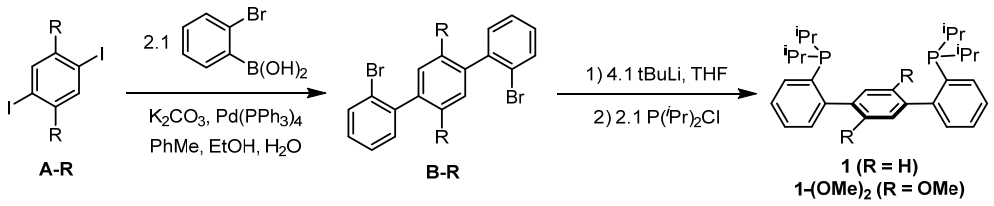

The synthesis of the parent *para*-terphenyl diphosphine ligand (**1**) was accomplished according to literature procedure (Scheme 1).[8] The synthesis of the more electron-rich *para*-terphenyl diphosphine ligand, **1-(OMe)$_2$**, which contains a 1,4-dimethoxybenzene central arene as opposed to a central phenylene, was accomplished using a similar synthetic route (Scheme 1). A Pd-catalyzed Suzuki coupling between 2-bromophenyl

boronic acid and 2,5-diiodo-1,4-dimethoxy benzene (**A**) provided the desired *para*-terphenyl dibromide precursor (**B**). Subsequent lithium halogen exchange using *tert*-butyl lithium (*t*BuLi) followed by addition P(*i*Pr)$_2$Cl yielded the desired ligand, **1-(OMe)$_2$**, following workup.

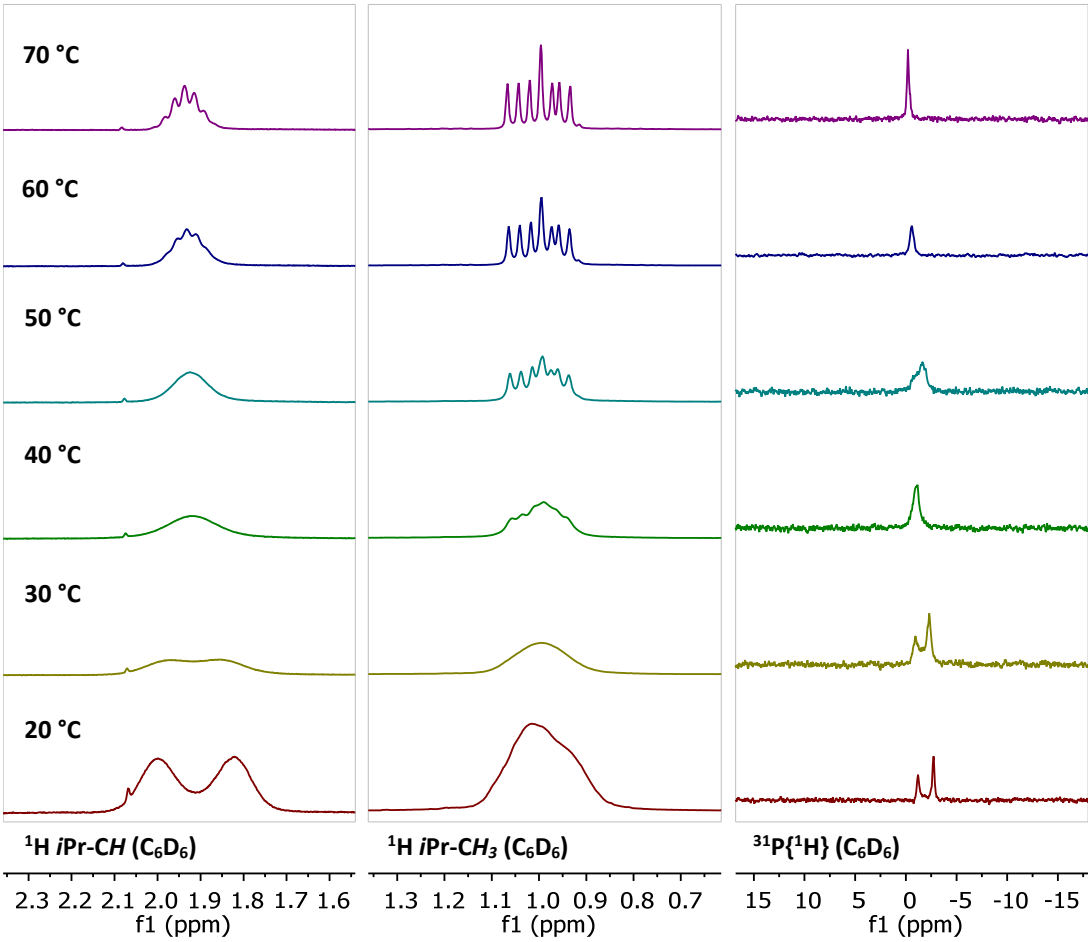

Figure 1. VT-NMR spectra for **1-(OMe)$_2$**.

In solution, **1-(OMe)$_2$** shows two broad *i*Pr methine resonances (2.05, 1.87 ppm) and a broad methyl signal by ^{1}H NMR. Two ^{31}P{^{1}H} signals (-1.18, -2.67 ppm) of inequivalent integration are also observed in contrast to **1**, which shows a single peak at 7.55 ppm (Figure 1). These data are consistent with hindered rotation around the aryl–

aryl bonds at room temperature as a result of the steric clash between the bulky phosphine moieties and the *ortho*-methoxy central arene substituents of **1-(OMe)$_2$**. Similar solution NMR behavior has been reported in a related *meta*-terphenyl diphosphine ligand.[9] To test this hypothesis, variable temperature (VT) NMR experiments were pursued with **1-(OMe)$_2$**. Heating a sample of **1-(OMe)$_2$** to 70 °C in C_6D_6 was sufficient for coalescence of the *i*Pr methine proton resonances and resulted in substantially sharper methyl signals (Figure 1). Additionally, a single ^{31}P resonance at -0.2 ppm was observed at 70 °C, confirming the presence of a single ligand rather that two distinct phosphorus-containing species in solution. The synthesis of **1-(OMe)$_2$** allows for a study of the effects of central arene electronics on the spectroscopic properties of supported metal complexes.

2.2 Synthesis and Characterization of Heterometallic Trinuclear M_2M'-Type Clusters

We have previously reported the chemistry of homometallic clusters coordinated by multidentate phosphinoarene ligands.[7a, 8, 10] Targeting heterometallic trinuclear clusters, dinuclear Pd_2 (**2**) and Ni_2 (**7**) precursors were treated with the tetracarbonyl anions of Fe and Co (Scheme 2). $[Na]_2[Fe(CO)_4]$ was found to react with **2** and **7** to yield $[Pd_2Fe]^0$ (**3**) and $[Ni_2Fe]^0$ (**8**) cores, respectively, while $[Na][Co(CO)_4]$ generated the corresponding $[Pd_2Co]^+$ (**4**) core following reaction with **2**. Reactions of **7** and $[Na][M(CO)_n]$ (M = Co (n = 4), Mn (n = 5)) precursors yielded multinuclear Ni-carbonyl clusters, which will further discussed in Section 2.3, rather than a $[Ni_2M]^+$ (M = Co, Mn) core. $Mo(CO)_3(MeCN)_3$ was found to react with **2** to yield the corresponding $[Pd_2Mo]^{2+}$ core (**6**), demonstrating that salt metathesis reactions with anionic transition metal carbonyl precursors were not required to construct heterometallic trinuclear complexes.

Scheme 2. Synthesis of heterometallic trinuclear complexes.

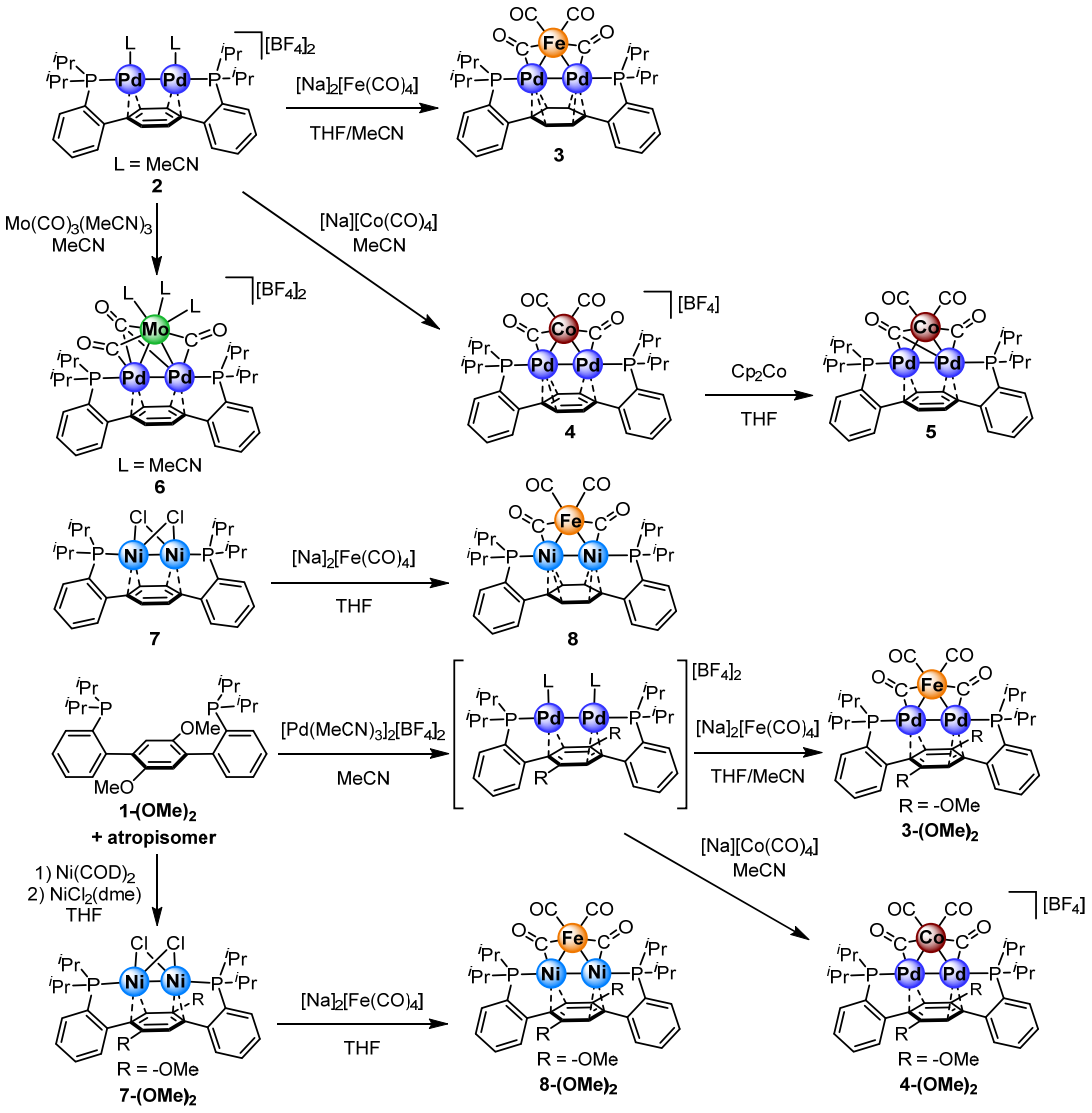

These complexes represent very rare examples of triangular clusters, with only two Pd_2Co, four Ni_2Fe, and no Pd_2Fe species structurally characterized previously.[4a, 4b, 4e-g, 4i] Spectroscopic and structural parameters of these reported clusters are challenging to compare due to differences in cluster oxidation state and the identity of supporting ligands. The present series maintains the same ligand environment while varying the identity of the major and minor metal components. To analyze the effect of ligand electronics on cluster properties, a

diphosphine variant with *para*-methoxy-substitution of the central arene, **1-(OMe)$_2$** (Scheme 2), was employed to support analogous multinuclear complexes. A one-pot metalation of **1-(OMe)$_2$** with $[Pd_2(MeCN)_6][BF_4]_2$ followed by the addition of $[Na]_2[Fe(CO)_4]$ or $[Na][Co(CO)_4]$ yielded the desired $[Pd_2Fe]^0$ (**3-(OMe)$_2$**) or $[Pd_2Co]^+$ (**4-(OMe)$_2$**) cores, respectively. Adapted literature procedures were used to synthesize the analogous Ni_2 precursor (**7-(OMe)$_2$**) via a comproportionation reaction with $Ni(COD)_2$ (COD = 1,5-cyclooctadiene) and $NiCl_2$dme (dme = 1,2-dimethoxyethane). **7-(OMe)$_2$** was allowed to react with $[Na]_2[Fe(CO)_4]$ to obtain the targeted $[Ni_2Fe]^0$ core (**8-(OMe)$_2$**). Multiple techniques have been utilized to compare the reported compounds: electrochemical measurements, NMR spectroscopy, Mössbauer spectroscopy, and IR spectroscopy in addition to structural comparisons from solid-state structures.

Single crystal X-ray diffraction (XRD) studies were performed for **3**, **4**, **6**, **3-(OMe)$_2$**, and **8** (Figure 2). The homodinuclear moiety (M_2) is bound to the phosphine and arene donors in a manner reminiscent of the precursors (**2** and **7**).[8, 10a, 11] The apical metal (M') of the $M_2M'(CO)_4$–type clusters display interactions with the M_2 core and two CO ligands, one bridging each M–M' interaction. For complex **6**, the all three CO ligands support the Pd_2 core-Mo interaction. One CO ligand bridges across one face of the Pd_2Mo core in a μ_3 fashion, while the remaining two each bridge a different Pd–Mo interaction. Despite the variation of apical and dinuclear core metal identity as well as ligand electronics, the clusters remain largely isostructural, with the exception of **6**. The metal-metal distances for $Pd_2M(CO)_4$–type clusters are similar between complexes **3**, **4**, and **3-(OMe)$_2$** with Pd–Pd distances ranging between 2.5643(3) and 2.5853(3)(2) Å and Pd–M' distances ranging between 2.5374(3) and 2.5541(6) Å. Owing the larger size of Mo compared to Fe or Co, complex **6** shows a considerably

expanded trinuclear core with a Pd–Pd distance 2.6220(2) Å and Pd–Mo distances of 2.8176(3) and 2.7516(3) Å. Complex **8** shows shorter metal-metal distances of 2.3931(8) and 2.4169(6) Å for Ni–Ni and Ni–Fe, respectively, due to the smaller size of Ni compared to Pd. Both average Pd–Pd and Ni–Ni distances are similar to the metal-metal distances in a previously reported mono-atom bridged complexes such as the dmdbt-Pd_2 complex (dmdbt = 4,6-dimethyldibenzothiophene) and complex **7**.[8, 10a]

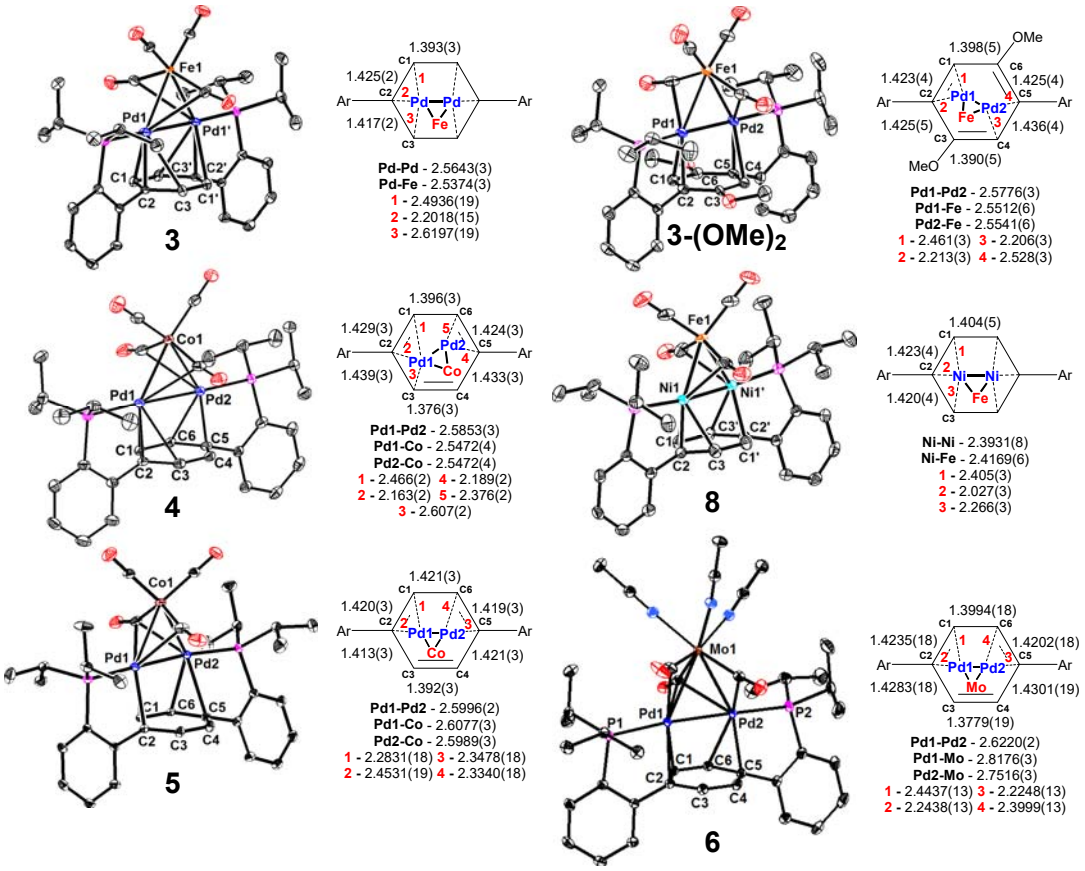

Figure 2. Solid-state structures and select bond metrics for the synthesized trinuclear compounds. Hydrogen atoms, solvent, and counter ions have been omitted for clarity.

The binding mode of the central arene and the NMR characteristics core for each complex allows for the interrogation of the effect of changing of the apical metal on the M_2 moiety. Isoelectronic compounds **3** and **4** show slightly different metal-arene interactions, changing

from *pseudo*-C_2 μ_2:(η^3,η^3) to μ_2:(η^3,η^2). The closest Pd–C contacts are slightly shorter in **4** compared to **3**, potentially a consequence of the cationic nature of **4** leading to stronger metal-arene interactions. Complex **6** and **3-(OMe)$_2$** both show different μ_2:(η^2,η^2) coordination modes in the solid-state with the M_2 moiety of the former binding to C1–C2 and C4–C5 while the latter coordinates to adjacent C–C bonds (C1–C2 and C5–C6) as seen in the Pd_2 precursor **2**. Complex **8** shows a *pseudo*-C_2 μ_2:(η^3,η^3) coordination mode reminiscent of **3**. In solution, complexes **3**, **4**, and **8** show single resonances (^{1}H NMR spectroscopy) for central arene protons (δ(ppm) **3**: 5.92; **4**: 6.39; **8**: 5.78), indicating fluxional central arene coordination on the NMR timescale. The significantly upfield shifted resonance for the central arene protons compared to **1** (7.55 ppm) is indicative of metal-arene interactions as observed by XRD. NMR data for the $M_2M'(CO)_4$-type clusters supported by **1-(OMe)$_2$** ligand also show an upfield shift of the central arene proton resonance (δ(ppm) **3-(OMe)$_2$**: 5.51; **4-(OMe)$_2$**: 5.80; **8-(OMe)$_2$**: 5.30) compared to free ligand (6.83 ppm) again consistent with strong metal-arene interactions. Distortions of the central arene consistent with a reduced arene or bis-allyl assignment as seen in previously characterized Co_2 and Fe_2 complexes, which will be discussed in greater detail in Section 2.3, are not consistent with the solid-state structures despite spectroscopic evidence for significant metal-arene interactions.[10c]

Solution infrared (IR) spectroscopy was used as a measure of the effect of the identity of the homodinuclear component (M_2) and supporting ligand on the cluster properties. The clusters containing the $Fe(CO)_4$ moiety display bands corresponding to C–O stretches (ν_{CO}(cm^{-1}) **3**: 1901 (s), 1874 (m), 1848 (s), 1843 (w, sh); **3-(OMe)$_2$**: 1898 (s), 1867 (m), 1838 (s, coincidental overlap with weak shoulder ν_{CO} stretch); **8**: 1896 (s), 1874 (m), 1821 (m), 1798 (w, sh)). Complex **8** shows a larger reduction in average carbonyl stretching frequency (20 cm^{-1}).

The effect of the more electron-rich central arene of **3-(OMe)$_2$** is seen in the average carbonyl stretching frequencies that shift by 7 cm^{-1} to lower energy compared to **3**, though the magnitude of the change is smaller. These differences indicate that the moiety in direct contact with Fe (Ni$_2$ or Pd$_2$) has a larger effect than the more distant arene ligand. Mössbauer data was obtained to further to probe the electronic differences between Fe-containing complexes (Figure 3-5). The isomer shifts and quadrupole splitting of all complexes (δ (mm s^{-1}) (ΔEq (mm·s^{-1})) **3**: -0.10 (1.08), **3-(OMe)$_2$**: -0.09 (1.13), **8**: -0.11 (0.83)) are within 0.02 mm s^{-1} range suggesting the presence of similar Fe centers despite the differences observed by IR spectroscopy. Complex **4** shows IR absorptions at higher energy (2057 (s), 2012 (m), 1915 (m), and 1878 (w, sh) cm^{-1}) compared to **2**, consistent with the expected trends for isoelectronic complexes based on higher nuclear charge for Co vs Fe. Complex **6** shows three IR absorptions (1900 (s), 1847 (s), and 1799 (s) cm^{-1}) consistent with the asymmetry of the solid-state structure. The C_{3v} symmetry of the Mo(CO)$_3$(MeCN)$_3$ precursor results in the appearance of only two IR absorptions: an A_1 set at 1920 cm^{-1} and an E set at 1796 cm^{-1}.[12] The average ν_{CO} stretching frequencies of complex **6** (1849 cm^{-1}) are slightly shifted to higher energy compared to the precursor (1837 cm^{-1}), consistent with binding of the Mo center to an electron-deficient dicationic Pd$_2$ core.

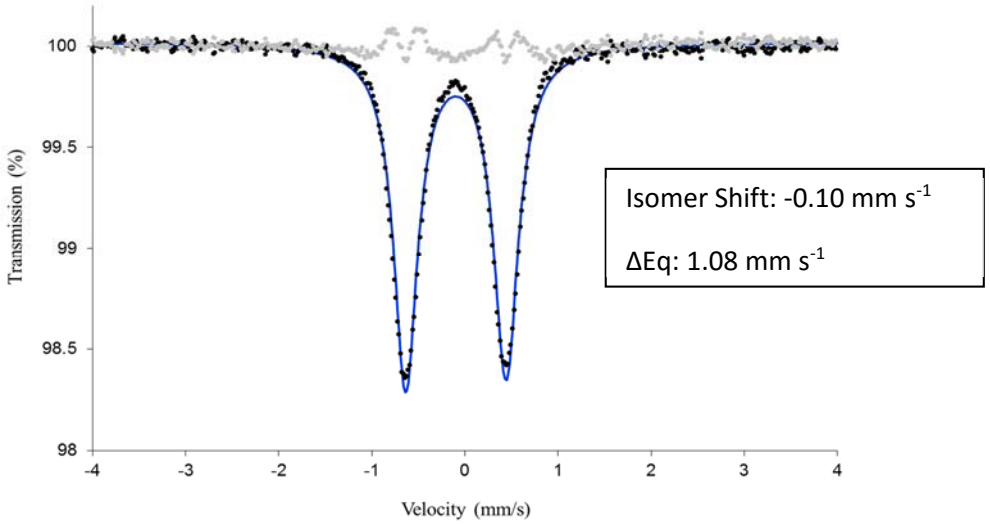

Figure 3. Zero-field ^{57}Fe Mössbauer spectrum for **3**, 80 K. Data: black dots; spectral fit: blue line; and residual: grey dots.

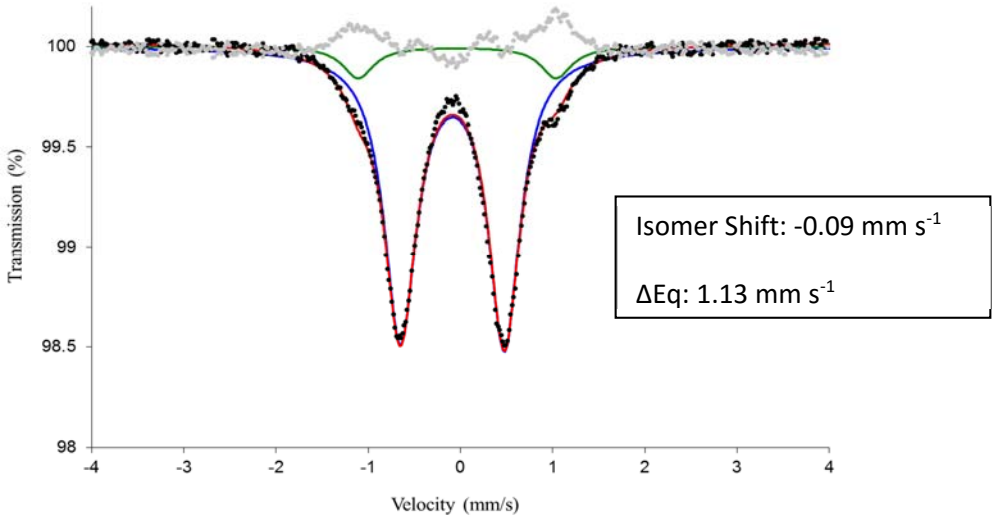

Figure 4. Zero-field ^{57}Fe Mössbauer spectrum for **3-(OMe)$_2$** and minor decomposition (green line) following removal from glovebox, 80 K. Data: black dots; spectral fit: red line; deconvolution: blue and green lines; residual: grey dots.

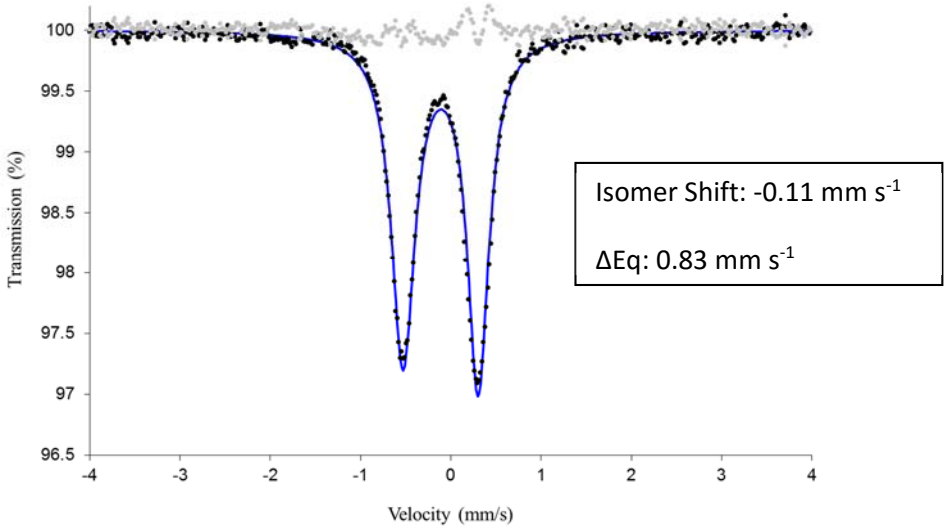

Figure 5. Zero-field ^{57}Fe Mössbauer spectrum for **8**, 80 K. Data: black dots; spectral fit: blue line; and residual: grey dots.

Computational studies were performed on simplified models of **3**, **4**, **3-(OMe)$_2$**, and **8** (see Table 3 for details and representative molecular orbitals for all compounds). Calculated metal-metal distances are in good agreement with solid-state parameters obtained from XRD studies (Table 1) with largest deviations in M–M and M–M' distances see for complex **7** at 0.046 and 0.020 Å, respectively. Differences in computed average carbonyl stretching frequencies largely agree with the experimental differences (Table 2). Select computed MOs are highlighted for a truncated model of **3** (**3-Me$_2$**) (Figure 3). Natural bond orbital (NBO) calculations reveal Wiberg bond indices (WBIs) consistent with weak bonds of comparable strength for both M–M (**3-Me$_2$**: 0.1647, **4-Me$_2$**: 0.1647, **3-(OMe)$_2$-Me$_2$**: 0.1658, **8-Me$_2$**: 0.1647) and M–M' (**3-Me$_2$**: 0.2147, **4-Me$_2$**: (0.1758, 0.1753), **3-(OMe)$_2$ -Me$_2$**: (0.2133, 0.2131), **8-Me$_2$**: 0.2140) interactions in all complexes (Figure 27). These results are consistent with a previously reported bonding picture with the formally 18-electron M(CO)$_4$ fragment donating electron density to the M$_2$ fragment, which states that M–M' interactions provide the largest

stabilization responsible for cluster formation.[13] These weak M–M' interactions suggest direct electronic communication between the $M(CO)_4$ moiety and the homodinuclear core.

Table 1. Comparison of Calculated and Experimental Bond Metrics

Complex	ν_{CO}(calc) (cm^{-1})	Average ν_{CO}(calc) (cm^{-1})	ν_{CO}(expt) (cm^{-1})	Average ν_{CO}(expt) (cm^{-1})
3	2029.2, 1980.3, 1948.4, 1927.5	1971.4	1901 (s), 1874 (m), 1848 (s), 1843 (w, sh)	1867
4	2110.7, 2076.0, 2023.8, 1991.2	2050.4	2057 (s), 2012 (m), 1915 (m), 1878 (w, sh)	1966
3-$(OMe)_2$	2024.3, 1976.3, 1931.4, 1909.3	1960.3	1898 (s), 1867 (m) 1838 (s, coincidental overlap with weak should stretch)	1860
8	2015.0, 1964.1, 1924.7, 1902.8	1951.7	1896 (s), 1874 (m) 1821 (m), 1798 (w, sh)	1847

Table 2. Comparison of Calculated and Experimental IR Parameters

Complex	$d(M\text{-}M)_{calc}$ (Å)	$d(M\text{-}M)_{expt}$ (Å)	$d(M\text{-}M')_{calc}$ (Å)	$d(M\text{-}M')_{expt}$ (Å)
3	2.5889	2.5643(3)	2.5379, 2.5382	2.5374(3)
4	2.5983	2.5853(3)	2.5463, 2.5464	2.6077(3), 2.5472(4)
3-$(OMe)_2$	2.5988	2.5776(3)	2.5398, 2.5402	2.5512(6), 2.5541(6)
8	2.3474	2.3931(8)	2.3970, 2.3976	2.4169(6)

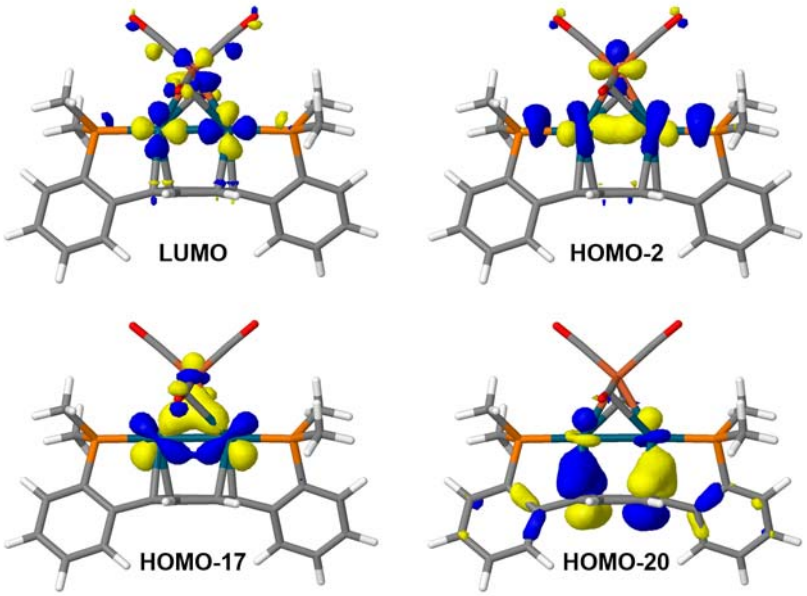

Figure 6. Select molecular orbitals calculated for a truncated version of **3** (**3-Me**$_2$) that show interactions between (clockwise from LUMO), M–M/M–M', M–M, M–arene, and M–M' moieties.

Cyclic voltammetry (CV) experiments were conducted on complexes of the trinuclear series (see Experimental Section for full conditions). Quasireversible reductions for all complexes were observed at (**3**: -2.43 V), (**4**: -1.31, -1.81 V), (**3-(OMe)**$_2$: -2.62 V), and (**8**: -2.29, -2.75 V) vs the ferrocene/ferrocenium (Fc/Fc^+) couple in tetrahydrofuran (THF) (Figure 7). Irreversible oxidations are observed for all complexes. While comparable CV data for Pd_2Fe and Ni_2Fe complexes are absent from the literature to the best of our knowledge, a systematic study of ligand variation in isoelectronic Pd_2Co complexes has been reported.[4g] The reported trinuclear complex $[Pd_2Co(\mu\text{-dppm})_2(\mu_3\text{-CO})_2(CO)_2][PF_6]$ (dppm = 1,1-bis(diphenylphosphino)methane) was reported to have two one-electron reductions with $E_{1/2}$ potentials comparable to **4** at -1.20 V and -1.63 V vs Fc/Fc^+ in THF despite significant differences in supporting ligands.

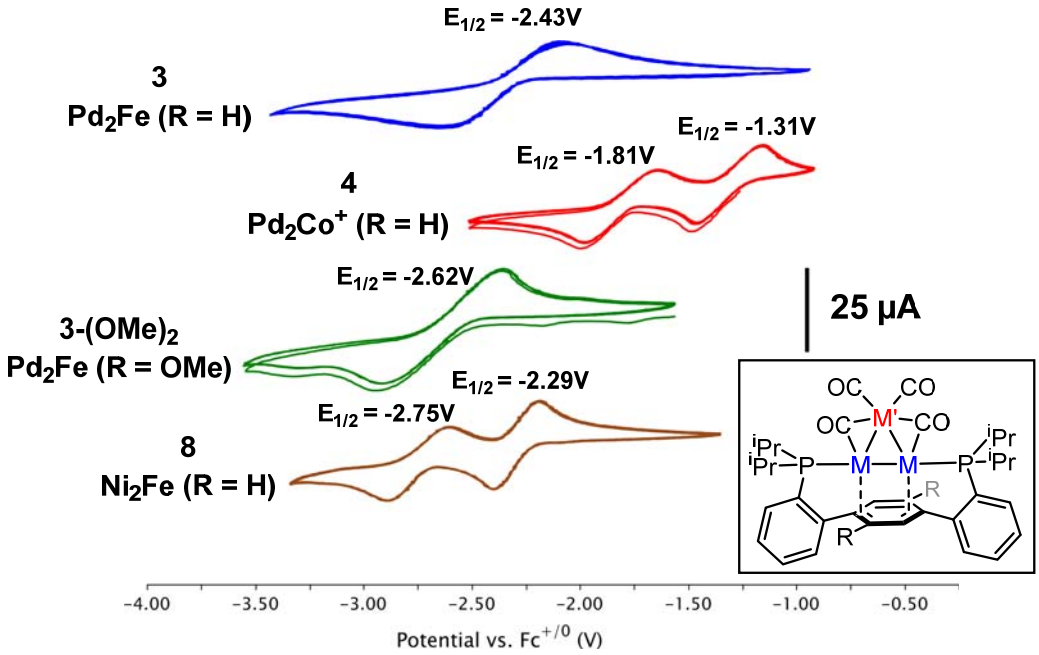

Figure 7. Cyclic voltammetry data for the reported $M_2M'(CO)_4$–type complexes.

Both Pd_2Fe complexes, **3** and **3-(OMe)$_2$**, display CV behavior with only a single, two-electron electrochemical reduction observed at more negative potentials than both peaks for **4**. The reduction of **3-(OMe)$_2$** is ~200 mV more negative than **3**, a consequence of the more electron-rich supporting arene. The Ni_2Fe complex **8** shows similar electrochemical behavior as **4**, with two reduction events, but at potentials ~1 V more negative. The more electron-rich Ni_2Fe complex, **8-(OMe)$_2$**, also shows two quasireversible reductions (-2.42, -2.88 V) shifted to more negative potentials by approximately ~130 mV compared to **8** (Figure 8). The increased charge of the Pd_2Co core relative to the Ni_2Fe or Pd_2Fe complexes likely contributes to the positive shift in the redox events for complex **4**, making the reduction more facile. Overall, the electrochemical data indicate that metal composition and supporting ligand play a significant role in cluster properties as the variation of apical metal (Fe to Co) and dinuclear core (Pd_2 to Ni_2) significantly affects redox behavior.

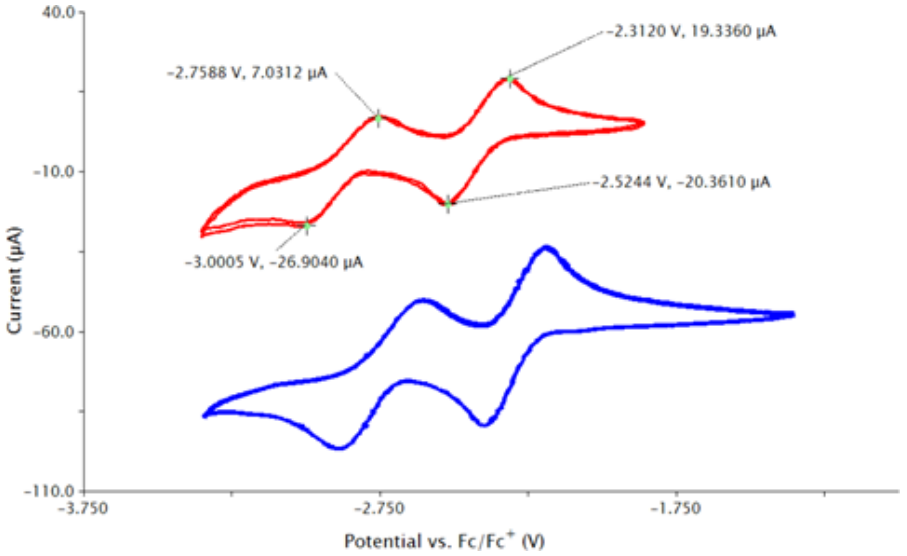

Figure 8. A comparison of cyclic voltammetry data for complexes **8** and **8-(OMe)$_2$**.

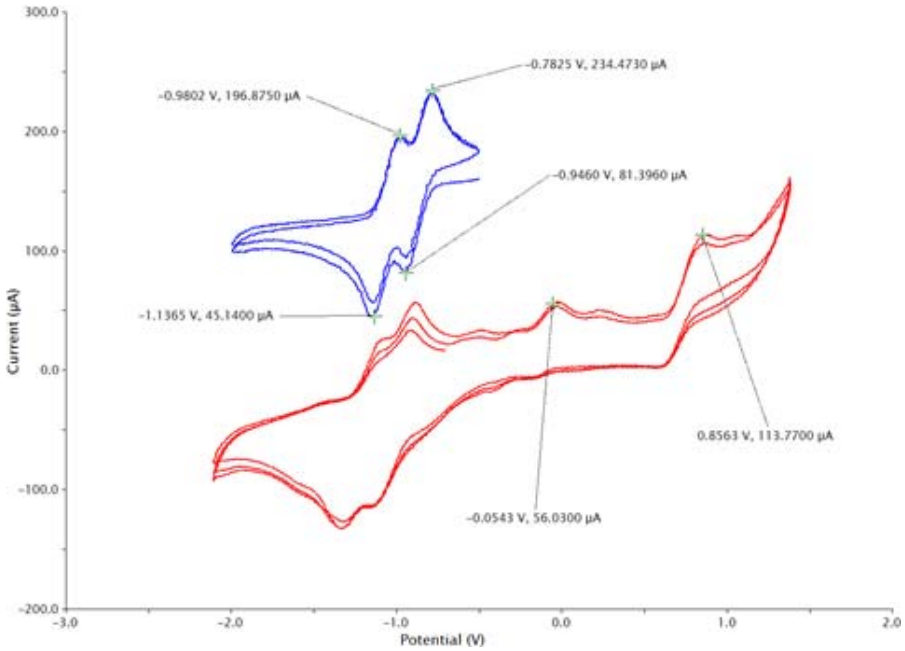

Figure 9. Cyclic voltammetry data for the complex **6**.

CV experiments in acetonitrile (MeCN) were also conducted on complex **6** (Figure 9). As with the aforementioned trinuclear clusters, irreversible oxidations are observed. Reminiscent of the electrochemical behavior of **4** and **8**, a pair of quasireversible reduction events (-0.64,

-1.28 V) are observed for complex **6**. These reductions occur at considerably more positive potentials compared to $M_2M'(CO)_4$-type clusters, which is likely attributable to the increased cationic charge of compound **6**.

In light of the electrochemical observations, chemical reductions were performed with **3**, **4**, **3-(OMe)$_2$**, and **8**. The Fe-containing complexes led to complex mixtures of products. The neutral $[Pd_2Co]^0$ core, complex **5**, was successfully isolated upon treatment of **4** with one equivalent of cobaltocene (Scheme 2). While unstable at room temperature, single crystals suitable for XRD analysis were obtained at -35 °C (Figure 2). Coordination of the dinuclear core to the central arene has shifted to μ_2:(η^2,η^2) and the bridging CO ligands have adopted a different geometry, with one bound μ_3 across the Pd_2Co core, indicative of increased back-bonding to the π-acidic ligands. In agreement, IR spectra of complex **5** display CO stretching frequencies of 2007 (s), 1920 (m, sh), 1879 (m), and 1837 (m) cm^{-1} that are shifted to lower energy compared to **4**. Increases in Pd–Co and Pd–Pd bond distances by 0.06 and 0.03 Å, respectively, are consistent with weakened M–M and M–M' interactions. Solution electron paramagnetic resonance (EPR) data for **5** obtained in a toluene glass at 77 K shows a rhombic signal (g = 2.128, 2.032, 1.930) with hyperfine coupling to the Co nucleus (A = 119, 65, 105) (Figure 10), and compares well to a comparable literature complex.[4g] The flexible coordination the central arene and CO ligands likely helps stabilize complex **5**, allowing for its isolation. Overall, the synthesis of a new series of heterometallic trinuclear complexes allowed for the systematic study of the effects of changes in metal composition and ligand electronics.

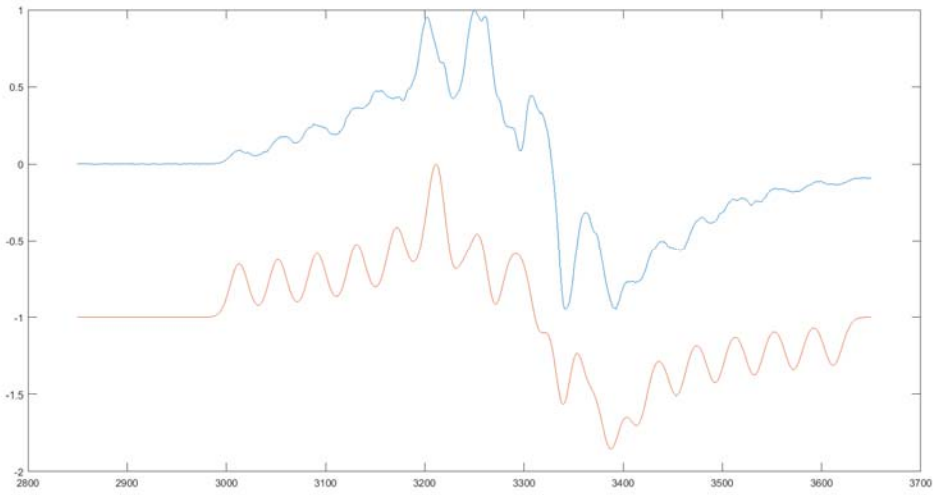

Figure 10. X-band EPR spectrum of **5** collected at 77K in a toluene glass (blue). EasySpin simulation of EPR data (red).

2.3 Synthesis and Characterization of Homometallic Di- and Trinuclear Carbonyl Complexes

Efforts targeting homometallic multinuclear complexes were also pursued. After multiple days of ultraviolet irradiation, a THF solution of compound **1** and $Fe_3(CO)_{12}$ yielded a Fe_2 complex, **9**, in 11% isolated yield (Scheme 3). Refluxing a toluene (PhMe) solution of compound **1** and $Co_2(CO)_8$ at 110 °C overnight cleanly afforded a Co_2 complex, **11**, in 54% isolated yield (Scheme 3). The analogous cofacial Ni_2 complex was prepared by the reduction of a previously synthesized Ni^I–Ni^I dichloride complex, **7**,[5g] with [Na][$Co(CO)_4$], or [Na][$Mn(CO)_5$] which served as a source of both reducing equivalents and carbon monoxide (CO) ligands. The Ni_2 complex, **12**, was isolated in 11% yield (Scheme 1). An alternative synthesis of complex **4** involved the careful addition of four equivalents of CO to two equivalents of $Ni(COD)_2$ and compound **1** (Scheme 3). However, this method was lower yielding and not used as the primary synthetic route. The low yields for compounds **9** and **12** are due to purification

procedures, which require isolation of crystalline material. The reaction mixtures for the syntheses of these complexes display the desired compounds as the major species by ^{31}P NMR spectroscopy. An added complication was the gradual conversion of **12** into a mixture of a $Ni_3(CO)_4$ complex (**13-CO**) and a mononickel carbonyl complex (**1-Ni(CO)**) in solution. **13-CO** could be independently synthesized by metalating **1** with three equivalents of $Ni(COD)_2$ in the presence of a five equivalents of carbon monoxide, which afforded the product in 74% yield (Scheme 3). Control of CO stoichiometry is necessary, as a large excess results in the excessive coordination of carbon monoxide to generate previously characterized transfacial dinuclear $Ni(CO)_n$ (n = 2-3) complexes.[8]

Scheme 3. Synthesis of homometallic multinuclear carbonyl complexes of Fe, Co, and Ni

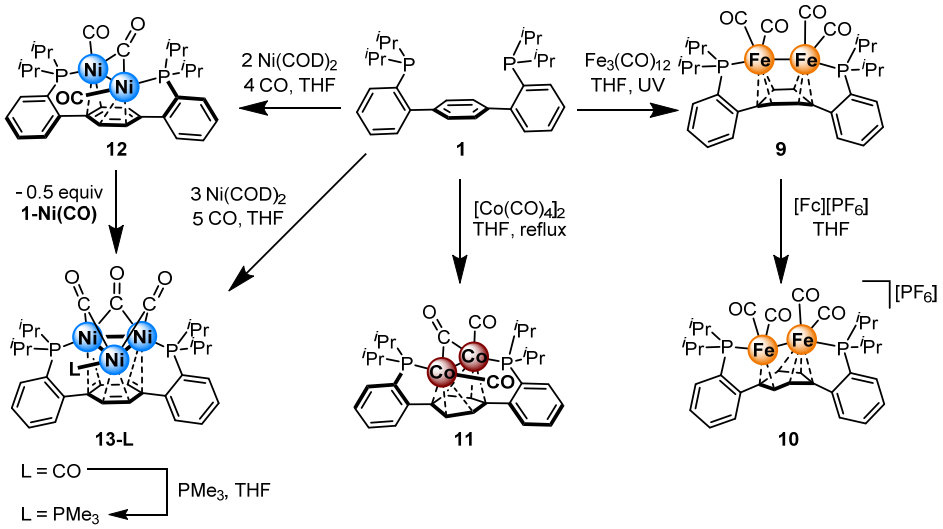

Single crystal XRD studies of complexes **9**, **11**, **12**, and **13-CO** confirmed the stabilization of multinuclear homometallic fragments by metal-arene interactions (Figure 11). The dinuclear core of complex **9** and **11** coordinate in a μ_2:(η^3,η^3) fashion to the central arene. In **9**, the phosphines coordinated to each Fe center are roughly

colinear with the Fe–Fe vector, resulting in a structure of *pseudo*-C_{2v} symmetry. The zig-zag arrangement of the P_2Co_2 moiety in **11**, imposed by the bridging and terminal CO ligands on Co, effects the overall *pseudo*-C_2 symmetry of the dicobalt complex. In complex **9**, the planes defined by C1-C2-C3 and C4-C5-C6 show an average dihedral angle of 26º with the C1-C3-C4-C6 plane. Central arene deplanarization is also observed in complex **11**, with a dihedral angle averaging approximately 23º between both the C2-C3-C4 and C5-C6-C1 planes with the C1-C2-C4-C5 plane. The deplanarized central arene carbons of complex **11** are *ortho* to the aryl substituents, oriented to match the Co–Co vector. The C–C bonds separating the η^3-M moieties are considerably elongated, averaging approximately 1.469 Å for C1–C6 and C3–C4 in complex **2** and 1.470 Å for C1–C2 and C4–C5 in complex **11**. These structural features are consistent with reduction of the arene to generate a bis-allyl motif and formal oxidation of the M_2 core by two electrons to yield a M^I–M^I unit (M = Fe, Co). Further supporting this assignment are short M–arene distances that are consistent with literature bisallyl Fe_2 or Co_2 complexes.[14] Bridging arene complexes of Fe_2 and Co_2 displaying a bis-allyl motif are very rare and typically have the two metal centers bound in transfacial manner.[15, 16] Compounds **9** and **11** represent unusual examples of cofacially coordinated μ_2-arene complexes. The Fe–Fe distance in complex **9** (2.7563(2) Å) is comparable to a cofacial μ_2:(η^3,η^3)-toluene Fe_2 complex at 2.746(1) Å,[15b] but shorter than typical bis-allyl diiron compounds which range between 2.927(3) and 3.138(3) Å.[14b-d] The Co–Co distance (2.6035(2) Å) in **11** is in the range for a formal single Co^0-Co^0 bond.[17]

In contrast to the Fe_2 and Co_2 systems, the Ni_2 core of complex **12** binds μ_2:(η^2,η^2) to adjacent C–C bonds of the central arene (Figure 11). In the solid-state, complex **12** shows partial localization of single bond character at C1–C6, C2–C3, and C4–C5, indicative of disrupted aromaticity. No deplanarization of the central arene ligand is observed, suggesting that bisallyl character is not present. While transfacial μ_2:(η^2,η^2)-arene Ni^0Ni^0 complexes are known,[18] complex **12** displays the first structurally characterized cofacial μ_2:(η^2,η^2) binding mode. The coordination sphere of Ni in complex **12** is reminiscent of $Ni_2(CO)_3(dppm)_2$ with a phosphine donor replaced by an arene double bond for each metal center and twisting of the dihedral angle defined by the two terminal carbonyl carbons and the Ni–Ni vector (dppm = bis(diphenyphosphino)methane).[10a]

An XRD study reveals that complex **13-CO** has similar structural features another previously reported trinickel complex supported by a related ligand scaffold (Figure 11).[7a] Instead of a third phosphine arm, Ni3 binds a terminal CO ligand. The Ni_3 core of complex **13-CO** binds μ_3:(η^2,η^2,η^2) to adjacent C–C bonds of the central arene. Central arene C–C bond distances range between 1.419(2) and 1.435(2) Å indicating strong Ni backbonding. This is also corroborated by short Ni-arene distances in **13-CO** which range between 2.130(2) to 2.185(2) Å with an average distance (2.157 Å) comparable to that of **12** (2.195 Å). The Ni–Ni distances in compound **13-CO** (2.4394(3), 2.4466(3), 2.4746(3) Å) are substantially shorter than those in **12** (2.6313(4) Å), which may be attributable to the more constrained triangular geometry. Consistent with the solid-state structure, the solution IR spectrum of **13-CO** shows bands at 2002, 1873, and 1830 cm^{-1}, indicative of terminal and bridging carbon monoxide coordination.[19]

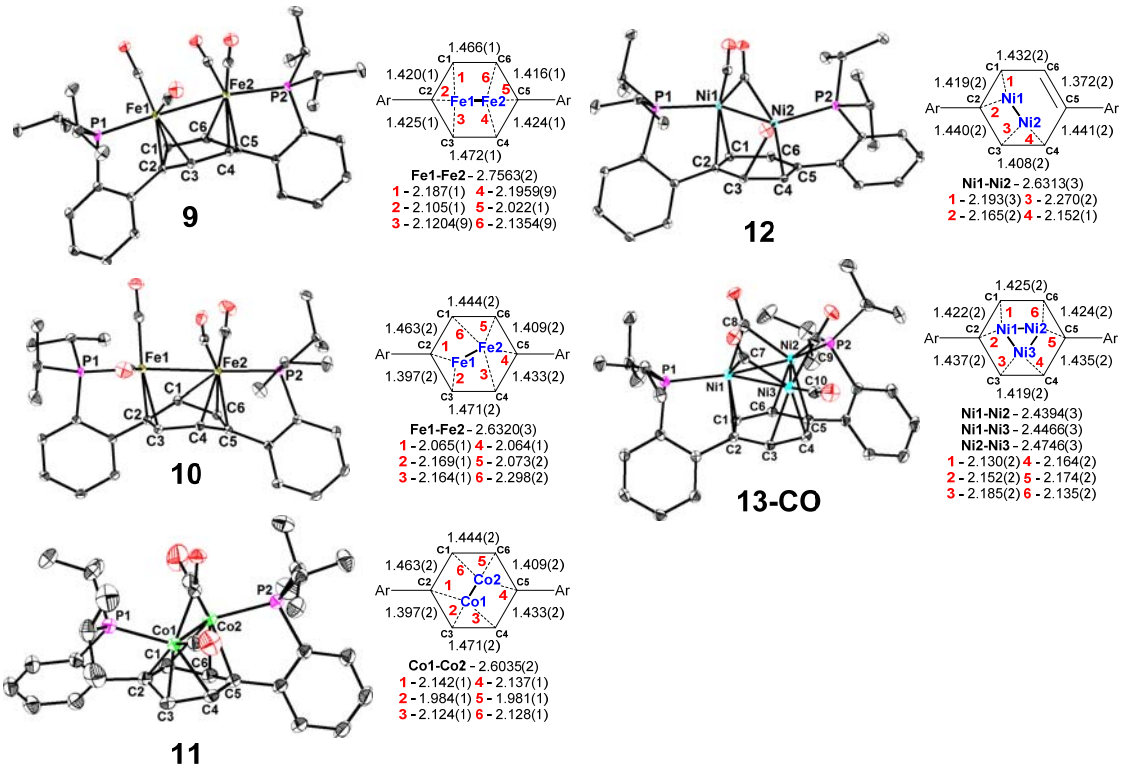

Figure 11. Solid-state structures and select bond metrics for synthesized compounds. Hydrogen atoms, solvent, and counter ions have been omitted for clarity.

The ^{1}H NMR chemical shifts of the central arene protons of complex **9**, **11**, and **12** are shifted upfield in comparison to the parent ligand, as a singlet at 4.39 ppm, a pair of 1:1 singlets at 4.29 and 3.95 ppm, and a singlet at 5.85 ppm, respectively, indicating that strong metal-arene interactions and disruption of aromaticity are preserved in solution. The NMR spectra of **9** are consistent with the high symmetry observed in the solid-state structure. Variable temperature (VT) NMR experiments were performed for complexes **11** and **12**. For **11**, VT ^{1}H NMR experiments show broadening of the central arene and methine protons upon heating, with coalescence observed around 80 °C (Figure 12). At 100 °C, the central arene and methine protons each show a single broad peak. The fluxional process consistent with the observed NMR features involves the interconversion of the two *pseudo*-C_2 isomers by partial rotation of the Co_2 unit around

the central arene ring. VT ^{1}H NMR studies with complex **12** show decoalescence of the central arene protons into a pair of doublets at -20 °C (Figure 13). Further cooling to -78 °C was not sufficient to resolve the central arene protons into four separate resonances, indicating that the complex was not locked out as the C_1 solid-state structure due to partial rotation of Ni_2-unit. In agreement, the ^{31}P NMR spectrum shows a single peak, even at -78 °C. The lower energetic barrier for the fluxional process in **12** versus **11** may be due to a smaller molecular distortion, particularly of the central ring, necessary for partial rotation of the M_2 unit of **12**.

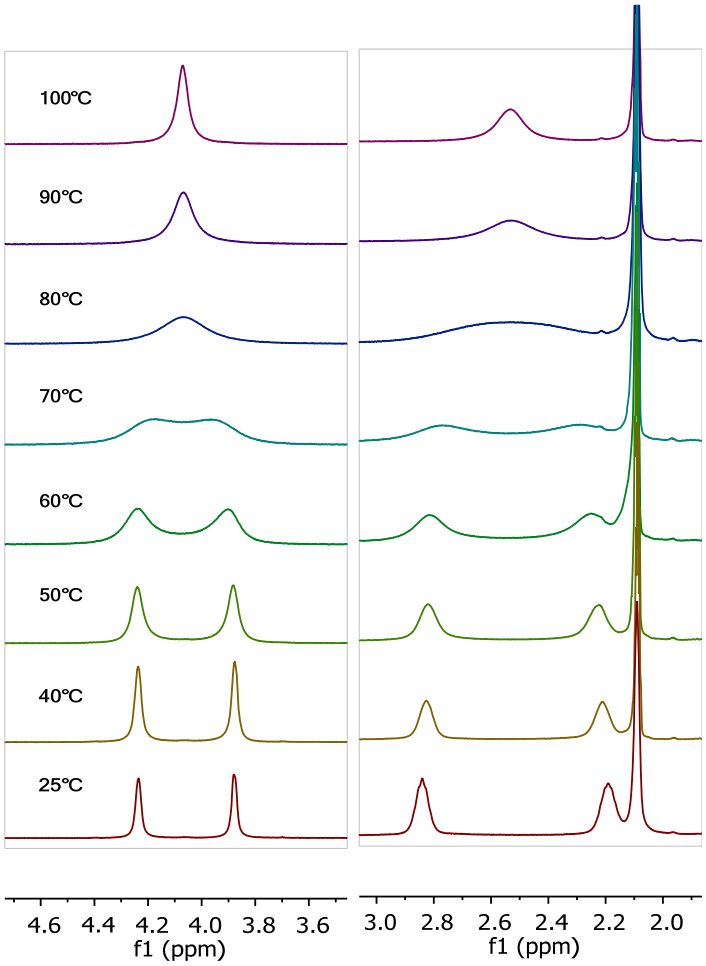

Figure 12. VT ^{1}H NMR (500 MHz, d_8-PhMe) spectra of **11** with central arene protons (Left) and methine protons (Right) shown.

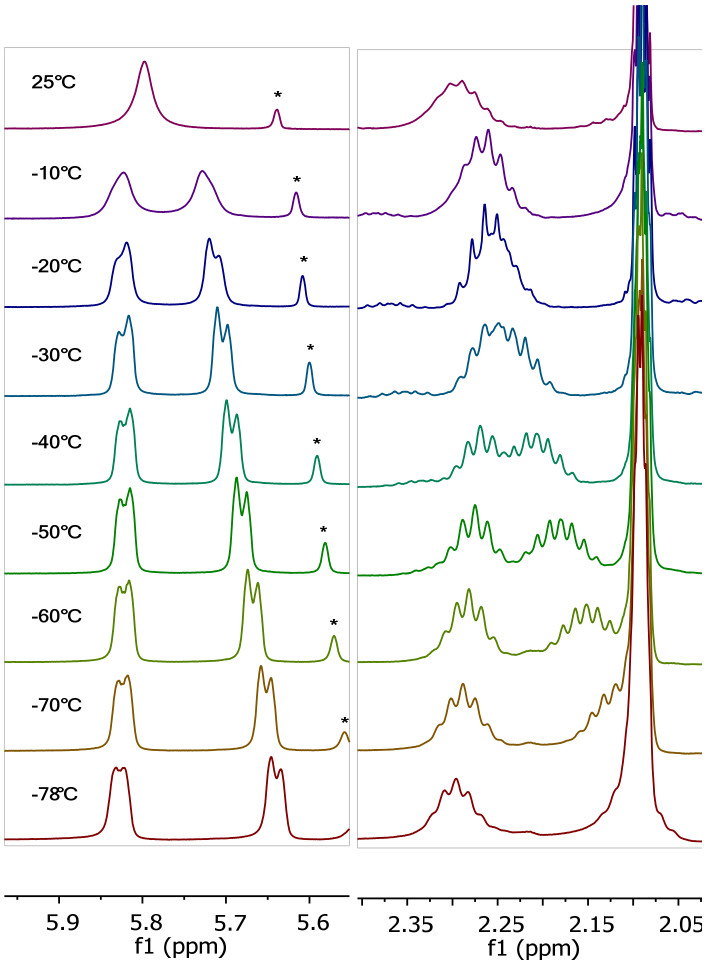

Figure 13. VT ^{1}H NMR (500 MHz, d_8-PhMe) spectra of **12** with central arene protons (Left) and methine protons (Right) shown. Starred peak corresponds to the partial decomposition of **12** to **13-CO** over course of experiment.

The weaker M-arene interactions of **12** compared to **9** or **11** may also contribute to the solution instability of the complex. The disproportionation of the Ni^0 centers and CO ligands of **12** may occur through a bimolecular process. A preliminary XRD structure containing two cocrystallized Ni complexes, one containing a Ni_3 core (molecule 1) reminiscent of **13-CO** while the other possesses a $Ni(CO)_2$ unit (molecule 2), which supports this hypothesis (Figure 14). The nickel center of molecule 2 is coordinated by only one phosphine donor, allowing the other to bind to molecule 1. While other disproportionation pathways may also be

operative, this structure provides evidence that two equivalents of **12** could exchange a nickel center via a transient dimer complex.

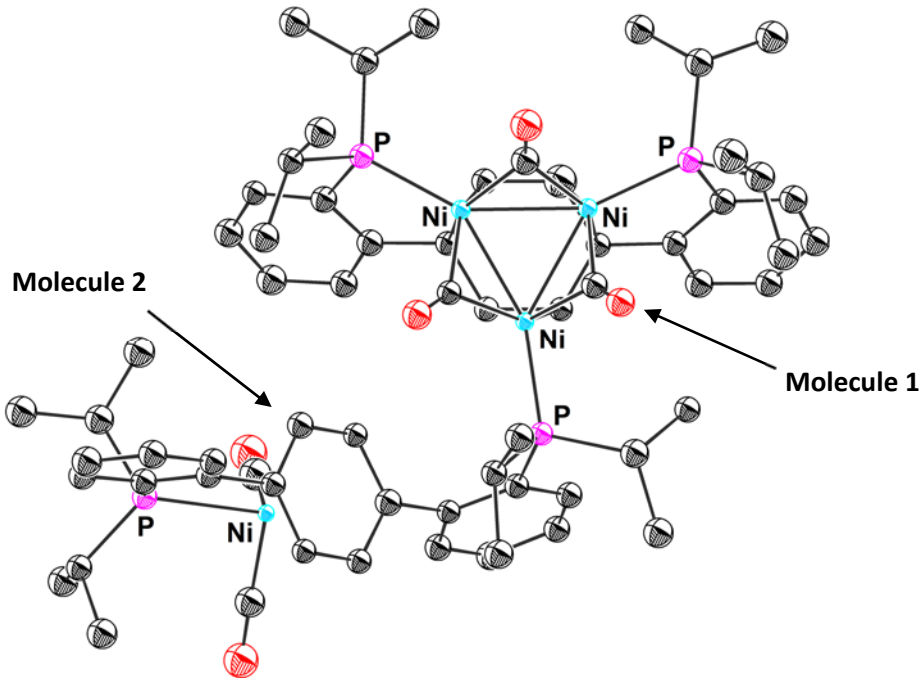

Figure 14. Preliminary solid-state structure highlighting a potential intermolecular pathway for the disproportionation of **12** to **13-CO** and a mononuclear Ni carbonyl complex in solution.

Solution NMR data for **13-CO** is consistent with the *pseudo*-C_{2v} solid-state structure. Two distinct resonances central arene protons are observed at 5.65 and 4.57 ppm, consistent with strong metal-arene backbonding. Two methine signals (2.30, 2.11 ppm) and a single resonance (50.32 ppm) are observed by ^{1}H and ^{31}P{^{1}H} NMR, respectively. The terminal carbon monoxide ligand of complex **13-CO** is readily substituted upon addition of trimethylphosphine (PMe_3) to yield complex **13-PMe$_3$** (Scheme 3). While single crystals suitable for XRD analysis have not been obtained to date due to the compound's high solubility, spectroscopic characterization of the complex indicates an intact triangulo-trinickel core. The C_s symmetry of complex **13-CO** has not been perturbed by PMe_3 substitution as

two ^{1}H NMR resonances corresponding to the methine protons are observed (2.41 and 2.24 ppm). The ^{31}P{^{1}H} NMR spectrum of **13-PMe$_3$** displays the terphenyl phosphines as a doublet at 51.49 ppm and the PMe_3 as a triplet at -6.61 ppm; the observed multiplicity is consistent with the assigned structure. Strong metal-arene interactions are also maintained based on the upfield-shifted ^{1}H NMR resonances at 5.12 and 4.67 ppm. The substitution of the terminal CO ligand is supported by the IR spectrum, showing only bands indicative of bridging CO ligands (1854, 1783 cm^{-1}) and the disappearance of the peak at 195.08 ppm (^{13}C NMR) observed for complex **13-CO**. The increased electron density of Ni3 induced by the ligand substitution is reflected in the 0.53 upfield shift of the arene C-*H* ^{1}H NMR peak compared to **13-CO** and the lower stretching energy of the bridging CO ligands. The lability of this terminal CO ligand suggests that coordination and activation of other molecules at the Ni_3 unit in **13-CO** may be possible.

The IR spectrum of complex **9** displays peaks corresponding to terminal CO stretches at 1966, 1914, 1903, and 1880 cm^{-1}. This is comparable to an asymmetrically substituted [FeFe]-hydrogenase model complex, (μ-pdt)[Fe^{I}(CO)$_2$(PMe$_3$)] [Fe^{I}(CO)$_2$(IMes)] (pdt = 1,3-propanedithiolate, IMes = 1,3-bis(2,4,6-trimethylphenyl)imidazol-2-ylidene), with CO stretches at 1972, 1933, 1897, and 1882 cm^{-1}.[20] Complex **11** shows peaks consistent with the presence of two terminal (1946 and 1928 cm^{-1}) and one bridging (1771 cm^{-1}) CO ligands, as observed in the solid-state.[21] Similarly, complex **12** shows IR absorptions for two terminal (1972, 1952 cm^{-1}) and one bridging (1803 cm^{-1}) CO ligands.[21]

Cyclic voltammetry (CV) studies of complex **9** revealed a quasireversible oxidation at -0.44 V versus the Fc/Fc^{+} couple (Figure 15). Complexes **11** and **12** did not show

reversible redox events in CV studies, and chemical oxidations led to decomposition. The addition of one equivalent of ferrocenium hexafluorophosphate to a THF solution of complex **9** resulted in a color change from orange-red to green. The one-electron oxidized complex, **10**, was isolated in 41% yield, but was found to be unstable in solution at ambient temperatures. However, crystals of complex **10** grown at -35 ºC were stable for weeks in the solid-state and proved suitable for XRD analysis.

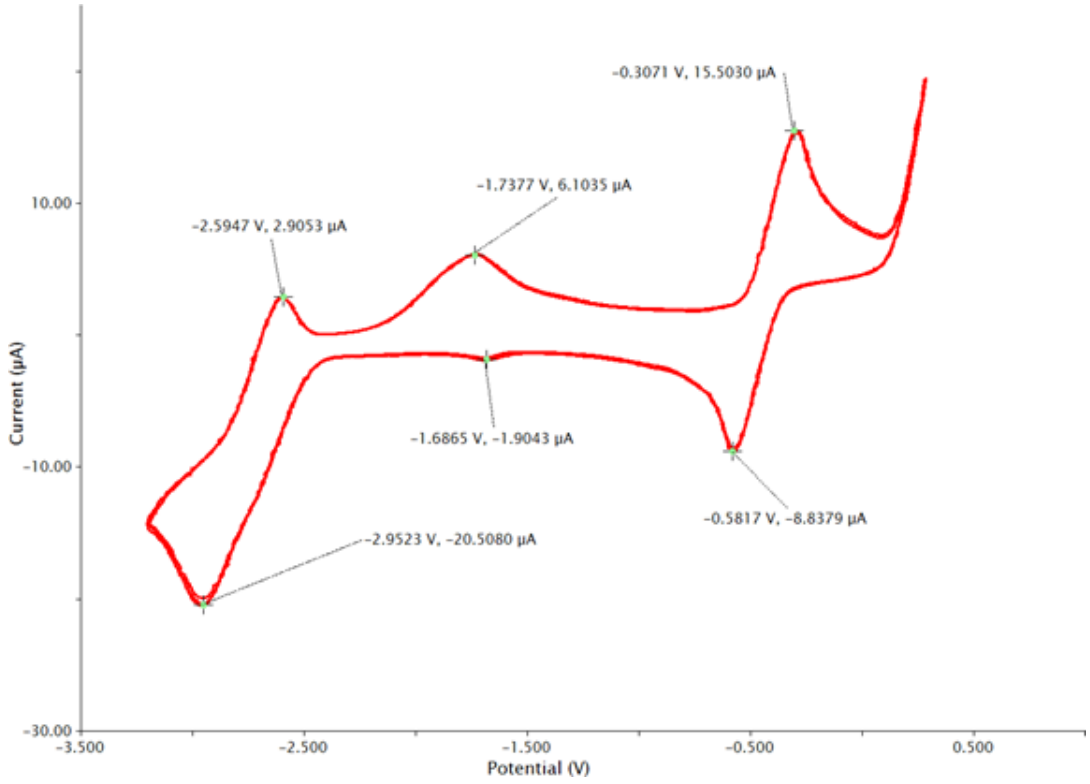

Figure 15. Cyclic voltammogram of **9** with potentials referenced to the Fc/Fc^{+} couple.

Oxidation of complex **9** results in significant structural changes to both the coordination mode of the Fe_2 core to the central arene and the nature of the central arene deplanarization (Figure 11). The diiron core binds in an μ_2:(η^2,η^4) fashion, consistent with a distorted neutral ene-diene assignment for the arene. The longest C–C distances are C1–C2 and C3–C4 (average of 1.467 Å), which correspond to the bonds

separating the metal-bound olefin and diene fragments. This is an unusual structural motif for an arene coordinated to a dinuclear unit. The Fe–Fe bond of **10** has contracted to 2.6320(3) Å, over 0.12 Å shorter compared to complex **9**. This is suggestive of a strengthened metal–metal bonding interaction and is in agreement with the shorter Fe–Fe bond of 2.423 Å observed in a comparatively more oxidized literature μ_2-arene Fe_2 complex.[15c] The IR spectrum of **10** shows peaks at 2010, 1972, 1938, and 1917 cm^{-1} consistent with terminal CO stretches. These values are indicative of weaker back-bonding from metal to CO in **10** compared to **9**, consistent with a higher formal oxidation state in the former. The aforementioned [FeFe]-hydrogenase model complex has been chemically oxidized by one electron and also shows higher terminal CO stretching frequencies at 2036, 1997, and 1987 cm^{-1},[20] with shifting of the IMes ligand from an apical to a basal position. Given the trans-spanning nature of the phosphine arms in compound **1**, such a rearrangement is not readily accommodated and instead M–arene coordination is perturbed from μ_2:(η^3,η^3) to give a *pseudo*-square pyramidal geometry around Fe1. The neutral ene-diene assignment of the central arene challenges a formal oxidation state assignment of **10** as $Fe^{I}Fe^{II}$ and underscores the potential redox participation of the central arene in the interconversion of **9** and **10**. Such ambiguity in formal oxidation state assignments is not uncommon for non-innocent ligands.[22] Although the central arene may also be regarded as a formal electron acceptor and redox non-innocent ligand, its most notable aspect is the ability to accommodate a variety of coordination modes and support reversible electron-transfer chemistry at the Fe_2-(μ_2-arene) unit.

CONCLUSIONS

In summary, the synthesis of new series of hetero- and homometallic multinuclear clusters was accomplished. In Section 2.2, access to a family of structurally related heterometallic trinuclear complexes allowed for the systematic study of the effects of changes in metal composition and ligand electronics. The identity of the minor, apical metal significantly impacts the C–O stretching frequency, as expected given the weak M–M' interaction and changes in Pd–arene interactions. The identity of the homodinuclear moiety metal of the bimetallic core also affects the CO stretching frequency, $^{31}P\{^{1}H\}$ NMR chemical shifts, and Mössbauer parameters. Ligand electronics were found to affect the spectroscopic features of the clusters, but to a lesser extent than changes in metal identity. Electrochemical behavior varied considerably with metallic composition and nature of the supporting arene. Overall, the present studies provide a quantitative evaluation of the effect of metal identity and supporting ligands in triangular low oxidation state metal clusters. Future studies with these complexes focuses on gaining further insight into heterometallic effects on chemical and physical properties of transition metal clusters.

The discussed homometallic multinuclear Fe, Co, and Ni complexes presented in Section 2.3 show that the combination of pendant donors surrounding an arene moiety provides a versatile multidentate platform to support a variety of multinuclear complexes of first-row transition metals. Beyond the intriguing structural aspects, the redox-induced reorganization of the arene highlights its flexible coordination modes and the ability to accommodate electron transfer chemistry. Future work will focus on employing the redox non-innocence and coordination lability of π-bound aromatic systems for reactivity.

EXPERIMENTAL SECTION

General considerations.

All air- and/or water-sensitive compounds were manipulated using standard vacuum or Schlenk line techniques or in an inert atmosphere glove box. The solvents for air- and moisture-sensitive reactions were dried over sodium benzophenone ketyl, calcium hydride, or by the method of Grubbs.[23] All NMR solvents were purchased from Cambridge Isotopes Laboratories, Inc. and dried over sodium benzophenone ketyl or calcium hydride. Unless mentioned otherwise, reagents were used as received from commercial suppliers without further purification. Bis(1,5-cyclooctadiene)nickel(0), nickel(II) dichloride dimethoxyethane adduct, $Fe_3(CO)_{12}$ stabilized with 10 wt. percent methanol, tetrakis(acetonitrile)palladium(II) tetrafluroborate, cobaltocene, and tris-(dibenzylideneacetone)dipalladium(0) were ordered from Strem Chemicals, Inc. 2-bromophenylboronic acid was purchased from Ark Pharm, Inc. Chlorodiisopropylphosphine, ferrocenium hexafluorophosphate, and carbon monoxide were purchased from Sigma Aldrich. Iodine monochloride, $Co_2(CO)_8$, [*n*Bu_4N][PF_6], and ferrocene were purchased from Alfa Aesar. 1,4-dimethoxy-2,5-diiodobenzene,[24] 1,4-bis(2-diisopropylphosphinophenyl)benzene,[8] compounds **1** and **7**,[8] $[Pd(MeCN)_3]_2[BF_4]_2$,[25] $Na[Co(CO)_4]$,[26] and $Na_2[Fe(CO)_4]$[27] were synthesized according to literature procedures. All ^1H, ^{13}C, and ^{31}P spectra were recorded on Varian Mercury 300 MHz, or Varian INOVA-500 or 600 MHz spectrometers at room temperature. Chemical shifts for ^1H and ^{13}C NMR data are reported relative to residual solvent peaks and are ^{13}C and ^1H decoupled, respectively, unless otherwise noted.[28] ^{31}P NMR chemical shifts are reported with respect to the deuterated solvent used to lock the instrument and are ^1H decoupled unless otherwise noted. IR spectra were obtained as solution samples using a CaF_2 window cell on a Thermo Scientific Nicolet

6700 FT-IR spectrometer or as thin films on a Bruker Alpha FT-IR spectrometer with a diamond ATR attachment. Elemental analyses were performed by Robertson Microlit Laboratories, Ledgewood, NJ.

Synthesis of 1,4-bis(2-bromophenyl)-2,5-(dimethoxy)benzene (B-R) (R = -OMe)

The Suzuki coupling to produce the terphenyl product was run as a modification of literature procedure.[8] A Schlenk tube fitted with a Teflon stopper was charged with 1,4-dimethoxy-2,5-diiodobenzene (5.00 g, 12.82 mmol, 1 equiv.), 2-bromo-phenylboronic acid (5.41 g, 26.9 mmol, 2.1 equiv.), and K_2CO_3 (10.63 g, 76.9 mmol, 6 equiv.). Toluene (270 mL), ethanol (65 mL), and water (65 mL) were then transferred to the Schlenk tube along with a magnetic stirbar. The mixture was degassed by two freeze pump thaw cycles and then put under positive nitrogen pressure. Under a strong counterflow of nitrogen, $Pd(PPh_3)_4$ (741 mg, 0.64 mmol, 0.05 equiv.) was added and the solution became a pale yellow color. The reaction mixture was then heated to 65 ºC and stirred for 16-24 hrs while monitoring the reaction by GC-MS. The volatiles were then removed on a rotovap and the residue triturated with water, then methanol, and finally dichloromethane to yield the product as an off-white powder. Yield: 4.22 g (67 %). ^{1}H NMR (500 MHz, $CDCl_3$) δ 7.42-7.36 (unresolved m, 4H, aryl-*H*), 7.23 (m, 2H, aryl-*H*), 6.82 (s, 2H, central aryl-*H*), 3.74 (s, 6H, O*CH*$_3$). ^{13}C NMR (126 MHz, $CDCl_3$) δ 150.20 (s), 129.61 (s), 132.64 (s), 131.68 (s), 130.35 (s), 128.82 (s), 127.04 (s), 124.13 (s), 114.45 (s), 56.39 (s). GC-MS (m/z): Calcd, 447.95 (M^+), Found: 448.1 (M^+). FAB-MS (m/z): Calcd, 447.9496 (M^+), Found: 447.9486 (M^+).

Synthesis of 1,4-bis(2-(diisopropylphophino)phenyl)-2,5-(dimethoxy)benzene (1-(OMe)$_2$)

Phosphination run as a modification of literature procedures.[8] A Schlenk tube fitted with a screw-in Telfon stopper was charged with 1,4-bis(2-bromophenyl)-2,5-dimethoxybenzene (1.5 g, 3.34 mmol, 1 equiv.) and a magnetic stirbar. Tetrahydrofuran (150 mL) was then to the Schlenk tube. The reaction was cooled to -78 ºC and *tert*-butyllithium (1.7 M pentane solution, 8 mL, 13.7 mmol, 4.1 equiv.) was added while stirring to generate a pale yellow solution. The reaction mixture was allowed to warm to room temperature and then stirred for an additional hour. During this time the solution became a cloudy suspension. Chlorodiisopropyl phosphine (1.12 mL, 7.02 mmol, 2.1 equiv.) was then added to the reaction via syringe. The solution immediately became a homogenous pale yellow solution which was allowed to stir for 16 hours. The volatiles were then removed under reduced pressure on the Schlenk line. The yellowish residue was then suspended in *ca.* 100 mL of toluene and filtered through a Celite pad. The filtrate was then dried under reduced pressure. This residue was then triturated with acetonitrile (*ca.* 20 mL) which removed colored impurities to leave the product as a white powder. Yield: 0.6 g (34 %). ^{1}H NMR spectra of product is broad at room temperature due to hindered rotation around aryl–aryl bonds. This is corroborated by ^{31}P NMR, where two distinct peaks are observed at room temperature. ^{1}H NMR (300 MHz, C_6D_6) δ 7.49 (m, 2H, aryl-*H*), 7.43 (m, 2H, aryl-*H*), 7.19 (m, 4H, aryl-*H*), 6.83 (s, 2H, central aryl-*H*), 3.43 (s, 6H, OC*H*$_3$), 2.05 (m, 2H, C*H*), 1.87 (m, 2H, C*H*), 1.06 (m, 24H, C*H*$_3$). ^{31}P{^{1}H} NMR (121 MHz, C_6D_6) δ -1.18 (s), -2.67 (s). This is due to the formation of two different atropisomers at room temperature due to hindered rotation around the aryl-aryl bonds. A single ^{31}P resonance is observed at -0.2 ppm at 70 ºC. ^{13}C{^{1}H} NMR (126 MHz, C_6D_6) δ 149.98

(s), 147.34 (d, J_{PC} = 30.5 Hz), 136.26 (d, J_{PC} = 22.0 Hz), 131.97 (s), 130.90 (s), 130.65 (s), 128.12 (s), 126.33 (s), 115.02 (s), 54.93 (s), 25.42 (broad s), 24.03 (broad s), 23.38 (broad s), 20.35 (broad s), 19.89 (broad s), 19.12 (broad s). GC-MS (m/z): Calcd: 522.28 (M^+), Found: 521.2761. FAB-MS (m/z): Calcd: 521.2738 (M^+), Found: 521.2761 (M^+).

Synthesis of Complex 3

Compound **2** was generated *in situ* from the reaction of 1,4-bis(2-diisopropylphosphinophenyl)benzene (**1**) (100 mg, 0.216 mmol, 1 equiv.) with $[Pd(MeCN)_3]_2[BF_4]_2$ (MeCN = acetonitrile) (136.8 mg, 0.216 mmol, 1 equiv.). This was accomplished by charging a 20 mL scintillation vial with the 1,4-bis(2-diisopropylphosphinophenyl)benzene and a magnetic stirbar before adding the $[Pd(MeCN)_3]_2[BF_4]_2$ as a solution in acetonitrile (*ca.* 5 mL) and allowing the mixture to stir over 1 hr at room temperature. During this time the solution became a homogeneous red. Formation of **1** could be confirmed by ^{31}P NMR of reaction mixture. $Na_2[Fe(CO)_4]$ was added as a partially solubilized suspension in tetrahydrofuran (*ca.* 2 mL) at room temperature. The solution immediately became a darker red and the reaction was allowed to stir for 1 hr. Volatiles were then removed under reduced pressure. The residue was suspended in acetonitrile and filtered onto a Celite pad. The solid was washed with additional acetonitrile until washes became colorless. The remaining material was dissolved in tetrahydrofuran filtered through the Celite pad. Removal of volatiles yielded the product as a red solid. Yield: 80 mg (44 %). Single crystals suitable for X-ray diffraction studies were grown from the vapor diffusion of hexanes into a concentrated tetrahydrofuran:benzene (1:1) solution at room

temperature. ^{1}H NMR (300 MHz, C_6D_6) δ 7.18 (s, 2H, aryl-*H*), δ 7.11-6.98 (m, 6H, aryl-*H*), δ 5.92 (s, 4H, central aryl-*H*), δ 2.26 (m, 4H, C*H*), δ 1.25 (dd, J_{PH} = 18.1, J_{HH} = 7.0 Hz, 12H, C*H*$_3$), δ 0.89 (dd, J_{PH} = 8.5, J_{HH} = 7.2 Hz, 12H, C*H*$_3$). ^{31}P{^{1}H} NMR (121 MHz, C_6D_6) δ 53.36 (s). ^{13}C{^{1}H} NMR (126 MHz, CD_2Cl_2) δ 225.26 (s), 149.04 (vt, J_{PC} = 14.0 Hz), 141.36 (vt, J_{PC} = 14.3 Hz), 132.80 (s), 132.17 (vt, J_{PC} = 7.0 Hz), 130.66 (s), 128.19 (s), 118.03 (s), 111.15 (s), 26.62 (vt, J_{PC} = 8.4 Hz), 19.33 (s), 18.64 (s). IR (CaF_2 window, C_6H_6, cm^{-1}) ν_{CO}: 1901 (s), 1874 (m), 1848 (s), 1843 (w, sh). Anal. Calcd. for: $C_{34}H_{40}FeO_4P_2Pd_2$ (**3**) (%): C, 48.42; H, 4.78. Found: C, 48.25; H, 5.08.

Synthesis of Complex 4

Compound **3** was generated in an analogous fashion to the procedure described in the synthesis of **3** again using 4-bis(2-diisopropylphosphinophenyl)benzene (40 mg, 0.0865 mmol, 1 equiv.) and $[Pd(MeCN)_3]_2[BF_4]_2$ (MeCN = acetonitrile) (54.7 mg, 0.0865 mmol, 1 equiv.). To the *in situ* generated acetonitrile solution of **2** was added $[Na][Co(CO)_4]$ (16.8 mg, 0.0865 mmol, 1 equiv.) as an acetonitrile solution (*ca.* 2 mL). The reaction mixture was allowed to stir for 1 hr at room temperature. During this time the reaction mixture turned a deep purple-red. The volatiles were then removed under reduced pressure. The residue was then suspended in benzene and collected on a Celite pad. The solid was then washed with additional benzene until the washes became colorless. The washed solid was then dissolved in tetrahydrofuran and filtered through the Celite pad. Removal of volatiles yielded the product as a purple-red solid. Yield: 40 mg, (49 %). Single crystals suitable for X-ray diffraction were grown by the vapor diffusion of hexanes into a concentrated tetrahydrofuran:benzene solution at room

temperature. ^{1}H NMR (300 MHz, CD_3CN) δ 7.92-7.62 (m, 8H, aryl-*H*), 6.39 s, 4H, central aryl-*H*), 2.72 (m, 4H, C*H*), 1.18 (m, 24H, C*H*$_3$). ^{31}P{^{1}H} NMR (121 MHz, CD_3CN) δ 61.83 (s). ^{19}F NMR (282 MHz, CD_3CN) δ 61.83 (s).^{13}C{^{1}H} NMR (126 MHz, CD_3CN) δ 203.70 (broad), 146.58 (vt, J_{PC} = 12.6 Hz), 136.83 (vt, J_{PC} = 17.7 Hz), 133.50 (s), 132.60 (s), 132.23 (s), 129.77 (s), 116.42 (s), 114.30 (s), 26.40 (s), 18.84 (s), 18.04 (s). IR (CaF_2 window, THF, cm^{-1}) ν_{CO}: 2057 (s), 2012 (m), 1915 (m), 1878 (w, sh). Anal. Calcd. for: $C_{34}H_{40}BCoF_4O_4P_2Pd_2$ (**4**) (%): C, 43.76; H, 4.32. Found: C, 43.58; H, 4.48.

Synthesis of Complex 5

Compound **4** (50 mg, 0.0535 mmol, 1 equiv.) was added to a 20 mL scintillation vial. Tetrahydrofuran (*ca.* 5 mL) was added to fully dissolve **4**. Cobaltocene (10.1 mg, 0.0535 mmol, 1 equiv.) was added as a tetrahydrofuran solution (1 mL) and the reaction mixture was allowed to stir for 1 hr. During this time the solution changed from purple-red to a green-brown. The volatiles were removed under reduced pressure. The residue was suspended in hexanes and collected over a Celite pad. The solid was washed with hexanes until only a pale green tinge remained in the washes which were initially brown. The remaining green colored material was dissolved in benzene and brought through the Celite pad. The benzene filtrate was then dried to a solid under reduced pressure. The benzene soluble material was then dissolved in minimal diethyl ether and then several drops of hexamethyldisiloxane were added. The product was then precipitated by the slow evaporation of diethyl ether. Yield: 14 mg (31 %). The product is unstable and prone to decomposition. Therefore characterization was obtained immediately after synthesis. Single crystals were obtained from the vapor diffusion of diethyl ether out of

a concentrated solution of **5**. IR (CaF_2 window, THF, cm^{-1}) ν_{CO}: 2007 (s), 1920 (m, sh), 1879 (m), 1837 (m). Anal. Calcd. for: $C_{34}H_{40}CoO_4P_2Pd_2$ (**5**) (%): C, 48.25; H, 4.76. Found: C, 48.24; H, 4.61.

Synthesis of Complex 3-(OMe)$_2$

A Schlenk tube fitted with a screw-in Telfon stopper was charged with **1-(OMe)$_2$** (100 mg, 0.191 mmol, 1 equiv.) and a magnetic stirbar. $[Pd(MeCN)_3]_2[BF_4]_2$ (MeCN = acetonitrile) (121 mg, 0.191 mmol, 1 equiv.) was transferred as an acetonitrile solution (*ca.* 20 mL) and the mixture was allowed to stir at room temperature for 1 hr. During this the time the reaction mixture became a homogenous deep red. $[Na]_2[Fe(CO)_4]$ (40.9 mg, 0.191, 1 equiv.) was then added as a partially solubilized tetrahydrofuran suspension (*ca.* 2 mL) and the reaction was allowed to stir for 1 hr at room temperature. The volatiles were then removed under reduced pressure. The residue was triturated with hexanes and collected over a Celite pad. The solid was then washed with additional hexanes until the washes became colorless. Then 10 mL of cold ether were used to wash the solid. The remaining solid was dissolved in benzene and brought through the Celite pad. Removal of volatiles yielded the product as a red solid. Yield: 40 mg (23 %). Crystals suitable for X-ray diffraction studies were grown from the vapor diffusion of hexanes into a concentrated tetrahydrofuran:benzene (1:1) solution. ^{1}H NMR (300 MHz, C_6D_6) δ 7.47 (d, J_{HH} = 7.6 Hz, 2H, aryl-*H*), 7.28 (m, 2H, aryl-*H*), 7.20 (m, 2H, aryl-*H*), 7.09 (t, J_{HH} = 7.4 Hz, 2H, aryl-*H*), 5.55 (s, 2H, central aryl-*H*), 2.94 (s, 6H, OC*H*$_3$), 2.40 (m, 2H, C*H*), 2.27 (m, 2H, C*H*), 1.33 (m, 12H, C*H*$_3$), 0.99 (aq, J_{HH} = 7.2 Hz, 6H, C*H*$_3$), 0.91 (aq, J_{HH} = 7.2 Hz, 6H, C*H*$_3$). ^{31}P{^{1}H} NMR (121 MHz, C_6D_6) δ 56.92 (s). ^{13}C{^{1}H} NMR (126

MHz, CD_2Cl_2) δ 225.48 (s), 147.08 (vt, J_{PC} = 14.7 Hz), 143.24 (vt, J_{PC} = 15.0 Hz), 140.86 (s), 132.70 (s), 132.20 (vt, J_{PC} = 7.6 Hz), 130.83 (s), 128.05 (s), 54.90 (s), 26.84 (d, J_{PC} = 8.6 Hz), 26.71 (d, J_{PC} = 8.4 Hz), 19.56 (vt, J_{PC} = 5.1 Hz), 19.41 (vt, J_{PC} = 4.6 Hz), 18.77 (s), 18.53 (s). IR (CaF_2 window, C_6H_6, cm^{-1}) ν_{CO}: 1898, 1867, 1838 (fourth IR stretch likely coincidentally underneath 1838 band by analogy to the IR of compound **3**). Anal. Calcd. for: $C_{36}H_{44}FeO_6P_2Pd_2$ (**3-(OMe)$_2$**) (%): C, 47.86; H, 4.91. Found: C, 48.14 H, 4.86.

Synthesis of Complex 8

A Schlenk tube fitted with a screw-in Teflon stopper was charged with **7** (300 mg, 0.462 mmol, 1 equiv.) and a magnetic stirbar. Tetrahydrofuran (*ca.* 20 mL) was then transferred to the Schlenk tube to yield a green homogeneous solution. $[Na]_2[Fe(CO)_4]$ (100.7 mg, 0.462 mmol, 1 equiv.) was added as a partially solubilized tetrahydrofuran suspension (*ca.* 10 mL). This addition resulted in an immediate color change from green to brown within a minute. The reaction mixture was allowed to stir at room temperature for 1 hr. Volatiles were then removed under reduced pressure. The dark brown residue was suspended in hexanes and filtered on a Celite pad. The solid was then washed with hexanes until the washes were colorless. The remaining solid was then washed with 10 mL cold diethyl ether. Finally, the product was dissolved with benzene and brought through the Celite pad. The benzene soluble material was lyophilized to yield the product as a brown powder. Yield: 160 mg (41 %). Crystals suitable for X-ray diffraction studies could be grown from the slow vapor diffusion of hexanes into a concentrated tetrahydrofuran:benzene (1:1) solution. However, the compound decomposes in solution over extended periods of time and the cleanest material was obtained

without crystallization. ^{1}H NMR (300 MHz, C_6D_6) δ 7.17 (d, J_{HH} = 7.4 Hz, 2H, aryl-*H*), 7.05-6.90 (m, 6H, aryl-*H*), 5.78 (s, 4H, central aryl-*H*), 2.32 (h, J_{HH} = 7.0 Hz, 4H, C*H*), 1.19 (m, 12H, CH_3), 0.89 (aq, J_{HH} = 7.0 Hz, CH_3). ^{31}P{^{1}H} NMR (121 MHz, C_6D_6) δ 43.18 (s). ^{13}C{^{1}H} NMR (126 MHz, C_6D_6) δ 225.38 (broad s), 150.24 (vt, J_{PC} = 14.2 Hz), 138.27 (vt, J_{PC} = 15.0 Hz), 131.40 (s), 130.23 (s), 130.09 (s), 127.70 (s), 103.31 (s), 102.02 (s), 25.18 (vt, J_{PC} = 9.7 Hz), 18.60 (s), 17.66 (s). IR (CaF_2 window, C_6H_6, cm^{-1}) ν_{CO}: 1896, 1874, 1821, 1798.3 (sh). Anal. Calcd. for: $C_{34}H_{40}FeO_4P_2Ni_2$ (**8**) (%): C, 54.60; H, 5.39. Found: C, 54.69; H, 5.35.

Synthesis of Complex 6

Compound **2** (82.7 mg, 0.089 mmol, 1 equiv.) was transferred to a 20 mL scintillation vial equipped with a magnetic stirbar. Acetonitrile (*ca.* 5 mL) was then added to dissolve the compound and then $Mo(CO)_3(MeCN)_3$ (27.2 mg, 0.089 mmol, 1 equiv.) was then added as a suspension in *ca.* 1 mL acetonitrile. Following addition of the molybdenum precursor the reaction mixture immediately became homogeneous. After 1 hr, volatiles were removed under reduced pressure and the solid residue was triturated with THF until washes became colorless leaving behind clean material as a red solid. Yield: 77 mg (75.2 %). ^{1}H NMR (300 MHz, CD_3CN) δ 7.86 – 7.80 (m, 2H, Ar*H*), 7.79 – 7.68 (m, 4H, Ar*H*), 7.55 (dd, *J* = 7.7, 1.5 Hz, 2H, Ar*H*), 6.50 (s, 4H, central-Ar*H*), 2.83 – 2.67 (m, 4H, C*H*), 1.26 – 1.10 (m, 24H, CH_3). ^{13}C NMR (126 MHz, CD_3CN δ 230.16 (s), 146.16 (vt, J_{CP} = 12.1 Hz), 135.07 (vt, J_{CP} = 18.5 Hz), 133.35 (s), 132.61 (s), 132.13 (vt, J_{CP} = 7.1 Hz), 129.91 (s), 126.56 (s), 123.43 (s), 25.69 (t, J_{CP} = 9.9 Hz), 18.06 (s), 17.41 (s). ^{31}P NMR (121 MHz, CD_3CN) δ 56.87. ^{19}F NMR (282 MHz, CD_3CN) δ -151.77.

Synthesis of Complex 4-(OMe)$_2$

1-(OMe)$_2$ (55.1 mg, 0.105 mmol, 1 equiv.) was transferred to a 20 mL scintillation vial equipped with a magnetic stirbar. $[Pd(MeCN)_3]_2[BF_4]_2$ (MeCN = acetonitrile) (66.7 mg, 0.105 mmol, 1 equiv.) was transferred as an acetonitrile solution (*ca.* 5 mL) and the mixture was allowed to stir at room temperature for 1 hr. During this the time the reaction mixture became a homogenous deep red. $[Na][Co(CO)_4]$ (20.88 mg, 0.105 mmol, 1 equiv.) was then added as a solution in *ca.* 5 mL acetonitrile and the reaction mixture was allowed to stir for 1 hr at room temperature. During this time the reaction mixture turned a deep purple-red. The volatiles were then removed under reduced pressure. The residue was then suspended in benzene and collected on a Celite pad. The solid was then washed with additional benzene until the washes became colorless. The washed solid was then dissolved in tetrahydrofuran and filtered through the Celite pad. Removal of volatiles yielded the product as a purple-red solid. ^{1}H NMR (300 MHz, CD_3CN) δ 7.90 – 7.62 (m, 1H), 5.80 (s, 0H), 3.25 (s, 1H), 2.83 – 2.61 (m, 1H), 1.36 – 1.25 (m, 1H), 1.20 – 1.07 (m, 3H). ^{31}P NMR (121 MHz, CD_3CN) δ 64.99. ^{19}F NMR (282 MHz, CD_3CN) δ -151.87.

Synthesis of Complex 7-(OMe)$_2$

Compound **1-(OMe)$_2$** (300 mg, 0.574 mmol, 1 equiv.) was transferred to a 20 mL scintillation vial equipped with a magnetic stirbar. $Ni(COD)_2$ (158.3 mg, 0.574 mmol, 1 equiv.) was then added as a suspension in THF (*ca.* 5 mL). The reaction mixture was allowed to stir for 10 min during which time the solution turned a deep red. $NiCl_2$dme (126 mg, 0.574 mmol, 1 equiv.) was then added as a suspension in minimal THF, resulting in formation of a green solution. The reaction mixture was allowed to stir for 24 hrs before volatiles were removed

under reduced pressure to yield a green powder which was carried on to the synthesis of **8-(OMe)$_2$** without further purification. ^{1}H NMR (300 MHz, Benzene-d_6) δ 7.43 (d, J = 7.8 Hz, 1H), 7.03 (t, J = 7.1 Hz, 1H), 6.90 (t, J = 7.3 Hz, 1H), 6.82 (d, J = 7.4 Hz, 1H), 6.30 (s, 1H), 3.78 (s, 3H), 1.86 (t, J = 6.9 Hz, 0H), 1.77 (q, J = 7.0 Hz, 1H), 1.37 (d, J = 6.9 Hz, 4H), 1.26 (d, J = 7.0 Hz, 4H), 1.01 (d, J = 6.9 Hz, 4H), 0.93 (d, J = 6.8 Hz, 4H). ^{31}P NMR (121 MHz, Benzene-d_6) δ 64.74.

Synthesis of Complex 8-(OMe)$_2$

Compound **7-(OMe)$_2$** (40 mg, 0.0563 mmol, 1 equiv.) was transferred to a 20 mL scintillation vial equipped with a magnetic stirbar as a solution in THF (*ca.* 4 mL). To the rapidly stirring solution was added $[Na]_2[Fe(CO)_4]$ (12.1 mg, 0.0563 mmol, 1 equiv.) as a suspension in *ca.* 1 mL THF. The reaction mixture was allowed to stir for 1 hr before volatiles were removed under reduced pressure to yield a brown residue. The residue was triturated with hexanes and filtered over a Celite pad until washes became colorless. The solid was then washed with a small portion of diethyl ether. The remaining material was dissolved in benzene and brought through the Celite pad and lyophilized to afford the product as a brown solid. ^{1}H NMR (300 MHz, C_6D_6) δ 7.41 (d, J = 7.7 Hz, 2H, Ar*H*), 7.15 – 7.05 (m, 4H, Ar*H*), 6.98 (t, J = 7.3 Hz, 2H, Ar*H*), 5.30 (s, 2H, central-Ar*H*), 3.27 (s, 6H, OCH_3), 2.73 – 2.57 (m, 2H, C*H*), 2.11 (m, 2H, C*H*), 1.49 – 1.39 (m, 6H, CH_3), 1.20 – 1.10 (m, 6H, CH_3), 0.98 – 0.90 (m, 12H, CH_3). ^{31}P NMR (121 MHz, C_6D_6) δ 44.99.

Synthesis of Complex 9

Compound **1** (300 mg, 0.648 mmol, 1 equiv) was transferred as a solution in *ca.* 10 mL THF into a quartz Schlenk tube fitted with a screw-in Teflon stopper along with a magnetic stir bar. $Fe_3(CO)_{12}$ (10 wt % MeOH stabilizer) (359.3 mg, 0.648 mmol, 1 equiv) was then added as a solution in *ca.* 20 mL THF. The reaction mixture was then thoroughly degassed and allowed to stir for 1 hr, during which time the solution turned from green to a deep red. The reaction mixture was then subjected to UV photolysis under a 200 W Hg-Xe lamp for 2-3 days until the desired product was determined to be the majority species by ^{31}P NMR. During photolysis, the solution was degassed every few hours. Volatiles were then removed under reduced pressure. The dark red/orange residue was washed with hexanes then diethyl ether until only a pale orange color remained in washes. The remaining material was dissolved in THF and filtered through a Celite pad and the filtrate dried under reduced pressure. The solid was then recrystallized by the vapor diffusion of hexanes into a concentrated THF solution. Resulting dark red/orange crystals were washed with hexanes and dried under reduced pressure. Yield: 48.4 mg (11 %) ^1H NMR (300 MHz, C_6D_6) δ 7.57 (d, 2H, aryl-*H*), 7.10 (t, 2H, aryl-*H*), 6.97 (t, 2H, aryl-*H*), 6.88 (t, 2H, aryl-*H*), 3.76 (s, 4H, central aryl-*H*), 2.20 (m, 4H, C*H*), 0.98 (dd, 12H, C*H*$_3$), 0.82 (dd, 12H, C*H*$_3$) ppm. ^{31}P NMR (121 MHz, C_6D_6) δ 90.59 (s) ppm. ^{13}C NMR (126 MHz, C_6D_6) δ 221.3 (d), 149.4 (d), 139.0 (d), 130.2 (d), 129.3 (s), 129.0 (s), 126.84 (s), 96.8 (s), 57.6 (s), 26.7 (d), 17.2 (d) ppm. IR (ATR film, cm^{-1}) ν_{CO}: 1966, 1914, 1903, 1880. Anal. Calcd. for: $C_{34}H_{40}Fe_2O_4P_2$ (**9**) (%): C, 59.50; H, 5.87. Found: C, 59.29; H, 5.74.

Synthesis of Complex 11

Compound **1** (100 mg, 0.216 mmol, 1 equiv) was transferred as a solution in *ca.* 15 mL toluene into a Schlenk tube fitted with a screw-in Teflon stopper along with a magnetic stir bar. $Co_2(CO)_8$ (74 mg, 0.216 mmol, 1 equiv) was then added as a solution in *ca.* 15 mL toluene. The brown reaction mixture was heated to 110 ºC for 1 hour. The solution was then degassed, 1 atm of fresh N_2 readmitted, and then heated at 110 ºC for an additional 2-3 hours. During this time the solution turned green. The reaction mixture was then dried under reduced pressure. The green powder was washed with *ca.* 10 mL of ether and the remaining material dissolved in THF and filtered through a Celite pad and dried under reduced pressure to yield a green powder as the clean product. Yield: 78 mg (54 %). ^{1}H NMR (300 MHz, C_6D_6) δ 7.51 (d, 2H, aryl-*H*), 7.14 (t, 2H, aryl-*H*), 7.05 (t, 2H, aryl-*H*), 6.93 (m, 2H, aryl-*H*), 4.29 (broad s, 2H, central aryl-*H*), 3.95 (d, 2H, central aryl-*H*), 2.90 (m, 2H, C*H*), 2.19 (m, 2H, C*H*), 1.15 (m, 12H, C*H*$_3$), 0.99 (dd, 6H, C*H*$_3$), 0.89 (dd, 6H, C*H*$_3$) ppm. ^{31}P NMR (121 MHz, C_6D_6) δ 80.20 (s) ppm. ^{13}C NMR (126 MHz, C_6D_6) δ 271.45 (s), 215.4 (s), 153.21 (d), 135.25 (d), 130.40 (s), 129.46 (s), 127.65 (s), 127.42 (m), 87.39 (s), 61.65 (d), 60.15 (s), 27.29 (t), 24.51 (s), 18.32 (s), 18.13 (s), 17.86 (s), 17.28 (s) ppm. IR (CaF_2 window, THF, cm^{-1}) ν_{CO}: 1946, 1928, 1771. Anal. Calcd. for: $C_{33}H_{40}Co_2O_3P_2$ (**11**) (%): C, 59.65; H, 6.07. Found: C, 59.90; H, 6.07.

Synthesis of Complex 12

Complex **7** (100.0 mg, 0.154 mmol, 1 equiv) was transferred as a solution in *ca.* 6 mL of THF into a 20 mL scintillation vial along with a magnetic stir bar. [Na][$Co(CO)_4$] (29.8 mg, 0.154 mmol, 1 equiv) was then added as a solution in *ca.* 4 mL of THF. The reaction mixture

was stirred for 30 minutes at room temperature, during which time the solution turned from green to brown/yellow. The solution was then dried under reduced pressure, and the resulting solid was triturated with diethyl ether, filtered through a Celite pad, and then dried under reduced pressure. The solid from the filtrate was recrystallized by the vapor diffusion of pentane into a concentrated THF solution to yield ruby red rectangular crystals. Complex **12** is *unstable* in solution and slowly decomposes to two different products by ^{31}P NMR at 50.32 (**13-CO**) and 32.31 ppm.[7a] Yield: 11 mg (11 %) ^{1}H NMR (300 MHz, C_6D_6) δ 7.26 (broad d, 2H, aryl-*H*), 7.15-6.96 (broad m, 6H, aryl-*H*), 5.85 (broad s, 4H, central aryl-*H*), 2.32 (m, 4H, C*H*), 1.44-0.80 (broad m, 24H, C*H*$_3$) ppm. ^{31}P NMR (121 MHz, C_6D_6) δ 34.80 (s) ppm. ^{13}C NMR (126 MHz, C_6D_6) δ 235.66 (s), 196.96 (s), 151.41 (d), 133.72 (d), 130.41 (s), 129.37 (s), 128,56 (d), 126.92 (s), 118.51 (d), 105.64 (broad s), 73.93 (broad s), 25.66 (broad s), 18.00 (broad s) ppm. IR (CaF_2 window, THF, cm^{-1}) ν_{CO}: 1972, 1956.4, 1803. Anal. Calcd. for: $C_{33}H_{40}Ni_2O_3P_2$ (**12**) (%): C, 59.69; H, 6.07. Found: C, 59.61; H, 6.10.

Synthesis of Complex 12 from 1

Compound **1** (20 mg, 0.039 mmol, 1 equiv) and Ni(COD)$_2$ (21.2 mg, 0.077 mmol, 2 equiv) were transferred as a solution in *ca.* 5 mL of THF into a Schlenk tube fitted with a screw-in Teflon stopper along with a magnetic stirbar. The solution was stirred for *ca.* 20 minutes at room temperature during which time the solution turned deep red. The reaction mixture was then thoroughly degassed. The solution was cooled to -78 °C, and *ca.* 4 equivalents of CO were admitted using a calibrated gas bulb. The solution was then allowed to slowly warm to room temperature while stirring over 30 minutes during which time the color changed

from red to orange and finally to pale yellow. The volatiles were then removed under reduced pressure. While complex **4** was found to be the majority product, a significant quantity of impurities of $P_2Ni_3(CO)_4$ as well as a transfacical polycarbonyl dinickel complex, with each phosphine coordinated to a $Ni(CO)_3$ or $Ni(CO)_2$ fragment, was observed which proved difficult to remove by recrystallization.[5g, 7a] Synthesis from complex **7** was therefore pursued as the predominant route to complex **12**.

Synthesis of Complex 10

Complex **9** (30.0 mg, 0.043 mmol, 1 equiv) was transferred as a solution in *ca.* 6 mL of THF to a 20 mL scintillation vial along with a magnetic stir bar. Ferrocenium hexafluorophosphate (14.5 mg, 0.043 mmol, 1 equiv) was then added as a solution in *ca.* 4 mL of THF. The reaction mixture was stirred for 30 minutes during which time the solution changed from red/orange to green/brown. The reaction mixture was then concentrated under reduced pressure, and *ca.* 5 mL of diethyl ether was added to precipitate out the product. The solid was washed with additional diethyl ether and then dissolved in minimal THF before filtering through a Celite pad and removing volatiles under reduced pressure. The emerald green residue was recrystallized by vapor diffusion of pentane into a concentrated THF solution at -35 ºC to yield dark green crystalline needles. Complex **10** is *unstable* in THF solution and decomposes overnight at room temperature to ill-defined species. Complex **10** also immediately decomposes in acetonitrile. As a crystalline solid, complex **10** is indefinitely stable at room temperature. Yield: 14.7 mg (41 %). ^{1}H NMR (300 MHz, d_8-THF*)* shows no signals between 200 and -70 ppm, consistent with a paramagnetic compound with a weakly

associated PF_6 counteranion. ^{31}P NMR (121 MHz, *d*$_8$-THF) shows no signals between 200 and -200 ppm, consistent with a paramagnetic compound with a weakly associated PF_6 counteranion. ^{19}F NMR (282 MHz, *d*$_8$-THF) shows a broadened doublet centered at -70.32 ppm, consistent with a weakly associated PF_6 counteranion. IR (ATR film, cm^{-1}) ν_{CO}: 2010, 1972, 1938, 1917. Anal. Calcd. for: $C_{34}H_{40}F_6Fe_2O_4P_3$ (**10**) (%): C, 49.13; H, 4.85. Found: C, 49.40; H, 4.85.

Synthesis of Complex 13-CO

A Schlenk tube fitted with a screw-in Teflon stopper was charged with 1,4-bis(2-diisopropylphosphino)phenyl)benzene (**1**) (500 mg, 1.08 mmol, 1 equiv) and $Ni(COD)_2$ (891.9 mg, 3.24 mmol, 3 equiv). THF (*ca.* 60 mL) was added and then the combined reaction mixture was degassed and sealed. After stirring for two hours a color change from yellow to dark red was observed. Following degassing the solution, the reaction mixture was cooled to -78ºC and 5 equivalents of CO was admitted using a calibrated gas bulb. The reaction was allowed to slowly warm to room temperature while stirring. During this time the solution turned a bright red/orange. While stirring for an addition 16 h, the solution slowly turned yellow/brown, at which time volatiles were removed under reduced pressure to yield a yellow/brown residue. The residue was dissolved in minimal THF and filtered through a celite pad. The product was recrystallized from the filtrate by the slow vapor diffusion of hexanes over 3 days at room temperature to afford pure product as large dark crystals (37% yield). ^1H NMR (300 MHz, C_6D_6) δ 7.42 (d, 2H, aryl-*H*), 7.09-6.89 (m, 6H, aryl-*H*), 5.65 (s, 2H, central aryl-*H*), 4.57 (s, 2H, central aryl-*H*), 2.30 (m, 2H, C*H*), 2.12 (m, 2H, C*H*), 1.25 (dd, 6H, C*H*$_3$),

1.06 (dd, 12H, C*H*$_3$), 0.89 (dd, 6H, C*H*$_3$). ^{31}P NMR (121 MHz, C_6D_6) δ 50.32 (s). ^{13}C NMR (126 MHz, C_6D_6) δ 246.87 (s), 245.58 (s), 195.08 (s), 151.56 (m), 134.28 (m), 131.62 (s), 129.32 (s), 127.60 (s), 126.33 (s), 91.06 (s), 70.98 (s), 66.64 (s), 26.87 (m), 24.30 (m), 20.18 (s), 18.84 (s), 18.03 (t), 17.58 (s). IR (CaF_2 window, THF, cm^{-1}) ν_{CO}: 2002, 1873, 1830. Anal. Calcd. for: $C_{34}H_{40}Ni_3O_4P_2$ (**13-CO**) (%): C, 54.40; H, 5.37. Found: C, 54.31; H, 5.28.

Synthesis of Complex 13-PMe$_3$

In an inert atmosphere glovebox, a 20 mL scintillation vial was charged with **13-CO** (102 mg, 0.136 mmol, 1 equiv) and dissolved in THF (*ca.* 10 mL). While stirring, PMe$_3$ (1 M in THF, 149 μL, 1.1 equiv) was added via syringe. The reaction slowly turned from yellow to bright orange over the 16h reaction time. Volatiles were removed under reduced pressure to yield an orange residue. Pure product was obtained by the vapor diffusion of hexanes out of a concentrated hexanes/hexamethyldisiloxane solution to yield an orange precipitate (74% yield). ^{1}H NMR (300 MHz, C_6D_6) δ 7.71 (m, 2H, aryl-*H*), 7.07 (m, 4H, aryl-*H*), 6.94 (t, 2H, aryl-*H*), 5.13 (d, 2H, central aryl-*H*), 4.67 (d, 2H, central aryl-*H*), 2.41 (m, 2H, C*H*), 2.24 (m, 2H, C*H*), 1.38 (dd, 6H, C*H*$_3$), 1.16 (m, 12H, C*H*$_3$), 1.00 (d, 9H, C*H*$_3$), 0.99 (dd, 6H, C*H*$_3$). ^{31}P NMR (121 MHz, C_6D_6) δ 51.50 (d, J = 16.6 Hz), 6.61 (t, J = 16.6 Hz). ^{13}C NMR (126 MHz, C_6D_6) δ 259.93 (s), 250.72 (s), 153.21 (m), 135.345 (m), 131.55 (s), 128.87 (s), 127.26 (t), 125.74 (t), 88.31 (s), 68.17 (s), 63.15 (s), 27.01 (m), 24.47 (m), 20.45 (s), 19.11 (t), 18.29 (t), 17.82 (s), 14.48 (d). IR (CaF_2 window, C_6H_6, cm^{-1}) ν_{CO}: 1854, 1783. Anal. Calcd. for: $C_{36}H_{49}Ni_3O_3P_3$ (**6**) (%): C, 54.13; H, 6.18. Found: C, 54.44; H, 6.10.

Electrochemistry Details

Electrochemical measurements of complex **3**, **4**, **6**, **3-(OMe)$_2$**, **8**, **8-(OMe)$_2$**, and **9** were taken on a Pine Instrument Company biopotentiostat model AFCBP1 as 3 millimolar solutions in tetrahydrofuran using 0.1 molar [*n*Bu$_4$N][PF$_6$] as the electrolyte with a platinum wire counter electrode, a glassy carbon working electrode, and a silver/silver nitrate reference electrode in 0.1 molar [*n*Bu$_4$N][PF$_6$] as an acetonitrile solution. Electrochemical measurements of compounds were internally referenced to ferrocene.

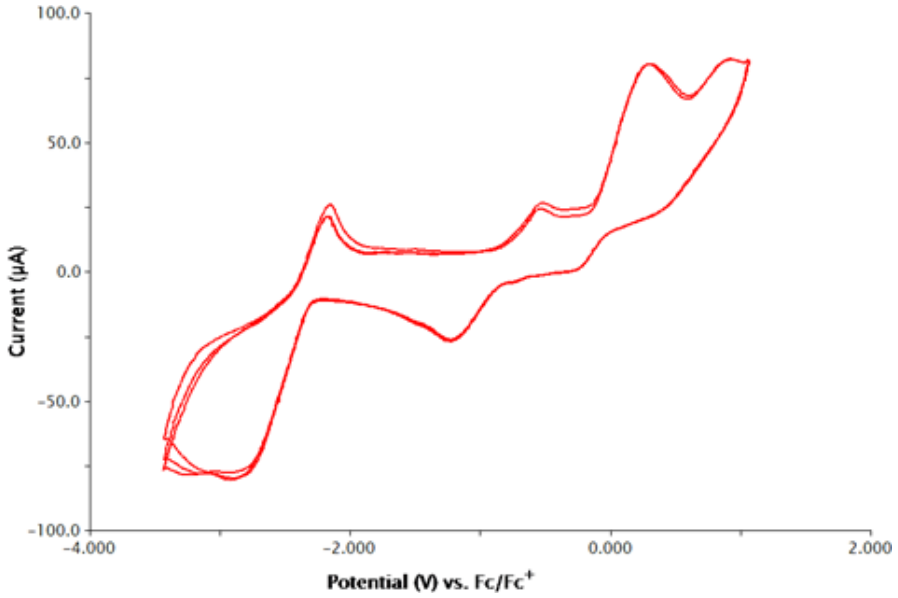

Figure 16. Complex **3** full cyclic voltammogram.

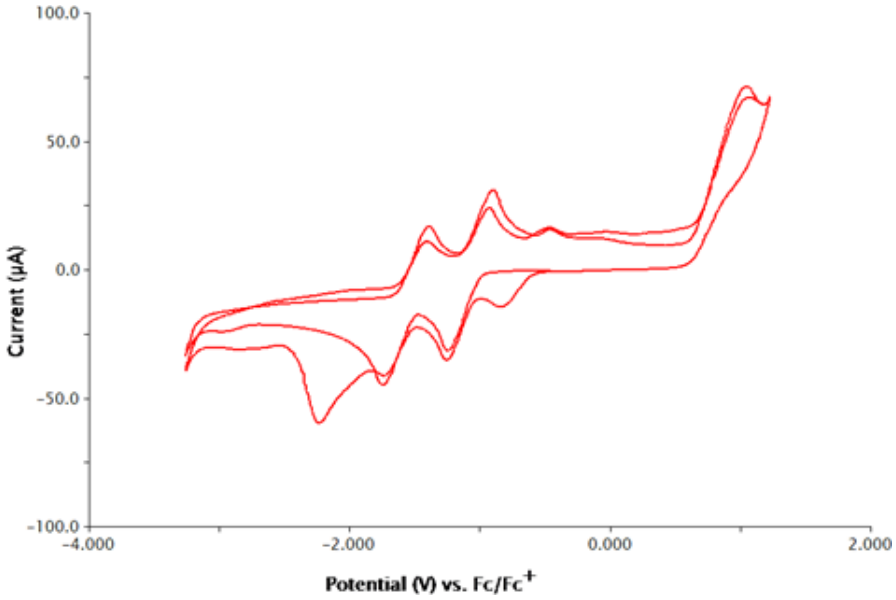

Figure 17. Complex **4** full cyclic voltammogram.

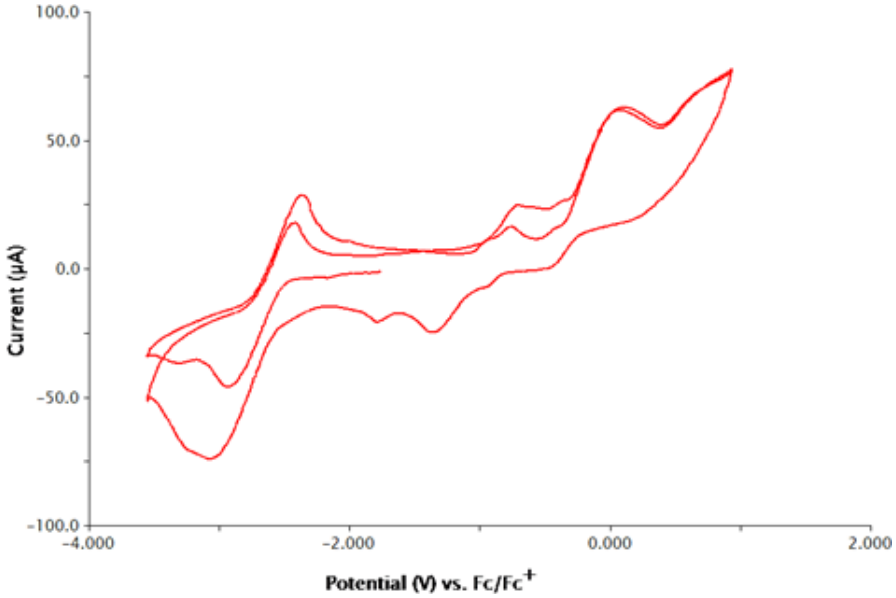

Figure 18. Complex **3-(OMe)$_2$** full cyclic voltammogram.

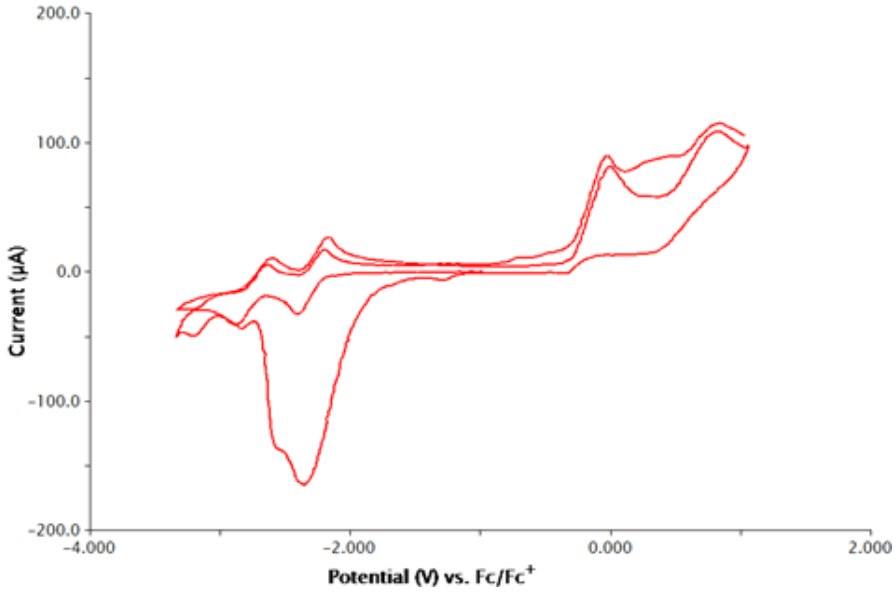

Figure S19. Complex **8** full cyclic voltammogram.

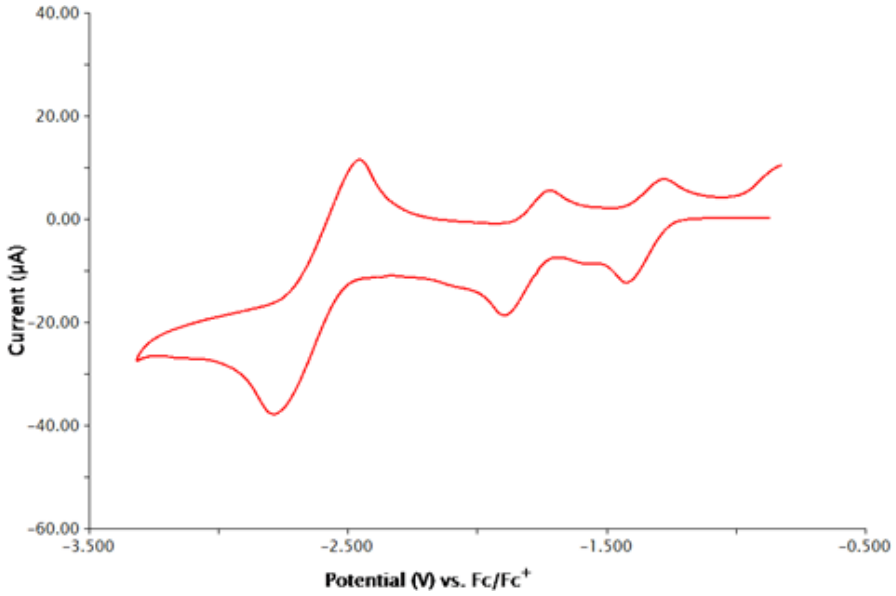

Figure 20. Complex **3-(OMe)$_2$** and **4** reductive scan as equimolar solution.

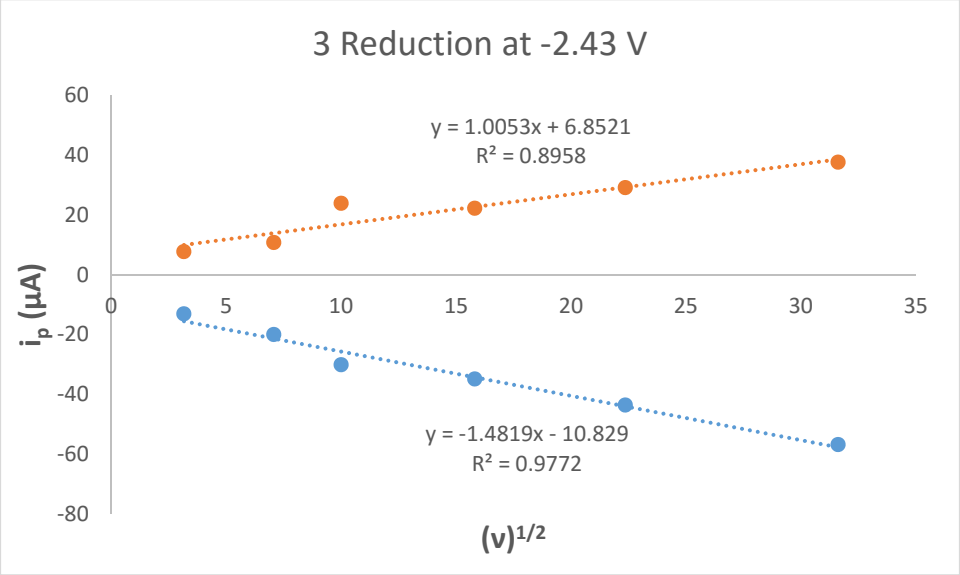

Figure 21. Plot of the scan rate dependence for the reduction of compound **3** with the cathodic (blue) and anodic scans (orange).

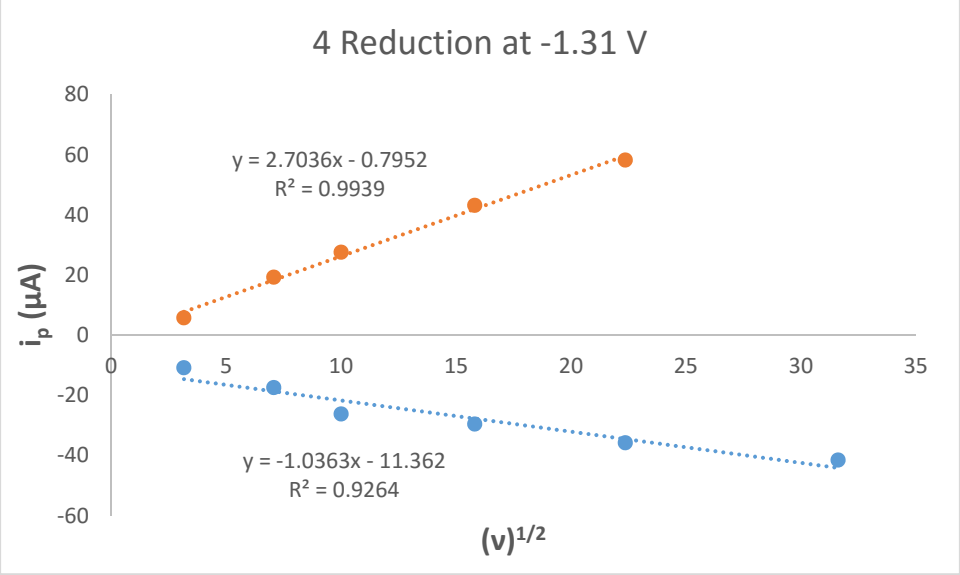

Figure 22. Plot of the scan rate dependence for the first reduction of compound **4** with the cathodic (blue) and anodic scans (orange).

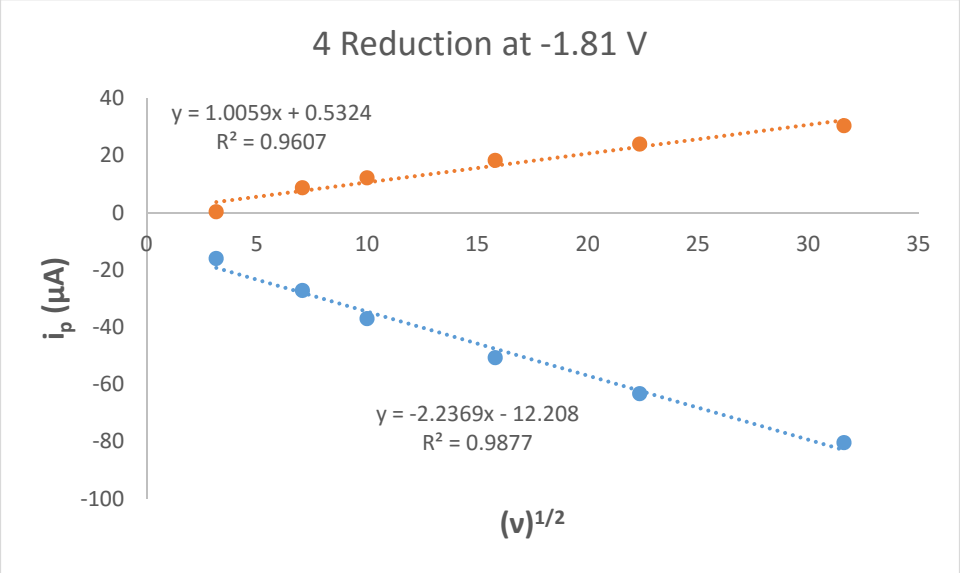

Figure 23. Plot of the scan rate dependence for the second reduction of compound **4** with the cathodic (blue) and anodic scans (orange).

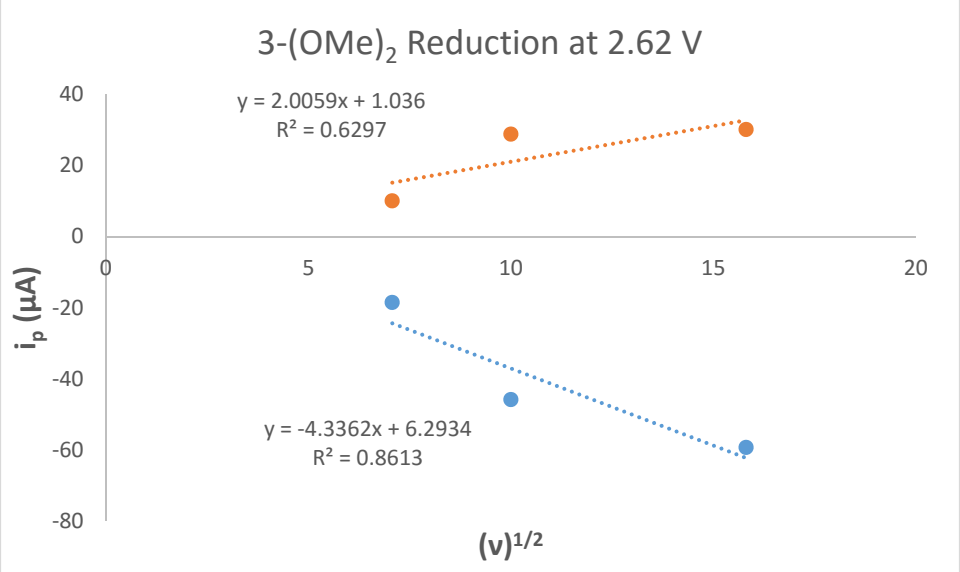

Figure 24. Plot of the scan rate dependence for the reduction of compound **3-(OMe)$_2$** with the cathodic (blue) and anodic scans (orange).

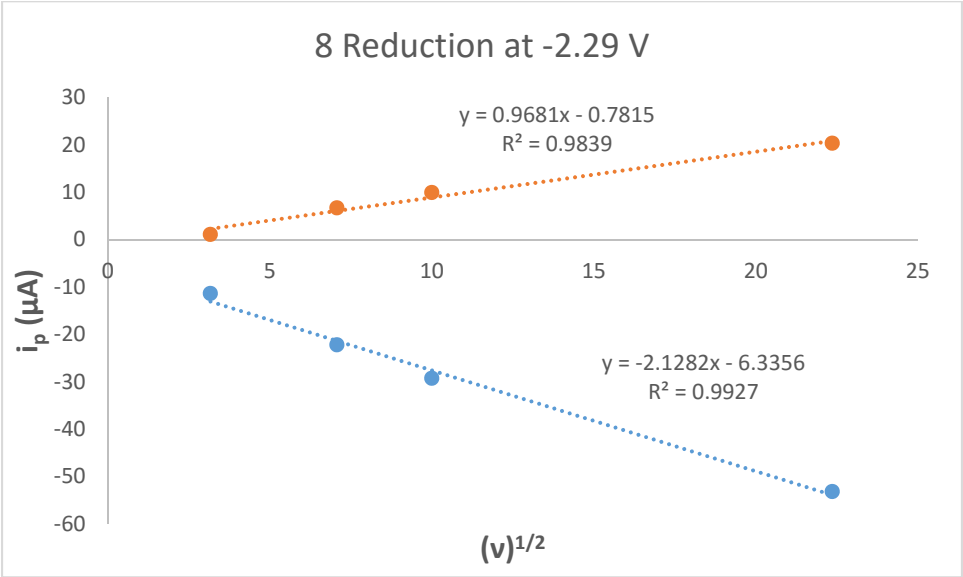

Figure 25. Plot of the scan rate dependence for the first reduction of compound **8** with the cathodic (blue) and anodic scans (orange).

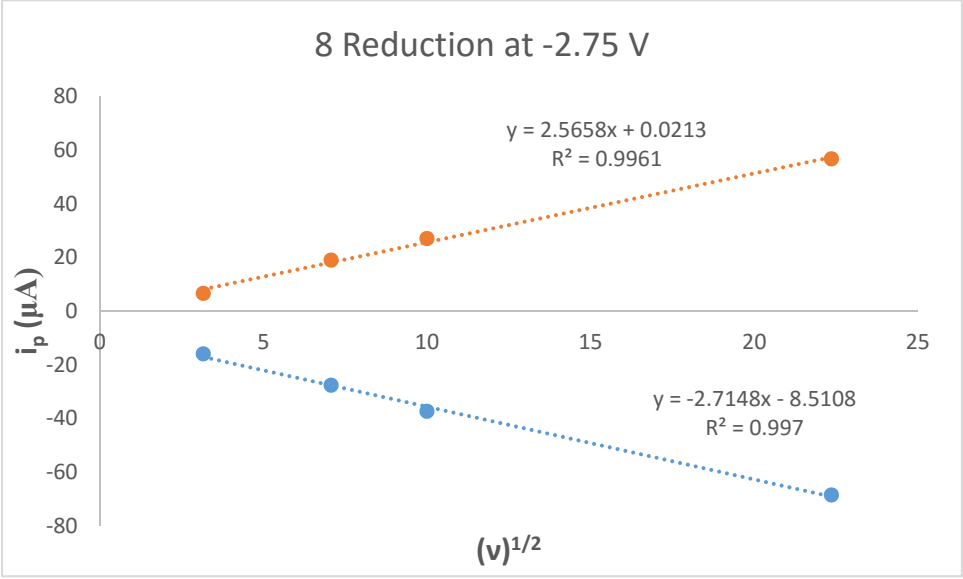

Figure 26. Plot of the scan rate dependence for the second reduction of compound **8** with the cathodic (blue) and anodic scans (orange).

Mössbauer Details

Spectra were recorded on a spectrometer from SEE Co. operating in the constant acceleration mode in a transmission geometry. Spectra were recorded with the temperature of the sample maintained at 80 K. The sample was kept in an SVT-400 Dewar from Janis, at zero field. Application of a magnetic field of 54 mT parallel to the γ-beam did not cause detectable changes in the spectra recorded at 80 K. The quoted isomer shifts are relative to the centroid of the spectrum of a metallic foil of α-Fe at room temperature. Samples were prepared by grinding polycrystalline material into a fine powder and then mounted in a cup fitted with a screw cap as a boron nitride pellet. Data analysis was performed using the program WMOSS (www. wmoss.org) and quadrupole doublets were fit to Lorentzian lineshapes.

Computational Details

All calculations were performed with DFT as implemented in Gaussian 09 Revision C.01.[29] Geometry optimizations and electronic structure calculations were performed with the TPSSh hybrid functional[30] that, incorporating 10% exact exchange (c.f. BLYP 0% and B3LYP 20%), has been shown to be effective for calculating transition metal-containing compounds.[31] The LANL2DZ basis set and effective core potential[32] for Pd atoms and the 6-31++G(d,p) basis set[33] for all other atoms was used. No solvent corrections were used. For all compounds isopropyl substituents on the phosphine ligands were truncated to methyl groups and have been designated with the -Me_2 suffix to the appropriate compound numbers. Geometry optimizations of **3-Me_2** and **3-$(OMe)_2$-Me_2** were performed under the C_2 point group, while **4-Me_2** and **8-Me_2** were optimized without symmetry constraints. Optimization stationary points were confirmed with subsequent frequency calculations that did not return imaginary frequency vibrations < -10 cm^{-1}. All molecular orbital illustrations are depicted with a 0.05 isosurface value. Natural bond order (NBO) calculations were performed to elucidate the nature of the M-M' interactions. There is an unresolved error with NBO3, as implemented in Gaussian09[8], when trying to do bonding analysis of these compounds. So to perform NBO bond analysis, the following procedure was used: the atomic coordinates from the Gaussian09 geometry optimizations were used to run single-point calculations in Orca (version 3.0.3[34]), and Orca was used to generate input files (*.47) for NBO6 [35] analysis. The NBO6 input files were modified by including the keywords BNDIDX and PLOT and listing analogous connectivity patterns in a $CHOOSE block before running. The natural localized molecular orbitals (NLMOs) were visualized using the pre-orthogonalized natural atomic orbitals basis set by opening the *.38 NBO6 output files with JMol.

Table 3. Select Molecular Orbital Illustrations for **3-Me$_2$**, **4-Me$_2$**, **3-(OMe)$_2$-Me$_2$**, and **8-Me$_2$**

3-Me$_2$	4-Me$_2$	3-(OMe)$_2$-Me$_2$	8-Me$_2$	Rep. MO
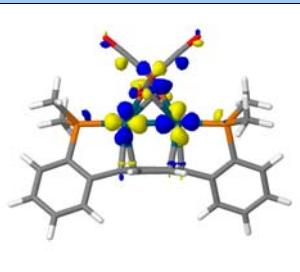 LUMO	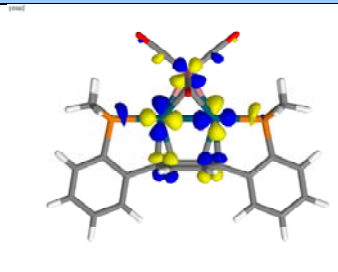 LUMO	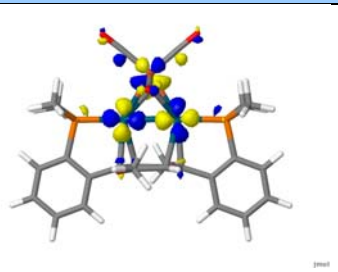 LUMO	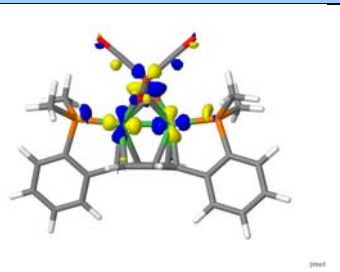 LUMO	M-M and M-M' antibonding
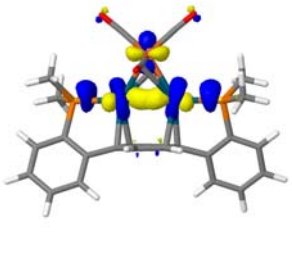 HOMO-2	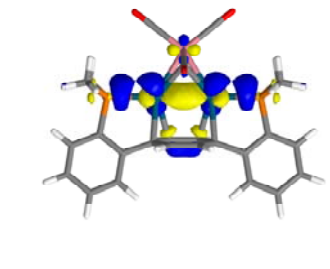 HOMO	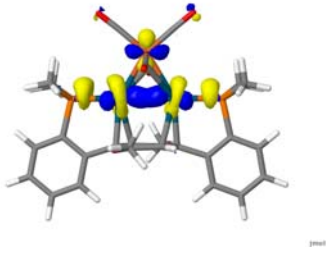 HOMO-2	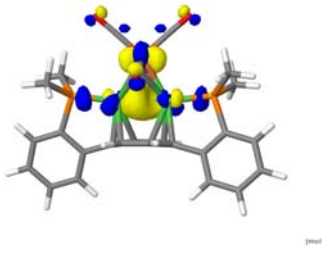 HOMO-1	M-M σ-bonding

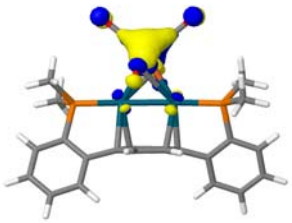 HOMO-4	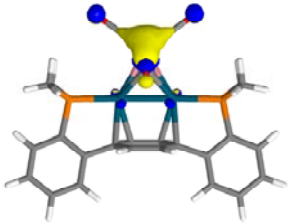 HOMO-5	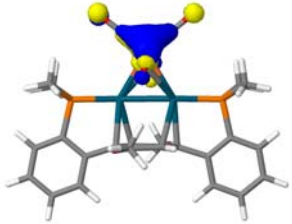 HOMO-4	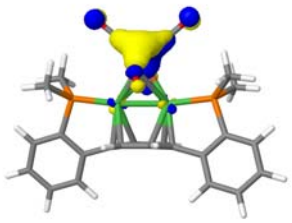 HOMO-4	M'-CO backbonding
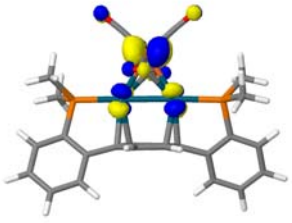 HOMO-5	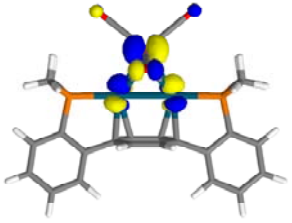 HOMO-16	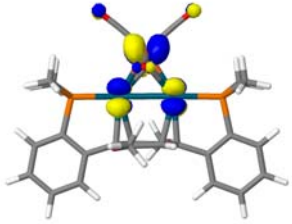 HOMO-5	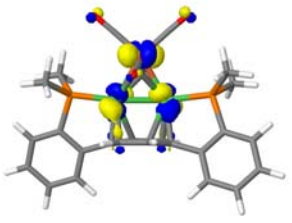 HOMO-7	M-M' π antibonding and M-M δ antibonding
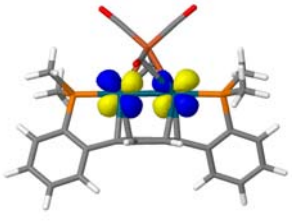 HOMO-10	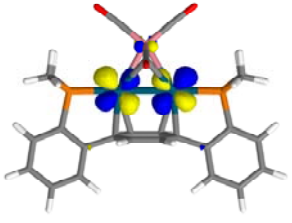 HOMO-13	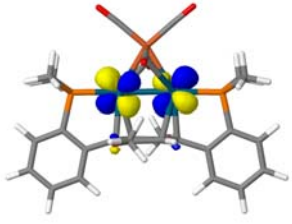 HOMO-10	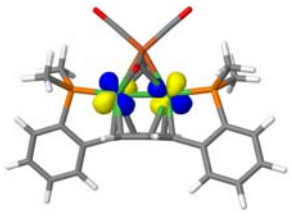 HOMO-9	M-M π-antibonding

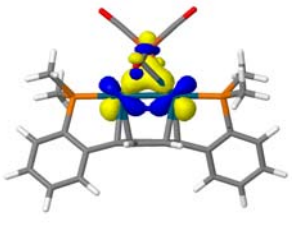 HOMO-17	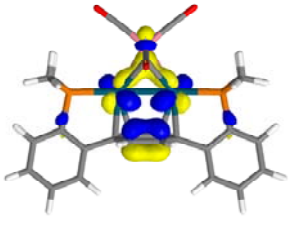 HOMO-18	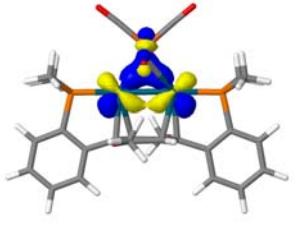 HOMO-18	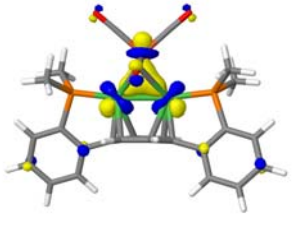 HOMO-17	M-M and M-M' bonding
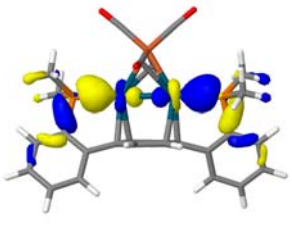 HOMO-19	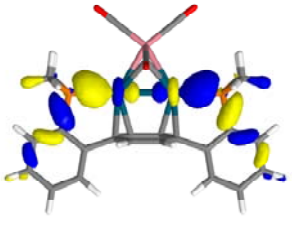 HOMO-17	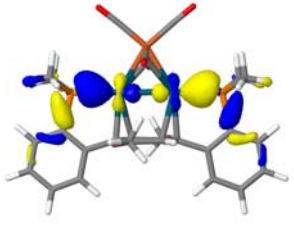 HOMO-20	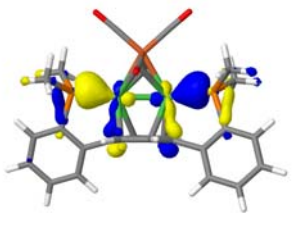 HOMO-18	M-P bonding
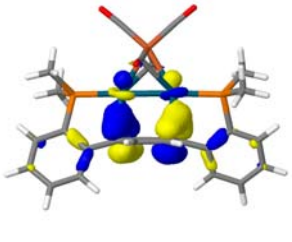 HOMO-20	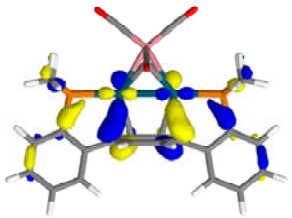 HOMO-23	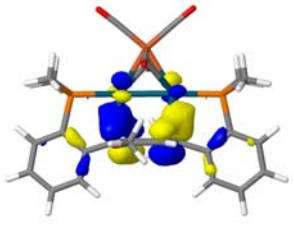 HOMO-21	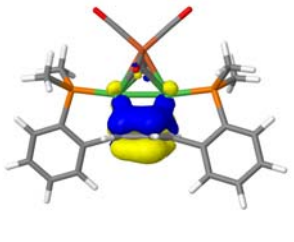 HOMO-19	M-arene bonding

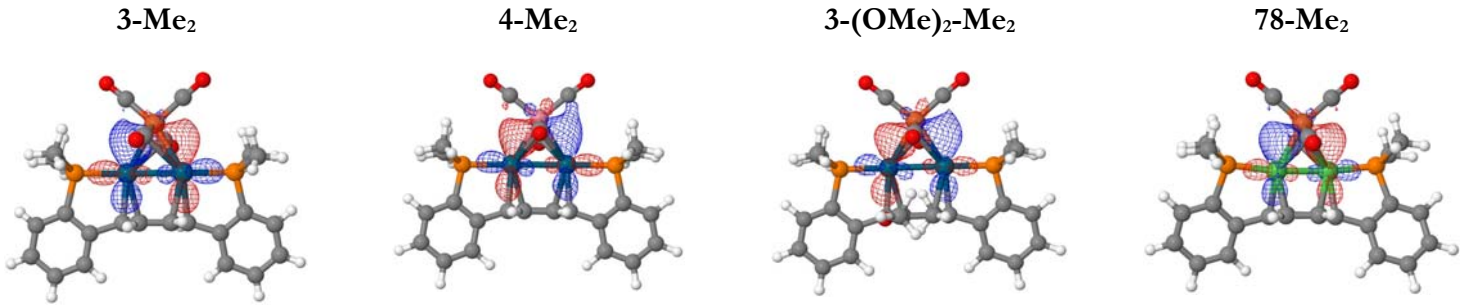

Figure 27. a) Metal–metal and metal-CO Wiberg bond indices and b) (group 10 metal center)–(apical metal center) (M–M') natural localized molecular orbitals (NLMOs) and their contributions to total M–M' bond orders

Crystallographic Information

CCDC 1056167-1056171 contain the supplementary crystallographic data for the published compounds in Section 2.2. CCDC 981915, 737475, 981916, and 981917 contain the supplementary crystallographic data for the published complexes in Section 2.3. These data can be obtained free of charge from The Cambridge Crystallographic Data Centre via www.ccdc.cam.ac.uk/data_request/cif.

Refinement Details

In each case, crystals were mounted on a glass fiber or nylon loop using Paratone oil, then placed on the diffractometer under a nitrogen stream. Low temperature (100 K) X-ray data were obtained on a Bruker APEXII CCD based diffractometer (Mo sealed X-ray tube, K_α = 0.71073 Å). All diffractometer manipulations, including data collection, integration and scaling were carried out using the Bruker APEXII software.[36] Absorption corrections were applied using SADABS.[37] Space groups were determined on the basis of systematic absences and intensity statistics and the structures were solved by direct methods using XS (incorporated into SHELXTL) and refined by full-matrix least squares on F^2. All non-hydrogen atoms were refined using anisotropic displacement parameters. Hydrogen atoms were placed in idealized positions and refined using a riding model. The structure was refined (weighted least squares refinement on F^2) to convergence.

Special refinement details for 10

10 was crystallized from a THF-hexanes vapor diffusion at -35 ºC in an inert atmosphere glovebox. It was found to crystallize with a disordered THF solvent molecule with one oxygen modelled isotropically. The structure also contains an outer-sphere hexafluorophosphate anion that was satisfactorily modelled.

Table 4. Crystal and refinement data for complexes reported in Section 2.2

Complex	**3**	**4**	**5**	**6**	**3-(OMe)$_2$**	**8**
empirical formula	$C_{17}H_{20}Fe_{0.50}O_2PPd$	$C_{40}H_{47.50}BCoF_4N_{1.50}O_4P_2Pd_2$	$C_{34}H_{40}CoO_4P_2Pd_2$	$C_{41}H_{52}B_2F_8MoN_4O_3P_2Pd_2$	$C_{36}H_{44}FeO_6P_2Pd_2$	$C_{17}H_{20}Fe_{0.50}NiO_2P$
formula wt	421.62	1033.77	846.33	1193.16	903.30	373.93
T (K)	100	100	100	100	100	100
a, Å	11.4622(6)	15.9326(8)	15.7355(5)	7.7570(7)	14.0587(5)	11.5996(6)
b, Å	13.3606(7)	16.5136(9)	13.6086(4)	15.4169(13)	14.2422(5)	13.1456(7)
c, Å	11.1153(5)	18.4384(10)	15.8392(5)	19.7029(18)	18.4208(6)	10.9589(5)
α, deg	90	90.490(3)	90	95.586(4)	90	90
β, deg	90	114.618(2)	90.1244(15)	91.721(4)	90	90
γ, deg	90	105.162(2)	90	95.546(4)	90	90
V, Å^3	1702.22(15)	4218.4(4)	3391.77(18)	2332.2(4)	3688.3(2)	1671.05(15)
Z	4	4	4	2	4	4
cryst syst	Orthorhombic	Triclinic	Monoclinic	Triclinic	Orthorhombic	Orthorhombic
space group	P 2_1 2_1 2	P $_{-1}$	P 1 21/n 1	P$_{-1}$	P 2_1 2_1 2_1	P 2_1 2_1 2
d_{calcd}, g/cm^3	1.645	1.628	1.657	1.699	1.627	1.486
θ range, deg	1.832 to 30.581	1.289 to 26.372	1.822 to 36.252	1.039 to 45.367	2.035 to 36.442	2.342 to 30.569
μ, mm^{-1}	1.595	1.367	1.662	1.170	1.482	1.675
abs cor	Semi-empirical from equivalents	Semi-empirical from equivalents	Semi-empirical from equivalents	Semi-empirical from equivalents	Semi-empirical from equivalents	Semi-empirical from equivalents
GOF[c]	1.172	1.077	1.175	1.042	1.070	1.082
R1,[a] wR2[b] (I > 2σ(I))	0.0142, 0.0352	0.0264, 0.0669	0.0378, 0.0791	0.0401, 0.1295	0.0325, 0.0638	0.0342, 0.0898

Table 5. Crystal and refinement data for complexes reported in Section 2.3

Complex	**9**	**11**	**12**	**10**	**13-CO**
empirical formula	$C_{34}H_{40}O_4P_2Fe_2$	$C_{39}H_{46}Co_2O_3P_2$	$C_{33}H_{40}Ni_2O_3P_2$	$C_{36}H_{44}F_6Fe_2O_{4.50}P_3$	$C_{34}H_{40}Ni_3O_4P_2$
formula wt	686.33	742.56	664.01	867.32	750.73
T (K)	100	100	100	100	100
a, Å	14.3107(5)	10.0645(4)	14.1146(4)	8.8633(4)	13.2747(6)
b, Å	11.4723(4)	11.1061(5)	15.1785(4)	15.6066(7)	14.3889(6)
c, Å	20.2029(7)	32.262(1)	15.6000(4)	27.166(1)	17.0160(7)
α, deg	90	90	90	90	90
β, deg	108.029(2)	91.975(2)	115.380(1)	98.310(2)	90
γ, deg	90	90	90	90	90
V, Å^3	3154.0(2)	3604.0(3)	3019.6(1)	3718.4(3)	3250.2(2)
Z	4	4	4	4	4
cryst syst	Monoclinic	Monoclinic	Monoclinic	Monoclinic	Orthorhombic
space group	$P2_1/c$	$P2_1/n$	$P2_1/c$	$P2_1/c$	$P2_12_12_1$
d_{calcd}, g/cm^3	1.4453	1.369	1.461	1.549	1.534
θ range, deg	3 to 73.66	1.94 to 36.81	1.972 to 30.656	2.000 to 30.598	1.85 to 37.24
μ, mm^{-1}	1.058	1.045	1.386	0.980	1.855
abs cor	Semi-empirical from equivalents	Semi-empirical from equivalents	Semi-empirical from equivalents	Semi-empirical from equivalents	Semi-empirical from equivalents
GOF[c]	1.076	1.517	0.983	1.602	1.091
R1,[a] wR2[b] ($I > 2\sigma(I)$)	0.0302, 0.1373	0.0373, 0.0624	0.0321, 0.1090	0.0267, 0.0732	0.0344, 0.0615

[a] $R1 = \Sigma||F_o|-|F_c|| / \Sigma|F_o|$ [b] $wR2 = \{ \Sigma [w(F_o^2-F_c^2)^2] / \Sigma [w(F_o^2)^2] \}^{1/2}$ [c] $GOF = S = \{ \Sigma [w(F_o^2-F_c^2)^2] / (n-p) \}^{1/2}$

EPR Details

Spectrum was collected on an X-band EPR (Frequency: 9.391 GHz; Power: 0.645 mW; Modulation Amplitude: 1 G) as a toluene glass at 77 K. EPR simulation run using EasySpin program for Matlab.[38] Simulation parameters: g = [2.128, 2.032, 1.930], lw = 2, HStrain = [20, 20, 20], Nucs = 'Co', A = [119 65 105].

REFERENCES

1.(a) Adams, R. D.; Cotton, F. A., *Catalysis by Di- and Polynuclear Metal Cluster Complexes*. Wiley-VCH: 1998; (b) Guczi, L., *Supported Bimetallic Catalysts Derived from Molecular Metal Complexes*. Elsevier Science Publishers B. V.: 1986; Vol. 29; (c) Braunstein, P.; Rosé, J., Heterometallic Clusters in Catalysis. In *Metal Clusters in Chemistry*, Braunstein, P.; Oro, L. A.; Raithby, P. R., Eds. Wiley-VCH: 1999.
2.Buchwalter, P.; Rosé, J.; Braunstein, P., *Chemical Reviews* **2015,** *115*, 28-126.
3.(a) Marquard, S. L.; Bezpalko, M. W.; Foxman, B. M.; Thomas, C. M., *J Am Chem Soc* **2013,** *135*, 6018-6021; (b) Krogman, J. P.; Foxman, B. M.; Thomas, C. M., *J Am Chem Soc* **2011,** *133*, 14582-14585; (c) Kuppuswamy, S.; Bezpalko, M. W.; Powers, T. M.; Wilding, M. J. T.; Brozek, C. K.; Foxman, B. M.; Thomas, C. M., *Chem. Sci.* **2014,** *5*, 1617-1626; (d) Napoline, J. W.; Krogman, J. P.; Shi, R.; Kuppuswamy, S.; Bezpalko, M. W.; Foxman, B. M.; Thomas, C. M., *Eur. J. Inorg. Chem.* **2013,** *2013*, 3874-3882; (e) Cooper, B. G.; Napoline, J. W.; Thomas, C. M., *Catal. Rev.* **2012,** *54*, 1-40; (f) Clouston, L. J.; Siedschlag, R. B.; Rudd, P. A.; Planas, N.; Hu, S. X.; Miller, A. D.; Gagliardi, L.; Lu, C. C., *J Am Chem Soc* **2013,** *135*, 13142-13148; (g) Rudd, P. A.; Liu, S. S.; Gagliardi, L.; Young, V. G.; Lu, C. C., *J Am Chem Soc* **2011,** *133*, 20724-20727; (h) Tereniak, S. J.; Carlson, R. K.; Clouston, L. J.; Young, V. G.; Bill, E.; Maurice, R.; Chen, Y. S.; Kim, H. J.; Gagliardi, L.; Lu, C. C., *J Am Chem Soc* **2014,** *136*, 1842-1855; (i) Banerjee, S.; Karunananda, M. K.; Bagherzadeh, S.; Jayarathne, U.; Parmelee, S. R.; Waldhart, G. W.; Mankad, N. P., *Inorganic Chemistry* **2014,** *53*, 11307-11315; (j) Collman, J. P.; Boulatov, R., *Angew. Chem. Int. Ed.* **2002,** *41*, 3948-3961.
4.(a) Jaouen, G.; Marinetti, A.; Mentzen, B.; Mutin, R.; Saillard, J. Y.; Sayer, B. G.; McGlinchey, M. J., *Organometallics* **1982,** *1*, 753-756; (b) Mlekuz, M.; Bougeard, P.; Sayer, B. G.; Peng, S.; McGlinchey, M. J.; Marinetti, A.; Saillard, J. Y.; Ben Naceur, J.; Mentzen, B.; Jaouen, G., *Organometallics* **1985,** *4*, 1123-1130; (c) Powers, T. M.; Gu, N. N. X.; Pout, A. R.; Baldwin, A. M.; Sanchez, R. H.; Alfonso, D. M.; Chen, Y. S.; Zheng, S. L.; Betley, T. A., *J Am Chem Soc* **2013,** *135*, 14448-14458; (d) Eames, E. V.; Sanchez, R. H.; Betley, T. A., *Inorganic Chemistry* **2013,** *52*, 5006-5012; (e) Braunstein, P.; Sappa, E.; Tiripicchio, A.; Camellini, M. T., *Inorganica Chimica Acta* **1980,** *45*, L191-L193; (f) Sironi, A.; Gervasio, G.; Sappa, E., *Journal of Cluster Science* **1994,** *5*, 535-548; (g) Bachert, I.; Braunstein, P.; McCart, M. K.; Biani, F. F. d.; Laschi, F.; Zanello, P.; Kickelbick, G.; Schubert, U., *Journal of Organometallic Chemistry* **1999,** *573*, 47-59; (h) Braunstein, P.; Ries, M.; Bellefon, C. d. M. d., *Journal of Organometallic Chemistry* **1988,** *355*, 533-550; (i) Braunstein, P.; Bellefon, C. d. M. d.; Ries, M.;

Fischer, J.; Bouaoud, S.-E.; Grandjean, D., *Inorganic Chemistry* **1988,** *27*, 1327-1337; (j) Braunstein, P.; Guarino, N.; de Méric de Bellefon, C.; Richert, J.-L., *Angewandte Chemie International Edition in English* **1987,** *26*, 88-89; (k) Archambault, C.; Bender, R.; Braunstein, P.; Bouaoud, S.-E.; Rouag, D.; Golhen, S.; Ouahab, L., *Chemical Communications* **2001**, 849-850; (l) Sappa, E.; Tiripicchio, A.; Braunstein, P., *Chemical Reviews* **1983,** *83*, 203-239; (m) Sappa, E.; Tiripicchio, A.; Braunstein, P., *Coordination Chemistry Reviews* **1985,** *65*, 219-284; (n) Braunstein, P.; De Meric de Bellefon, C.; Ries, M., *Inorganic Chemistry* **1990,** *29*, 1181-1186; (o) Lal De, R.; Von Seyerl, J.; Huttner, G., *Journal of Organometallic Chemistry* **1979,** *178*, 319-324; (p) Bender, R.; Braunstein, P.; Metz, B.; Lemoine, P., *Organometallics* **1984,** *3*, 381-384; (q) Vahrenkamp, H., *Pure Appl Chem* **1991,** *63*, 643-649; (r) Barr, R. D.; Green, M.; Howard, J. A. K.; Marder, T. B.; Stone, F. G. A., *J Chem Soc Chem Comm* **1983**, 759-760; (s) Carriedo, G. A.; Howard, J. A. K.; Stone, F. G. A., *Journal of Organometallic Chemistry* **1983,** *250*, C28-C32.
5.(a) Tard, C.; Pickett, C. J., *Chemical Reviews* **2009,** *109*, 2245-2274; (b) Gloaguen, F.; Rauchfuss, T. B., *Chem Soc Rev* **2009,** *38*, 100-108; (c) Darensbourg, M. Y.; Lyon, E. J.; Smee, J. J., *Coordination Chemistry Reviews* **2000,** *206*, 533-561; (d) Camara, J. M.; Rauchfuss, T. B., *Nat Chem* **2012,** *4*, 26-30; (e) Shibata, T., *Adv Synth Catal* **2006,** *348*, 2328-2336; (f) Mazzoni, R.; Salmi, M.; Zanotti, V., *Chem-Eur J* **2012,** *18*, 10174-10194; (g) Velian, A.; Lin, S.; Miller, A. J. M.; Day, M. W.; Agapie, T., *J. Am. Chem. Soc.* **2010,** *132*, 6296-6297; (h) Beck, R.; Johnson, S. A., *Chemical Communications* **2011,** *47*, 9233-9235; (i) Laskowski, C. A.; Hillhouse, G. L., *Chem. Sci.* **2011,** *2*, 321-325; (j) Laskowski, C. A.; Hillhouse, G. L., *Organometallics* **2009,** *28*, 6114-6120; (k) Delaet, D. L.; Delrosario, R.; Fanwick, P. E.; Kubiak, C. P., *J Am Chem Soc* **1987,** *109*, 754-758; (l) Lee, C. H.; Laitar, D. S.; Mueller, P.; Sadighi, J. P., *J Am Chem Soc* **2007,** *129*, 13802-13803; (m) Simon-Manso, E.; Kubiak, C. P., *Organometallics* **2005,** *24*, 96-102; (n) Lemke, F. R.; Delaet, D. L.; Gao, J. L.; Kubiak, C. P., *J Am Chem Soc* **1988,** *110*, 6904-6906; (o) Friedle, S.; Reisner, E.; Lippard, S. J., *Chem Soc Rev* **2010,** *39*, 2768-2779; (p) Ritleng, V.; Chetcuti, M. J., *Chemical Reviews* **2007,** *107*, 797-858; (q) Haak, R. M.; Wezenberg, S. J.; Kleij, A. W., *Chemical Communications* **2010,** *46*, 2713-2723; (r) Wheatley, N.; Kalck, P., *Chemical Reviews* **1999,** *99*, 3379-3419.
6.Gavrilova, A. L.; Bosnich, B., *Chemical Reviews* **2004,** *104*, 349-383.
7.(a) Suseno, S.; Horak, K. T.; Day, M. W.; Agapie, T., *Organometallics* **2013,** *32*, 6883-6886; (b) Lin, S.; Herbert, D. E.; Velian, A.; Day, M. W.; Agapie, T., *JACS* **2013,** *135*, 15830-15840; (c) Chao, S. T.; Lara, N. C.; Lin, S.; Day, M. W.; Agapie, T., *Angew. Chem. Int. Ed.* **2011,** *50*, 7529-7532.
8.Velian, A.; Lin, S. B.; Miller, A. J. M.; Day, M. W.; Agapie, T., *J Am Chem Soc* **2010,** *132*, 6296-6297.
9.Kelley, P.; Lin, S.; Edouard, G.; Day, M. W.; Agapie, T., *J Am Chem Soc* **2012,** *134*, 5480-5483.
10.(a) Lin, S. B.; Herbert, D. E.; Velian, A.; Day, M. W.; Agapie, T., *J Am Chem Soc* **2013,** *135*, 15830-15840; (b) Chao, S. T.; Lara, N. C.; Lin, S. B.; Day, M. W.; Agapie, T., *Angew. Chem. Int. Ed.* **2011,** *50*, 7529-7532; (c) Horak, K. T.; Velian, A.; Day, M. W.; Agapie, T., *Chemical Communications* **2014,** *50*, 4427-4429.
11.(a) Murahashi, T.; Takase, K.; Oka, M.-a.; Ogoshi, S., *J Am Chem Soc* **2011,** *133*, 14908-14911; (b) Ishikawa, Y.; Kimura, S.; Takase, K.; Yamamoto, K.; Kurashige, Y.; Yanai, T.; Murahashi, T., *Angewandte Chemie International Edition* **2015,** *54*, 2482-2486.
12.(a) Cristiani, F.; De Filippo, D.; Deplano, P.; Devillanova, F.; Diaz, A.; Trogu, E. F.; Verani, G., *Inorganica Chimica Acta* **1975,** *12*, 119-122; (b) Siclovan, O. P.; Angelici, R. J., *Inorganic Chemistry* **1998,** *37*, 432-444.

13.Bender, R.; Braunstein, P.; Bouaoud, S.-E.; Rouag, D.; Harvey, P. D.; Golhen, S.; Ouahab, L., *Inorganic Chemistry* **2002,** *41*, 1739-1746.
14.(a) Aguirre-Etcheverry, P.; Ashley, A. E.; Balazs, G.; Green, J. C.; Cowley, A. R.; Thompson, A. L.; O'Hare, D., *Organometallics* **2010,** *29*, 5847-5858; (b) Kerber, R. C.; Miran, M. J.; Waldbaum, B.; Rheingold, A. L., *Organometallics* **1995,** *14*, 2002-2008; (c) Putnik, C. F.; Welter, J. J.; Stucky, G. D.; D'Aniello Jr., M. J.; Sosinsky, B. A.; Kirner, J. F.; Muetterties, E. L., *JACS* **1978,** *100*, 4107-4116; (d) Knox, S. A. R.; Morton, D. A. V.; Orpen, A. G.; Turner, M. L., *Inorganica Chimica Acta* **1994,** *220*, 201-214.
15.(a) Lu, C. C.; Saouma, C. T.; Day, M. W.; Peters, J. C., *J Am Chem Soc* **2007,** *129*, 4-5; (b) Schneider, J. J.; Specht, U.; Goddard, R.; Krüger, C.; Ensling, J.; Gütlich, P., *Chem. Ber.* **1995,** *128*, 941-945; (c) Jonas, K.; Koepe, G.; Schieferstein, L.; Mynott, R.; Kruger, C.; Tsay, Y. H., *Angew. Chem. Int. Ed. Engl.* **1983,** *22*, 620-621.
16.A CSD search of dinuclear Co or Fe complexes bound to a cyclic C6-fragment yielded 1 cofacial and 1 transfacial Fe2 complex and 1 transfacial Co2 complex with a μ2:(η3,η3) binding mode.
17.Casati, N.; Macchi, P.; Sironi, A., *Angew. Chem. Int. Ed.* **2005,** *44*, 7736-7739.
18.(a) Johnson, S. A.; Taylor, E. T.; Cruise, S. J., *Organometallics* **2009,** *28*, 3842-3855; (b) Bach, I.; Porschke, K. R.; Goddard, R.; Kopiske, C.; Kruger, C.; Rufinska, A.; Seevogel, K., *Organometallics* **1996,** *15*, 4959-4966.
19.(a) Mezailles, N.; LeFloch, P.; Waschbusch, K.; Ricard, L.; Mathey, F.; Kubiak, C. P., *Journal of Organometallic Chemistry* **1997,** *541*, 277-283; (b) Osborn, J. A.; Stanley, G. G., *Angew Chem Int Edit* **1980,** *19*, 1025-1026.
20.Liu, T. B.; Darensbourg, M. Y., *J Am Chem Soc* **2007,** *129*, 7008-7009.
21.(a) Osborn, J. A.; Stanley, G. G.; Bird, P. H., *J Am Chem Soc* **1988,** *110*, 2117-2122; (b) Vogl, E. M.; Bruckmann, J.; Kruger, C.; Haenel, M. W., *Journal of Organometallic Chemistry* **1996,** *520*, 249-252.
22.(a) Munha, R. F.; Zarkesh, R. A.; Heyduk, A. F., *Dalton T* **2013,** *42*, 3751-3766; (b) Luca, O. R.; Crabtree, R. H., *Chem Soc Rev* **2013,** *42*, 1440-1459; (c) Annibale, V. T.; Song, D. T., *Rsc Adv* **2013,** *3*, 11432-11449; (d) Eisenberg, R.; Gray, H. B., *Inorganic Chemistry* **2011,** *50*, 9741-9751; (e) Chirik, P. J.; Wieghardt, K., *Science* **2010,** *327*, 794-795.
23.Pangborn, A. B.; Giardello, M. A.; Grubbs, R. H.; Rosen, R. K.; Timmers, F. J., *Organometallics* **1996,** *15*, 1518-1520.
24.Zhao, Y. L.; Liu, L. H.; Zhang, W. Y.; Sue, C. H.; Li, Q. W.; Miljanic, O. S.; Yaghi, O. M.; Stoddart, J. F., *Chem-Eur J* **2009,** *15*, 13356-13380.
25.Murahashi, T.; Nagai, T.; Okuno, T.; Matsutani, T.; Kurosawa, H., *Chemical Communications* **2000**, 1689-1690.
26.Edgell, W. F.; Lyford, J., *Inorganic Chemistry* **1970,** *9*, 1932-1933.
27.Strong, H.; Krusic, P. J.; San Filippo, J., *Inorganic Syntheses*. 1986; Vol. 24.
28.Fulmer, G. R.; Miller, A. J. M.; Sherden, N. H.; Gottlieb, H. E.; Nudelman, A.; Stoltz, B. M.; Bercaw, J. E.; Goldberg, K. I., *Organometallics* **2010,** *29*, 2176-2179.
29.1) Gaussian 09, Revision C.01, Frisch, M. J.; Trucks, G. W.; Schlegel, H. B.; Scuseria, G. E.; Robb, M. A.; Cheeseman, J. R.; Scalmani, G.; Barone, V.; Mennucci, B.; Petersson, G. A.; Nakatsuji, H.; Caricato, M.; Li, X.; Hratchian, H. P.; Izmaylov, A. F.; Bloino, J.; Zheng, G.; Sonnenberg, J. L.; Hada, M.; Ehara, M.; Toyota, K.; Fukuda, R.; Hasegawa, J.; Ishida, M.; Nakajima, T.; Honda, Y.; Kitao, O.; Nakai, H.; Vreven, T.; Montgomery, Jr., J. A.; Peralta, J. E.; Ogliaro, F.; Bearpark, M.; Heyd, J. J.; Brothers, E.; Kudin, K. N.; Staroverov, V. N.; Kobayashi, R.; Normand, J.; Raghavachari, K.; Rendell, A.; Burant, J. C.; Iyengar, S. S.; Tomasi, J.; Cossi, M.; Rega, N.; Millam, J. M.; Klene, M.; Knox, J. E.; Cross, J. B.; Bakken,

V.; Adamo, C.; Jaramillo, J.; Gomperts, R.; Stratmann, R. E.; Yazyev, O.; Austin, A. J.; Cammi, R.; Pomelli, C.; Ochterski, J. W.; Martin, R. L.; Morokuma, K.; Zakrzewski, V. G.; Voth, G. A.; Salvador, P.; Dannenberg, J. J.; Dapprich, S.; Daniels, A. D.; Farkas, Ö.; Foresman, J. B.; Ortiz, J. V.; Cioslowski, J.; Fox, D. J. Gaussian, Inc., Wallingford CT, 2009.
30.(a) Tao, J. M.; Perdew, J. P.; Staroverov, V. N.; Scuseria, G. E., *Phys. Rev. Lett.* **2003,** *91*; (b) Staroverov, V. N.; Scuseria, G. E.; Tao, J. M.; Perdew, J. P., *J. Chem. Phys.* **2003,** *119*, 12129-12137.
31.(a) Jensen, K. P., *Inorganic Chemistry* **2008,** *47*, 10357-10365; (b) Buhl, M.; Kabrede, H., *J. Chem. Theory Comput.* **2006,** *2*, 1282-1290; (c) Waller, M. P.; Braun, H.; Hojdis, N.; Buhl, M., *J. Chem. Theory Comput.* **2007,** *3*, 2234-2242.
32.Hay, P. J.; Wadt, W. R., *J. Chem. Phys.* **1985,** *82*, 270-283.
33.Ditchfield, R.; Hehre, W. J.; Pople, J. A., *J. Chem. Phys.* **1971,** *54*, 724-728.
34.Neese, F., Wiley Interdiscip. Rev.: Comput. Mol. Sci., 2012, 2, 73-78.
35.NBO 6.0. Glendening, E. D., Badenhoop, J. K., Reed, A. E., Carpenter, J. E., Bohmann, J. A., Morales, C. M., Landis, C. R., Weinhold, F. (Theoretical Chemistry Institute, University of Wisconsin, Madison, WI, 2013), http://nbo6.chem.wisc.edu/
36.APEX2, Version 2 User Manual, M86-E01078, Bruker Analytical X-ray Systems, Madison, WI, June 2006.
37.Sheldrick, G. M. "SADABS (Version 2008/1): Program for Absorption Correction for Data from Area Detector Frames", University of Göttingen, 2008.
38.Stoll, S.; Schweiger, A., *J Magn Reson* **2006,** *178*, 42-55.

CHAPTER 3

SYNTHESIS AND REACTIVITY OF METAL COMPLEXES SUPPORTED BY A NON-INNOCENT HYDROQUINONE PARA-TERPHENYL DIPHOSPHINE LIGAND

Abstract

A novel *para*-terphenyl diphosphine ligand was synthesized with a non-innocent hydroquinone moiety as the central arene (**1-H**). *Pseudo*-tetrahedral 4-coordinate Ni^0 and Pd^0-quinone (**2** and **3**, respectively) complexes proved accessible by metalating **1-H** with the corresponding $M^{II}(OAc)_2$ precursors. O_2 does not react with the Pd^0-quinone species (**3**) and protonation occurs at the quinone moiety indicating that the coordinated oxidized quinonoid moiety prevents reactivity at the metal. A 2-coordinate Pd^0-hydroquinone complex (**4-H**) was prepared using a one-pot metalation with Pd^{II} followed by reduction. The reduced quinonoid moiety in **4-H** shows metal-coupled reactivity with small molecules. **4-H** was capable of reducing a variety of substrates including dioxygen, nitric oxide, nitrous oxide, 1-azido adamantane, trimethylamine *n*-oxide, and 1,4-benzoquinone quantitatively producing **3** as the Pd-containing reaction product. Mechanistic investigations of dioxygen reduction revealed that the reaction proceeds through a η^2-peroxo intermediate (**Int1**) at low temperatures followed by subsequent ligand oxidation at higher temperatures in a reaction that consumed half an equivalent of O_2 and produced water as a final oxygenic byproduct. Control compounds with methyl protected phenolic moieties (**4-Me**), displaying a Ag^I center incapable of O_2 binding (**7-H**) or a cationic Pd-H motif (**6-H**) allowed for the independent examination of potential reaction pathways. The reaction of **4-Me** with dioxygen at low temperature produces a species (**8-Me**) analogous to **Int1** demonstrating that initial dioxygen activation is an inner sphere Pd-based process where the hydroquinone moiety only subsequently participates in the reduction of O_2, at higher temperatures, by H^+/e^- transfers.

INTRODUCTION

Dioxygen is commonly employed as an oxidant in biology where active site architecture regulates the delivery of reducing equivalents and protons to the substrate.[1] Similar strategies for electron[2] or proton management[3] using non-innocent ligand frameworks have been developed in synthetic systems. However, ligands capable of both proton and electron transfers during small molecule activation remain uncommon.[3b, 4] Aerobic oxidation chemistry using Pd[5] has seen many advances recently due to the appeal of employing dioxygen as a stoichiometric oxidant in a strategy akin to biological oxidase catalysts. Pd-catalyzed aerobic oxidations utilizing the reversible two proton-two electron couple of 1,4-benzoquinone as an additive has important applications in organic methodology.[6] The use 1,4-benzoquinone and its derivatives as stoichiometric or catalytic oxidants in their own right has also recently been reviewed.[7] Recent mechanistic studies have highlighted the complicated reaction pathways available in the combination of redox active metal (Pd), redox active organic additive that can also act as ligand (1,4-benzoquinone), and O_2.[6a, 8] Although in catalysis with Pd, 1,4-benzoquinone is used as a direct oxidant, we are particularly interested in the reactivity of the reduced counterpart, as a venue for providing protons and electrons for substrate activation in the presence of a reactive metal site. At the same time, the effect of the nature of the quinonoid fragment (reduced vs oxidized) on the chemistry of Pd with O_2 is particularly relevant to organic methodology. To that end, proximity to the reactive metal site is instrumental. Efforts to directly incorporate quinonoid moieties into ligand frameworks for Pd have been reported.[9] Though the interconversion of the hydroquinone and quinone forms of these ligands has been observed in some instances, the reduction of dioxygen with these Pd systems has not been reported. The use of π-bound quinonoid moieties as ligands has seen a several applications.[10]

Our group has reported the use of bis- and trisphosphinoarylbenzene ligands as scaffolds for mono- and multinuclear, π-bound transition metal complexes.[11] Non-innocence of the central arene moiety has been observed with cationic Ni–H complexes with respect to H-migration as well as with dinuclear Fe and Co carbonyl complexes with respect to partial reduction of the ring.[11e, 11g] The incorporation of a catechol moiety into the ligand scaffold capable of transferring multiple electrons and protons or other electrophiles during dioxygen reduction has also been recently reported for a Mo complex.[11c] In that case, there is no evidence that the metal center undergoes inner sphere chemistry with O_2, although electronic coupling with the quinonoid moiety and transfer of electrophile from catechol is instrumental for reactivity. With its established inner sphere chemistry with O_2, Pd provides an ideal case study for the effect of a pendant non-innocent group capable of transferring both electrons and protons. Moreover, given the utilization of Pd, hydroquinone, and O_2 in catalysis the present studies have implications to organic methodology. We report the synthesis of a *para*-terphenyldiphosphine ligand containing a 1,4-hydroquinone moiety and the cooperative small molecule activation observed in a Pd^0 complex.

RESULTS AND DISCUSSION

Section 3.1 Ligand Synthesis

The desired ligand, **1-H** (Scheme 1), was readily synthesized in five steps from commercially available starting materials. 2,5-diiodo-1,4-hydroquinone was synthesized according to literature procedures in two steps from 1,4-dimethoxybenzene. Methoxymethyl acetal (MOM) protection of both OH moieties to produce compound **A** was accomplished in dichloromethane (DCM) using diisopropyl ethyl amine as the base. A palladium-catalyzed Suzuki coupling with 2-bromophenyl boronic acid as the coupling partner yielded the desired

terphenyl ligand precursor (**B**). Subsequent lithium halogen exchange with *tert*-butyl lithium (*t*BuLi) followed by addition the chloro diisopropyl phosphine yielded the desired ligand (**1-H**). Much like the dimethoxy variant presented in Chapter 2 (Section 2.1 **1-(OMe)$_2$**), hindered rotation results in multiple $^{31}P\{^1H\}$ resonances (1.80, -0.06 ppm) at room temperature as well as a broadened ^1H spectrum.

Scheme 1. Synthesis of 1-H

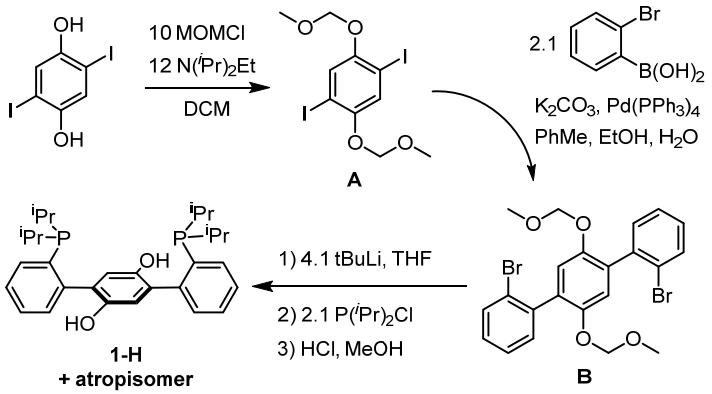

Section 3.2 Synthesis of Hydroquinone and Quinone Diphosphine-Supported Metal Complexes

Ni and Pd complexes supported by both the hydroquinone and quinone forms of compound **1-H** were targeted. Metalations with Ni^{II} or Pd^{II} diacetate proceeded in tetrahydrofuran (THF), though elevated temperatures were required for nickel. Both reactions yielded the corresponding M^0-quinone complexes **2** and **3** (~60% yield) as green and purple solids, respectively (Scheme 2).

The quinone assignment for the central arene was corroborated by strong ν_{CO} infrared (IR) absorptions at 1597 and 1603 cm^{-1} for complex **2** and **3** respectively. While the quinone form of **1-H** could not be isolated, likely due to reactivity with the phosphine moieties, a shift to lower ν_{CO} stretching frequencies relative to 2,5-diphenyl-1,4-benzoquinone (1640 cm^{-1})[12] is consistent with data reported for other π-bound Ni and Pd quinone complexes.[13] Solution

NMR data in CD_2Cl_2 for **2** and **3** are consistent with either C_2 symmetric structures or a fast exchange process on the NMR time scale that exchanges the front and back of the molecules (as drawn). Both complexes show sharp singlets (**2**: 6.13 ppm, **3**: 6.10 ppm) corresponding to the central quinone protons and two distinct methine resonances (**2**: 2.52, 2.24 ppm, **3**: 2.46, 2.33 ppm) in the ^1H NMR spectra. By $^{31}P\{^1H\}$ NMR, single resonances are observed at 54.30 and 55.02 ppm for **2** and **3** respectively. Strong metal-to-ligand charge transfer bands for both complexes give both complexes their distinct colors (**2**: ε_{389} = 5000 M^{-1} cm^{-1}, ε_{456} = 1700 M^{-1} cm^{-1}, ε_{623} = 650 M^{-1} cm^{-1}; **3**: ε_{316} = 8300 M^{-1} cm^{-1}, ε_{375} = 6200 M^{-1} cm^{-1}, ε_{544} = 2400 M^{-1} cm^{-1}).[14] Formally these metalations result in the two proton / two electron oxidation of the hydroquinone moiety with the acetates and the M^{II} center serving as the proton and electron acceptors respectively.

Scheme 2. Synthesis of reported metal complexes

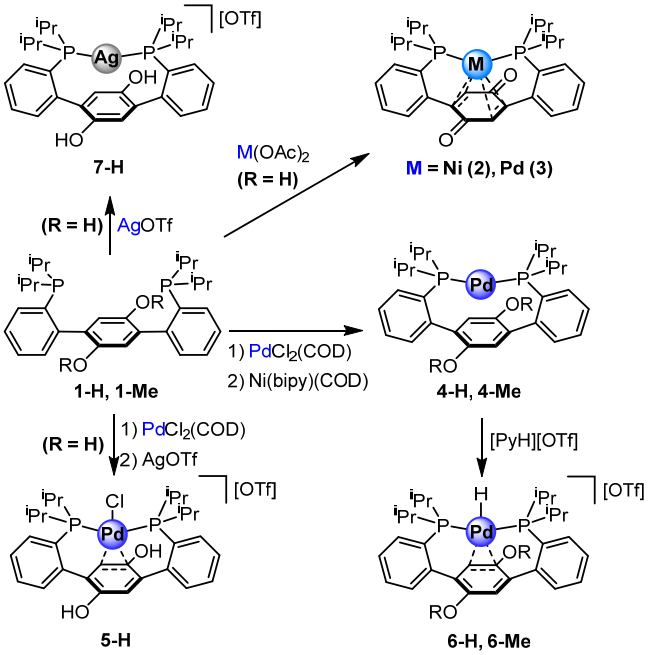

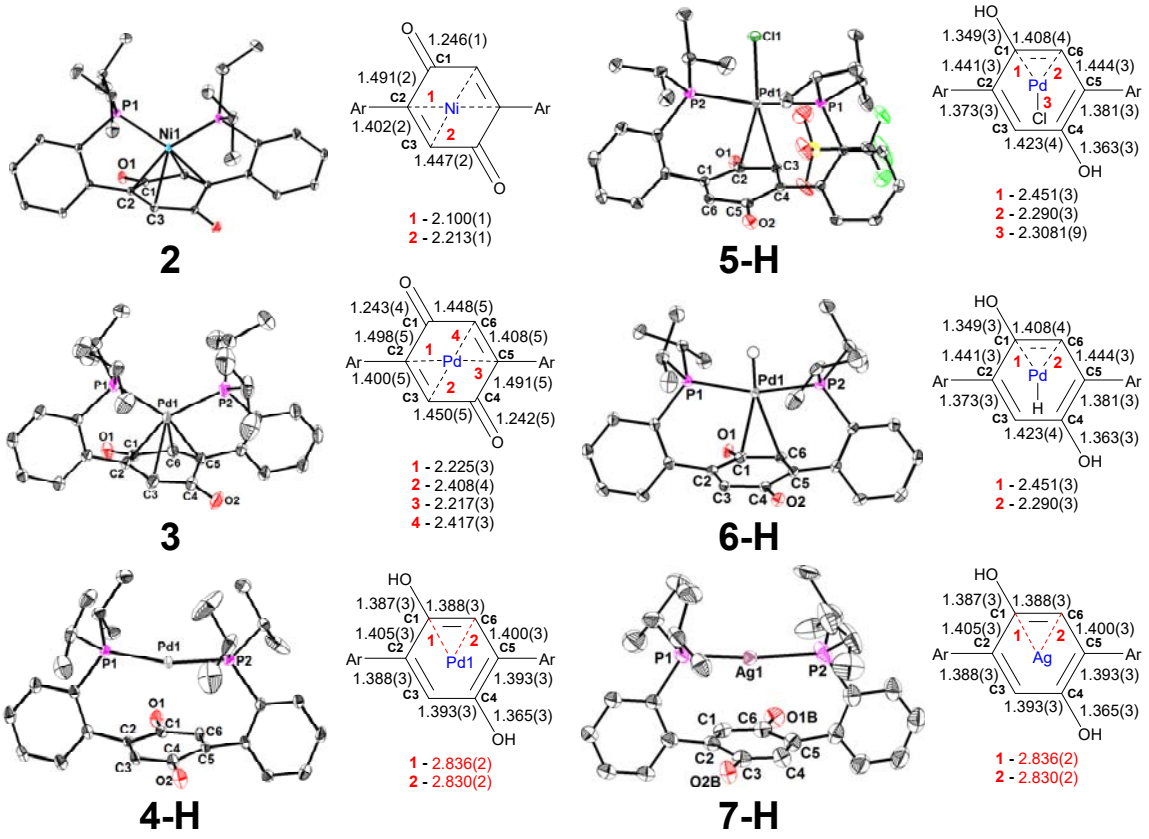

Figure 1. Solid-state structures and selected bond distances for complexes **2**, **3**, **4-H**, **5-H**, **6-H**, and **7-H** (top to bottom). Cocrystallized solvent, counteranions, and most hydrogen atoms omitted for clarity. Bond lengths highlighted in red are too long to represent substantial interactions. Disorder of the hydroquinone oxygen positions has been omitted for clarity for complexes **6-H** and **7-H**.

Single crystal X-ray diffraction (XRD) studies of **2** and **3** (Figure 1) confirm short C-O distances (**2**: 1.246(1) Å; **3**: 1.243(4) 1.242(5) Å) consistent with the quinone assignment for the central arene. Both complex **2** and **3** bind the quinone moiety in an η^4 fashion similar to previously reported metal-quinone complexes.[13a-c, 15] While η^4 binding has precedent for Pd, it should be noted that the majority Pd-quinone structures show η^2 coordination.[13c-e, 15b, 16] Both complex **2** and **3** display a distorted tetrahedral geometry with similar τ_4' values of 0.54 and 0.55 respectively using the two phosphine donors and the centroids of the coordinated C–C double bonds as the ligand contacts. Strong metal-arene interactions are evident from short

average M–C distances of 2.16 and 2.32 Å for **2** and **3** respectively. Substantial backbonding into the quinone C–C double bonds is also evident from the elongated C–C distances of 1.402(2) Å for **2** and 1.400(5) and 1.408(5) Å for **3**. A deplanarization of the quinone moiety is also observed with a C1-(C2-C3-C5-C6 centroid)-C4 angle of 162.2° for **3** and 160.2 ° for the analogous angle in **2**.

Cyclic voltammetry (CV) studies of **2** and **3** in THF were also pursued to establish the redox chemistry of π-bound quinone moiety. Free quinone in DMSO shows two reductions to the corresponding radical anion and the closed shell dianion at -0.91 V and -1.71 V versus Fc/Fc^{+}.[4c] Complex **2** shows a quasireversible reduction event centered at -1.59 V, possibly a two-electron process, and an irreversible oxidation event at 0.77 V versus Fc/Fc^{+} (Figure 2). Complex **3** shows a more complicated CV data with two quasireversible reductions centered at -1.97 and -1.68 V and an irreversible oxidation at 0.54 v versus Fc/Fc^{+} (Figure 3). However, additional oxidation events are observed at -1.09 and -0.4 V corresponding to the reduction events suggesting the formation of multiple species upon two-electron reduction of **3**. Literature electrochemical data for Pd complexes with quinonoid moieties incorporated into the ligand scaffold show reductions at far milder potentials suggesting that the direct coordination of Ni or Pd to the quinone π-system results in significant changes in the electronic properties of the ligand.[9b, 9d, 9e]

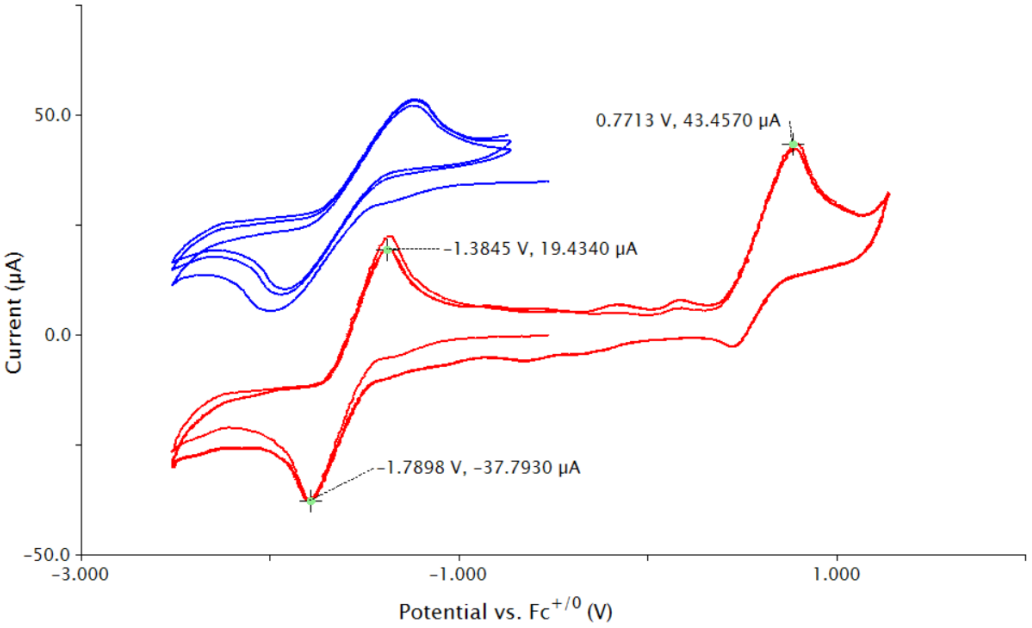

Figure 2. Cyclic voltammetry data for complex **2**.

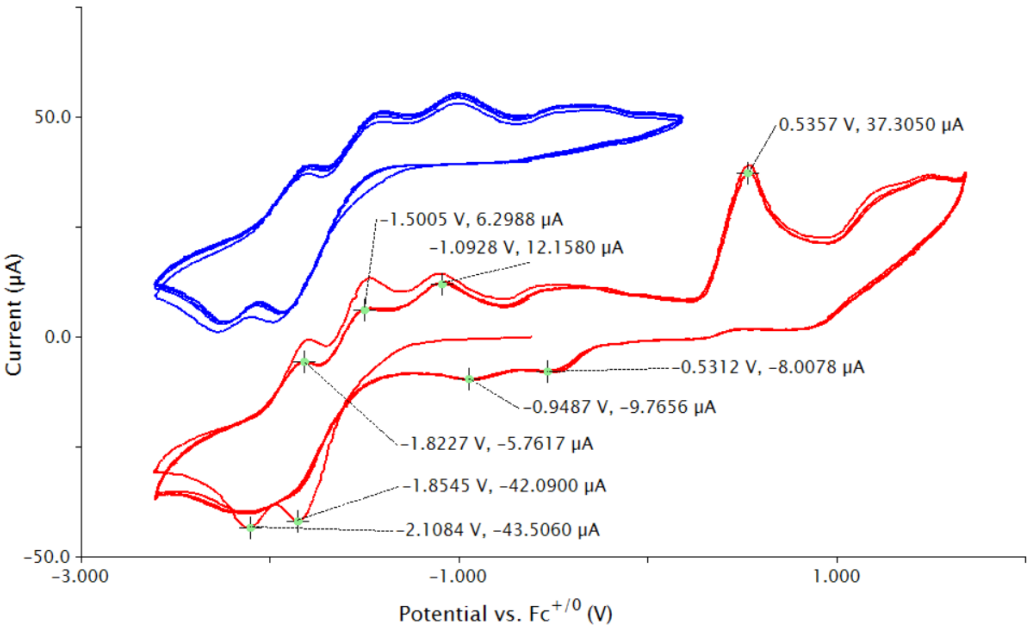

Figure 3. Cyclic voltammetry data for complex **3**.

Efforts to regenerate the hydroquinone form of the central arene by reduction of the quinone in **3** directly was attempted. Conceptually, this transformation corresponds to the delivery of two protons and electrons to the central quinone moiety (Scheme 3), which can be

accomplished with dihydrogen (Pathway 1), discrete sources of protons and electrons (Pathway 2), or through the successive delivery of two hydrogen atoms (Pathway 3).

Scheme 3. Summary of reduction attempts of **3**

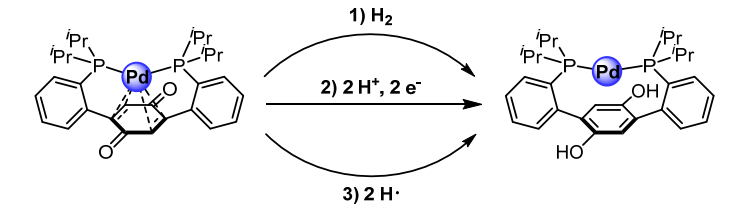

Pathway 1	Pathway 2	Pathway 3
-No direct reaction of 3 with dihydrogen -External catalyst required -Pd/C or Pt/C most selective -Inconsistent scale up	-Electrochemical studies with weak acids looked promising -Stoichiometric studies showed best resuts with KC_8 or sodium napthalenide	-No H-atom transfer from TEMPOH observed -Consistent with BDFE for 1,4-benzoquinone and TEMPOH

Complex **3** proved incapable of rehydrogenating itself with dihydrogen even at elevated temperatures with multiple atmospheres of pressure. The coordinatively saturated nature of the Pd^0 center likely prevents dihydrogen coordination. Furthermore Pdo binding to the π-accepting quinone moiety results in an electron-poor metal center which would disfavor oxidative addition to form a Pd^{II} dihydride. The addition of an external heterogeneous hydrogenation catalyst proved sufficient to generate modest conversions to the desired hydroquinone though some demetalation and other phosphorus-containing species were also observed. Pd/C or Pt/C proved to be the most selective hydrogenation catalysts, however inconsistent results in scale ups were observed with this approach.

The regeneration of the hydroquinone moiety with discrete reductants and acids was also pursued. Given the isolation of stable electrochemical reductions, similar CV studies in the presence of *para-t*Bu benzoic acid were pursued (Figure 4). The addition of acid to complex **3** in cyclic voltammetry experiments resulted in substantial changes in the reductive behavior (Figure 4). An improvement in the chemical reversibility of complex **3** was observed with a

broad quasireversible oxidative (-0.81 V vs Fc/Fc^+) with a very large peak-to-peak separation (1.47 V). The presence of a weak proton source facilitates the reductive and oxidative processes for complex **3** while also substantially improving the potential at which chemical reduction can occur.

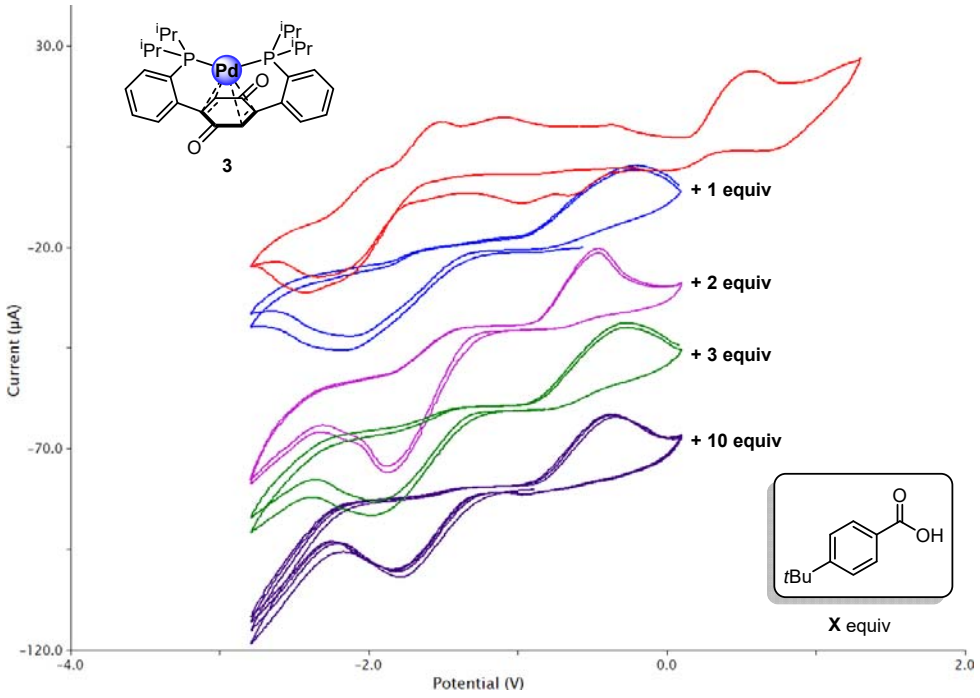

Figure 4. Cyclic voltammetry data for **3** in the presence of varying equivalents of *para-t*Bu benzoic acid.

The obtained CV data suggest strong reductants (~ -1.5 V vs Fc/Fc^+) would still be required for effective reduction of **3** in the presence of two equivalents of *para-t*Bu benzoic acid. No reaction was observed when using Zn^0 or Mg^0 as the reductants. A slow reaction was observed with a Na^0 mirror, however a decomposition product was observed to be the major species by NMR. Kinetically faster reductants were then surveyed and it was found that sodium napthalenide and potassium graphite were capable of a rapid reaction to yield the hydroquinone-Pd^0 complex as the major species. However, removal of naphthalene or other impurities proved challenging due to their similar solubility in hydrocarbon solvents.

Finally, a reaction between complex **3** and 1-hydroxy-2,2,6,6-tetramethyl-piperidine (TEMPOH) (BDFE = 71.0 kcal/mol) was attempted. Unfortunately, no formation of product was observed, which is likely attributable to the weak O–H bond of the first H-atom delivered to 1,4-benzoquinone (65.2 kcal/mol) despite the strength of the first O–H bond in 1,4-hydroquinone (81.5 kcal/mol).

The direct synthesis of Ni^0 and Pd^0 complexes with the hydroquinone form of **1-H** was pursued without using complex **3** as a precursor. Attempted metalations of **1-H** with $Ni(COD)_2$ (COD = 1,5-cyclooctadiene) generated complicated mixtures of species. However, both Pd^0 (**4-H**) and Pd^{II} (**5-H**) species supported by **1-H** proved isolable (Scheme 1). **4-H** was synthesized as brown powder in 84% yield using a one-pot synthesis involving initial metalation with $PdCl_2(COD)$ in THF followed by reduction with Ni(bipy)(COD) (bipy = 2,2'-bipyridine). Treatment of **1-H** with $PdCl_2(COD)$ followed by halide abstraction with silver triflate resulted in the formation of a cationic monochloride species, **5-H**, which could be isolated as a dark red powder in 32% yield. Both **4-H** and **5-H** are stable as solids, but substantial decomposition to a complicated mixture of species in solution is observed over time.

Solution NMR spectra for both **4-H** (C_6D_6) and **5-H** (CD_3CN) show a sharp singlet (**4-H**: 6.94 ppm, **5-H**: 6.72 ppm) and a broad resonance (**4-H**: 4.14 ppm, **5-H**: 8.18 ppm) by ^1H NMR that correspond to the central hydroquinone CH and OH protons, respectively. One methine resonance at 1.88 and 3.12 ppm by ^1H NMR and a sharp singlet at 33.85 and a broad resonance at 34.22 ppm by $^{31}P\{^1H\}$ NMR are observed for **4-H** and **5-H,** respectively. These data are consistent with *pseudo-*C_2 symmetry or fast exchange processes on the NMR time scale. Single crystals suitable for XRD analysis were obtained for **4-H** and **5-H** (Figure 1). Complex **4-H** was found to cocrystallize with a decomposition product where the central arene was

converted to a 2,3-dihydro-1,4-benzoquinone moiety. Formation of this species suggests that decomposition of **4-H** in solution may occur via a metal-mediated isomerization of the hydroquinone moiety. The hydroquinone assignment for the central arene of **4-H** is supported by C–O distances of 1.387(3) and 1.365(3) Å, which are consistent with single bonds. The Pd^0 center in **4-H** is two coordinate as long Pd1–C1 and Pd1–C6 distances of 2.836(2) and 2.830(2) Å respectively represents a negligible metal-arene interaction. Consistent with this assignment, all the C–C bond distances of the central hydroquinone moiety do not vary substantially, ranging between 1.388(3) and 1.405(3) Å and are in line with structures of reported 2,5-diphenyl-1,4-hydroquinone moieties.[17] The P1-Pd1-P2 angle of 165.08(2)° also supports this assignment and is also likely enforced by the *trans*-spanning nature of the rigid *para*-terphenyl framework. These data indicate no disruption of aromaticity is occurring as would be expected upon metal coordination, making the best description of **4-H** a 14 e^-, two-coordinate Pd^0 complex with a spectator hydroquinone moiety.

In complex **5-H**, the C–O bond lengths of 1.349(3) and 1.363(3) Å are comparable to **4-H** and consistent with the hydroquinone assignment for the central arene. Furthermore, complex **5-H** crystallizes with a clear hydrogen bonding interaction between a hydroquinone OH moiety and a neighboring triflate. The Pd^{II} center shows an η^2 interaction with the central arene trans to the Cl ligand with Pd1–C1 and Pd1–C6 distances of 2.451(3) and 2.290(3) Å respectively. Disrupted aromaticity in the hydroquinone moiety is evident from the alternating shorter (C1–C6, C2–C3, C4–C5) and longer (C1–C2, C3–C4, C5–C6) C–C bond lengths which indicate partially localized olefinic character resulting from Pd coordination. The geometry about Pd is square planar with a τ_4' value of 0.10 using the two phosphines, chloride, and centroid of the C1–C6 bond as metal contacts. Complexes **3**, **4-H**, and **5-H** demonstrate

the flexible nature of the Pd-central arene coordination (η^0, η^2, η^4) and how Pd oxidation state (**4-H** to **5-H**) and hydroquinone/quinone interconversion can influence preferred binding modes.

*Section 3.3 Small Molecule Activation by **4-H** and Synthesis of Control Compounds*

Hydroquinone-Pd^0 (**4-H**) and quinone-Pd^0 (**3**) complexes were investigated for reactivity with small molecules toward utilization of protons and electrons stored in the central arene. Clean oxidation of **4-H** to **3** was observed with a variety of gaseous oxidants including dioxygen, nitric oxide, and nitrous oxide, which were all confirmed to produce water as the oxygenic reaction byproduct by ^{1}H NMR spectroscopy when reaction volatiles were transferred between J-Young tubes. 1-azido adamantane was also found to effect the transformation with the formation of 1-amino adamantine confirmed by gas chromatography-mass spectrometry (GC-MS). Additionally, trimethylamine *n*-oxide, 1,4-benzoquinone, and 2,4,6-tri(*tert*butyl)phenoxyl radical were also found to react with **4-H** to form **3**. With all the surveyed small molecule substrates, no further oxidation of **3** was observed.

A more detailed mechanistic understanding of the rapid reactivity of **4-H** with dioxygen was pursued. The reactions of Pd and Pt complexes with molecular dioxygen have been recently reviewed.[18] The direct activation of dioxygen by low-coordinate Pd^0 complexes has been reported and typically yields an η^2-peroxo.[16a, 19] However, a bis-(η^1-superoxo)[20] and a terminal η^1-superoxo[21] have been reported. Therefore it is possible that initial dioxygen activation can occur at the Pd^0 center prior to subsequent activation of the hydroquinone moiety. The reaction of Pd^{II} hydrides with dioxygen to yield hydroperoxo complexes has also been reported though the reaction mechanism varies with different supporting ligands.[6a, 8, 22] Therefore, the possibility of proton transfer to the Pd center from the hydroquinone moiety

prior to dioxygen activation must also be considered. The autooxidation of some hydroquinones by dioxygen in the absence of catalyst has been reported, most notably in the anthraquinone process which is the primary means of industrial hydrogen peroxide production.[23] As a net change in Pd oxidation state does not occur in the conversion of **4-H** to **3**, it is possible that the reaction with dioxygen is entirely mediated by the ligand without involvement of the metal center. Previous studies with a related catechol diphosphine ligand have shown that dioxygen activation likely occurs by an initial outer sphere electron transfer step offering another mechanistic proposal.[11c] Cooperative activation of dioxygen by both Pd center and the ligand in a concerted process is also plausible.

In order to address the aforementioned mechanistic possibilities, suitable complexes to investigate different reactivity patterns were synthesized. To test for Pd-only initial dioxygen activation, a Pd^0 complex supported by a previously reported diphosphine ligand with a para-dimethoxy substituted central arene was synthesized (**4-Me**, see section 2.1 for detailed synthesis) using the same synthetic route as **4-H** with the product obtained as an orange solid in 98% yield (Scheme 1). Solution NMR data (C_6D_6) are consistent with *pseudo*-C_2 symmetry or a fast exchange processes on the NMR time scale with chemical shifts comparable to **4-H**. Sharp singlets are observed for the central arene CH and OMe proton resonances at 6.86 and 3.49 ppm respectively. One methine resonance at 1.96 ppm by ^{1}H NMR and a sharp singlet at 33.81 by $^{31}P\{^1H\}$ NMR are also seen.

To test for the potential reactivity of Pd-H species, complex **4-H** and **4-Me** were protonated with one equivalent of pyridinium triflate to yield **6-H** and **6-Me** respectively (Scheme 1). Solution NMR data for both species (CD_3CN) are quite similar and consistent with *pseudo*-C_2 symmetry or fast exchange processes on the NMR time scale. Reminiscent of **5-H**, the central arene CH proton resonances appear as sharp singlets at 6.79 and 6.99 ppm

for **6-H** and **6-Me,** respectively. The OH and OMe protons appear as a broad resonance at 7.42 and a sharp singlet at 3.73 ppm, respectively. A single methine proton resonance is observed (**6-H**: 2.46 ppm; **6-Me:** 2.48 ppm). Both complexes coincidentally show the Pd–H resonances as a triplets (**6-H**: J_{PH} = 8.5 Hz, **6-Me**: J_{PH} = 9.0 Hz) at -16.33 ppm, while the $^{31}P\{^{1}H\}$ NMR shows a doublet centered at 41.57 ppm for **6-H** and a broadened singlet at 41.93 ppm for **6-Me**.

Single crystals suitable for XRD analysis were obtained for **6-H** (Figure 1). The hydroquinone oxygens were nearly equivalently disordered across the C1/C4 and C3/C6 positions, only the majority species has been shown in Figure 1 for clarity. While this disorder precludes assessment of the C–O bond lengths, the central arene bond distances show an alternation of long and short distances analogous to **4-H** suggestive of disrupted aromaticity in a hydroquinone moiety rather than a quinone assignment. The Pd-center shows η^2 coordination to C1–C6 akin to **5-H** though the Pd1–C1 and Pd1–C6 distances are longer at 2.501(4) and 2.477(3) Å respectively. **6-H** and **6-Me** are cationic and therefore represent a Pd-H that could potentially arise from intermolecular proton transfer between equivalents of **4-H**. These complexes will provide insight into the behavior of Pd–H species on the current ligand platforms and probe how the non-innocence of the hydroquinone moiety affects reactivity. An alternative Pd-H accessible from **4-H** could be neutral, corresponding to (formal) intramolecular proton transfer from the hydroquinone moiety to the Pd center. Such a compound has not been observed or isolated to date.

To probe for ligand-only reactivity, a Ag^{I} complex, **7-H**, was synthesized by metalation of **1-H** with silver triflate in THF. The product was isolated as colorless needles in 68% yield following recrystallization. Solution NMR data (CD_3CN) is consistent with *pseudo*-C_2 symmetry

or a fast exchange process on the NMR time scale. The central hydroquinone OH and CH proton resonances appear as a broad singlet at 6.98 ppm and a sharp singlet at 6.85 ppm respectively. Additionally, a single methine resonance at 2.52 ppm is observed. The $^{31}P\{^{1}H\}$ NMR shows two pairs of doublets centered at 28.33 with J_{PAg} values of 559.7 and 484.9 Hz owing to coupling to ^{107}Ag (52% abundance) and ^{109}Ag (48% abundance) nuclei.

Single crystals of **7-H** suitable for XRD analysis were obtained. Like **6-H**, nearly equivalent disorder of the hydroquinone oxygens is present precluding detailed analysis of the C–O bond lengths. Ag1-C1 and Ag1-C6 distances are in excess of 2.9 Å consistent with a negligible metal-arene interaction similar to that of **4-H**. C–C bond lengths in the hydroquinone moiety do no show an alternation of longer and shorter bond distances. This structural information indicates that **7-H** serves as a suitable electronic and structural control for dioxygen reactivity with the hydroquinone moiety, as no substantial metal-arene interaction perturbs the reactivity of the central arene moiety as seen in **4-H**.

Section 3.4 Studies of Initial Dioxygen Activation

The reactivity of dioxygen with all control compounds was pursued (Scheme 4). At room temperature **4-Me** was found to rapidly react with dioxygen to form a complicated mixture of species. This reactivity differs from that of previously reported bis(phosphine) Pd^0 complexes which are known to form (η^2-peroxo) complexes stable enough to be structurally characterized.[19a, 19b, 19f, 19l, 19q] Compound **7-H** showed no reaction for multiple weeks at room temperature when exposed to one atmosphere of dioxygen (Scheme 3). This indicates that direct oxidation of the hydroquinone moiety of the ligand by dioxygen is not a facile reaction pathway and it likely does not occur in the reaction of **4-H**. Compound **6-H** showed a color change upon mixing to generate a bright pink species that shows a peak at λ_{max} = 520 nm. By

$^{31}P\{^{1}H\}$ and ^{1}H spectroscopy, the starting material is consumed within 6 hours, resulting in the formation of a new major species, **3(H)$^{+}$**. No peaks are observed upfield of 0 ppm, suggesting the lack of a Pd-H moiety. An identical UV/Vis spectrum was obtained upon addition of one equivalent of pyridinium triflate to **3** in THF leading to the assignment of this product as the protonated quinone species. **6-Me** showed reaction with dioxygen upon mixing at room temperature to generate a complicated mixture of species. To test for the direct oxidation of the hydroquinone moiety in **6-H** by dioxygen, **5-H** was treated with O_2, since dioxygen activation across Pd^{II}-Cl bond has not been reported to the best of our knowledge. No reaction with dioxygen was observed for complex **5-H**. Similar to **7-H**, these results suggest that oxidation of the hydroquinone moiety to the corresponding quinone is likely metal-mediated as no evidence for direct ligand chemistry has been seen.

Studies of dioxygen reactivity at lower temperatures were pursued to detect intermediates for mechanistic insight. Dioxygen addition to **4-H** at -78 °C resulted in the formation of a new species (**Int1**, Scheme 5, a) by $^{31}P\{^{1}H\}$ NMR (THF). **Int1** shows two coupling doublets 35.38 and 30.77 ppm (J_{PP} = 32 Hz) consistent with an asymmetric species in solution (Scheme 5, c). Low temperature solution IR data showed no absorptions consistent with a C–O double bond, indicating that no conversion of the hydroquinone moiety to a quinone or semiquinone form had occurred. While observed to be stable at -78 °C for up to an hour, **Int1** was found to be quite thermally sensitive with 80% conversion to **3** occurring at -50 °C over an hour. These data suggest that a Pd-only binding and activation of dioxygen is occurring at lower temperatures without any participation of the hydroquinone.

Scheme 4. Summary of room temperature reactivity

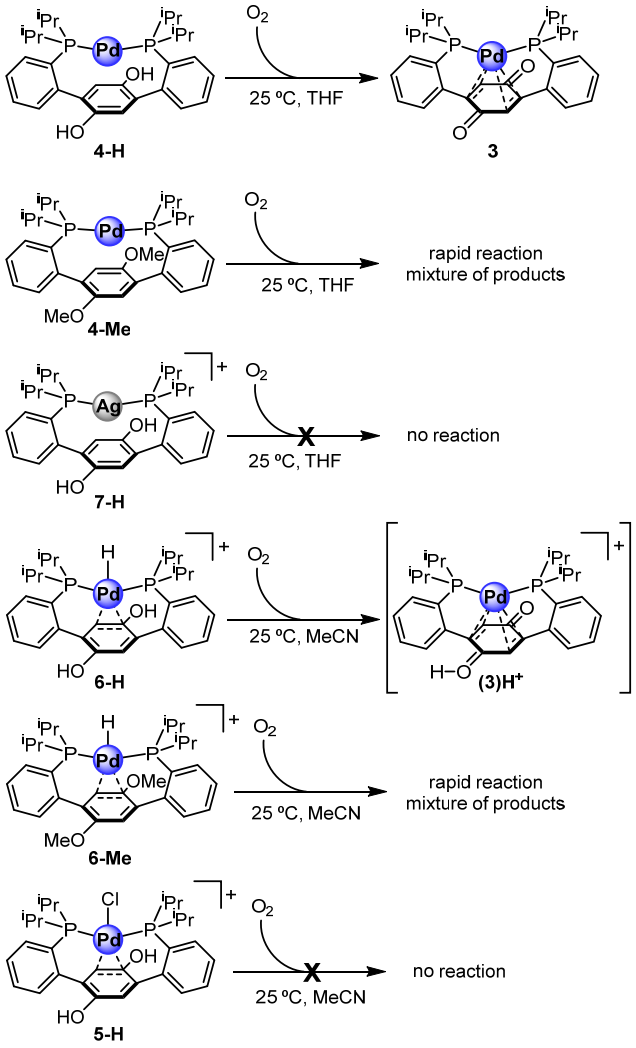

To test if the hydroquinone moiety was necessary for initial activation, dioxygen was added to a solution of **4-Me** at -78 °C, in which the phenolic moieties are protected with methyl groups (Scheme 5, b). The formation of a new species, **8-Me**, was observed upon mixing by NMR (d_8-THF) (Scheme 5, c). Similar to **Int1**, $^{31}P\{^1H\}$ NMR shows two coupling doublets at 34.04 and 29.87 ppm (J_{PP} = 24.0 Hz) again consistent with an asymmetric species suggesting the formation of a very similar species by NMR. By ^1H NMR, two signals for the central arene CH (6.87 and 6.66 ppm) and OMe (3.56 and 3.47 ppm) protons are observed. Three distinct methine proton signals that integrate 1:1:2 appear at 3.67, 3.59, and 1.98 ppm). Unlike **Int1**, **8-**

Me was found to be stable for over four weeks at -78 °C in THF and for over multiple hours at -40 °C with no sign of decomposition. This information further supports the assignment of direct dioxygen binding at the Pd^0 center without involvement of the hydroquinone moiety. Furthermore, the increased stability of **8-Me** suggests that the hydroquinone moiety, when present, facilitates further reactivity with the Pd-coordinated O_2 moiety.

Scheme 5. Proposed dioxygen activation mechanism for **4-H** and **4-Me**

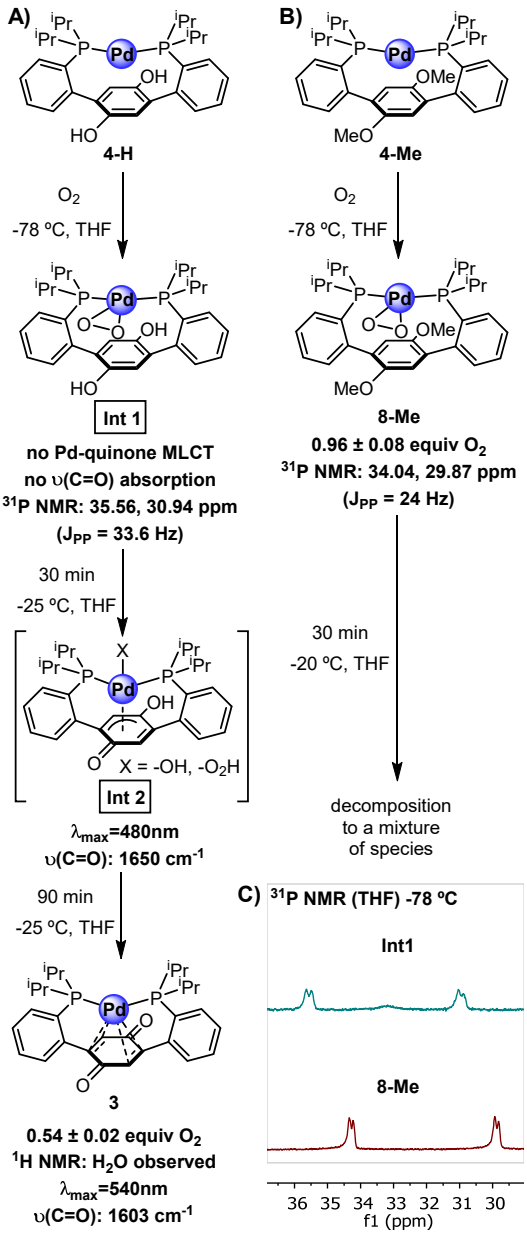

No reaction of **6-H** or **6-Me** with dioxygen was observed at -30 °C by $^{31}P\{^{1}H\}$ NMR (CD_3CN), suggesting that the activation of dioxygen by **4-H** likely does not occur via a cationic Pd-H species. However, reactivity from a neutral complex generated by intramolecular protonation to form a Pd-H moiety and deprotonated hydroquinone cannot be ruled out. The similarity of **Int1** and **8-Me** by NMR further suggests that the activation of dioxygen by **4-H** does not occur via a Pd-H species, given that the precursor to **8-Me** does not have acidic protons. Gas quantification experiments using a Toepler pump was used to determine the equivalents of dioxygen consumed by each reaction (Table 1). At 25 °C, **4-H** and **6-H** were found to consume 0.54 ± 0.02 and 0.95 ± 0.04 equivalents of dioxygen, respectively. Oxygen addition to **4-Me** at -78 °C showed consumption of 0.96 ± 0.08 equivalents of dioxygen. During the freeze-pump-thaw cycles of **Int1** during Toepler pump experiments a noticeable purple hue developed in the reaction vessel indicating the partial formation of **3** regardless of attempts to keep reaction mixtures from warming up substantially. These experiments with **4-H** were likely unsuccessful due to the decreased thermal stability of **Int1** compared to **8-Me** as seen in NMR experiments.

The binding of a single equivalent of dioxygen to **4-Me** at low temperatures rules out the formation of a bis-(η^1-superoxo) (Scheme 6, a). The literature example of a η^1-(superoxo) complex was observed to convert to the corresponding η^2-peroxo over 80 minutes at temperatures above -82 °C.[21] Therefore, the most plausible assignment for **8-Me** and, due to similarities by $^{31}P\{^{1}H\}$ NMR, **Int1**, is an η^2-peroxo species (Scheme 6, a).[24] Furthermore, η^1-(superoxo) would be expected to bind the oxygenic ligand in a position *trans* to the central arene moiety as seen in the case of **5-Cl** resulting in equivalent phosphine donors on the NMR time scale. Differences in reaction rates at low temperature and the amount of dioxygen consumed make reactivity derived from a Pd-H species less likely (Scheme 6, b). The absence

of oxidation of **7-H** rules out hydroquinone oxidation akin to that of the anthraquinone process (Scheme 6, c).[23] It is also noteworthy that the reactivity appears to proceed through an initial inner sphere intermediate unlike previous reports on molybdenum carbonyl complexes (Scheme 6, d). Finally, cooperative activation of dioxygen between the Pd center and hydroquinone ligand is also ruled out as no evidence for hydroquinone oxidation by IR was observed for **Int1**. Additionally, the same type of intermediate can be accessed with **4-Me** which does not have the ability to transfer protons / H-atoms (Scheme 6, e).

Scheme 6. Possible Dioxygen Activation Mechanisms

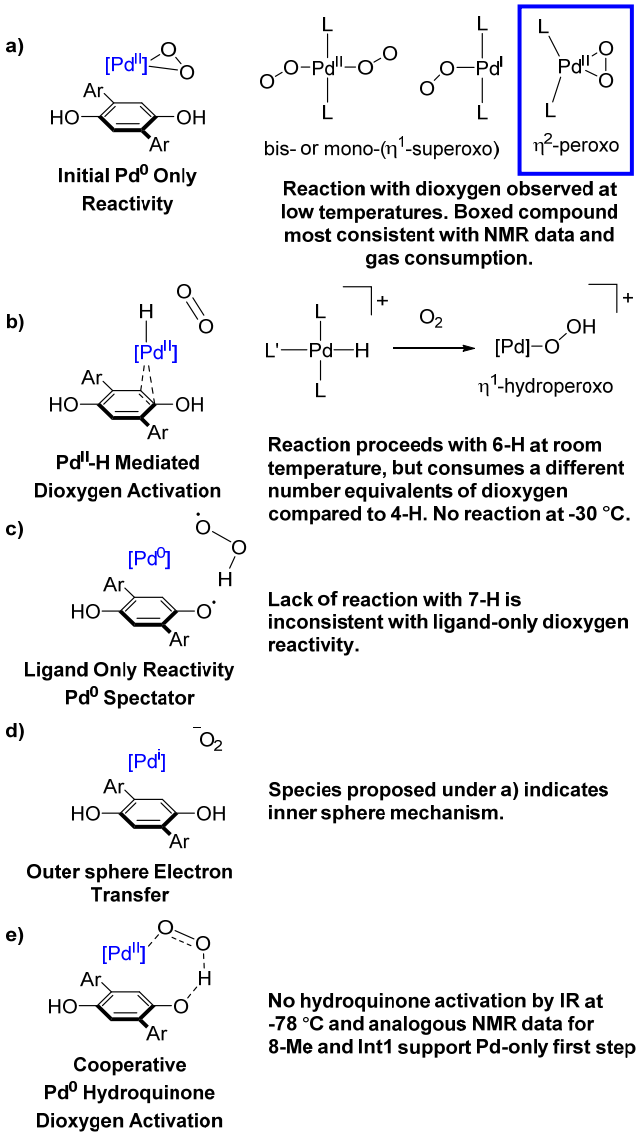

As both **4-H** and **4-Me** activate dioxygen at low temperatures to likely form η^2-peroxo species, the electrophilic or nucleophilic character of the oxygenic moiety of **8-Me** was tested with external substrates. As a test for electrophilic character, **8-Me** was mixed with cyclohexene, 2,4,6-tri*tert*butylphenol, methyl *para*-tolyl sulfide, or triphenylphosphine.[25] No formation of cyclohexanone or sulfoxide product was observed by GC or GC-MS spectroscopy. No formation of 2,4,6-tritertbutylphenoxyl radical was observed by UV/Vis spectroscopy suggesting that an H-atom abstraction pathway is not occurring (BDFE (kcal mol^{-1}) in DMSO: 2,4,6-tri(*tert*butyl)phenol = 80.6, 1,4-hydroquinone = 80.0).[4c] The formation of triphenylphosphine oxide was detected by GC-MS. However low temperature NMR experiments show this reaction to proceed by initial triphenylphosphine substitution of **1-Me** to form $(PPh_3)_2Pd(\eta^2\text{-}O_2)$ by comparison to literature $^{31}P\{^1H\}$ chemical shifts[18a] and independent synthesis from $Pd(PPh_3)_4$ and dioxygen (Figure 22). Subsequent phosphine oxidation therefore likely does not involve terphenyl diphosphine. As a test for nucleophilic character, cyclohexane carboxyaldehyde or *para*-trifluoromethyl benzylalcohol were added to **8-Me**.[25a, 25b] In both cases oxidation products, cyclohexene and the corresponding benzaldehyde, were observed by GC and GC-MS analysis respectively, suggesting nucleophilic character for **8-Me**. These data taken together with the control reactions indicate that dioxygen activation at **4-H** occurs through a Pd-only mediated formation of a (η^2-peroxo) species with nucleophilic character. Hydroquinone activation occurs subsequently through an inter- or intramolecular proton transfer.

Low temperature NMR experiments were run to probe whether both intermolecular proton transfer occur. First, intermolecular proton transfer was tested by studying the reaction of dioxygen with a mixture of **4-Me** and the Ag^I complex, **7-H** (Figure 23). At -78 in THF, **8-Me** was formed in the presence of **7-H** upon the addition of dioxygen. Warming the

reaction mixture to -40 °C did not result in any detectable reaction over more than 30 minutes suggesting intermolecular proton transfer is not occurring at these temperatures. In contrast, **Int1** shows significant conversion over 30 min, even at -50 °C. The dioxygen reactivity of **4-H** in the presence of **7-H** was also tested (Figure 23). As with **4-Me**, oxygen addition at -78 °C in THF resulted in the formation of **Int1** in the presence of **7-H**. Warming the reaction to -40 °C showed near quantitative conversion of **Int1** to form **3** within 10 minutes without any detectable consumption with **7-H**. While these experiments do not rule out intermolecular proton transfer during conversion of **Int1**, they do suggest that such proton transfer to the analogous (η^2-peroxo) species supported by **4-Me** without a pendant hydroquinone moiety either does not occur or is not sufficient for subsequent reactivity of the O_2 moiety.

Oxygen addition at -78 °C to a THF solution of **4-H** resulted in a color change from yellow/brown to orange/brown within thirty seconds consistent with the rapid formation of **Int1** by UV/Vis (Figure 5). Warming the UV/Vis solution of **Int1** to -25 °C resulted in the conversion to a new intermediate (Figure 6), in contrast to the NMR experiments, with a λ_{max} of 480 nm over the course of approximately 30 minutes. This suggests that at lower concentrations, the rates of steps following the formation of **Int1** (and **Int2**) are slowed enough to allow the observation of an additional intermediate. Low temperature solution IR data at -35 °C showed the appearance of an absorption at 1601 cm^{-1} attributable to the formation of a substantial quantity of **3**. However, a small absorption at 1650 cm^{-1} (Figure 18) was also observed that may be attributed to the transient formation of **Int2**, which suggests stepwise activation of the hydroquinone moiety. **Int2** was observed to gradually convert to **3**, the final reaction product, over the course of 3 hours at -25 °C (Figure 7). Cooling the solution of **Int2** to -78 °C could not arrest the conversion to **3**, though the reaction was slower. The formation of **Int2** and **3** both occur with isosbestic points indicating that these

transformations correspond to the clean interconversion of these species. These data show that **Int2** possesses an activated hydroquinone with at least partial quinone character by IR spectroscopy. The UV/Vis spectra of **Int2** is inconsistent with a Pd^{o} protonated quinone, as such structure is assigned to be the product of **6-H** with dioxygen, which can be prepared independently, and shows a peak at λ_{max} = 520 nm. Therefore, it is proposed that **Int2** is a Pd^{II} species with the metal center coordinated to a semiquinone moiety (Scheme 5, a). An anionic oxygenic fragment could be released or still remain coordinated to the metal center in a distorted geometry. If the oxygenic fragment is released, **Int2** would formally correspond to **(3)H**$^{+}$ which is inconsistent with the spectroscopic data. Therefore, it is proposed that an oxygenic moiety remains coordinated, and because of coordination *trans* to the central arene, a second proton transfer is slow allowing observation of this intermediate. As one equivalent of dioxygen is assigned to be bound in **Int1** while only half an equivalent is consumed by the net reaction to **3**, a dioxygen release must occur during the conversion of **Int1** to **3** via an intermolecular disproportionation process. If the oxygen release has already occurred by the time formation of **Int2** then the proposed anionic oxygenic fragment may be a hydroxide ligand. However, if dioxygen release occurs in the conversion of **Int2** to **3**, then the bound oxygenic fragment may be a hydroperoxo species. Unfortunately, the instability of these intermediates and fluorescence from the ligand prevented detailed IR or resonance Raman spectroscopy to further characterize the identity of the reaction intermediates. As intermediate **Int2** is not observed at the higher concentrations of the NMR experiments, the steps following the formation of **Int2** must be slower than its generation. The concentration effect could be a consequence of the intermolecular reaction required for the proposed disproportionation.

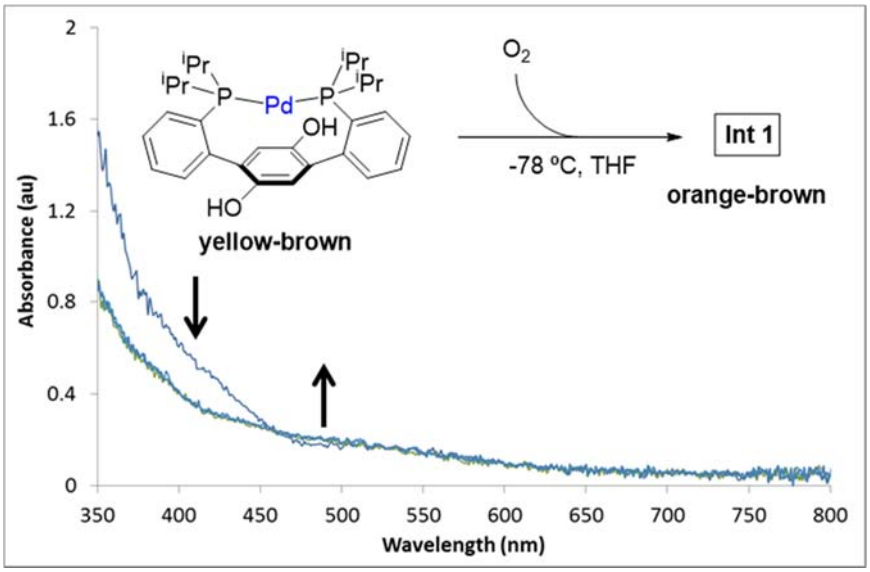

Figure 5. Solution UV/Vis spectrum for **4-H** after warming to -78 °C following O_2 addition.

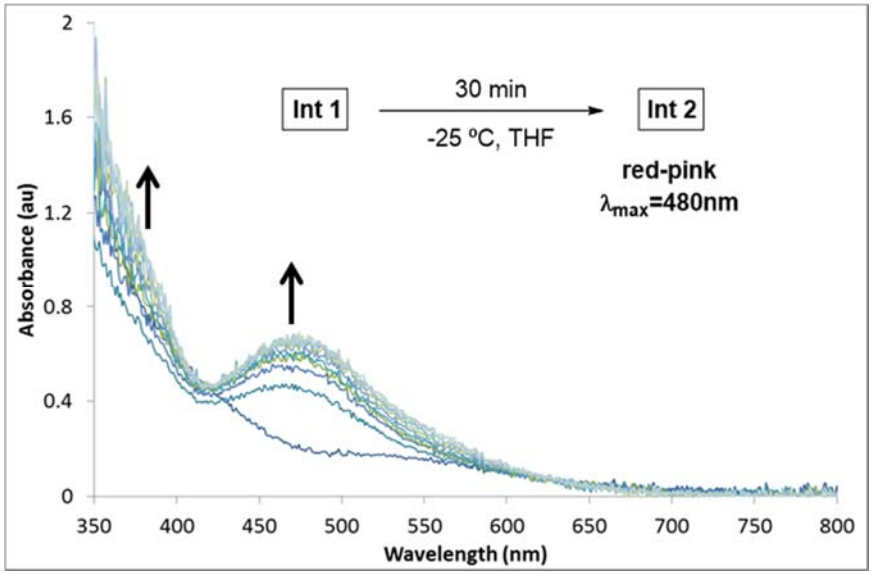

Figure 6. Solution UV/Vis spectrum for **4-H** after warming to -25 °C with O_2 addition over 30 minutes.

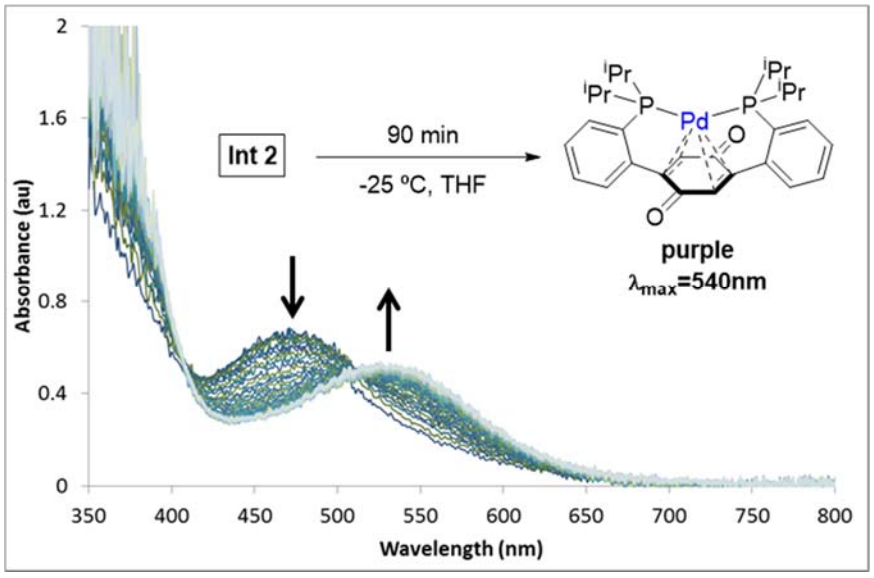

Figure 7. Solution UV/Vis spectrum for the decay of **Int2** at -25 °C over multiple hours.

Kinetics analysis of the conversion of **Int2** into **3** were run to determine the reaction order and gain insight into the reaction mechanism. Two assumptions went into making the calculations: 1) complete conversion to **3** had occurred and 2) the concentration of **Int2** is equal to the final concentration of **3** as inferred from the presence of an isosbestic point. Utilizing the UV/Vis data displayed in Figure 7, and the above assumptions extinction coefficients can be calculated for both **Int2** and **3** at 480 nm and 535 nm. A check of these calculated coefficients were plugged into calculations for the expected summed absorbance values at 480 nm and 535 nm for comparison to experimental data. Good agreement was observed as shown in Figure 8 and Figure 9. This absorbance data was converted into concentrations of **Int1** and **3** using the assumption 2 and plotted (Figure 10) against time. Plotting the natural log of **Int2** concentration against the natural log of time (Figure 11) showed a curved line not consistent with first order process. Plotting the inverse of **Int2** concentration against time (Figure 12) gave a straight line over approximately 120 minutes though noisy data disrupted the fitting of data and greater conversion. However, the linear

regression of the initial 110 minutes (Figure 13) gave an R^2 value of 0.97 suggesting the interconversion of **Int2** and **3** is a second order process.

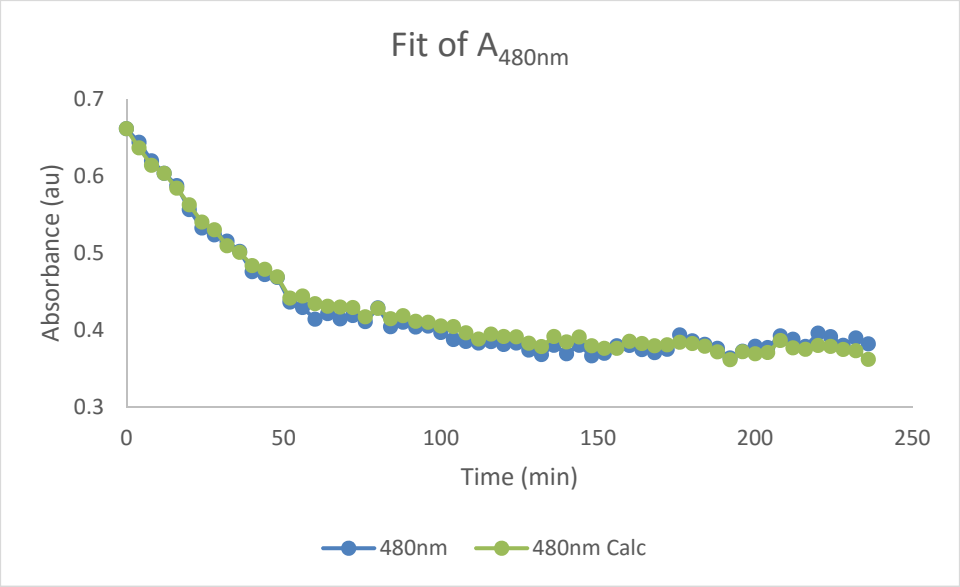

Figure 8. Solution UV/Vis spectrum for the decay of **Int2** at -25 °C over multiple hours.

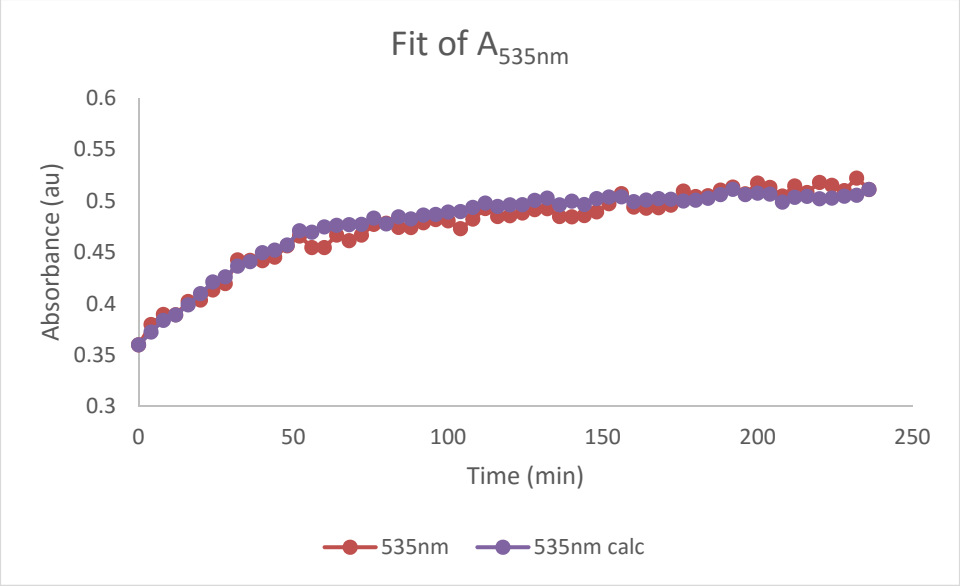

Figure 9. Solution UV/Vis spectrum for the decay of **Int2** at -25 °C over multiple hours.

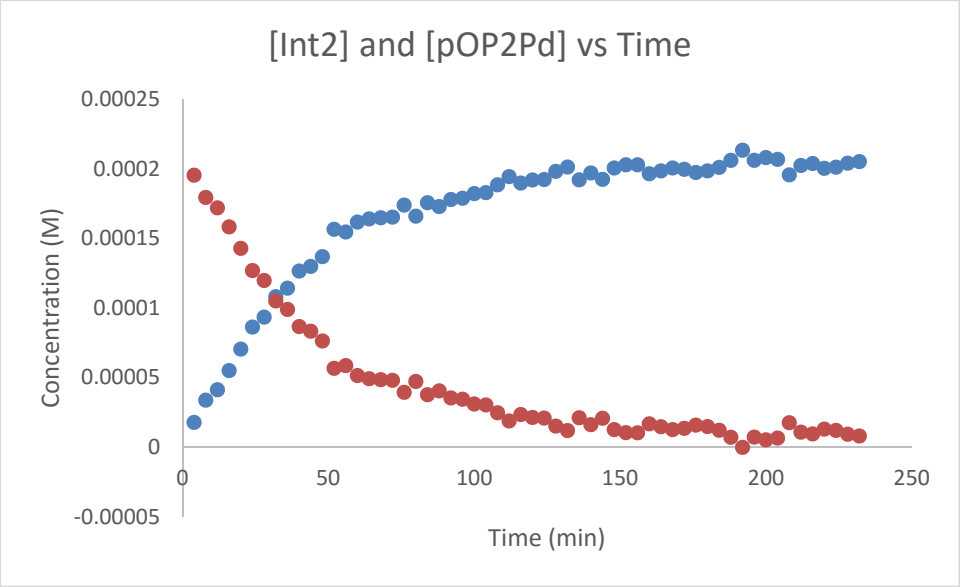

Figure 10. Solution UV/Vis spectrum for the decay of **Int2** at -25 °C over multiple hours.

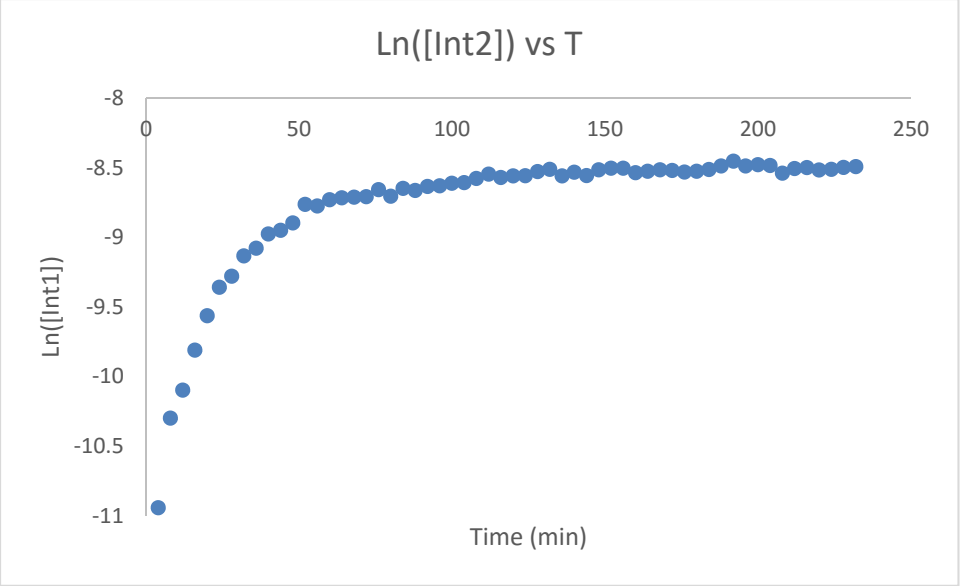

Figure 11. Solution UV/Vis spectrum for the decay of **Int2** at -25 °C over multiple hours.

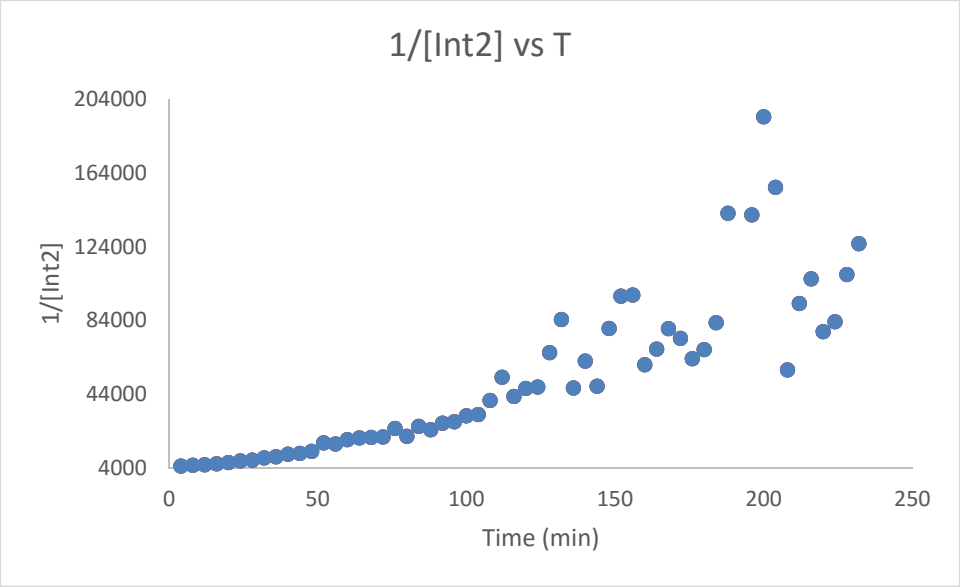

Figure 12. Solution UV/Vis spectrum for the decay of **Int2** at -25 °C over multiple hours.

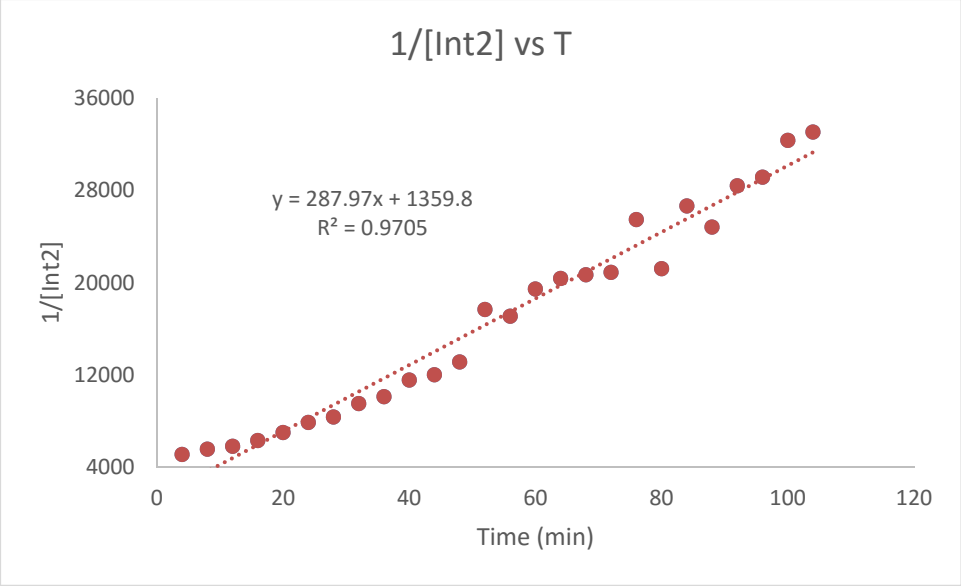

Figure 13. Solution UV/Vis spectrum for the decay of **Int2** at -25 °C over multiple hours.

In catalytic Pd-meditated organic transformations that utilize benzoquinone as a stoichiometric oxidant, the regeneration of $Pd^{II}X_2$ species required for substrate oxidation relies on the transfer of reducing equivalents from Pd^0 to the quinone moiety.[6] Compound **3**

allows investigation of the propensity of a Pd^0 center coordinated to the π-system of the quinone to undergo oxidation or protonation. As supported by CV data and air stability, the oxidation of **3** to form a Pd^{II}-quinone complex requires strong oxidant. Excess (5 equivalents) aqueous hydrogen peroxide was found to slowly bleach the characteristic UV/Vis features of **3** (88% conversion over 12 hours) at room temperature, however well-defined reaction products could not be isolated. The present reactivity suggests that loss of the benzoquinone ligand might be necessary prior to (or in concert with) oxidation of Pd^0, for example with O_2.[6a] In the present system, **4-H** undergoes facile reaction with O_2, showing that upon removal of hydroquinone coordination, oxidation of Pd^0 occurs readily. As Pd^{II}-H species are known intermediates in benzoquinone mediated chemistry, further studies were performed with **6-H**.[6a]

Scheme 7. Proposed Dioxygen Activation Mechanism of **6-H**

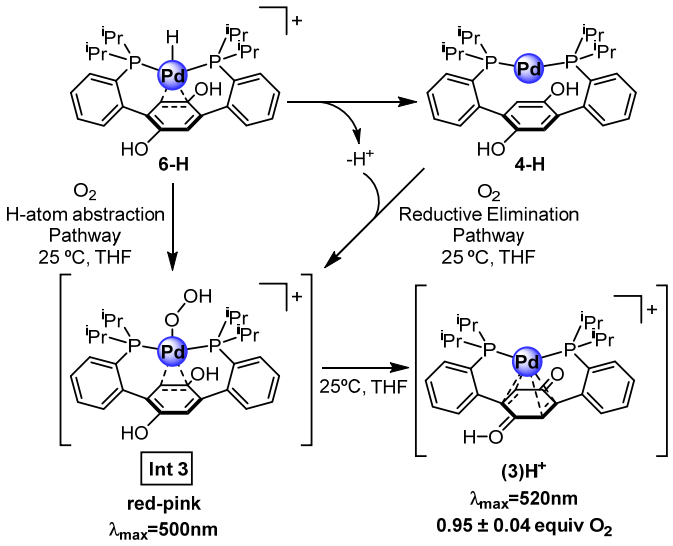

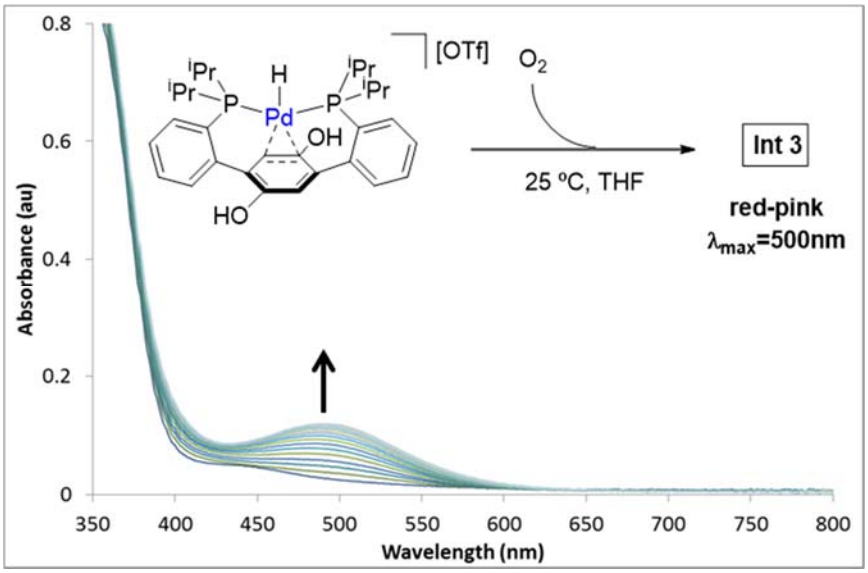

Figure 14. Solution UV/Vis spectrum for **6-H** at 25 °C following O_2 addition over multiple hours.

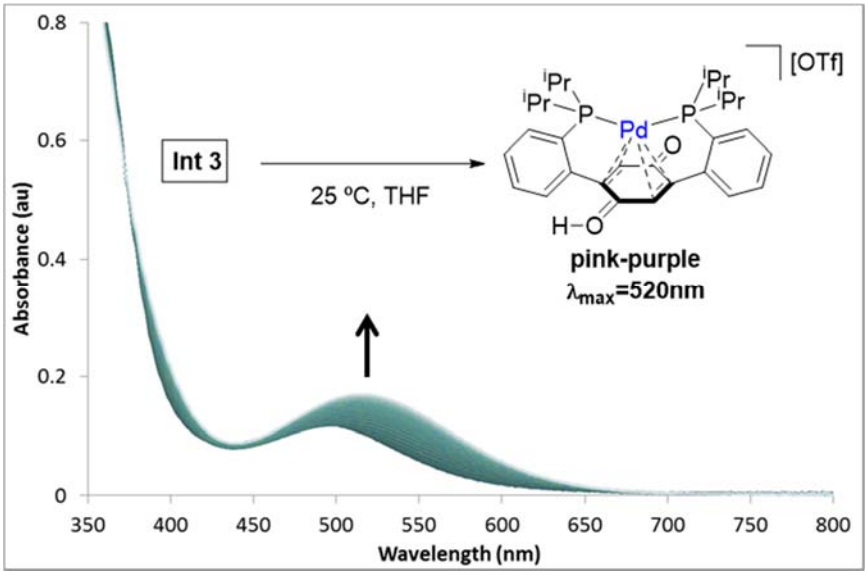

Figure 15. Solution UV/Vis spectrum for the conversion of **Int3** to **(3)H**$^+$ after over multiple 12 hours.

By UV/Vis spectroscopy, **6-H** was found to convert to a pink compound with λ_{max} of 500 nm over several hours following oxygen addition at room temperature (Figure 14). The subsequent conversion to the final product that has a λ_{max} of 520 nm (Figure 15) requires

greater than 16 hours for completion as judged by the slowly shifting λ_{max} in the UV/Vis spectrum. Toepler pump experiments indicate the overall reaction consumes a single equivalent of dioxygen. Based on literature precedence this reaction may proceed via the initial formation of a hydroperoxo species in a geometry akin to **5-H** where the central hydroquinone moiety is *trans* to the oxygenic ligand. Whether this transformation occurs via a reductive elimination / deprotonation route or a hydrogen-atom abstraction pathway as proposed in the literature is unknown at this point (Scheme 7).[22b, 22c] Subsequent deprotonation of the hydroquinone moiety by the hydroperoxide results in release of H_2O_2 and formal reduction of the metal center by the pendant hydroquinone.[26] Given the difference in rate of oxidation between **6-H** and **4-H**, a cationic Pd-H is not an intermediate consistent with the fast reaction of **4-H** with O_2. Previously, benzoquinone has been reported to promote reductive elimination of carboxylic acid from Pd-H complexes.[6a] The final product (**3(H)$^+$**) in the reaction of **6-H** with O_2, lacking diagnostic Pd-H peaks by ^{1}H NMR spectroscopy, indicates that formation of such hydritic species by formal oxidation via protonation at the metal is unfavorable. The π-acidic benzoquinone moiety bound to Pd^0 makes the metal center electron deficient and stabilizes the lower oxidation state.

CONCLUSIONS

A novel non-innocent ligand platform capable of cooperatively mediating the multiproton-multielectron reduction of multiple substrates at a Pd^0 center has been synthesized based on a hydroquinone-diphosphine moiety. Reduction of O_2 was studied in detail. The reaction occurs by an initial Pd-mediated step which involves binding of one equivalent of dioxygen to form a nucleophilic η^2-peroxo species assigned by comparison to complex **8-Me**, displaying a dimethylated hydroquinone moiety. Subsequent activation of the

hydroquinone moiety occurs at higher temperatures with a second intermediate observable by UV/Vis spectroscopy at low concentrations. The reported reactivity represents an overall transformation that requires both the redox active metal capable of binding O_2 as well as the non-innocent pendant hydroquinone within the same molecule. A related Pd^0 complex (**4-Me**), lacking the hydroquinone moiety, or Ag^I-hydroquinone complex (**7-H**), lacking a metal center capable of binding O_2, do not reproduce the reactivity independently or even in combination. Overall, the described results highlight the potential for the reduction of small molecule substrates by utilizing auxiliary redox-active and acid-base non-innocent moieties to store reducing equivalents. From the perspective of oxidation organic methodology utilizing the Pd-benzoquinone combination, O_2 does not react with the isolated Pd^0-benzoquinone species and protonation occurs at the quinone moiety indicating that the oxidized quinonoid moiety prevents reactivity at the coordinated metal.

EXPERIMENTAL SECTION

General considerations.

All air- and/or water-sensitive compounds were manipulated using standard vacuum or Schlenk line techniques or in an inert atmosphere glove box. The solvents for air- and moisture-sensitive reactions were dried over sodium benzophenone ketyl, calcium hydride, or by the method of Grubbs.[27] All NMR solvents were purchased from Cambridge Isotopes Laboratories, Inc. and dried over sodium benzophenone ketyl or calcium hydride. Unless mentioned otherwise, reagents were used as received from commercial suppliers without further purification. Nickel(II)acetate, palladium(II)acetate, chlorodiisopropylphosphine, boron tribromide, silver trifluoromethanesulfonate, 1.7 M *t*BuLi in pentane, diisopropylethylamine, 1,4-dimethoxybenzene, were purchased from Sigma Aldrich. (1,5-cyclooctadiene)palladium(II)chloride, bis(1,5-cyclooctadiene)-Ni(0), tetrakis-(triphenylphosphine)palladium(0), tris-(dibenzylideneacetone)-dipalladium(0), were purchased from Strem Chemicals Inc.Iodine monochloride was purchased from Alfa Aesar. , 2-Bromophenylboronic acid was purchased from Ark Pharm. 2.1 M methyl chloromethyl ether (MOMCl) in toluene,[28] (2,2'-bipyridine)(1,5-cyclooctadiene)nickel(0),[29] 1,4-dimethoxy-2,5-diiodobenzene,[30] 2,5-diiodo-1,4-hydroquinone,[31] and **1-Me**[32] were made according to literature procedures. All ^{1}H, ^{13}C, and ^{31}P spectra were recorded on Varian Mercury 300 MHz, or Varian INOVA-500 or 600 MHz spectrometers at room temperature. Chemical shifts for ^{1}H and ^{13}C NMR data are reported relative to residual solvent peaks.[33] ^{31}P NMR chemical shifts are reported with respect to the deuterated solvent used to lock the instrument. Solution IR spectra were obtained as solution samples using a CaF_2 window cell on a Thermo Scientific Nicolet 6700 FT-IR spectrometer. *In situ* solution IR spectra were recorded on an iC10 ReactIR (Mettler Toledo) equipped with a K4 conduit and a SiComp Sentinel sensor in a

custom-made glass vessel. The UV/Vis spectra were recorded on a Varian Cary Bio 50 spectrophotometer. Low-temperature UV/Vis spectra were obtained using a Varian dip-probe (661.202-UV, 10 mm) and custom-made glass vessel. Elemental analyses were performed by Robertson Microlit Laboratories, Ledgewood, NJ.

Synthesis of 2,5-diiodo-1,4-bis(methoxymethylether)hydroquinone (A)

The synthesis of 2,5-diiodo-1,4-bis(methoxymethylether)hydroquinone has been previously reported, however this protocol provides an alternative synthetic route. 2,5-diiodo-1,4-hydroquinone (2 g, 5.53 mmol, 1 equiv) was added to a 3-neck flask under a counterflow of nitrogen. Degassed, anhydrous dichloromethane (100 mL) was then added with a cannula to yield a suspension. Diisopropylethylamine (11.6 mL, 66.3 mmol, 12 equiv) was then added with a syringe and the reaction mixture allowed to stir for 1 minute. Methylchloromethylether was then added (~2.1 M in PhMe, 26.3 mL, 55.3 mmol, 10 equiv) with a syringe and the reaction was allowed to stir for 3-4 hours during which time the solution became homogenous. The reaction was monitored by GC-MS until all starting material was consumed. The reaction mixture was then washed with a saturated sodium bicarbonate solution. The organic layer was then collected and dried with magnesium sulfate before volatiles were removed by rotary evaporation to yield the clean product as an off-white residue. Characterization matched previous literature reports. Yield: 2.07 g (83 %).

Synthesis of 2,5-bis(2-bromophenyl)-1,4-(methoxymethylether)hydroquinone (B)

The Suzuki coupling to produce the terphenyl product was run as a modification of literature procedure.[34] A Schlenk tube fitted with a Teflon stopper was charged with 2,5-diiodo-1,4-bis(methoxymethylether)hydroquinone (500 mg, 1.11 mmol, 1 equiv.), 2-bromophenylboronic acid (468.6 mg, 2.33 mmol, 2.1 equiv.), and K_2CO_3 (921.3 mg, 6.67 mmol, 6 equiv.). Toluene (26 mL), ethanol (6 mL), and water (6 mL) were then transferred to the Schlenk tube along with a magnetic stirbar. The mixture was degassed by two freeze pump thaw cycles and then put under positive nitrogen pressure. Under a strong counterflow of nitrogen, $Pd(PPh_3)_4$ (64.2 mg, 0.056 mmol, 0.05 equiv.) was added and the solution became a pale yellow color. The reaction mixture was then heated to 65 ºC and stirred for 16-24 hrs while monitoring the reaction by GC-MS. The volatiles were then removed on a rotovap and the residue extracted using dichloromethane and water. The organic layer was then collected and dried using magnesium sulfate before volatiles were removed on a rotovap. Following recrystallation from dichloromethane-methanol the product was obtained as off-white crystalline powder. Yield: 400 mg (71 %). ^{1}H NMR (500 MHz, $CDCl_3$) δ 7.67 (d, J_{HH} = 8.0 Hz, Ar*H*, 2H), 7.37 (m, Ar*H*, 4H), 7.25 – 7.20 (m, Ar*H*, 2H), 7.06 (s, central-Ar*H*, 2H), 5.02 (broad s, OC*H*$_2$O, 4H), 3.33 (s, OC*H*$_3$, 6H). ^{13}C NMR (126 MHz, $CDCl_3$) δ 149.23 (s), 139.54 (s), 132.68 (s), 132.17 (broad s), 131.93 (s), 129.00 (s), 127.11 (s), 124.21 (s), 118.74 (s), 96.14 (s), 56.20 (s). GC-MS (m/z): Calcd, 508.0 (M^+). Found: 508.0 (M^+), FAB-MS (m/z): Calcd, 506.9630 (M+). Found: 506.9623 (M^+).

Synthesis of 2,5-bis(2-(diisopropylphosphino)phenyl)-1,4-hydroquinone (1-H)

Phosphination run as a modification of literature procedures. A Schlenk tube fitted with a screw-in Telfon stopper was charged with 2,5-bis(2-bromophenyl)-1,4-bis(methoxymethylether)hydroquinone (1 g, 1.96 mmol, 1 equiv.) and a magnetic stirbar. Tetrahydrofuran (60 mL) was then to the Schlenk tube. The reaction was cooled to -78 ºC and *tert*-butyllithium (1.7 M pentane solution, 5.4 mL, 8.07 mmol, 4.1 equiv.) was added while stirring to generate a pale yellow solution. The reaction mixture was allowed to warm to room temperature and then stirred for an additional hour. During this time the solution became a cloudy suspension. Chlorodiisopropyl phosphine (0.656 mL, 4.13 mmol, 2.1 equiv.) was then added to the reaction via syringe. The solution immediately became a homogenous pale yellow solution which was allowed to stir for 16 hours. The volatiles were then removed under reduced pressure on the Schlenk line. Acidified methanol (13 mL concentrated HCl, 60 mL MeOH) was quickly degassed on the Schlenk line and then cannula transferred to the dried reaction residue which formed a pale yellow homogeneous solution. The reaction mixture was allowed to stir for 4 hrs at 70 °C to ensure complete removal of the methoxymethylether protecting group before all volatiles were removed under reduced pressure. The reaction was then brought into a wet inert atmosphere glovebox and extracted with dichloromethane. The organic layer was washed with saturated aqueous potassium carbonate followed by saturated ammonium chloride. The organic layer was then dried over magnesium sulfate and the volatiles were then removed under reduced pressure. After drying the residue overnight with heating to 60 °C the reaction was then brought into the dry inert atmosphere glovebox. The residue was washed with cold pentanes and then cold ether to yield the pure product as an off-white solid. Yield: 460 mg (47 %). ^{1}H NMR spectra of product is broad at room temperature due to hindered rotation around aryl–aryl bonds. This is corroborated by ^{31}P

NMR where two distinct peaks are observed at room temperature. ^{1}H NMR (300 MHz, C_6D_6) δ 7.22 (broad s, Ar*H*, 4H), 7.05 (broad s, Ar*H*, 4H), 5.78 (broad s, O*H*, 1H), 5.42 (broad s, O*H*, 1H), 1.93 (broad s, C*H*, 2H), 1.71 (broad s, C*H,* 2H), 0.84 (unresolved m, C*H₃*, 24H). ^{13}C{^{1}H} NMR (126 MHz, C_6D_6) δ 145.76 (s), 134.38 (d, J_{PC} = 45.8 Hz), 131.94 (s), 129.24 (s), 127.01 (s), 121.76 (s), 120.72 (s), 25.35 (s), 21.97 (s), 21.33 (s), 19.89 (s), 19.27 (s), 18.18 (s). At room temperature, **1** shows two distinct ^{31}P NMR signals due to hindered rotation around the aryl-aryl bonds. ^{31}P{^{1}H} NMR (121 MHz, C_6D_6) δ 1.80 (s), -0.06 (s). FAB-MS (m/z): Calcd: 495.2578 (M^+). Found: 495.2582 (M^+).

Synthesis of Complex 2

Compound **1-H** (100 mg, 0.202 mmol, 1 equiv.) was dissolved in tetrahydrofuran (6 mL) and transferred to a Schlenk tube fitted with a screw-in Teflon stopper. $Ni(OAc)_2$ (35.7 mg, 0.202 mmol, 1 equiv.) was suspended in tetrahydrofuran and then added to the solution of **1**. The Schlenk tube was then sealed and heated to 80 °C for 16 hours outside the glovebox during which time to solution became a cloudy green. The reaction mixture was then dried under reduced pressure and brought back into the inert atmosphere glovebox. The crude residue was suspended in diethyl ether and filtered onto a Celite pad. The green solid was washed with additional diethyl ether until the washes became colorless. The product was brought through the Celite pad using tetrahydrofuran. The combined tetrahydrofuran filtrate was dried under reduced pressure to yield the clean product as a green powder. Yield: 65 mg (58 %). ^{1}H NMR (500 MHz, CD_2Cl_2) δ 7.62 (d, J_{HH} = 7.6 Hz, Ar*H*, 2H), 7.58 (t, J_{HH} = 7.4 Hz, Ar*H*, 2H), 7.50 (t, J_{HH} = 6.7 Hz, Ar*H*, 2H), 7.45 (t, J_{HH} = 7.5 Hz, Ar*H*, 2H), 6.16 (s, central Ar*H*, 2H), 2.56 (m, C*H*, 2H), 2.28 (m, C*H*, 2H), 1.32 – 1.24 (m, C*H₃*, 12H), 1.21 (dd, J_{PH} =

16.1 Hz, J_{HH} = 7.0 Hz, C*H₃*, 6H), 1.09 (dd, J_{PH} = 15.8 Hz, J_{HH} = 7.0 Hz, C*H₃*, 6H). $^{13}C\{^1H\}$ NMR (126 MHz, CD_2Cl_2) δ 162.79 (s), 146.43 – 145.62 (m), 138.53 – 136.77 (m), 130.95 (d, J_{PC} = 16.1 Hz), 127.68 (s), 120.33 – 117.76 (m), 96.46 (s), 27.29 (m), 19.99 (s), 17.97 (s), 17.82 (s), 17.43 (s). $^{31}P\{^1H\}$ NMR (121 MHz, CD_2Cl_2) δ 54.30 (s). IR (CaF_2 window, THF, cm^{-1}) ν_{C-O}: 1597. Anal. Calcd. for: $C_{30}H_{38}NiO_2$ (**2)** (%): C, 65.36; H, 6.95. $C_{31}H_{40}Cl_2NiO_2$ (**2•DCM)** (%): C, 58.53; H, 6.34. Found: C, 58.94; H, 6.18.

Synthesis of Complex 3 using $Pd(OAc)_2$

Compound **1-H** (100mg, 0.202 mmol, 1 equiv.) was dissolved in tetrahydrofuran (10 mL) and transferred to a 20 mL scintillation vial. Palladium diacetate (45.4 mg, 0.202 mmol, 1 equiv.) was added as a tetrahydrofuran solution, which in the immediate formation of a deep purple solution. The reaction mixture was allowed to stir for 16 hours before volatiles were removed under reduced pressure to yield a purple residue. The residue was filtered through a Celite pad with tetrahydrofuran. The combined tetrahydrofuran filtrate was dried under reduced pressure to yield the product as a purple powder. Yield: 70 mg (58 %).

Synthesis of Complex 3 using $Pd_2(dba)_3$ and O_2

Compound **1-H** (300 mg, 0.606 mmol, 1 equiv.) was dissolved in tetrahydrofuran (10 mL) and then transferred to a 20 mL scintillation vial. Tris(dibenzylideneacetone dipalladium(0) (277.7 mg, 0.303 mmol, 0.5 equiv.) was then partially dissolved in tetrahydrofuran (10 mL) and added to the solution of **1**. The reaction mixture was allowed to stir for 30 minutes. The scintillation vial was then removed from the inert atmosphere glovebox and exposed to air

and allowed to stir for 1 hour. The reaction immediately turned a deep purple upon exposure to air. The reaction mixture was then poured onto a silica plug that had been wet packed with ethyl acetate (Note: the product is not indefinitely stable on silica and should be eluted quickly from the plug column). Excess dibenzylideneacetone was eluted with ethyl acetate as evidenced by a yellow band. The product was then eluted with methanol taking care to collect only the purple band. The methanol filtrate was then dried under reduced pressure. The purple residue was dried on the Schlenk line overnight and brought into the glovebox where it was dissolved in dry dichloromethane and redried under reduced pressure to yield the product as a purple powder. Yield: 219.7 mg (60 %). ^{1}H NMR (300 MHz, CD_2Cl_2) δ 7.62 – 7.54 (m, Ar*H*, 2H), 7.53 – 7.48 (m, Ar*H*, 4H), 7.47 – 7.37 (m, Ar*H*, 2H), 6.10 (s, central Ar*H*, 2H), 2.46 (dtt, C*H*, 2H), 2.33 (m, C*H*, 2H), 1.13 (m, C*H*$_3$, 24H). ^{13}C{^{1}H} NMR (126 MHz, CD_2Cl_2) δ 165.45 (s), 146.28 – 145.30 (m), 140.90 – 139.75 (m), 132.41 (s), 130.78 (s), 129.82 (s), 128.81 (vt, J_{PC} = 7.9 Hz), 127.82 (d, J_{PC} = 2.5 Hz), 102.64 (s), 28.18 – 27.56 (m), 26.85 – 25.79 (m), 19.38 (t, J_{PC} = 3.7 Hz), 18.70 (vt, J_{PC} = 3.6 Hz), 18.34 (s), 18.05 (s). ^{31}P{^{1}H} NMR (121 MHz, CD_2Cl_2) δ 55.02 (s). IR (CaF_2 window, THF, cm^{-1}) $\nu_{C\text{-}O}$: 1603. Anal. Calcd. for: $C_{30}H_{38}FO_4P_2Pd$ (**3)** (%): C, 60.16; H, 6.39. Anal. Calcd. for: $C_{31}H_{40}Cl_2O_4P_2Pd$ (**3•DCM)** (%): C, 54.44; H, 5.90. Found: C, 54.90; H, 6.00.

Synthesis of Complex 4-H

Compound **1-H** (300 mg, 0.606 mmol, 1 equiv.) was dissolved in tetrahydrofuran (10 mL) and transferred to a Schlenk tube fitted with a screw-in Teflon stopper. (1,5-cyclooctadiene)palladium(II) dichloride (173.2 mg, 0.606 mmol, 1 equiv.) was then added as a partially dissolved suspension in tetrahydrofuran (15 mL). The reaction mixture was allowed

to stir for 2 hours during which time the reaction became a homogeneous orange solution. (1,5-cyclooctadiene)(2,2'-bipyridine)nickel(0) (195.6 mg, 0.606 mmol, 1 equiv.) was then dissolved in tetrahydrofuran (15 mL) and transferred to the reaction mixture. This resulted in an immediate color change to a heterogeneous brown/orange suspension. After stirring for 15 minutes the reaction mixture was filtered through a Celite pad with washing with additional tetrahydrofuran until washes became less colored. The combined tetrahydrofuran filtrate was dried under reduced pressure to yield a brown residue. This residue was then redissolved in benzene and lyophilized to yield the product as a brown powder. Yield: 305 mg (84 %). *Note*: the product is not indefinitely stable in solution and eventually decomposes to a mixture of species. However, it is stable in the solid state. ^{1}H NMR (300 MHz, C_6D_6) δ 7.41 – 7.29 (m, Ar*H*, 4H), 7.12 – 7.03 (m, Ar*H*, 4H), 6.94 (s, central Ar*H*, 2H), 4.14 (s, O*H*, 2H), 1.88 (m, C*H*, 4H), 1.35 (m, C*H*$_3$, 12H), 0.95 (m, C*H*$_3$, 12H). ^{13}C{^{1}H} NMR (126 MHz, C_6D_6) δ 145.26 (s), 144.83 (vt, J_{PC} = 10.2 Hz), 135.02 (vt, J_{PC} = 9.7 Hz), 132.01 (s), 129.67 (s), 128.57 (s), 128.19 (s), 124.22 (s), 29.15 (vt, J_{PC} = 6.1 Hz), 27.82 (vt, J_{PC} = 6.2 Hz), 22.04 (vt, J_{PC} = 8.3 Hz), 21.82 (vt, J_{PC} = 9.1 Hz), 20.80 – 20.30 (m). ^{31}P{^{1}H} NMR (121 MHz, C_6D_6) δ 33.85 (s). Anal. Calcd. for: $C_{30}H_{40}O_2P_2Pd$ (**4)** (%): C, 59.95; H, 6.71. Found: C, 60.21; H, 6.71.

Synthesis of Complex 5-H

Compound **1-H** (100.7 mg, 0.204 mmol, 1 equiv.) was dissolved in tetrahydrofuran (8 mL) and added to a 20 mL scintillation vial containing (1,5-cyclooctadiene)palladium(II) dichloride (58.1 mg, 0.204 mmol, 1 equiv.). The reaction mixture was allowed to stir for 2 hours during which time the solution became a homogeneous orange. Silver triflate (52.3 mg, 0.204 mmol, 1 equiv.) was then added as a tetrahydrofuran solution resulting in an immediate color change

to a dark red. The solution was allowed to stir for 30 minutes before filtering the solution through a Celite pad. Tetrahydrofuran washes eluted further product from the Celite pad. The combined tetrahydrofuran filtrate was dried under reduced pressure to yield a red residue. This residue was recrystallized from acetonitrile:diethyl ether to yield the product as dark red crystals. Yield: 56.1 mg (31.6 %). *Note*: the product is not indefinitely stable in solution and eventually decomposes to a mixture of species. However, it is stable in the solid state. ^{1}H NMR (300 MHz, CD_3CN) δ 8.18 (broad s, O*H*, 2H), 7.86 (m, Ar*H*, 2H), 7.79 – 7.65 (m, Ar*H*, 4H), 7.59 (m', Ar*H*, 2H), 6.72 (s, central Ar*H*, 2H), 3.12 (m, C*H*, 4H), 1.42 – 1.07 (m, C*H*$_3$, 24H). ^{13}C{^{1}H} NMR (126 MHz, CD_3CN) δ 148.17 (s), 143.58 (s), 133.80 (s), 133.23 (s), 132.55 (s), 130.76 (s), 130.14 (s), 128.81 (s), 128.28 (s), 27.35 (s), 26.89 (vt, J_{PC} = 11.5 Hz), 19.61 (s), 19.34 (s), 18.74 (s). ^{31}P{^{1}H} NMR (121 MHz, CD_3CN) δ 34.22 (s). ^{19}F NMR (282 MHz, CD_3CN) δ -79.40 (s). Anal. Calcd. for: $C_{31}H_{44}F_3O_5P_2PdS$ (**5)** (%): C, 47.40; H, 4.51. Found: C, 47.62; H, 5.13.

Synthesis of Complex 6-H

Pyridinium triflate (44.7 mg, 0.195 mmol, 1 equiv.) was partially dissolved in tetrahydrofuran (4 mL) in a 20 mL scintillation vial. Compound **4-H** (117.2 mg, 0.195 mmol, 1 equiv.) was the added as a tetrahydrofuran solution which resulted in an immediate lightening of the solution from yellow/brown to yellow. After stirring for 16 hours the reaction mixture was dried under reduced pressure to yield the product as a foamy yellow/orange solid in quantitative yield. ^{1}H NMR (300 MHz, CD_3CN) δ 7.84 – 7.75 (m, Ar*H*, 2H), 7.71 – 7.53 (m, Ar*H*, 6H), 7.42 (broad s, O*H*, 2H), 6.79 (s, central Ar*H*, 4H), 2.46 (m, C*H*, 4H), 1.19 – 1.01 (m, C*H*$_3$, 18H), 0.94 (m, C*H*$_3$, 6H), -16.33 (t, J_{PH} = 8.5 Hz, Pd*H*, 1H). ^{13}C{^{1}H} NMR (126

MHz, CD_3CN) δ 144.58 (s), 143.99 (vt, J_{PC} = 7.2 Hz), 132.28 (s), 131.11 (s), 130.12 (s), 128.38 (s), 126.64 (s), 125.97 (vt, J_{PC} = 19.2 Hz), 110.30 (s), 28.11 (vt, J_{PC} = 13.1 Hz), 27.30 (vt, J_{PC} = 12.5 Hz), 19.68 (s), 19.44 (s), 18.60 (s), 18.41 (s). $^{31}P\{^1H\}$ NMR (121 MHz, CD_3CN) δ 41.57 (d, J_{PH} = 6.7 Hz). ^{19}F NMR (282 MHz, CD_3CN) δ -79.34 (s). Anal. Calcd. for: $C_{31}H_{41}F_3O_5P_2PdS$ (**6)** (%): C, 49.57; H, 5.50. Found: C, 49.32; H, 5.36.

Synthesis of Complex 7-H

Compound **1-H** (129.5 mg, 0.262 mmol, 1 equiv.) was dissolved in tetrahydrofuran (8 mL) and then added to a 20 mL scintillation vial with silver triflate (67.2 mg, 0.262 mmol, 1 equiv.). The reaction mixture was allowed to stir for 3 hours to yield a pale pink solution before being dried under reduced pressure. The residue was then dissolved in minimal acetonitrile and filtered through a Celite pad, which removed the pinkish color. The product was then recrystallized from an acetonitrile:diethyl ether vapor diffusion to yield white crystalline needles. Yield: 134 mg (68 %). ^1H NMR (500 MHz, CD_3CN) δ 7.81 – 7.77 (m, Ar*H*, 2H), 7.72 – 7.68 (t, J_{HH} = 7.6 Hz, 2H), 7.63 (t, J_{HH} = 7.7 Hz, Ar*H*, 2H), 7.58 (dq, J_{HH} = 7.5 Hz, J_{HH} = 1.8 Hz, Ar*H*, 2H), 6.98 (broad s, O*H*, 2H), 6.85 (s, central Ar*H*, 2H), 2.52 (m, C*H*, 4H), 1.32 – 1.15 (m, C*H*$_3$, 12H), 1.02 (m, C*H*$_3$, 12H). $^{13}C\{^1H\}$ NMR (126 MHz, CD_3CN) δ 147.80 (s), 144.47 (vt, J_{PC} = 8.7 Hz), 132.62 (d), 131.00 (s), 130.30 (s), 128.58 (s), 126.91 (d, J_{PC} = 5.3 Hz), 126.88 – 126.48 (m), 118.16 (s), 26.12 (dd), 25.78 – 25.34 (m), 20.93 (vt, J_{PC} = 5.9 Hz), 20.65 (vt, J_{PC} = 5.9 Hz), 19.50 (m). $^{31}P\{^1H\}$ NMR (121 MHz, CD_3CN) δ 28.33 (d, J_{PAg} = 559.7 Hz), 28.33 (d, J_{PAg} = 484.9 Hz). ^{19}F NMR (282 MHz, CD_3CN) δ -79.32 (s). Anal. Calcd. for: $C_{31}H_{40}AgF_3O_5P_2S$ (**7)** (%): C, 49.54; H, 5.37. Found: C, 49.77; H, 5.15.

Synthesis of Complex 4-Me

Compound **1-Me** (327.3 mg, 0.626 mmol, 1 equiv.) was dissolved in tetrahydrofuran (10 mL) and transferred to a Schlenk tube fitted with a screw-in Teflon stopper. (1,5-cyclooctadiene)palladium(II) dichloride was then added as a partially dissolved suspension in tetrahydrofuran (15 mL). The reaction mixture was allowed to stir for 2 hours during which time the solution became a homogeneous yellow/orange. (1,5-cyclooctadiene)(2,2'-bipyridine)nickel(0) was added as a solution in tetrahydrofuran (20 mL) which resulted in immediate consumption of the purple nickel complex and the formation of a heterogeneous orange solution. The reaction mixture was stirred for an additional 30 minutes before filtering through a Celite pad. Additional tetrahydrofuran was used to wash product through the Celite pad. The combined tetrahydrofuran filtrate was dried under reduced pressure to yield an orange residue. This residue was redissolved in benzene and lyophilized to yield the product as an orange powder. Yield: 385.8 mg (98 %). ^{1}H NMR (300 MHz, C_6D_6) δ 7.63 (m, Ar*H*, 2H), 7.45 (m, Ar*H*, 12H), 7.22 (m, Ar*H*, 4H), 6.86 (s, central Ar*H*, 2H), 3.49 (s, OC*H*$_3$, 6H), 1.96 (m, C*H*, 4H), 1.36 (m, C*H*$_3$, 12H), 1.00 (m, C*H*$_3$, 12H). ^{13}C{^{1}H} NMR (126 MHz, C_6D_6) δ 149.30 (s), 147.29 (vt, J_{PC} = 10.0 Hz), 133.88 (vt, J_{PC} = 10.9 Hz), 131.25 (s), 129.95 (s), 126.81 (s), 125.74 (s), 55.09 (s), 28.58 (vt, J_{PC} = 6.2 Hz), 28.40 (t, J_{PC} = 6.3 Hz), 22.18 (vt, J_{PC} = 8.6 Hz), 21.97 (vt, J_{PC} = 8.8 Hz), 20.82 (s), 20.52 (s). ^{31}P{^{1}H} NMR (121 MHz, C_6D_6) δ 33.81 (s). Anal. Calcd. for: $C_{32}H_{44}O_2P_2Pd$ (**9)** (%): C, 61.10; H, 7.05. Found: C, 60.62; H, 6.81.

Synthesis of Complex 6-Me

Pyridinium triflate (94.8 mg, 0.413 mmol, 1 equiv.) was partially dissolved in tetrahydrofuran (5 mL) in a 20 mL scintillation vial. Compound **4-Me** (260.3 mg, 0.413 mmol,

1 equiv.) was then added as a tetrahydrofuran solution (10 mL) which resulted in an immediate color change from orange to yellow. After stirring for 16 hours the reaction mixture was dried under reduced pressure to yield the product as a foamy yellow/orange solid in quantitative yield. ^{1}H NMR (300 MHz, CD_3CN) δ 7.86 – 7.75 (m, Ar*H*, 2H), 7.75 – 7.51 (m, Ar*H*, 6H), 6.99 (s, central Ar*H*, 2H), 3.73 (s, OC*H*$_3$, 1H), 2.55 – 2.42 (m, C*H*, 4H), 1.17 – 1.01 (m, C*H*$_3$, 12H), 1.00 – 0.84 (m, C*H*$_3$, 12H), -16.33 (t, J_{PH} = 9.0 Hz, Pd*H*, 1H).^{13}C{^{1}H} NMR (126 MHz, CD_3CN) δ 148.03 (s), 144.17 (vt, J_{PC} = 7.0 Hz), 132.17 (s), 130.98 (s), 128.39 (s), 127.92 (s), 125.55 (vt, J_{PC} = 19.0 Hz), 107.70 (s), 56.49 (d), 27.76 (vt, J_{PC} = 13.3 Hz), 27.18 (vt, J_{PC} = 13.2 Hz), 19.63 (s), 19.24 (s), 18.55 (s), 18.22 (s). ^{31}P{^{1}H} NMR (121 MHz, CD_3CN) δ 41.93 (s). ^{19}F NMR (282 MHz, CD_3CN) δ -79.37 (s). Anal. Calcd. for: $C_{33}H_{45}F_3O_5P_2PdS$ (**10)** (%): C, 50.87; H, 5.82. Found: C, 50.19; H, 5.47.

In Situ Preparation of Complex 8-Me

4-Me (11.6 mg, 0.0184 mmol, 1 equiv) was dissolved d_8-THF and transferred to a J-Young tube. The solution was then frozen and the headspace removed under vacuum. Excess O_2 (1 atm) was then added and the solution was carefully mixed to avoid warming the solution. Immediate and quantitative conversion to **8-Me** was observed by NMR at -78 °C. *Note:* The compound is stable at low temperatures with no decomposition detected by NMR for hours at -40 °C or two weeks at -78 °C. However, around 0 °C decomposition to a mixture of species in observed. Solutions can be degassed to remove excess O_2 by placing solutions under dynamic vacuum at -78 °C if prepared in a Schlenk tube or by multiple freeze-pump-thaw cycles if care is taken not to warm the solution above -40 °C. All NMR characterization was obtained at -40 °C. ^{1}H NMR (500 MHz, d_8-THF) δ 7.62 (dd, J_{HH} = 7.8 Hz, J_{HH} = 5.1 Hz, Ar*H*,

1H), 7.54 (dd, J_{HH} = 7.8, J_{HH} = 5.1 Hz, Ar*H*, 1H), 7.52 – 7.46 (m, Ar*H*, 4H), 7.44 – 7.38 (m, Ar*H*, 2H), 6.87 (s, central aryl Ar*H*, 1H), 6.66 (s, central aryl Ar*H*, 1H), 3.56 (s, OC*H*$_3$, 3H), 3.47 (s, OC*H*$_3$, 3H), 2.67 (m, C*H*, 1H), 2.59 (m, C*H*, 1H), 1.98 (m, C*H*, 2H), 1.37 (m, C*H*$_3$, 12H), 1.13 – 1.04 (m, C*H*$_3$, 6H), 0.85 (m, C*H*$_3$, 6H). $^{13}C\{^1H\}$ NMR (126 MHz, d_8-THF) δ 151.03 (s), 149.81 (s), 146.60 (d, J_{PC} = 16.0 Hz), 145.46 (d, J_{PC} = 16.1 Hz), 133.84 (s), 133.06 (s), 132.99 (s), 132.77 (s), 130.28 (s), 130.09 (s), 129.66 (d, J_{PC} = 6.1 Hz), 129.52 (d, J_{PC} = 5.8 Hz), 129.14 (s), 128.95 (d, J_{PC} = 7.2 Hz), 128.78 (s), 128.61 (d, J_{PC} = 6.6 Hz), 128.21 (s), 127.97 (s), 127.87 (s), 127.67 (s), 127.48 (s), 126.06 (s), 125.53 (s), 113.70 (d, J_{PC} = 13.2 Hz), 54.43 (s), 28.36 (d, J_{PC} = 14.2 Hz), 27.26 (d, J_{PC} = 11.5 Hz), 25.48 (d, J_{PC} = 20.2 Hz), 22.70 (d, J_{PC} = 18.0 Hz), 22.37 (d, J_{PC} = 15.1 Hz), 20.04 (s), 19.53 (d, J_{PC} = 13.1 Hz), 19.33 (d, J_{PC} = 7.1 Hz), 18.86 (d, J_{PC} = 5.6 Hz), 17.26 (d, J_{PC} = 4.5 Hz), 16.32 (d, J_{PC} = 6.0 Hz). $^{31}P\{^1H\}$ NMR (202 MHz, d_8-THF) δ 34.04 (d, $^2J_{PP}$ = 23.8 Hz), 29.87 (d, $^2J_{PP}$ = 24.0 Hz).

Synthesis of Complex (3)H$^+$

6-H (13.9 mg, 0.019 mmol, 1 equiv) was dissolved in CD_3CN and transferred to a J-Young tube. The solution was then frozen and the headspace removed under vacuum. Excess O_2 (1 atm) was then added and the sample was allowed to thaw to room temperature with inversion to ensure adequate mixing. A gradual color change from yellow/orange to a pink/red solution was observed over 6^+ hours. NMR revealed quantitative conversion to a new species, **(3)H$^+$**, that could be isolated as a red powder following removal of volatiles. ^1H NMR (300 MHz, CD_3CN) δ 7.76 – 7.51 (m, 8H), 6.39 (s, 2H), 2.63 (m, 2H), 2.54 (m, 2H), 1.24 – 0.96 (m, 24H). ^{13}C NMR (126 MHz, CD_3CN) δ 142.35 (d, J_{PC} = 13.7 Hz), 139.70 (d, J_{PC} = 37.2 Hz), 133.34 (s), 132.23 (s), 131.57 (s), 129.09 (d, J_{PC} = 13.6 Hz), 127.38 (s), 105.94 (s), 28.10 (d, J_{PC} = 19.1

Hz), 26.35 (d, J_{PC} = 26.1 Hz), 18.73 (s), 18.07 (s), 17.83 (s), 17.23 (s). ^{31}P NMR (121 MHz, CD_3CN) δ 64.39. ^{19}F NMR (282 MHz, CD_3CN) δ -79.34.

Volumetric Measurement of O_2 Consumption

Toepler Pump Experimental Details

To determine the stoichiometry of reaction of O_2 with compounds **4-**H, **4-Me**, and 6-H, a solution of the compound to be tested was degassed via three freeze-pump-thaw cycles on a high vacuum line. While the solution (benzene for **4-H**, THF for **4-Me** and **6-H**) was still frozen, a known amount of O_2 (~3-5 equiv) was measured with a volumetric Schlenk bulb (33.28 mL or 43.48 mL). The exact procedure then varied depending on the compound used. For **4-H** and **6-H**, the solution of compound was then warmed to room temperature and while stirring vigorously the O_2 was then added to the reaction mixture. For **4-Me**, the solution was warmed to -78 °C and while stirring vigorously the dioxygen was added to the reaction mixture while this temperature was maintained. All reactions were allowed to stir for 1hr. During this time, the solution of **4-H** and **6-H** were observed to change color from brown/yellow and pale yellow to purple and pink respectively. No substantial color changed was observed following O_2 addition to **4-Me** at low temperature. The solution was again frozen, and the gas present in the headspace was measured by Toepler pump (30.23 mL volume). Three freeze-pump-thaw cycles were carried out on the final reaction solution to recover all unreacted gases. Table **1** summarizes all the separate runs of volumetric measurements.

Table 1. Results of volumetric O_2 measurements. Volumetric bulb volume = 33.28 mL[a] or 43.48 mL[b], Toepler pump volume = 30.25 mL.

Run	Cmpd	T (K)	mmol Cmpd	O_2 added (mmHg)	Final O_2 (mmHg)	mmol O_2 Consumed	Equiv Consumed
1[a]	**4-H**	295	0.0902	151	197	0.0507	0.56
2[a]	**4-H**	295	0.0928	152	197	0.0490	0.53
3[b]	**4-H**	295	0.0850	182	234	0.0454	0.53
4[b]	**6-H**	295	0.0808	186	224	0.0712	0.88
5[b]	**6-H**	295	0.0800	190	227	0.0758	0.95
6[b]	**6-H**	295	0.0750	187	226	0.0703	0.94
7[b]	**4-Me**	295	0.0849	157	172	0.0882	1.04
8[b]	**4-Me**	295	0.0885	157	178	0.0783	0.89
9[b]	**4-Me**	295	0.0909	159	176	0.0863	0.95

ReactIR Spectra

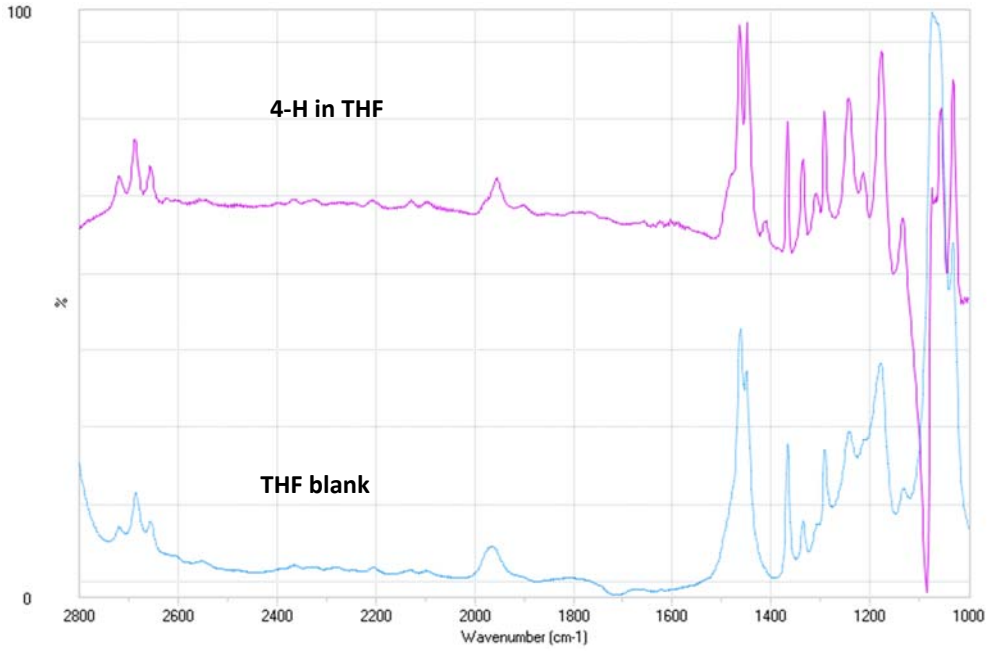

Figure 16. Solution ReactIR spectrum for **4-H** at -78 °C before O_2 addition.

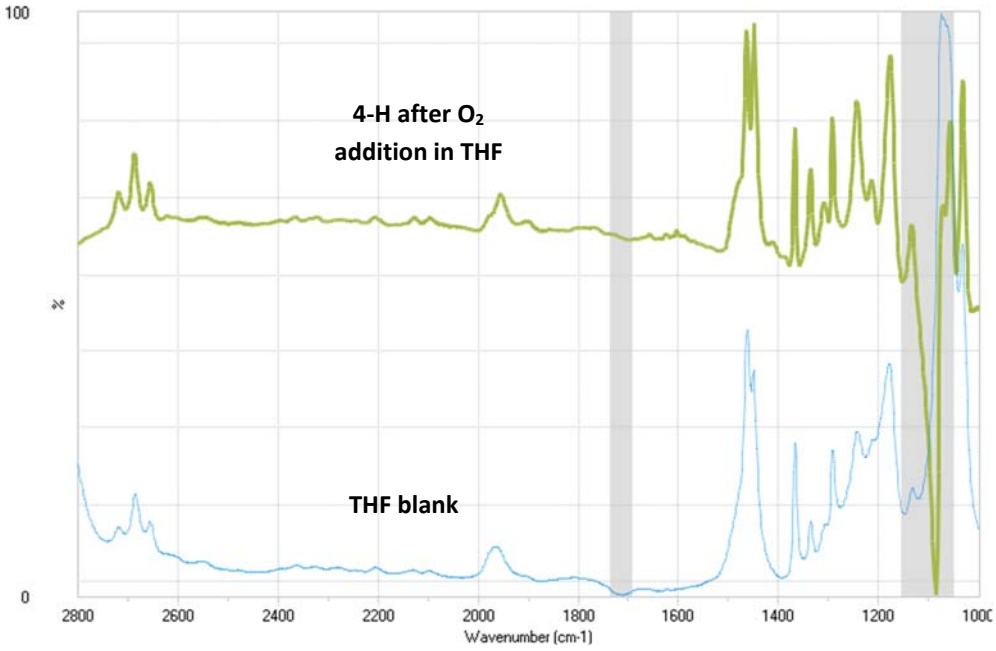

Figure 17. Solution ReactIR spectrum for **4-H** at -78 °C after O_2 addition.

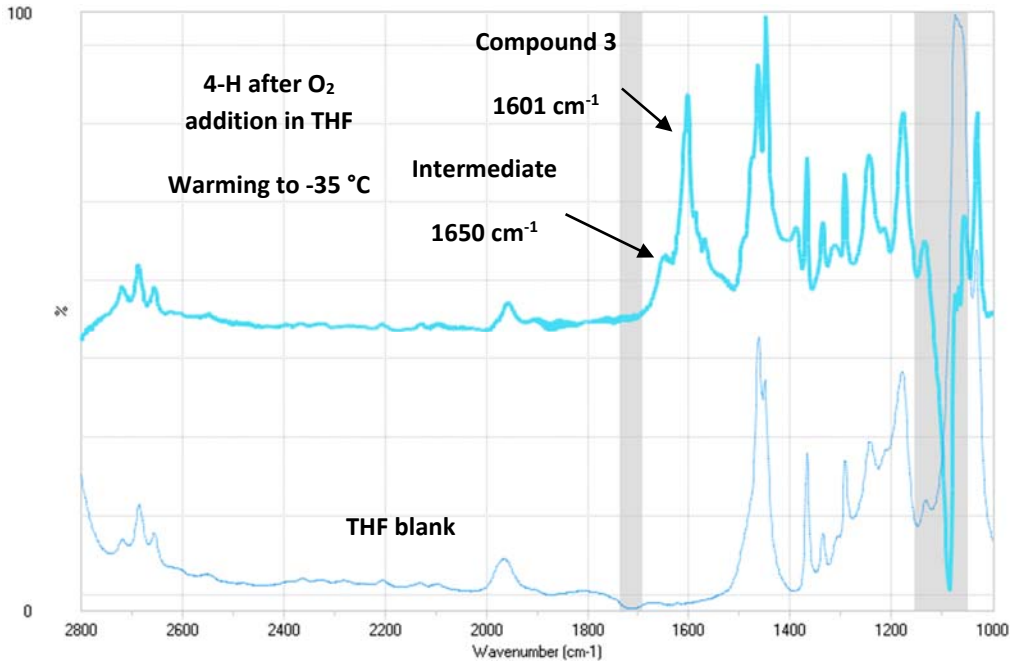

Figure 18. Solution ReactIR spectrum for **4-H** after warming to -35 °C after O_2 addition.

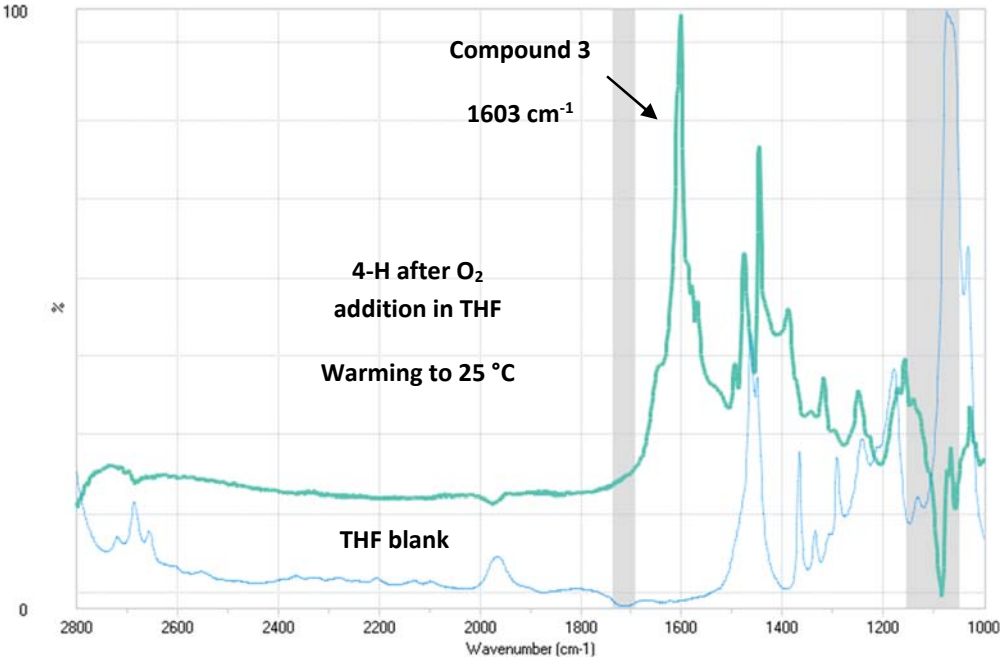

Figure 19. Solution ReactIR spectrum for **4-H** after warming to 25 °C after O_2 addition.

UV/Vis Spectra

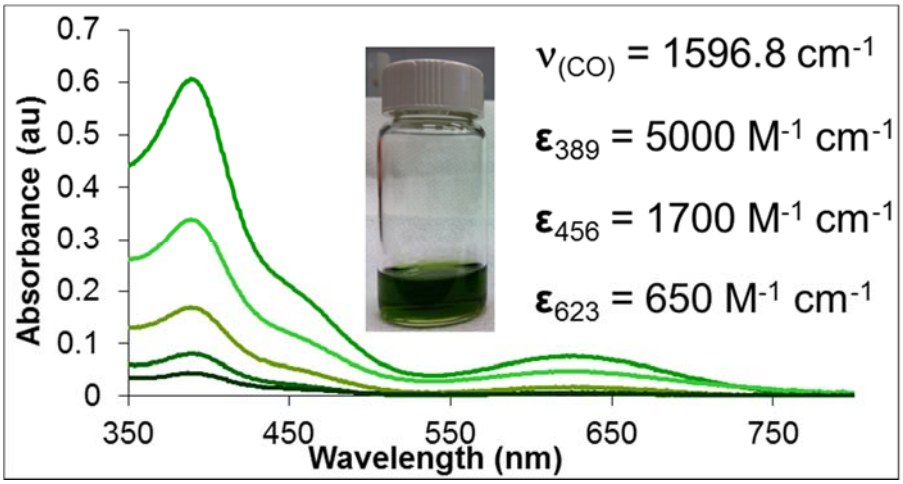

Figure 20. Solution UV/Vis spectrum for **2**.

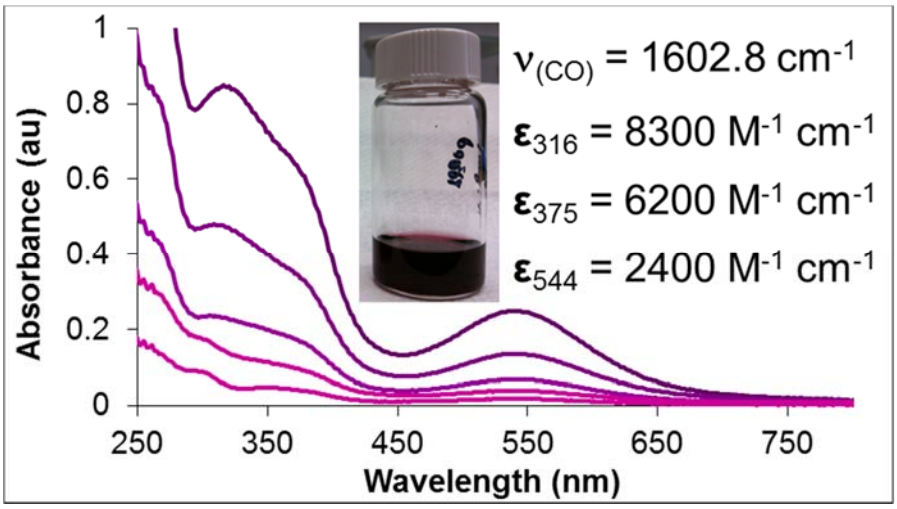

Figure 21. Solution UV/Vis spectrum for **3**.

Oxidation of 4-H to 3 by Various Substrates

Dioxygen

4-H (10.1 mg, 0.0170 mmol, 1 equiv) was transferred to a Schlenk tube as a solution in ca. 2 mL of THF. The solution was degassed by three freeze-pump-thaw cycles and then cooled to -78 °C. Excess O_2 (1 atm) was then added and allowed to stir vigorously for several minutes. The reaction mixture was then degassed under dynamic vacuum at -78 °C while stirring vigorously for 8 minutes. The reaction mixture was then warmed to room temperature. During this time the solution immediately turned purple indicative of the formation of **3**. Volatiles were then removed under reduced pressure and NMR of the residue taken in C_6D_6, which confirmed the quantitative formation of **3**. If the reaction is run in a J-Young tube in C_6D_6 the formation of water could be confirmed by vacuum transferring the volatiles of the reaction into another J-Young tube.

Nitric Oxide

4-H (10.0 mg, 0.0167 mmol, 1 equiv) was dissolved in C_6D_6 and transferred to a J-Young tube. The sample was frozen and the headspace removed. Nitric oxide (1 equiv) was measured in a calibrated gas bulb and then condensed into the J-Young tube. The sample was then warmed to room temperature. The solution turned purple as soon it thawed indicating the rapid formation of **3**. This was confirmed by NMR which showed quantitative conversion to **3**. The formation of water could be confirmed by vacuum transferring the volatiles of the reaction into another J-Young tube.

Nitrous Oxide

4-H (9.9 mg, 0.0165 mmol, 1 equiv) was dissolved in C_6D_6 and transferred to a J-Young tube. The sample was frozen and the headspace removed. Excess nitrous oxide (1 atm) was then added to the J-Young tube. The sample was then warmed to room temperature. The reaction was then monitored by NMR. The slow formation of **3** was observed by NMR over the course of 12 hrs, however simultaneous decomposition of **4-H** typical of solution samples allowed to stand has also occurred. A color change from brown-yellow to a purple was observed over the course of the reaction. The formation of water could be confirmed by vacuum transferring the volatiles of the reaction into another J-Young tube.

2,4,6-Tri(tertbutyl) Phenoxyl Radical

4-H (10.0 mg, 0.0167 mmol, 1 equiv) was dissolved in ca. 1 mL of THF and transferred to a 20 mL scintillation vial equipped with a magnetic stirbar. 2,4,6-tri*tert*butyl phenoxyl radical (8.2 mg, 0.033 mmol, 2 equiv) as then added as a solution in ca. 1 mL THF. This resulted in the immediate formation of a purple solution consistent with formation of **3**. The volatiles were then removed under reduced pressure. Successful conversion to **3** was confirmed by ^{31}P NMR.

1-Azido Adamantane

4-H (10.6 mg, 0.0180 mmol, 1 equiv) was dissolved in ca. 1 mL of THF and transferred to a 20 mL scintillation vial equipped with a magnetic stirbar. 1-Azido adamantane (3.2 mg,

0.0180 mmol, 1 equiv) was added as a solution in ca. 1 mL of THF and the reaction was allowed to stir for 2 hrs. During this time the solution turned from yellow-brown to purple, indicative of conversion to **3**. The volatiles were then removed under reduced pressure. Successful conversion to **3** was confirmed by ^{31}P NMR. The formation of 1-amino adamantine was confirmed by GC-MS comparisons to the retention time and mass data for an authentic sample.

Trimethylamine n-oxide

4-H (10.0 mg, 0.0166 mmol, 1 equiv) was dissolved in ca. 1 mL of MeCN and transferred to a 20 mL scintillation vial equipped with a magnetic stirbar. Trimethylamine *n*-oxide (1.3 mg, 0.0173 mmol, 1.04 equiv) was added as a solution in ca. 1 mL of MeCN and the reaction was allowed to stir for 2 hrs. During this time the solution turned from yellow-brown to purple, indicative of conversion to **3**. The volatiles were then removed under reduced pressure. Successful conversion to **3** was confirmed by ^{31}P NMR.

1,4-Benzoquinone

4-H (10.0 mg, 0.0166 mmol, 1 equiv) was dissolved in ca. 1 mL of THF and transferred to a 20 mL scintillation vial equipped with a magnetic stirbar. 1,4-Benzoquinone (1.8 mg, 0.167 mmol, 1 equiv) was then added as a solution in ca. 1 mL of THF and the reaction was allowed to stir for 2 hrs. During this time there was a rapid color change from brown-yellow to purple, indicative of conversion to **3**. The volatiles were then removed under reduced pressure. Successful conversion to **3** was confirmed by ^{31}P NMR.

Representative Conditions for Testing Substrate Oxidation by 8-Me

Para-trifluoromethyl benzyl alcohol

In a Schlenk tube equipped with a magnetic stirbar, **4-Me** (11.3 mg, 0.0180 mmol, 1 equiv) and 1,3,5-trimethoxybenzene (3.7 mg, 0.0180 mmol, 1 equiv), for an internal standard, was dissolved in ca. 5 mL of THF. The solution was degassed by a series of three freeze-pump-thaw cycles, then cooled to -78 °C. Excess O_2 (1 atm) was then added the solution was stirred vigorously to ensure complete conversion to **8-Me** The solution was then degassed under dynamic vacuum at -78 °C while stirring vigorously for several minutes. The reaction was then put under a N_2 atmosphere and para-trifluoromethyl benzyl alcohol (24.6 μL, 0.180 mmol, 10 equiv) was added via syringe. The reaction mixture was allowed to stir for 4 hrs before a GC-MS aliquot was taken under a strong counterflow of N_2. GC-MS indicated partial conversion to the corresponding benzaldehyde and unreacted benzyl alcohol by comparison to retention time and mass data for authentic samples. Addition of more equivalents of O_2 did not lead to further conversion to product.

Para-trifluoromethyl-benzaldehyde

No oxidation of the benzaldehyde was observed by GC-MS.

Cyclohexane Carboxaldehyde

Partial conversion to cyclohexene observed by GC by comparison to retention time for an authentic sample.

Cyclohexene

No oxidation of cyclohexene was observed by GC. In particular, no cyclohexanone was observed by comparison to retention time for an authentic sample.

Triphenylphosphine

Partial conversion to triphenylphosphine oxide observed by GC-MS by comparison to retention time and MS data for an authentic sample. However, low temperature ^{31}P NMR experiments indicate that substitution of **1-Me** by 2 equivalents of PPh_3 to yield $(PPh_3)_2Pd(\eta^2\text{-}O_2)$ occurs (^{31}P shift observed at 33.18 ppm consistent with literature data obtained in DMF (33.4 ppm) or $CDCl_3$ (33.2 ppm)). By comparison to the ^{31}P integration of against an internal standard of $OP(OMe)_3$, the disappearance of **8-Me** occurs at the same rate of **1-Me** and $(PPh_3)_2Pd(\eta^2\text{-}O_2)$ formation. Subsequent formation of phosphine oxide observed by GC-MS likely occurs from this complex rather than **8-Me**.

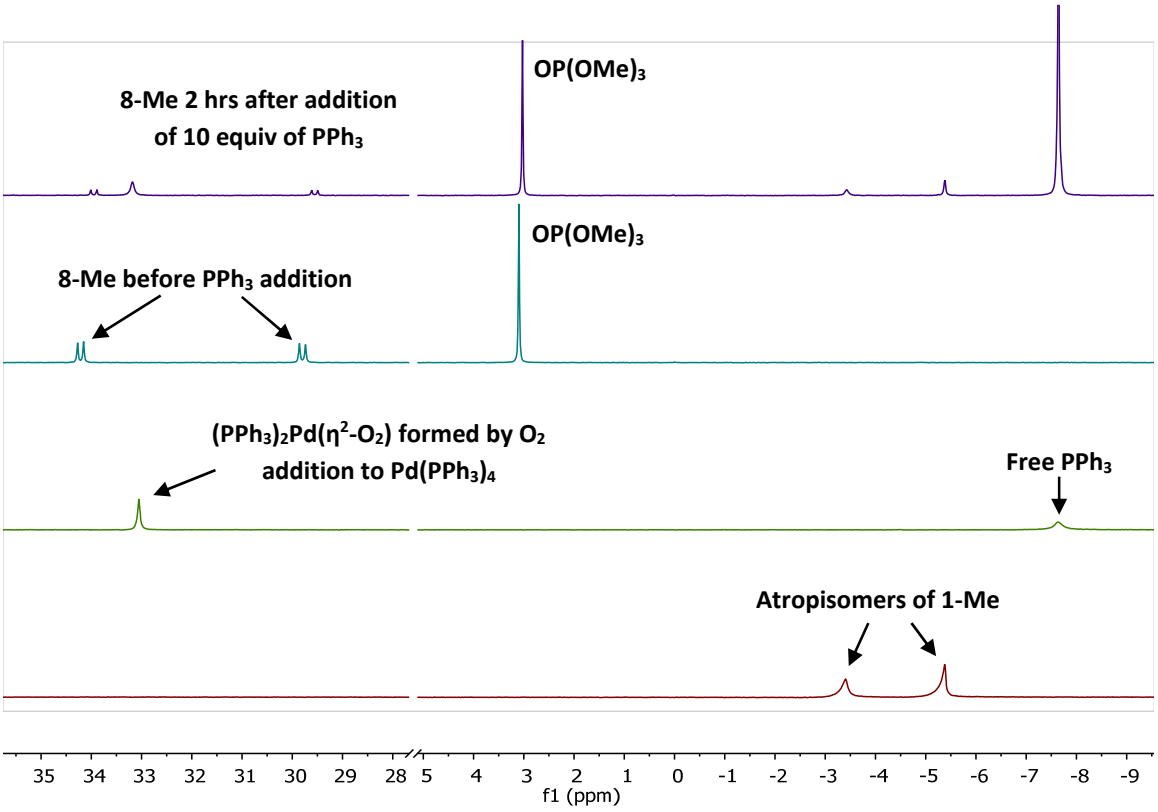

Figure 22. NMR spectra taken at -78 °C in THF confirming the substitution of PPh_3 for **1-Me** in solution in compound **8-Me**.

Methyl-para-tolyl sulfide

No oxidation of the aryl-alkyl sulfide was observed.

Electrochemical Details

Electrochemical measurements of complex **2** and **3** were taken on a Pine Instrument Company biopotentiostat model AFCBP1 as 3 millimolar solutions in tetrahydrofuran using 0.1 molar [*n*Bu_4N][PF_6] as the electrolyte with a platinum wire counter electrode, a glassy carbon working electrode, and a silver/silver nitrate reference electrode in 0.1 molar [*n*Bu_4N][PF_6] as an acetonitrile solution. Electrochemical measurements of compounds were internally referenced to ferrocene.

Crystallographic Information

CCDC 1440560-1440565 contain the supplementary crystallographic data for this paper. These data can be obtained free of charge from The Cambridge Crystallographic Data Centre via www.ccdc.cam.ac.uk/data_request/cif.

Refinement details

In each case, crystals were mounted on a glass fiber or nylon loop using Paratone oil, then placed on the diffractometer under a nitrogen stream. Low temperature (100 K) X-ray data were obtained on a Bruker APEXII CCD based diffractometer (Mo sealed X-ray tube, K_α = 0.71073 Å). All diffractometer manipulations, including data collection, integration and scaling were carried out using the Bruker APEXII software.[35] Absorption corrections were applied using SADABS.[36] Space groups were determined on the basis of systematic absences and intensity statistics and the structures were solved by direct methods using XS (incorporated into SHELXTL) and refined by full-matrix least squares on F^2. All non-hydrogen atoms were refined using anisotropic displacement parameters. Hydrogen atoms were placed in idealized positions and refined using a riding model. The structure was refined (weighted least squares refinement on F^2) to convergence.

Table 2. Crystal and refinement data for reported complexes.

Complex	**2**	**3**	**4-H**	**5-H**	**6-H**	**7-H**
empirical formula	$C_{15}H_{19}Cl_{0.06}Ni_{0.50}OP$	$C_{32}H_{43}O_{2.5}P_2Pd$	$C_{69}H_{88}O_4P_4Pd_2$	$C_{35}H_{48}F_3ClO_6P_2PdS$	$C_{31}H_{41}F_3O_5P_2PdS$	$C_{32.33}H_{43.33}AgF_3O_{5.33}P_2S$
formula wt	277.84	636.00	1318.07	857.58	751.04	776.20
T (K)	100	200	100	100	100	99.98
a, Å	16.8334(5)	24.0630(6)	12.900(3)	13.040(6)	19.7535(3)	31.152(3)
b, Å	16.8334(5)	24.0630(6)	13.564(3)	19.284(8)	19.7535(3)	31.152(3)
c, Å	20.9194(8)	20.9789(6)	19.638(3)	15.679(6)	19.7535(3)	20.2695(18)
α, deg	90	90	106.655(6)	90	110.8200	90
β, deg	90	90	91.342(6)	108.373(18)	110.8200	90
γ, deg	90	90	97.356(5)	90	110.8200	120
V, Å^3	5927.8(4)	12147.4(7)	3258.4(12)	3742(3)	5617.9(3)	17035
Z	16	16	4	4	6	18
cryst syst	Tetragonal	Tetragonal	Triclinic	Monoclinic	Rhombohedral	Trigonal
space group	P2/ncc	P-42$_1$c	P-1	P12$_1$/n1	R3cR	R3c
d_{calcd}, g/cm^3	1.245	1.391	1.344	1.515	1.332	1.362
θ range, deg	1.711 to 36.343	1.197 to 37.310	1.583 to 37.026	1.729 to 36.211	2.17 to 29.22	2.147 to 30.664
μ, mm^{-1}	0.797	0.745	0.696	0.767	0.685	0.723
abs cor	Semi-empirical from equivalents	Semi-empirical from equivalents	Semi-empirical from equivalents	Semi-empirical from equivalents	Semi-empirical from equivalents	Semi-empirical from equivalents
GOF[c]	0.952	1.167	0.874	1.022	0.972	0.904
R1,[a] wR2[b] ($I > 2\sigma(I)$)	0.0406, 0.1039	0.0527, 0.0995	0.0521, 0.0944	0.0529, 0.1286	0.0318, 0.0720	0.0475, 0.1239

[a] $R1 = \Sigma||F_o|-|F_c|| / \Sigma|F_o|$ [b] $wR2 = \{ \Sigma [w(F_o^2-F_c^2)^2] / \Sigma [w(F_o^2)^2] \}^{1/2}$ [c] $GOF = S = \{ \Sigma [w(F_o^2-F_c^2)^2] / (n-p) \}^{1/2}$

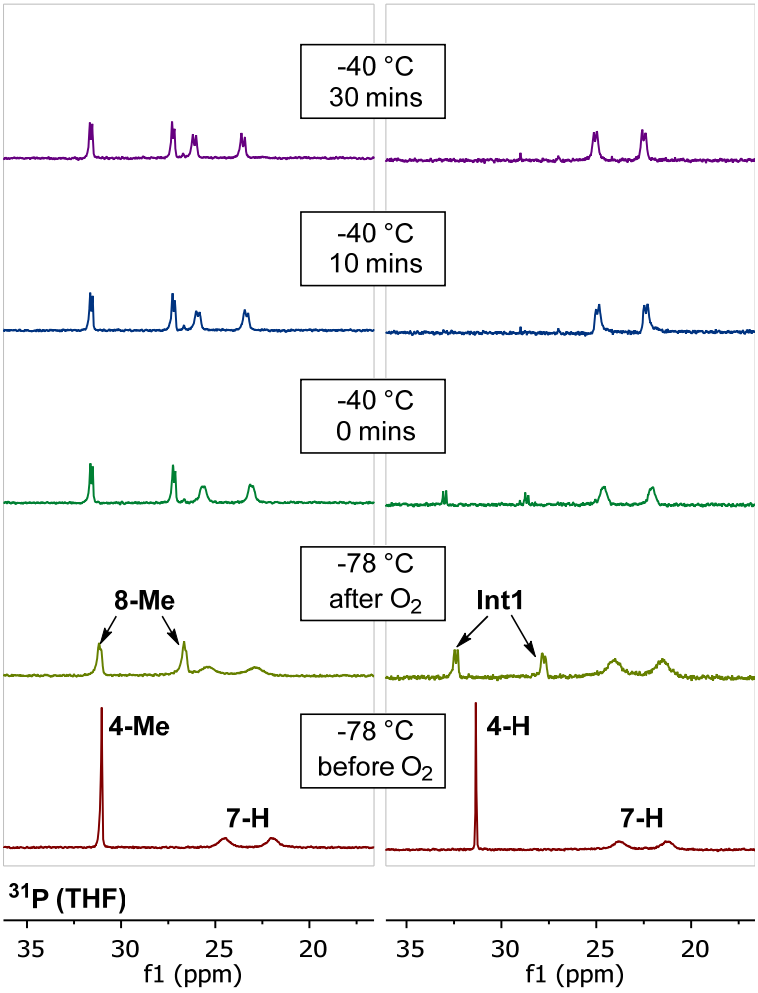

Figure 23. NMR spectra taken at -78 °C in THF confirming the substitution of PPh_3 for **1-Me** in solution in compound **8-Me**.

REFERENCES

1.(a) Costas, M.; Mehn, M. P.; Jensen, M. P.; Que, L., *Chem. Rev.* **2004,** *104*, 939-986; (b) Sono, M.; Roach, M. P.; Coulter, E. D.; Dawson, J. H., *Chem. Rev.* **1996,** *96*, 2841-2888; (c) Whittaker, J. W., *Chem. Rev.* **2003,** *103*, 2347-2363.

2.(a) Chirik, P. J.; Wieghardt, K., *Science* **2010,** *327*, 794-795; (b) Eisenberg, R.; Gray, H. B., *Inorg. Chem.* **2011,** *50*, 9741-9751; (c) Haneline, M. R.; Heyduk, A. F., *J. Am. Chem. Soc.* **2006,** *128*, 8410-8411; (d) Luca, O. R.; Crabtree, R. H., *Chem. Soc. Rev.* **2013,** *42*, 1440-1459; (e) Lyaskovskyy, V.; de Bruin, B., *ACS Catal.* **2012,** *2*, 270-279; (f) Pierpont, C. G., *Coord. Chem. Rev.* **2001,** *216–217*, 99-125; (g) Praneeth, V. K. K.; Ringenberg, M. R.; Ward, T. R., *Angew. Chem. Int. Ed.* **2012,** *51*, 10228-10234; (h) Brown, S. N., *Inorg. Chem.* **2012,** *51*, 1251-1260.

3.(a) Chang, C. J.; Chng, L. L.; Nocera, D. G., *J. Am. Chem. Soc.* **2003,** *125*, 1866-1876; (b) Chaudhuri, P.; Hess, M.; Müller, J.; Hildenbrand, K.; Bill, E.; Weyhermüller, T.; Wieghardt, K., *J. Am. Chem. Soc.* **1999,** *121*, 9599-9610; (c) Hull, J. F.; Himeda, Y.; Wang, W.-H.; Hashiguchi, B.; Periana, R.; Szalda, D. J.; Muckerman, J. T.; Fujita, E., *Nat. Chem.* **2012,** *4*, 383-388; (d) Langer, R.; Leitus, G.; Ben-David, Y.; Milstein, D., *Angew. Chem. Int. Ed.* **2011,** *50*, 2120-2124; (e) Umehara, K.; Kuwata, S.; Ikariya, T., *J. Am. Chem. Soc.* **2013,** *135*, 6754-6757; (f) Vogt, M.; Nerush, A.; Diskin-Posner, Y.; Ben-David, Y.; Milstein, D., *Chem. Sci.* **2014,** *5*, 2043-2051; (g) Carver, C. T.; Matson, B. D.; Mayer, J. M., *J. Am. Chem. Soc.* **2012,** *134*, 5444-5447; (h) Gunanathan, C.; Milstein, D., *Acc. Chem. Res.* **2011,** *44*, 588-602; (i) Kohl, S. W.; Weiner, L.; Schwartsburd, L.; Konstantinovski, L.; Shimon, L. J. W.; Ben-David, Y.; Iron, M. A.; Milstein, D., *Science* **2009,** *324*, 74-77; (j) Rakowski DuBois, M.; DuBois, D. L., *Chem. Soc. Rev.* **2009,** *38*, 62-72.

4.(a) Costentin, C.; Drouet, S.; Robert, M.; Savéant, J.-M., *Science* **2012,** *338*, 90-94; (b) Purse, B. W.; Tran, L.-H.; Piera, J.; Åkermark, B.; Bäckvall, J.-E., *Chem. Eur. J.* **2008,** *14*, 7500-7503; (c) Warren, J. J.; Tronic, T. A.; Mayer, J. M., *Chem. Rev.* **2010,** *110*, 6961-7001; (d) McSkimming, A.; Colbran, S. B., *Chem. Soc. Rev.* **2013,** *42*, 5439-5488; (e) Collman, J. P.; Devaraj, N. K.; Decreau, R. A.; Yang, Y.; Yan, Y. L.; Ebina, W.; Eberspacher, T. A.; Chidsey, C. E. D., *Science* **2007,** *315*, 1565-1568; (f) Lu, F.; Zarkesh, R. A.; Heyduk, A. F., *Eur. J. Inorg. Chem.* **2012**, 467-470.

5.(a) Campbell, A. N.; White, P. B.; Guzei, I. A.; Stahl, S. S., *J. Am. Chem. Soc.* **2010,** *132*, 15116-15119; (b) Gligorich, K. M.; Sigman, M. S., *Chem. Commun.* **2009**, 3854-3867; (c) Muzart, J., *Chem. Asian J.* **2006,** *1*, 508-515; (d) Schultz, M. J.; Sigman, M. S., *Tetrahedron* **2006,** *62*, 8227-8241; (e) Shi, Z. Z.; Zhang, C.; Tang, C. H.; Jiao, N., *Chem. Soc. Rev.* **2012,** *41*, 3381-3430; (f) Sigman, M. S.; Jensen, D. R., *Acc. Chem. Res.* **2006,** *39*, 221-229; (g) Stahl, S. S., *Science* **2005,** *309*, 1824-1826; (h) Stoltz, B. M., *Chem. Lett.* **2004,** *33*, 362-367; (i) Piera, J.; Backvall, J. E., *Angew. Chem. Int. Ed.* **2008,** *47*, 3506-3523.

6.(a) Decharin, N.; Stahl, S. S., *J. Am. Chem. Soc.* **2011,** *133*, 5732-5735; (b) Diao, T.; Stahl, S. S., *Polyhedron* **2014,** *84*, 96-102; (c) Popp, B. V.; Thorman, J. L.; Stahl, S. S., *J. Mol. Cat.* **2006,** *251*, 2-7.

7.Wendlandt, A. E.; Stahl, S. S., *Angew. Chem. Int. Ed.* **2015,** *54*, 14638-14658.

8.Popp, B. V.; Stahl, S. S., *J. Am. Chem. Soc.* **2007,** *129*, 4410-4422.

9.(a) Kumar, A.; Purkait, K.; Dey, S. K.; Sarkar, A.; Mukherjee, A., *Rsc Adv* **2014,** *4*, 35233-35237; (b) Scheuermann, S.; Kretz, T.; Vitze, H.; Bats, J. W.; Bolte, M.; Lerner, H. W.; Wagner, M., *Chem. Eur. J.* **2008,** *14*, 2590-2601; (c) Sembiring, S. B.; Colbran, S. B.; Bishop, R.; Craig, D. C.; Rae, A. D., *Inorg. Chim. Acta* **1995,** *228*, 109-117; (d) Sembiring, S. B.; Colbran, S. B.; Craig, D. C., *Inorg. Chem.* **1995,** *34*, 761-762; (e) Sembiring, S. B.; Colbran, S. B.; Craig, D. C., *J. Chem. Soc., Dalton Trans.* **1999**, 1543-1554.

10.(a) Kim, S. B.; Pike, R. D.; Sweigart, D. A., *Acc. Chem. Res.* **2013,** *46*, 2485-2497; (b) Moussa, J.; Amouri, H., *Angew. Chem. Int. Ed.* **2008,** *47*, 1372-1380; (c) Reingold, J. A.; Uk Son, S.; Bok Kim, S.; Dullaghan, C. A.; Oh, M.; Frake, P. C.; Carpenter, G. B.; Sweigart, D. A., *Dalton Trans.* **2006**, 2385-2398; (d) Damas, A.; Ventura, B.; Axet, M. R.; Degli Esposti, A.; Chamoreau, L. M.; Barbieri, A.; Amouri, H., *Inorg. Chem.* **2010,** *49*, 10762-10764; (e) Le Bras, J.; Amouri, H.; Vaissermann, J., *Organometallics* **1998,** *17*, 1116-1121; (f) Moussa, J.; Rager, M. N.; Chamoreau, L. M.; Ricard, L.; Amouri, H., *Organometallics* **2009,** *28*, 397-404.
11.(a) Buss, J. A.; Edouard, G. A.; Cheng, C.; Shi, J.; Agapie, T., *J. Am. Chem. Soc.* **2014,** *136*, 11272-11275; (b) Chao, S. T.; Lara, N. C.; Lin, S.; Day, M. W.; Agapie, T., *Angew. Chem. Int. Ed.* **2011,** *50*, 7529-7532; (c) Henthorn, J. T.; Lin, S. B.; Agapie, T., *J. Am. Chem. Soc.* **2015,** *137*, 1458-1464; (d) Herbert, D. E.; Lara, N. C.; Agapie, T., *Chem. Eur. J.* **2013,** *19*, 16453-16460; (e) Horak, K. T.; Velian, A.; Day, M. W.; Agapie, T., *Chem. Commun.* **2014,** *50*, 4427-4429; (f) Kelley, P.; Lin, S.; Edouard, G.; Day, M. W.; Agapie, T., *J. Am. Chem. Soc.* **2012,** *134*, 5480-5483; (g) Lin, S.; Day, M. W.; Agapie, T., *J. Am. Chem. Soc.* **2011,** *133*, 3828-3831; (h) Suseno, S.; Agapie, T., *Organometallics* **2013,** *32*, 3161-3164; (i) Suseno, S.; Horak, K. T.; Day, M. W.; Agapie, T., *Organometallics* **2013,** *32*, 6883-6886; (j) Velian, A.; Lin, S.; Miller, A. J. M.; Day, M. W.; Agapie, T., *J. Am. Chem. Soc.* **2010,** *132*, 6296-6297.
12.Moore, H. W.; Sing, Y.-L. L.; Sidhu, R. S., *J. Org. Chem.* **1980,** *45*, 5057-5064.
13.(a) Glick, M. D.; Dahl, L. F., *J. Organomet. Chem.* **1965,** *3*, 200-&; (b) Klein, H. F.; Auer, E.; Dal, A.; Lemke, U.; Lemke, M.; Jung, T.; Rohr, C.; Florke, U.; Haupt, H. J., *Inorg. Chim. Acta* **1999,** *287*, 167-172; (c) Canovese, L.; Visentin, F.; Santo, C.; Bertolasi, V., *J. Organomet. Chem.* **2014,** *749*, 379-386; (d) Milani, B.; Anzilutti, A.; Vicentini, L.; Santi, A. S. O.; Zangrando, E.; Geremia, S.; Mestroni, G., *Organometallics* **1997,** *16*, 5064-5075; (e) Tschoerner, M.; Trabesinger, G.; Albinati, A.; Pregosin, P. S., *Organometallics* **1997,** *16*, 3447-3453.
14.(a) Schrauzer, G. N.; Dewhirst, K. C., *J. Am. Chem. Soc.* **1964,** *86*, 3265-3270; (b) Schrauzer, G. N.; Kratel, G., *J. Organomet. Chem.* **1964,** *2*, 336-346.
15.(a) Aleksand.Gg; Struchko.Yt, *Zh. Strukt. Khim.* **1973,** *14*, 1067-1074; (b) Yamamoto, Y.; Ohno, T.; Itoh, K., *Organometallics* **2003,** *22*, 2267-2272; (c) Selvakumar, K.; Zapf, A.; Spannenberg, A.; Beller, M., *Chem. Eur. J.* **2002,** *8*, 3901-3906.
16.(a) Clegg, W.; Eastham, G. R.; Elsegood, M. R. J.; Heaton, B. T.; Iggo, J. A.; Tooze, R. P.; Whyman, R.; Zacchini, S., *J. Chem. Soc., Dalton Trans.* **2002**, 3300-3308; (b) Kulik, A. V.; Bruk, L. G.; Temkin, O. N.; Khabibulin, V. R.; Belsky, V. K.; Zavodnik, V. E., *Mendeleev Commun.* **2002**, 47-48; (c) Liu, J. K.; Jacob, C.; Sheridan, K. J.; Al-Mosule, F.; Heaton, B. T.; Iggo, J. A.; Matthews, M.; Pelletier, J.; Whyman, R.; Bickley, J. F.; Steiner, A., *Dalton Trans.* **2010,** *39*, 7921-7935.
17.Kaftory, M.; Tanaka, K.; Toda, F., *J. Org. Chem.* **1985,** *50*, 2154-2158.
18.(a) Scheuermann, M. L.; Goldberg, K. I., *Chem. Eur. J.* **2014,** *20*, 14556-14568; (b) Boisvert, L.; Goldberg, K. I., *Acc. Chem. Res.* **2012,** *45*, 899-910.
19.(a) Aboelella, N. W.; York, J. T.; Reynolds, A. M.; Fujita, K.; Kinsinger, C. R.; Cramer, C. J.; Riordan, C. G.; Tolman, W. B., *Chem. Commun.* **2004**, 1716-1717; (b) Adjabeng, G.; Brenstrum, T.; Frampton, C. S.; Robertson, A. J.; Hillhouse, J.; McNulty, J.; Capretta, A., *J. Org. Chem.* **2004,** *69*, 5082-5086; (c) Erhardt, S.; Grushin, V. V.; Kilpatrick, A. H.; Macgregor, S. A.; Marshall, W. J.; Roe, D. C., *J. Am. Chem. Soc.* **2008,** *130*, 4828-4845; (d) Fantasia, S.; Egbert, J. D.; Jurcik, V.; Cazin, C. S. J.; Jacobsen, H.; Cavallo, L.; Heinekey, D. M.; Nolan, S. P., *Angew. Chem. Int. Ed.* **2009,** *48*, 5182-5186; (e) Fantasia, S.; Nolan, S. P., *Chem. Eur. J.* **2008,** *14*, 6987-6993; (f) Gramage-Doria, R.; Armspach, D.; Matt, D.; Toupet, L., *Chem. Eur. J.* **2012,** *18*, 10813-10816; (g) Halligudi, S. B.; Bhatt, K. N.; Khan, N. H.; Kurashy, R. I.; Venkatsubramanian, K., *Polyhedron* **1996,** *15*, 2093-2101; (h) Jurcik, V.; Schmid, T. E.;

Dumont, Q.; Slawin, A. M. Z.; Cazin, C. S. J., *Dalton Trans.* **2012,** *41*, 12619-12623; (i) Konnick, M. M.; Guzei, I. A.; Stahl, S. S., *J. Am. Chem. Soc.* **2004,** *126*, 10212-10213; (j) Labios, L. A.; Millard, M. D.; Rheingold, A. L.; Figueroa, J. S., *J. Am. Chem. Soc.* **2009,** *131*, 11318-11319; (k) Miyaji, T.; Kujime, M.; Hikichi, S.; Moro-oka, Y.; Akita, M., *Inorg. Chem.* **2002,** *41*, 5286-5295; (l) Sergeev, A. G.; Neumann, H.; Spannenberg, A.; Beller, M., *Organometallics* **2010,** *29*, 3368-3373; (m) Stahl, S. S.; Thorman, J. L.; Nelson, R. C.; Kozee, M. A., *J. Am. Chem. Soc.* **2001,** *123*, 7188-7189; (n) Tsubomura, T.; Murota, H.; Takao, K., *Inorg. Chem. Commun.* **2013,** *35*, 110-112; (o) Walther, D.; Lamm, K.; Gorls, H., *Z. Anorg. Allg. Chem.* **2009,** *635*, 1187-1195; (p) Yamashita, M.; Goto, K.; Kawashima, T., *J. Am. Chem. Soc.* **2005,** *127*, 7294-7295; (q) Yoshida, T.; Tatsumi, K.; Matsumoto, M.; Nakatsu, K.; Nakamura, A.; Fueno, T.; Otsuka, S., *Nouv. J. Chim.* **1979,** *3*, 761-774.
20.Cai, X. C.; Majumdar, S.; Fortman, G. C.; Cazin, C. S. J.; Slawin, A. M. Z.; Lhermitte, C.; Prabhakar, R.; Germain, M. E.; Palluccio, T.; Nolan, S. P.; Rybak-Akimova, E. V.; Temprado, M.; Captain, B.; Hoff, C. D., *J. Am. Chem. Soc.* **2011,** *133*, 1290-1293.
21.Scheuermann, M. L.; Boyce, D. W.; Grice, K. A.; Kaminsky, W.; Stoll, S.; Tolman, W. B.; Swang, O.; Goldberg, K. I., *Angew. Chem. Int. Ed.* **2014,** *53*, 6492-6495.
22.(a) Denney, M. C.; Smythe, N. A.; Cetto, K. L.; Kemp, R. A.; Goldberg, K. I., *J. Am. Chem. Soc.* **2006,** *128*, 2508-2509; (b) Keith, J. M.; Muller, R. P.; Kemp, R. A.; Goldberg, K. I.; Goddard, W. A.; Oxgaard, J., *Inorg. Chem.* **2006,** *45*, 9631-9633; (c) Konnick, M. M.; Decharin, N.; Popp, B. V.; Stahl, S. S., *Chem. Sci.* **2011,** *2*, 326-330; (d) Konnick, M. M.; Gandhi, B. A.; Guzei, I. A.; Stahl, S. S., *Angew. Chem. Int. Ed.* **2006,** *45*, 2904-2907.
23.(a) Goor, G.; Glenneberg, J.; Jacobi, S., Hydrogen Peroxide. In *Ullmann's Encyclopedia of Industrial Chemistry*, Wiley-VCH Verlag GmbH & Co. KGaA: 2000; (b) Nishimi, T.; Kamachi, T.; Kato, K.; Kato, T.; Yoshizawa, K., *Eur. J. Org. Chem.* **2011,** *2011*, 4113-4120.
24.Resonance Raman experiments in 2-methyl tetrahydrofuran using wavelengths accessible to an Ar ion laser were attempted for Int1 and 8-Me. Depending on the excitation wavelength no signals from compound were detected of fluorescence from the ligand precluded the observation of bands corresponding to the O-O stretch in the peroxo species.
25.(a) Geiger, R. A.; Chattopadhyay, S.; Day, V. W.; Jackson, T. A., *Dalton Trans.* **2011,** *40*, 1707-1715; (b) Kim, J.; Shin, B.; Kim, H.; Lee, J.; Kang, J.; Yanagisawa, S.; Ogura, T.; Masuda, H.; Ozawa, T.; Cho, J., *Inorg. Chem.* **2015,** *54*, 6176-6183; (c) Miller, C. G.; Gordon-Wylie, S. W.; Horwitz, C. P.; Strazisar, S. A.; Peraino, D. K.; Clark, G. R.; Weintraub, S. T.; Collins, T. J., *J. Am. Chem. Soc.* **1998,** *120*, 11540-11541; (d) Park, J.; Morimoto, Y.; Lee, Y.-M.; Nam, W.; Fukuzumi, S., *J. Am. Chem. Soc.* **2011,** *133*, 5236-5239.
26.As with Int1 and 8-Me, resonance Raman experiments using an Ar ion laser were attempted on aliquots of Int2 and Int3 from UV/Vis experiments. However, again ligand fluoresence precluded the observation of bands corresponding to any O-O stretches.
27.Pangborn, A. B.; Giardello, M. A.; Grubbs, R. H.; Rosen, R. K.; Timmers, F. J., *Organometallics* **1996,** *15*, 1518-1520.
28.Berliner, M. A.; Belecki, K., *J. Org. Chem.* **2005,** *70*, 9618-9621.
29.Eisch, J. J.; Piotrowski, A. M.; Han, K. I.; Kruger, C.; Tsay, Y. H., *Organometallics* **1985,** *4*, 224-231.
30.Wariishi, K.; Morishima, S.; Inagaki, Y., *Org. Process Res. Dev.* **2003,** *7*, 98-100.
31.Zhang, J. X.; Cui, Y. P.; Wang, M. L.; Liu, J. Z., *Chem. Commun.* **2002**, 2526-2527.
32.Horak, K. T.; Lin, S.; Rittle, J.; Agapie, T., *Organometallics* **2015,** *34*, 4429-4432.
33.Fulmer, G. R.; Miller, A. J. M.; Sherden, N. H.; Gottlieb, H. E.; Nudelman, A.; Stoltz, B. M.; Bercaw, J. E.; Goldberg, K. I., *Organometallics* **2010,** *29*, 2176-2179.

34.Velian, A.; Lin, S. B.; Miller, A. J. M.; Day, M. W.; Agapie, T., *J Am Chem Soc* **2010,** *132*, 6296-6297.
35.APEX2, Version 2 User Manual, M86-E01078, Bruker Analytical X-ray Systems, Madison, WI, June 2006.
36.Sheldrick, G. M. "SADABS (Version 2008/1): Program for Absorption Correction for Data from Area Detector Frames", University of Göttingen, 2008.

CHAPTER 4

SYNTHESIS AND REACTIVITY OF METAL COMPLEXES SUPPORTED BY A PYRIDINE DIPHOSPHINE LIGAND WITH TUNABLE ELECTRONICS UTILIZING REMOTE LEWIS ACID BINDING

The text for this chapter was reproduced in part from:

Horak, K. T.; VanderVelde, D. G.; Agapie, T. *Organometallics*, **2015**, *34*, 4753-4765.

Abstract

Metal complexes supported by ligands with chemically modifiable pendant groups are of interest for controlling reactivity. We report on the coordination chemistry and reactivity of a multidentate phosphine ligand framework that contains Lewis acid binding sites. 3,5-Bis-(2-phosphinophenyl)-pyridine coordinates low oxidation state metal centers such as Ni^0 and Pd^0 via the phosphine donors and the π-system of the heterocycle. Electrophilic reagents such as $B(C_6F_5)_3$, Me^+, and BCy_2OTf were demonstrated to bind the available pyridine nitrogen, generating the Ni complexes (**2Ni-B(C$_6$F$_5$)$_3$**, **2Ni-Me**, **2Ni-BCy$_2$OTf**). Analogous compounds were prepared for Pd (**2Pd**, **2Pd-B(C$_6$F$_5$)$_3$**, **2Pd-H**). The effect of Lewis acid binding was evaluated by single crystal X-ray diffraction studies and spectroscopy. Lewis acid binding to **2Pd** leads to a stronger η^1 interaction between the metal and the heterocycle π-system. Ni binds in an η^2 fashion, but the Lewis acid-free species is not monomeric. Ni coordination results in disruption of pyridine aromaticity as indicated by localization of double- and single-bond character in the solid state. CO adducts were prepared for Lewis acid-free (**4Ni(CO)**) and Lewis acid–bound species (H^+–, Me^+–, and $B(C_6F_5)_3$–bound; **4Ni(CO)-H**, **4Ni(CO)-Me**, **4Ni(CO)-B(C$_6$F$_5$)$_3$**) that show a significant shift of the CO stretching frequency from 1930 cm^{-1} to 1966-1976 cm^{-1}, respectively, clearly indicating communication of ligand electronics to the metal center. A NO adduct (**5Ni**) with negligible metal-pyridine interactions was obtained upon sequential reaction of **2Ni** with $[OMe_3][BF_4]$ then $[NO][BF_4]$. Treatment of **2Ni** with silanes and boranes results in pyridine dearomatization involving heteroatom-H bond activation with the heteroatom binding to the pyridine nitrogen, and the hydrides delivered to the *ortho* positon of pyridine. This demonstrates that the electronics of the pendant

pyridine are drastically affected upon metal binding and enables unusual ligand-based substrate activation. The described chemistry highlights a strategy for tuning the properties of metal centers by ligand post-synthetic modifications.

INTRODUCTION

Alterations to ligand electronics can dramatically alter the properties of transition metal complexes. Efforts to develop chemically switchable ligands that show variable ligand electronics have been explored.[1] One such strategy has involved the binding of the Lewis acids to sites on the ligand framework to remotely tune the electronics.[2] This approach is amenable to the late-stage, modular tuning of ligand electronics, and serves as a way to rapidly assemble a range of complexes from a common precursor thereby avoiding the potentially time-consuming independent synthesis of multiple ligands. For SXS[3] and PXP[4] pincer ligands, where X is either an aryl or pyridine carbon or a pyridine or pyrazine nitrogen, remote hydroxyl, amino, or basic N-heterocycle sites have been incorporated into the ligand scaffold. However, the systematic functionalization of these groups with Lewis acids has not been reported, to the authors' knowledge. Our group has previously studied *meta*-substituted bis(phosphinoaryl)benzene ligand systems that bind in a P-arene-P pincer geometry (Figure 1).[5] Related diphosphines with other pendant π-systems have been reported.[6] *m*P_2Ni was found to coordinate a variety of ligands, and Ni methylidene and Ni imide complexes were implicated as intermediates that perform further intramolecular chemistry, such as CH amination. Complexes displaying Ni-ligand multiple bonding have been elegantly synthesized and studied by Hillhouse *et al.* and others.[7] As an alternative to the central arene donor in *m*P_2Ni, pyridine is known to bind a variety of electrophiles under mild conditions that can significantly alter the electronics and reaction chemistry of the heterocycle.[8] The properties of metal complexes bound to pyridine π-systems have been shown to be influenced by N-functionalization of the pyridine.[9] Herein, we report the synthesis and characterization of π-bound nickel and palladium complexes supported by a diphosphine ligand containing a π-coordinated pyridine

moiety that can be functionalized with electrophiles to alter the properties of the metal complex.

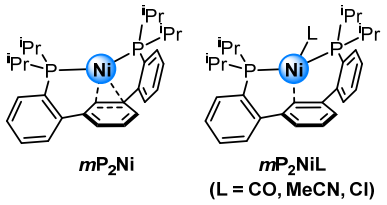

Figure 1. Ni complexes of *meta*-terphenyldiphosphine ligands.

RESULTS AND DISCUSSION

Section 4.1 Ligand Synthesis

Scheme 1. Synthesis of ligand 1

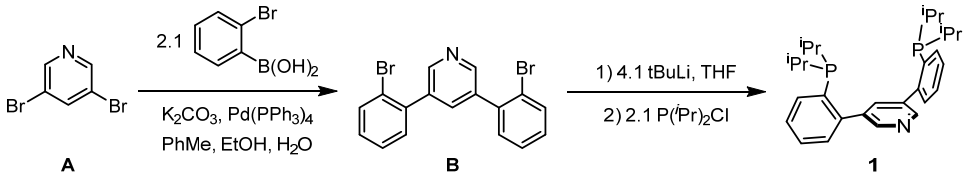

The desired ligand (**1**) was synthesized in two steps from commercially available starting materials. 3,5-(2-bromophenyl)pyridine (**B**) was synthesized from 3,5-dibromopyridine (**A**) and 2-bromophenylboronic acid in a palladium-catalyzed Suzuki coupling reaction and could be isolated as a colorless material following recrystallization. Subsequent phosphination was accomplished using a lithium halogen exchange reaction with *tert*-butyl lithium (*t*BuLi) followed by the addition of $P(^{i}Pr)_2Cl$ as an electrophile. Following workup, **1** could be isolated in gram quantities as a colorless powder.

Section 4.2 Synthesis and Electrophile Reactivity of Ni and Pd Complexes.

Metallations with nickel and palladium precursors were targeted as these metals are known to readily bind to related P-arene-P ligands (Scheme 2).[5a, 5b, 10] Mixing benzene solutions of **1**

and bis(1,5-cyclooctadiene)nickel(0) ($Ni(COD)_2$) in a stoichiometric ratio yielded **2Ni** as a brown solid after removal of volatile materials. The corresponding palladium complex (**2Pd**) was synthesized cleanly starting from palladium dimethyl (N,N,N',N'-tetramethylethylenediamine) (TMEDA) with mild heating to 70 °C for 16 hours. After workup **2Pd** could be isolated as an orange solid.

Scheme 2. Synthesis of nickel and palladium complexes

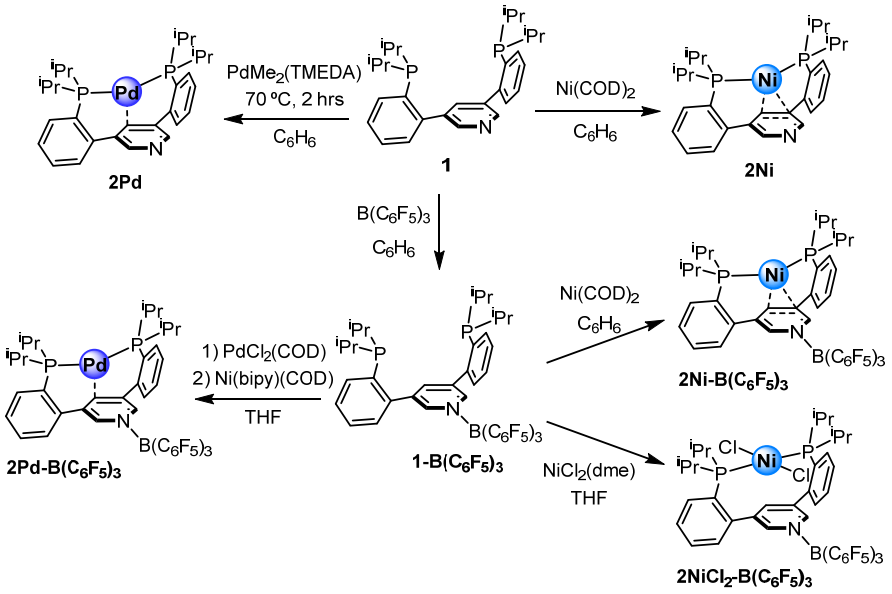

Solution NMR spectroscopic data for **2Ni** and **2Pd** are consistent with pseudo-C_s structures with single ^{31}P resonances at 40.32 and 33.76 ppm and two distinct isopropyl methine ^{1}H resonances at (2.28, 2.07) and (2.12, 1.86) ppm respectively. *m*P_2Ni has previously been shown to have a C_1 structure in the solid-state arising from η^2 coordination to the central arene π-system despite possessing pseudo-C_s solution NMR characteristics. This suggests that solution NMR data for **2Ni** and **2Pd** could arise from changes in metal-pyridine **π-system** coordination modes on the NMR time scale, resulting in apparent symmetry across the plane perpendicular to the pyridine ring containing the nitrogen and *para*-pyridyl carbon. The ^{31}P NMR spectrum at room temperature for **2Ni** is a broad singlet, which is suggestive of a slow

dynamic process. This is corroborated by the ^{1}H NMR where broadened resonances for the central pyridine protons are observed at 7.82 and 4.35 ppm for the *ortho*-pyridyl (C3 and C4 protons) and *para*-pyridyl (C1 proton) signals respectively. The proton signals are significantly upfield shifted from that of the free ligand at 8.96 and 7.89 ppm. This indicates significant disruption of pyridine electronic environment upon binding of the nickel center as seen with Ni complexes on related ligand platforms.[5a, 11] The *H*-C1 shows the largest upfield shift, consistent with that proton being directly bonded to the carbon atom that shows the strongest interactions with the nickel center. Cooling a sample of **2Ni** in d_8-toluene to -80 °C freezes out the fluxional process evident at room temperature leading to the observation of two pairs of coupling ^{31}P resonances at (46.07, 40.63 ppm ($^{2}J_{PP}$ = 75.0 Hz)) and (23.69, 22.79 ppm ($^{2}J_{PP}$ = 85.6 Hz)) of equal integration (Figure 2). These data suggest a dimerization process may be occurring likely arising due to pyridine coordination to a Ni center in another equivalent of complex. The pyridine protons of **2Pd** appear at 8.29 and 7.90 ppm for C3/C4 and C1 protons respectively. Interestingly, the *H*-C1 does not show any upfield shift and instead the *H*-C3/C4 show the larger upfield deviation from **1**. This is suggestive of comparatively weaker metal-pyridine π-system interaction and is consistent with palladium being less effective at backbonding than nickel.

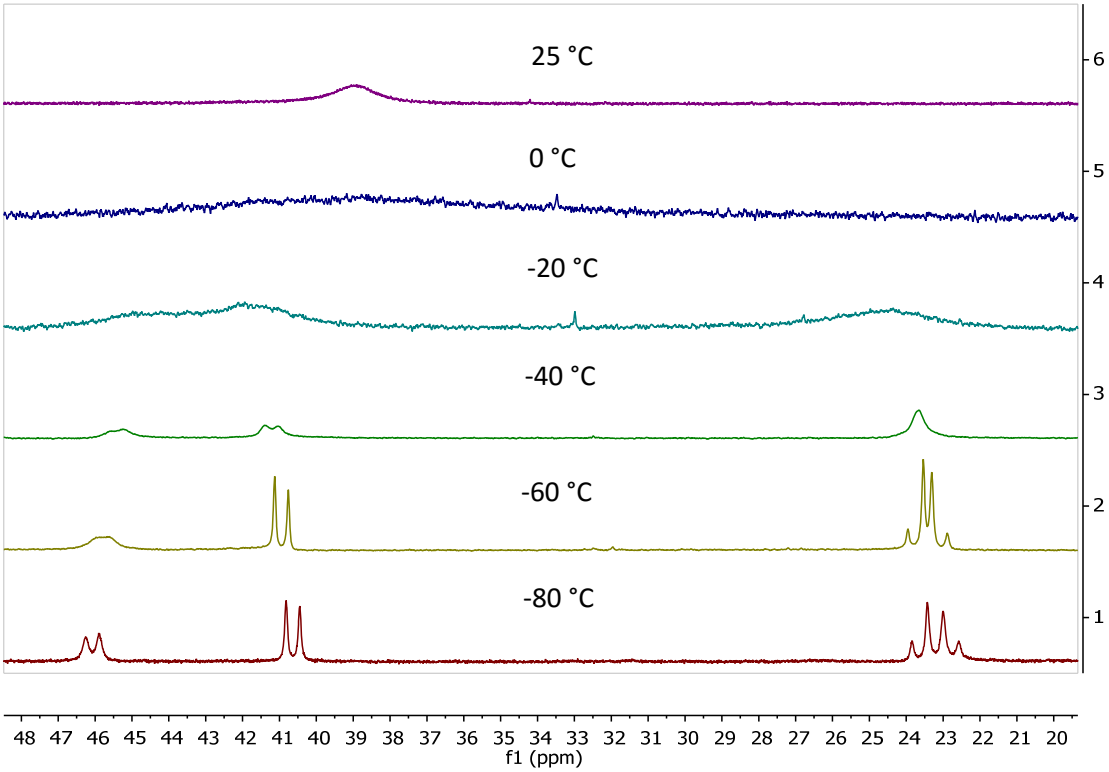

Figure 2. Variable temperature NMR (202 MHz ^{31}P, d_8-toluene) data for **2Ni**.

Attempts to selectively functionalize the pyridine nitrogen of **1** with Lewis acids prior to metallation were challenged by lack of selectivity relative to binding to phosphine. However, tris(pentafluorophenyl)borane ($B(C_6F_5)_3$) was found to coordinate to **1** exclusively through the pyridine nitrogen to yield **1-B(C_6F_5)$_3$** by NMR spectroscopy. **1-B(C_6F_5)$_3$** shows a single ^{31}P resonance at -5.58 ppm, which is close to that of the **1** (-5.75 ppm). The C3/C4 and C1 protons are also only slightly shifted and appear at 8.82 and 8.04 ppm respectively. ^{19}F NMR show three resonances at -131.46, -155.96, and -162.87 ppm shifted from the resonances of free borane (-130.29, -143.60, and -161.54 ppm), and consistent with four-coordinate boron.[12] These data are inconsistent with borane binding to a phosphine moiety as a significant ^{31}P shift is expected[13] in addition to asymmetry in the pyridine protons if only one equivalent of borane was bound. The observed binding selectivity is assigned to the large steric profile of

the borane, which disfavors binding to more sterically hindered phosphine donors compared to the pyridine nitrogen.

Scheme 3. Electrophile functionalization of pyridine nitrogen

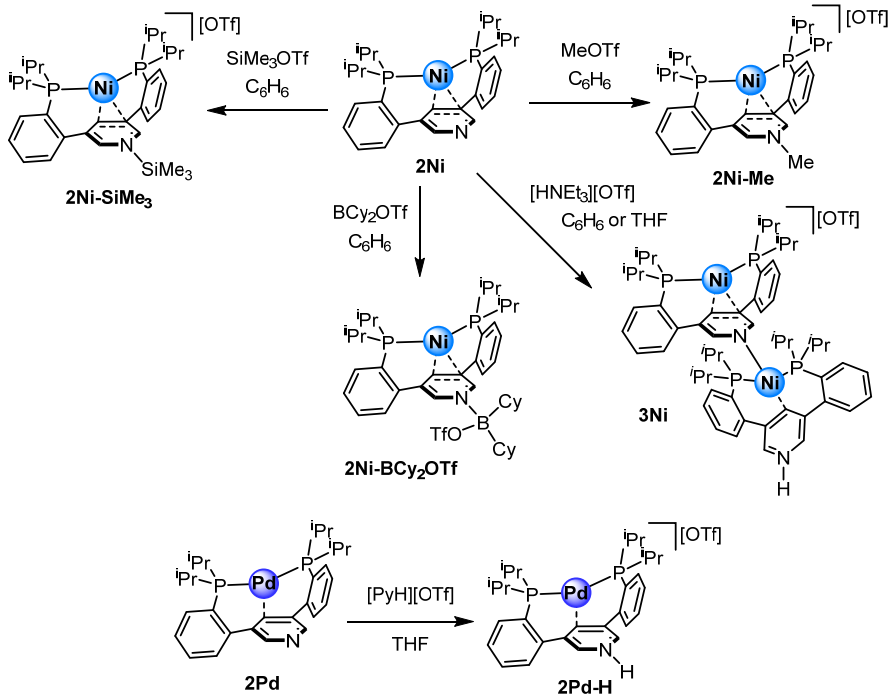

Analogous metallation procedures with $Ni(COD)_2$ were found to be effective with **1-B(C_6F_5)$_3$**, yielding **2Ni-B(C_6F_5)$_3$** as a dark brown solid in (Scheme 2). Additionally, a clean metallation with $NiCl_2$(dme) was observed to yield **2NiCl$_2$-B(C_6F_5)$_3$**. A one-pot procedure starting from Pd^{II} was found to be the most effective way to access **2Pd-B(C_6F_5)$_3$**. Initial metallation of $PdCl_2$(COD) produced a homogeneous orange solution, presumed to be a $PdCl_2$ complex supported by **1-B(C_6F_5)$_3$**. This was followed by reduction with (2,2'-bipyridine)(COD)nickel(0) to yield the desired Pd^0 complex. After workup **2Pd-B(C_6F_5)$_3$** was isolated as a bright pink solid.

^{1}H NMR data of **2Ni-B(C_6F_5)$_3$** and **2Pd-B(C_6F_5)$_3$** show single ^{31}P resonances at 41.94 and 34.06 ppm and two distinct isopropyl methine ^{1}H resonances at (2.07, 1.78) and (2.02,

1.69) ppm, respectively. These data are consistent with a pseudo-C_s symmetric structure or a fluxional process in solution. Interesting only small differences in ^{31}P NMR shifts are seen between **2Ni** and **2Ni-B(C_6F_5)$_3$** despite the binding of B(C_6F_5)$_3$ to the pyridine nitrogen, indicating that ^{31}P NMR is either not a good indicator of electronic changes caused by Lewis acid binding or that the P-atoms are not significantly affected. ^{19}F NMR data show sets of three signals (**2Ni-B(C_6F_5)$_3$**: -131.35, -157.46, -163.85 ppm; **2Pd-B(C_6F_5)$_3$** -131.04, -157.36, -163.73 ppm), at similar chemical shifts as for **1-B(C_6F_5)$_3$**, consistent with pyridine coordination of B(C_6F_5)$_3$. In contrast to ^{31}P NMR, the ^{1}H NMR spectra of compound **2Ni-B(C_6F_5)$_3$** show a further upfield shift of the pyridine protons, with the *H*-C1 signal showing at 3.18 ppm compared to 4.35 ppm for **2Ni**. This shift is likely due to the electronic effect caused by binding of the Lewis acid. The electron withdrawing B(C_6F_5)$_3$ group to the pyridine nitrogen results in the central pyridine ring becoming a better π-acceptor ligand for the electron-rich Ni^0 center. Consequently, strong metal-pyridine π-system interactions result in an even greater upfield shift of the *H*-C1 compared to **2Ni**. Consistent with the NMR data for analogous nickel complex, **2Pd-B(C_6F_5)$_3$** also shows a significant upfield shift in the central pyridine protons with the *H*-C3/C4 signals at 7.69 and *H*-C1 signal at 6.39 ppm. While **2Pd** showed a *H*-C1 pyridine resonance essentially the same as free phosphine, **1**, the upfield shift in **2Pd-B(C_6F_5)$_3$** indicates a significant metal-pyridine π-system interaction that results from the more electron deficient borane-bound pyridine.

2NiCl$_2$-B(C_6F_5)$_3$ is not expected to have a metal-pyridine π-system interaction based on previous reports from group for a related ***m*P$_2$NiCl$_2$** compound.[5a] Consistent with this assignment is the absence of upfield shifted NMR resonances corresponding to the central pyridine ring. Instead a substantial downfield shift of the central pyridine C1-*H* resonance compared to free ligand is observed (δ(ppm) **2NiCl$_2$-B(C_6F_5)$_3$**: 10.84, **1-B(C_6F_5)$_3$**: 8.04). A

comparable shift in the C3/C4 proton resonances is not observed again highlighting to increased sensitivity of the C1 protons to the metal center (δ(ppm) **2NiCl$_2$-B(C$_6$F$_5$)$_3$**: 8.57, **1-B(C$_6$F$_5$)$_3$**: 8.82). **2NiCl$_2$-B(C$_6$F$_5$)$_3$** shows two distinct methine proton resonances (2.46, 1.56 ppm) and a single ^{31}P signal at 7.51 ppm. These data are consistent with a pseudo-C_s symmetric structure or a fluxional process in solution. This unusual chemical shift for the C1 proton (10.42 ppm) has been previously observed in a related complex, ***m*P$_2$NiCl$_2$**, again supporting a similar structural assignment.

To expand the series of Lewis acids investigated, functionalization of the pyridine nitrogen was attempted starting with metallated species, **2Ni** and **2Pd**, by reaction with various electrophiles. **2Ni** was found to react quantitatively with methyl triflate and dicyclohexylboron triflate to yield **2Ni-Me** and **2Ni-BCy$_2$OTf,** respectively (Scheme 3), that were both obtained as dark brown solids. Trimethylsilyl triflate was also found to generate a new green species, **2Ni-SiMe$_3$**, by NMR. However, this compound was not stable likely due to loss of silylation of the glass, though the use of presilylated NMR tubes improved the lifetime of the compound. NMR evidence indicates selective derivatization of the pyridine nitrogen by the electrophile rather than a nickel-based reaction such as an oxidative addition. **2Ni-Me** displays a single ^{31}P resonance at 31.13 ppm and two distinct isopropyl methine ^{1}H resonances at 2.57 and 2.45 ppm, consistent with a C_s symmetric structure or a fluxional process in solution. The methyl protons that do not correspond to the isopropyl substituents of **2Ni-Me** appear at 2.77 ppm and do not show ^{31}P coupling. This chemical shift and lack of 3-bond coupling to phosphorus indicate that methylation has not occurred at the metal center, but rather at the pyridine nitrogen. Of particular note is the chemical shift for the *H*-C1 of the pyridine which appears as a triplet (J =5.03 Hz) at 1.95 ppm, *further* upfield than the aliphatic isopropyl methine protons. ^{31}P decoupling the ^{1}H spectrum results in an singlet resonance for the *H*-C1,

indicating that coupling to two equivalent ^{31}P nuclei results in the observed triplet. This significantly upfield shifted *H*-C1 and *H*-C3/C4 (6.76 ppm) resonances again indicates a substantial Ni-pyridine π-system interaction that is stronger than either **2Ni** or **2Ni-B(C_6F_5)$_3$**. This likely arises from the cationic nature of the electrophile bound to the pyridine nitrogen ($B(C_6F_5)_3$ vs Me^+) which results in a substantially more electron deficient central pyridine. For **2Ni-BCy$_2$OTf** the cyclohexyl substituents complicate the aliphatic region of the ^1H NMR spectrum. However, the *H*-C1 can be assigned to a peak at 3.45 ppm, close to that of **2Ni-B(C_6F_5)$_3$**. The ^{31}P NMR chemical shift 42.29 ppm again is only slightly shifted from **2Ni**.

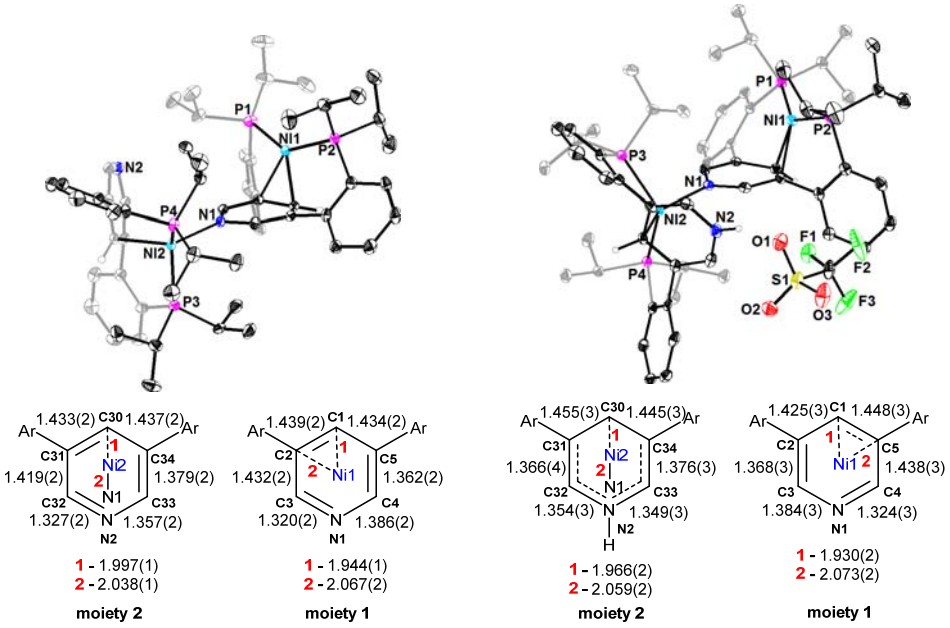

Figure 3. Solid-state structures and selected bond metrics for (left to right) **2Ni** and **3Ni**. Hydrogen atoms and solvent have been omitted for clarity.

The reaction of triethylammonium triflate (Scheme 3) with **2Ni** selectively forms a dinuclear mono-protonated species, **3Ni**, (Figure 1), which precipitates out of reaction mixtures when run in benzene though tetrahydrofuran is also compatible as a solvent (vide infra). Pyridinium triflate was found to cleanly react with **2Pd** to produce a mononuclear

complex, as a pink material (**2Pd-H**). Reactions of **2Pd** with other electrophiles yielded complex mixtures of products and were not pursued further. In line with other complexes, **2Pd-H** is C_s symmetric in solution with a ^{31}P NMR resonance at 32.08 ppm and two distinct isopropyl methine ^{1}H resonances at 2.77 and 2.30 ppm in d_3-acetonitrile. Upfield shifted *H*-C3/C4 (7.28 ppm) and *H*-C1 (6.16 ppm) resonances are observed, and are consistent with metal-pyridine π-system interactions that are stronger than in **2Pd** and comparable to those seen in **2Pd-B(C$_6$F$_5$)$_3$**. Importantly, the proton resonance derived from the pyridinium triflate is seen as a broad resonance at 9.88 ppm. This is a region is consistent with a pyridinium moiety not a palladium hydride. Furthermore, no apparent coupling to ^{31}P nuclei is observed, which would be expected in the case of a Pd-H moiety. These results agree with the results of reactivity **2Ni** with electrophiles, which demonstrate that selective derivatization of the pyridine nitrogen is also possible with Pd.

Solid-state structures were obtained by single crystal X-ray diffraction (XRD) studies. **2Ni** was found to crystallize as a dinuclear species with the pyridine nitrogen of one equivalent of complex (moiety 1) binding to the nickel center of the other (moiety 2) (Figure 3). The observed dimerization in the solid state agrees well with the ^{31}P solution NMR data obtained for **2Ni** at -80 °C suggesting the reversible pyridine coordination is responsible for the observed broadening of ^{1}H and ^{31}P signals at room temperature. Consistent with structures of Ni^0 complexes on related ligands,[5a, 5c, 11] the metal center in moiety 1 of **2Ni** binds to the central pyridine in an η^2 fashion with Ni–C1 and Ni–C2 distances of 1.944(1) and 2.067(1) Å respectively. Disrupted aromaticity is evident from the central pyridine bond metrics by comparing bond distances for C2–C3 (1.432(2) Å) to C4–C5 (1.362(2) Å) and C3–N1 (1.320(2) Å) to C4–N1 (1.386(2) Å). The significant differences seen in each of these pairs of bond distances highlights the partial localization of double bond character around the central

pyridine ring. Significant backbonding from Ni is also evident from the C1–C2 distance (1.439(2) Å), which is longer than all other C–C bond in the pyridine.

Moiety 2 of **2Ni** shows η^1 coordination of nickel to the central pyridine, a binding mode shift observed upon acetonitrile coordination in a related Ni^0 complex supported by a *meta*-substituted bis(phosphinoaryl)benzene ligand (Figure 1).[5a] This binding mode change results in a longer Ni–C30 contact of 1.997(1) Å. Aromaticity still appears to be disrupted within the pyridine ring, though to a lesser extent than seen in moiety 1 since the compared distances (C31–C32: 1.419(2) C33–C34: 1.379(2)) and (C32–N2: 1.327(2) C33–N2: 1.357(2)) show smaller differences. This portion of the structure of **2Ni** demonstrates the potential for flexible metal-pyridine π-system interactions that varies with ligand coordination.

Structurally characterized complexes of Ni and Pd with a π-bound pyridine are very rare. The only example to the authors' knowledge is a bis-N-heterocyclic carbene complex of Ni bound η^2 to the C3-C4 positions of a pyridine coordinated via the nitrogen to $AlMe_3$.[14] Though an analogous coordination mode is observed in moiety 1 of **2Ni**, the average Ni–C distances are longer by 0.025 Å in **2Ni**. This is consistent with weaker backbonding into the coordinated C_2 fragment as evidenced from the 0.17 Å shorter C–C distance in **2Ni**. Disrupted aromaticity is also evident in the literature compound though differences in C–C and C–N distances range between 0.01-0.035 Å. This is likely attributable to electronic differences attributable to the N-heterocyclic carbene ligands as well as the coordination of $AlMe_3$ rather than the Ni center of moiety 2.

The solid-state structure of **3Ni** is reminiscent of that of **2Ni**, again with a 3-coordinate nickel complex (moiety 1) binding through its pyridine nitrogen to a protonated equivalent of complex (moiety 2). The bond metrics for moiety 1 of **3Ni** are similar to the analogous ones

of **2Ni**, indicative only of minor perturbation as the site of protonation is quite remote. More substantial changes are seen in bond metrics of moiety 2 of **3Ni**. A different pattern of disruption of aromaticity is observed with similar C31–C32/C33–C34 (1.366(4), 1.376(3) Å) and C32–N2/C33–N2 (1.354(3), 1.349(3) Å) bond distances seen on opposite sides of the pyridine ring relative to the N2-C30 vector. Consistently, C30–C31 and C30–C34 distances are both lengthened, at 1.455(3) and 1.445(3) Å, respectively. Contraction of the Ni–C30 distance to 1.930(2) Å suggests a stronger interaction between the metal and the π-system compared to **2Ni**. These distances are consistent with partial isolation of C30 from the π-system of the pyridine, which results in delocalization across the remaining 5-atoms. The above structural parameters demonstrate the plasticity of pyridine π-system and its potential to rearrange as a function of Lewis acid functionalization of the pyridine nitrogen.

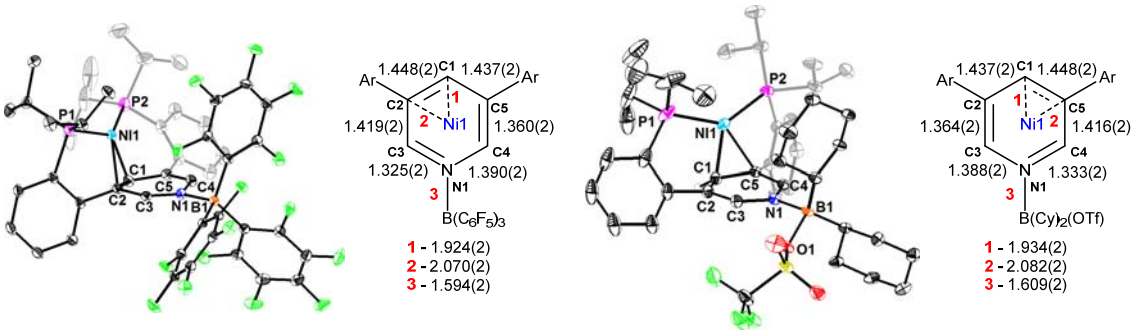

Figure 4. Solid-state structures and selected bond metrics for **2Ni-B(C_6F_5)$_3$** and **2Ni-BCy$_2$OTf**. Hydrogen atoms have been omitted for clarity.

2Ni-B(C_6F_5)$_3$ and **2Ni-BCy$_2$OTf** both crystallize as discrete complexes (Figure 4). They display four-coordinate boron centers. The nickel center is coordinated in an η^2 fashion to the central pyridine in a manner comparable to moiety 1 of **2Ni** and **3Ni**. Furthermore, the distortions of observed in the pyridine moiety are very similar between **2Ni-B(C_6F_5)$_3$, 2Ni-BCy$_2$OTf** and moiety 1 of **2Ni** and **3Ni**. Overall, the structural parameters of these complexes are indicative of stronger interactions between the metal center and the π-bound

heterocycle compared to moiety 2 of **2Ni** where the pyridine nitrogen is not coordinated. However, this comparison must be taken cautiously given that the metal center in moiety 2 of **2Ni** is four-coordinate, while the other compounds display three-coordinate metal centers. In the case of **2Ni**, the comparison is complicated by the dinuclear nature of the crystallized complex. In contrast, Pd complexes and carbon monoxide adducts of Ni complexes (vide infra) provide better points of reference as they are mononuclear in both Lewis acid-bound and –free states.

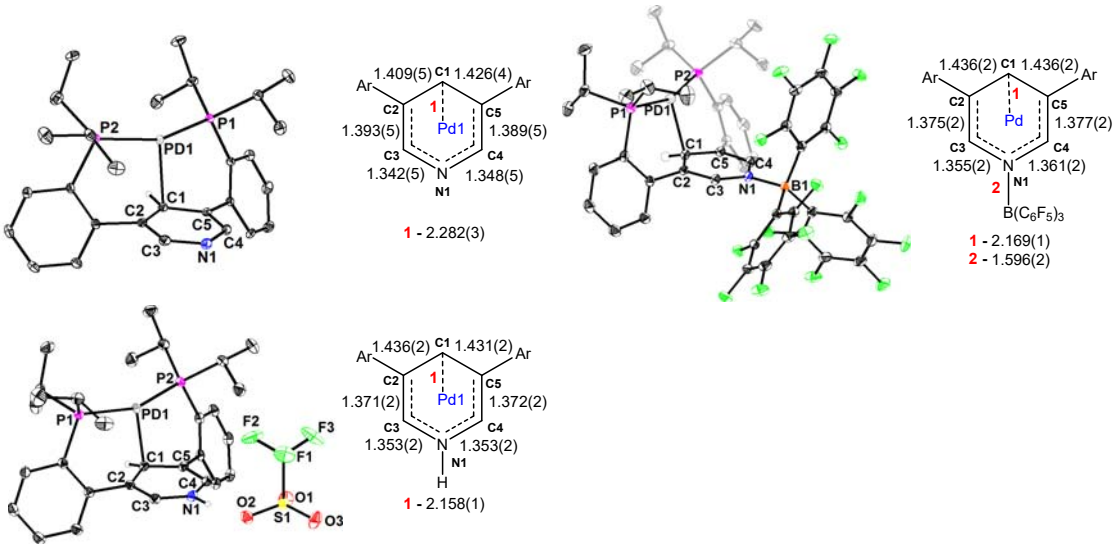

Figure 5. Solid-state structures and selected bond metrics for **2Pd**, **2Pd-B(C_6F_5)$_3$**, and **2Pd-H**. Hydrogen atoms have been omitted for clarity.

As mentioned above, **2Pd**, **2Pd-B(C_6F_5)$_3$**, and **2Pd-H** crystallize as the discrete monomers allowing the direct comparison of the effect of the electrophile on the structural parameters (Figure 5). All complexes show η^1 coordination to the central pyridine ring with Pd–C1 distances of 2.282(3), 2.169(1), and 2.158(1) Å respectively. The significant shortening of the Pd–C1 distance is attributed at a stronger interaction between the electron rich Pd^0 and the more electron deficient borane and proton functionalized pyridine moieties. Symmetric distortions of central pyridine bond metrics relative to the N1-C1 vector are seen, with C2–

C3 and C4–C5 (0.002 Å average change) as well as C3–N1 and C4–N1 (0.004 Å average change) showing negligible differences. However, between complexes differences can be observed. An elongation of C1–C2 and C1–C5 bonds is seen in **2Pd-B(C_6F_5)$_3$** and **2Pd-H** (ranging between 1.436(2) to 1.431(2) Å) vs **2Pd** (1.409(5) and 1.426(4) respectively) again suggestive of a stronger metal-pyridine interaction. C2–C3 and C4–C5 distances shorten by an average of 0.015 and 0.038 Å while C3–N1 and C4–N1 elongate by an average of 0.013 and 0.008 Å for **2Pd-B(C_6F_5)$_3$** and **2Pd-H** respectively relative to **2Pd**. The geometry around palladium is T-shaped with a P1–Pd1–P2 angle of 155.65(3), 160.89(2), 156.97(1) ° for **2Pd**, **2Pd-B(C_6F_5)$_3$**, and **2Pd-H** respectively. For comparison, the P1–Ni–P2 angles are between 133 and 139 in compounds **2Ni-B(C_6F_5)$_3$** and **2Ni-BCy$_2$OTf**, moiety 1 of **2Ni** and **3Ni**. Due to the metal center's increased size, the coordination angle of the diphosphine is larger with palladium. Additionally, the coordination flexibility of the palladium complexes may be limited and a binding akin to that of molecule 1 of **2Ni** may not be sterically accessible.

Section 4.3 Binding of Small Molecules to Ni Complexes

To further study the effect of pyridine modification of ligand electronics on the properties of the metal centers, a series of carbon monoxide adducts was pursued to take advantage of CO as a spectroscopic reporter based on its infrared stretching frequency (Scheme 4). Treatment of with one equivalent of CO was found to quantitatively convert **2Ni**, **2Ni-B(C_6F_5)$_3$**, and **2Ni-Me** to the corresponding mono-CO adducts, **4Ni(CO)**, **4Ni(CO)-B(C_6F_5)$_3$**, and **4Ni(CO)-Me** respectively. The ν_{CO} for **4Ni(CO)** appears 1930 cm^{-1}. The related complex supported by the *meta*-terphenyl diphosphine ligand shows a more activated CO (ν_{CO} = 1916 cm^{-1}) indicative of the more electron rich benzene vs pyridine resulting in a metal center more prone to undergo π-backbonding with CO.[5a] The binding of Lewis acids to

the pyridine nitrogen results in a shift to higher ν_{CO} values as the pyridine ring becomes more electron deficient and competes as an acceptor ligand with the CO (ν_{CO} (cm^{-1}): **4Ni(CO)-B(C_6F_5)$_3$** (1976) and **4Ni(CO)-Me** (1966)). The addition of an equivalent of pyridinium triflate to **4Ni(CO)** results in the quantitative formation of **4Ni(CO)-H** which shows a ν_{CO} of 1975 cm^{-1}. Interestingly, **4Ni(CO)-B(C_6F_5)$_3$** and **4Ni(CO)-H** show similar ν_{CO} frequencies despite the difference in charge. It is notable that changing the supporting π-system from benzene to pyridine has a smaller effect (~14 cm^{-1}) on ν_{CO} compared to binding Lewis acids to the pyridine nitrogen (36 to 45 cm^{-1}).

Scheme 4. Synthesis of small molecule-coordinated Ni complexes

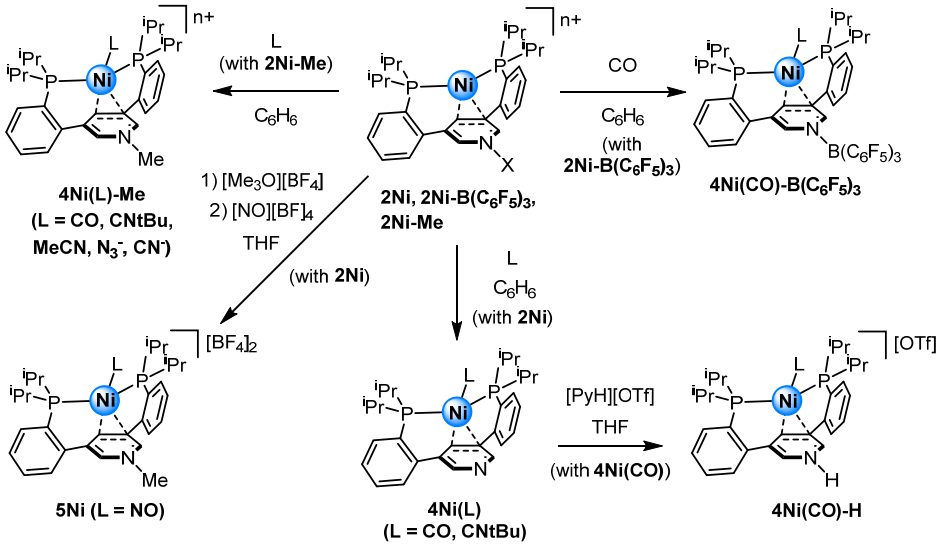

NMR data indicate that the introduction of the CO ligand significantly alters the metal-pyridine interaction (Figure 6). Each complex shows NMR data that is consistent with a C_s symmetric species or a fluxional process in solution as seen from the sharp ^{31}P singlet (δ(ppm): **4Ni(CO)** (33.83), **4Ni(CO)-B(C_6F_5)$_3$** (31.84), **4Ni(CO)-Me** (34.74), and **4Ni(CO)-H** (35.69 in CD_3CN**)**) and two distinct ^1H signals observed for the isopropyl methines (δ(ppm): **4Ni(CO)** (2.33, 2.06), **4Ni(CO)-B(C_6F_5)$_3$** (2.17, 1.74), **4Ni(CO)-Me** (2.27, 1.98), and

4Ni(CO)-H (2.82, 2,49 in CD_3CN)). The signal for the *H*-C1 ((δ(ppm): **4Ni(CO)** (6.23), **4Ni(CO)-B(C_6F_5)$_3$** (4.61), **4Ni(CO)-Me** (4.53), and **4Ni(CO)-H** (4.80 in CD_3CN)) and C3/C4 ((δ(ppm): **4Ni(CO)** (6.23), **4Ni(CO)-B(C_6F_5)$_3$** (4.61), **4Ni(CO)-Me** (4.53), and **4Ni(CO)-H** (4.80 in CD_3CN)) shifts downfield indicating a weaker metal–pyridine interaction, a consequence of competing π-backbonding between metal and pyridine vs CO. Corroborating the similarities in the IR data, both **4Ni(CO)-B(C_6F_5)$_3$** and **4Ni(CO)-Me** show similar chemical shifts for the *H*-C1 despite the charge difference.

Solid-state structures for **4Ni(CO)** and **4Ni(CO)-H** were obtained allowing for comparison to the CO-free analogs and evaluation of the effect of pyridine derivatization with monometallic Ni species (Figure 7). Both **4Ni(CO)** and **4Ni(CO)-H** show η^2 coordination to the central pyridine moiety, differing from **mP$_2$Ni-CO** which shows η^1 coordination.[5a] The shortest Ni–C_{ring} distance is 2.254(1) Å in **mP$_2$Ni-CO** which is longer than in both **4Ni(CO)** (2.119(1) Å) and **4Ni(CO)-H** (2.029(1) Å) consistent with stronger interactions between the electron rich Ni^0 center and the electron deficient heterocycle relative to benzene. These differences in the interactions with the π-systems are corroborated by the ν_{CO} values. Disrupted aromaticity is observed in both **4Ni(CO)** and **4Ni(CO)-H** with significant differences in bond metrics observed for C2–C3 vs C4–C5 as well as C3–N1 vs C4–N1 indicating partial localization of double and single bonds. The shortest Ni-pyridine interactions for **4Ni(CO)** and **4Ni(CO)-H**, 2.119(1) and 2.029(1) Å respectively, are elongated relative to moiety 2 of **2Ni** (1.997(1) Å) and **3Ni** (1.966(2) Å), respectively, consistent with the CO ligand being overall more acidic than the N-bound pyridine and leaving the metal center less prone to backbonding to the π-system of pyridine. It is worth noting that the pattern of aromaticity disruption (localized double bond character) and coordination mode are different between **4Ni(CO)** and **4Ni(CO)-H** vs moiety 2 of **2Ni** and **3Ni** despite

both complexes being 4-coordinate at nickel. This structural difference may be a consequence of CO being smaller than substituted pyridine and accommodating η^2-coordination to the central π-system.

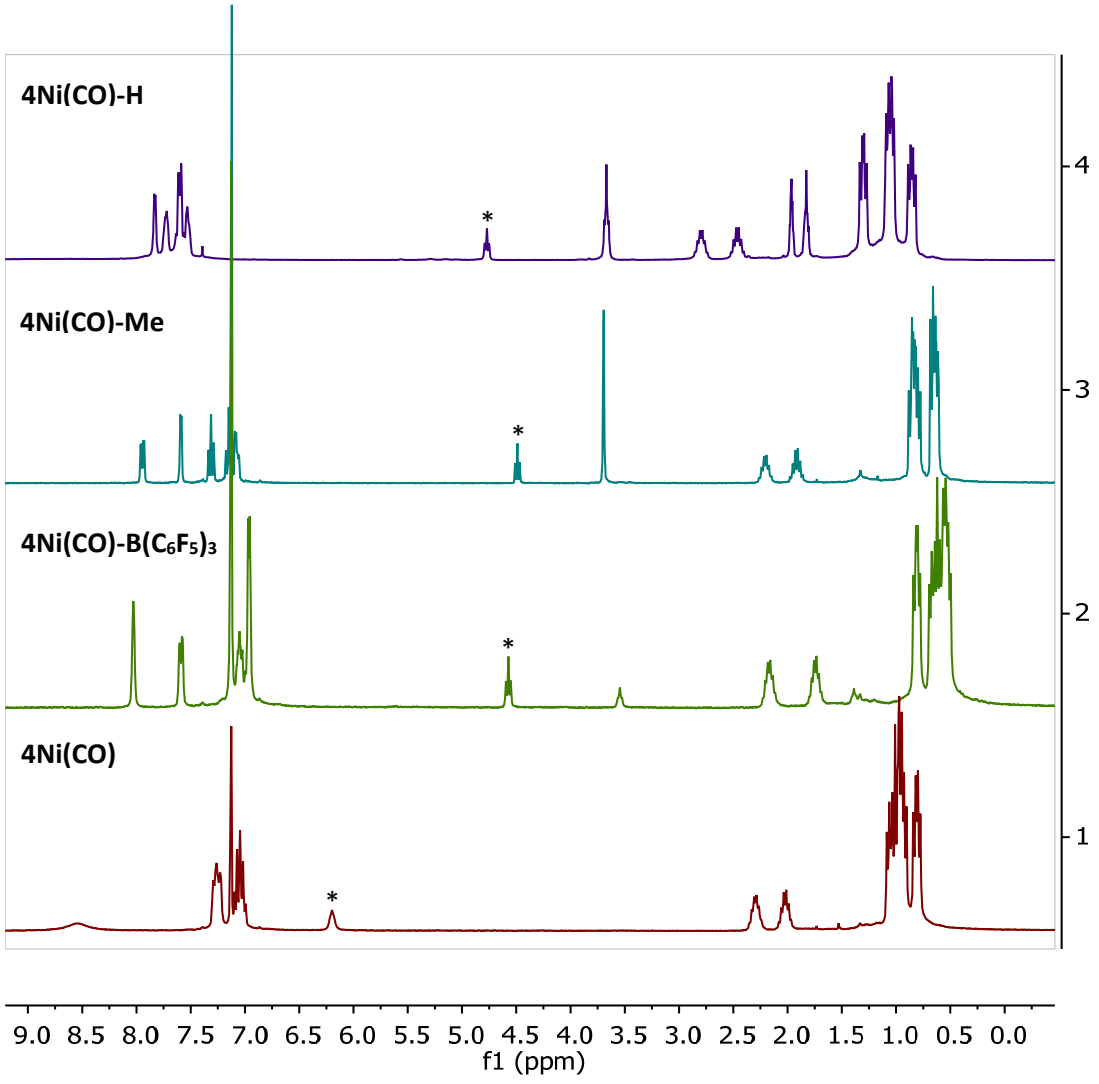

Figure 6. ^{1}H NMR comparison for all isolated Ni monocarbonyl complexes. Peaks denoted by an asterisk indicate the C1 proton of the central pyridine ring. All spectra are taken in C_6D_6 with the exception of **4Ni(CO)-H** which was obtained in CD_3CN.

Comparison between **4Ni(CO)-H** and **4Ni(CO)** provides insight into the effect of protonation on pyridine coordination to metal. **4Ni(CO)-H** shows shorter Ni-C contacts vs **4Ni(CO)** consistent with stronger interaction between the metal and pyridine in **4Ni(CO)-**

H. Additionally, the C1–C5 distance of the Ni-coordinated C_2 moiety is shorter in **4Ni(CO)** (1.416(2) Å) compared to **4Ni(CO)-H** (1.441(2) Å), suggesting weaker backbonding into the pyridine in **4Ni(CO)**. These effects are likely due to the more electron deficient pyridinium moiety being a better π-acceptor from the electron rich Ni^0 center compared to pyridine.

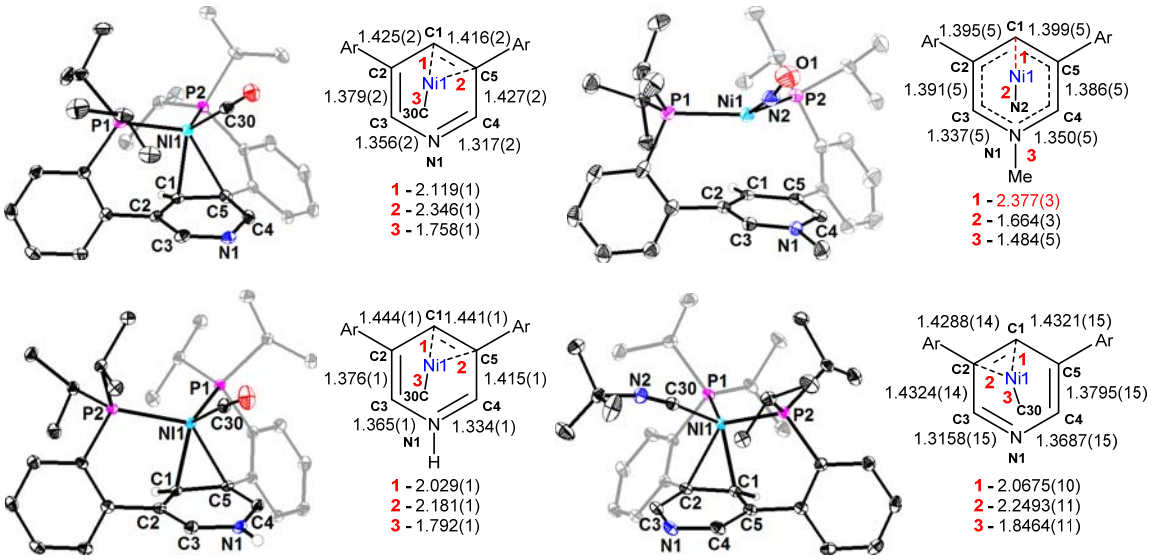

Figure 7. Solid-state structures and selected bond distances of **4Ni(CO)**, **4Ni(CO)-H**, **5Ni**, and **4Ni(CN*t*Bu)**. Hydrogen atoms and solvent have been omitted for clarity.

To test the ability of ligands derivatized at pyridine to support coordination of other donors to Ni, reaction with nitrosonium ion was pursued as an isoelectronic analog of carbon monoxide. **2Ni** reacts with trimethyloxonium tetrafluoroborate ($[OMe_3][BF_4]$) in THF to *in situ* generate the N-methylated complex. Subsequently, $[NO][BF_4]$ was added causing color change from a dark brown to a blue-brown solution. Following work up, the desired complex, **5Ni**, was isolated as a dark blue crystalline solid. NMR spectra recorded in d_3-acetonitrile indicated the formation of a species that showed a broad ^{31}P signal at 31.31 ppm. The chemical shift of the C1 (7.55 ppm) and C3/C4 protons (9.01 ppm) appear in the aromatic region suggesting weaker metal-pyridine π-system interactions than any of the CO complexes. This is corroborated by the solid-state structure. The structure of **5Ni** shows substantial differences

from all other nickel complexes synthesized. A negligible Ni-pyridine interaction is present as seen from the long Ni–C1 distance of 2.377(3) Å. The sum of the P–Ni–P and P–Ni–N angles is equal to 350.78 ° and is approaching the theoretical value for ideal trigonal planar coordination. Therefore, this complex represents a rare example of a structurally characterized three-coordinate Ni-NO complex where both other donors are phosphines.[15] Central pyridine distances also indicate a negligible Ni-heterocycle interaction as C–C (1.386(5) to 1.399(5) Å) and C–N distances, 1.337(5) and 1.350(5) Å for C3–N1 and C4–N1 respectively, are quite similar. The NO stretching frequency for **5Ni** appears at 1846 cm^{-1} (IR). The Ni–N2–O1 angle is 163.1(4) ° which is consistent with literature linear nitrosyl moieties bound to Ni.[16] These data indicate that the pyridinium ring cannot compete with the nitrosonium ligand for coordination of nickel.

Following the initial success with nitrosonium coordination, the binding of other small molecules was pursued. **2Ni** was found to readily bind *tert*-butyl isocyanide to produce **4Ni(CN*t*Bu)** although the partial formation of free ligand was also observed (Scheme 4). Analogous reactions with **2Ni-B(C_6F_5)$_3$** resulted in a complicated mixture of products, likely resulting from the steric profile of the B(C_6F_5)$_3$ moiety. **2Ni-Me** was found to readily coordinate *tert*-butyl isocyanide to yield **4Ni(CN*t*Bu)-Me**. The addition of other small molecules such as cyanide, azide, and acetonitrile to **2Ni-Me** results in quantitative binding to the Ni-center to produce **4Ni(CN)-Me**, **4Ni(N_3)-Me**, and **4Ni(MeCN)-Me** respectively. Including **5Ni**, N-methylated Ni complexes coordinate a variety of small molecules of charge varying from anionic (CN^- and N_3^-), to neutral (MeCN, CN*t*Bu, and CO), and even cationic in the case of nitrosonium.

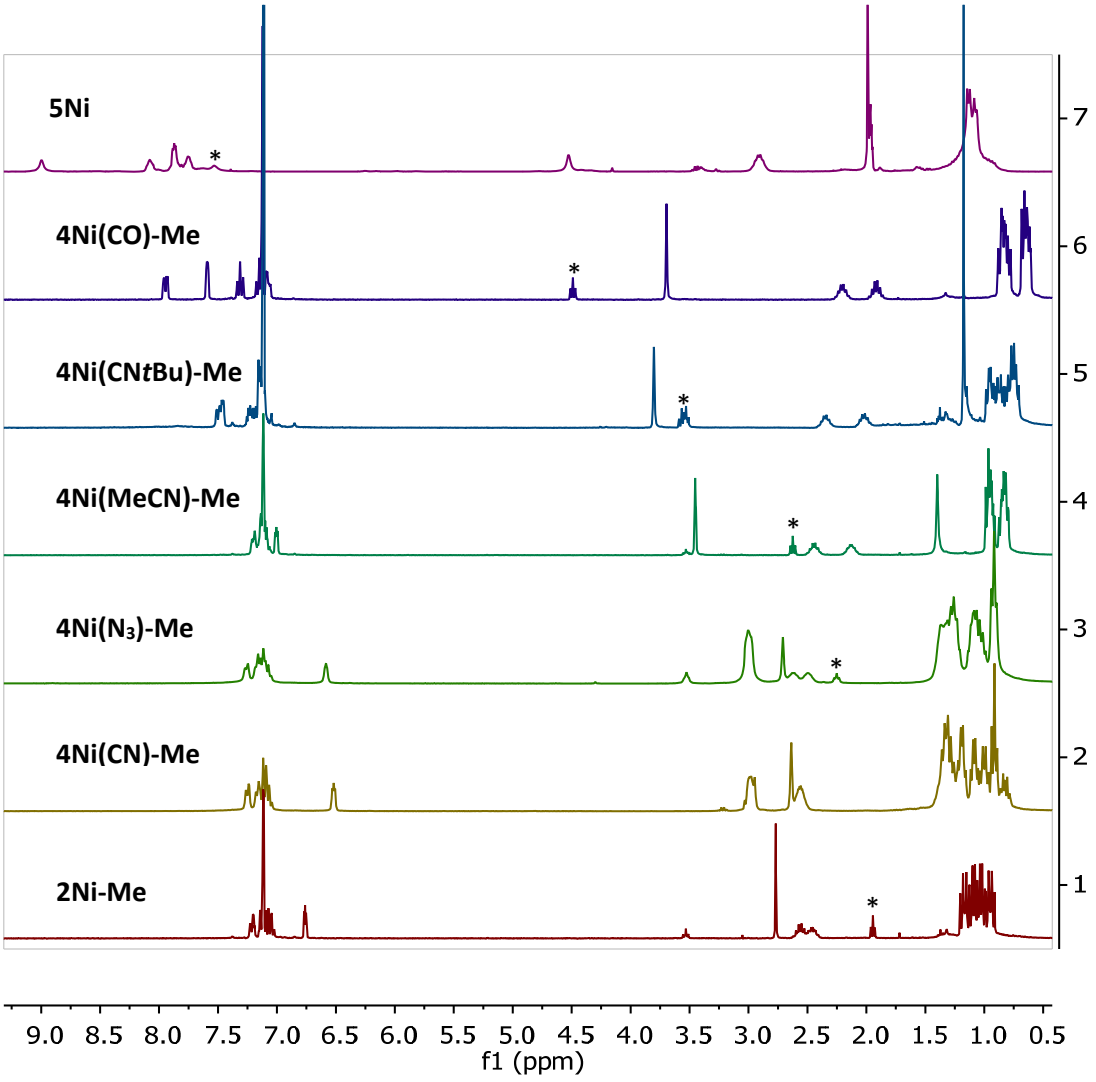

Figure 8. ^{1}H NMR comparison for all isolated N-methylated Ni complexes. Peaks denoted by an asterisk indicate the C1 proton of the central pyridine ring. All spectra are taken in C_6D_6 with the exception of **5Ni** which was obtained in CD_3CN.

As carbon monoxide is expected to be a better π-acid than *tert*-butyl isocyanide, **4Ni(CO)** is expected to display a weaker Ni-pyridine π-system interaction compared to **4Ni(CN*t*Bu)** as the coordinated ligand competes better for electron density with the heterocycle. This is borne out in the comparison of solution NMR data for **4Ni(CO)** and **4Ni(CN*t*Bu)**. Both complexes show substantially upfield shifted resonances for the central pyridine protons (**4Ni(CN*t*Bu)** δ(ppm) *H*-C1: 5.51, *H*-C3/C4 8.17; **4Ni(CO)** δ(ppm) *H*-C1: 6.23, *H*-C3/C4

8.58) consistent with a strong Ni-pyridine π-system interaction. However, for both *H*-C1 and *H*-C3/C4 resonances for **4Ni(CNtBu)** appear further downfield compared to **4Ni(CO)** (Δδ(ppm) *H*-C1: 0.72, *H*-C3/C4: 0.41) indicating more backbonding from the Ni center into the pyridine ring for **4Ni(CNtBu)**. Both complexes show a comparable pair of ^{1}H resonances (δ(ppm): **4Ni(CO)** (2.35, 2.06), **4Ni(CN*t*Bu)** (2.41, 2.11)) corresponding to the methine protons. Single resonances are observed by ^{31}P NMR (δ(ppm): **4Ni(CO)** 33.83, **4Ni(CN*t*Bu)** 36.56). Overall the effect of a change in π-acidity of the donor ligand moves the C1-H chemical shift by roughly half that resulting from the binding of $B(C_6F_5)_3$ to the pyridine nitrogen (*H*-C1 δ(ppm): **4Ni(CO)-B(C_6F_5)$_3$** 4.61). Crystals suitable for XRD experiments were obtained for **4Ni(CN*t*Bu)** allowing for comparisons in the solid-state with **4Ni(CO)** (Figure 7). Both complexes show η^2 coordination modes with a shorter average Ni–C distance (**4Ni(CO)** 2.23 Å, **4Ni(CN*t*Bu)** 2.16 Å) seen for **4Ni(CN*t*Bu)** consistent with a stronger Ni-pyridine π-system interaction. Otherwise, central pyridine bond lengths are consistent localized double bond character due to Ni coordination.

In a similar way, NMR comparisons across the series of **4Ni(L)-Me** (L = CN^-, N_3^-, MeCN, CN*t*Bu, CO) and **5Ni** allows for an assessment the strength of the Ni-pyridine π-system interaction with a wide variety of small molecules while holding the pyridine substitution constant (Figure 8). A clear trend in the chemical shift of the C1-*H* proton can be seen with the more π-acidic donors resulting in a more downfield resonance (C1-*H* δ(ppm): **5Ni** 7.55 (CD_3CN), **4Ni(CO)-Me** 4.49, **4Ni(CN*t*Bu)-Me** 3.57, **4Ni(MeCN)-Me** 2.62, **4Ni(N_3)-Me** 2.25, **4Ni(CN)-Me** 2.95 (under TBA peak), **2Ni-Me** 1.94) (Figure 8). These results corroborate the interplay between the electronics of the small molecule and the N-functionalized pyridine by looking at the chemical shift of the *H*-C1 proton.

Overall the crystal structures reported here indicate that the interactions of Ni^0 and Pd^0 with aromatic π-systems become stronger upon changing the pendant donor from benzene to pyridine to Lewis acid functionalized pyridine. This trend is maintained upon binding of additional ligands such CO. The electronic effect of these interactions with pendant π-systems is reflected in extent of CO bond weakening. The metal pyridine π-system interaction can also be modulated with the π-acidity of coordinated ligand.

Section 4.4 Pyridine Dearomatization by Small Molecule Reactivity

With the influence of the aromatic ligand on the metal center demonstrated, the activation of the heterocycle by the metal toward reactivity was also investigated. With the aromaticity of pyridine partially disrupted by metal coordination, reactivity at the N=C moiety was targeted. **2Ni** showed no reactivity under an atmosphere of dihydrogen at room temperature in benzene, and increasing the temperature was found to yield free phosphine, **1**, presumably with loss of nickel black. However, reactions with pinacol borane and phenylsilane led to the formation of new species, **6Ni** and **7Ni**, respectively, at room temperature by NMR spectroscopy (Scheme 5).

Attempts to obtain X-ray diffraction quality single crystal of **6Ni** and **7Ni** have been unsuccessful to date. A suite of NMR experiments were employed for the structural characterization of these compounds. Both complexes show asymmetric coupling ^{31}P doublets at (56.23, 44.70 ppm ($^2J_{PP}$ = 55.7 Hz)) and (56.09, 44.77 ($^2J_{PP}$ = 56.2)) for **6Ni** and **7Ni,** respectively. Furthermore, asymmetric signals for the central pyridine protons are observed that are consistent with the hydroboration or hydrosilylation of a C–N bond of the pyridine rather than a 1,4 selective reaction or a formal oxidative addition at the nickel center. The formation of a methylene moiety with diastereotopic hydrogens is supported by two doublet proton resonances for **6Ni** (4.51, 3.78 ppm ($^2J_{HH}$ = 13.7 Hz)) and **7Ni** (4.13, 3.77 ppm ($^2J_{HH}$

= 13.2 Hz)) are correlated by gCOSY and couple to the same ^{13}C resonance at 52.40 or 55.15 ppm, respectively, by gHSQCAD. The assignments for the remaining central pyridine protons are completed using a combination of gHSQCAD and gHMBCAD experiments, which confirm the location of the C1 and the remaining *ortho*-pyridine protons at 4.11 and 6.83 ppm and 4.13 and 6.40 ppm for **6Ni** and **7Ni** respectively (Figure 9). The Si*H* signal of **7Ni** appears as a multiplet at 5.29 ppm. Complete assignments of the central pyridine carbons have also been made (See Experimental Section), which support the 1,2 substitution pattern assignment.

Scheme 5. Reactivity at pyridine beyond Lewis acid binding: synthesis of dearomatized pyridine complexes

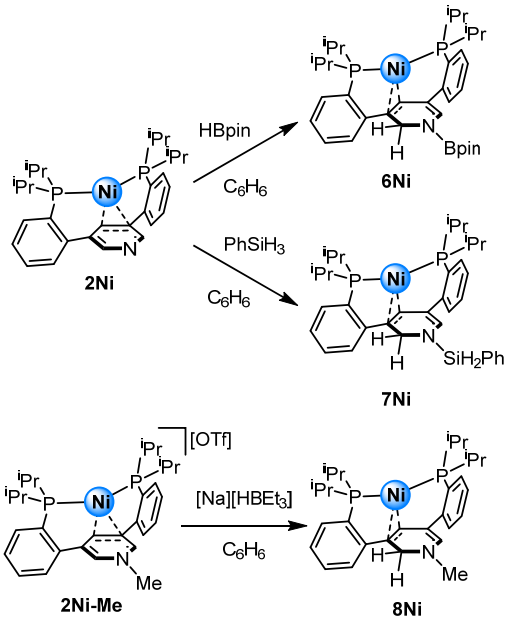

To further support the NMR-based structural assignments for **6Ni** and **7Ni**, the reactivity of hydrides with **2Ni-Me** was tested to determine if a similar dearomatization occurs. **2Ni-Me** was found to cleanly react with sodium triethylborohydride to yield the asymmetric species **8Ni**. Similar to **6Ni** and **7Ni** coupling ^{31}P doublets are seen at 56.52 and 44.05 ppm ($^{2}J_{PP}$ = 56.4 Hz). The pattern of ^{1}H resonances and the connectivity of the dearomatized central pyridine ring was found to be similar to that of **6Ni**. The methylene protons are observed at

3.49 and 3.09 ppm ($^{2}J_{HH}$ = 12.0 Hz), while the C1 and remaining *ortho*-pyridine proton are observed at 4.09 and 5.85 ppm respectively.

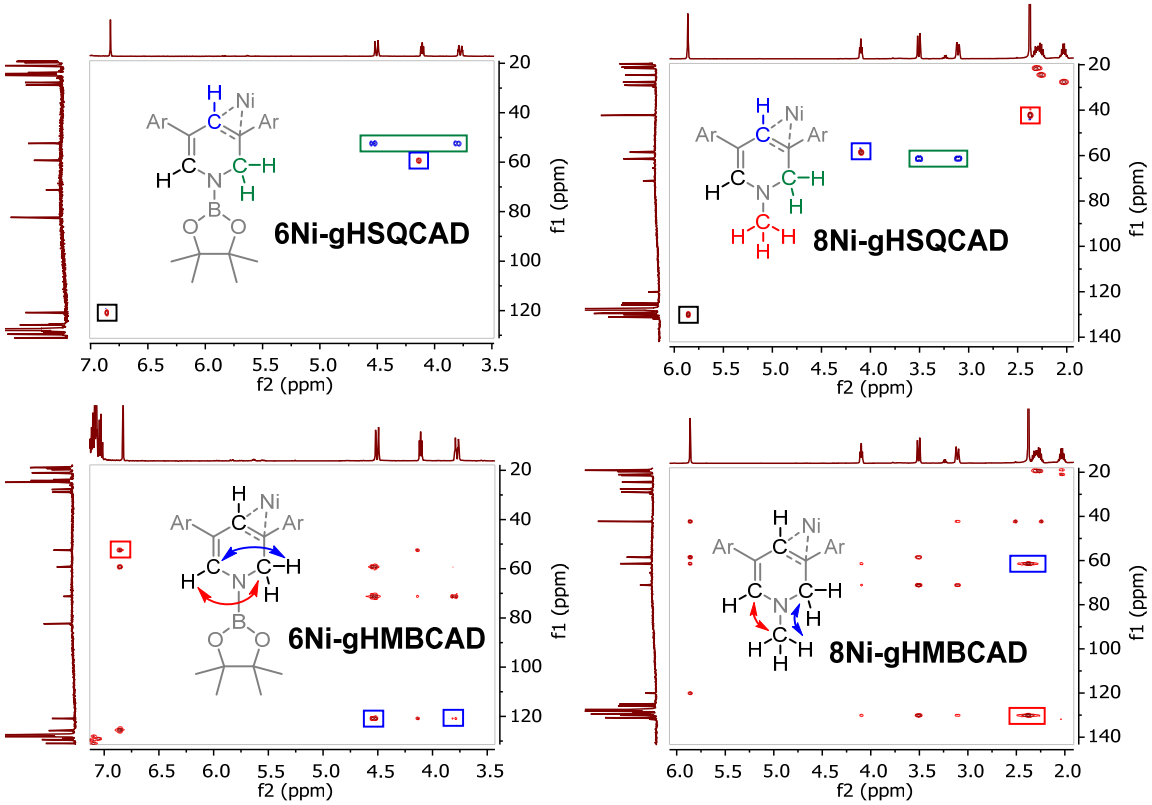

Figure 9. Select portions of the gHSQCAD and gHMBCAD spectra for **6Ni** (Left) and **8Ni** (Right).

Complexes **6Ni**, **7Ni**, and **8Ni** are reminiscent of transition metal bound NAD(P)H analogs.[17] The use of pyridine and other heterocycles to store proton and electron equivalents in metal-complexes has been previously explored for a variety of transformations.[18] In the context of π-bound ligands, catechol moieties have been shown to act as a source of both electrons and electrophile equivalents during dioxygen activation.[19] **6Ni**, **7Ni**, and **8Ni** demonstrate the ability of the pyridine to serve as a reservoir of reducing equivalents in the present system. Access to these reduced species is however sensitive to the steric and electronic properties of the reagents. Diphenylsilane and triethylsilane did not react with **2Ni** even at

elevated temperatures. The addition of sodium triethylborohydride to **2Ni-BCy$_2$OTf** did not result in the formation of a dearomatized product by ^{31}P NMR. Although the final products **6Ni**, **7Ni**, and **8Ni** show delivery of hydride to the pyridine, mechanistically the initial site of reactivity, metal vs heterocycle, has not been established. A precise understanding of the factors that govern the pyridine reduction reactivity require further investigation, as do methodologies to transfer the reducing equivalents to an external substrate.

Section 4.5 Preliminary Mo Metalation Reactions

Preliminary attempts have been made to expand the scope of metals supported by ligands **1** and **1-B(C$_6$F$_5$)$_3$** beyond Ni and Pd. Initials efforts focused on metalation conditions with molybdenum carbonyl precursors as such compounds have served as precursors for a variety of compounds capable of interesting multielectron transformations on *para*-terphenyl diphosphine ligands.[19-20] The stirring of **1** with Mo(CO)$_3$(MeCN)$_3$ at 100 °C for 16 hours in toluene produced a major species at 55.17 ppm (~80 %) and a minor species at 55.89 ppm (~20 %). Efforts to separate these complexes with solvent washes or by recrystallization proved unsuccessful. However, protonation of this mixture with pyridinium triflate and recrystallization was sufficient to cleanly afford **9Mo(CO)$_3$-H** (Scheme 6). To date to decarbonylate or oxidize **9Mo(CO)$_3$-H** have proven unsuccessful. The reaction with trimethylamine *n*-oxide was found to cleanly afford the deprotonation product, **9Mo(CO)$_3$**, which could then be identified as the major species in the initial metalation of **1** with Mo(CO)$_3$(MeCN)$_3$. The current hypothesis is that the minor species is dimolybenum complex where the pyridine nitrogen coordinates to a second metal. The metallation of **1-B(C$_6$F$_5$)$_3$** with Mo(CO)$_3$(MeCN)$_3$ under identical reaction conditions produces a single new species, **9Mo(CO)$_3$-B(C$_6$F$_5$)$_3$**, consistent with the aforementioned hypothesis as boron

prefunctionalization of the pyridine nitrogen would prevent the formation of the proposed dimolybdenum species.

Scheme 6. Synthesis of molybdenum carbonyl complexes supported by 1 and 1-B(C_6F_5)$_3$

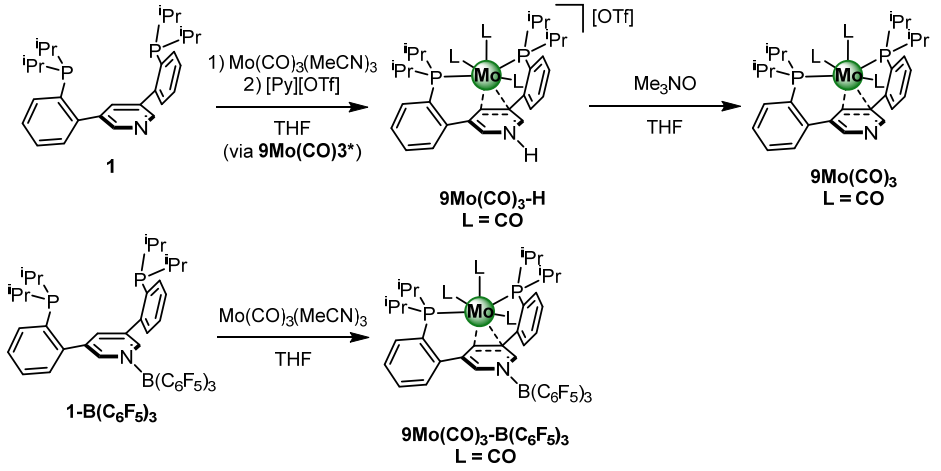

Solution NMR data obtained for **9Mo(CO)$_3$** and **9Mo(CO)$_3$-B(C$_6$F$_5$)$_3$** (C_6D_6) as well as **9Mo(CO)$_3$-H** (CD_3CN) are consistent with strong metal-pyridine π-system interactions and a C_s symmetric species or a fluxional process on the NMR timescale. All compounds show a pair of resonances corresponding to the methine protons (δ(ppm): **9Mo(CO)$_3$** (2.67, 2.36), **9Mo(CO)$_3$-B(C$_6$F$_5$)$_3$** (2.48, 2.05), **9Mo(CO)$_3$-H** (3.31, 2.58)) and a single ^{31}P signal (δ(ppm): **9Mo(CO)$_3$** 55.17, **9Mo(CO)$_3$-B(C$_6$F$_5$)$_3$** 55.97, **9Mo(CO)$_3$-H** 54.63). The ^{1}H resonances for the central pyridine protons appear at upfield resonances compared to the free ligands (*H*-(C1) δ(ppm): **9Mo(CO)$_3$** 6.15, **9Mo(CO)$_3$-B(C$_6$F$_5$)$_3$** 4.97, **9Mo(CO)$_3$-H** 5.35) (*H*-(C3/4) δ(ppm): **9Mo(CO)$_3$** 8.39, **9Mo(CO)$_3$-B(C$_6$F$_5$)$_3$** 8.11, **9Mo(CO)$_3$-H** 7.96). These data suggest that a substantial Mo-pyridine π-system interaction which is stronger for the more electron deficient B(C_6F_5)$_3$- and H^+-functionalized central pyridine ring. **9Mo(CO)$_3$-H** shows a broad ^{1}H signal corresponding to the pyridinium resonance at 12.37 ppm.

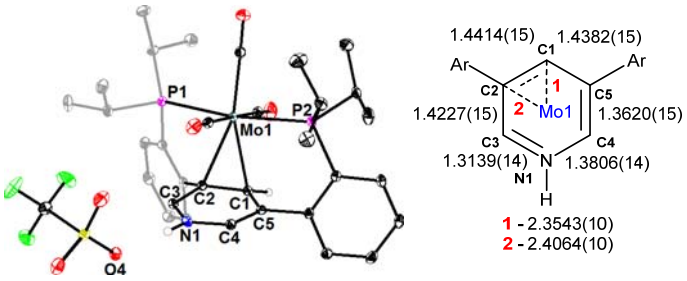

Figure 10. Solid-state structures and selected bond distances for **9Mo(CO)$_3$-H**. Hydrogen atoms and solvent have been omitted for clarity.

Crystals of **9Mo(CO)$_3$-H** suitable for XRD analysis were obtained from a THF/pentane vapor diffusion (Figure 10). A *pseudo*-octahedral coordination environment around the Mo-center is observed, which shows η^2 coordination to the central pyridine ring. Substantial backbonding from Mo is evident from the long C1–C2 bond distance (1.4414(15) Å), which exceeds that of all other C–C bonds in the pyridine ring. The alternation of long and short bonds in the central pyridine ring is indicative of localization of double bond character due to Mo coordination. Efforts to open up the coordination sphere of the Mo center by removing the carbon monoxide ligands is being pursued.

CONCLUSIONS

A new P-pyridine-P ligand that readily binds nickel and palladium via phosphine donors and the heterocycle π-system was developed. The interaction between the transition metal and the π-system results in partial disruption of aromaticity. Metal coordination to the phosphine donors and pyridine π-system leaves the pyridine nitrogen available for Lewis acid functionalization. Binding of groups such as boranes, H^+, or Me^+ results in stronger interactions of the metal center with the pyridine π-

system, as reflected in both the NMR spectroscopy and structural characteristics of the complexes. The observed differences in binding are caused by the varied ability of pyridines to act as π-backbonding ligands; the functionalized heterocycles are more electron-deficient resulting in a stronger interaction with the electron rich M^0 centers. CO and NO adducts of Ni were synthesized. Comparison of the CO stretching frequencies indicate that functionalization of the pyridine nitrogen has a significant effect on the coordinated diatomic ligand, leading to up to 46 cm^{-1} shift to higher energy upon $B(C_6F_5)_3$ binding. Dearomatization of the pyridine ring was observed in stoichiometric reactions between phenylsilane or pinacol borane and **2Ni**, with the heteroatom binding to nitrogen and the hydrogen *ortho* to N. This ligand-based reactivity is likely a consequence of the activation of the pyridine ring by the metal center, through disruption of aromaticity. Overall, the described results highlight a strategy for tuning the electronic properties and reactivity of metal centers by post-synthetic modifications of the complex instead of the more typical, and expensive, re-synthesis of electronically altered ligands.

EXPERIMENTAL SECTION

General considerations

Unless otherwise specified, all air- and moisture-sensitive compounds were manipulated using glovebox or using standard Schlenk line techniques with an N_2 atmosphere. Anhydrous tetrahydrofuran (THF) was purchased from Aldrich in 18 L Pure-Pac™ containers. Anhydrous pentanes, hexanes, benzene, toluene, diethyl ether, and THF were purified by sparging with nitrogen for 15 minutes and then passing under nitrogen pressure through a column of activated A2 alumina (Zapp's).[21] Benzene-d_6, tetrahydrofuran-d_8, and acetonitrile-d_3 was purchased from Cambridge Isotope Laboratories, Inc., dried over sodium/benzophenone ketyl (benzene and THF) or calcium hydride (MeCN) and vacuum transferred prior to use. Unless indicated otherwise, all commercial chemicals were used as received. $Ni(COD)_2$, $PdMe_2$TMEDA, $PdCl_2$COD, and $Pd(PPh_3)_4$ were purchased from Strem Chemicals Inc.. 3,5-dibromopyridine, pinacol borane, dicyclohexylboron triflate, methyl triflate, 1M sodium triethylborohydride in toluene, 1.7 M *t*BuLi in pentane, chlorodiisopropyl phosphine, and CO (lecture bottle) was purchased from Sigma Aldrich. Phenylsilane was purchased from Sigma Alrich and was dried over calcium hydride and distilled prior to use. Tris(pentafluorophenyl)borane was purchased from Sigma Aldrich as sublimed prior to use. 2-bromophenylboronic acid was purchased from Ark Pharm, Inc. and used as received. ^{1}H, ^{13}C, and ^{31}P NMR spectra were recorded on Varian Mercury 300 or Varian INOVA-500 spectrometers at room temperature unless indicated otherwise. Chemical shifts for ^{1}H and ^{13}C NMR data are reported relative to residual solvent peaks and are decoupled with respect to each other unless otherwise noted.[22] ^{31}P NMR chemical shifts are reported with respect to the deuterated solvent used to lock the instrument and are ^{1}H decoupled unless otherwise noted. Powder and thin film ATR-IR measurements were obtained by placing a powder or drop of

solution of the complex on the surface of a Bruker APLHA ATR-IR spectrometer probe and allowing the solvent to evaporate (Platinum Sampling Module, diamond, OPUS software package) at 2 cm^{-1} resolution. Elemental analyses were performed by Robertson Microlit Laboratories, Ledgewood, NJ.

Synthesis of 3,5-(2-bromophenyl)pyridine (B)

3,5-dibromopyridine (8.50 g, 35.9 mmol, 1 equiv), 2-bromophenylboronic acid (15.13 g, 75.3 mmol, 2.1 equiv), and potassium carbonate (29.8 g, 215.6 mmol, 6 equiv) were added to a Schlenk tube fitted with a screw-in Teflon stopper. A magnetic stirbar, 810 mL of toluene, 195 mL of water, and 195 mL of ethanol were then added the resulting biphasic solution was thoroughly degassed by two sequential freeze-pump-thaw cycles on a Schlenk line. Under a strong counterflow of nitrogen, $Pd(PPh_3)_4$ (2.07 g, 1.79 mmol, 0.05 equiv) was then added to the reaction mixture. The reaction flask was then sealed and heated to 65 °C for 16 hrs. At this point, GC-MS analysis of an aliquot of the organic fraction indicated complete conversion to the desired product. Volatiles were removed by rotary evaporation to yield a light orange residue. Salts were removed by a water:dichloromethane extraction. After drying with magnesium sulfate and filtering, the organic fraction was dried under reduced pressure. The product was recrystallized from dichloromethane:methanol at -35 °C and obtained as a white crystalline solid. Yield: 7.93 g (59 %) ^{1}H NMR (500 MHz, C_6D_6) δ 8.75 (d, $^4J_{HH}$ = 2.2 Hz, Py*H*, 2H), 7.51 (t, $^4J_{HH}$ = 2.2 Hz, Py*H*, 1H), 7.40 (ddd, $^3J_{HH}$ = 8.0, $^4J_{HH}$ = 1.2, $^5J_{HH}$ = 0.5 Hz, Ar*H*, 2H), 6.92 (ddd, $^3J_{HH}$ = 7.6, $^4J_{HH}$ = 1.9, $^5J_{HH}$ = 0.5 Hz, Ar*H*, 2H), 6.87 (td, $^3J_{HH}$ = 7.5, $^4J_{HH}$ = 1.2 Hz, Ar*H*, 2H), 6.72 (ddd, $^3J_{HH}$ = 8.0, $^3J_{HH}$ = 7.3, $^4J_{HH}$ = 1.8 Hz, Ar*H*, 2H). ^{13}C NMR (126 MHz, C_6D_6) δ 149.52 (s), 139.37 (s), 137.50 (s), 136.08 (s), 133.51 (s), 131.65 (s), 129.63 (s), 127.71 (s), 123.2 4 (s). MS (m/z): Calcd, 389.9316 (M^+). Found: 389.9327 (FAB-MS, M^+).

Synthesis of Compound 1

B (4 g, 10.3 mmol, 1 equiv) was dissolved in 60 mL of THF and transferred to a Schlenk tube fitted with a screw-in Teflon stopper. The reaction mixture was then cooled to -78 °C and then *t*BuLi (1.7 M pentanes, 24.8 mL, 42.2 mmol, 4.1 equiv) was added via syringe resulting in an immediate color change to a deep red. The reaction mixture was then allowed to warm to room temperature and stir for 2 hrs. The reaction mixture was again cooled to -78 ºC and then chlorodiisopropyl phosphine (3.6 mL, 22.6 mmol, 2.2 equiv) was added via syringe. The reaction was warmed to room temperature and allowed to stir for 16 hrs during which time the solution lightened to a homogenous orange brown. Volatiles were then removed under reduced pressure to yield a thick residue. This residue was dissolved in toluene a filtered through a Celite pad to remove salts. The volatiles of the filtrate were then removed under reduced pressure. The resulting residue was suspended in acetonitrile (*ca.* 20 mL) and then resulting solution allowed to stand for 1 hour. During this time the residue initially became soluble before the product began to precipitate as a yellow solid. This product was collected via filtration and washed with additional acetonitrile until the washes became colorless. After drying the collected solid under reduced pressure, the product was obtained as a pale yellow solid. Yield: 2.82 g (59 %). ^{1}H NMR (500 MHz, C_6D_6) δ 8.94 (dd, $^{3}J_{HH}$ = 2.2 Hz, $^{5}J_{PH}$ = 1.3 Hz, Py*H*, 2H), 7.87 (td, $^{3}J_{HH}$ = 2.2 Hz, $^{5}J_{PH}$ = 1.1 Hz, Py*H*, 1H), 7.45 – 7.36 (m, Ar*H*, 2H), 7.35 – 7.27 (m, Ar*H*, 2H), 7.15 – 7.09 (m, Ar*H*, 4H), 1.86 (pd, $^{3}J_{HH}$ = 6.9, $^{2}J_{PH}$ =1.6 Hz, C*H*, 4H), 0.95 (dd, $^{3}J_{PH}$ = 14.6, $^{3}J_{HH}$ =6.9 Hz, C*H*$_3$, 12H), 0.85 (dd, $^{3}J_{PH}$ = 11.5, $^{3}J_{HH}$ = 6.9 Hz, C*H*$_3$, 12H). ^{13}C NMR (126 MHz, C_6D_6) δ 150.33 (d, $^{5}J_{PC}$ = 5.9 Hz), 147.55 (d, $^{2}J_{PC}$ = 28.3 Hz), 140.29 (t, $^{5}J_{PC}$ = 4.9 Hz), 137.11 (d, $^{3}J_{PC}$ = 6.2 Hz), 135.64 (d, $^{1}J_{PC}$ = 24.6 Hz), 133.04 (d, $^{2}J_{PC}$ = 2.9 Hz), 130.96 (d, $^{3}J_{PC}$ = 5.4 Hz), 129.01 (s), 127.42 (s), 25.01 (d, $^{1}J_{PC}$ = 15.6 Hz), 20.47 (d, $^{2}J_{PC}$ =

20.2 Hz), 19.75 (d, $^{2}J_{PC}$ = 11.0 Hz). ^{31}P NMR (121 MHz, C_6D_6) δ -5.75. MS (m/z): Calcd, 464.2638 (M+). Found: 464.2636 (FAB-MS, M^+).

Synthesis of Complex 1-B(C_6F_5)$_3$

Compound **1** (562 mg, 1.21 mmol, 1 equiv.) was dissolved in benzene (*ca.* 10 mL) and transferred to a 20 mL scintillation vial equipped with a magnetic stirbar. B(C_6F_5)$_3$ (620.7 mg, 1.21 mmol, 1 equiv.) was then added as a benzene solution (*ca.* 10 mL). The reaction mixture was allowed to stir for 3 hours, during which time the solution became a slightly lighter shade of yellow. The reaction mixture was then frozen in a -35 °C freezer and the benzene removed by lyophilization to yield the desired product by NMR and was used without further purification. Yield: 1.06 g (90 %) ^{1}H NMR (500 MHz, C_6D_6) δ 8.82 (s, Py*H*, 2H), 8.04 (s, Py*H*, 1H), 7.26 – 7.18 (m, Ar*H*, 4H), 7.08 – 6.97 (m, Ar*H*, 4H), 1.70 (pd, $^{1}J_{HH}$ = 6.9, $^{1}J_{PH}$ = 2.3 Hz, C*H*, 4H), 0.82 (dd, $^{2}J_{PH}$ = 14.6, $^{1}J_{HH}$ = 6.9 Hz, C*H*$_3$, 12H), 0.72 (dd, $^{2}J_{PH}$ = 12.3, $^{1}J_{HH}$ = 6.9 Hz, C*H*$_3$, 12H). ^{13}C NMR (126 MHz, C_6D_6) δ 149.20 (s), 147.97 – 146.77 (m), 145.99 (d, $^{5}J_{PC}$ = 7.0 Hz), 142.87 (d, $^{2}J_{PC}$ = 26.8 Hz), 141.22 (m), 139.65 – 138.95 (m), 139.18 (d, $^{3}J_{PC}$ = 5.7 Hz), 136.37 (m), 134.65 (d, $^{1}J_{PC}$ = 25.1 Hz), 132.83 (d, $^{2}J_{PC}$ = 2.4 Hz), 130.22 (d, $^{4}J_{PC}$ = 5.3 Hz), 129.35 (s), 128.76 (s), 128.17 (s), 23.68 (d, $^{1}J_{PC}$ = 13.6 Hz), 19.23 (d, $^{2}J_{PC}$ = 18.1 Hz), 18.93 (d, $^{2}J_{PC}$ = 11.4 Hz). ^{31}P NMR (121 MHz, C_6D_6) δ -5.58. ^{19}F NMR (282 MHz, C_6D_6) δ -131.46 (s), -155.96 (s), -162.87 (s). MS (m/z): Calcd, 976.2484 (M+). Found: 976.2389 (FAB-MS, M+).

Synthesis of Complex 2Ni

Compound **1** (1.00 g, 2.15 mmol, 1 equiv.) was transferred as a tetrahydrofuran solution (*ca.* 20 mL) into a Schlenk flask fitted with a screw-in Teflon stopper and equipped with a magnetic stirbar. Ni(COD)$_2$ (593.3 mg, 2.15 mmol, 1 equiv.) was then added as a

tetrahydrofuran suspension (*ca.* 20 mL). The reaction mixture was then sealed and allowed to stir for 16 hrs, during which time to solution changed color from a yellow to a dark red brown. All volatiles were then removed under reduced pressure. The residue was then dissolved in benzene and filtered through a Celite pad. The volatiles of the filtrate were removed under reduced pressure to yield the product as a dark brown clumpy solid. Yield: 833 mg (74 %) ^{1}H NMR (300 MHz, C_6D_6) δ 7.82 (broad s, Py*H*, 2H), 7.47 (d, J = 6.9 Hz, Ar*H*, 2H), 7.22 (d, J = 6.0 Hz, Ar*H*, 2H), 7.10 (m, Ar*H*, 4H), 4.35 (s, Py*H*, 1H), 2.28 (m, C*H*, 2H), 2.07 (m, C*H*, 2H), 1.07 (m, C*H*$_3$, 7.6 Hz, 18H), 0.91 (m, C*H*$_3$, 6H). ^{13}C NMR (126 MHz, C_6D_6) δ 150.84 (s), 142.31 (s), 136.58 (s), 132.64 (s), 129.12 (s), 128.42 (s), 128.19 (s), 106.12 (s), 59.21 (s), , 27.02 (s), 24.61 (d, $^{1}J_{PC}$ = 15.6 Hz), 22.27 (s), 20.07 (d, $^{1}J_{PC}$ = 20.1 Hz), 19.25 (s). ^{31}P NMR (121 MHz, C_6D_6) δ 40.38 (s). Anal. Calcd. for: $C_{29}H_{39}NP_2Ni$ (**2Ni**) (%): C, 66.69; H, 7.53; N, 2.68. Found: C, 65.15; H, 6.89; N, 2.21.

Synthesis of Complex 2Pd

Compound **1** (211.9 mg, 0.457 mmol, 1 equiv.) was transferred as a benzene solution (*ca.* 10 mL) into a Schlenk flask fitted with a screw-in Telfon stopper and equipped with a magnetic stirbar. $PdMe_2$(TMEDA) (127.05 mg, 0.503 mmol, 1.1 equiv.) was then added as a benzene suspension (*ca.* 20 mL). The reaction mixture was then sealed and heated to 60 °C for 16 hrs, during which time the reaction changed color from yellow to a bright orange. The solution was then filtered through a Celite pad, and the volatiles of the resulting filtrate were removed under reduced pressure to yield clean product as an orange solid without further purification. Yield: 197.6 mg (76 %). ^{1}H NMR (500 MHz, C_6D_6) δ 8.29 (s, Py*H*, 2H), 7.90 (s, Py*H*, 1H), 7.24 (m, Ar*H*, 4H), 7.15 – 7.10 (m, Ar*H*, 2H), 7.05 (m, Ar*H*, 2H), 2.22 – 2.01 (m, C*H*, 2H), 1.86 (p, $^{3}J_{HH}$ = 7.2 Hz, C*H*, 2H), 1.28 (dd, $^{3}J_{PH}$ = 7.8, $^{3}J_{HH}$ = 7.6 Hz, C*H*$_3$, 6H), 1.08 (dd, $^{3}J_{PH}$ =

8.0, $^{3}J_{HH}$ =7.5 Hz, C*H*$_3$, 6H), 0.96 (dd, $^{3}J_{PH}$ = 7.9, $^{3}J_{HH}$ = 7.7 Hz, C*H*$_3$, 6H), 0.73 (dd, $^{3}J_{PH}$ = 5.9, $^{3}J_{HH}$ = 5.8 Hz, C*H*$_3$, 6H). ^{13}C NMR (126 MHz, C_6D_6) δ 147.39 (vt, $^{2}J_{PC}$ = 11.1 Hz), 146.18 (s), 134.51 (vt, $^{1}J_{PC}$ = 13.6 Hz), 131.64 (s), 131.44 (vt, $^{3}J_{PC}$ =5.0 Hz), 130.68 (s), 128.61 (s), 127.24 (s), 105.30 (s), 27.87 (vt, $^{2}J_{PC}$ = 5.7 Hz), 21.75 (vt, $^{2}J_{PC}$ = 7.8 Hz), 20.66 (vt, $^{3}J_{PC}$ = 5.5 Hz), 17.07 (s). ^{31}P NMR (121 MHz, C_6D_6) δ 33.76 (s). Anal. Calcd. for: $C_{29}H_{39}NP_2Pd$ (**2Pd**) (%): C, 61.11; H, 6.90; N, 2.46. Found: C, 60.87; H, 6.70; N, 2.45.

Synthesis of Complex 2Ni-B(C_6F_5)$_3$

Compound **1-B(C_6F_5)$_3$** (126.7 mg, 0.129 mmol, 1 equiv.) was transferred as a benzene solution (*ca.* 10 mL) into a Schlenk flask fitted with a screw-in Telfon stopper and equipped with a magnetic stirbar. Ni(COD)$_2$ (35.7 mg, 0.129 mmol, 1 equiv.) was then added as a benzene suspension (*ca.* 10 mL). The reaction was allowed to stir for 16 hrs, during which time the solution changed color from a pale yellow to dark brown. The volatiles were then removed under reduced pressure. The brown residue was then dissolved in benzene and filtered through a Celite pad. The volatiles of the filtrate were removed under reduced pressure to yield the product as a dark brown solid. Yield: 94 mg (70 %) ^{1}H NMR (500 MHz, C_6D_6) δ 7.42 (d, J_{HH} = 7.0 Hz, Ar*H*, 2H), 7.37 (s, Py*H*, 2H), 7.01 (m, Ar*H*, 2H), 7.00 – 6.94 (m, Ar*H*, 2H), 3.18 (s, Py*H*, 1H), 2.07 (m, C*H*, 2H), 1.85 – 1.70 (m, C*H*, 2H), 0.88 (dd, $^{3}J_{PH}$ = 14.7, $^{3}J_{HH}$ = 7.5 Hz, C*H*$_3$, 6H), 0.85 – 0.77 (m, 18H). ^{13}C NMR (126 MHz, C_6D_6) δ 149.07 (s), 147.45 (vt, $^{2}J_{PC}$ = 10.9 Hz), 147.15 (s), 140.72 (s), 138.74 (s), 138.19 (s), 136.30 (m), 135.93 – 135.32 (m), 135.07 (s), 131.77 (d, $^{3}J_{PC}$ = 7.3 Hz), 131.13 (s), 130.48 (s), 130.09 – 129.14 (m), 128.89 (s), 128.61 (s), 119.66 (s), 104.74 (s), 49.97 – 47.80 (m), 28.42 – 26.47 (m), 22.26 – 20.89 (m), 20.15 – 18.18 (m). ^{31}P NMR (121 MHz, C_6D_6) δ 41.97 (s). ^{19}F NMR (282 MHz, C_6D_6) δ -131.42 (s), -157.56

(s), -163.95 (s). Anal. Calcd. for: $C_{47}H_{39}BF_{15}NP_2Ni$ (**2Ni-B(C_6F_5)$_3$**) (%): C, 54.48; H, 3.80; N, 1.35. Found: C, 55.71; H, 3.79; N, 1.28.

Synthesis of Complex 2Pd-B(C_6F_5)$_3$

Compound **1-B(C_6F_5)$_3$** (110.3 mg, 0.113 mmol, 1 equiv.) was dissolved in tetrahydrofuran (*ca.* 5 mL) and transferred to a 20 mL scintillation vial equipped with a magnetic stirbar. $PdCl_2COD$ (32.3 mg, 0.113 mmol, 1 equiv.) was then added as a suspension in tetrahydrofuran (*ca.* 5 mL). The reaction mixture was allowed to stir for 3 hrs, during which time the solution changed color from a yellow suspension to a homogeneous orange color. Ni(bpy)(COD) (36.5 mg, 0.113 mmol, 1 equiv.) was then added as a tetrahydrofuran solution (*ca.* 10 mL) resulting in an immediate color change from orange to a pink purple solution heterogeneous solution. The reaction mixture was allowed to stir for 30 mins before filtering through a Celite pad. The volatiles of the filtrate were then removed under reduced pressure to yield a pink purple solid. Yield: 96.7 mg (79 %). ^{1}H NMR (500 MHz, C_6D_6) δ 7.69 (s, Py*H*, 2H), 7.47 (s, Ar*H*, 2H), 7.09 – 7.04 (m, Ar*H*, 4H), 7.01 (m, Ar*H*, 2H), 6.39 (s, Py*H*, 1H), 2.02 (m, C*H*, 2H), 1.69 (p, $^3J_{HH}$ = 7.0 Hz, C*H*, 2H), 1.03 (dd, $^3J_{PH}$ = 8.0, $^3J_{HH}$ = 7.7 Hz, C*H*$_3$, 6H), 0.88 (dd, $^3J_{PH}$ = 7.9, $^3J_{HH}$ =7.8 Hz, C*H*$_3$, 6H), 0.78 (q, $^3J_{PH}$ = 7.9, $^3J_{HH}$ = 7.8 Hz, C*H*$_3$, 6H), 0.66 (dd, $^3J_{PH}$ =J = 6.5, $^3J_{HH}$ = 6.2 Hz, C*H*$_3$, 6H). ^{13}C NMR (126 MHz, C_6D_6) δ 148.97 (s), 147.04 (s), 145.25 (t), 140.80 (s), 138.81 (s), 138.22 (s), 138.00 (s), 136.37 (s), 131.56 (t, J = 16.5 Hz), 131.51 (s), 130.35 (s), 130.07 (s), 128.63 (s), 126.81 (t, J = 6.1 Hz), 120.10 (s), 86.87 (s), 27.80 (vt, $^2J_{PC}$ = 6.9 Hz), 21.32 (vt, $^3J_{PC}$ = 9.0 Hz), 19.77 (vt, $^3J_{PC}$ = 6.9 Hz), 19.30 (m), 17.22 (s). ^{31}P NMR (121 MHz, C_6D_6) δ 34.06 (s). ^{19}F NMR (282 MHz, C_6D_6) δ -131.04 (s), -157.36 (s), -163.73 (s). Anal. Calcd. for: $C_{47}H_{39}BF_{15}NP_2Pd$ (**2Pd-B(C_6F_5)$_3$**) (%): C, 52.17; H, 3.63; N, 1.29. Found: C, 51.80; H, 3.69; N, 1.71.

Synthesis of Complex 2Ni-Me

Compound **2Ni** (213 mg, 0.408 mmol, 1 equiv.) was dissolved in benzene (*ca.* 12 mL) and transferred to a 20 mL scintillation vial equipped with a magnetic stirbar. MeOTf (44.7 μL, 0.408 mmol, 1 equiv.) was added by Hamilton syringe to a rapidly stirring reaction mixture, which resulted in a color change from red brown to a darker brown. After stirring for 30 mins, volatiles were then removed under reduced pressure to yield the desired product as a dark brown solid without the need for further purification. Yield: 260 mg (93 %). ^{1}H NMR (300 MHz, C_6D_6) δ 7.25 – 7.18 (m, Ar*H*, 2H), 7.16 – 7.11 (m, Ar*H*, 4H), 7.10 – 7.01 (m, Ar*H*, 2H), 6.78 – 6.73 (m, Py*H*, 2H), 2.77 (t, $^{4}J_{HH}$ = 1.4 Hz, NC*H*$_3$, 3H), 2.57 (m, C*H*, 2H), 2.45 (m, C*H*, 2H), 1.99 – 1.90 (t, $^{2}J_{PH}$ = 5.0 Hz, 1H), 1.22 – 1.13 (m, C*H*$_3$, 6H), 1.13 – 1.06 (m, C*H*$_3$, 6H), 1.06 – 0.99 (m, C*H*$_3$, 6H), 0.99 – 0.91 (m, C*H*$_3$, 6H). ^{13}C NMR (126 MHz, C_6D_6) δ 147.30 (s), 133.92 (s), 131.41 (s), 129.38 (s), 129.18 (s), 128.52 (s), 128.42 (s), 128.19 (s), 104.91 (s), 44.95 (s), 41.69 (s), 26.42 (s), 23.30 (s), 19.43 (s), 18.97 (s), 18.65 (s), 18.38 (s). ^{31}P NMR (121 MHz, C_6D_6) δ 31.13 (s). ^{19}F NMR (282 MHz, C_6D_6) δ -77.43 (s). Anal. Calcd. for: $C_{31}H_{42}F_3NNiO_3P_2S$ (**2Ni-Me**) (%): C, 54.25; H, 6.17; N, 2.04. $C_{37}H_{48}F_3NNiO_3P_2S$ (**2Ni-Me·(C_6H_6)**) (%): C, 58.13; H, 6.33; N, 1.83. Found: C, 57.24; H, 6.01; N, 1.70.

Synthesis of Complex 2Ni-BCy$_2$OTf

Compound **2Ni** (113.4 mg, 0.217 mmol, 1 equiv.) was dissolved in benzene (*ca.* 5 mL) and transferred to a 20 mL scintillation vial equipped with a magnetic stirbar. Dicyclohexylboron triflate (70.8 mg, 0.217 mmol, 1 equiv.) was added as a benzene solution (*ca.* 5 mL), which resulted in an immediate color change from red brown to a dark green solution before gradually turning a dark brown similar to that of **2Ni-B(C_6F_5)$_3$**. The solution was allowed to stir for 3 hrs before volatiles were removed under reduced pressure yielding the desired

complex as a dark brown solid without the need for further purification. Yield: 120 mg (65 %). ^{1}H NMR (300 MHz, C_6D_6) δ 7.43 (s, Py*H*, 2H), 7.41 (s, Ar*H*, 2H), 7.11 – 7.00 (m, Ar*H*, 6H), 3.45 (s, Py*H*, 1H), 2.33 (s, 2H), 2.13 (m, 1H), 2.00 – 1.80 (m, 8H), 1.71 (s, 1H), 1.43 (m, 10H), 1.30 (m, 2H), 1.10 – 0.99 (m, 6H), 0.97 – 0.81 (m, 18H). ^{13}C NMR (126 MHz, C_6D_6) δ 147.86 (s), 142.37 (s), 136.04 (s), 133.94 (s), 131.16 (s), 130.29 (s), 104.49 (s), 29.29 (s), 28.83 (s), 28.15 (s), 27.74 (s), 27.41 (s), 27.02 (s), 21.40 (s), 19.71 (s), 18.79 (s). ^{31}P NMR (121 MHz, C_6D_6) δ 42.29. ^{19}F NMR (282 MHz, C_6D_6) δ -77.35.

Synthesis of Complex 2Pd-H

Compound **2Pd** (34.7 mg, 0.0609 mmol, 1 equiv.) was dissolved in tetrahydrofuran (*ca.* 4 mL) and transferred to a 20 mL scintillation vial equipped with a magnetic stirbar. Pyridinium triflate (13.95 mg, 0.0609 mmol, 1 equiv.) was then added as a tetrahydrofuran solution (*ca.* 4 mL). This resulted in an immediate color change from orange to a bright pink solution. The reaction mixture was allowed to stir for 1 hr before all volatiles were removed under reduced pressure to yield clean product as a pink solid without further purification. Yield: 40.3 mg (92 %) ^{1}H NMR (500 MHz, CD_3CN) δ 9.88 (s, PyN*H*, 1H), 7.75 – 7.66 (m, Ar*H*, 2H), 7.66 – 7.54 (m, Ar*H*, 4H), 7.47 – 7.36 (m, Ar*H*, 2H), 7.28 (s, Py*H*, 2H), 6.16 (s, Py*H*, 1H), 2.77 (m, C*H*, 2H), 2.30 (m, C*H*, 2H), 1.28 (dd, $^{3}J_{PH}$ = 9.2, $^{3}J_{HH}$ = 6.9 Hz, C*H*$_3$, 6H), 1.15 (dd, $^{3}J_{PH}$ = 8.8, $^{3}J_{HH}$ = 6.8 Hz, C*H*$_3$, 6H), 1.11 – 1.01 (m, C*H*$_3$, 12H). ^{13}C NMR (126 MHz, CD_3CN) δ 144.81 (s), 132.24 (s), 130.99 (s), 130.38 (s), 129.79 (s), 129.14 (s), 123.78 (s), 77.26 (s), 27.52 (vt, $^{1}J_{PC}$ = 7.6 Hz), 21.71 (vt, $^{1}J_{PC}$ = 9.6 Hz), 19.69 – 19.18 (m), 19.05 (s), 16.82 (s). ^{31}P NMR (121 MHz, CD_3CN) δ 32.08 (s). ^{19}F NMR (282 MHz, CD_3CN) δ -79.33 (s). Anal. Calcd. for: $C_{30}H_{40}F_3NO_3P_2PdS$ (**2Pd-H**) (%): C, 50.04; H, 5.60; N, 1.95. Found: C, 50.25; H, 5.58; N, 1.81.

Synthesis of Complex 3Ni

Compound **2Ni** (53.8 mg, 0.103 mmol, 1 equiv.) was dissolved in benzene (*ca.* 5 mL) and transferred to a 20 mL scintillation vial equipped with a magnetic stirbar. Triethylammonium triflate (27.9 mg, 0.111 mmol, 1.08 equiv.) was added as a benzene solution (*ca.* 5 mL). The reaction mixture was allowed to stir for 3 hrs before volatiles were removed under reduced pressure. The material could be recrystallized from tetrahydrofuran:hexanes to yield the desired product as brown crystals sufficient for identification of the compound in the solid state. In acetonitrile the complex breaks up likely due to acetonitrile coordination. The sensitivity of the complex precluded further detailed characterization by NMR or elemental analysis. In d_8-tetrahydrofuran the ^{31}P NMR shows two very broad signals consistent with the solid state structure. By ^{1}H NMR very broad signals were observed precluding assignment and ^{13}C was too broad to observe assignable peaks. Yield: 36.8 mg (60 %). ^{31}P NMR (121 MHz, *d*$_8$-THF) δ 42.12 (broad s), 25.68 (broad s). ^{19}F NMR (282 MHz, *d*$_8$-THF) δ -78.96 (s).

Synthesis of Complex 4Ni(CO)

Compound **2Ni** (71.7 mg, 0.137 mmol, 1 equiv.) was dissolved in benzene (*ca.* 20 mL) and transferred to a Schlenk flask fitted with a screw-in Teflon stopper and equipped with a magnetic stirbar. This solution was degassed and CO (1.3 equiv.) admitted to the reaction flask. The solution stirred for 3 hrs during which time a lightening of the solution was observed. All volatiles were then removed under vacuum. The resulting brown residue was dissolved in benzene and transferred to a 20 mL scintillation vial. Lyophilization of the solvent yielded the desired clean product as a brown powder without further purification. Yield: 71.4 mg (94.5 %) ^{1}H NMR (500 MHz, C_6D_6) δ 8.58 (broad s, Py*H*, 2H), 7.34 – 7.26 (m, Ar*H*, 4H), 7.11 (t, $^{3}J_{HH}$ = 7.4 Hz, Ar*H*, 2H), 7.06 (t, $^{3}J_{HH}$ = 7.3 Hz, Ar*H*, 2H), 6.23 (s, Py*H*, 1H), 2.63 – 2.20 (m, C*H*,

2H), 2.19 – 1.94 (m, C*H*, 2H), 1.13 – 1.04 (m, C*H*$_3$, 6H), 1.00 (dd, $^3J_{PH}$ =14.6, $^3J_{HH}$ = 6.9 Hz, C*H*$_3$, 12H), 0.84 (dd, $^3J_{PH}$ = 6.8, $^3J_{HH}$ = 6.6 Hz, C*H*$_3$, 6H). ^{13}C NMR (126 MHz, C_6D_6) δ 197.31 (s), 148.37 (s), 145.30 (s), 134.32 (s), 130.54 (s), 129.60 (s), 129.06 (s), 128.20 (s), 83.07 (s), 28.52 (vt, $^1J_{PC}$ =10.6 Hz), 25.74 (vt, $^1J_{PC}$ = 6.5 Hz), 19.72 (t, $^2J_{PC}$ = 4.9 Hz), 18.81 (vt, $^2J_{PC}$ = 4.7 Hz), 18.14 (s), 17.70 (s). ^{31}P NMR (121 MHz, C_6D_6) δ 33.81 (s). IR(thin film, ATIR) ν_{CO}: 1930 cm^{-1}. Anal. Calcd. for: $C_{30}H_{39}NNiOP_2$ (**4Ni(CO)**) (%): C, 65.48; H, 7.14; N, 2.55. Found: C, 65.23; H, 6.87; N, 2.34.

Synthesis of Complex 4Ni(CO)-B(C_6F_5)$_3$

Compound **2Ni-B(C_6F_5)$_3$** (48.2 mg, 0.046 mmol, 1 equiv.) was dissolved in benzene (*ca.* 10 mL) and transferred to a Schlenk flask fitted with a screw-in Teflon stopper and equipped with a magnetic stirbar. This solution was degassed and CO (1.3 equiv.) admitted to the reaction flask. The solution stirred for 3 hrs during which time a lightening of the solution was observed. All volatiles were then removed under vacuum. The resulting brown residue was dissolved in benzene and transferred to a 20 mL scintillation vial. Lyophilization of the solvent yielded the desired clean product as a brown powder without further purification. Yield: 42.6 mg (86 %). ^{1}H NMR (300 MHz, C_6D_6) δ 8.03 (s, Py*H*, 2H), 7.59 (dd, $^3J_{HH}$ = 7.7, $^4J_{HH}$ = 2.9 Hz, Ar*H*, 2H), 7.04 (m, Ar*H*, 2H), 6.96 (d, $^3J_{HH}$ = 4.7 Hz, Ar*H*, 4H), 4.57 (t, $^2J_{PH}$ = 6.8 Hz, Py*H*, 1H), 2.17 (h, $^3J_{HH}$ = 7.0 Hz, C*H*, 2H), 1.74 (h, $^3J_{HH}$ = 6.9 Hz, C*H*, 2H), 0.87 – 0.73 (m, C*H*$_3$, 6H), 0.59 (m, C*H*$_3$, 18H). ^{13}C NMR (126 MHz, C_6D_6) δ 197.39 (s), 149.10 (s), 147.15 (s), 147.03 – 146.11 (m), 140.95 (s), 138.64 (s), 138.41 (s), 136.47 (m), 131.61 – 130.78 (m), 130.41 (d, $^2J_{PC}$ = 32.4 Hz), 129.19 (s), 128.66 (s), 128.18 (s), 119.03 (s), 113.82 (s), 68.61 (s), 27.30 (vt, $^1J_{PC}$ = 10.2 Hz), 24.29 (vt, $^1J_{PC}$ = 6.7 Hz), 19.07 – 18.32 (m), 17.92 – 16.97 (m), 16.69 (s). ^{31}P NMR (121 MHz, C_6D_6) δ 31.84 (s). ^{19}F NMR (282 MHz, C_6D_6) δ -130.79 (s), -

157.28 (s), -163.66 (s). IR(thin film, ATIR) ν_{CO}: 1976 cm^{-1}. Anal. Calcd. for: $C_{48}H_{39}BF_{15}NNiOP_2$ (**4Ni-B(C_6F_5)$_3$**) (%): C, 54.27; H, 3.70; N, 1.32. $C_{60}H_{51}BF_{15}NNiOP_2$ (**4Ni(CO)-B(C_6F_5)$_3$·2(C_6H_6)**) (%): C, 59.14; H, 4.22; N, 1.15. Found: C, 58.57; H, 4.32; N, 1.12.

Synthesis of Complex 4Ni(CO)-H

Compound **2Ni** (72.9 mg, 0.140 mmol, 1 equiv.) was dissolved in benzene (*ca.* 20 mL) and transferred to a Schlenk flask fitted with a screw-in Telfon stopper and equipped with a magnetic stirbar. This solution was degassed and CO (1.3 equiv.) admitted to the reaction flask. The solution stirred for 3 hrs during which time a lightening of the solution was observed consistent with the formation of **4Ni(CO)**. All volatiles were then removed under vacuum. The residue was then redissolved in tetrahydrofuran (*ca.* 4 mL) and transferred to a 20 mL scintillation vial equipped with a magnetic stirbar. Pyridinium triflate (31.98 mg, 0.140 mmol, 1 equiv.) was then added as a tetrahydrofuran solution (*ca.* 2 mL), which resulted in a color change from brown to a red brown. This reaction was allowed to stir for 1 hr before all volatiles were removed under reduced pressure to yield the desired product as a red brown powder. Yield: 52.0 mg (67.7 %). ^{1}H NMR (500 MHz, CD_3CN) δ 11.78 (broad s, N*H*, 1H), 7.84 (d, $^4J_{HH}$ = 3.7 Hz, Py*H*, 2H), 7.75 (m, Ar*H*, 2H), 7.63 (m, Ar*H*, 4H), 7.54 (m, Ar*H*, 2H), 4.79 (t, $^2J_{PH}$ = 6.1 Hz, Py*H*, 1H), 2.82 (h, $^3J_{HH}$ = 6.9 Hz, C*H*, 2H), 2.49 (h, $^3J_{HH}$ = 7.0 Hz, C*H*, 2H), 1.32 (dd, $^3J_{PH}$ = 12.2, $^3J_{HH}$ = 7.1 Hz, C*H*$_3$, 6H), 1.08 (m, C*H*$_3$, 12H), 0.88 (dd, $^3J_{PH}$ = 13.6, $^3J_{HH}$ = 7.0 Hz, C*H*$_3$, 6H). ^{13}C NMR (126 MHz, CD_3CN) δ 198.82 (s), 145.31 (vt, $^2J_{PC}$ = 11.5 Hz), 132.41 – 131.83 (m), 131.62 (d, $^1J_{PC}$ = 12.5 Hz), 130.50 (s), 129.66 (s), 129.10 (s), 113.51 (vt, $^3J_{PC}$ = 5.7 Hz), 66.74 (s), 27.55 (vt, $^1J_{PC}$ = 10.7 Hz), 24.75 (vt, $^2J_{PC}$ = 7.6 Hz), 19.22 (s), 18.19 (s), 17.54 (s), 17.01 (s). ^{31}P NMR (121 MHz, CD_3CN) δ 35.69 (s). ^{19}F NMR (282 MHz, CD_3CN)

δ -79.25 (s). IR(thin film, ATIR) ν_{CO}: 1975 cm^{-1}. Anal. Calcd. for: $C_{31}H_{40}F_3NNiO_4P_2S$ (**4Ni(CO)-H**) (%): C, 53.16; H, 5.76; N, 2.00. Found: C, 51.96; H, 5.39; N, 2.54.

Synthesis of Complex 4Ni(CO)-Me

Compound **2Ni-Me** (35.9 mg, 0.052 mmol, 1 equiv.) was dissolved in benzene (*ca.* 10 mL) and transferred to a Schlenk flask fitted with a screw-in Teflon stopper and equipped with a magnetic stirbar. This solution was degassed and CO (1.3 equiv.) admitted to the reaction flask. The solution stirred for 3 hrs during which time a lightening of the solution. All volatiles were then removed under vacuum. The resulting red brown residue was dissolved in acetonitrile and transferred to a 20 mL scintillation vial. Removal of the volatiles under reduced pressure yielded the desired clean product as a red brown powder without further purification. Yield: 34.7 mg (93 %). ^{1}H NMR (500 MHz, C_6D_6) δ 7.95 (dd, $^3J_{HH}$ = 7.8, $^4J_{HH}$ = 3.5 Hz, Ar*H*, 2H), 7.65 (d, $^4J_{HH}$ = 4.0 Hz, Py*H*, 2H), 7.37 (dd, $^3J_{HH}$ = 9.3, $^4J_{HH}$ = 5.7 Hz, Ar*H*, 2H), 7.22 (dd, J = 9.0, 5.8 Hz, Ar*H*, 2H), 7.16 (m, Ar*H*, 2H), 4.51 (t, $^2J_{PH}$ = 6.2 Hz, Py*H*, 1H), 3.75 (s, NC*H*$_3$, 3H), 2.34 – 2.22 (m, C*H*, 2H), 1.98 (p, $^3J_{HH}$ = 6.7 Hz, C*H*, 2H), 0.89 (m, C*H*$_3$, 12H), 0.70 (dd, $^3J_{PH}$ = 13.5, $^3J_{HH}$ = 6.8 Hz, C*H*$_3$, 12H). ^{13}C NMR (126 MHz, C_6D_6) δ 145.02 (vt, $^2J_{PC}$ = 11.4 Hz), 136.12 (s), 131.82 – 131.01 (m), 130.79 (s), 130.57 (s), 130.41 (s), 129.33 (s), 128.21 (s), 115.61 (s), 67.44 (s), 45.67 (s), 27.75 (vt, $^1J_{PC}$ = 10.4 Hz), 24.84 (vt, $^1J_{PC}$ = 7.1 Hz), 19.36 (s), 18.39 (s), 17.75 (s), 17.42 (s). ^{31}P NMR (121 MHz, C_6D_6) δ 34.74 (s). ^{19}F NMR (282 MHz, C_6D_6) δ -77.53 (s). IR(thin film, ATIR) ν_{CO}: 1966 cm^{-1}. Anal. Calcd. for: $C_{32}H_{42}F_3NNiO_4P_2S$ (**4Ni(CO)-Me**) (%): C, 53.80; H, 5.93; N, 1.96. Found: C, 54.09; H, 5.98; N, 1.71.

Synthesis of Complex 5Ni

Compound **2Ni** (98.8 mg, 0.189 mmol, 1 equiv.) was dissolved in tetrahydrofuran (*ca.* 5 mL) and transferred to a 20 mL scintillation vial equipped with a magnetic stirbar. While stirring vigorously, $[OMe_3][BF_4]$ (28.0 mg, 0.189 mmol, 1 equiv.) was added as a suspension in tetrahydrofuran (*ca.* 5 mL). The reaction mixture was allowed to stir for *ca.* 2 hrs during which time the $[Me_3O][BF_4]$ solubilized and a significant darkening of the solution to a color similar to **2Ni-Me** was observed. At this point, $[NO][BF_4]$ was added as a suspension in tetrahydrofuran (*ca.* 5 mL) and the vial was rapidly sealed. The reaction mixture was allowed to stir for 16 hrs during which time to solution a heterogenous brown with visible blueish precipitate forming upon standing. The reaction mixture was then filtered over a Celite pad and washed with copious tetrahydrofuran until washes became colorless leaving a blue colored precipitate. The product was eluted from the Celite pad using acetonitrile, and volatiles of the blue filtrate were removed under reduced pressure. The product could be purified by crystallization from acetonitrile:diethyl ether to yield the desired complex as blue crystals. Yield: 34 mg (24.3 %). The compound is unstable in solution and prone to decomposition. Peaks associated with the dominant decomposition product are indicated in the appropriate NMR spectra. ^{1}H NMR (500 MHz, CD_3CN) δ 9.01 (s, Py*H*, 2H), 8.16 – 8.05 (m, Ar*H*, 2H), 7.89 (m, Ar*H*, 4H), 7.81 – 7.74 (m, Ar*H*, 2H), 7.55 (s, Py*H*, 1H), 4.54 (s, NC*H*$_3$, 3H), 2.94 (m, C*H*, 4H), 1.19 – 1.04 (m, C*H*$_3$, 24H). ^{31}P NMR (121 MHz, CD_3CN) δ 31.31 (broad s). ^{13}C NMR (126 MHz, CD_3CN) δ 143.96 (s), 143.35 (s), 140.35 (d, $^{2}J_{PC}$ = 14.0 Hz), 134.41 (s), 133.27 (s), 132.20 (s), 132.09 (s), 131.46 (s), 131.07 (s), 128.50 (s), 128.04 (d, $^{1}J_{PC}$ = 24.4 Hz), 49.13 (s), 27.19 (s), 24.17 (s), 18.89 (s), 17.25 (s). IR(powder, ATIR) ν_{NO}: 1846 cm^{-1}. Anal. Calcd. for: $C_{30}H_{42}B_2F_8N_2NiOP_2$ (**5Ni**) (%): C, 48.63; H, 5.71; N, 3.78. $C_{30}H_{42}B_2F_8N_2NiOP_2$ (**5Ni-Me·MeCN**) (%): C, 49.15; H, 5.80; N, 5.37. Found: C, 48.13; H, 5.42; N, 5.15.

Synthesis of Complex 6Ni

Compound **2Ni** (24.6 mg, 0.047 mmol, 1 equiv.) was dissolved in benzene (*ca.* 2 mL) and transferred to a 20 mL scintillation vial equipped with a magnetic stirbar. Pinacol borane (6.9 μL, 0.047 mmol, 1 equiv.) was then added via Hamilton syringe. The reaction mixture was allowed to stir for 6 hrs before volatiles were removed under reduced pressure yielding the product without further purification. Yield: 29.1 mg (95 %). ^{1}H NMR (500 MHz, C_6D_6) δ 7.78 (dd, $^{3}J_{HH}$ = 7.4, $^{4}J_{HH}$ =2.9, Ar*H*, 1H), 7.55 (ddd, $^{3}J_{HH}$ = 7.3, $^{4}J_{HH}$ = 3.8, $^{4}J_{HH}$ = 2.2 Hz, Ar*H*, 1H), 7.33 (ddd, $^{3}J_{HH}$ = 8.8, $^{4}J_{HH}$ = 4.5, $^{4}J_{HH}$ = 2.2 Hz, Ar*H*, 1H), 7.13 – 7.10 (m, Ar*H*, 1H), 7.10 – 7.06 (m, Ar*H*, 2H), 7.05 – 7.00 (m, Ar*H*, 1H), 6.83 (d, $^{4}J_{HH}$ = 1.5 Hz, Py-(C3)*H*, 1H), 4.51 (dd, $^{1}J_{HH}$ = 13.6, $^{4}J_{HH}$ = 1.6 Hz, Py-(C4)*H*, 1H), 4.14 – 4.08 (m, Py-(C1)*H*, 1H), 3.78 (dtd, $^{1}J_{HH}$ = 13.6, $^{4}J_{PH}$ = 3.3, $^{3}J_{HH}$ = 1.2 Hz, Py-(C4)*H*, 1H), 2.35 – 2.21 (m, C*H*, 2H), 2.00 (pd, $^{3}J_{HH}$ = 7.0, $^{3}J_{HH}$ = 5.0 Hz, C*H*, 1H), 1.83 – 1.73 (m, C*H*, 1H), 1.25 – 1.15 (m, overlapping *i*Pr and pinacol CH_3, 9H), 1.12 (s, pinacol CH_3, 6H), 1.09 – 0.99 (m, *i*Pr CH_3, 12H), 0.98 (s, pinacol CH_3, 3H), 0.95 – 0.84 (m, *i*Pr CH_3, 6H). ^{13}C NMR (126 MHz, C_6D_6) δ 155.90 (d, $^{2}J_{PC}$ = 32.8 Hz), 150.24 (d, $^{2}J_{PC}$ = 15.2 Hz), 148.59 (d, $^{3}J_{PC}$ = 11.3 Hz), 148.33 (d, $^{2}J_{PC}$ = 11.5 Hz), 131.87 (d, $^{1}J_{PC}$ = 20.1 Hz), 131.01 (s), 129.66 (d, $^{1}J_{PC}$ = 8.4 Hz), 129.45 (s), 129.21 – 128.87 (m), 128.20 (s), 125.75 (m), 125.48 (s, Py(C2)), 120.81 (d, $^{4}J_{PC}$ = 5.3 Hz, Py(C3)), 82.33 (s), 71.21 (d, $^{2}J_{PC}$ = 14.6 Hz, Py(C5)), 59.22 (d, $^{2}J_{PC}$ = 10.9 Hz, Py(C1)), 52.41 (s, Py(C4)), 28.83 (d, $^{1}J_{PC}$ = 10.8 Hz), 27.73 (d, $^{1}J_{PC}$ = 15.1 Hz), 24.85 (s), 24.56 (s), 24.23 (d, $^{2}J_{PC}$ = 11.2 Hz), 23.83 (d, $^{2}J_{PC}$ = 15.7 Hz), 21.12 (d, $^{2}J_{PC}$ = 12.8 Hz), 20.91 (d, $^{2}J_{PC}$ = 7.9 Hz), 19.72 (d, $^{2}J_{PC}$ = 8.6 Hz), 19.38 (d, $^{2}J_{PC}$ = 11.3 Hz), 19.27 (d, $^{2}J_{PC}$ = 7.5 Hz), 18.97 (s), 18.88 (s), 18.78 (s). ^{31}P NMR (121 MHz, C_6D_6) δ 56.23 (d, J = 55.8 Hz), 44.70 (d, J = 55.6 Hz).

Synthesis of Complex 7Ni

Compound **2Ni** (213.4 mg, 0.408 mmol, 1 equiv.) was dissolved in benzene (*ca.* 10 mL) and transferred to a 20 mL scintillation vial equipped with a magnetic stirbar. Phenylsilane (50.4 μL, 0.408 mmol, 1 equiv.) was then added via Hamilton syringe. The reaction mixture was allowed to stir for 1 hr before volatiles were removed under reduced pressure yielding the product without further purification. Yield: 245 mg (95 %). ^{1}H NMR (500 MHz, C_6D_6) δ 7.70 (m, Ar*H*, 1H), 7.63 (m, Ar*H*, 1H), 7.50 (m, Ar*H*, 1H), 7.37 (t, $^{3}J_{HH}$ = 6.6 Hz, Ar*H*, 1H), 7.15 – 7.00 (m, Ar*H*, 6H), 6.40 (d, $^{4}J_{HH}$ = 7.9 Hz, Py-(C3)*H*, 1H), 5.29 (m, Si*H*$_2$, 2H), 4.18 – 4.09 (m, Py-(C1)*H*, 1H), 4.01 (d, $^{1}J_{HH}$ = 13.2 Hz, Py-(C4)*H*, 1H), 3.77 (dd, $^{1}J_{HH}$ = 13.1, $^{4}J_{HH}$ = 3.7 Hz, Py-(C4)*H*, 1H), 2.29 (m, C*H*, 2H), 2.05 (m, C*H*, 1H), 1.78 (m, C*H*, 1H), 1.24 (m, C*H*$_3$, 12H), 1.14 – 0.98 (m, C*H*$_3$, 6H), 0.94 (m, C*H*$_3$, 6H). ^{13}C NMR (126 MHz, C_6D_6) δ 155.77 (d, $^{2}J_{PC}$ = 33.4 Hz), 150.32 (d, $^{2}J_{PC}$ = 15.2 Hz), 148.80 (d, $^{1}J_{PC}$ = 10.9 Hz), 148.55 (d, $^{1}J_{PC}$ = 11.2 Hz), 135.69 (s), 134.91 (s), 133.13 (s), 131.72 (d, $^{3}J_{PC}$ = 7.2 Hz), 131.50 (d, $^{3}J_{PC}$ = 6.9 Hz), 131.16 (s), 130.11 (s), 129.76 (s), 129.59 (s), 129.43 (s), 128.90 (s), 128.30 – 127.87 (m), 125.83 (s), 125.58 (s), 124.96 (s, Py(C2)), 123.65 (d, J = 5.0 Hz, Py(C3)), 70.71 (d, $^{2}J_{PC}$ = 13.9 Hz, Py(C5)), 59.00 (d, $^{2}J_{PC}$ = 11.2 Hz, Py(C1)), 55.13 (s, Py(C4)), 28.71 (d), 27.68 (d, $^{1}J_{PC}$ = 15.3 Hz), 24.03 (d, $^{1}J_{PC}$ = 15.7 Hz), 21.44 (d, $^{1}J_{PC}$ = 12.7 Hz), 20.95 (m), 19.71 (d, $^{2}J_{PC}$ = 8.4 Hz), 19.45 (d, $^{2}J_{PC}$ = 10.9 Hz), 19.25 (d, $^{2}J_{PC}$ = 6.4 Hz), 19.10 (d, $^{2}J_{PC}$ = 4.5 Hz), 18.97 (d, $^{2}J_{PC}$ = 11.7 Hz), 18.86 (s). ^{31}P NMR (121 MHz, C_6D_6) δ 56.09 (d, *J* = 56.2 Hz), 44.77 (d, *J* = 56.1 Hz).

Synthesis of Complex 8Ni

Compound **2Ni-Me** (83.7 mg, 0.121 mmol, 1 equiv.) was dissolved in benzene (*ca.* 10 mL) and transferred to a 20 mL scintillation vial equipped with a magnetic stirbar. While stirring vigorously, sodium triethylborohydride (1 M toluene solution, 122 μL, 0.122 mmol, 1 equiv.)

was then added via Hamilton syringe resulting in an immediately lightening of the solution and precipitation of salts. The reaction was allowed to stir for 1 hr before the reaction mixture was filtered through a Celite pad. The volatiles of the filtrate were removed under reduced pressure yield the desired product without further purification. Yield: 62.4 mg (95 %). ^{1}H NMR (300 MHz, C_6D_6) δ 7.81 (dd, $^{3}J_{HH}$ = 7.7, $^{4}J_{HH}$ = 3.0, Ar*H*, 1H), 7.46 (dd, $^{3}J_{HH}$ = 7.7, $^{4}J_{HH}$ = 4.0, Ar*H*, 1H), 7.34 (dd, $^{3}J_{HH}$ = 7.4, $^{3}J_{HH}$ = 5.7, Ar*H*, 1H), 7.21 – 7.08 (m, Ar*H*, 1H), 7.10 – 7.03 (m, Ar*H*, 3H), 7.00 (m, Ar*H*, 1H), 5.85 (m, Py-(C3)*H*, 1H), 4.09 (t, $^{2}J_{PH}$ = 5.9 Hz, Py-(C1)*H*, 1H), 3.49 (d, $^{1}J_{HH}$ = 12.0 Hz, Py-(C4)*H*, 1H), 3.09 (d, $^{1}J_{HH}$ = 12.0 Hz, Py*H*, 1H), 2.36 (s, NC*H*$_3$, 3H), 2.34 – 2.17 (m, C*H*, 2H), 2.00 (m, C*H*, 1H), 1.81 (m, C*H*, 1H), 1.31 – 1.09 (m, C*H*$_3$, 12H), 1.03 – 0.84 (m, C*H*$_3$, 12H). ^{13}C NMR (126 MHz, C_6D_6) δ 156.12 (d, $^{2}J_{PC}$ = 33.1 Hz), 150.66 (d, $^{1}J_{PC}$ = 13.7 Hz), 148.75 (d, $^{1}J_{PC}$ = 11.9 Hz), 131.99 (d, $^{2}J_{PC}$ = 27.6), 131.17 (s), 130.10 (d, $^{4}J_{PC}$ = 5.5 Hz, Py(C3)), 129.58 (s), 129.33 (s), 129.29 – 129.16 (m), 125.82 (d, $^{3}J_{PC}$ = 4.3 Hz), 125.06 (d, $^{3}J_{PC}$ = 4.1 Hz), 120.05 (s, Py(C2)), 71.13 (d, $^{2}J_{PC}$ = 14.4 Hz, Py(C5)), 61.43 (d, $^{3}J_{PC}$ = 7.4 Hz, Py(C4)), 58.48 (d, $^{2}J_{PC}$ = 10.8 Hz, Py(C1)), 42.29 (s), 29.84 (s), 29.09 (d, $^{1}J_{PC}$ = 10.3 Hz), 27.63 (d, $^{1}J_{PC}$ = 15.2 Hz), 24.49 (d, $^{1}J_{PC}$ = 15.8 Hz), 21.51 (d, $^{1}J_{PC}$ = 12.9 Hz), 21.19 – 20.59 (m), 19.67 (m), 19.40 – 18.80 (m), 10.73 (s). ^{31}P NMR (121 MHz, C_6D_6) δ 56.52 (d, *J* = 56.5 Hz), 44.05 (d, *J* = 56.4 Hz). Anal. Calcd. for: $C_{30}H_{43}NNiP_2$ (**8Ni)** (%): C, 66.94; H, 8.05; N, 2.60. Found: C, 67.16; H, 7.96; N, 2.43.

Synthesis of Complex 2NiCl$_2$-B(C$_6$F$_5$)$_3$

1-B(C$_6$F$_5$)$_3$ (22.7 mg, 0.023 mmol, 1 equiv.) was dissolved in THF (*ca.* 2 mL) and transferred to a 20 mL scintillation vial equipped with a magnetic stirbar. $NiCl_2$(dme) (dme = dimethoxyethane) (5.1 mg, 0.023 mmol, 1 equiv.) was transferred as a suspension in miminal THF and the combined reaction mixture was allowed to stir overnight at room temperature.

Volatiles were then removed under reduced pressure and the residue dissolved in benzene and filtered through a Celite pad. The benzene filtrate was then lyophilized to afford the product as an orange-yellow powder. ^{1}H NMR (300 MHz, C_6D_6) δ 10.84 (s, 1H, Py-(C1)*H*), 8.57 (s, 2H, Py-(C3/C4)*H*), 7.41 (d, *J* = 7.6 Hz, 2H, Ar*H*), 7.03 – 6.94 (m, 4H, Ar*H*), 6.84 (t, *J* = 7.6 Hz, 2H, Ar*H*), 2.46 (s, 2H, C*H*), 1.63 – 1.52 (m, 2H, C*H*), 1.48 (m, 6H, CH_3), 1.10 (m, 6H, CH_3), 0.91 (m, 12H, CH_3). ^{31}P NMR (121 MHz, C_6D_6) δ 7.51. ^{19}F NMR (282 MHz, C_6D_6) δ -130.88, -155.80, -162.71.

Synthesis of Complex 2Ni-SiMe$_3$

2Ni (29.0 mg, 0.056 mmol, 1 equiv.) was dissolved in C_6D_6 and transferred to a J-young tube that had been previously silylated with trimethylsilyl chloride. Trimethylsilyl triflate (10.1 μL, 0.056 mmol, 1 equiv.) was added via Hamilton syringe and the tube was capped and inverted several times to ensure adequate mixing. The reaction mixture immediately turned from brown to a green/brown color during inversion. NMR data confirmed the quantitative conversion to **2Ni-SiMe$_3$** by ^{31}P NMR. The product is semistable in solution but will decompose to a mixture of species over time though this can be slowed in silylated glassware. ^{1}H NMR (300 MHz, C_6D_6) δ 7.26 – 7.00 (m, 10H, overlapping Ar*H* and Py-(C3/4)*H*), 2.70 (m, 2H, C*H*), 2.63 – 2.49 (m, 2H, C*H*), 1.99 (t, *J* = 5.4 Hz, 1H, Py-(C1)*H*), 1.26 – 1.18 (m, 6H, CH_3), 1.17 – 1.06 (m, 12H, CH_3), 1.00 (m, 6H, CH_3), 0.30 (s, 9H,SiCH_3). ^{31}P NMR (121 MHz, C_6D_6) δ 26.58. ^{19}F NMR (282 MHz, C_6D_6) δ -77.33.

Synthesis of Complex 4Ni(CN*t*Bu)

2Ni (14.9 mg, 0.029 mmol, 1 equiv.) was dissolved in C_6D_6 and transferred to a J-young tube. *Tert*-butyl isocyanide (3.23 μL, 0.029 mmol, 1 equiv.) was added via Hamilton syringe and the tube was capped and inverted several times to ensure adequate mixing. NMR data confirmed the formation of **4Ni(CN*t*Bu)** along with some small decomposition to free ligand (~17 %) by ^{31}P NMR. ^{1}H NMR (300 MHz, C_6D_6) δ 8.17 (s, 2H, Py-(C3/4)*H*), 7.47 (m, 2H, Ar*H*), 7.33 – 7.28 (m, 2H, Ar*H*), 5.51 (s, 1H, Py-(C1)*H*), 2.41 (m, 2H, C*H*), 2.11 (m, 2H, C*H*), 1.17 – 1.02 (m, 27H, overlapping CH_3 and C(CH_3)$_3$), 0.90 – 0.81 (m, 6H, CH_3). ^{31}P NMR (121 MHz, C_6D_6) δ 36.56. Crystals grown from this NMR reaction were used to obtain the solid-state structure for **4Ni(CN*t*Bu)**.

Synthesis of Complex 4Ni(CN*t*Bu)-Me

2Ni-Me (17.5 mg, 0.025 mmol, 1 equiv.) was dissolved in C_6D_6 and transferred to a NMR tube. *Tert*-butyl isocyanide (2.9 μL, 0.025 mmol, 1 equiv.) was then added by Hamilton syringe and the tube was capped and inverted several times to ensure adequate mixing. NMR data confirmed the quantitative formation of **4Ni(CN*t*Bu)-Me** by NMR. ^{1}H NMR (300 MHz, C_6D_6) δ 7.53 – 7.44 (m, 1H), 7.27 – 7.13 (m, 2H), 3.80 (t, J = 1.8 Hz, 1H), 3.62 – 3.54 (m, 0H), 2.35 (dq, J = 10.7, 3.5 Hz, 1H), 2.01 (dt, J = 13.4, 6.7 Hz, 1H), 1.18 (s, 3H), 1.00 – 0.91 (m, 1H), 0.91 – 0.83 (m, 1H), 0.82 – 0.69 (m, 2H). ^{31}P NMR (121 MHz, C_6D_6) δ 35.13. ^{19}F NMR (282 MHz, C_6D_6) δ -77.49.

Synthesis of Complex 4Ni(MeCN)-Me

2Ni-Me (20.0 mg, 0.029 mmol, 1 equiv.) was dissolved in MeCN. Volatiles were then removed under reduced pressure to afford **4Ni(MeCN)-Me** in quantitative yield. ^{1}H NMR (300 MHz, C_6D_6) δ 7.23 – 7.17 (m, 2H, Ar*H*), 7.16 – 7.07 (m, 6H, overlapping Ar*H* and Py-(C3/4)*H*), 7.02 – 6.98 (m, 2H, Ar*H*), 3.45 (s, 3H, NCH_3), 2.62 (t, *J* = 6.1 Hz, 1H, Py-(C1)*H*), 2.44 (m, 2H, C*H*), 2.20 – 2.05 (m, 2H, C*H*), 1.40 (s, 3H, CH_3CN), 1.00 – 0.90 (m, 12H, CH_3), 0.83 (m, 12H, CH_3). ^{31}P NMR (121 MHz, C_6D_6) δ 32.03. ^{19}F NMR (282 MHz, C_6D_6) δ -77.67.

Synthesis of Complex 4Ni(CN)-Me

2Ni-Me (15.3 mg, 0.022 mmol, 1 equiv.) was dissolved in THF (*ca.* 5 mL) and transferred to a 20 mL scintillation vial equipped with a magnetic stirbar. Tetrabutylammonium cyanide (6.0 mg, 0.022 mmol, 1 equiv.) was then added as a solution in *ca.* 1 mL THF and the reaction was allowed to stir for 3 hrs. Volatiles were then removed under reduced pressure. ^{31}P NMR data in C_6D_6 shows the clean conversion to a new species, however, removal of the tetrabutylammonium triflate with solvent washes of recrystallization proved difficult. Partial NMR data obtained for **4Ni(CN)-Me**. ^{1}H NMR (300 MHz, C_6D_6) δ 7.25 (d, *J* = 7.4 Hz, 2H, Ar*H*), 7.19 – 7.03 (m, 6H, Ar*H*), 6.55 – 6.49 (m, 2H, Py-(C3/4)*H*), 3.05 – 2.92 (m, 1H, Py-(C1)*H* overlapping with tetrabutylammonium triflate peaks), 2.64 (s, 3H, NCH_3), 2.56 (m, 4H, C*H*). ^{31}P NMR (121 MHz, C_6D_6) δ 36.02. ^{19}F NMR (282 MHz, C_6D_6) δ -77.67.

Synthesis of Complex 4Ni(N_3)-Me

2Ni-Me (22.0 mg, 0.032 mmol, 1 equiv.) was dissolved in THF (*ca.* 5 mL) and transferred to a 20 mL scintillation vial equipped with a magnetic stirbar. Tetrabutylammonium azide (9.1

mg, 0.032 mmol, 1 equiv.) was then added as a solution in *ca.* 1 mL THF and the reaction was allowed to stir for 3 hrs. Volatiles were then removed under reduced pressure. ^{31}P NMR data in C_6D_6 shows the clean conversion to a new species, however, removal of the tetrabutylammonium triflate with solvent washes of recrystallization proved difficult. Partial NMR data obtained for **4Ni(N$_3$)-Me**. ^{1}H NMR (300 MHz, C_6D_6) δ 7.26 (d, *J* = 7.5 Hz, 2H, Ar*H*), 7.13 (m, 6H, Ar*H*), 6.58 (s, 2H, Py-(C3/4)*H*), 2.71 (s, 3H, NC*H*$_3$), 2.67 – 2.56 (m, 2H, C*H*), 2.48 (s, 2H, C*H*), 2.25 (t, *J* = 6.2 Hz, 1H, Py-(C1)*H*). ^{31}P NMR (121 MHz, C_6D_6) δ 32.07. ^{19}F NMR (282 MHz, C_6D_6) δ -77.67.

Synthesis of 9Mo(CO)$_3$* from 1

1 (412.9 mg, 0.890 mmol, 1 equiv.) was dissolved in toluene (*ca.* 10 mL) and transferred to a Schlenk tube fitted with a screw-in Teflon stopper and a magnetic stirbar. $Mo(CO)_3(MeCN)_3$ (297 mg, 0.980 mmol, 1.1 equiv.) was then added as a suspension in *ca.* 10 mL of toluene and the reaction vessel was sealed and heated to 100 °C for 16 hrs. During this time the reaction mixture turned a red/orange color. Reaction volatiles were removed under reduced pressure. NMR in C_6D_6 revealed the predominant formation of **9Mo(CO)$_3$** along with an impurity (~20 %) with a very similar NMR characteristics (both ^{31}P and ^{1}H) believed to be a dimolybdenum complex where the pyridine nitrogen of one equivalent of **9Mo(CO)$_3$** is coordinated so a $Mo(CO)_n(L)_m$ species. Efforts to remove this impurity with solvent washes or recrystallizations proved unsuccessful so that material was carried forward as synthesized.

Synthesis of Complex 9Mo(CO)$_3$-H

9Mo(CO)$_3$* (55 mg) was dissolved in THF (*ca.* 5 mL) and transferred to a 20 mL scintillation vial equipped with a magnetic stirbar. Pyridinium triflate (18.9 mg, 0.082 mmol, 1 equiv. using effective mass if all **9Mo(CO)$_3$**) was then added as a solution in *ca.* 2 mL of THF and the reaction mixture was allowed to stir for 3 hrs at room temperature. Reaction volatiles were then removed under reduced pressure. The residue was then recrystallized from THF/pent vapor diffusion to yield clean **9Mo(CO)$_3$-H**. ^{1}H NMR (300 MHz, CD_3CN) δ 11.80 (broad s, 1H, Py-(N1)*H*), 7.96 (s, 2H, Py-(C3/4)*H*), 7.76 (m, 2H, Ar*H*), 7.60 – 7.54 (m, 2H, Ar*H*), 7.52 – 7.44 (m, 2H, Ar*H*), 7.24 (m, 2H, Ar*H*), 5.35 (s, 1H, Py-(C1)*H*), 3.28 (m, 2H, C*H*), 2.64 – 2.43 (m, 2H, C*H*), 1.59 – 1.40 (m, 6H, CH_3), 1.25 (m, 6H, CH_3), 1.15 (m, 12H, CH_3). ^{13}C NMR (126 MHz, CD_3CN) δ 217.62 (t, J_{CP} = 12.0 Hz), 211.49 (t, J_{CP} = 7.4 Hz), 207.86 (t, J_{CP} = 8.0 Hz), 145.19 (vt, J_{CP} = 10.4 Hz), 139.05 (s), 137.82 (vt, J_{CP} = 14.4 Hz), 130.79 (s), 130.14 (s), 129.91 (s), 128.95 (s), 119.46 (s), 69.68 (s), 34.23 (t, J_{CP} = 9.0 Hz), 27.29 (vt, J_{CP} = 11.3 Hz), 19.68 (s), 19.15 (s), 18.82 (s), 17.85 (s). ^{31}P NMR (121 MHz, CD_3CN) δ 54.63. ^{19}F NMR (282 MHz, CD_3CN) δ -79.35.

Synthesis of Complex 9Mo(CO)$_3$ from Complex 9Mo(CO)$_3$-H

9Mo(CO)$_3$-H (22.5 mg, 0.028 mmol, 1 equiv.) was dissolved in MeCN (*ca.* 5 mL) and transferred to a 20 mL scintillation vial equipped with a magnetic stirbar. Trimethylamine *n*-oxide (2.2 mg, 0.028 mmol, 1 equiv.) was then added as a solution in *ca.* 1 mL of MeCN) The reaction mixture was allowed to stir for 3 hrs at room temperature. Reaction volatiles were then removed under reduced pressure. Rather than decarbonylation, deprotonation and clean formation of **9Mo(CO)$_3$** without the impurity was obtained in quantitative yield. ^{1}H NMR (500 MHz, C_6D_6) δ 8.39 (s, 2H, Py-(C3/4)*H*), 7.16 (d, *J* = 7.8 Hz, 2H, Ar*H*), 7.00 (t, *J* = 7.5

Hz, 2H, Ar*H*), 6.90 (t, *J* = 7.5 Hz, 2H, Ar*H*), 6.77 (dd, *J* = 7.7, 1.9 Hz, 2H, Ar*H*), 6.15 (t, *J* = 2.0 Hz, 1H, Py-(C1)*H*), 2.67 (m, 2H, C*H*), 2.42 – 2.29 (m, 2H, C*H*), 1.52 (m, 6H, CH_3), 1.24 (m, 6H, CH_3), 1.00 (m, 12H, CH_3). ^{13}C NMR (126 MHz, C_6D_6) δ 222.27 (t, J_{CP} = 10.5 Hz), 212.98 (s), 211.76 (d, J_{CP} = 9.0 Hz), 148.33 (s), 146.51 (t, J_{CP} = 11.2 Hz), 139.91 (vt, J_{CP} = 11.5 Hz), 130.06(s), 129.31 (vt, J_{CP} = 4.1 Hz), 128.62 (s), 128.41 (s), 86.09 (s), 33.60 (vt, J_{CP} = 7.9 Hz), 28.22 (vt, J_{CP} = 10.5 Hz), 20.29 (s), 19.74 (vt, J_{CP} = 3.8 Hz), 19.27 (s), 18.48 (s). ^{31}P NMR (121 MHz, C_6D_6) δ 55.17. ^{19}F NMR (282 MHz, C_6D_6) δ -78.17.

Synthesis of Complex 9Mo(CO)$_3$-B(C$_6$F$_5$)$_3$

1-B(C$_6$F$_5$)$_3$ (56 mg, 0.057 mmol, 1 equiv.) was dissolved in toluene (*ca.* 5 mL) and transferred to a Schlenk tube fitted with a screw-in Teflon stopper and a magnetic stirbar. Mo(CO)3(MeCN)3 (17.4 mg, 0.057 mmol, 1 equiv.) was then added as a suspension in *ca.* 5 mL of toluene and then the reaction vessel was sealed and heated to 100 °C for 16 hrs. Reaction volatiles were then removed under reduced pressure to yield the desired product. ^{1}H NMR (300 MHz, C_6D_6) δ 8.11 (s, 2H, Py-(C3/4)*H*), 7.09 – 6.85 (m, 8H, Ar*H*), 4.99 – 4.95 (m, 1H, Py-(C1)*H*), 2.48 (m, 2H, C*H*), 2.10 – 1.97 (m, 2H, C*H*), 1.27 (dd, *J* = 15.4, 7.1 Hz, 6H, CH_3), 1.06 – 0.93 (m, 6H, CH_3), 0.88 – 0.77 (m, 12H, CH_3). ^{31}P NMR (121 MHz, C_6D_6) δ 55.97. ^{19}F NMR (282 MHz, C_6D_6) δ -130.44, -156.55 (t, *J* = 20.9 Hz), -163.32.

Crystallographic Information

CCDC 1400900-1400909 contain the supplementary crystallographic data for this paper. These data can be obtained free of charge from The Cambridge Crystallographic Data Centre via www.ccdc.cam.ac.uk/data_request/cif.

Refinement Details.

In each case, crystals were mounted on a glass fiber or nylon loop using Paratone oil, then placed on the diffractometer under a nitrogen stream. Low temperature (100 K) X-ray data were obtained on a Bruker APEXII CCD based diffractometer (Mo sealed X-ray tube, K_α = 0.71073 Å) or a Bruker PHOTON100 CMOS based diffractometer (Mo micro-focus sealed X-ray tube, K_α = 0.71073 Å). All diffractometer manipulations, including data collection, integration, and scaling were carried out using the Bruker APEXII software.[23] Absorption corrections were applied using SADABS.[24] Space groups were determined on the basis of systematic absences and intensity statistics and the structures were solved by direct methods using XS[25], by intrinsic phasing using XT (incorporated into SHELXTL), or by charge flipping using Olex2 and refined by full-matrix least squares on F^2.[26] All non-hydrogen atoms were refined using anisotropic displacement parameters. Hydrogen atoms were placed in the idealized positions and refined using a riding model. The structure was refined (weighed least squares refinement on F^2) to convergence. Graphical representation of structures with 50% probability thermal ellipsoids was generated using Diamond visualization software.[27] Data collection and refinement details are included in the Supporting Information.

Table 1. Crystal and refinement data for reported complexes.

Complex	**2Ni**	**2Pd**	**2Ni-B(C_6F_5)$_3$**	**2Pd-B(C_6F_5)$_3$**	**3Ni**
empirical formula	$C_{63}H_{90}N_2Ni_2P_4$	$C_{29}H_{39}NP_2Pd$	$C_{46}H_{43}B_5F_{15}NNiP_2$	$C_{47}H_{39}BF_{15}NP_2Pd$	$C_{65}H_{85}F_3N_2Ni_2O_3P_4S$
formula wt	1116.66	569.95	1069.51	1081.94	1272.71
T (K)	100	100(2)	99.99	100.03	100.01
a, Å	18.7148(7)	8.6112(7)	40.5679(17)	13.4502(7)	20.003(3)
b, Å	13.0646(5)	17.8635(16)	12.1876(4)	14.6571(7)	13.924(2)
c, Å	25.9359(9)	8.8154(11)	20.6773(7)	22.5392(11)	22.832(4)
α, deg	90	90	90	90	90
β, deg	109.324(2)	99.464(4)	114.405(2)	91.080(2)	22.832(4)
γ, deg	90	90	90	90	90
V, Å^3	5984.1(4)	1337.6(2)	9309.9(6)	4442.6(4)	6267.1(18)
Z	4	4	4	4	4
cryst syst	Monoclinic	Monoclinic	Monoclinic	Monoclinic	Monoclinic
space group	P 1 21/n 1	P 21	C 1 2/c 1	P 1 21/c 1	P 1 21/n 1
d_{calcd}, g/cm^3	1.239	1.415	1.526	1.618	1.349
θ range, deg	1.630-30.557	2.342 to 45.810	1.759 to 30.538	2.280 to 36.326	1.720-28.677
μ, mm^{-1}	1.058	0.831	0.582	0.589	0.792
abs cor	Semi-empirical from equivalents	Semi-empirical from equivalents	Semi-empirical from equivalents	Semi-empirical from equivalents	Semi-empirical from equivalents
GOF[c]	0.775	0.885	1.017	1.014	1.003
R1,[a] wR2[b] (I > 2σ(I))	0.0364, 0.0843	0.0639, 0.1107	0.0361, 0.0867	0.0414, 0.0897	0.0437, 0.0840

Table 2. Crystal and refinement data for reported complexes.

Complex	**2Ni-BCy$_2$OTf**	**2Pd-H**	**4Ni(CO)**	**4Ni(CO)-H**	**5Ni**
empirical formula	$C_{42}H_{61}BF_3NNiO_3P_2S$	$C_{30}H_{40}F_3NO_3P_2PdS$	$C_{30}H_{39}NNiOP_2$	$C_{31}H_{40}F_3NNiO_4P_2S$	$C_{64}H_{90}B_4F_{16}N_6Ni_2O_2P_4$
formula wt	848.43	720.03	550.27	700.35	1563.95
T (K)	100.01	100.01	100.0	99.98	100.11
a, Å	15.7224(11)	12.2515(8)	11.5436(5)	12.7394(14)	11.4094(4)
b, Å	12.6201(9)	11.1901(7)	15.7065(6)	15.2760(17)	11.4298(4)
c, Å	22.1023(15)	24.2291(15)	15.3374(5)	16.7217(19)	30.3230(12)
α, deg	90	90	90	90	92.4620(10)
β, deg	109.324(2)	102.437(3)	90.135(2)	101.186(2)	100.545(2)
γ, deg	90	90	90	90	107.826(2)
V, Å^3	4170.8(5)	3243.8(4)	2780.81(18)	3192.3(6)	3680.2(2)
Z	4	4	4	4	2
cryst syst	Monoclinic	Monoclinic	Monoclinic	Monoclinic	Triclinic
space group	P 1 21/c 1	P 1 21/c 1	P 1 21/c 1	P 1 21/c 1	P -1
d_{calcd}, g/cm^3	1.351	1.474	1.314	1.457	1.411
θ range, deg	2.522 to 30.530	1.702 to 30.570	1.764 to 30.552	1.822 to 30.519	2.981 to 78.736
μ, mm^{-1}	0.645	0.783	0.836	0.828	2.208
abs cor	Semi-empirical from equivalents	Semi-empirical from equivalents	Semi-empirical from equivalents	Semi-empirical from equivalents	Semi-empirical from equivalents
GOF[c]	1.041	1.076	1.005	1.050	1.078
R1,[a] wR2[b] (I > 2σ(I))	0.0417, 0.1143	0.0211, 0.0508	0.0321, 0.0724	0.0248, 0.0634	0.0810, 0.2035

Table 3. Crystal and refinement data for reported complexes.

Complex	**4Ni(CN*t*Bu)**	**9Mo(CO)$_3$-H**
empirical formula	$C_{34}H_{48}BF_3N_2NiP_2$	$C_{33}H_{40}F_3MoNO_6P_2S$
formula wt	605.39	793.60
T (K)	99.98	99.95
a, Å	17.460(2)	10.1276(2)
b, Å	10.8834(13)	24.7845(6)
c, Å	16.865(2)	14.5371(3)
α, deg	90	90
β, deg	94.574(7)	110.2770(10)
γ, deg	90	90
V, Å^3	3194.6(7)	3422.79(13)
Z	4	4
cryst syst	Monoclinic	Monoclinic
space group	P 1 2_1/c 1	P 1 2_1/c 1
d_{calcd}, g/cm^3	1.259	1.540
θ range, deg	1.170 to 36.520	2.296 to 30.525
μ, mm^{-1}	0.733	0.599
abs cor	Semi-empirical from equivalents	Semi-empirical from equivalents
GOF[c]	0.963	1.041
R1,[a] wR2[b] (I > 2σ(I))	0.0363, 0.1185	0.0211, 0.0493

[a] $R1 = \Sigma||F_o|-|F_c|| / \Sigma|F_o|$ [b] $wR2 = \{ \Sigma [w(F_o^2-F_c^2)^2] / \Sigma [w(F_o^2)^2] \}^{1/2}$ [c] $GOF = S = \{ \Sigma [w(F_o^2-F_c^2)^2] / (n-p) \}^{1/2}$

REFERENCES

1.(a) Allgeier, A. M.; Mirkin, C. A., *Angew Chem Int Edit* **1998,** *37*, 894-908; (b) Cisnetti, F.; Gibard, C.; Gautier, A., *J Organomet Chem* **2015,** *782*, 22-30.
2.(a) Cesar, V.; Castro, L. C. M.; Dombray, T.; Sortais, J. B.; Darcel, C.; Labat, S.; Miqueu, K.; Sotiropoulos, J. M.; Brousses, R.; Lugan, N.; Lavigne, G., *Organometallics* **2013,** *32*, 4643-4655; (b) Benhamou, L.; Cesar, V.; Gornitzka, H.; Lugan, N.; Lavigne, G., *Chem Commun* **2009**, 4720-4722; (c) Azoulay, J. D.; Rojas, R. S.; Serrano, A. V.; Ohtaki, H.; Galland, G. B.; Wu, G.; Bazan, G. C., *Angew Chem Int Edit* **2009,** *48*, 1089-1092; (d) Benhamou, L.; Vujkovic, N.; Cesar, V.; Gornitzka, H.; Lugan, N.; Lavigne, G., *Organometallics* **2010,** *29*, 2616-2630.
3.Bergbreiter, D. E.; Frels, J. D.; Rawson, J.; Li, J.; Reibenspies, J. H., *Inorganica Chimica Acta* **2006,** *359*, 1912-1922.
4.(a) Walter, M. D.; White, P. S.; Schauer, C. K.; Brookhart, M., *New Journal of Chemistry* **2011,** *35*, 2884-2893; (b) Mehendale, N. C.; Lutz, M.; Spek, A. L.; Klein Gebbink, R. J. M.; van Koten, G., *J Organomet Chem* **2008,** *693*, 2971-2981; (c) Rivada-Wheelaghan, O.; Dauth, A.; Leitus, G.; Diskin-Posner, Y.; Milstein, D., *Inorganic Chemistry* **2015,** *54*, 4526-4538; (d) Weisman, A.; Gozin, M.; Kraatz, H.-B.; Milstein, D., *Inorganic Chemistry* **1996,** *35*, 1792-1797; (e) Ashkenazi, N.; Vigalok, A.; Parthiban, S.; Ben-David, Y.; Shimon, L. J. W.; Martin, J. M. L.; Milstein, D., *Journal of the American Chemical Society* **2000,** *122*, 8797-8798; (f) Gauvin, R. M.; Rozenberg, H.; Shimon, L. J. W.; Ben-David, Y.; Milstein, D., *Chemistry – A European Journal* **2007,** *13*, 1382-1393.
5.(a) Herbert, D. E.; Lara, N. C.; Agapie, T., *Chem-Eur J* **2013,** *19*, 16453-16460; (b) Chao, S. T.; Lara, N. C.; Lin, S. B.; Day, M. W.; Agapie, T., *Angew. Chem. Int. Ed.* **2011,** *50*, 7529-7532; (c) Kelley, P.; Lin, S. B.; Edouard, G.; Day, M. W.; Agapie, T., *Journal of the American Chemical Society* **2012,** *134*, 5480-5483.
6.(a) Smith, R. C.; Protasiewicz, J. D., *Organometallics* **2004,** *23*, 4215-4222; (b) Morgan, B. P.; Smith, R. C., *J Organomet Chem* **2008,** *693*, 11-16; (c) Baratta, W.; Herdtweck, E.; Martinuzzi, P.; Rigo, P., *Organometallics* **2001,** *20*, 305-308; (d) Chen, C.-S.; Lin, C.-S.; Yeh, W.-Y., *J Organomet Chem* **2011,** *696*, 1474-1478; (e) Robertson, G. B.; Whimp, P. O., *Inorganic Chemistry* **1974,** *13*, 2082-2088; (f) Robertson, G. B.; Tucker, P. A.; Whimp, P. O., *Inorganic Chemistry* **1980,** *19*, 2307-2315; (g) Bennett, M. A.; Clark, P. W.; Robertson, G. B.; Whimp, P. O., *Journal of the Chemical Society, Chemical Communications* **1972**, 1011-1012; (h) Barrett, B. J.; Iluc, V. M., *Organometallics* **2014,** *33*, 2565-2574; (i) Barrett, B. J.; Iluc, V. M., *Inorganic Chemistry* **2014,** *53*, 7248-7259; (j) Okamoto, K.; Omoto, Y.; Sano, H.; Ohe, K., *Dalton Transactions* **2012,** *41*, 10926-10929; (k) Dixon, F. M.; Farrell, J. R.; Doan, P. E.; Williamson, A.; Weinberger, D. A.; Mirkin, C. A.; Stern, C.; Incarvito, C. D.; Liable-Sands, L. M.; Zakharov, L. N.; Rheingold, A. L., *Organometallics* **2002,** *21*, 3091-3093; (l) Dixon, F. M.; Masar, M. S.; Doan, P. E.; Farrell, J. R.; Arnold, F. P.; Mirkin, C. A.; Incarvito, C. D.; Zakharov, L. N.; Rheingold, A. L., *Inorganic Chemistry* **2003,** *42*, 3245-3255; (m) Xu, F.-B.; Li, Q.-S.; Wu, L.-Z.; Leng, X.-B.; Li, Z.-C.; Zeng, X.-S.; Chow, Y. L.; Zhang, Z.-Z., *Organometallics* **2003,** *22*, 633-640.
7.(a) Harrold, N. D.; Hillhouse, G. L., *Chemical Science* **2013,** *4*, 4011-4015; (b) Haas, T.; Kaspar, K.; Forner, K.; Drexler, M.; Fischer, H., *J Organomet Chem* **2011,** *696*, 946-955; (c) Laskowski, C. A.; Miller, A. J. M.; Hillhouse, G. L.; Cundari, T. R., *Journal of the American Chemical Society* **2011,** *133*, 771-773; (d) Iluc, V. M.; Miller, A. J. M.; Anderson, J. S.; Monreal, M. J.; Mehn, M. P.; Hillhouse, G. L., *Journal of the American Chemical Society* **2011,** *133*, 13055-13063; (e) Iluc, V. M.; Hillhouse, G. L., *Journal of the American Chemical Society* **2010,** *132*, 15148-15150; (f) Waterman, R.; Hillhouse, G. L., *Journal of the American Chemical Society* **2008,**

130, 12628-12629; (g) Kogut, E.; Wiencko, H. L.; Zhang, L.; Cordeau, D. E.; Warren, T. H., *Journal of the American Chemical Society* **2005,** *127*, 11248-11249; (h) Melenkivitz, R.; Mindiola, D. J.; Hillhouse, G. L., *Journal of the American Chemical Society* **2002,** *124*, 3846-3847; (i) Mindiola, D. J.; Hillhouse, G. L., *Journal of the American Chemical Society* **2002,** *124*, 9976-9977; (j) Mindiola, D. J.; Hillhouse, G. L., *Journal of the American Chemical Society* **2001,** *123*, 4623-4624.
8.Bull, J. A.; Mousseau, J. J.; Pelletier, G.; Charette, A. B., *Chem Rev* **2012,** *112*, 2642-2713.
9.(a) Takao, T.; Kawashima, T.; Kanda, H.; Okamura, R.; Suzuki, H., *Organometallics* **2012,** *31*, 4817-4831; (b) Kawashima, T.; Takao, T.; Suzuki, H., *Angew Chem Int Edit* **2006,** *45*, 7615-7618; (c) Harrison, D. P.; Welch, K. D.; Nichols-Nielander, A. C.; Sabat, M.; Myers, W. H.; Harman, W. D., *Journal of the American Chemical Society* **2008,** *130*, 16844-16845; (d) Mehnert, C. P.; Haggitt, J.; Green, M. L. H., *J Organomet Chem* **1998,** *550*, 63-70.
10.Suseno, S.; Agapie, T., *Organometallics* **2013,** *32*, 3161-3164.
11.Velian, A.; Lin, S. B.; Miller, A. J. M.; Day, M. W.; Agapie, T., *J Am Chem Soc* **2010,** *132*, 6296-6297.
12.Jiang, Y.; Blacque, O.; Fox, T.; Berke, H., *Journal of the American Chemical Society* **2013,** *135*, 7751-7760.
13.Welch, G. C.; Prieto, R.; Dureen, M. A.; Lough, A. J.; Labeodan, O. A.; Holtrichter-Rossmann, T.; Stephan, D. W., *Dalton Transactions* **2009**, 1559-1570.
14.CSD search run: 6-member ring with one N, any bonds between vicinal atoms, H or C substitution, Pd or Ni bound to any C atoms in the ring.
15.Iluc, V. M.; Miller, A. J. M.; Hillhouse, G. L., *Chem Commun* **2005**, 5091-5093.
16.(a) Haller, K. J.; Enemark, J. H., *Inorganic Chemistry* **1978,** *17*, 3552-3558; (b) Landry, V. K.; Parkin, G., *Polyhedron* **2007,** *26*, 4751-4757; (c) MacBeth, C. E.; Thomas, J. C.; Betley, T. A.; Peters, J. C., *Inorganic Chemistry* **2004,** *43*, 4645-4662; (d) Muñoz, S. B.; Foster, W. K.; Lin, H.-J.; Margarit, C. G.; Dickie, D. A.; Smith, J. M., *Inorganic Chemistry* **2012,** *51*, 12660-12668; (e) Wright, A. M.; Wu, G.; Hayton, T. W., *Journal of the American Chemical Society* **2012,** *134*, 9930-9933; (f) Puiu, S. C.; Warren, T. H., *Organometallics* **2003,** *22*, 3974-3976; (g) Varonka, M. S.; Warren, T. H., *Organometallics* **2010,** *29*, 717-720.
17.McSkimming, A.; Colbran, S. B., *Chem Soc Rev* **2013,** *42*, 5439-5488.
18.(a) Gunanathan, C.; Milstein, D., *Accounts of Chemical Research* **2011,** *44*, 588-602; (b) Kundu, S.; Brennessel, W. W.; Jones, W. D., *Inorganic Chemistry* **2011,** *50*, 9443-9453; (c) Gunanathan, C.; Shimon, L. J. W.; Milstein, D., *Journal of the American Chemical Society* **2009,** *131*, 3146-3147; (d) Gunanathan, C.; Milstein, D., *Angewandte Chemie International Edition* **2008,** *47*, 8661-8664; (e) Gunanathan, C.; Gnanaprakasam, B.; Iron, M. A.; Shimon, L. J. W.; Milstein, D., *Journal of the American Chemical Society* **2010,** *132*, 14763-14765; (f) Ohtsu, H.; Tanaka, K., *Angewandte Chemie International Edition* **2012,** *51*, 9792-9795; (g) Koizumi, T.-a.; Tanaka, K., *Angewandte Chemie International Edition* **2005,** *44*, 5891-5894; (h) McSkimming, A.; Bhadbhade, M. M.; Colbran, S. B., *Angew Chem Int Edit* **2013,** *52*, 3411-3416.
19.Henthorn, J. T.; Lin, S.; Agapie, T., *Journal of the American Chemical Society* **2015,** *137*, 1458-1464.
20.(a) Buss, J. A.; Agapie, T., *Nature* **2016,** *529*, 72-75; (b) Buss, J. A.; Edouard, G. A.; Cheng, C.; Shi, J.; Agapie, T., *Journal of the American Chemical Society* **2014,** *136*, 11272-11275.
21.Pangborn, A. B.; Giardello, M. A.; Grubbs, R. H.; Rosen, R. K.; Timmers, F. J., *Organometallics* **1996,** *15*, 1518-1520.
22.Fulmer, G. R.; Miller, A. J. M.; Sherden, N. H.; Gottlieb, H. E.; Nudelman, A.; Stoltz, B. M.; Bercaw, J. E.; Goldberg, K. I., *Organometallics* **2010,** *29*, 2176-2179.

23.APEX2, Version 2 User Manual, M86-E01078, Bruker Analytical X-ray Systems, Madison, WI, June 2006.
24.Sheldrick, G.M. "SADABS (version 2008/1): Program for Absorption Correction for Data from Area Detector Frames", University of Göttingen, 2008.
25.Sheldrick, G.M. (2008). Acta Cryst. A64, 112-122.
26.Dolomanov, O.V. (2009). OLEX2. J. Appl. Cryst. 42, 339-341.
27.Brandenburg, K. (1999). DIAMOND. Crystal Impact GbR, Bonn, Germany.

Chapter 5

SYNTHESIS OF SITE-DIFFERENTIATED [$FE_4(\mu_4\text{-}O)$] COMPLEXES SUPPORTED BY PYRAZOLATE LIGANDS POSSESSING PENDANT HYDROGEN BOND DONORS

Abstract

The synthesis of site-differentiated [$Fe_4(\mu_4\text{-}O)$] clusters supported by a hexa(pyridyl) tris(alkoxide)ligand and two different types of pyrazolates is described. Building off previous results with phenyl pyrazolate supporting ligands, sterically smaller scaffolds are explored using parent pyrazolate and 3-aminophenyl pyrazolate. The aminophenyl substituents were utilized to successfully construct a secondary coordination sphere hydrogen bonding network capable of forming stabilizing interactions with terminal chloride and hydroxide ligands bound to the apical Fe center. Terminal chloride and azide complexes were also synthesized with the parent pyrazolate ligand to directly compare spectroscopic parameters with the analogous complexes containing hydrogen bonding networks. Cyclic voltammetry experiments and Mössbauer spectroscopy were utilized to better understand the properties of the described clusters.

INTRODUCTION

The biological activation of many small molecules including dihydrogen, dioxygen, carbon dioxide, water, and dinitrogen is accomplished at complicated multimetallic active sites capable of managing the delivery of protons and electrons to and/or from the substrate.[1] The use of multiple metal centers to store oxidizing equivalents is exemplified by the [Mn_4Ca] cluster in the oxygen evolving complex (OEC) of photosystem II (PSII), which catalyzes the conversion of water into molecular oxygen.[1h, 2] The reverse reaction, dioxygen reduction to water, can be accomplished by cytochrome *c* oxidase as well as multicopper oxidases, such as laccase.[1g, 3] Beyond the careful control of cluster nuclearity and metal identity, Nature also frequently employs hydrogen bonding networks or acid/base moieties to help facilitate these chemical transformations.[4] In P450 enzymes a complicated hydrogen bonding network helps to stabilize dioxygen binding and is also instrumental in mediating proton transfer.[4a, 5]

The use of secondary coordination sphere effects has become increasingly common in synthetic systems relevant to biological dioxygen reduction[6] or water oxidation[7] in recent years. In Fe complexes, terminal Fe(III)- and Fe(IV)-oxo as well as Fe(III)-sulfide and -selenide compounds derived from their elemental sources have been isolated utilizing tris(amido)amine scaffolds with stabilizing hydrogen bonding networks (Figure 2).[8] More recently, nitrite reduction to nitric oxide and a terminal oxo moiety has also been recently observed in an azafulvene tripodal scaffold with Fe (Figure 2).[9] These results demonstrate the ability of these types of scaffolds to fundamentally change the types of accessible Fe complexes by stabilizing reactive oxygenic species. While this strategy has been most commonly employed in monometallic systems, examples of dinuclear systems have also been reported.[10]

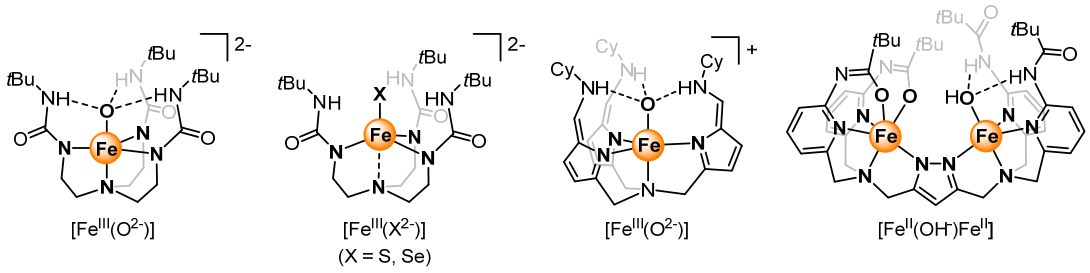

Figure 2. Literature examples of Fe and Cu complexes with pendant hydrogen-bonding moieties.

Our group has recently reported the synthesis of a series of tetrairon (μ_4-oxido) ([$Fe_4(\mu_4$-O)]) clusters (Figure 2).[11] Notably, these complexes showed four isolable oxidation states with localized redox behaviour isolated in the triiron core rather than the site-differentiated apical iron center based on solid-state structural analysis and Mössbauer data. While the apical Fe center is 4-coordinate as synthesized, the isolation of a series of complexes with nitric oxide (NO) coordinated to the apical iron center also proved accessible enabling the use of NO molecule as an IR reporter for the electronics of apical metal as a function of the triiron core oxidation state (Figure 2). Additional studies with oxygen atom transfer reagents with these clusters resulted in C–H or C–F bond activation and coordination of the resultant phenoxide to the apical iron center as shown in Figure 2. While no characterization of the reactive species is presently available these data suggest the ability oxygen atom transfer reagents to work in conjunction with [$Fe_4(\mu_4$-O)] core to accomplish the intramolecular activation of strong aryl-X bonds. Herein we report efforts to further elaborate the range of accessible [$Fe_4(\mu_4$-O)]-type clusters by further functionalizing the existing the pyrazolates scaffold to include hydrogen bonding moieties in an effort to stabilize reactive oxygenic species at the apical Fe. Efforts to open the steric congestion at the

apical Fe center to promote intermolecular reactivity and expand the variety of small molecules capable of binding were also pursued.

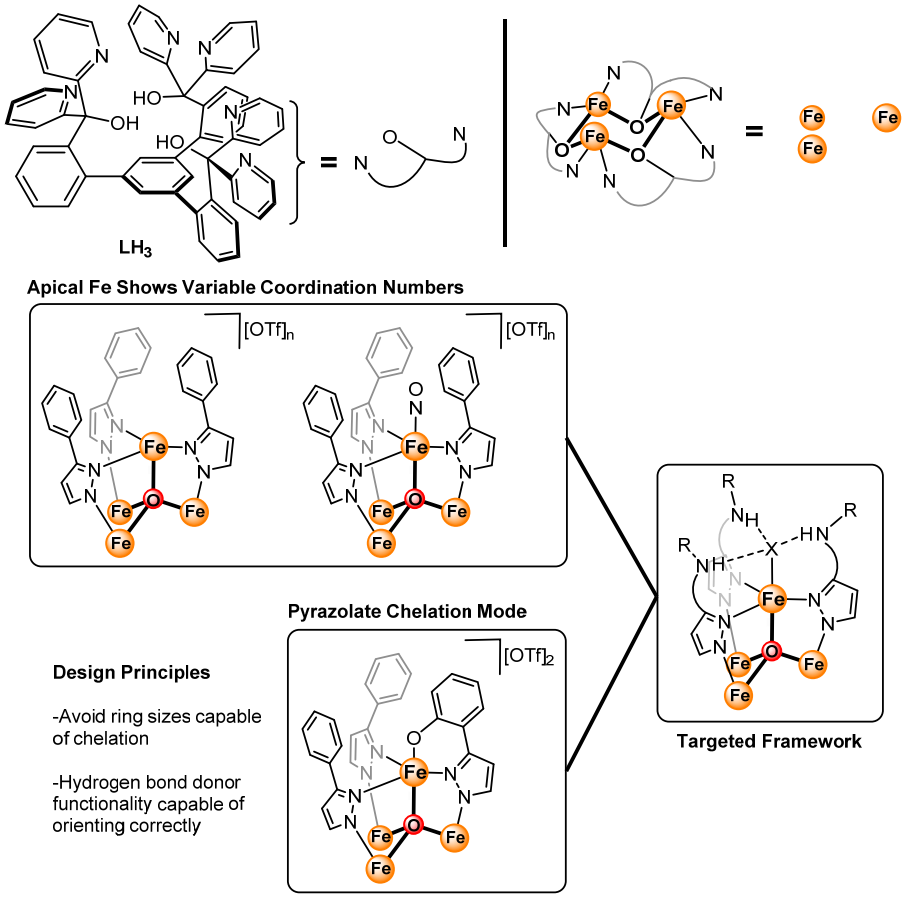

Figure 2. Outline of the design principles for the targeted ligand framework

RESULTS AND DISCUSSION

Section 5.1 Ligand Synthesis

The general synthetic strategy aimed to construct hydrogen bonding networks by modifying the established strategies employed for previously reported [$Fe_4(\mu_4\text{-}O)$] phenyl pyrazolate-supported clusters in our group. Starting from 3-amino pyrazole (**(NH_2)PzH**), multiple hydrogen bonding scaffolds were targeted (Scheme 1). **(NH_2)PzH** is precedented to undergo Buchwald-Hartwig couplings with a variety of aryl and aromatic heterocyclic substrates to selectively afford mono-functionalized

product.[12] These conditions were utilized to afford 3-aminophenyl pyrazole (**(PhNH)PzH**) in multigram quantities. **(PhNH)PzH** could then be quantitatively deprotonated using sodium hexamethyldisilazide (NaHMDS) for afford the corresponding pyrazolate salt of the ligand (**(PhNH)PzNa**). The N-acetylation of **(NH$_2$)PzH** was accomplished according to a reported patent procedure to afford **(AcNH)PzH**, however, due to the initial successes observed with **(PhNH)PzNa** further efforts with this ligand were not pursued.

Scheme 1. Synthesis of hydrogen bonding pyrazole derivatives

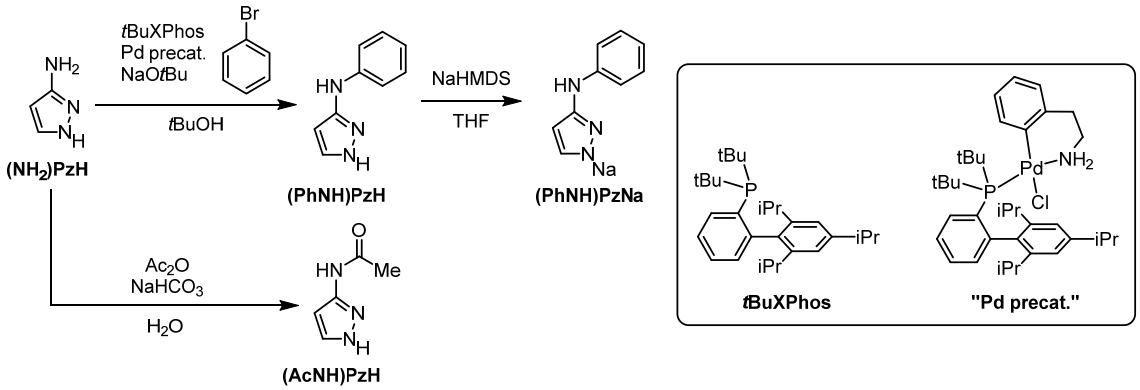

Section 5.2 Synthesis of [Fe$_4$(μ_4-O)] Complexes Supported by Parent Pyrazolate

Initial studies were carried out with parent pyrazole to access a less sterically crowded environment around the apical Fe and promote intermolecular reactivity and the coordination of small molecules. Initial syntheses involved the non-oxidative installation of the pyrazolates and apical Fe center from a cationic [Fe^{III}_3(μ_3-O)Cl_3] complex discussed in Appendix A. However, the reaction was sluggish and yielded inconsistent results despite the initial success on smaller scales. The optimized synthetic route involved the use of an oxidative route starting from the previously reported $Fe^{II}_3(OAc)_3$ complex, **1**,[13] more akin to strategies utilized in the reported pyrazolate-supported complexes.[11] The use of methyl triflate to remove acetates as reported for

phenylpyrazolate-supported clusters yielded messy reaction mixtures that were difficult to purify. Consequently, the use of alternative methods of acetate removal were pursued.

Scheme 2. Synthesis of [$Fe_4(\mu_4\text{-}O)$] clusters supported by pyrazolate

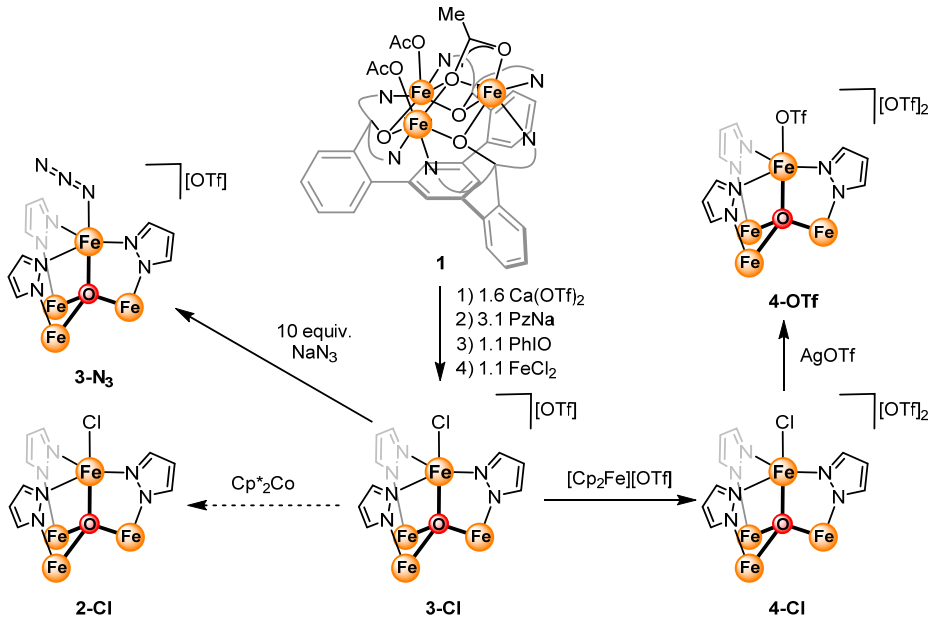

Preliminary results had shown that the synthesis of [$Fe_4(\mu_4\text{-}O)$] clusters supported by phenyl pyrazolate ligands from the previously reported calcium oxo hydroxo cluster was possible. Additionally, acetate removal from **1** with calcium triflate to produce a [$Fe^{II}_3(OAc)_2(OTf)$] complex has also been described. Therefore, the use of calcium triflate as an acetate sink was explored. Gratifyingly, this approach proved successful to reproducibly access the desired [$Fe_4(\mu_4\text{-}O)$] complex, **3-Cl**, in a one-pot procedure. Calcium triflate addition to **1** in THF resulted in the *in situ* formation of a [$Fe^{II}_3(OAc)_2(OTf)$] complex as a yellow/brown suspension. The subsequent addition of sodium pyrazolate resulted in the formation of a homogeneous red/orange solution. The addition of iodosylbenzene (PhIO) resulted in the formation of a brown solution s, which is presumably the [$Fe_3Na(\mu_4\text{-}O)$] cluster by analogy to previously reported

syntheses. Installation of the apical Fe center could then be accomplished utilizing $FeCl_2$. The calcium salts proved more readily removed due to their lower solubility in DCM thus allowing for the clean isolation of **3-Cl** as a brown powder. Electrospray ionization mass spectrometry (ESI-MS) provided mixed results for these clusters likely attributable to the decreased steric protection and moisture and oxygen sensitivity.

Crystals suitable for single crystal X-ray diffraction (XRD) studies were obtained for **3-Cl** (Figure 3). In the solid-state, **3-Cl** displays a structure reminiscent of the phenylpyrazolate-supported clusters previously reported by our group with the Fe_3 core bridged to the apical Fe center by the (μ_4-O) and pyrazolate ligands. The apical Fe center is 5-coordinate, likely to the reduced steric protection without the phenyl substituents, with a terminal chloride ligand trans to the (μ_4-O). A τ_5 parameter of 0.968 for the apical Fe center indicates a trigonal bipyramidal geometry. Fe–(μ_4-O) distances to the Fe_3 core are consistent with an [$Fe^{III}Fe^{II}_2$] assignment with two longer (2.071(4), 2,145(3) Å) and one shorter (2.024(4) Å) distances. These data suggest that chloride coordination to the apical Fe center is sufficient to induce a redox rearrangement compared to other reported [$Fe^{III}_4Fe^{II}_2(\mu_4\text{-O})$] clusters, which show localization of an apical Fe^{II} center in the apical position in four and five coordinate geometries. This is likely attributable to the anionic charge of the chloride ligand, a hypothesis that is supported by the localization of an apical Fe^{III} center in [$Fe_4(\mu_4\text{-O})$] clusters with chelating phenoxide pyrazolate ligands.

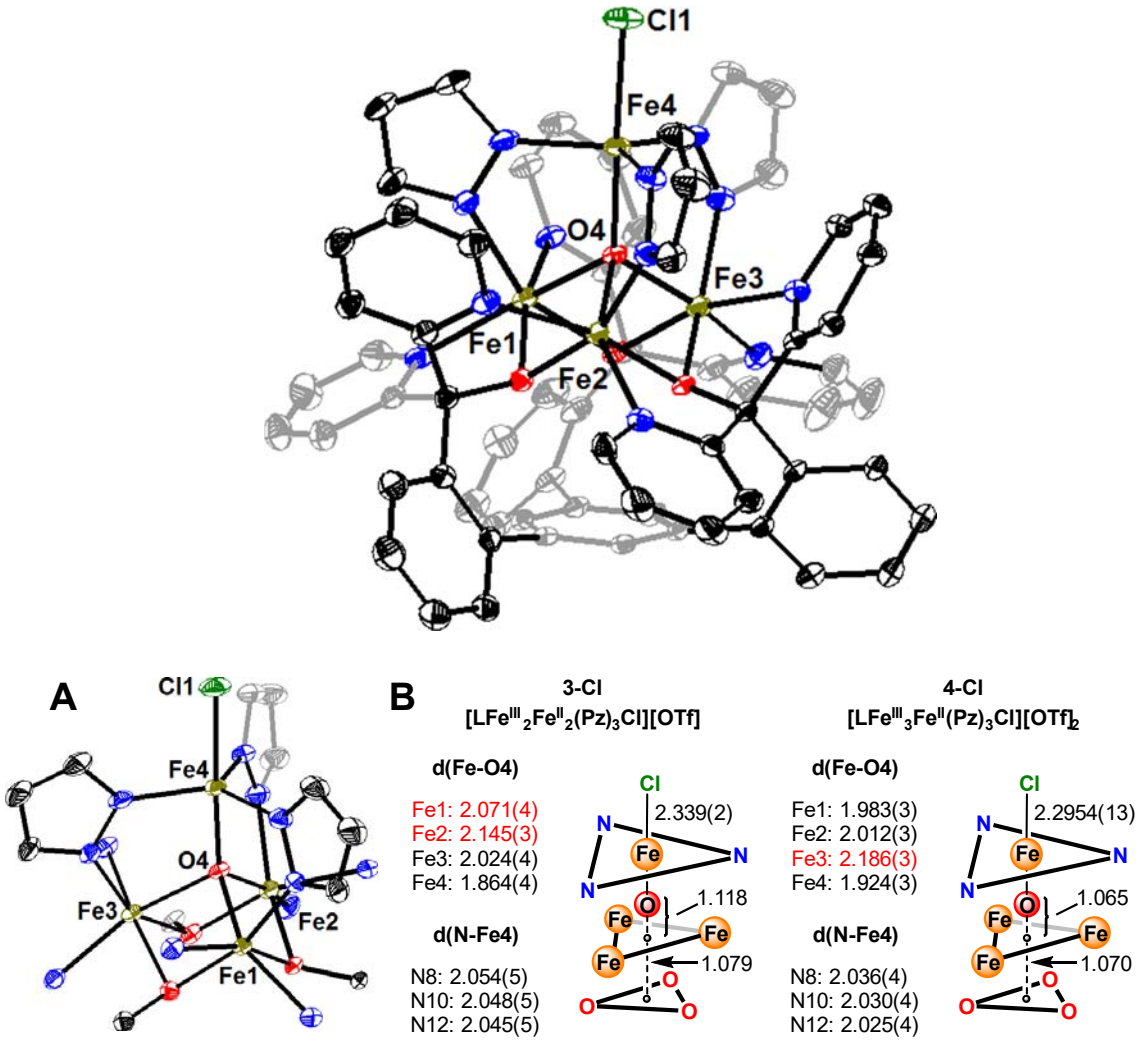

Figure 3. Solid-state structure **3-Cl** (top), and the truncated the [$Fe_4(\mu_4\text{-}O)$] core of **3-Cl** (A). Select bond metrics for **3-Cl** (B, Left) and **4-Cl** (B, Right). Hydrogen atoms, counterions, solvent molecules, and most of the supporting tris(alkoxide) hexa(pyridyl) ligand have been omitted for clarity.

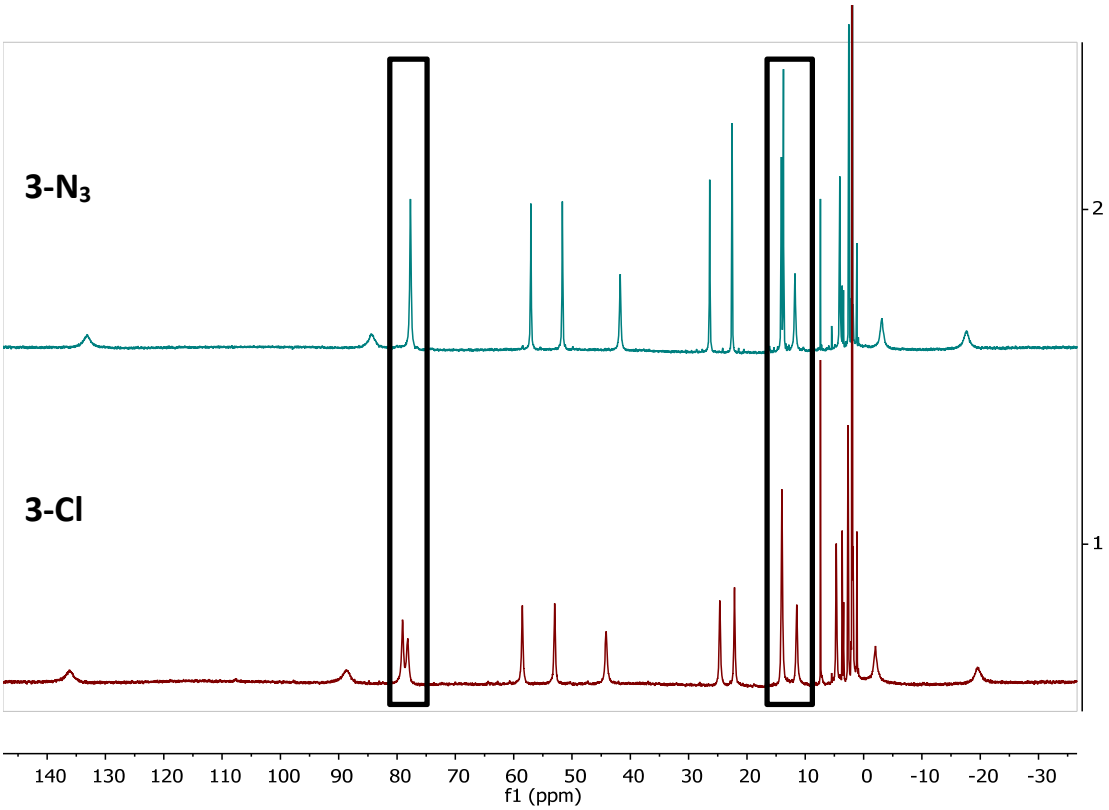

Figure 4. Comparison of NMR spectra for **3-Cl** (red trace) and **3-N$_3$** (blue trace) in CD_3CN. Boxed regions highlight the largest distinguishing features resulting from chloride substitution.

Substitution of the apical chloride was attempted. The addition of an excess of sodium azide yielded the desired terminal azide compound, **3-N$_3$** (Scheme 2). Confirmation of the presence of the azide ligand was confirmed by infrared (IR) spectroscopy, which showed an absorption at 2060 cm^{-1}. This stretch is more activated than in sodium azide (2129 cm^{-1})[14] and comparable to another reported trigonal bipyramidal Fe^{III} terminal azide complex supported by an amine tris(thiolate) ligand (2048 cm^{-1}).[15] By NMR spectroscopy, **3-N$_3$** appears quite similar to **3-Cl** (Figure 4) indicating there are no substantial structural or electronic differences between the two complexes. A preliminary solid-state structure (R1 = 39.35%) also supports the formation of a terminal azide complex (Figure 5). Attempts to photolyze **3-N$_3$** with a

75 W Xenon lamp did not result in decomposition of the terminal azide to an Fe-nitride and dinitrogen. Attempts to repeat these reactions in different cluster oxidation states with a more powerful lamp are currently being pursued.

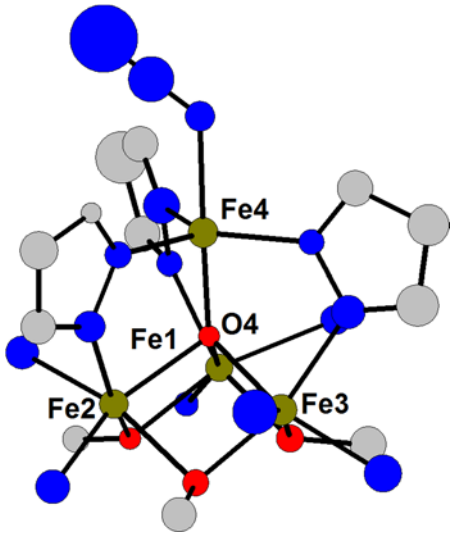

Figure 5. Preliminary solid-state structure of the [$Fe_4(\mu_4$-O)] core of **3-N_3.**

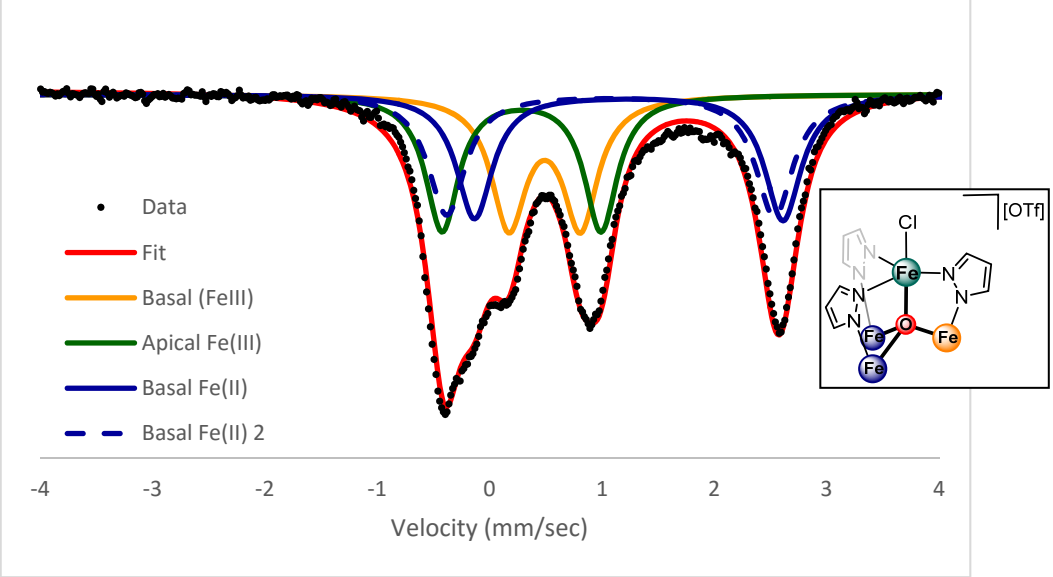

Figure 6. Zero-field ^{57}Fe Mössbauer spectrum at 80 K of **3-Cl** (black dots) and global fit (red trace) with simulated parameters (i) δ (mm/s) = 0.490, |ΔEq| (mm/s) = 0.637 (blue trace); (ii) δ (mm/s) = 0.284, |ΔEq| (mm/s) = 1.413 (orange trace); (iii) δ (mm/s) = 1.238, |ΔEq| (mm/s) = 2.745 (green trace); (iv) δ (mm/s) = 1.076, |ΔEq| (mm/s) = 2.915 (purple trace).

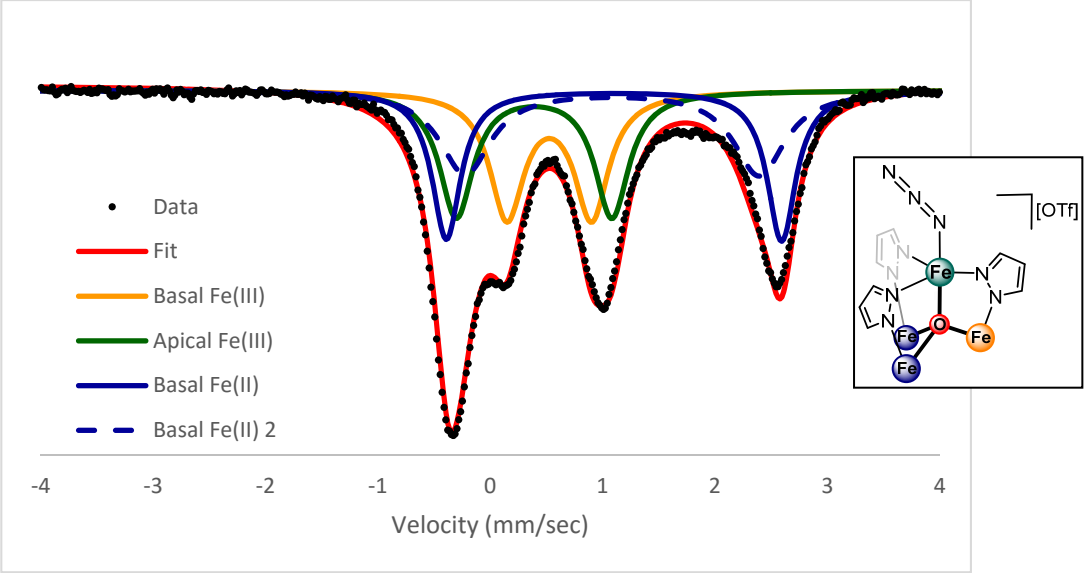

Figure 7. Zero-field ^{57}Fe Mössbauer spectrum at 80 K of **3-N$_3$** (black dots) and global fit (red trace) with simulated parameters (i) δ (mm/s) = 0.525, |ΔEq| (mm/s) = 0.754 (blue trace); (ii) δ (mm/s) = 0.390, |ΔEq| (mm/s) = 1.384 (orange trace); (iii) δ (mm/s) = 1.101, |ΔEq| (mm/s) = 2.983 (green trace); (iv) δ (mm/s) = 1.084, |ΔEq| (mm/s) = 2.615 (purple trace).

Mössbauer spectra were collected for **3-Cl** and **3-N$_3$** (Figure 6, 7) with simulated parameters summarized in Table 1. In both cases the data can be best fit as two Fe^{II} centers and two Fe^{III} centers. Based on the solid-state data for **3-Cl** and by comparison to previously synthesized phenoxide complexes in related clusters, the Fe^{III} component with the larger quadrupole splitting (Figure 5, 6 orange traces) was assigned as the apical Fe center for both complexes (**3-Cl** δ (mm/s): 0.284, |ΔEq| (mm/s): 1.413; **3-N$_3$** δ (mm/s): 0.390, |ΔEq| (mm/s): 1.384). Further support for this assignment comes from a pair of anionic monometallic Fe^{III} complexes supported by an amine tris(thiolate) ligand ($[N(CH_2CH_2S)_3]^{3-}$). Both the $[Et_4N][Fe^{III}Cl(NS_3)]$ and $[Et_4N][Fe^{III}(N_3)(NS_3)]$ complex for this ligand were isolated with solid-state characterization confirming a trigonal bipyramidal 5-coordinate geometry akin to the apical Fe center in **3-Cl** and **3-N$_3$**. These complexes also have comparable reported

Mössbauer isomer shifts ([Et_4N][$Fe^{III}X(NS_3)$]: X = Cl^- δ (mm/s): 0.258, |ΔEq| (mm/s): 0.982; X = N_3^- δ (mm/s): 0.352, |ΔEq| (mm/s): 0.731). Furthermore, the trend of larger isomer shifts and smaller quadrupole splitting for the terminal azide compared to the chloride is reproduced in both pairs of complexes. Taken together these data all support the assignment of the apical Fe center as an Fe^{III} with an [$Fe^{III}Fe^{II}_2$] core for both **3-Cl** and **3-N_3**.

Table 1. Summary of Mössbauer parameters for complexes **3-Cl** and **3-N_3**

		parameters		
Cmpd.	Formula	δ (mm/s)	|ΔEq| (mm/s)	%
3-Cl	[$LFe_3OFe(Pz)_3Cl$][OTf]	0.490	0.637	25
		0.284	1.413	25
		1.238	2.745	25
		1.076	2.915	25
4-Cl	[$LFe_3OFe(Pz)_3Cl$][$OTf]_2$	0.483	0.635	25
		0.320	0.679	25
		0.496	0.927	25
		1.086	2.946	25
3-N_3	[$LFe_3OFe(Pz)_3(N_3)$][OTf]	0.525	0.754	25
		0.390	1.384	25
		1.101	2.983	25
		1.084	2.615	25
	[Et_4N][$FeCl(NS_3)$]	0.258	0.982	-
	[Et_4N][$Fe(N_3)(NS_3)$]	0.352	0.731	-

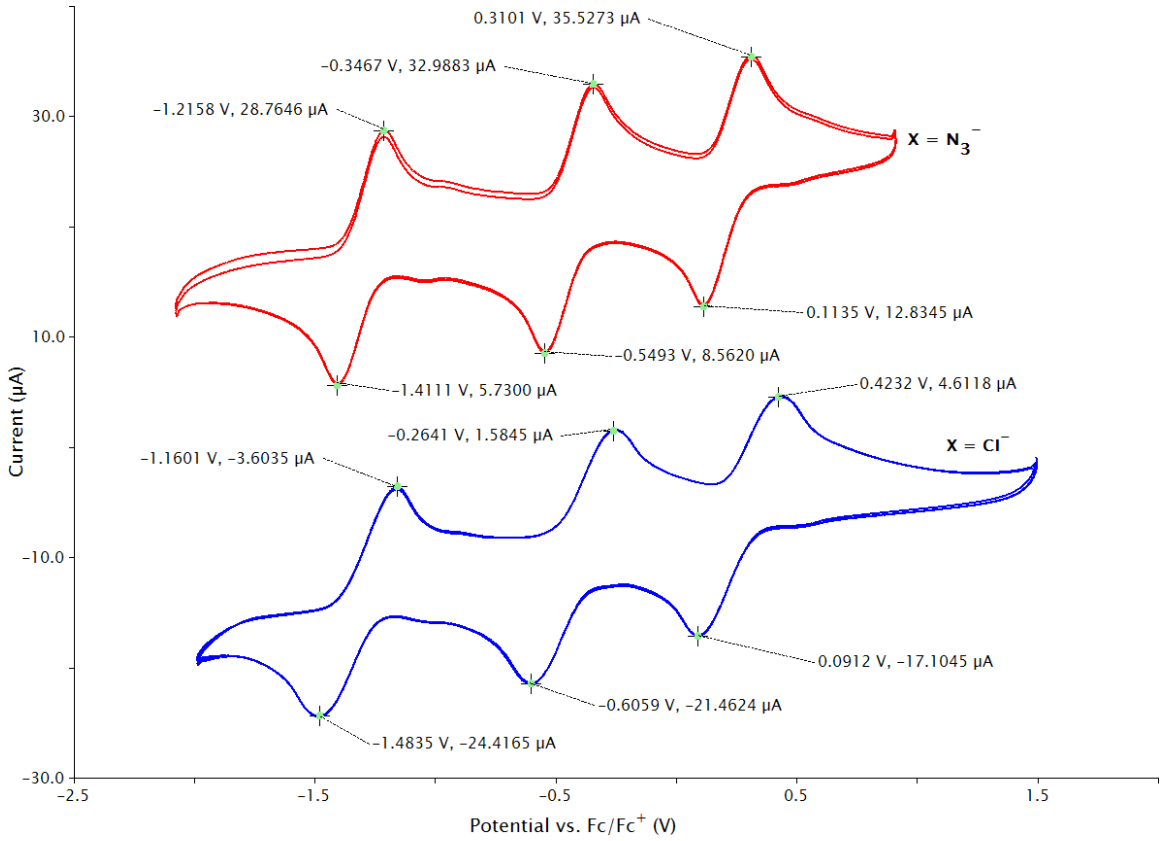

Figure 8. Stacked and normalized cyclic voltammograms (CVs) of **3-Cl** (blue trace) and **3-N$_3$** (red trace) in DCM at a scan rate of 100 mV/s. CVs were recorded a concentration of 2 mM and 1 mM for **3-Cl** and **3-N$_3$** respectively using a glassy carbon, platinum wire, and silver wire as working, counter, and reference electrodes respectively. 0.1 M [*n*Bu$_4$N][PF$_6$] was used as the supporting electrolyte.

Cyclic voltammetry (CV) studies of **3-Cl** and **3-N$_3$** were performed (Figure 8). Both complexes nearly identical electrochemical behavior with two quasireversible oxidations (**3-Cl**: -0.435, 0.26 V vs Fc/Fc$^+$; **3-N$_3$**: -0.448, 0.22 V vs Fc/Fc$^+$) corresponding to the [$Fe^{III}_2Fe^{II}_2$]/[$Fe^{III}_3Fe^{II}$] and [$Fe^{III}_3Fe^{II}$]/[Fe^{III}_4] couples respectively, and one quasireversible reduction (**3-Cl**: -1.32 vs Fc/Fc$^+$; **3-N$_3$**: -1.31 V vs Fc/Fc$^+$) corresponding to the [$Fe^{III}_2Fe^{II}_2$]/[$Fe^{III}Fe^{II}_3$] observable for both complexes. Compared to previously reported [Fe$_4$(µ$_4$-O)] clusters supported by phenylpyrazolate ligands, the oxidation to the [Fe^{III}_4] state is unusual. For both [LFe$_4$(µ$_4$-O)(PhPz)$_3$][OTf]$_2$ and

$[LFe_4(\mu_4\text{-}O)(NO)(PhPz)_3][OTf]_2$ two reductions at (-1.733, -0.727 V vs Fc/Fc^+) and (-1.662, -0.712 V vs Fc/Fc^+) and one oxidation at 0.018 and 0.005 V vs Fc/Fc^+ were observed for each complex respectively. While these complexes were reported to yield an $[Fe^{II}_4]$ cluster utilizing decamethylcobaltocene as the reductant, no such oxidation state is electrochemically accessible with **3-Cl** or **3-N_3** in DCM. This suggests that chloride or azide coordination in **3-Cl** and **3-N_3** results in a significantly more electron-rich cluster that is substantially harder to reduce as seen from the shifts in the $[Fe^{III}_2Fe^{II}_2]/[Fe^{III}Fe^{II}_3]$ ($\Delta E_{½}$ ~ -600 mV) and $[Fe^{III}_2Fe^{II}_2]/[Fe^{III}_3Fe^{II}]$ ($\Delta E_{½}$ ~ -450 mV) couples relative to $[LFe_4(\mu_4\text{-}O)(NO)(PhPz)_3][OTf]_2$ which also possesses a 5-coordinate apical Fe center.

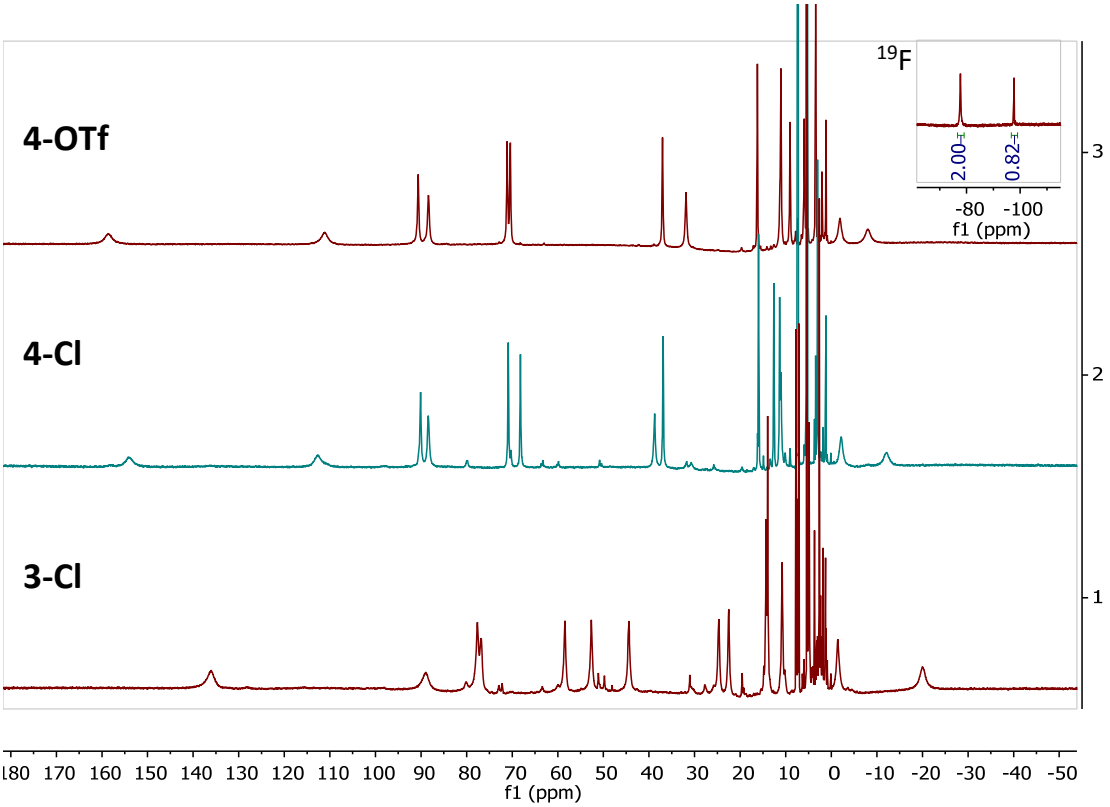

Figure 9. Comparison of NMR spectra for **3-Cl** (bottom red trace), **4-Cl** (blue trace), and **4-OTf** (top red trace) in CD_2Cl_2. Inset shows the ^{19}F NMR spectra for **4-OTf**.

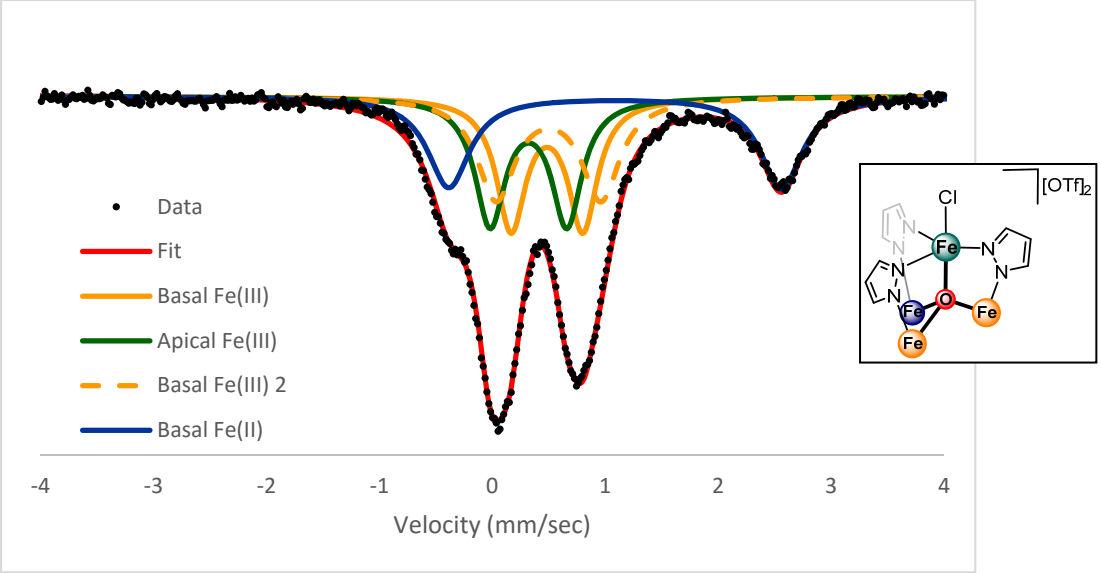

Figure 10. Zero-field ^{57}Fe Mössbauer spectrum at 80 K of **4-Cl** (black dots) and global fit (red trace) with simulated parameters (i) δ (mm/s) = 0.483, |ΔEq| (mm/s) = 0.635 (blue trace); (ii) δ (mm/s) = 0.320, |ΔEq| (mm/s) = 0.679 (orange trace); (iii) δ (mm/s) = 0.496, |ΔEq| (mm/s) = 0.927 (green trace); (iv) δ (mm/s) = 1.086, |ΔEq| (mm/s) = 2.946 (purple trace).

Attempts to isolate **3-Cl** in different oxidation states utilizing chemical oxidations and reductants was attempted. A clean oxidation with ferrocenium triflate was observed to yield the $[LFe^{III}_3Fe^{II}(\mu_4\text{-}O)(Pz)_3Cl][OTf]_2$ complex, **4-Cl** (Scheme 2). Substantial differences between **3-Cl** and **4-Cl** are observed by ^{1}H NMR spectroscopy (Figure 9). Single crystals suitable of XRD analysis were obtained for **4-Cl** (Figure 3). A comparable overall cluster geometry is observed for the one-electron oxidized complex. τ_5 parameter of 0.941 for the apical Fe center again indicates an approximately trigonal bipyramidal geometry. Fe–(μ_4-O) distances to the Fe_3 core are now consistent with an $[Fe^{III}_2Fe^{II}]$ assignment with one longer (2.186(3) Å) and two shorter (1.983(3), 2.012(3) Å) distances. The O4-Fe_3 centroid distance shortens from 1.118 to 1.065 Å, which results in an elongation of the Fe4–O4 distance from 1.864(4) to 1.924(3) Å. Mössbauer data was also collected for **4-Cl** (Figure 10). **4-Cl** shows simulated parameters

summarized in Table 1. The data clearly indicates the presence of an [$Fe^{III}_3Fe^{II}$] cluster confirming successful one-electron oxidation. This data is consistent with a formal oxidation of the Fe_3 core rather than an apical Fe-based redox process. Fe4–Cl and Fe4–N distances contract in **4-Cl**, likely to compensate for the decreased donor strength of the (μ_4-O) to Fe4 as the Fe_3 core becomes more oxidized. Otherwise **3-Cl** and **4-Cl** remain largely isostructural as expected given the rigidity of the tris(pyrazole) supporting framework.

Attempts to reduce **3-Cl** yielded inconsistent results. Attempts to access the [Fe^{III}_4] oxidation state of the cluster was attempted using silver triflate. In an NMR scale reaction halide abstraction rather than one electron oxidation appears to be the most consistent with the data. This is supported by the similarity of NMR features to the starting material (Figure 9) and the approximately 2:1 ratio of peaks observed in the ^{19}F NMR (Figure 9, inset) consistent with free triflate in solution with a single triflate coordinated the apical Fe center. The use of stronger metallocene-based oxidants is currently being pursued to access the [Fe^{III}_4] cluster oxidation state without the risk of halide abstraction. Efforts to install terminal oxygenic fragments on **3-Cl** utilizing silver nitrite and tetrabutylammonium *meta*-periodate cleanly yielded **4-Cl** suggesting the use of **4-OTf** or another less coordinating ligand coordinated to the apical Fe center might be necessary for productive chemistry.

Section 5.3 Synthesis of [Fe_4(μ_4-O)] Complexes with a Hydrogen Bonding Network

Efforts then turned to the synthesis of related clusters supported by pyrazolates capable of forming a hydrogen bonding network to moieties coordinated to the apical Fe center. Previous results with phenoxide pyrazole ligands and pyridine pyrazole indicated that both 5 and 6-member chelates from the pyrazolate were feasible.

Therefore the use of the 3-aminophenyl pyrazole ligand (**(PhNH)PzH**) was pursued due to the smaller, 4-member ring size which would likely prevent chelation. Analogous cluster construction procedures for **3-Cl** were utilized allowing for the isolation of the analogous $[LFe^{III}_2Fe^{II}_2(\mu_4\text{-}O)(PhNHPz)_3Cl][OTf]$ complex, **6-Cl**, in a one pot synthesis from **1** (Scheme 3). A preliminary solid-state structure obtained for the complex confirmed the connectivity of the tetranuclear core (Figure 11). While a detailed comparison of bond metrics is prohibited by the comparatively lower quality of the crystal structure (R1 = 20.65%), a substantial elongation of the Fe–Cl bond distance (~ 2.68 Å) has occurred compared to **3-Cl** (2.339(2) Å). This elongation is consistent with a previous report on a three-fold symmetric ligand capable of hydrogen bonding to a terminal Fe–Cl ligand.[16] However, this Fe–Cl distance is unusually long though a better solid-state structure is required to support this claim. The three N–Cl distances for the aminophenyl moieties are all roughly 3 Å long consistent with a hydrogen bonding interaction. Geometrically the three NH hydrogen bond donors are arranged in a nearly C_3 arrangement about the chloride ligand. As a consequence of the hydrogen bonding to the chloride, the ligand loses electron density and forms a weaker interaction with the Fe center.

The $[Fe^{III}_2Fe^{II}_2]$ oxidation state was confirmed by the Mössbauer data obtained for **6-Cl** (Figure 12). The apical Fe center has been assigned as the Fe^{III} component with the larger quadrupole splitting (δ (mm/s) = 0.504, $|\Delta Eq|$ (mm/s) =1.066), however no Mössbauer data for comparable hydrogen bonded Fe–Cl moieties have been reported in the literature for structurally characterized complexes making confirmation of this assignment more tenuous. The remaining components of the Mössbauer

spectrum are comparable to reported parameters for Fe^{III} and Fe^{II} enters is related complexes (Table 2).

Scheme 3. Synthetic routes to [$Fe_4(\mu_4\text{-}O)$] clusters supported by **(PhNH)Pz** ligands

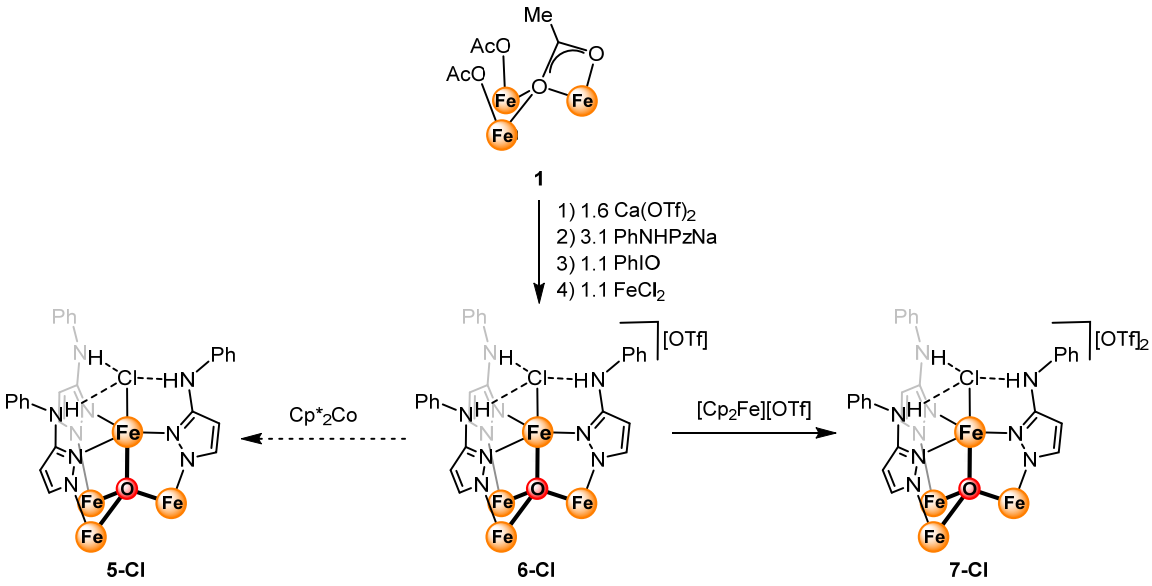

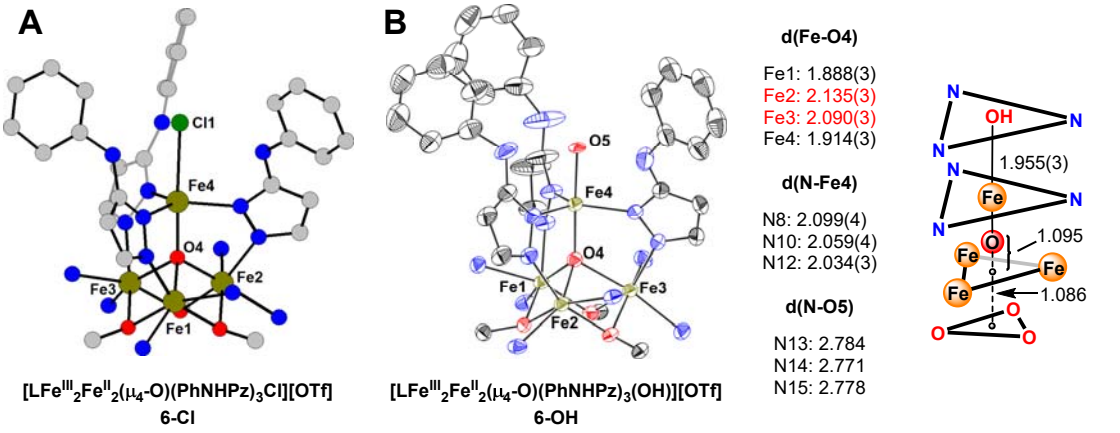

Figure 11. Solid-state structure of the [$Fe_4(\mu_4\text{-}O)$] core of **6-Cl** (A) and **6-OH** (B). Select bond metrics for **6-OH** (B, Right). Hydrogen atoms, counterions, solvent molecules, and most of the supporting tris(alkoxide) hexa(pyridyl) ligand have been omitted for clarity.

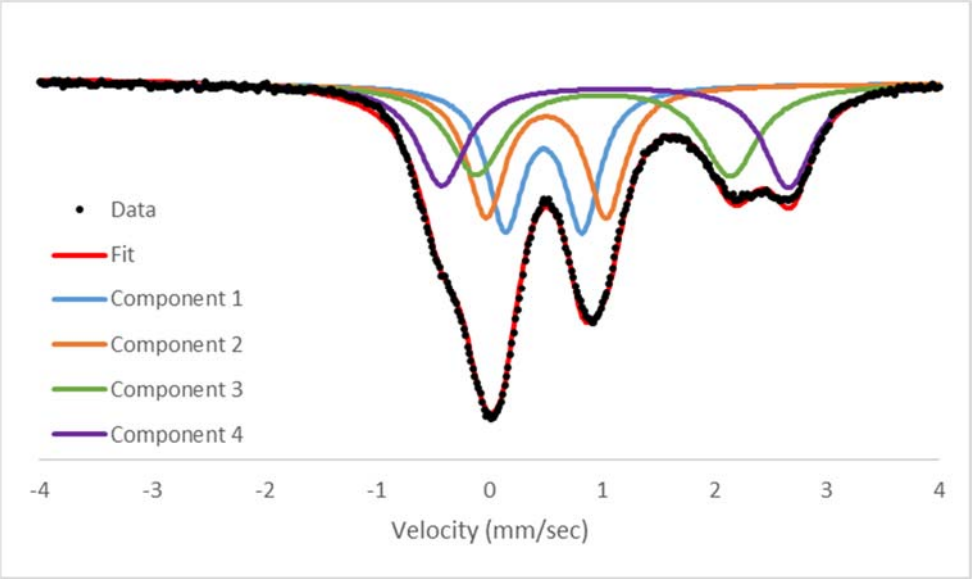

Figure 12. Zero-field ^{57}Fe Mössbauer spectrum at 80 K of **6-Cl** (black dots) and global fit (red trace) with simulated parameters (i) δ (mm/s) = 0.483, |ΔEq| (mm/s) = 0.685 (blue trace); (ii) δ (mm/s) = 0.504, |ΔEq| (mm/s) =1.066 (orange trace); (iii) δ (mm/s) = 1.012, |ΔEq| (mm/s) = 2.254 (green trace); (iv) δ (mm/s) = 1.118, |ΔEq| (mm/s) = 3.080 (purple trace).

The electrochemical behavior of **6-Cl** in DCM was also studied using cyclic voltammetry experiments (Figure 13). While the sample was not entirely pure as evidenced by small shoulders on redox events, **6-Cl** also displays one quasireversible (-1.15 V vs Fc/Fc^{+}) reduction and two quasireversible oxidations (-0.42, 0.16 V vs Fc/Fc^{+}) again indicating chloride binding substantially shifts the redox potentials compared to $[LFe_4(\mu_4\text{-}O)(NO)(PhPz)_3][OTf]_2$. Interestingly, despite the presence of electron-donating aminophenyl substituents compared to **3-Cl** there not appear to be a shift in reduction potentials to more negative values. In fact the reduction potential corresponding to the $[Fe^{III}_2Fe^{II}_2]/[Fe^{III}Fe^{II}_3]$ couple of **6-Cl** is actually approximately +150 mV more positive that **3-Cl**. However, the oxidation events corresponding to the $[Fe^{III}_2Fe^{II}_2]/[Fe^{III}_3Fe^{II}]$ and $[Fe^{III}_3Fe^{II}]/[Fe^{III}_4]$ couples respectively occur at similar (+10 mV) and lower (-98 mV) potentials. This suggests that at higher oxidation states the

electron-donating aminophenyl substituents do facilitate oxidation of the complex. At higher potentials ~ 0.6 V vs Fc/Fc^+ another irreversible oxidation is observed, however this could correspond to a ligand oxidation of one of the aminophenyl substituents rather than a $[Fe^{III}_4]/[Fe^{IV}Fe^{III}_3]$ couple. However, further characterization of this third oxidation event is required.

Table 2. Summary of Mössbauer parameters for complex **6-Cl**

		parameters		
Cmpd.	Formula	δ (mm/s)	|ΔEq| (mm/s)	%
4	$[LFe_3OFe(PhNHPz)_3Cl][OTf]$	0.483	0.685	25
		0.504	1.066	25
		1.012	2.254	25
		1.118	3.080	25

Attempts to chemically access different redox states of **6-Cl** was attempted. Much like **3-Cl**, the reduction of **5-Cl** proved sluggish and provided inconsistent results. However, the addition of ferrocenium triflate resulted in the formation of the one electron oxidized complex, **7-Cl** (Scheme 3). Solution NMR indicates, **7-Cl** looks quite distinct from **6-Cl** (Figure 14). Future attempts to access the $[Fe^{III}_4]$ complex will be made. Solid-state characterization and Mössbauer spectroscopy will be pursued to better assess differences that arise upon one-electron oxidation of the $[Fe_4(\mu_4\text{-}O)]$ core.

A serendipitous result was obtained from attempts to synthesize $[Fe_4(\mu_4\text{-}O)]$-type clusters using $Fe(OTf)_2$ rather than $FeCl_2$ as the fourth equivalent of Fe. With older batches of $Ca(OTf)_2$ and PhIO, the formation of a new species by NMR that was later confirmed to the a terminal hydroxide moiety by XRD analysis was observed (Figure 11). The Fe–O(H) distance of 1.955(3) Å is consistent with comparable species in the literature stabilize by hydrogen bonding interactions.[10a, 17] Fe–O4 distances to the Fe3 core are consistent with an $[Fe^{III}Fe^{II}_2]$ assignment as evidenced with the two long

(2.135(3), 2.090(3) Å) and one short (1.888(3) Å) bond length. A distortion from the pseudo-C_3-fold symmetric distribution of the aminophenyl hydrogen bond donors is observed consistent with the assignment as a hydroxo ligand.

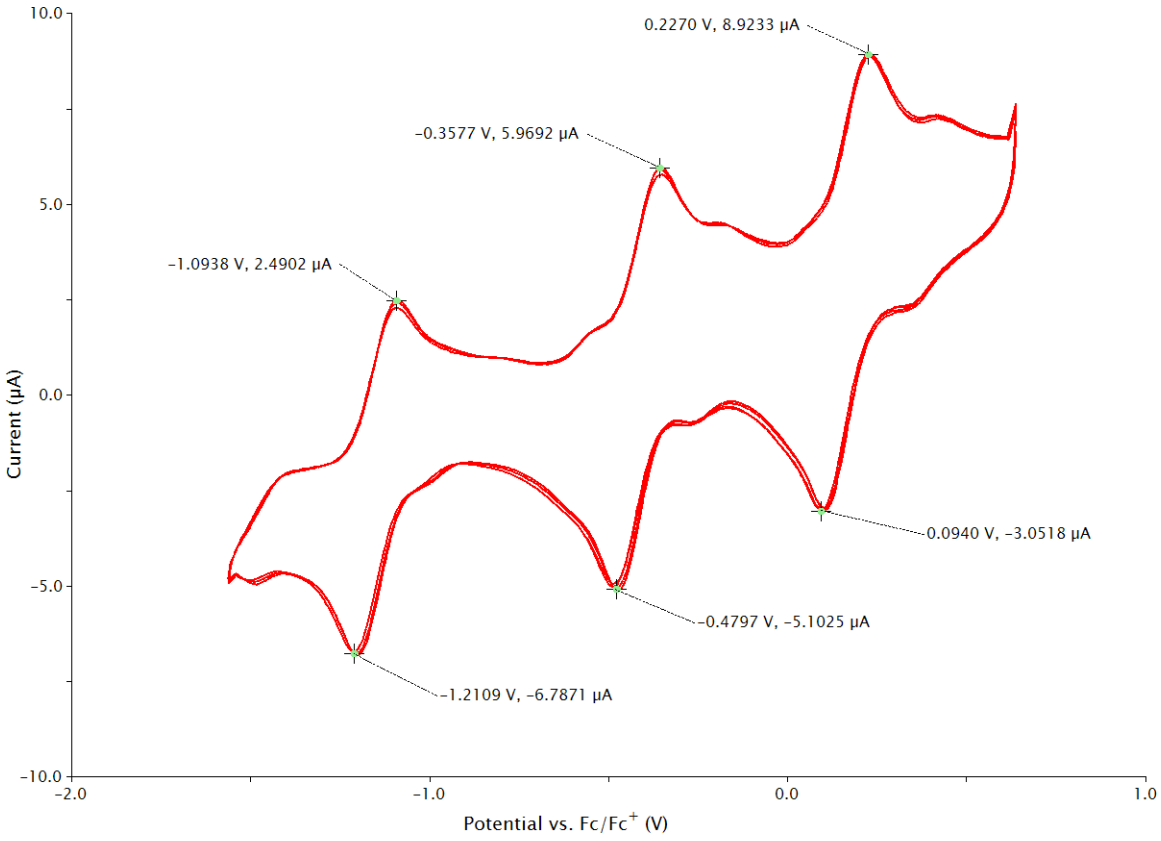

Figure 13. Cyclic voltammogram (CV) data for **6-Cl** (red trace) in DCM at a scan rate of 50 mV/s. CVs were recorded a concentration of 1 mM using a glassy carbon, platinum wire, and silver wire as working, counter, and reference electrodes respectively. 0.1 M [*n*Bu$_4$N][PF$_6$] was used as the supporting electrolyte.

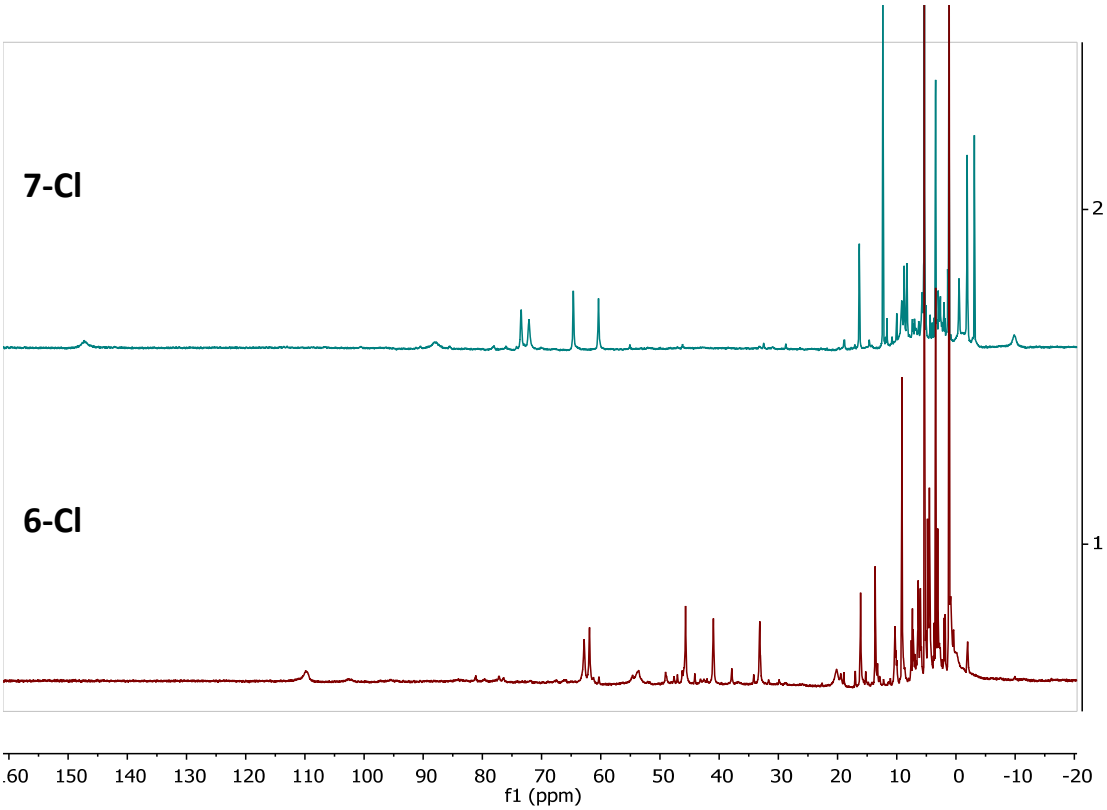

Figure 14. ^{1}H NMR comparison for **6-Cl** (red trace) and **7-Cl** (blue trace) in CD_2Cl_2.

Scheme 4. Synthesis of [$Fe_4(\mu_4$-O)] clusters with a terminal hydroxide ligand

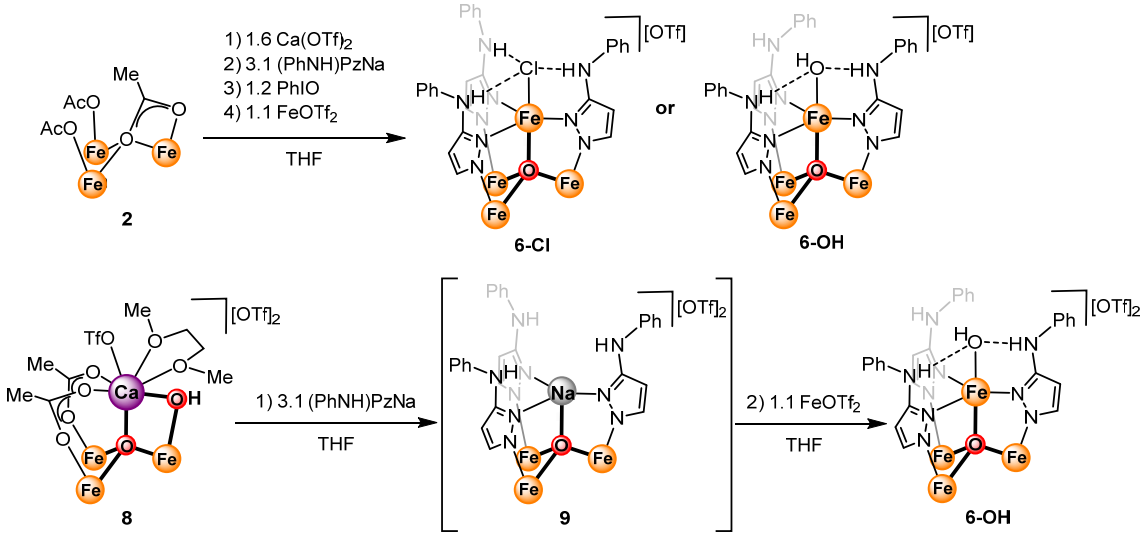

However, efforts to reproducibly synthesize **6-OH** from **1** proved challenging. Depending on the source starting materials **6-Cl** was observed to be the majority

species produced on multiple occasions. As the source of the terminal hydroxide ligand is likely from adventitious water or hydroxide impurities coordinated to the calcium or iron triflate precursors, efforts to rationally synthesize **6-OH** from alternative precursors was pursued. A previously reported [$Fe_3Ca(\mu_4\text{-}O)(\mu_2\text{-}OH)$] complex was utilized as a precursor as both the oxo and hydroxo ligand content need to synthesize **6-OH** is already present in the precursor. This route proved successful on smaller scales though incomplete transmetalation was often observed in reactions. Future efforts will focus on the scaling up of this route. Additionally, efforts to utilize salt metathesis routes to convert **6-Cl** into **6-OH** with precursors such as [NMe_4][OH], KOH, or NaOH will also be pursued. Once reproducible routes to **6-OH** are established, efforts will turn to the stabilization of terminal oxo species utilizing the stabilizing effects of the hydrogen bonding network provided by the **(PhNH)PzH** ligands.

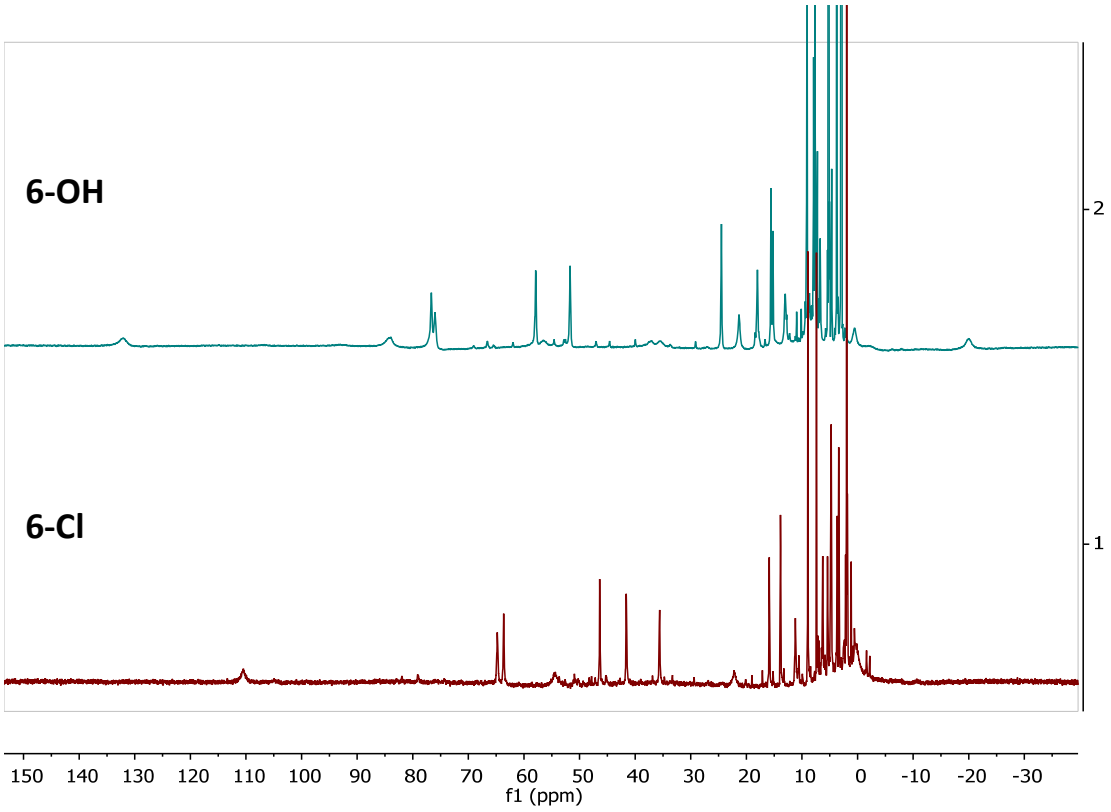

Figure 14. ^{1}H NMR comparison for **6-Cl** (red trace) and **6-OH** (blue trace) in CD_3CN.

Section 5.4 Miscellaneous Crystal Structures

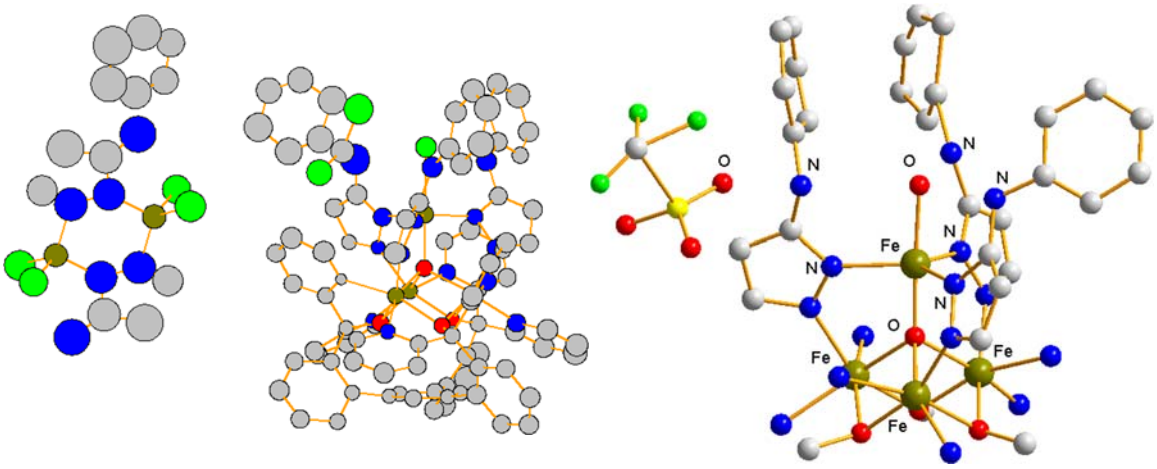

CONCLUSIONS

In conclusion, two new pyrazolate ligands have been explored study the effect of reduced steric bulk and hydrogen bonding networks on the small molecule activation reactivity of site-differentiated [$Fe_4(\mu_4$-O)] clusters. The reduction of steric bulk allows access to terminal chloride complexes where the apical Fe center prefers the Fe^{III} oxidation state rather than Fe^{II} as seen with reported clusters. With the parent pyrazolate ligand, clean substation of the chloride ligand for azide can be observed. Mössbauer parameters for the apical Fe center are in good agreement with previously reported literature complexes. Efforts to construct hydrogen bonding networks surrounding the apical Fe center have also proven successful. Compared the **3-Cl** and **4-Cl**, preliminary solid-state structures obtained for **6-Cl** shows an unusually long Fe–Cl bond consistent with hydrogen bonding from all three aminophenyl NH moieties to the chloride ligand. This unusually long elongation may also be attributable to the unusual stability of these pyrazolate-supported scaffolds to stabilize coordinatively-

unsaturated, 4-coordinate apical Fe centers using phenyl pyrazolate ligands. Efforts to synthesize terminal oxo and hydroxo moieties in a rational fashion are currently under development in the group.

EXPERIMENTAL SECTION

General considerations.

Unless otherwise specified, all air- and moisture-sensitive compounds were manipulated using glovebox or using standard Schlenk line techniques with an N_2 atmosphere. Anhydrous tetrahydrofuran (THF) was purchased from Aldrich in 18 L Pure-Pac™ containers. Anhydrous pentanes, hexanes, benzene, toluene, diethyl ether, and THF were purified by sparging with nitrogen for 15 minutes and then passing under nitrogen pressure through a column of activated A2 alumina (Zapp's).[18] Benzene-d_6, tetrahydrofuran-d_8, and acetonitrile-d_3 was purchased from Cambridge Isotope Laboratories, Inc., dried over sodium/benzophenone ketyl (benzene and THF) or calcium hydride (MeCN) and vacuum transferred prior to use. Unless indicated otherwise, all commercial chemicals were used as received. ^{1}H, ^{13}C, and ^{31}P NMR spectra were recorded on Varian Mercury 300 or Varian INOVA-500 spectrometers at room temperature unless indicated otherwise. Chemical shifts for ^{1}H and ^{13}C NMR data are reported relative to residual solvent peaks and are decoupled with respect to each other unless otherwise noted.[19] Powder and thin film ATR-IR measurements were obtained by placing a powder or drop of solution of the complex on the surface of a Bruker APLHA ATR-IR spectrometer probe and allowing the solvent to evaporate (Platinum Sampling Module, diamond, OPUS software package) at 2 cm^{-1} resolution. **(PhNH)PzH**[12] and **1**[13] were synthesized according to literature procedures.

Synthesis of Complex 3-Cl

Compound **1** (300 mg, 0.250 mmol, 1 equiv) and calcium triflate (135.2 mg, 0.400 mmol, 1.6 equiv) were transferred to a Schlenk tube fitted with a screw-in Teflon stopper and

equipped with a magnetic stirbar. THF (*ca.* 20 mL) were then added the combined mixture was allowed to stir for 1 hr during which time the solution changed from an orange suspension to a yellow-brown suspension. Sodium pyrazolate (67.5 mg, 0.750 mmol, 3 equiv) was then added as a solution in *ca.* 5 mL THF. The reaction mixture immediately turned a deep red color and became more homogeneous and was allowed to stir for 2 hrs. Iodosylbenzene (55.0 mg, 0.250 mmol, 1 equiv) was then added as a suspension in THF (*ca.* 5 mL). The reaction mixture was allowed to stir for 3 hrs during which time the solution became brown. $FeCl_2$ (34.8 mg, 0.275 mmol, 1.1 equiv) was then added as a suspension in THF (*ca.* 5 mL) and the reaction mixture was allowed to stir for 16 hrs. Reaction volatiles were then removed under reduced pressure. The residue was washed with DCM and filtered through a Celite pad until washes became clear to remove salts. Volatiles from the filtrate were then removed under reduced pressure to yield **3-Cl** as a brown powder. Yield: 317.5 mg (87 %). ^{1}H NMR (300 MHz, CD_3CN) δ 137.35 (s, 1H), 89.43 (s, 1H), 79.77 (s), 78.92 (s), 59.05 (s), 53.43 (s), 44.69 (s), 24.52 (s), 22.32 (s), 14.07 (s), 11.53 (s), -2.07 (s), -19.99 (s). ^{19}F NMR (282 MHz, CD_3CN) δ -79.28. ^{57}Fe Mössbauer: δ (mm/s) (|ΔEq| (mm/s)): 0.490 (0.637), 0.284 (1.413), 1.238 (2.745), 1.076 (2.915).

Synthesis of Complex 3-N_3

Complex **3-Cl** (106.9 mg, 0.066 mmol, 1 equiv) was transferred to a 20 mL scintillation vial equipped with a magnetic stirbar. Sodium azide (43.1 mg, 0.660 mmol, 10 equiv) was then added as a suspension in THF (*ca.* 5 mL). The combined reaction mixture was allowed to stir for 16 hrs. Reaction volatiles were then removed under reduced pressure. The residue was washed with DCM and filtered through a Celite pad until washes became colorless. Volatiles

from the filtrate were then removed under reduced pressure yielding the product as a brown solid. Yield: 80 mg (75 %). ^{1}H NMR (300 MHz, CD_3CN) δ 134.98 (s), 85.41 (s), 78.71 (s), 57.78 (s), 52.28 (s), 42.41 (s), 26.25 (s), 22.79 (s), 14.18 (s), 13.84 (s), 11.84 (s), -3.25 (s), -18.16 (s). ^{19}F NMR (282 MHz, CD_3CN) δ -79.31. IR: ν(N_3): 2060 cm^{-1}. ^{57}Fe Mössbauer: δ (mm/s) (|ΔEq| (mm/s)): 0.525 (0.754), 0.390 (1.384), 1.101 (2.983), 1.084 (2.615).

Synthesis of Complex 4-Cl

Complex **3-Cl** (106.9 mg, 0.069 mmol, 1 equiv) was transferred to a 20 mL scintillation vial equipped with a magnetic stirbar. Ferrocenium triflate (23.2 mg, 0.069 mmol, 1 equiv) was then added as a solution in *ca.* 5 mL of DCM. The reaction mixture was allowed to stir for 1 hr. Reaction volatiles were then removed under reduced pressure. The residue was washed with benzene and filtered through a Celite pad to remove the majority of the ferrocene byproduct. The residue was then washed with DCM to elute the product. The volatiles of the DCM filtrate were then removed under reduced pressure. The obtained product was then recrystallized from a DCM:Et_2O vapor diffusion yielding the product as a brown precipitate. Yield: 101 mg (86 %). ^{1}H NMR (300 MHz, CD_2Cl_2) δ 154.10 (s), 112.63 (s), 90.11 (s), 88.40 (s), 70.87 (s), 68.20 (s), 38.78 (s), 36.90 (s), 15.95 (s), 12.62 (s), 11.32 (s), 11.04 (s), -2.16 (s), -12.07 (s). ^{19}F NMR (282 MHz, CD_2Cl_2) δ -77.96. ^{57}Fe Mössbauer: δ (mm/s) (|ΔEq| (mm/s)): 0.483 (0.635), 0.320 (0.679), 0.496 (0.927), 1.086 (2.946).

Synthesis of Complex 6-Cl

Compound **1** (700 mg, 0.583 mmol, 1 equiv) and calcium triflate (317 mg, 1.75 mmol, 1.6 equiv) were transferred to a Schlenk tube fitted with a screw-in Teflon stopper and equipped with a magnetic stirbar. THF (*ca.* 40 mL) were then added the combined mixture was allowed to stir for 1 hr during which time the solution changed from an orange suspension to a yellow-brown suspension. **(PhNH)PzNa** (317 mg, 1.75 mmol, 3 equiv) was then added as a solution in *ca.* 5 mL THF. The reaction mixture immediately turned a deep red color and became more homogeneous and was allowed to stir for 2 hrs. Iodosylbenzene (128.3 mg, 0.583 mmol, 1 equiv) was then added as a suspension in THF (*ca.* 5 mL). The reaction mixture was allowed to stir for 3 hrs during which time the solution became a deep purple. $FeCl_2$ (81.3 mg, 0.641 mmol, 1.1 equiv) was then added as a suspension in THF (*ca.* 5 mL) and the reaction mixture was allowed to stir for 16 hrs. During this time the reaction mixture change color from purple to a blue/purple color. Reaction volatiles were then removed under reduced pressure. The residue was washed with DCM and filtered through a Celite pad until washes became clear to remove salts. Volatiles from the filtrate were then removed under reduced pressure to yield mostly pure **6-Cl** as a blue/purple powder. Yield: 750 mg (73 %). During purification attempts, it was found dissolving this material in acetonitrile and filtering through a second Celite pad afforded clean **6-Cl** suitable for further analysis. However, much of the material had been split between different purification protocols making an accurate estimate a yield via this method challenging. ^{1}H NMR (300 MHz, CD_3CN) δ 110.86 (s), 65.12 (s), 63.95 (s), 46.55 (s), 41.69 (s), 35.66 (s), 22.54 (s), 15.97 (s), 13.89 (s), 11.26 (s). ^{19}F NMR (282 MHz, CD_3CN) δ -79.30. ^{57}Fe Mössbauer: δ (mm/s) (|ΔEq| (mm/s)): 0.483 (0.685), 0.504 (1.066), 1.012 (2.254), 1.118 (3.080).

Synthesis of Complex 7-Cl

Complex **6-Cl** (80 mg, 0.046 mmol, 1 equiv) was transferred to a 20 mL scintillation vial equipped with a magnetic stirbar. Ferrocenium triflate (15.3 mg, 0.046 mmol, 1 equiv) was then added as a solution in *ca.* 5 mL of DCM. The reaction mixture was allowed to stir for 1 hr. During this time a color change from blue to green/blue was observed. The reaction mixture was concentrated (*ca.* 1 mL) under reduced pressure and then Et_2O (*ca.* 20 mL) was added to precipitate the product. The reaction mixture was filtered onto a Celite pad and washed with Et_2O until the filtrate became colorless. The residue was then washed with DCM to elute the product. The volatiles of the DCM filtrate were then removed under reduced pressure. The obtained product was then recrystallized from a DCM:Et_2O vapor diffusion yielding the product as a brown precipitate. Yield: 71.7 mg (83 %). ^{1}H NMR (300 MHz, CD_2Cl_2) δ 147.38 (s), 88.11 (s), 73.48 (s), 72.16 (s), 64.65 (s), 60.41 (s), 16.33 (s), 12.34 (s), -9.87 (s). ^{19}F NMR (282 MHz, CD_2Cl_2) δ -76.74.

Mössbauer Details

Zero-field ^{57}Fe Mössbauer spectra were recorded at 80 K in the constant acceleration mode on a spectrometer from See Co (Edina, MN) equipped with an SVT-400 cryostat (Janis, Wilmington, WA). The quoted isomer shifts are relative to the centroid of the spectrum of a α-Fe foil at room temperature. Samples were prepared by grinding polycrystalline material (20 mg) into a fine powder and pressed into a homogeneous pellet with boron nitride in a cup fitted with a screw cap. The data were fitted to Lorentzian lineshapes using the program WMOSS (www.wmoss.org).

Mössbauer simulation details for compounds 3-Cl, 3-N_3, 4-Cl, and 6-Cl.

All spectra were simulated by four pairs of symmetric quadrupole doublets with equal populations and Lorentzian lineshapes, and refined to a minimum by the method of least squares optimization (a total of 13 fitting parameters per spectrum). For all spectra, the observed resonances spanned the region from -1–3 mm s^{-1}. Any resonances appearing above 2 mm s^{-1} indicate the presence of high spin Fe(II) centers and must correspond to species with isomer shifts ~1 mm s^{-1}, given the range of observed resonances. In short, the Mössbauer data were modeled to be consistent with our previously reported triiron-oxo/hydroxyl clusters,[8] and our previously reported tetranuclear iron clusters.[2]

Table 1. Crystal and refinement data for reported complexes.

Complex	**3-Cl**	**4-Cl**	**6-OH**
empirical formula	$C_{79}H_{48}ClF_3Fe_4N_{12}O_{10}S$	$C_{72}H_{55}ClF_5Fe_4N_{13}O_{11}S_2$	$C_{96.60}H_{77.19}F_3Fe_4N_{15}O_{10.77}S$
formula wt	1673.20	1696.26	1933.04
T (K)	99.97	100.01	100.0
a, Å	12.4451(10)	12.2975(7)	17.2031(6)
b, Å	26.739(2)	17.0691(10)	17.6939(5)
c, Å	24.0447(18)	18.4705(11)	18.0034(6)
α, deg	90	76.376(2)	118.107(2)
β, deg	96.775(2)	86.452(2)	103.647(2)
γ, deg	90	85.738(2)	103.659(2)
V, Å^3	7945.2(11)	3753.6(4)	4294.5(3)
Z	4	2	2
cryst syst	Monoclinic	Triclinic	Triclinic
space group	P 1 21/c 1	P -1	P -1
d_{calcd}, g/cm^3	1.399	1.501	1.495
θ range, deg	2.244 to 29.127	2.312 to 30.552	2.887 to 79.265
μ, mm^{-1}	0.847	0.929	6.197
abs cor	Semi-empirical from equivalents	Semi-empirical from equivalents	Semi-empirical from equivalents
GOF[c]	1.043	1.021	1.017
R1,[a] wR2[b] ($I > 2\sigma(I)$)	0.0872, 0.2200	0.0940, 0.2788	0.0658, 0.1569

[a] $R1 = \Sigma||F_o|-|F_c|| / \Sigma|F_o|$ [b] $wR2 = \{ \Sigma [w(F_o^2-F_c^2)^2] / \Sigma [w(F_o^2)^2] \}^{1/2}$ [c] $GOF = S = \{ \Sigma [w(F_o^2-F_c^2)^2] / (n-p) \}^{1/2}$

REFERENCES

1.(a) Holm, R. H.; Kennepohl, P.; Solomon, E. I., *Chemical Reviews* **1996,** *96*, 2239-2314; (b) Ragsdale, S. W., *Chemical Reviews* **2006,** *106*, 3317-3337; (c) Fontecilla-Camps, J. C.; Amara, P.; Cavazza, C.; Nicolet, Y.; Volbeda, A., *Nature* **2009,** *460*, 814-822; (d) Can, M.; Armstrong, F. A.; Ragsdale, S. W., *Chemical Reviews* **2014,** *114*, 4149-4174; (e) Hoffman, B. M.; Lukoyanov, D.; Yang, Z. Y.; Dean, D. R.; Seefeldt, L. C., *Chemical Reviews* **2014,** *114*, 4041-4062; (f) Lubitz, W.; Ogata, H.; Rudiger, O.; Reijerse, E., *Chemical Reviews* **2014,** *114*, 4081-4148; (g) Solomon, E. I.; Heppner, D. E.; Johnston, E. M.; Ginsbach, J. W.; Cirera, J.; Qayyum, M.; Kieber-Emmons, M. T.; Kjaergaard, C. H.; Hadt, R. G.; Tian, L., *Chemical Reviews* **2014,** *114*, 3659-3853; (h) Yano, J.; Yachandra, V., *Chemical Reviews* **2014,** *114*, 4175-4205.
2.McEvoy, J. P.; Brudvig, G. W., *Chemical Reviews* **2006,** *106*, 4455-4483.
3.Solomon, E. I.; Sundaram, U. M.; Machonkin, T. E., *Chemical Reviews* **1996,** *96*, 2563-2606.
4.(a) Zhao, M.; Wang, H.-B.; Ji, L.-N.; Mao, Z.-W., *Chemical Society Reviews* **2013,** *42*, 8360-8375; (b) Warren, J. J.; Mayer, J. M., *Biochemistry* **2015,** *54*, 1863-1878.
5.(a) Meunier, B.; de Visser, S. P.; Shaik, S., *Chemical Reviews* **2004,** *104*, 3947-3980; (b) Denisov, I. G.; Makris, T. M.; Sligar, S. G.; Schlichting, I., *Chemical Reviews* **2005,** *105*, 2253-2278; (c) Ortiz de Montellano, P. R., *Chemical Reviews* **2010,** *110*, 932-948.
6.Rigsby, M. L.; Wasylenko, D. J.; Pegis, M. L.; Mayer, J. M., *Journal of the American Chemical Society* **2015,** *137*, 4296-4299.
7.(a) Taguchi, T.; Gupta, R.; Lassalle-Kaiser, B.; Boyce, D. W.; Yachandra, V. K.; Tolman, W. B.; Yano, J.; Hendrich, M. P.; Borovik, A. S., *Journal of the American Chemical Society* **2012,** *134*, 1996-1999; (b) Sano, Y.; Weitz, A. C.; Ziller, J. W.; Hendrich, M. P.; Borovik, A. S., *Inorganic Chemistry* **2013,** *52*, 10229-10231; (c) Cook, S. A.; Borovik, A. S., *Accounts of Chemical Research* **2015,** *48*, 2407-2414.
8.(a) MacBeth, C. E.; Golombek, A. P.; Young, V. G.; Yang, C.; Kuczera, K.; Hendrich, M. P.; Borovik, A. S., *Science* **2000,** *289*, 938-941; (b) Larsen, P. L.; Gupta, R.; Powell, D. R.; Borovik, A. S., *Journal of the American Chemical Society* **2004,** *126*, 6522-6523; (c) Lacy, D. C.; Gupta, R.; Stone, K. L.; Greaves, J.; Ziller, J. W.; Hendrich, M. P.; Borovik, A. S., *Journal of the American Chemical Society* **2010,** *132*, 12188-12190.
9.(a) Moore, C. M.; Szymczak, N. K., *Chemical Science* **2015,** *6*, 3373-3377; (b) Matson, E. M.; Park, Y. J.; Fout, A. R., *Journal of the American Chemical Society* **2014,** *136*, 17398-17401.
10.(a) Ng, G. K. Y.; Ziller, J. W.; Borovik, A. S., *Inorganic Chemistry* **2011,** *50*, 7922-7924; (b) Larsen, P. L.; Parolin, T. J.; Powell, D. R.; Hendrich, M. P.; Borovik, A. S., *Angewandte Chemie* **2003,** *115*, 89-93; (c) Zinn, P. J.; Powell, D. R.; Day, V. W.; Hendrich, M. P.; Sorrell, T. N.; Borovik, A. S., *Inorganic Chemistry* **2006,** *45*, 3484-3486; (d) Lee, J. H.; Park, J.; Lah, M. S.; Chin, J.; Hong, J.-I., *Organic Letters* **2007,** *9*, 3729-3731.
11.de Ruiter, G.; Thompson, N. B.; Lionetti, D.; Agapie, T., *Journal of the American Chemical Society* **2015,** *137*, 14094-14106.
12.Moss, T. A.; Addie, M. S.; Nowak, T.; Waring, M. J., *Synlett* **2012**, 285-289.
13.Tsui, E. Y.; Kanady, J. S.; Day, M. W.; Agapie, T., *Chemical Communications* **2011,** *47*, 4189-4191.
14.MacDonald, M. R.; Ziller, J. W.; Evans, W. J., *Inorganic Chemistry* **2011,** *50*, 4092-4106.
15.Davies, S. C.; Durrant, M. C.; Hughes, D. L.; Richards, R. L.; Sanders, J. R., *Journal of the Chemical Society, Dalton Transactions* **2000**, 4694-4701.
16.Sickerman, N. S.; Park, Y. J.; Ng, G. K. Y.; Bates, J. E.; Hilkert, M.; Ziller, J. W.; Furche, F.; Borovik, A. S., *Dalton Transactions* **2012,** *41*, 4358-4364.

17.(a) MacBeth, C. E.; Gupta, R.; Mitchell-Koch, K. R.; Young, V. G.; Lushington, G. H.; Thompson, W. H.; Hendrich, M. P.; Borovik, A. S., *Journal of the American Chemical Society* **2004,** *126*, 2556-2567; (b) Mukherjee, J.; Lucas, R. L.; Zart, M. K.; Powell, D. R.; Day, V. W.; Borovik, A. S., *Inorganic Chemistry* **2008,** *47*, 5780-5786.
18.Pangborn, A. B.; Giardello, M. A.; Grubbs, R. H.; Rosen, R. K.; Timmers, F. J., *Organometallics* **1996,** *15*, 1518-1520.
19.Fulmer, G. R.; Miller, A. J. M.; Sherden, N. H.; Gottlieb, H. E.; Nudelman, A.; Stoltz, B. M.; Bercaw, J. E.; Goldberg, K. I., *Organometallics* **2010,** *29*, 2176-2179.

APPENDIX A

TOWARDS THE SYNTHESIS OF HETEROMETALLIC MULTINUCLEAR COMPLEXES AS MODELS OF [NIFE]-CARBON MONOXIDE DEHYDROGENASE

Abstract

Synthetic models of [NiFe] carbon monoxide dehydrogenase (CODH) were targeted with the aim of isolating open heterobimetallic edge sites in [Fe_3Ni] clusters that mimic parts of both the [Fe_3NiS_4]-cubane and exo Fe site of the enzymatic active site. While a cationic [$Fe^{II}_3(\mu_3\text{-}S)$] cluster could be accessed, its application to higher nuclearity clusters proved challenging, and no nickel containing clusters could be isolated. A [$Fe^{III}_2Fe^{II}Ni^{II}(\mu_4\text{-}O)$] cluster could be isolated with the apical nickel center supported by both a chelating bis(oximate) ligand (**PRABOH$_2$**) and an acetate ligand. However, efforts to open a heterobimetallic edge site with electrophiles resulted in loss of both the nickel center and **PRABOH$_2$** ligand. While overall unsuccessful, this project provided insight into several design principles for the rational construction of heterometallic trinuclear complexes supported by the previously reported tris(alkoxide) hexa(pyridyl) ligand framework.

INTRODUCTION

The reduction of carbon dioxide and subsequent conversion into lower oxygen content products and liquid fuels is an area of active research due its relative abundance and identity as a greenhouse gas.[1] In biology, the selective two proton / two electron reduction of carbon dioxide (CO_2) to carbon monoxide (CO) can be reversibly mediated by the enzyme carbon monoxide dehydrogenase (CODH) at a heterobimetallic [Fe_4Ni] cluster (Figure 1).[2] In a CO_2-coordinated solid-state structure obtained for the enzyme, the core of inorganic cofactor structurally resembles an [Fe_4S_4] cubane with one metal vertex replaced with a nickel center, which shows an elongated interaction with S4, resulting in an open cubane structure.[2b] Instead, S4 binds a fourth Fe center exo to the cubane. At this unique [NiFe] heterobimetallic edge site is where the reversible conversion of CO_2 and CO occurs through the mechanism proposed in Figure 1B.

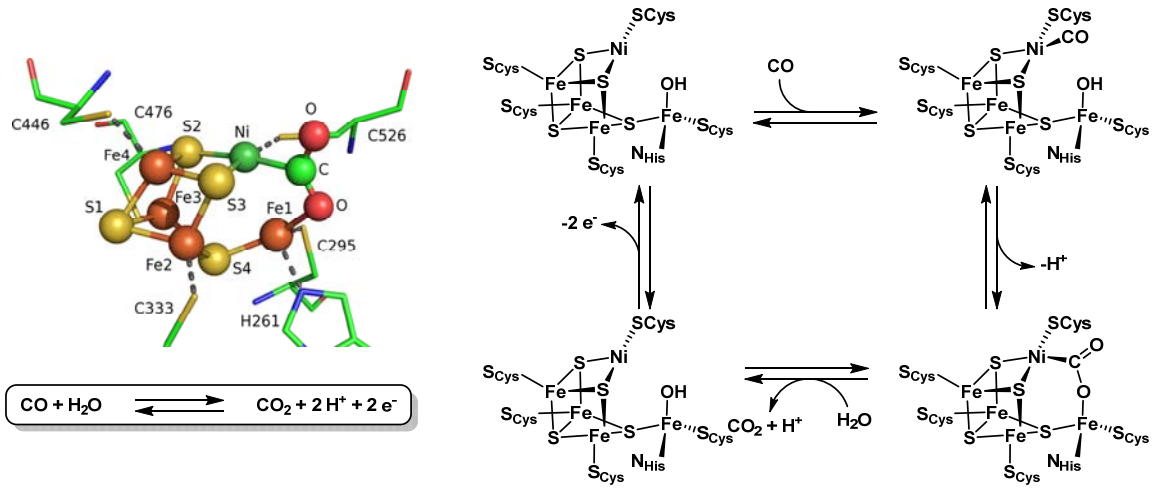

Figure 1. A) Active site structure of [NiFe]-CODH and B) proposed enzymatic catalytic cycle. Image credit for the pymol figure for [NiFe]-CODH goes to Dr. Davide Lionetti.

To better understand the enzymatic mechanism, many synthetic models of the [NiFe] CODH active site have been developed (Figure 2).[3] While a complete structural model of the active site have not been reported to date, likely attributable to the complexity and asymmetry of the target [Fe_4Ni] cluster, various aspects of the native cofactor, including heterometallic [NiFe] complexes,[3b] the [Fe_3Ni] cubane,[3a, 3c] and relevant fundamental chemical transformations at monometallic Ni complexes,[3d] the have been successfully incorporated in synthetic complexes. However, the coordination of CO_2 or hydroxide attack onto CO has not been demonstrated at [NiFe] complexes to date.

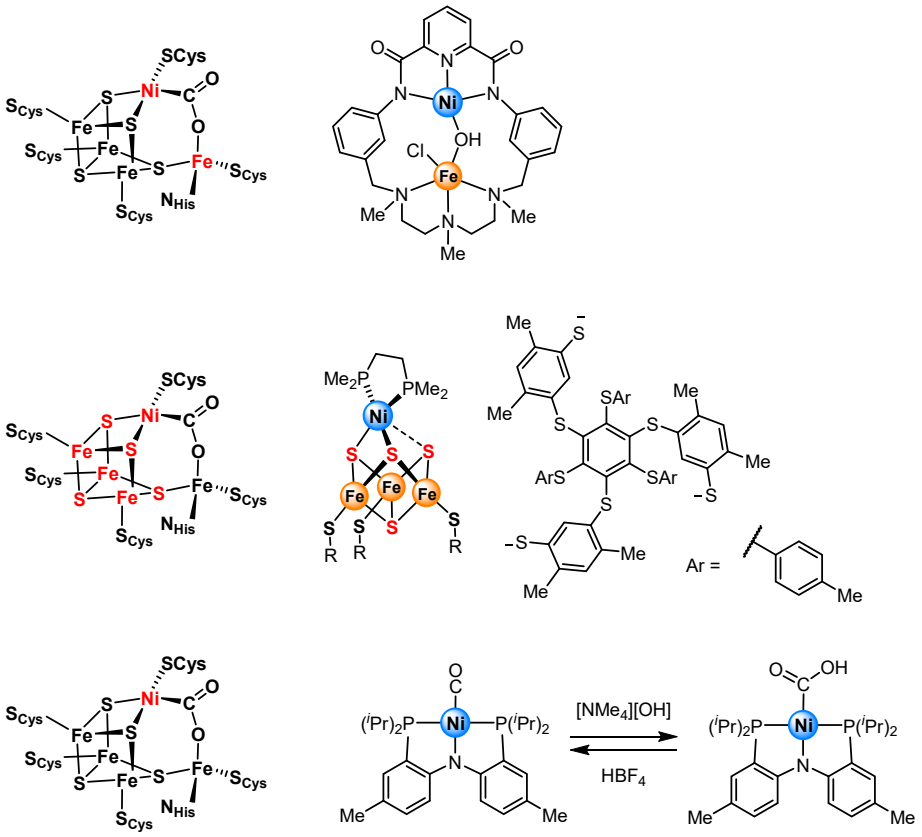

Figure 2. Select reported [NiFe] CODH model complexes and the modeled portions of the enzymatic active site.

Our group has previously reported the rational synthesis of numerous heterometallic multinuclear clusters supported by a tris(alkoxide) hexa(pyridyl) ligand framework (**LH_3**, Figure 3).[4] While these systems have provided insight into relationship between redox-active metals and the Lewis acidity of redox-inactive metals in $[M_3M'(\mu_4\text{-}O)(\mu_2\text{-}OH)]$ (M = Mn, Fe) and Mn_3MO_4 cubanes, the extension of these clusters to small molecule activation has not been reported. Herein, we discuss the attempts to synthesize $[Fe_3Ni(\mu_4\text{-}X)]$-type clusters with open edge sites capable of coordinating carbon dioxide to mimic the enzymatic active site of [NiFe] CODH (Figure 3). This strategy aims to model the [NiFe] heterobimetallic edge site as well as two additional Fe centers contained within the cubane moiety. Triiron tris(acetate) precursors support by **LH_3** have previously been reported in our group and will serve as an entry point into this chemistry. The triiron core is rigidly locked into a chair cyclohexane-like arrangement, which for the remainder of figures in this appendix will be abbreviated as a triangular arrangement of Fe centers as this core geometry remains invariant throughout the described chemistry (Figure 3).

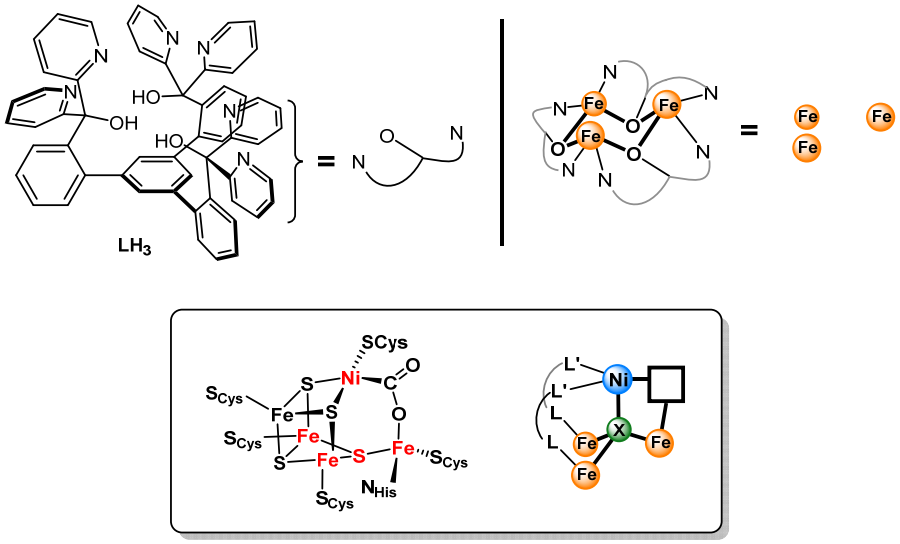

Figure 3. Targeted $[Fe_3Ni(\mu_4\text{-}X)]$ complexes as novel models of the [NiFe] CODH.

RESULTS AND DISCUSSION

Section A.1 Ligand Syntheses

Scheme 1. Syntheses of surveyed ligands

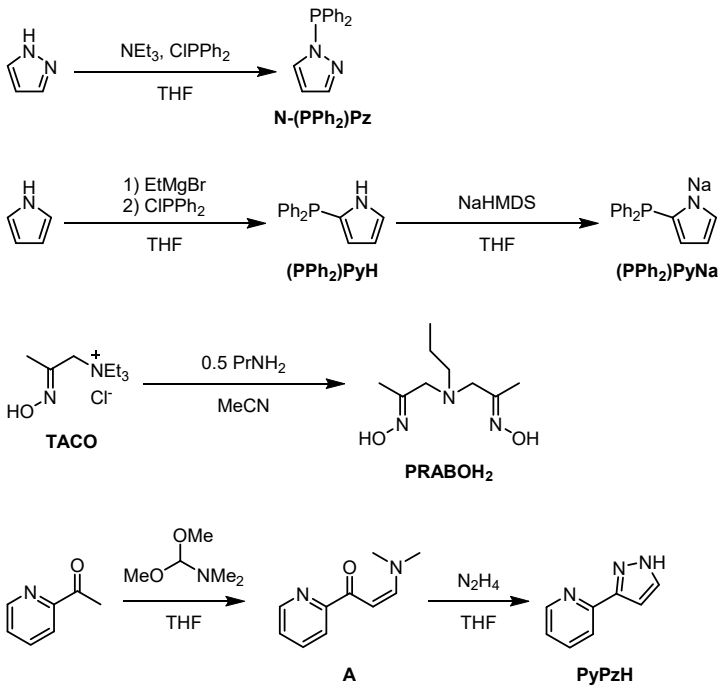

Many ligands were surveyed to determine which ligands would be most suitable to the stabilization of heterometallic [Fe_3M]-type complexes. With the aim of supporting low-valent apical Ni centers, **N-(PPh_2)Pz** and **(PPh_2)PyH** were synthesized according to literature protocols (Scheme 1).[5] The softer phosphine donors would be expected to preferentially bind the apical metal based on steric clash with the **LH_3** ligand to form a N-anchored three-atom bridge to the Fe_3 core. Conceptually, these ligands would replace bridging acetate ligands commonly observed in other multimetallic complexes reported by our group. The reaction of **(PPh_2)PzH** with sodium hexamethyldisilazide (NaHMDS) cleanly afforded the deprotonated pyrrole moiety, **(PPh_2)PzNa**. This opens up multiple avenues for ligand incorporation into clusters with both salt metathesis or protonlysis routes viable depending on ligand precursor utilized.

Multidentate chelating ligand architectures were also pursued to provide additional donors to support the apical metal center. To this end, **PRABOH$_2$** and **PyPzH** were also synthesized according to literature procedures (Scheme 1).[6] Unpublished results in the group had studied the use of these ligands in tetranuclear clusters suggesting their application to the synthesis of [Fe$_3$Ni] clusters would be worth pursuing.[7]

Section A.2 Attempts to Synthesize [Fe$_3$Ni(μ_4-S)] Clusters

To better mimic the active site of [NiFe] CODH, an interstitial sulfide was targeted. The addition of bis(trimethylsilyl)sulfide (S(SiMe$_3$)$_2$) to a cationic [Fe$^{II}_3$(OAc)$_2$(OTf)] (OTf = trifluoromethanesulfonate or triflate) complex (**2**) in acetonitrile (MeCN) cleanly afforded the desired Fe$_3$(μ_3-S) (**3**) cluster in quantitative yield by NMR with loss of trimethylsilylacetate. This represents a different synthetic strategy compared to other tetranuclear oxido-containing clusters reported from our group which require an oxidative installation of the interstitial atom. Compound **3** could also be cleanly be isolated from the corresponding [Fe$^{II}_3$(OAc)$_3$] complex (**1**) in a one-pot procedure in MeCN by first generating **2** *in situ* by adding half an equivalent of calcium triflate to act as an acetate sink. S(SiMe$_3$)$_2$ was then added resulting in an immediate color change to a red solution characteristic of **3**.

Scheme 2. Syntheses of Fe$_3$(μ_3-S) Cluster

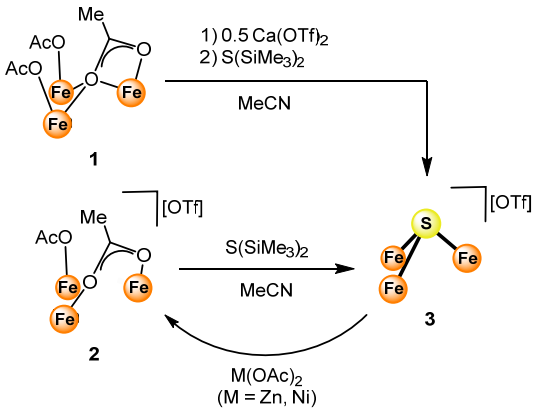

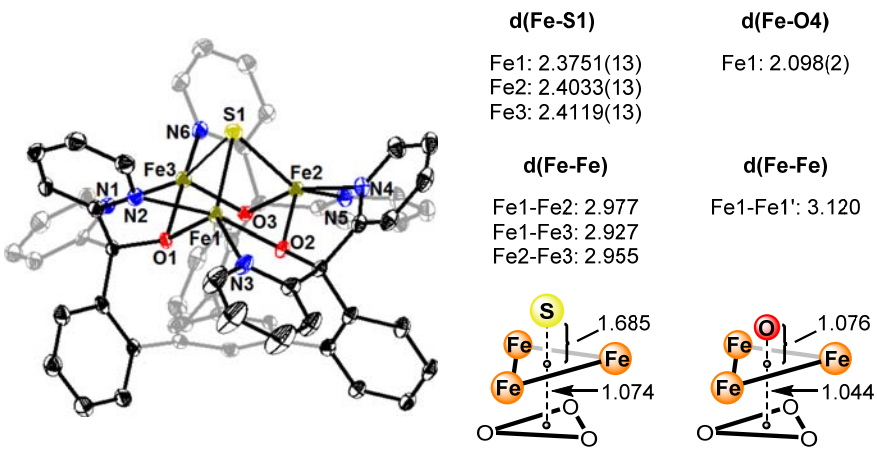

Figure 4. Solid-state structure of complex **3**. Hydrogen atoms, solvent molecules, and counterions have been omitted for clarity. Select bond metrics for **3** and the cationic $[Fe^{II}_3(\mu_3\text{-}O)(MeCN)_3]$ cluster are also presented.

The $[Fe^{II}_3(\mu_3\text{-}S)]$ assignment was confirmed by single crystal X-ray diffraction (XRD) analysis with samples recrystallized from acetonitrile/ether vapor diffusion (Figure 4). In the solid-state, each Fe center is five-coordinate and shows distorted square pyramidal geometry with an intermediate τ_5 parameter for each Fe center (Fe1: 0.43, Fe2: 0.34, Fe3: 0.31). This differs substantially from a crystallographically characterized $[Fe^{II}_3(\mu_3\text{-}O)]$ complex with the same metal oxidation states. The smaller oxide interstitial atom enables where acetonitrile coordination to each Fe center, resulting in 6-coordinate *pseudo*-octahedral metal centers. Consistent with the larger size of the interstitial sulfur atom relative to the oxygen Fe–X distances are considerably elongated in compound **3**, ranging from 2.3751(13) to 2.4119(13) Å, compared to 2.098(2) Å in the case of the $[Fe^{II}_3(\mu_3\text{-}O)]$ complex. As a consequence, the distances between the Fe_3-centroid and the interstitial atom elongates from 1.076 to 1.685 Å representing a substantial 0.61 Å shift. The sum of the angles around the interstitial atom are also markedly different shrinking with the larger sulfur atom to 228.18 ° versus

288.19 ° in the case of the (μ_3-O) ligand. Counterintuitively, the Fe–Fe distances contract for compound **3** (2.977, 2.927, 2.955 Å) relative to the [Fe^{II}_3(μ_3-O)] complex (3.120 Å), which necessarily results in a elongation of the Fe_3 centroid to (alkoxide-O)$_3$ centroid distance from 1.044 to 1.074 Å.

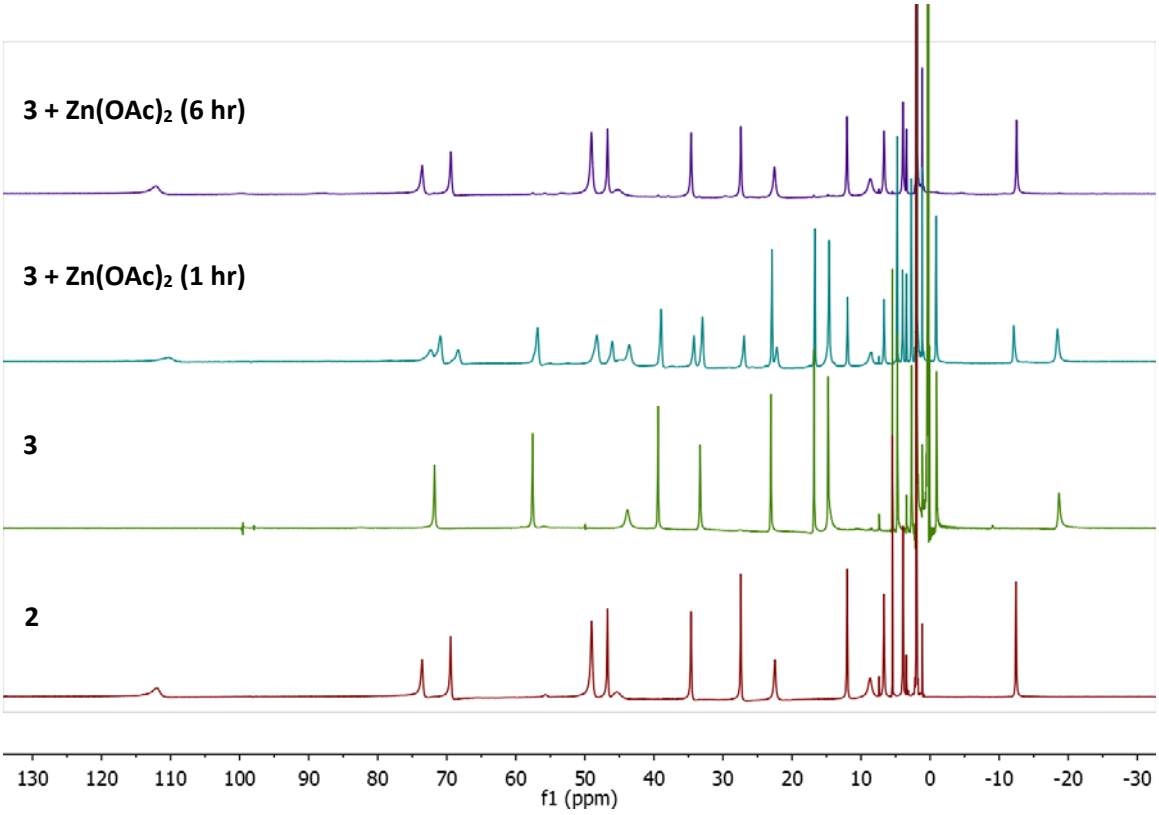

Figure 5. ^{1}H NMR data showing the quantitative conversion of **3** into **2** following addition of Zn(OAc)$_2$.

Despite the convenient ability to isolate compound **3**, the installation of the fourth metal center proved challenging. Previously reported tetranuclear clusters have always required supporting ligands such as acetates or pyrazolates. Therefore the binding to **N-(PPh$_2$)Pz** and **(PPh$_2$)PyNa** to compounds **3** was pursued. However, these reactions only resulted in a complicated mixture of products by NMR that could not be purified or characterized. The addition of Ni^{II}- or Zn^{II}(OAc)$_2$ salts also resulted in

the conversion of **3** back into the bis(acetate) complex **2** over multiple hours (Figure 5). A dark precipitate also formed consistent with loss of insoluble metal chalcogenides byproducts. Attempts to oxidize compound **3** with ferrocenium salts also resulted in complicated mixtures by NMR from which Fe_3Cl_n complexes could be crystallized indicating loss of the interstitial sulfide. As a result it became apparent that the installation of the fourth metal center using **3** was difficult due to the propensity to lose the sulfide either as metal chalogenides or as elemental sulfur. Efforts to construct [NiFe] CODH model complexes turned to alternative strategies.

Section A.3 Attempts to Synthesize [$Fe_3Ni(\mu_4$-O)] Clusters

After attempts to construct higher nuclearity clusters with compound **3** proved unsuccessful, efforts turned to the synthesis [Fe_3Ni] clusters with a (μ_4-O) ligand to build off of established results in the group with asymmetric [$Fe_3M(\mu_4$-O)]-type clusters.[7] Previous results in the group suggested that [Fe_4O] and [Fe_3ZnO] clusters had been accessible using **PyPzH** or **PRABOH$_2$** in conjunction with acetate ligands.[7] Therefore, the use of these ligands when constructing [Fe_3Ni] clusters was pursued. Due to the low propensity of Ni^{II} to coordinate carbon dioxide efforts focused on the isolation of [Fe_3Ni] possessing a bridging or terminal hydroxide ligand whose nucleophilic attack on carbon monoxide or isoelectronic analogs could be studied.

Initial efforts focused on transmetalation reactions from a previously reported [$Fe_3Ca(\mu_4$-O)(μ_2-OH)] complex (**4**) which had served as the precursor to a variety of heterometallic [Fe_3M]-type clusters. The addition of $Ni(OTf)_2$ was found to result in the quantitative recovery of starting material. As numerous other $M(OTf)_n$ salts have previously been shown to transmetallate in [Mn_3CaO_4] and [$M_3Ca(\mu_4$-O)(μ_2-OH)] (M = Mn, Fe) clusters,[4c, 4d, 8] it was proposed that the low solubility of the nickel precursor led

to the lack of observed reactivity. To improve the solubility of the nickel precursor, transmetalation reactions with $Ni(MeCN)_6(OTf)_2$ were attempted, however again no conversion was observed (Scheme 3). A clean reaction to form a new species was observed if $NiCl_2(dme)$ was used as the nickel source. However, a solid-state structure obtained of the product indicated the formation of a cationic $[Fe^{III}_3Cl_3(\mu_3\text{-}O)]$ cluster (**5**) indicating loss of the calcium center without nickel incorporation. A structurally related $[Fe^{II}_3Cl_3]$ complex (**6**) without the bridging oxido ligand could be accessed directly from **LH$_3$** by adapting the synthetic protocols for **1** to utilize $FeCl_2$ rather than $Fe(OAc)_2$ as the iron precursor. Of note a more efficient synthesis has been recently developed by Charlie Arnett in the group, which involves the addition of trimethylsilylchloride to **1**. This protocol avoids the difficult to remove triethylammonium derived salts and should be used and the synthesis for complex **6** in the future. A preliminary solid-state structure with highly disordered solvent was obtained for **6** allowing direct comparison to complex **5** (Figure 6).

Scheme 3. Synthesis of Fe_3Cl_3–type compounds

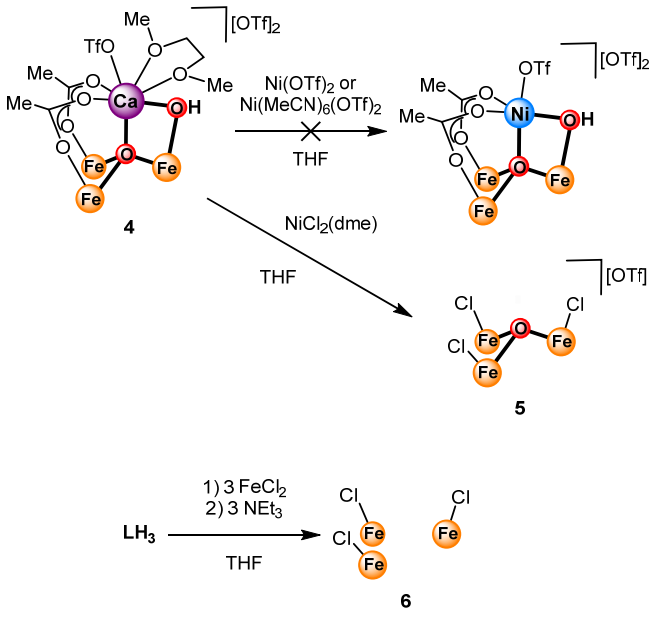

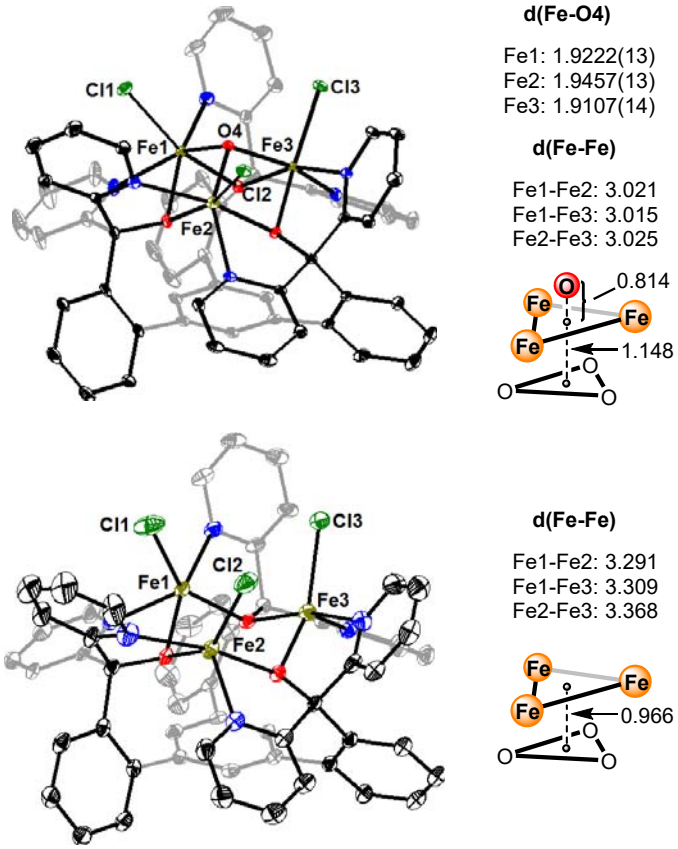

Figure 6. Solid-state structures of **5** (top) and **6** (bottom). Hydrogen atoms, solvent molecules, and counterions have been omitted for clarity.

The (μ_3-O) ligand of **5** helps enforce shorter average Fe–Fe distances (3.02 Å) compared to **6** (3.32 Å) by approximately 0.3 Å. As a result the Fe_3 centroid to $(alkoxide\text{-}O)_3$ centroid distance is longer in **5** compared to **6**, 1.148 and 0.966 Å respectively, due to the geometric constraints of the chair cyclohexane-like core of the complex. Complex **6** shows distorted square planar geometries around each Fe center with τ_5 parameters of 0.393, 0.436, and 0.330 for Fe1, Fe2, and Fe3 respectively. The metrics of **5** can also be compared to the cationic $[Fe^{II}_3(MeCN)_3(\mu_3\text{-}O)]$. Consistent with higher oxidation state of each Fe center (Fe^{III} vs Fe^{II}) in complex **5**, shorter Fe-O4 (d(Å): Fe1: 1.9222(13), Fe2: 1.9457(13), Fe3: 1.9107(14)), Fe-Fe (d(Å): Fe1-Fe2: 3.021,

Fe1-Fe3: 3.015, Fe2-Fe3: 3.025), and Fe_3 centroid to (alkoxide-O)$_3$ centroid distances (0.814 Å) are observed.

As transmetalation reactions directly from **4** proved unsuccessful, efforts to substitute supporting ligands prior to transmetalation was attempted. Previous results had shown that **PRABOH$_2$** substitution onto **4** resulted in selective protonlysis with the (μ_2-OH) resulted in the formation of complex **7** (Scheme 4). From complex **7** the addition of Ni(MeCN)$_6$(OTf)$_2$ was found to cleanly yield a new species by NMR (**8**).

Scheme 4. Synthesis and reactions of **PRABOH$_2$** stabilized Fe_3Ni complexes

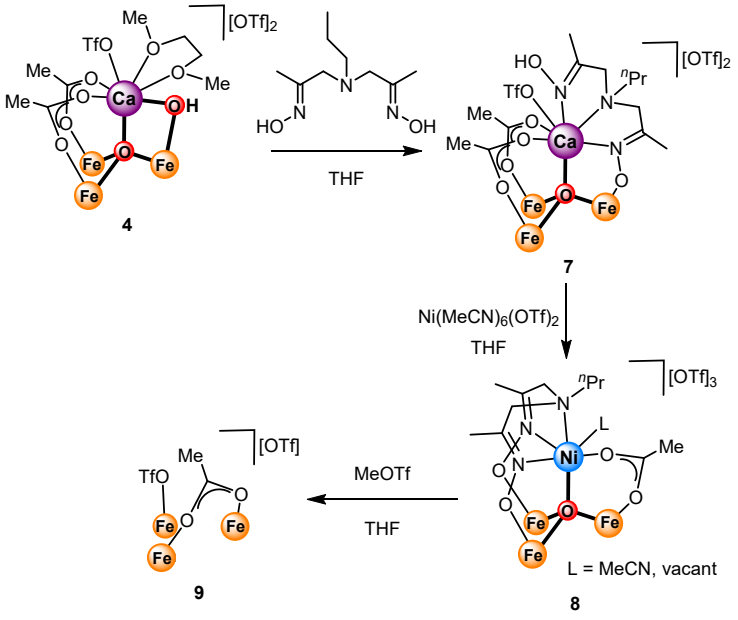

Two solid-state structures for **8** was obtained, which confirmed the formation of a dicationic [Fe_3Ni] complex with a formal oxidation state assignment of [$Fe^{III}_2Fe^{II}Ni^{II}$] indicating cluster reduction from the Fe^{III}_3 oxidation state of **7** has occurred. Transmetalation of calcium for nickel results the **PRABOH$_2$** substitution for another acetate resulting in both oximate oxygens coordinating to Fe2 and Fe3, which is likely attributable to the small size of nickel compared to calcium. The remaining three nitrogeneous donors of the **PRABOH$_2$** ligand form a facially coordinating chelate for

the apical Ni center. Different geometries around the apical Ni center are observed in the different solid-state structures with one showing a 5-coordinate *pseudo*-square planar geometry (τ_5 = 0.44) while acetonitrile coordination in the second structure results in a *pseudo*-octahedral nickel geometry. While the *pseudo*-octahedral structure is of low-quality (R1 = 16.3%), the crystal structure of the 5-coordinate nickel was of sufficient quality to thoroughly analyze the bonding metrics. Elongation of the Fe1–O4 distance (2.079(3) Å) relative to the comparable distances for Fe2 and Fe3, 1.942(3) and 1.960(3) Å respectively, is indicative of localization of the Fe^{II} center in the Fe1 position. The Ni1–O4 distance is slightly shorter than the Fe–O4 distances at 1.924(3) Å. Complex **8** shows O4 to Fe_3 centroid (0.929 Å) and Fe_3 centroid to (alkoxide-O)$_3$ centroid (1.096 Å) distances that are intermediate to **5** and the [Fe_3(MeCN)$_3$(μ_3-O)] centroid, however structural and oxidation state differences preclude further interpretation of these comparisons.

Efforts to open up a bimetallic edge site by acetate removal were then pursued. As trimethylsilyl triflate had previously been shown to oxidize clusters, the addition of methyl triflate to **8** was attempted. NMR reactions indicated the formation of a previously reported [Fe_3(OAc)(OTf)$_2$] complex (**9**) suggesting loss of the apical nickel center along with the **PRABOH$_2$** ligand had also occurred. Consequently, further efforts to install hydroxide ligands or bind carbon dioxide to complex **8** were discontinued.

Similar attempts to construct [Fe_3Ni] clusters with a previously synthesized Fe_3 mono(**PyPz**) bis(acetate) precursor (**7**). The addition of Ni(MeCN)$_6$(OTf)$_2$ to complex **10** did not result in the formation of a [Fe_3Ni] complex, but rather the loss of the PyPz ligand from the triiron core. Low quality crystals identified an iron-containing product

as a different structural form of the $[Fe_3(OAc)(OTf)_2]$ complex (**11**). If iodosylbenzene (PhIO) was added prior to $Ni(MeCN)_6(OTf)_2$ a complicated mixture of species was formed by NMR, however low quality crystals confirmed the formation of a $[Fe_3Ni]$ species. Unfortunately, efforts to reproduce these results of purify reactions products proved unsuccessful and this approach to [NiFe] heterobimetallic clusters was also discontinued.

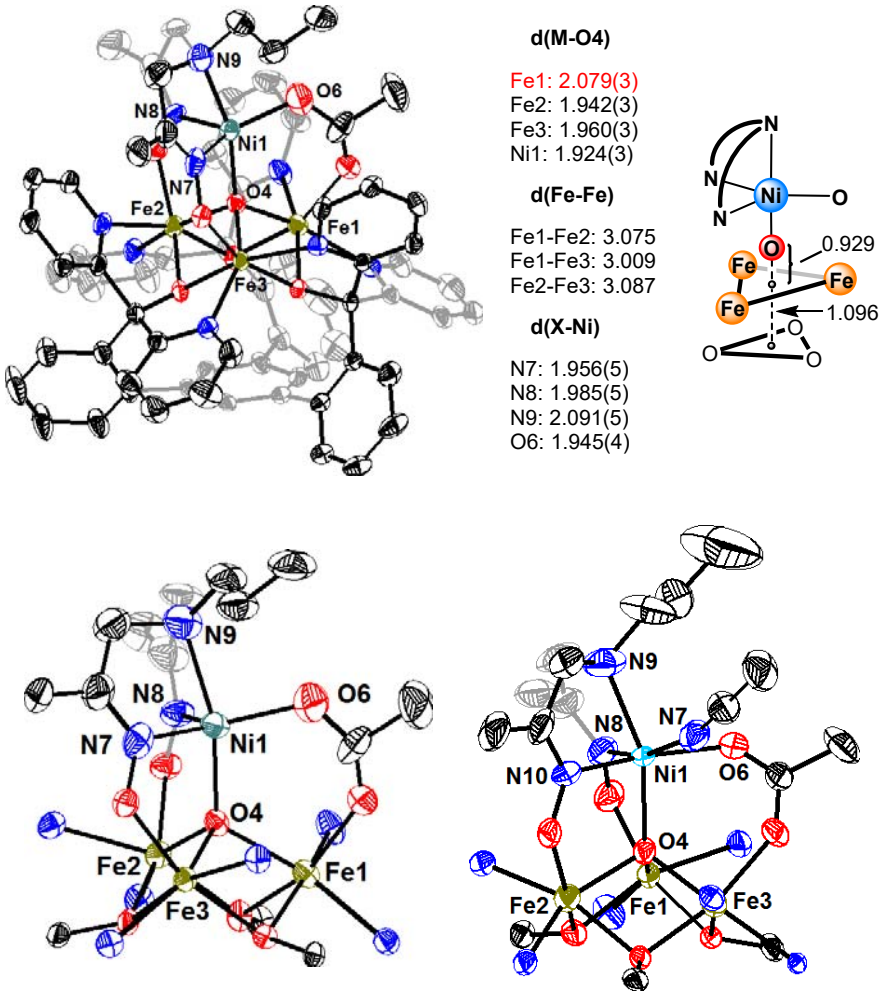

Figure 7. Solid-state structures of **8** with and without acetonitrile coordination. Hydrogen atoms, solvent molecules, and counterions have been omitted for clarity.

Scheme 5. Attempted synthesis of [Fe_3Ni] complexes

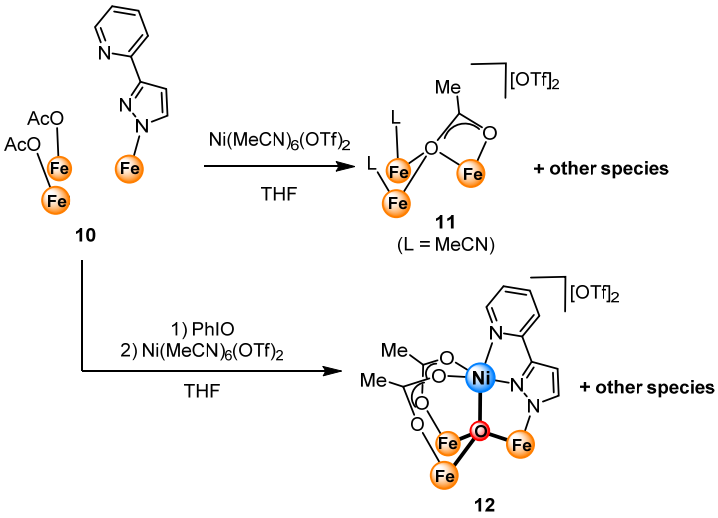

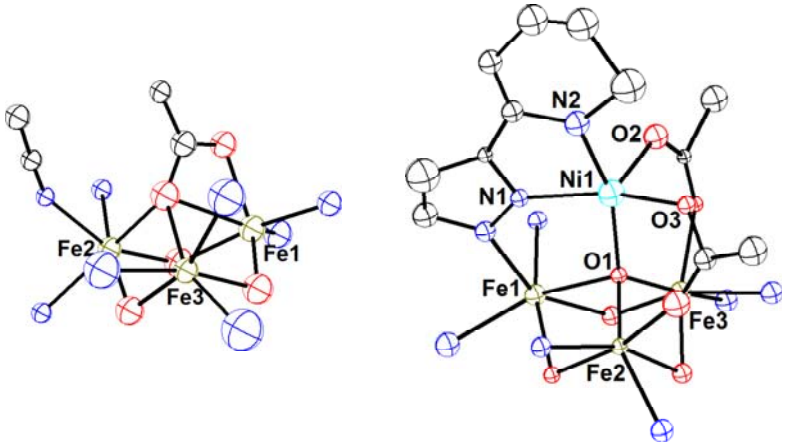

Figure 8. Preliminary solid-state structures for **11** and **12**.

CONCLUSIONS

Multiple attempts to rationally synthesize and study [Fe_3Ni] complexes as CODH active site models proved unsuccessful. However, several key caveats to design of tetranuclear clusters for subsequent projects could be gleaned from these studies. The first is the difficulty with utilizing the heavier main group elements as the interstitial atoms in higher nuclearity clusters. The substantial elongation of Fe–X bonds seen between compound **3** and the [$Fe^{II}_3(MeCN)_3(\mu_3\text{-}O)$] cluster (~0.3 Å)and the increase in the Fe_3 centroid to X distance (~0.6 Å) result in *pseudo*-square pyramidal 5-coordinate

Fe centers which are reluctant to coordinate sixth ligands. The loss of metal chalcogenide salts during attempts to construct tetranuclear clusters also proved problematic. Furthermore, the softer nature of the sulfide donor made oxidations while retaining the (μ_3-S) moiety infeasible as the formation of chloride species was observed in these reactions, likely arising from reaction with dichloromethane as the solvent. In combination, the inability to easily bind exogenous ligands, incorporate fourth metal centers, or oxidize the cluster resulted in a complex that, while structurally different from previously reported complexes in our group, was not compatible with the targeted biomimetic complexes.

The second design principle is the strengths and limitations of the utilizing stabilizing chelating architectures to access tetranuclear clusters. The use of **PRABOH$_2$** allowed for the isolation of [Fe$_3$Ni] clusters which was not possible with acetate ligands present in **4** demonstrating the type of donors available to the apical metal during transmetalation reactions also plays a role. However, this tight chelation of the apical metal can also result in synthetic complications when attempting to remove ligands with exogeneous electrophiles such as methyl triflate. While in principle the chelating nature of **PRABOH$_2$** was intended to promote removal of the remaining acetate ligand, loss of the chelating ligand and apical metal together proved to be the favorable reaction. The use of exogeneous metal salts to remove cluster-bound ligands has been previously been demonstrated in the synthesis of compound **2,** which is conveniently synthesized from compound **1** in MeCN with half an equivalent of calcium triflate. This was also implicated in reactions of **10** with Ni(MeCN)$_6$(OTf)$_2$ as crystals of **11** were obtained indicating removal of the **PyPz** ligand by the nickel center under reaction conditions. Taken together these data suggest a balance between chelating to the apical metal and

binding strength to the Fe_3 core exists to maintain a stable tetranuclear cluster. Though recent success with three-fold symmetric pyrazolate $[Fe_4O]$-type clusters has allowed for the stabilization of a vacant coordination site on the apical metal center, access to reactive dinuclear edge sites continues to be a challenge to due to asymmetry and reduced stability of these synthetic targets.

EXPERIMENTAL SECTION

General considerations.

All air- and/or water-sensitive compounds were manipulated using standard vacuum or Schlenk line techniques or in an inert atmosphere glove box. The solvents for air- and moisture-sensitive reactions were dried over sodium benzophenone ketyl, calcium hydride, or by the method of Grubbs.[9] All NMR solvents were purchased from Cambridge Isotopes Laboratories, Inc. and dried over sodium benzophenone ketyl or calcium hydride. Unless mentioned otherwise, reagents were used as received from commercial suppliers without further purification. **1**,[10] **2**,[7] **4**,[8a] **10**,[7] **N-(PPh$_2$)Pz**,[5b] **(PPh$_2$)PyH**,[5a] **PRABOH$_2$**,[6a] and **PyPzH**[6b] were synthesized according to reported procedures. Methyl triflate, bis(trimethylsilyl)sulfide, iodobenzene diacetate, and triethylamine was purchased from Sigma Aldrich, dried over calcium hydride, and then distilled prior to use. Calcium triflate, zinc acetate, nickel triflate, nickel acetate, nickel dichloride dimethoxyethane adduct, iron chloride were purchase from Strem Chemicals Inc. All ^{1}H, ^{13}C, and ^{31}P spectra were recorded on Varian Mercury 300 MHz, or Varian INOVA-500 or 600 MHz spectrometers at room temperature. Chemical shifts for ^{1}H and ^{13}C NMR data are reported relative to residual solvent peaks.[11] ^{31}P NMR chemical shifts are reported with respect to the deuterated solvent used to lock the instrument. Elemental analyses were performed by Robertson Microlit Laboratories, Ledgewood, NJ.

Synthesis of Complex 3 from 2

2 (196 mg, 0.151 mmol, 1 equiv) was partially dissolved in acetonitrile (20 mL) and then transferred to a Schlenk tube fitted with a screw-in Teflon stopper. While stirring bis(trimethylsilyl)sulfide (50 μL, 0.237 mmol, 1.56 equiv) was added as a acetonitrile solution

(1 mL). The reaction was then allowed to stir for 16 hours during which time the solution changed color from bright yellow to a deep red. The reaction mixture was then pumped down to yield a dark red solid. This residue was then suspended in minimal acetonitrile as filtered onto a Celite pad. The remaining red solid was brought through the Celite pad with dichloromethane. The dichloromethane filtrate was then dried under reduced pressure. The crude product was the purified by recrystallization from the vapor diffusion of diethyl ether into a concentrated dichloromethane solution. The pure product was obtained a dark red crystals and a red powder. Yield: 90 mg (49 %).

Synthesis of Complex 3 from 1

1 (299 mg, 0.249 mmol, 1 equiv) was suspended in acetonitrile (20 mL) and transferred to a Schlenk tube fitted with a screw-in Teflon stopper. Calcium triflate (42.1 mg, 0.124 mmol, 0.5 equiv) was then added as a solution in acetonitrile, which resulted in a gradual color change from a pale orange suspension to a homogeneous bright yellow color characteristic of $[LFe_3(OAc)_2][OTf]$ after 30 minutes. Bis(trimethylsilyl)sulfide (66.7 μL, 0.374 mmol, 1.5 equiv) was then added as a solution in acetonitrile. The reaction was then allowed to stir for 16 hours during which time a color change from bright yellow to a deep red was observed. The reaction mixture was then dried under reduced pressure to yield a red residue. The residue was then suspended in tetrahydrofuran and filtered onto a Celite pad. The red solid was then washed with additional tetrahydrofuran until washed became colorless before the product was brought through with dichloromethane. The combined dichloromethane filtrate was the dried under reduced pressure to yield the pure product without further purification as a red powder. Yield: 261 mg (87 %). ^{1}H NMR (300 MHz, CD_3CN) δ(ppm) 71.8, 57.5, 43.8, 39.3, 33.4, 23.0, 16.8,

14.7, 14.4, -0.98, -18.76. ^{19}F NMR (282 MHz, CD_3CN) δ(ppm) -79.2. Anal. Calcd. for: $C_{58}H_{39}F_3Fe_3N_6O_6S_2$ (**3**) (%): C, 57.83; H, 3.26; N, 6.98. Anal. Calcd. for: $C_{59}H_{41}Cl_2F_3Fe_3N_6O_6S_2$ (**3**•(CH_2Cl_2)) (%): C, 54.95; H, 3.20; N, 6.52. Found: C, 55.10; H, 3.16; N, 6.74.

Synthesis of Complex 5

Complex **4** (359 mg, 0.204 mmol, 1 equiv) was dissolved in acetonitrile (15 mL). This solution was then transferred to a 20 mL scintillation vial containing nickel dichloride dimethoxyethane adduct (67.5 mg, 0.303 mmol, 1.5 equiv). The reaction mixture was then allowed to stir for 16 hours during which time the $NiCl_2$(dme) became homogeneous. The reaction mixture was dried under reduced pressure to yield an orange residue. The residue was suspended in tetrahydrofuran and filtered onto a Celite pad. The orange solid was then washed with tetrahydrofuran until the washes became colorless. The product was then brought through with dichloromethane. The combined dichloromethane filtrate was then dried under reduced pressure to yield the pure product without further purification as an orange powder. Yield: 164 mg (61.8 %).^{1}H NMR (300 MHz, CD_3CN) δ(ppm) 126.9, 97.3, 61.5, 59.3, 58.3, 53.2, 14.7, 13.5, 8.7, 6.8. ^{19}F NMR (282 MHz, CD_3CN) δ(ppm) -78.9. Anal. Calcd. for: $C_{58}H_{39}Cl_3F_3Fe_3N_6O_7S_2$ (**5**) (%): C, 53.80; H, 3.04; N, 6.49. Anal. Calcd. for: $C_{59}H_{41}Cl_5F_3Fe_3N_6O_7S_2$ (**5**•(CH_2Cl_2)) (%): C, 51.36; H, 3.00; N, 6.09. Found: C, 51.27; H, 3.00; N, 5.82.

Synthesis of Complex 6

LH_3 (303.4 mg, 0.353 mmol, 1 equiv.) and $FeCl_2$ (134.3 mg, 1.059 mmol, 3 equiv.) was transferred into a Schlenk tube fitted with a screw-in Teflon stopper and equipped with a magnetic stirbar. Dichloromethane (*ca.* 40 mL) was then added. Triethylamine (152.8 μL, 1.09 mmol, 3.1 equiv.) was then added and the reaction vessel sealed and allowed to stir for 16 hrs at room temperature. Reaction volatiles were then removed under reduced pressure. The residue was then triturated with tetrahydrofuran and the solids collected on a Celite pad. The product was then eluted with copious dichloromethane. The filtrate volatiles were then removed under reduced pressure. Following purification with tetrahydrofuran washes, the product becomes largely insoluble and difficult to work with. Complete removal of triethylammonium salts proved difficult proved challenging and the low solubility of the product in dichloromethane precluded recrystallization on substantial scales. An improved synthesis, which should be used for all future preparations, has been developed by Charlie Arnett in the Agapie group. ^{1}H NMR (300 MHz, CD_2Cl_2) δ 108.90, 76.86, 73.32), 61.31, 51.72, 42.25, 26.22, 15.86, 12.84, 9.96, 8.73, 8.10, -7.56.

Synthesis of Complex 8

Compound **4** (102.8 mg, 0.059 mmol, 1 equiv.) was transferred to a 20 mL scintillation vial equipped with a magnetic stirbar. **$PRABOH_2$** (11.8 mg,0.059 mmol, 1 equiv.) was then added as a tetrahydrofuran solution (*ca.* 4 mL) and the reaction mixture was allowed to stir for 6 hrs at room temperature to ensure formation of **7**. $Ni(MeCN)_6(OTf)_2$ (35.4 mg, 0.059 mmol, 1 equiv.) was then added as a solution in THF (*ca.* 4 mL) and the combined reaction mixture

allowed to stir for 16 hrs at room temperature. The reaction volatiles were then removed under reduced pressure. The residue was then triturated with dichloromethane a filtered through a Celite pad to remove salts from the product. The DCM filtrates were then dried under reduced pressure and the product obtained as a brown solid. Yield: 77 mg (80 % calculated if no MeCN coordinated to Ni center). ^{1}H NMR (300 MHz, CD_3CN) δ 185.37, 184.47, 164.06, 94.29, 92.43, 90.76, 86.93, 84.69, 83.16, 81.44, 78.88, 78.28, 76.66, 74.83, 48.61, 45.90, 37.37, 17.36, 16.66, 12.08, 9.33, 8.49, -0.53, -1.91, -4.73, -18.95, -27.69. ^{19}F NMR (282 MHz, CD_3CN) δ -79.08.

Crystallographic Information

Refinement Details

In each case, crystals were mounted on a glass fiber or nylon loop using Paratone oil, then placed on the diffractometer under a nitrogen stream. Low temperature (100 K) X-ray data were obtained on a Bruker APEXII CCD based diffractometer (Mo sealed X-ray tube, K_α = 0.71073 Å). All diffractometer manipulations, including data collection, integration and scaling were carried out using the Bruker APEXII software.[12] Absorption corrections were applied using SADABS.[13] Space groups were determined on the basis of systematic absences and intensity statistics and the structures were solved by direct methods using XS (incorporated into SHELXTL) and refined by full-matrix least squares on F^2. All non-hydrogen atoms were refined using anisotropic displacement parameters. Hydrogen atoms were placed in idealized positions and refined using a riding model. The structure was refined (weighted least squares refinement on F^2) to convergence.

Table 1. Crystal and refinement data for complexes reported in Appendix A

Complex	**3**	**5**	**6**	**8**	**8 (MeCN-bound)**
empirical formula	$C_{66}H_{55}F_3Fe_3N_8O_7S_2$	$C_{62}H_{42}Cl_3F_3Fe_3N_8O_7S$	$C_{57}H_{39}Cl_3Fe_3N_6O_3$	$C_{78}H_{59}F_6Fe_3N_9Ni_{0.94}O_{16}S_2$	$C_{136}H_{0.50}F_{12}Fe_6Ni_2O_{26}S_4$
formula wt	1360.85	1373.99	1129.84	1779.20	3138.82
T (K)	100	100	100	100.01	99.99
a, Å	12.5685(13)	11.5004(4)	14.1495(8)	19.3212(6)	15.9295(7)
b, Å	32.915(4)	14.8380(5)	16.7479(9)	16.7299(5)	22.5961(10)
c, Å	14.5295(15)	18.0383(6)	27.1921(14)	25.9311(8)	26.0003(11)
α, deg	90	97.2724(11)	90	90	101.7460(10)
β, deg	98.698(3)	106.1004(11)	94.550(2)	111.6010(10)	102.1610(10)
γ, deg	90	91.9710(12)	90	90	97.1460(10)
V, Å^3	5941.5(11)	2925.77(17)	6423.5(6)	7793.3	8819.2(7)
Z	4	4	4	4	2
cryst syst	Monoclinic	Triclinic	Monoclinic	Monoclinic	Triclinic
space group	P1 2_1/c 1	P-1	P 1 2_c 1	P 1 2_1/c 1	P-1
d_{calcd}, g/cm^3	1.521	1.928	1.485	1.516	1.182
θ range, deg	1.547 to 28.513	2.374 to 36.523	2.165 to 30.536	2.275 to 30.509	2.429 to 30.154
μ, mm^{-1}	0.866	1.292	1.014	0.912	0.808
abs cor	Semi-empirical from equivalents	Semi-empirical from equivalents	Semi-empirical from equivalents	Semi-empirical from equivalents	Semi-empirical from equivalents
GOF[c]	1.038	1.921	2.987	1.019	1.377
R1,[a] wR2[b] ($I > 2\sigma(I)$)	0.0721, 0.1729	0.0826, 0.2622	0.1300, 0.4038	0.0762, 0.1699	0.1631, 0.4159

[a] $R1 = \Sigma||F_o|-|F_c|| / \Sigma|F_o|$ [b] $wR2 = \{ \Sigma [w(F_o^2-F_c^2)^2] / \Sigma [w(F_o^2)^2] \}^{1/2}$ [c] $GOF = S = \{ \Sigma [w(F_o^2-F_c^2)^2] / (n-p) \}^{1/2}$

REFERENCES

1.(a) Jones, J.-P.; Prakash, G. K. S.; Olah, G. A., *Israel Journal of Chemistry* **2014,** *54*, 1451-1466; (b) Qiao, J.; Liu, Y.; Hong, F.; Zhang, J., *Chemical Society Reviews* **2014,** *43*, 631-675; (c) Ren, D.; Deng, Y.; Handoko, A. D.; Chen, C. S.; Malkhandi, S.; Yeo, B. S., *ACS Catalysis* **2015,** *5*, 2814-2821.
2.(a) Can, M.; Armstrong, F. A.; Ragsdale, S. W., *Chemical Reviews* **2014,** *114*, 4149-4174; (b) Jeoung, J.-H.; Dobbek, H., *Science* **2007,** *318*, 1461-1464; (c) Jeoung, J.-H.; Dobbek, H., *Journal of the American Chemical Society* **2009,** *131*, 9922-9923.
3.(a) Ciurli, S.; Ross, P. K.; Scott, M. J.; Yu, S. B.; Holm, R. H., *Journal of the American Chemical Society* **1992,** *114*, 5415-5423; (b) Huang, D.; Holm, R. H., *Journal of the American Chemical Society* **2010,** *132*, 4693-4701; (c) Panda, R.; Zhang, Y.; McLauchlan, C. C.; Venkateswara Rao, P.; Tiago de Oliveira, F. A.; Münck, E.; Holm, R. H., *Journal of the American Chemical Society* **2004,** *126*, 6448-6459; (d) Yoo, C.; Kim, J.; Lee, Y., *Organometallics* **2013,** *32*, 7195-7203.
4.(a) de Ruiter, G.; Thompson, N. B.; Lionetti, D.; Agapie, T., *Journal of the American Chemical Society* **2015,** *137*, 14094-14106; (b) Kanady, J. S.; Tsui, E. Y.; Day, M. W.; Agapie, T., *Science* **2011,** *333*, 733-736; (c) Tsui, E. Y.; Agapie, T., *Proceedings of the National Academy of Sciences* **2013,** *110*, 10084-10088; (d) Tsui, E. Y.; Tran, R.; Yano, J.; Agapie, T., *Nat Chem* **2013,** *5*, 293-299.
5.(a) Dunn, P. L.; Reath, A. H.; Clouston, L. J.; Young Jr, V. G.; Tonks, I. A., *Polyhedron* **2014,** *84*, 111-119; (b) Yang, Y.; Liu, Z.; Liu, B.; Duchateau, R., *ACS Catalysis* **2013,** *3*, 2353-2361.
6.(a) Goldcamp, M. J.; Edison, S. E.; Squires, L. N.; Rosa, D. T.; Vowels, N. K.; Coker, N. L.; Krause Bauer, J. A.; Baldwin, M. J., *Inorganic Chemistry* **2003,** *42*, 717-728; (b) Yang, T.; Chen, G.; Sang, Z.; Liu, Y.; Yang, X.; Chang, Y.; Long, H.; Ang, W.; Tang, J.; Wang, Z.; Li, G.; Yang, S.; Zhang, J.; Wei, Y.; Luo, Y., *Journal of Medicinal Chemistry* **2015,** *58*, 6389-6409.
7.Thesis of Dr. Davide Lionetti, Appendix A
8.(a) Herbert, D. E.; Lionetti, D.; Rittle, J.; Agapie, T., *Journal of the American Chemical Society* **2013,** *135*, 19075-19078; (b) Suseno, S.; McCrory, C. C. L.; Tran, R.; Gul, S.; Yano, J.; Agapie, T., *Chemistry – A European Journal* **2015,** *21*, 13420-13430.
9.Pangborn, A. B.; Giardello, M. A.; Grubbs, R. H.; Rosen, R. K.; Timmers, F. J., *Organometallics* **1996,** *15*, 1518-1520.
10.Tsui, E. Y.; Kanady, J. S.; Day, M. W.; Agapie, T., *Chemical Communications* **2011,** *47*, 4189-4191.
11.Fulmer, G. R.; Miller, A. J. M.; Sherden, N. H.; Gottlieb, H. E.; Nudelman, A.; Stoltz, B. M.; Bercaw, J. E.; Goldberg, K. I., *Organometallics* **2010,** *29*, 2176-2179.
12.APEX2, Version 2 User Manual, M86-E01078, Bruker Analytical X-ray Systems, Madison, WI, June 2006.
13.Sheldrick, G. M. "SADABS (Version 2008/1): Program for Absorption Correction for Data from Area Detector Frames", University of Göttingen, 2008.

APPENDIX B

MODELING THE [FEFE]-HYDROGENASE H-CLUSTER: COMBINING A PEPTIDE-SUPPORTED [FE_4S_4] CLUSTER AND A SYNTHETIC DIIRON SUBSITE MIMIC

Abstract

The synthesis of biomimetic model complexes of the full H-cluster of [FeFe]-hydrogenase was targeted. Intended to be a more synthetically modular approach than that reported by the Pickett group, the [Fe_4S_4] cluster would be supported by short peptides of variable amino acid composition containing a conserved CX_2CX_2C motif. The incorporation of the diiron subsite would then be accomplished via thioester exchange with a specialized model complex shown to work in the literature. The synthesis of a variety of peptides was accomplished though the solubility of the sequences proved problematic for characterization. [Fe_4S_4] incorporation into a peptide containing the sequence NH_2-GCIACGACGW-$(CO)NH_2$ could be confirmed spectroscopically. However, subsequent addition of the diiron subsite mimic yielded unclear results. Furthermore, the correct binding of the diiron unit to the cluster could not be confirmed. Instead, evidence for peptide acetylation resulting from thioester exchange with polar residues side chains was observed. This unanticipated complication in subsite incorporation resulted in the discontinuation of the project.

INTRODUCTION

As a fuel, molecular hydrogen is both carbon-neutral and renewable, if produced by solar-driven electrolysis.[1] Currently, steam reforming of hydrocarbons, primarily methane, is the dominant industrial method for hydrogen production.[2] This process is both energy intensive and ultimately dependent on fossil fuels, making it an ineffectual method of producing hydrogen for use as an alternative fuel. Current electrolysis cells typically require precious metals, typically platinum,[2] to function without high energetic penalties in the form of catalytic overpotentials. While inorganic materials such as molybdenum sulfide and phosphide have emerged recently as promising low overpotential electrocatalysts for hydrogen evolution, further research is required to continue to improve future devices.[3]

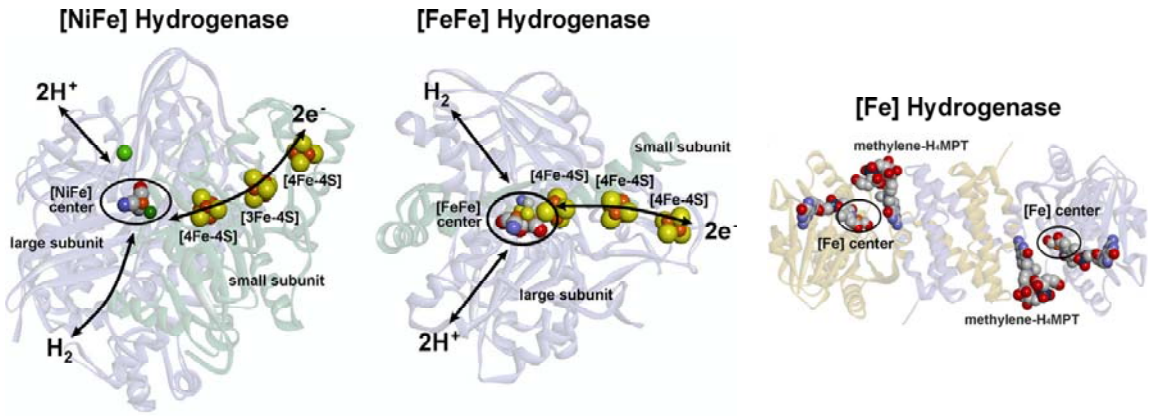

Figure 1. Protein crystal structures of the three classes of hydrogenases. Figure adapted from Lubitz,W. *Chem. Rev.* **2014**, *114*, 4081-4148.

Inspiration for suitable replacement proton reduction electrocatalysts can be found in nature. The hydrogenases are a family of enzymes capable of catalyzing the reversible interconversion of protons and electrons with molecular hydrogen.[4] These enzymes operate at negligible overpotentials and undergo thousands of turnovers per second while using only the earth-abundant metals iron and nickel.[4a] Protein X-ray crystallography studies have structurally characterized the active sites of three distinct classes of hydrogenase enzymes:

[FeFe]-, [NiFe]-, and [Fe]-only hydrogenase (Figure 1), which each show diverse metallic content and active site structure.[5] Biomimetic model complexes of each class of hydrogenase have sought to mimic the chemical properties and reactivity of their native enzymatic counterparts to better understand the biological systems and aid in the rational design of future electrocatalysts.[4] The enzymatic active site inorganic cofactor of [FeFe]-hydrogenase, dubbed the H-cluster, consists of [Fe_4S_4] cluster linked to an unusual diiron subsite by a bridging cysteine ligand (Figure 2, Left). The diiron subsite itself possess multiple, biologically unusual carbon monoxide and cyanide ligands and an azadithiolate ligand which bridges the two iron centers in a butterfly conformation with both sulfur donors. While two model complexes have been reported that incorporate both a diiron subsite model and a tethered redox cofactor (Figure 2, Right), H-cluster mimics remain uncommon in the literature.[6] Herein we discuss attempts to synthesize a six iron model complex of the H-cluster that utilizes and peptide to support a [Fe_4S_4] moiety that will be tethered to a diiron subsite mimic previously reported by Pickett and coworkers.[6b]

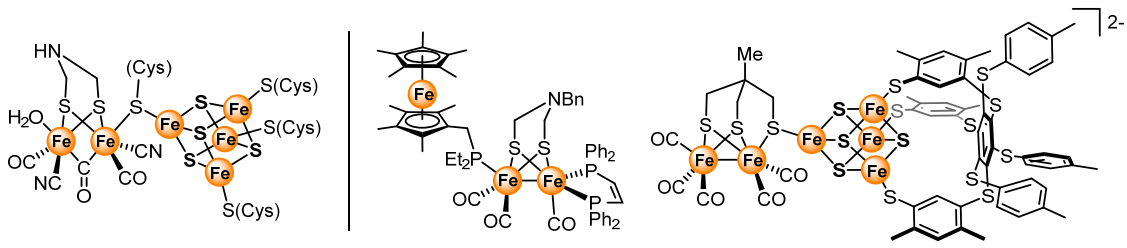

Figure 2. Schematic representation of the [FeFe]-hydrogenase active site (Left), and synthetic model complexes mimicking both the diiron subsite and [Fe_4S_4] cluster (Right).

RESULTS AND DISCUSSION

Section B.1 Peptide Synthesis

Scheme 1. General scheme for Fmoc-based solid phase peptide synthesis

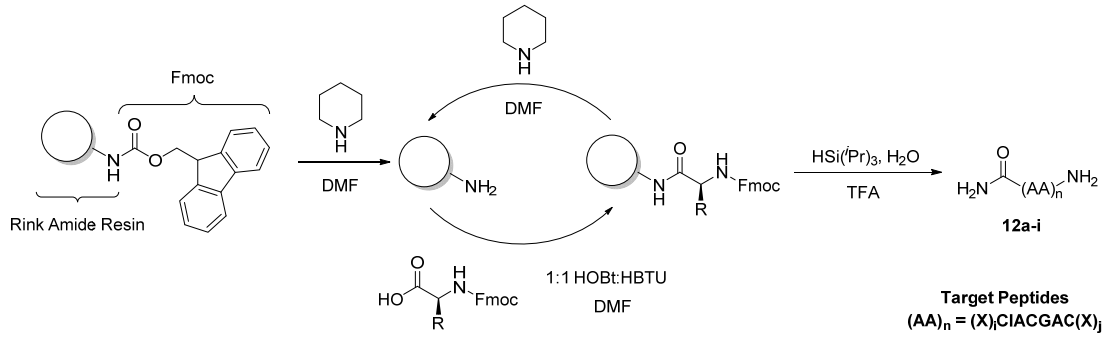

9-fluorenylmethyloxycarbonyl-based (Fmoc) protection schemes were employed to produce tricysteine peptides on a rink amide resin using solid-phase peptide synthesis protocols (Figure 4).[7] Subsequent cleavage from solid support using trifluoroacetic acid yielded C-terminally amidated, unpurified peptides on a multiple 100 mg scale. Sequences of the general form NH_2-$(X)_i$CIACGAC$(X)_j$-$CONH_2$ based on literature peptides were designed to include an internal CX_2CX_2C motif previously shown to bind $[Fe_4S_4]$-clusters (Table 1). $(X)_j$ sequences generally consisted of one to two glycine residues followed by a tryptophan to serve as a convenient UV/Vis (ε_{280nm} = 5600 $M^{-1}cm^{-1}$) and ^{1}H-NMR handle, while $(X)_i$ sequences were typically a single glycine.

Unfortunately, the majority of peptides (**1a**-**1i**) synthesized possessed limited solubility making purification by reverse-phase high performance liquid chromatography (RP-HPLC) difficult (Table 1). N-terminally acetylated peptides were virtually insoluble in all solvents except DMF and DMSO. Ultimately, the literature peptide, **1h**, was selected for preparatory-scale RP-HPLC as it presented the highest solubility in aqueous-acetonitrile solvent systems and was known to efficiently bind $[Fe_4S_4]$-clusters. The limited solubility of most of these peptides is likely a reflection of the cluster-binding environment in ferredoxin proteins, which are often buried in hydrophobic portions of the protein away from bulk solvent. The identity

and purity of **1h** was confirmed by electrospray ionization mass spectrometry (ESI-MS) and ^{1}H-NMR spectroscopy.

Table 1. Compiled list of synthesized peptides. ‡ Synthesized of glycine preloaded Wang resin.

Peptide #	N-term.	$(AA)_n$	C-Term.	Solubility
1a‡	*p*-F-aryl-C(O)-	GCIACGWCGG	-OH	<10mg/mL in DMF or DMSO
1b‡	Acetyl-	GCIACGWCGG	-OH	<10mg/mL in DMF or DMSO
1c‡	H-	GCIACGACGG	-OH	<10mg/mL in DMF or DMSO
1d	H-	GCIACGWCGG	$-NH_2$	<10mg/mL in DMF or DMSO
1e	H-	CGGCGGC	$-NH_2$	~20mg/mL MeCN:H_2O
1f	H-	CGGCGGCW	$-NH_2$	<10mg/mL in DMF or DMSO
1g	Acetyl-	CGGCGGCW	$-NH_2$	<10mg/mL in DMF or DMSO
1h	**H-**	**GCIACGACGW**	**$-NH_2$**	**~20mg/mL MeCN:H_2O**
1i	H-	RGCIACGACGW	$-NH_2$	~20mg/mL MeCN:H_2O

Section B.2 Attempted Assembly of Peptide-supported H-cluster Model Complexes

To assemble the peptide-supported H-cluster, a synthetic strategy analogous to that reported for the synthesis of **6** was adopted (Scheme 2).[6b] Previous studies of peptide-supported $[Fe_4S_4]$-clusters employed reconstitution protocols that took advantage of the CX_2CX_2C motif to self-assemble clusters from dissolved iron and sulfide salts under anaerobic conditions.[8] Tetracysteine peptides demonstrated near complete reconstitution yields, while omission of a single cysteine typically showed diminished efficiencies of ~50%.[9] To circumvent the reduced yields, use of a preformed cluster allowed for facile cluster binding via thiolate exchange. Similar strategies were previously shown by Holm to achieve near quantitative cluster incorporation in peptides.[10]

Scheme 2. Proposed synthetic scheme for the synthesis of a peptide supported H-cluster model complex

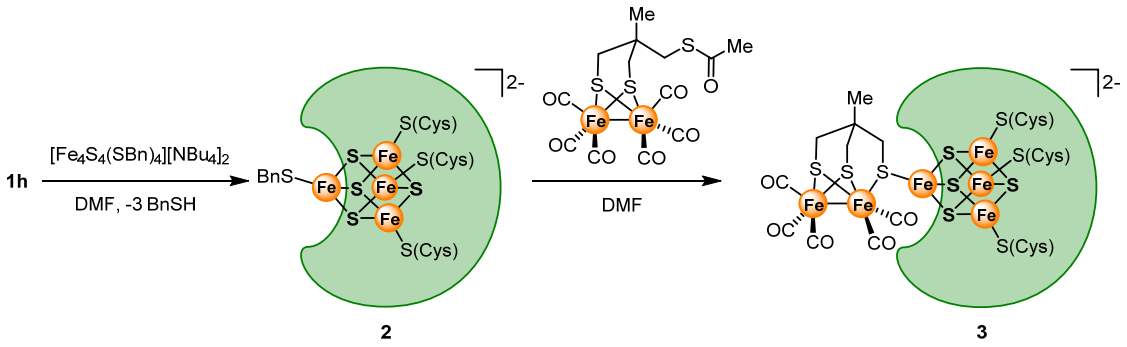

Preformed $[Fe_4S_4]$-clusters have been extensively studied,[11] and the benzyl thiolate and tetrabutylammonium variant, $[Fe_4S_4(SBn)_4][NBu_4]_2$, was readily synthesized. Reaction of **1h** with the preformed cluster produced a dark brown solid for which broadened ^{1}H-NMR resonances could be observed and assigned to benzyl thiolate and peptide protons (Scheme 3). ESI-MS confirmed the formation of **2** which showed signals corresponding to $[\mathbf{2}]^{2-}$ and $[\mathbf{2}\text{-}(SBn)]^{2-}$ ions. Electron paramagnetic resonance (EPR) spectroscopy of samples of **2** showed no signal confirming negligible degradation of the $[Fe_4S_4]^{2+}$ cluster to an EPR active $[Fe_3S_4]^{+}$ species. Furthermore, reduction with disodium dithionite produced **4** for which a rhombic, $S = {}^1/_2$, EPR signal with g-values of 1.88, 1.93, and 2.06 was observed (Figure 3), in close agreement with literature values for ferredoxin proteins.[12] An independently synthesized reduced $[Fe_4S_4]$-cluster precursor, $[Fe_4S_4(SBn)_4[NBu_4]_3$, produced an axial EPR signature with g-values of 1.93 and 2.04, supporting intact cluster binding to **4**.[12] Reactions of the reduced cluster precursor with **1h** directly yielded **4** without the use of chemical reductants (Figure 4).

With the $[Fe_4S_4]$-cluster bound to **1h**, incorporation of the diiron subsite was attempted. In literature reports a diiron subsite containing thiolate masked by an acetyl group was employed.[6b] Thioester exchange and subsequent loss of a carbon monoxide ligand formed the

μ_2-thiolate to generate six Fe cluster and release the acetylated thiolate. A similar approach was attempted for the peptide-bound compound **2**. Despite repeated attempts, reactions of the diiron subsite with **2** never showed evidence of formation of the target complex, **4**. ESI-MS confirmed consumption of the diiron subsite complex, however only acetylated **2** and diiron decomposition products were detected (Scheme 4). These data suggest quantitative acetylation of peptide side chains or N-terminus of **2** without displacement of the benzyl thiolate.

Scheme 3. Synthesis of peptide-supported $[Fe_4S_4]$ clusters

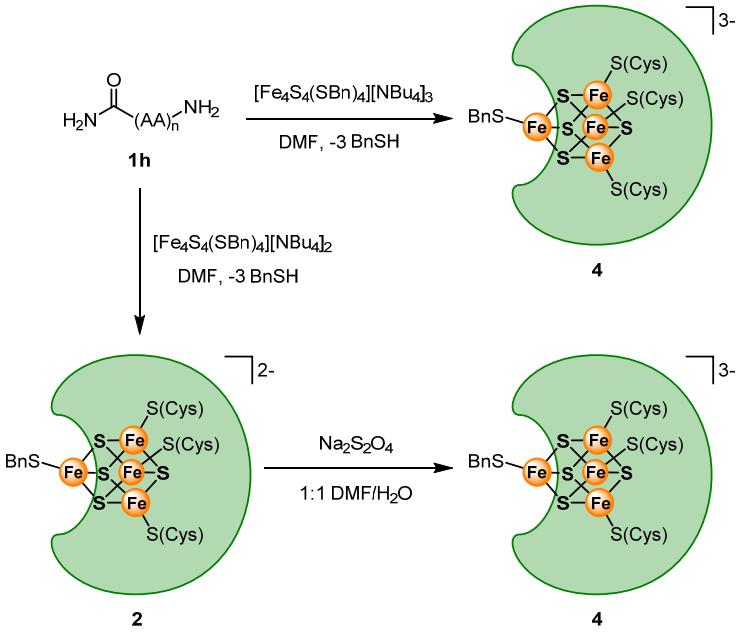

EPR spectroscopy of reaction mixtures revealed an unusual feature centered around 3320 G, which could not be attributed to known $[Fe_4S_4]$-cluster degradation products (Figure 5). Upon reduction with disodium dithionite, the signal typical of a $[Fe_4S_4]^+$ cluster appeared (Figure 6), confirming the presence of an intact, peptide-bound cluster.

Scheme 4. Attempted incorporation of the diiron subsite to **4**

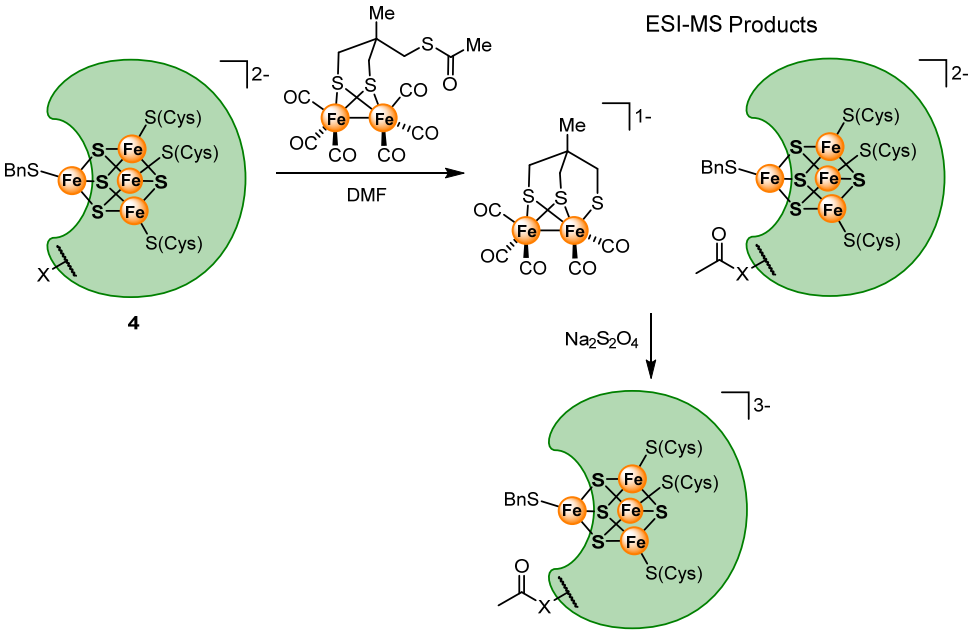

In theory, prior acetylation of the N-terminus of **1h** should be sufficient to minimize side reactions with the diiron subsite complex. However, the limited solubility of such a peptide would make RP-HPLC purification on reasonable scales challenging. Future peptides, will include additional polar amino acids to improve solubility while avoiding of sites capable of competing with the thioester exchange required for diiron linkage to the $[Fe_4S_4]$-cluster.

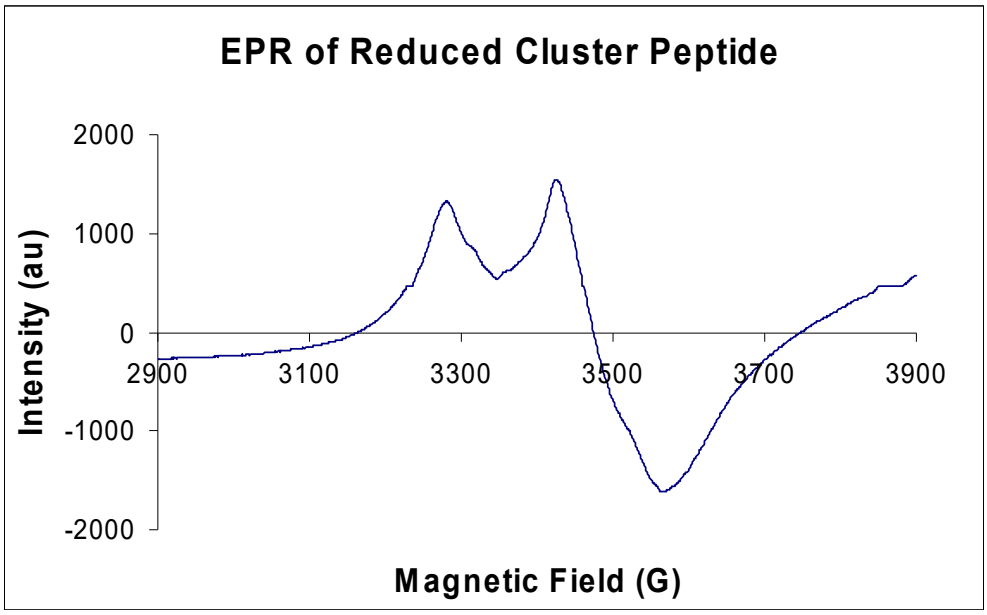

Figure 3. EPR spectrum of **4** produced by the metalation of **1h** with the reduced cluster precursor.

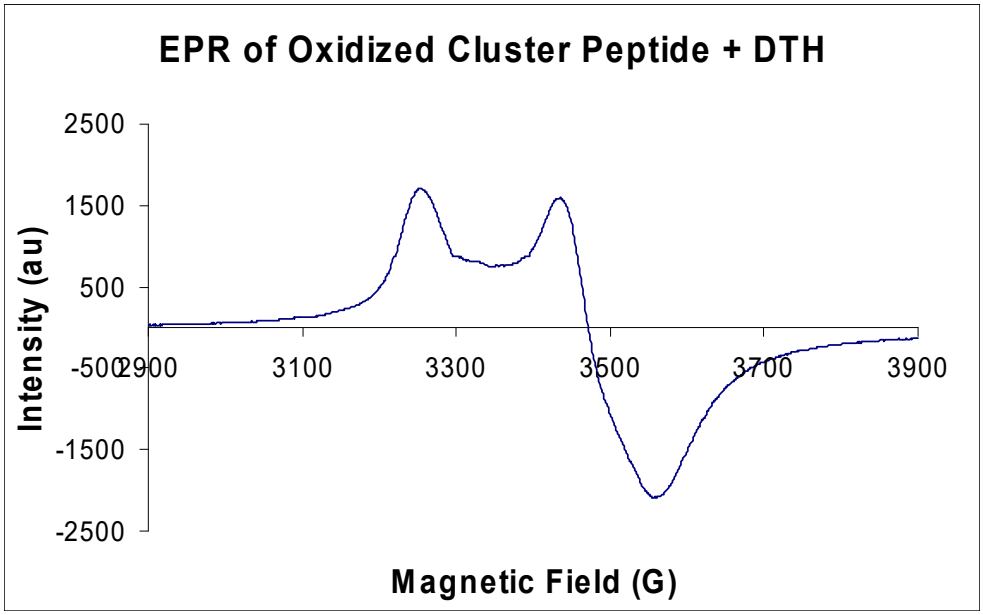

Figure 4. EPR spectrum of **4** produced by the reduction of **2** with dithionite.

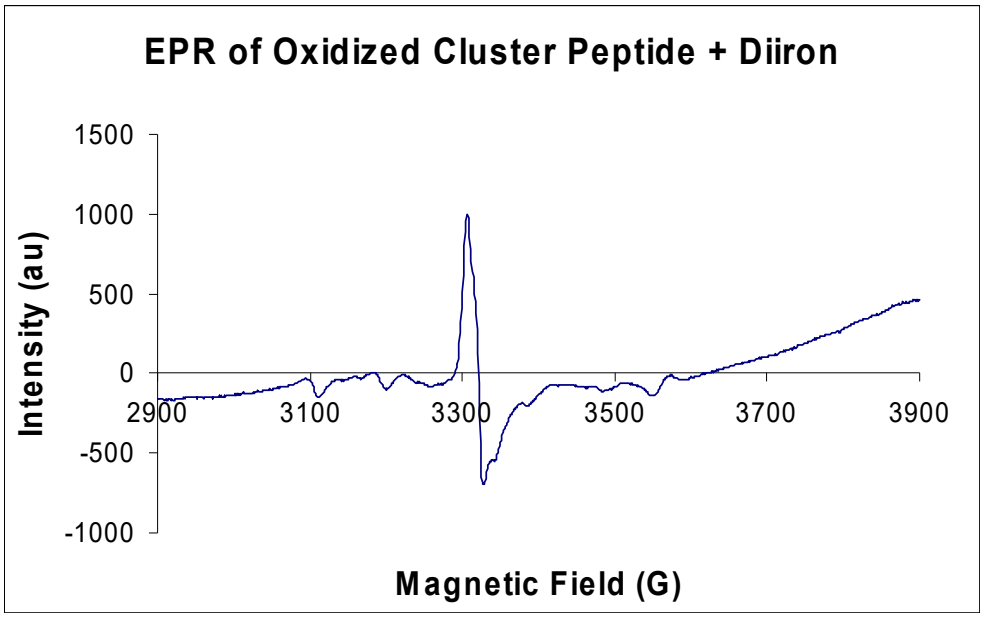

Figure 5. EPR spectrum of the reaction of **2** with the diiron subsite model complex.

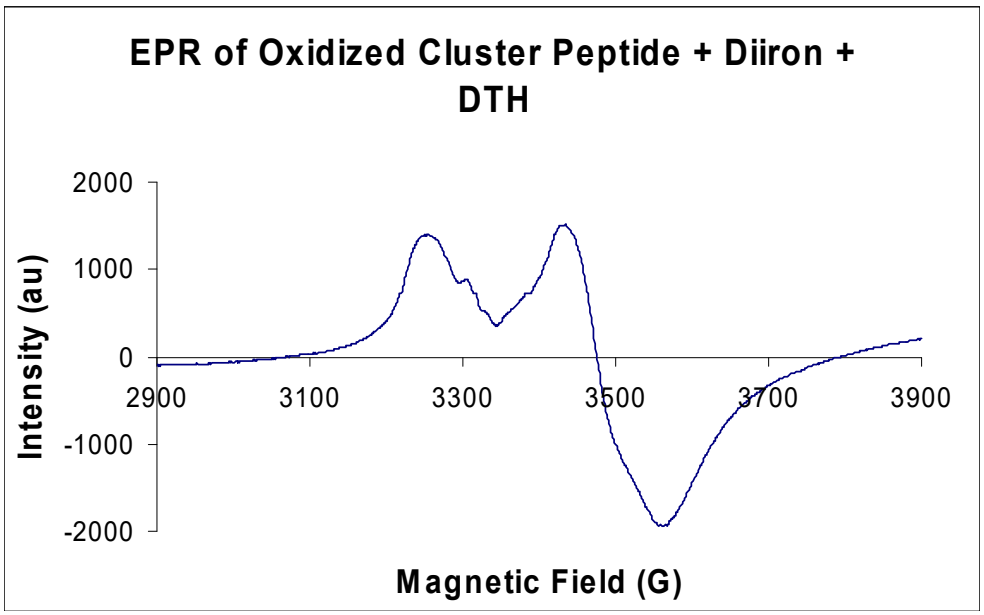

Figure 6. EPR spectrum of the reaction of **2** with the diiron subsite model complex following reduction with dithionite.

CONCLUSIONS

In conclusion, attempts to synthesize peptide-supported H-cluster model complexes was attempted. Peptide syntheses were successfully accomplished utilizing Fmoc-based approaches, however sequence optimization was required to access peptides of sufficient solubility to properly characterize and utilize in reactions. Incorporation of preformed [Fe_4S_4] clusters into the peptides proved successful with degradation not observed by EPR or ESI-MS. Unfortunately, attempts construct the full six Fe cluster proved unsuccessful as acetylation of the peptide backbone was interfering with thioester exchange with the last thiolate ligand coordinated to the [Fe_4S_4] cluster.

EXPERIMENTAL SECTION

General considerations.

Unless otherwise specified, all compounds were manipulated in a glovebox under a nitrogen atmosphere. Solvents for all reactions were dried by the Grubb's method. All purchased chemicals were used as ordered without further purification. Fmoc-protected amino acids, solid-phase resins and coupling reagents were purchased from Advanced Chemtech. Trifluoroacetic acid (TFA), triisopropyl silane (TIS), diisopropylethylamine (DIEA), and piperidine were purchased from Sigma Aldrich. HPLC-grade acetonitrile was purchased from VWR International. All deuterated NMR solvents were purchased from Cambridge Isotopes. ^{1}H-NMR and ^{31}P-NMR were recorded on a Varian 300 MHz with chemical shifts reported with respect to internal solvent at ambient temperatures unless otherwise noted. Mass spectrometry data was obtained using the Caltech Institute of Technology Mass Spectrometry Facility ESI-MS instrument. RP-HPLC was run on Agilent instruments utilizing a preparatory-scale C18 column. EPR experiments were run on an X-band Bruker instrument at 1 mmolar concentrations and 10 K unless otherwise noted. Other EPR instrument settings include microwave frequency 9.378 GHz, microwave power 5.115 mW, receiver gain 1.00e+003, modulation frequency 100 kHz, modulation amplitude 5.00 G, time constant 40.060 ms. $Fe_2(CO)_6CH_3C(CH_2S)_2CH_2SCOCH_3$,[6b] $[Fe_4S_4(SBn)_4][NBu_4]_2$,[11a] and $[Fe_4S_4(SBn)_4][NBu_4]_3$[12] were synthesized according to literature procedures.

Peptide synthesis and purification of Compound 1h

Peptide synthesis of **1a**-**1i** were done using identical methods. All peptide synthesis was done open to air using undried, reagent-grade solvents. Peptide synthesis conditions were

adapted from literature protocols.[18] Rink amide resin (850 mg, 0.5 mmol, 1 equiv) was added to a 50 mL peptide synthesis vessel (Chemglass, CG-1860-03) and swelled in *ca.* 40 mL of dichloromethane for 3 hours after which the solvent was removed by vacuum filtration. The resin was then washed 3 times with *ca.* 30 mL of DMF. Alternating Fmoc deprotection and amide coupling reactions were used to synthesize **1h** by the stepwise addition of amino acids. Fmoc deprotection was deemed complete by Kaiser test with *ca.* 20 mL of 20% (v/v) piperidine in DMF agitated on a shaker for 25-30 minutes, and the resin was washed 3 times with *ca.* 30 mL DMF, then 3 times with *ca.* 30 mL of dichloromethane, then 3 times again with DMF. For amide couplings, the Fmoc-protected amino acid (2 mmol, 4 equiv), 10 mL of freshly made 0.2 M solution of 1:1 HBTU:HOBt in DMF (2 mmol, 4 equiv), and 15 mL of a 0.2 M DIEA solution in DMF (3 mmol, 6 equiv) were mixed and allowed to stand at room temperature for 2 minutes. The activated amino acid was then transferred to the deprotected resin agitated on a shaker for 3 hours or until deemed complete by Kaiser test. Excess unreacted coupling reagents and amino acids were removed by washing 3 times with *ca.* 30 mL DMF, then 3 times with *ca.* 30 mL of dichloromethane, then 3 times again with DMF. Following the final Fmoc deprotection, peptides were cleaved from the resin support with 20 mL of a 95:2.5:2.5 TFA:TIS:H_2O stirred for 3 hours. A orange-yellow solution was collected by filtration and combined with TFA washes of the resin (*ca.* 10 mL) and the solvent removed *in vacuo*. The yellowish residue was triturated with 30 mL ether, then 3 times with 30 mL of hexanes, and then 3 more times with ether. The resulting off-white powder was carried on to RP-HPLC purification. Saturated solutions of crude **1h** (*ca.* 15-20 mg/mL) in 1:1 MeCN:H_2O acidified with 0.1% TFA were passed through 0.1 micron syringe filters (Pall Corporation). 2 mL injections of **1h** solution were separated on a preparatory-scale C18 column using a gradient from 0% solvent B-30% solvent B over 45 minutes at a flow rate of 20 mL/min,

where solvent A is 5:95 MeCN:H_2O acidified with 0.1% TFA and solvent B is 95:5 MeCN:H_2O acidified with 0.1% TFA. Fractions containing **1h** were combined and lyophilized to yield a *ca.* 40 mg fluffy white powder in 8.5% overall yield. ^{1}H-NMR (300 MHz, d_6-DMSO) δ 10.77 (s, 1H, Trp(N-H)), 8.57 (d, 1H), 8.23 (t, 1H), 7.55 (d, 1H), 7.40 (s, 1H), 7.29 (d, 1H), 6.53 (s, 1H), and multiple poorly resolved chemical shifts in both aliphatic and aromatic regions. MS (m/z): calcd. 939.12 $[M+H]^+$; found 939.2 $[M+H]^+$, 961.5 $[M+Na]^+$ (ESI-MS).

Synthesis of Complex 2

12h as the trifluoroacetate salt (10.0 mg, 9.5 μmol, 1 equiv) was stirred in 4 mL DMF for 30 minutes then was transferred to solution of $[Fe_4S_4(SBn)_4][NBu_4]_2$ (12.7 mg, 9.5 μmol, 1 equiv) in 1 mL of DMF. The resulting mixture was allowed to stir overnight at room temperature. Aliquots of the reaction mixture were used for characterization. ^{1}H-NMR (300 MHz, d_6-DMSO) δ 10.76 (broad, Trp(N-H)) and multiple, poorly resolved, broadened signals in both aliphatic and aromatic regions. MS (m/z): calcd. 705.0 $[M-2(NBu_4)]^{2-}$; found 705.2 $[M-2(NBu_4)]^{2-}$, 643.0 $[M-SBn-2(NBu_4)]^{2-}$ (ESI-MS).

Reduction of Complex 2 with $Na_2S_2O_4$.

500 μL of a freshly prepared 10 mmolar disodium dithionite solution in H_2O (5 μmol, 5 equiv) was added to a 500 μL aliquot of a 2 mmolar solution of **2** in DMF (1 μmol, 1 equiv). The mixture was stirred for 30 minutes before EPR aliquots were frozen. EPR g-values (2.06, 1.93, 1.88).

Synthesis of Complex 4

Analogous protocol used for the synthesis of **2** with the addition of the reduced cluster precursor $[Fe_4S_4(SBn)_4][NBu_4]_3$ (14.9 mg, 9.5 μmol, 1 equiv). EPR g-values (2.04, 1.92, 1.88). MS (m/z): calcd. 705.0 $[M\text{-}2(NBu_4)]^{2-}$; found 705.2 $[M\text{-}2(NBu_4)]^{2-}$, 643.0 $[M\text{-}SBn\text{-}2(NBu_4)]^{2-}$, 1652.2 $[M\text{-}(NBu_4)]^{-}$ (ESI-MS).

Reaction of Complex 2 with $Fe_2(CO)_6CH_3C(CH_2S)_2CH_2SCOCH_3$.

250 μL of a freshly prepared 2 mmolar solution of $Fe_2(CO)_6CH_3C(CH_2S)_2CH_2SCOCH_3$ in DMF was added to 250 μL of a 2 mmolar solution of **2** in DMF. The mixture was stirred for 30 minutes and aliquot was frozen for EPR. 5 equiv $Na_2S_2O_4$ was added. After stirring for an additional 30 minutes an aliquot was frozen for EPR.

Reaction of Complex 4 with $Fe_2(CO)_6CH_3C(CH_2S)_2CH_2SCOCH_3$.

250 μL of a freshly prepared 2 mmolar solution of $Fe_2(CO)_6CH_3C(CH_2S)_2CH_2SCOCH_3$ in DMF was added to 250 μL of a 2 mmolar solution of **2** in DMF. The mixture was stirred for 30 minutes and aliquot was frozen for EPR. 5 equiv $Na_2S_2O_4$ was added. After stirring for an additional 30 minutes an aliquot was frozen for EPR.

REFERENCES

1.Lewis, N. S.; Nocera, D. G., *P Natl Acad Sci USA* **2006,** *103*, 15729-15735.
2.Kubas, G. J., *J Organomet Chem* **2009,** *694*, 2648-2653.
3.(a) Benck, J. D.; Hellstern, T. R.; Kibsgaard, J.; Chakthranont, P.; Jaramillo, T. F., *ACS Catalysis* **2014,** *4*, 3957-3971; (b) Chen, X.; Wang, D.; Wang, Z.; Zhou, P.; Wu, Z.; Jiang, F., *Chemical Communications* **2014,** *50*, 11683-11685.
4.(a) Lubitz, W.; Ogata, H.; Rüdiger, O.; Reijerse, E., *Chem Rev* **2014,** *114*, 4081-4148; (b) Tard, C.; Pickett, C. J., *Chem Rev* **2009,** *109*, 2245-2274.
5.(a) Volbeda, A.; Garcin, E.; Piras, C.; deLacey, A. L.; Fernandez, V. M.; Hatchikian, E. C.; Frey, M.; FontecillaCamps, J. C., *J Am Chem Soc* **1996,** *118*, 12989-12996; (b) Peters, J. W.; Lanzilotta, W. N.; Lemon, B. J.; Seefeldt, L. C., *Science* **1998,** *282*, 1853-1858; (c) Shima, S.; Pilak, O.; Vogt, S.; Schick, M.; Stagni, M. S.; Meyer-Klaucke, W.; Warkentin, E.; Thauer, R. K.; Ermler, U., *Science* **2008,** *321*, 572-575.
6.(a) Camara, J. M.; Rauchfuss, T. B., *Nat Chem* **2012,** *4*, 26-30; (b) Tard, C.; Liu, X. M.; Ibrahim, S. K.; Bruschi, M.; De Gioia, L.; Davies, S. C.; Yang, X.; Wang, L. S.; Sawers, G.; Pickett, C. J., *Nature* **2005,** *433*, 610-613.
7.Blanco-Canosa, J. B.; Dawson, P. E., *Angew Chem Int Edit* **2008,** *47*, 6851-6855.
8.Gibney, B. R.; Mulholland, S. E.; Rabanal, F.; Dutton, P. L., *P Natl Acad Sci USA* **1996,** *93*, 15041-15046.
9.Mulholland, S. E.; Gibney, B. R.; Rabanal, F.; Dutton, P. L., *J Am Chem Soc* **1998,** *120*, 10296-10302.
10.Laplaza, C. E.; Holm, R. H., *J Am Chem Soc* **2001,** *123*, 10255-10264.
11.(a) Averill, B. A.; Herskovi.T; Holm, R. H.; Ibers, J. A., *J Am Chem Soc* **1973,** *95*, 3523-3534; (b) Laskowski, E. J.; Frankel, R. B.; Gillum, W. O.; Papaefthymiou, G. C.; Renaud, J.; Ibers, J. A.; Holm, R. H., *J Am Chem Soc* **1978,** *100*, 5322-5337; (c) Reynolds, J. G.; Laskowski, E. J.; Holm, R. H., *J Am Chem Soc* **1978,** *100*, 5315-5322; (d) Cai, L. S.; Weigel, J. A.; Holm, R. H., *J Am Chem Soc* **1993,** *115*, 9289-9290.
12.Laplaza, C. E.; Holm, R. H., *Abstr Pap Am Chem S* **2001,** *221*, U722-U722.

NMR Data

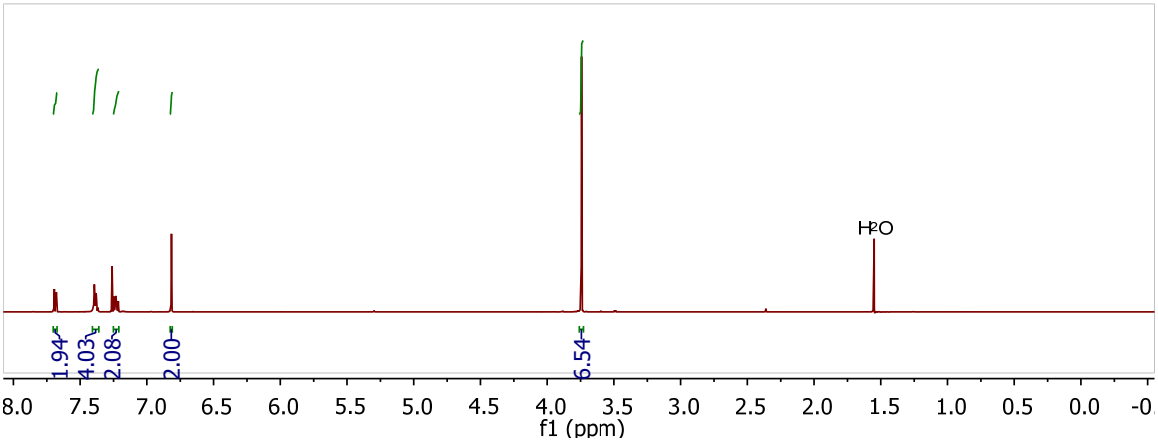

Figure 1. ^{1}H-NMR (500 MHz, $CDCl_3$) spectrum of **B**.

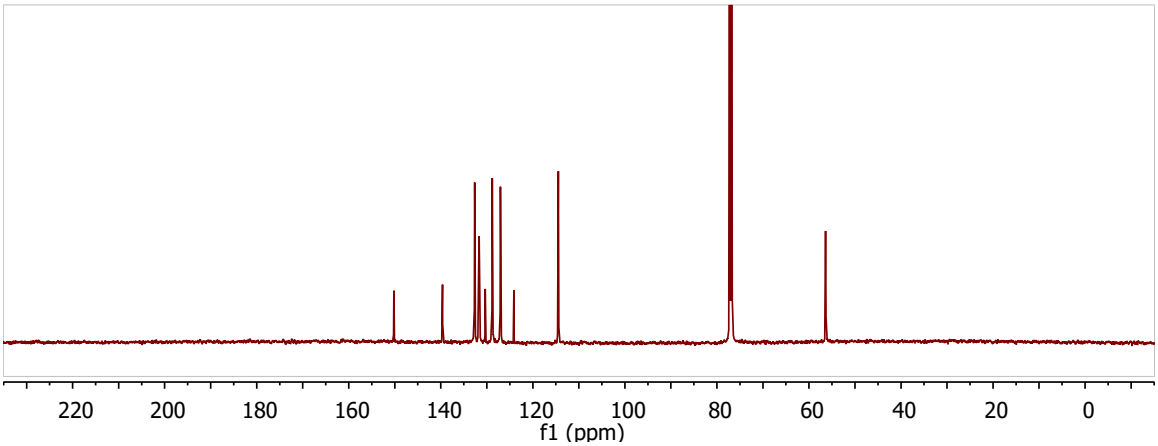

Figure 2. ^{13}C{^{1}H}-NMR (126 MHz, $CDCl_3$) spectrum of **B**.

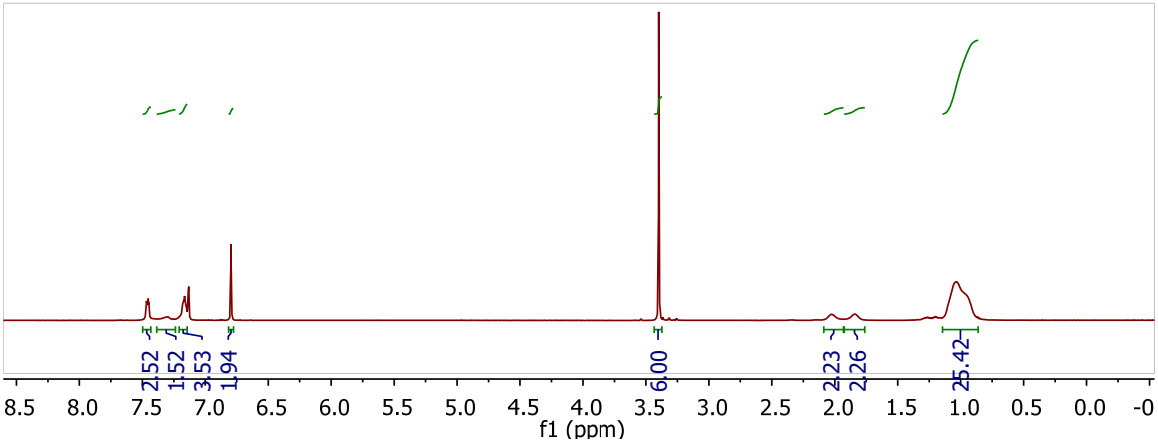

Figure 3. ^{1}H-NMR (500 MHz, C_6D_6) spectrum of **1-(OMe)$_2$**.

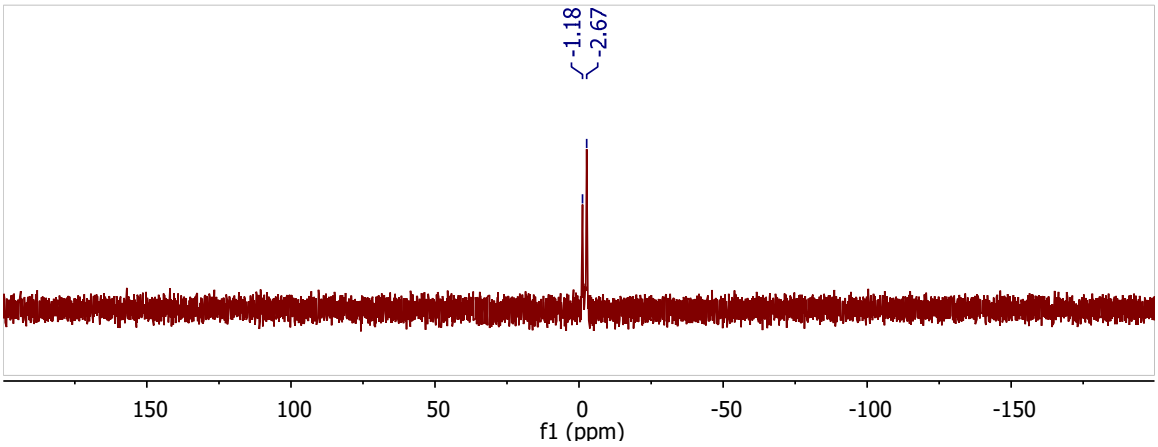

Figure 4. $^{31}P\{^{1}H\}$-NMR (121 MHz, C_6D_6) spectrum of **1-(OMe)$_2$**.

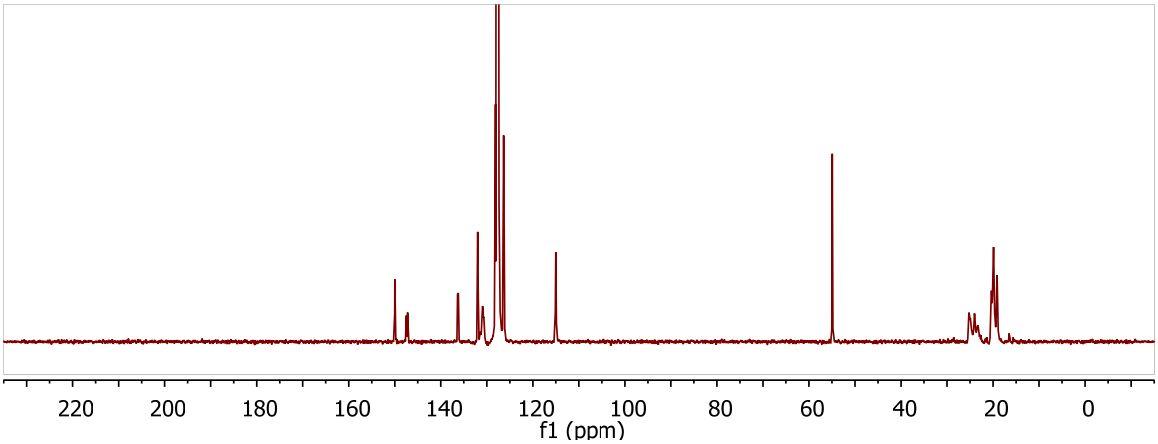

Figure 5. $^{13}C\{^{1}H\}$-NMR (126 MHz, C_6D_6) spectrum of **1-(OMe)$_2$**.

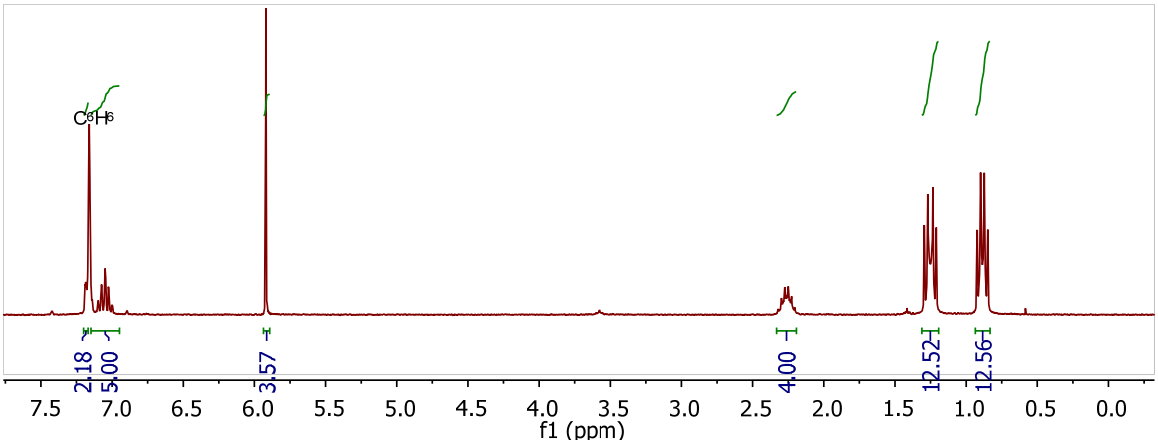

Figure 6. ^{1}H-NMR (300 MHz, C_6D_6) spectrum of complex **3**.

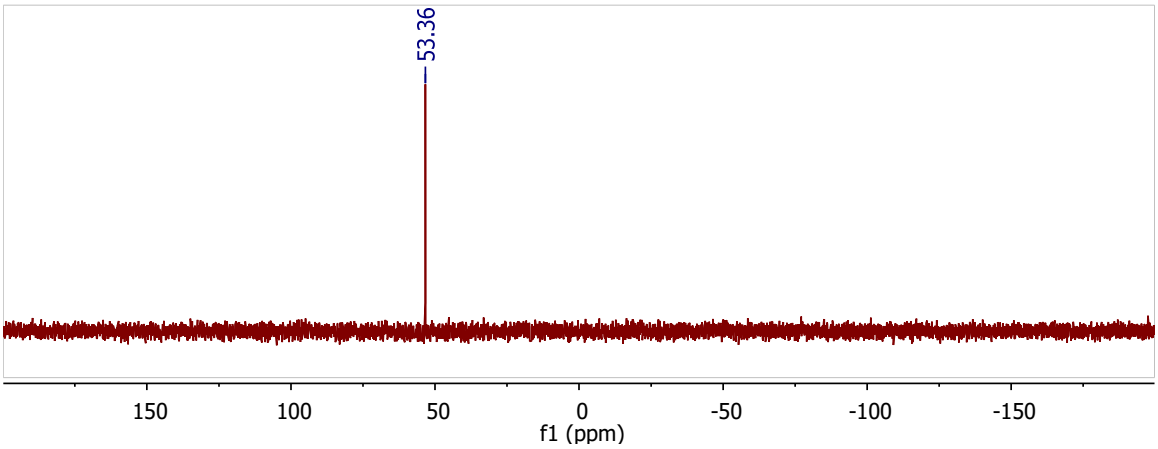

Figure 7. $^{31}P\{^{1}H\}$-NMR (121 MHz, C_6D_6) spectrum of complex **3**.

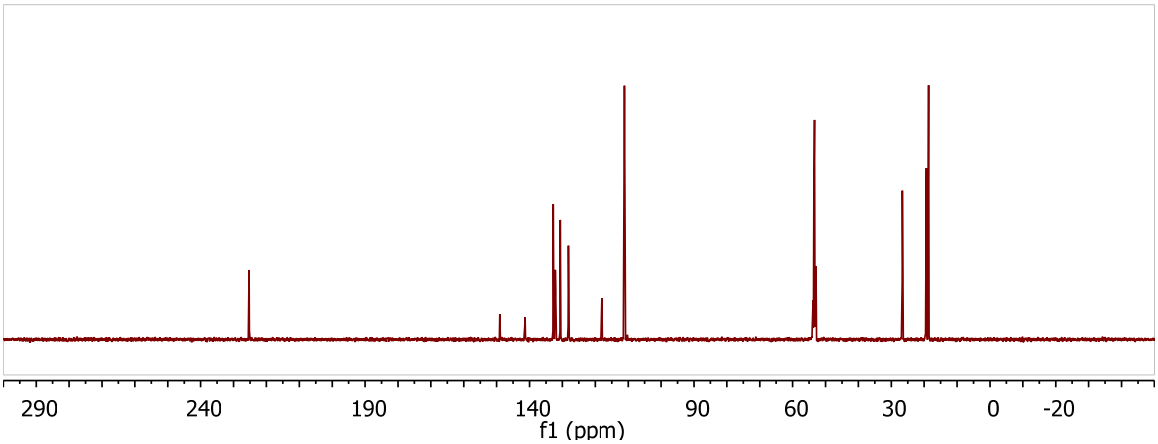

Figure 8. $^{13}C\{^{1}H\}$-NMR (126 MHz, CD_2Cl_2) spectrum of complex **3**.

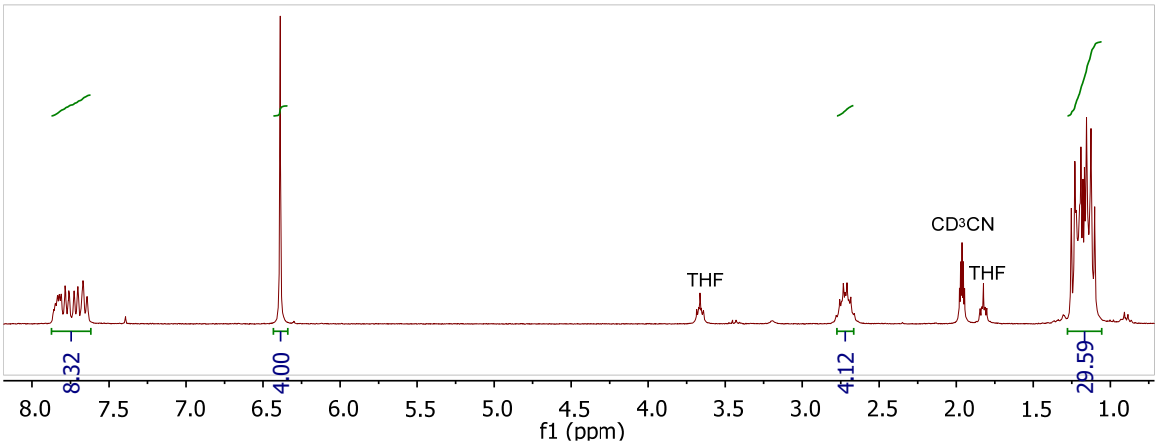

Figure 9. ^{1}H-NMR (300 MHz, CD_3CN) spectrum of complex **4**.

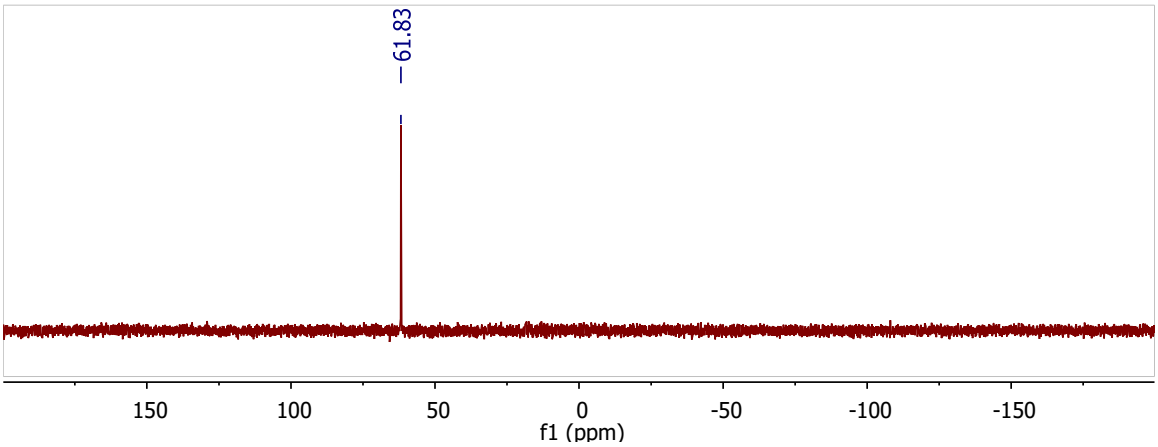

Figure 10. $^{31}P\{^{1}H\}$-NMR (121 MHz, CD_3CN) spectrum of complex **4**.

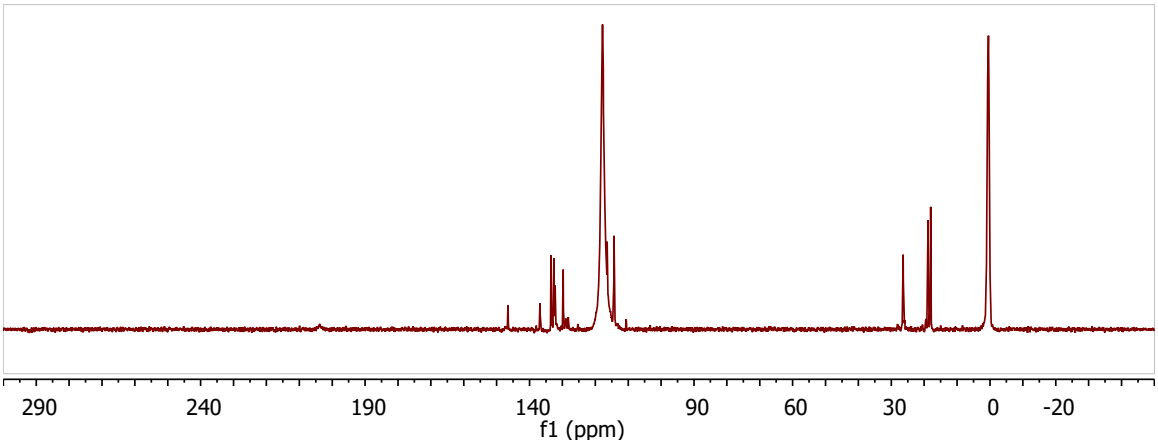

Figure 11. $^{13}C\{^{1}H\}$-NMR (126 MHz, CD_3CN) spectrum of complex **4**.

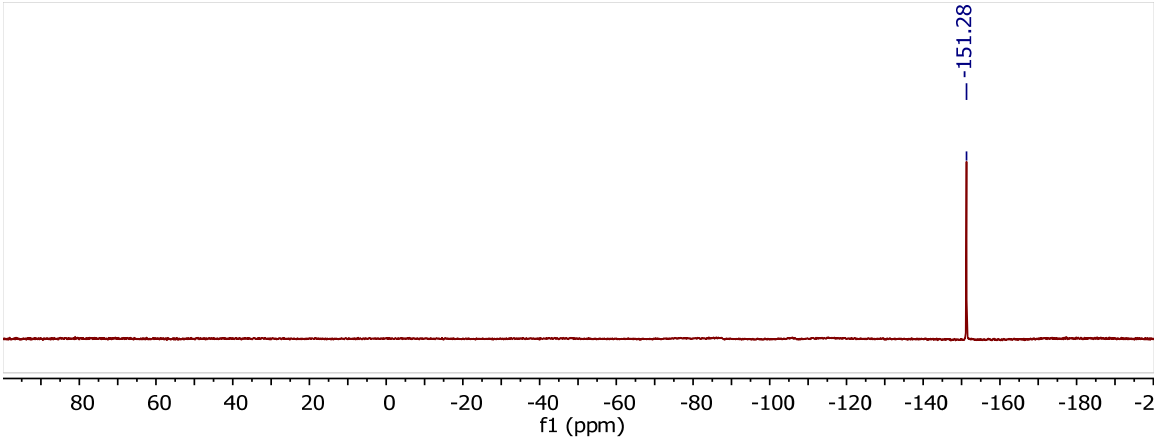

Figure 12. ^{19}F-NMR (282 MHz, CD_3CN) spectrum of complex **4**.

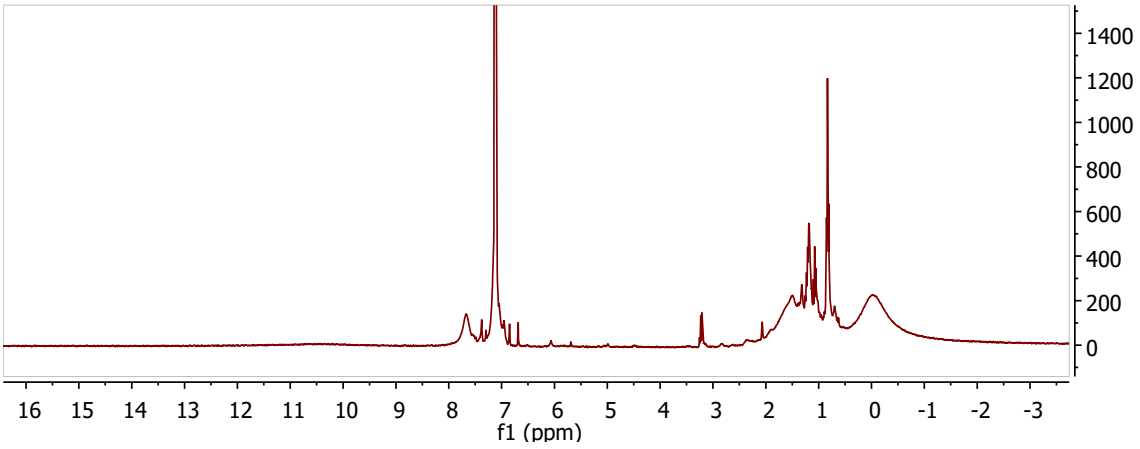

Figure 13. ^{1}H-NMR (300 MHz, C_6D_6) spectrum of complex **5**.

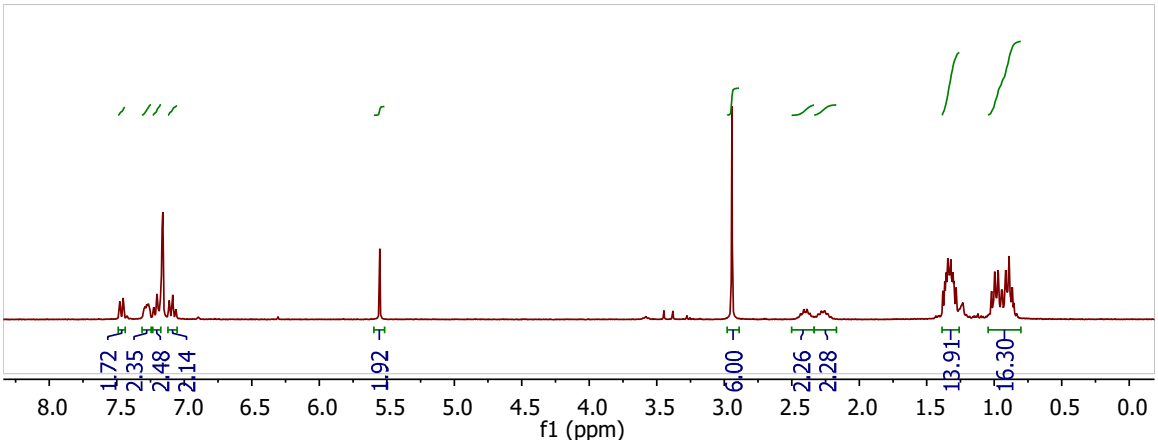

Figure 14. ^{1}H-NMR (300 MHz, C_6D_6) spectrum of complex **3-(OMe)$_2$**.

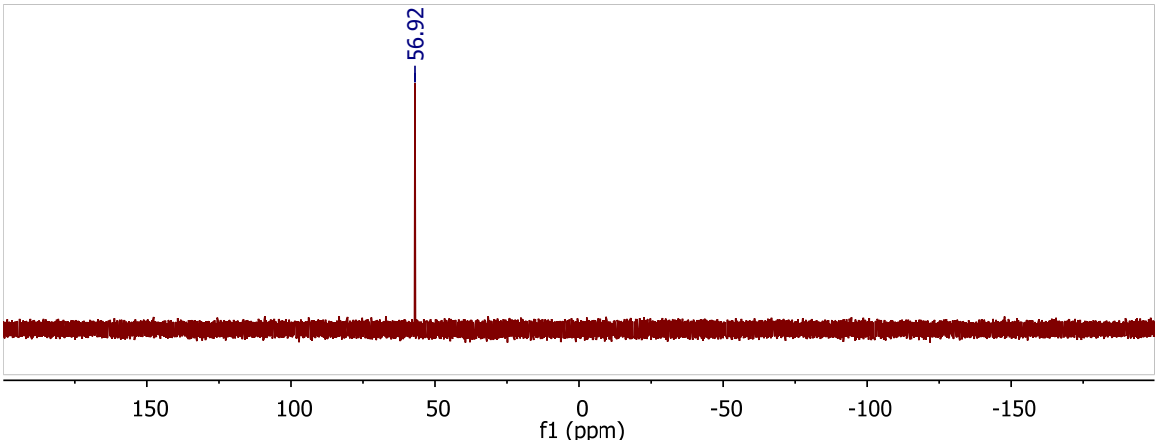

Figure 15. ^{31}P{^{1}H}-NMR (121 MHz, C_6D_6) spectrum of complex **3-(OMe)$_2$**.

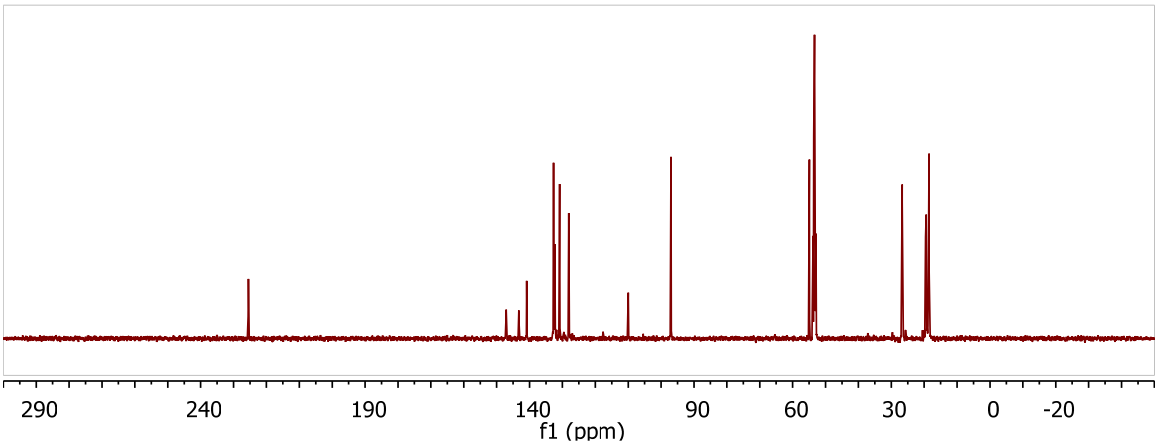

Figure 16. $^{13}C\{^{1}H\}$-NMR (126 MHz, CD_2Cl_2) spectrum of complex **3-(OMe)$_2$**.

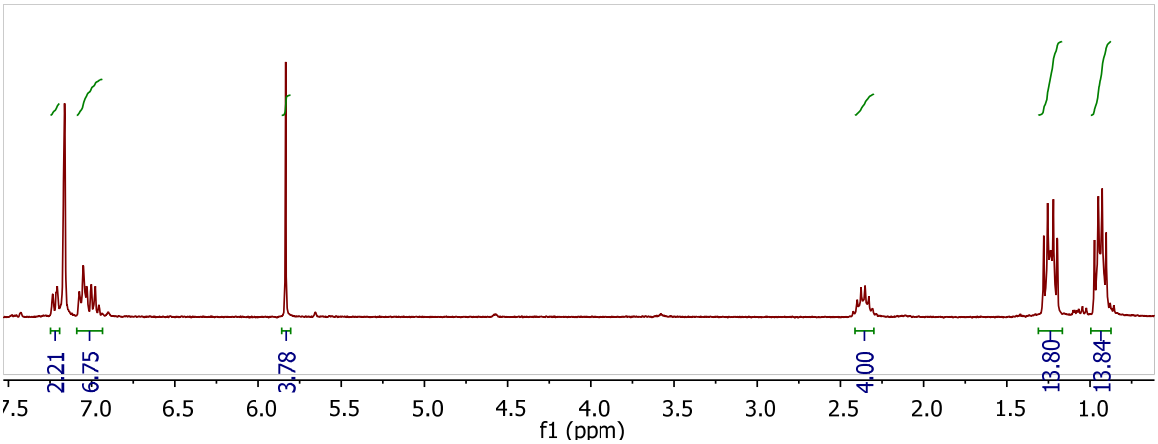

Figure 17. ^{1}H-NMR (300 MHz, C_6D_6) spectrum of complex **8**.

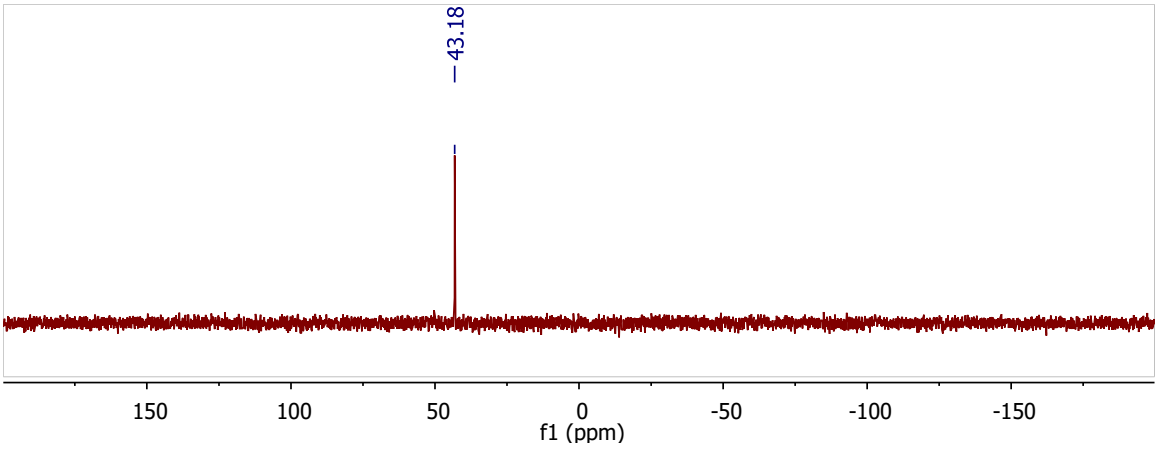

Figure 18. $^{31}P\{^{1}H\}$-NMR (121 MHz, C_6D_6) spectrum of complex **8**.

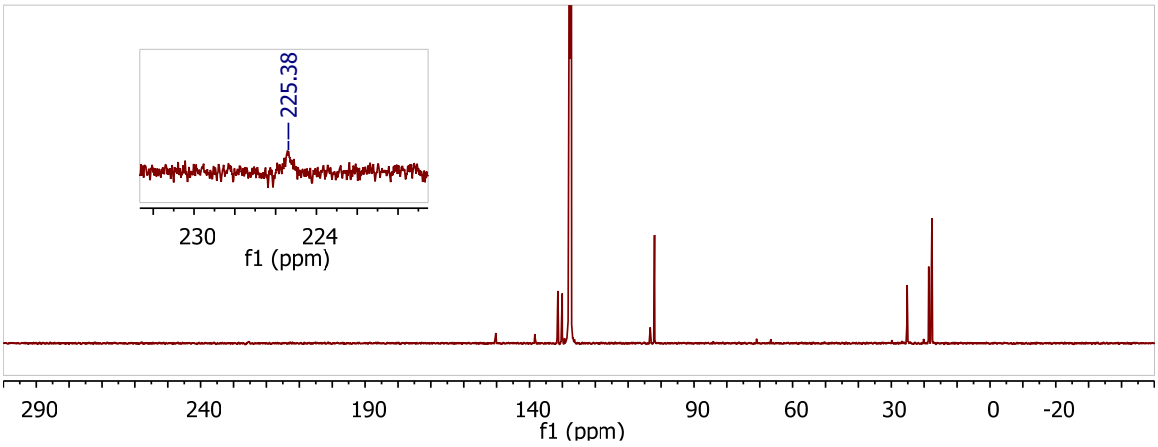

Figure 19. $^{13}C\{^{1}H\}$-NMR (126 MHz, C_6D_6) spectrum of complex **8**.

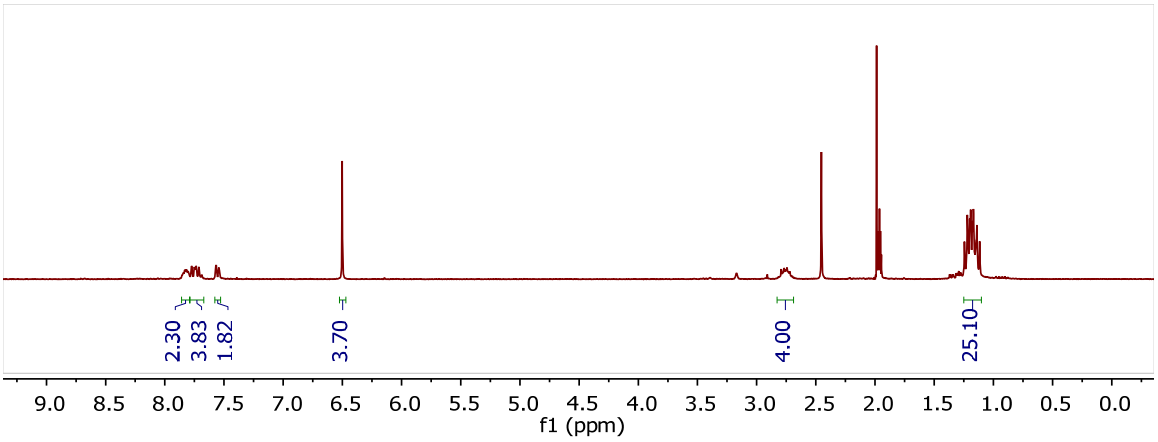

Figure 20. ^{1}H NMR (300 MHz, C_6D_6) spectrum of **6**.

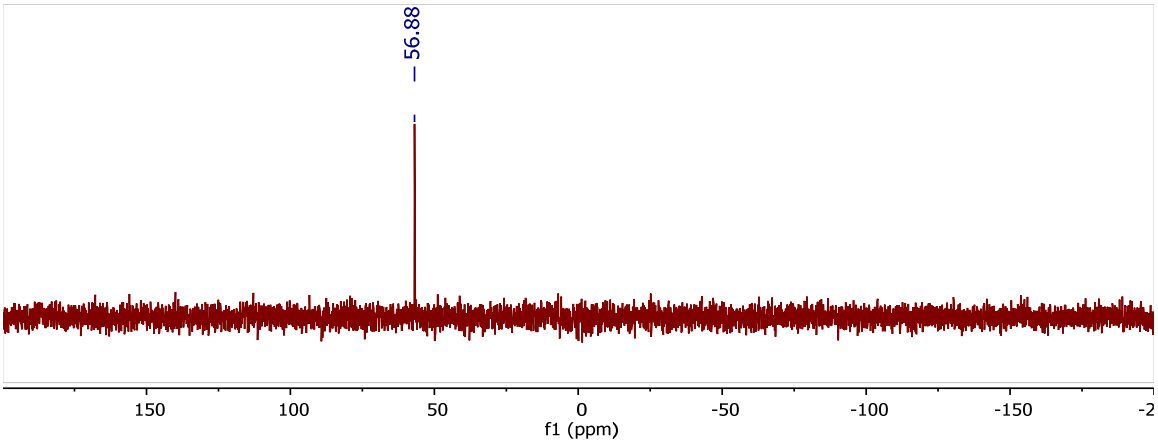

Figure 21. ^{31}P NMR (121 MHz, C_6D_6) spectrum of **6**.

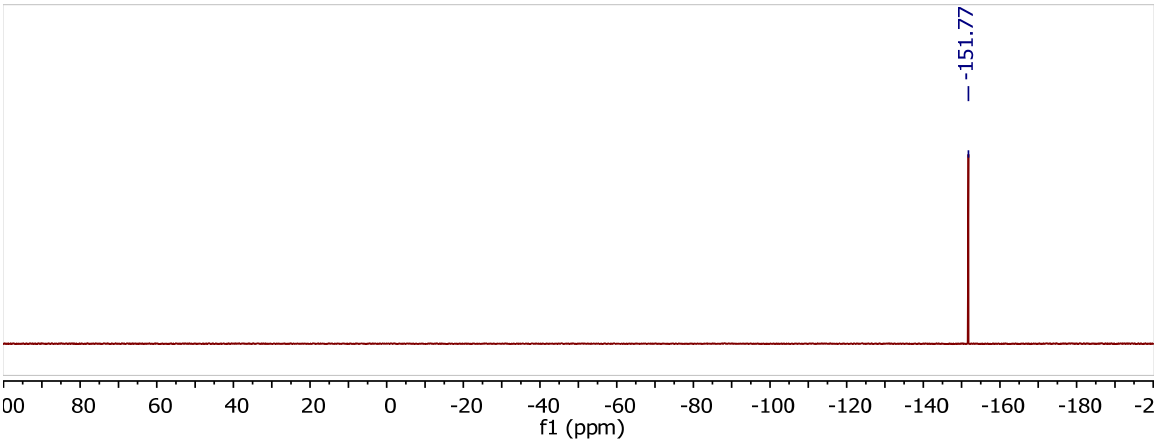

Figure 22. ^{13}C NMR (126 MHz, C_6D_6) spectrum of **6**.

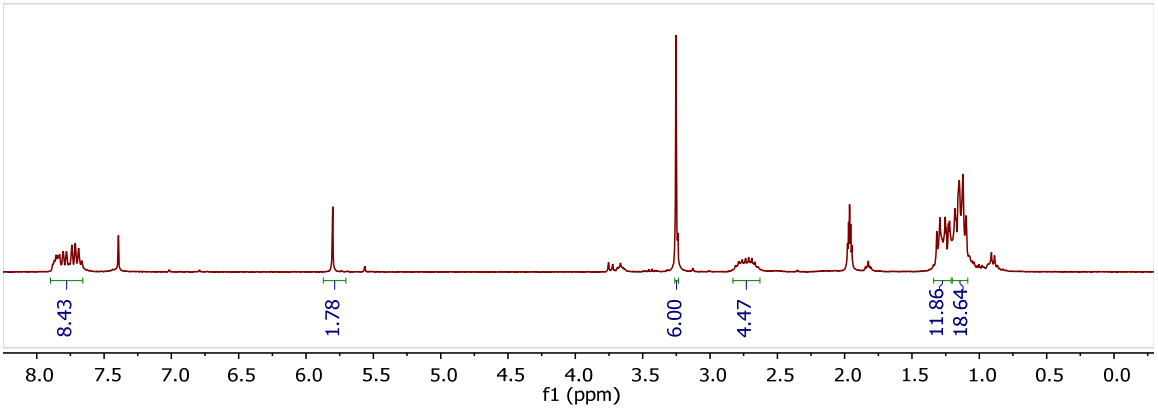

Figure 23. ^{1}H NMR (300 MHz, C_6D_6) spectrum of **4-(OMe)$_2$**.

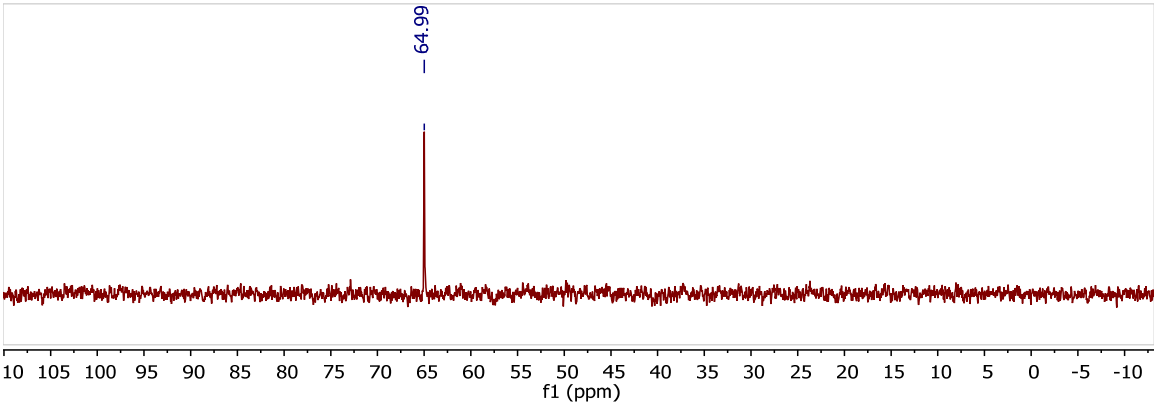

Figure 24. ^{31}P NMR (121 MHz, C_6D_6) spectrum of **4-(OMe)$_2$**.

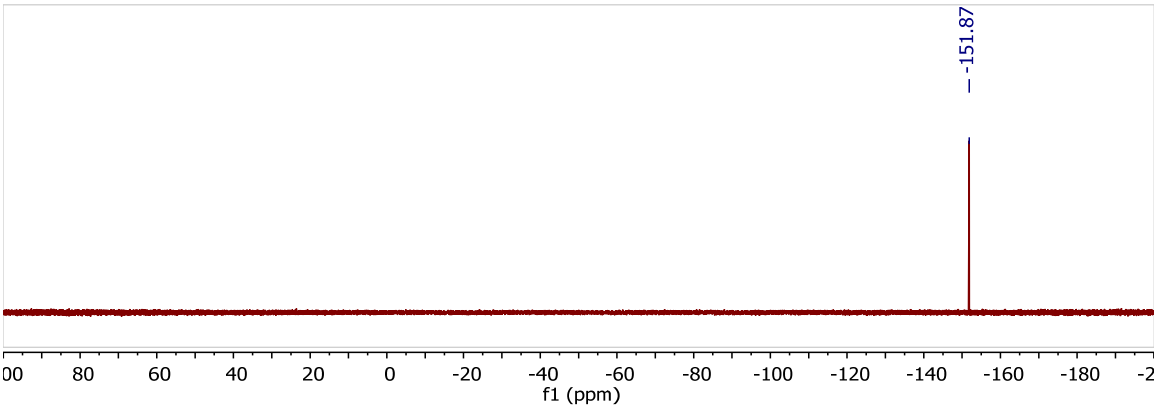

Figure 25. ^{19}F-NMR (282 MHz, CD_3CN) spectrum of complex **4-(OMe)$_2$**.

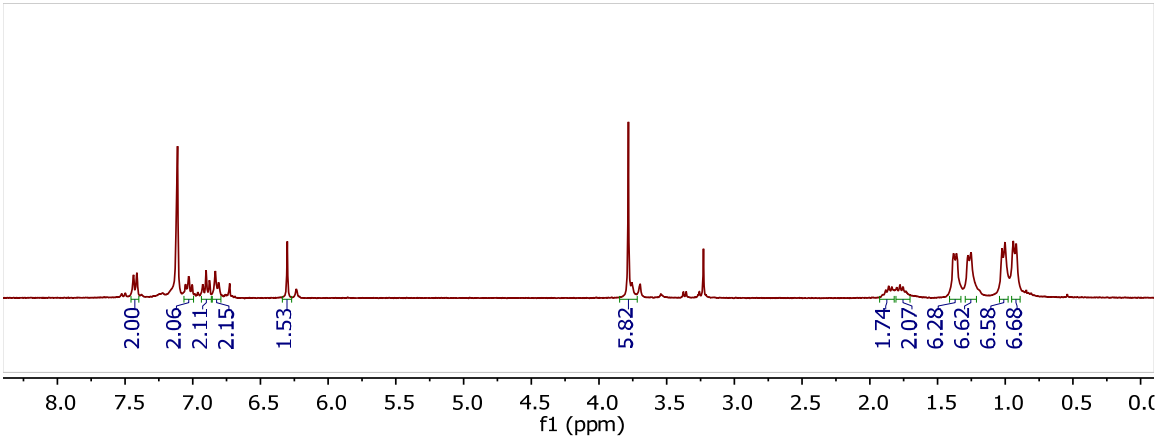

Figure 26. ^{1}H NMR (300 MHz, C_6D_6) spectrum of **7-(OMe)$_2$**.

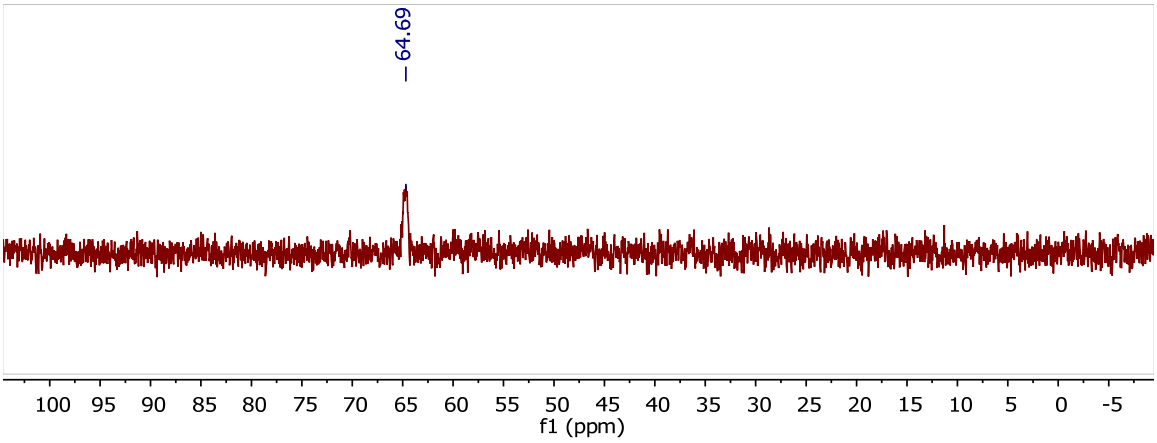

Figure 27. ^{31}P NMR (121 MHz, C_6D_6) spectrum of **7-(OMe)$_2$**.

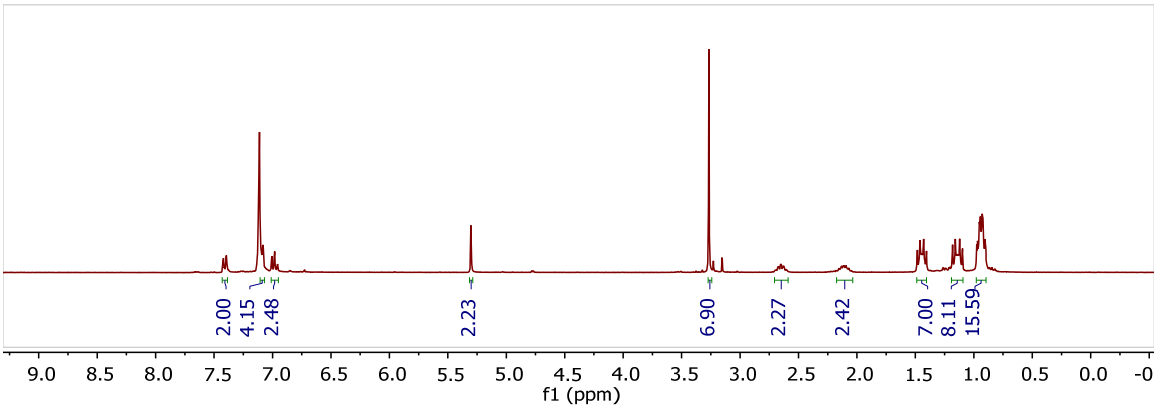

Figure 28. ^{1}H NMR (300 MHz, C_6D_6) spectrum of **8-(OMe)$_2$**.

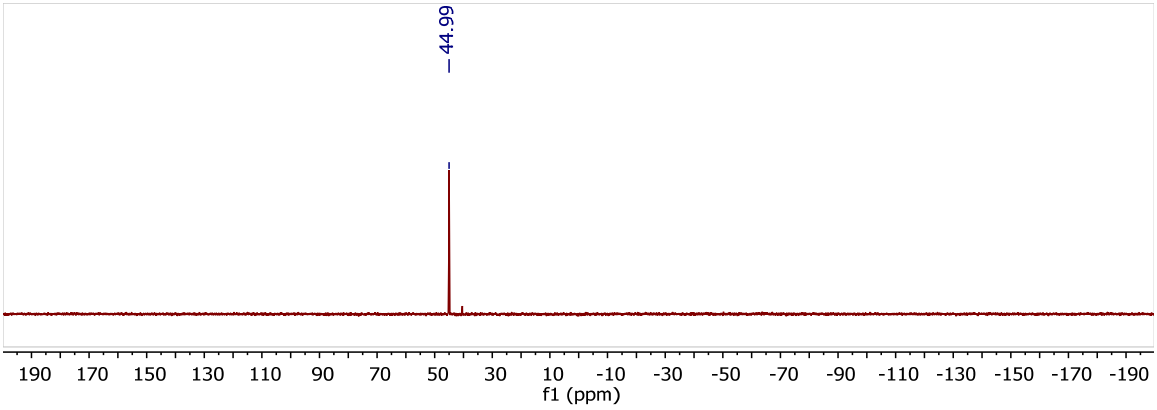

Figure 29. ^{31}P NMR (121 MHz, C_6D_6) spectrum of **8-(OMe)$_2$**.

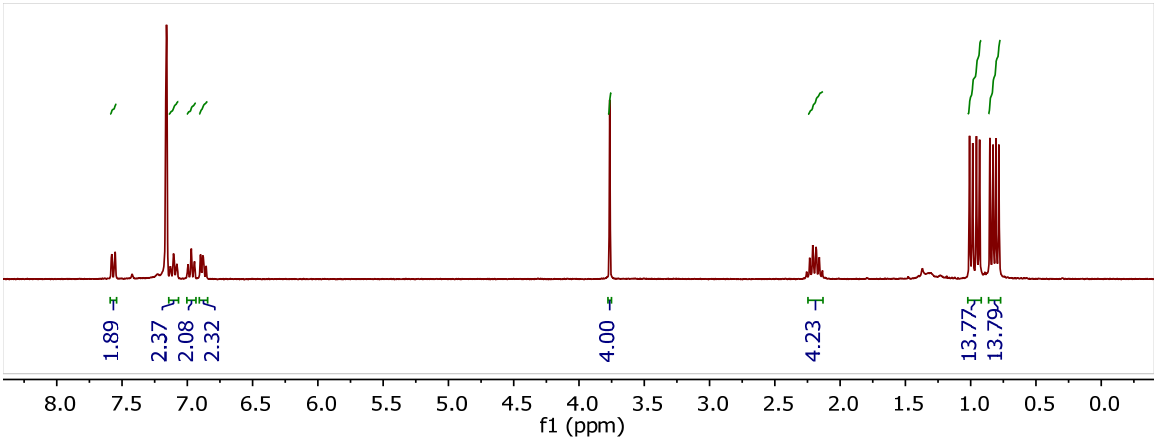

Figure 30. ^{1}H NMR (300 MHz, C_6D_6) spectrum of **9**.

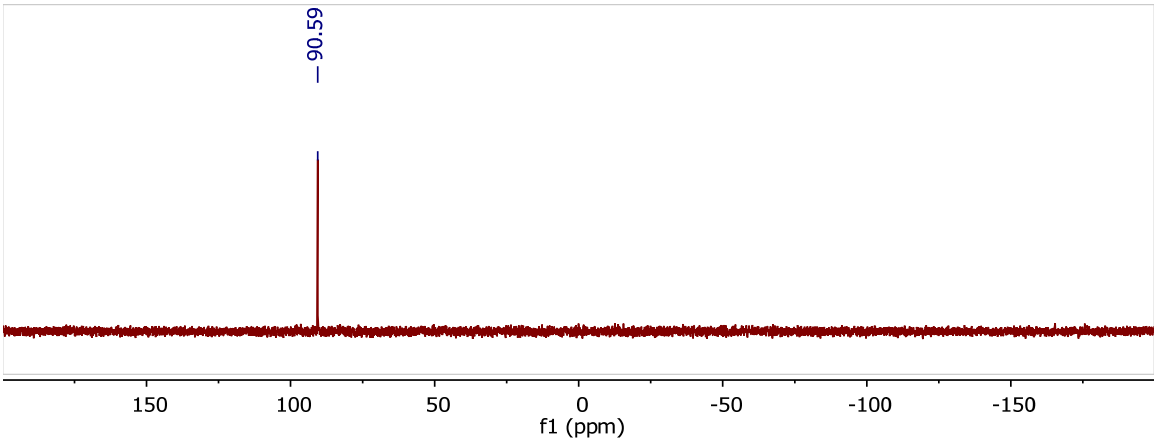

Figure 31. ^{31}P NMR (121 MHz, C_6D_6) spectrum of **9**.

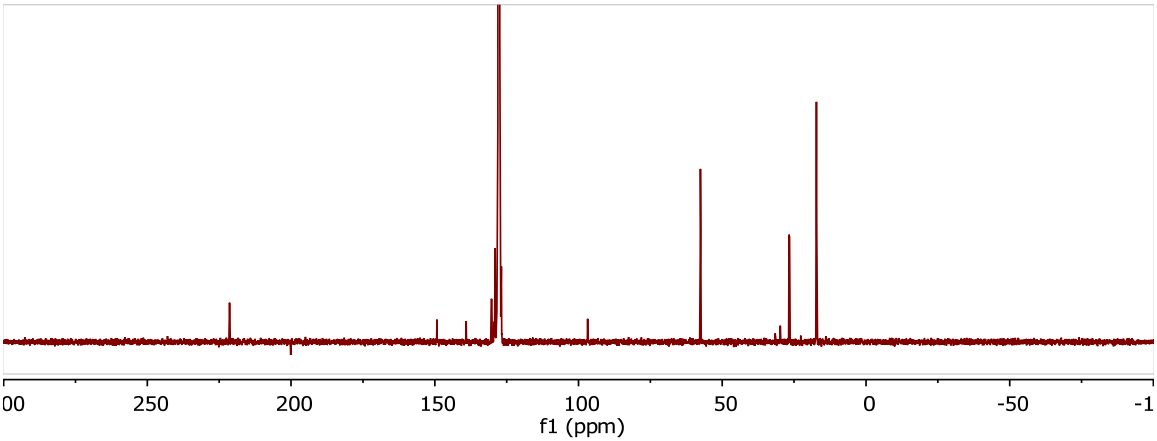

Figure 32. ^{13}C NMR (126 MHz, C_6D_6) spectrum of **9**.

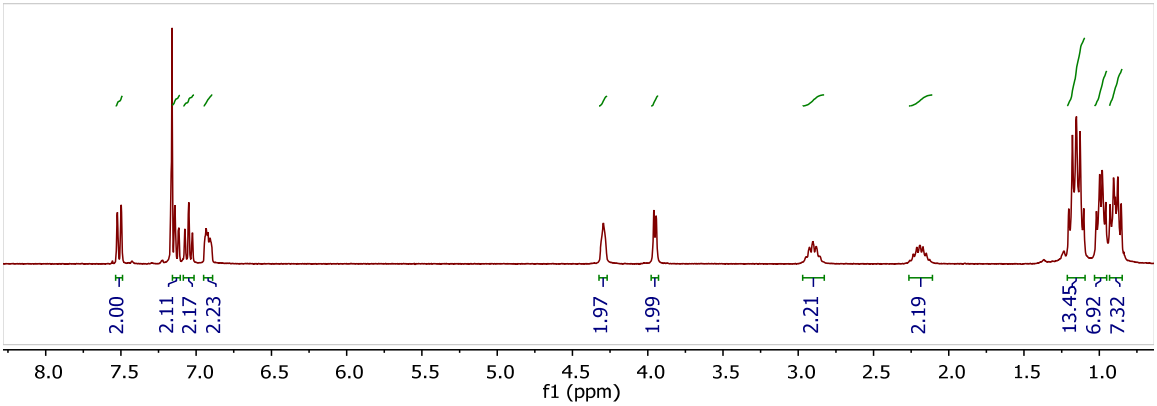

Figure 33. ^{1}H NMR (300 MHz, C_6D_6) spectrum of **11**.

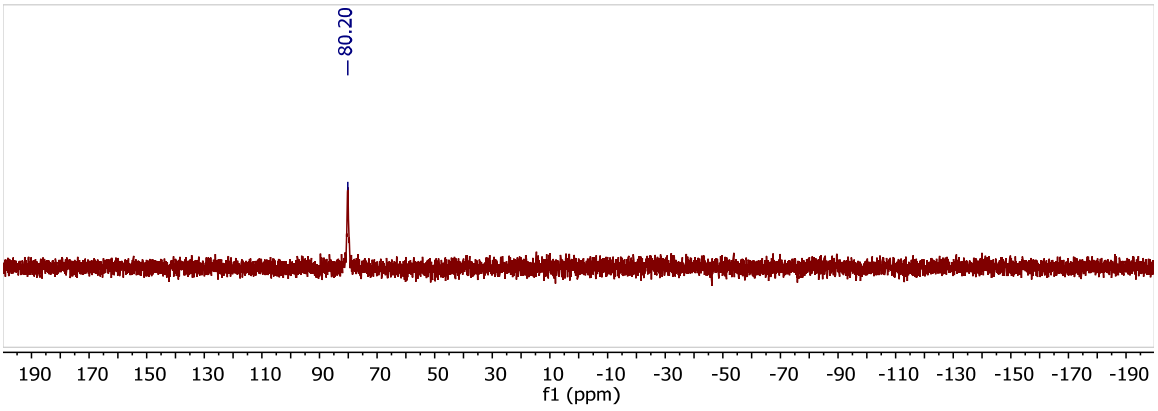

Figure 34. ^{31}P NMR (121 MHz, C_6D_6) spectrum of **11**.

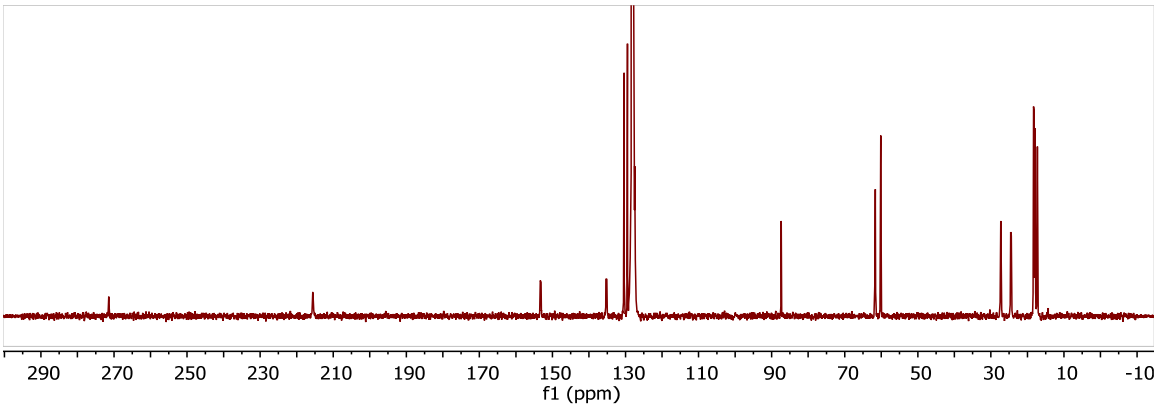

Figure 35. ^{13}C NMR (126 MHz, C_6D_6) spectrum of **11**.

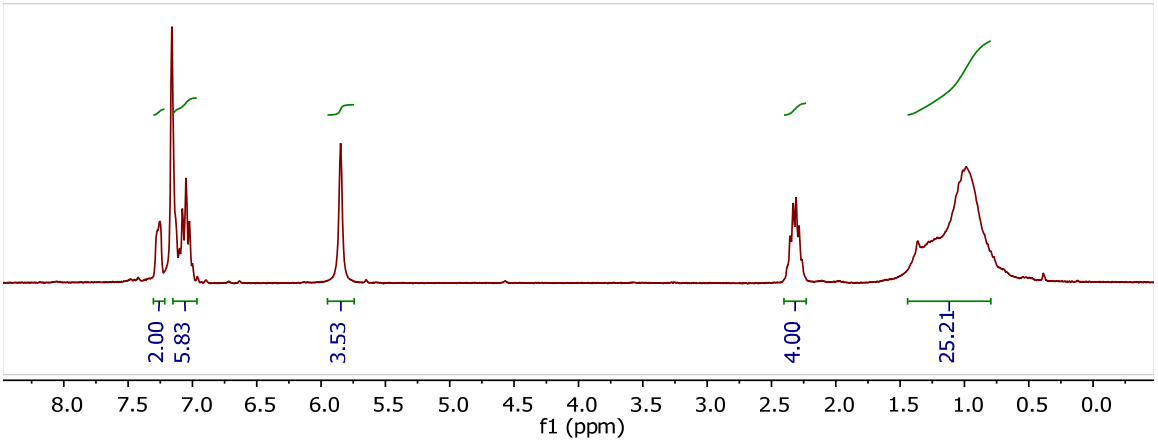

Figure 36. ^{1}H NMR (300 MHz, C_6D_6) spectrum of **12**.

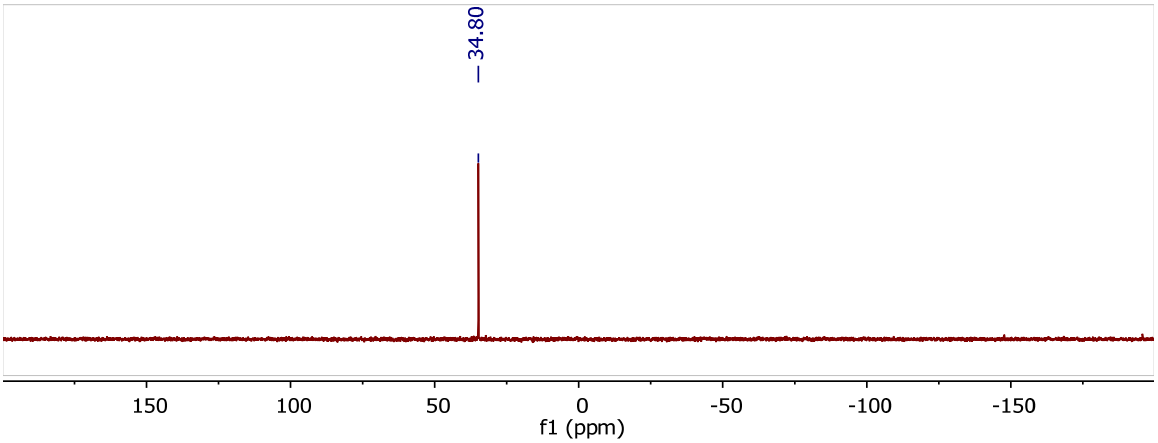

Figure 37. ^{31}P NMR (121 MHz, C_6D_6) spectrum of **12**.

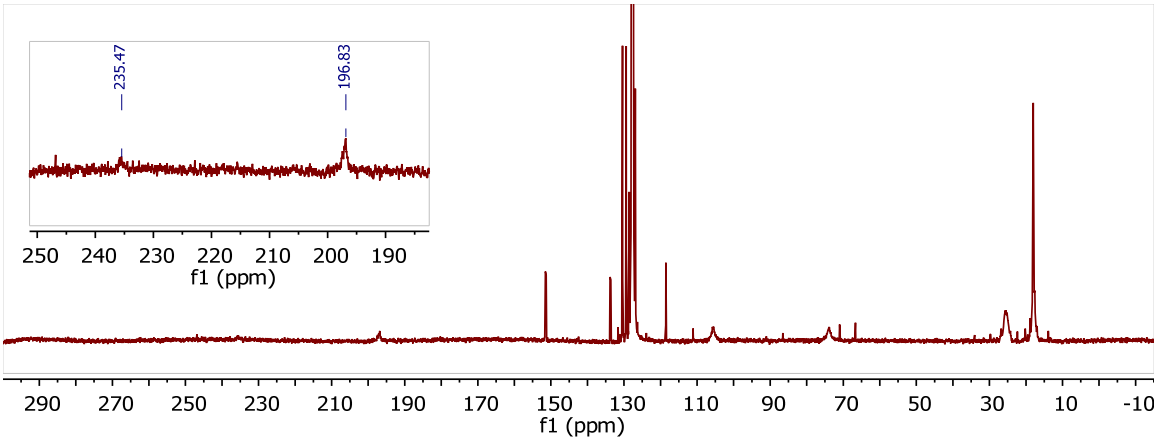

Figure 38. ^{13}C NMR (126 MHz, C_6D_6) spectrum of **12**.

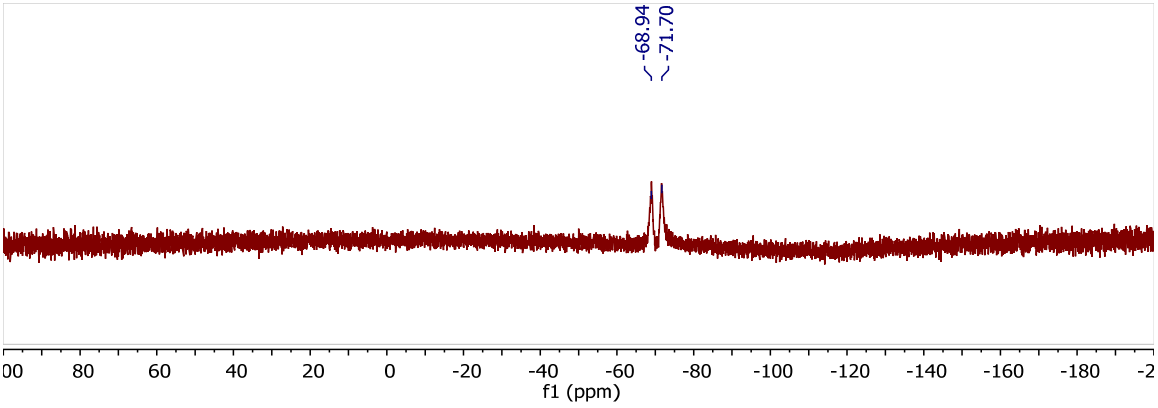

Figure 39. ^{19}F NMR (282 MHz, d_8-THF) spectrum of **10**.

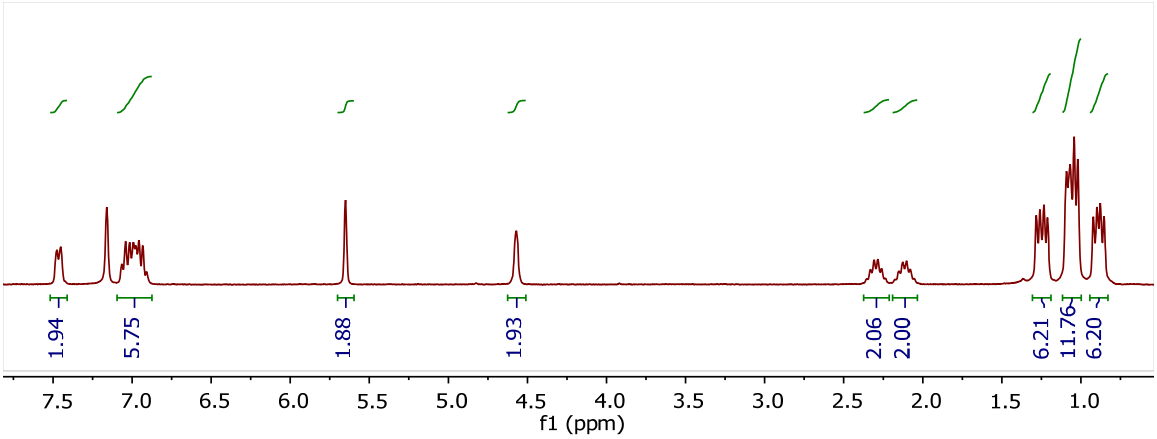

Figure 40. ^{1}H NMR (300 MHz, C_6D_6) spectrum of **13-CO**.

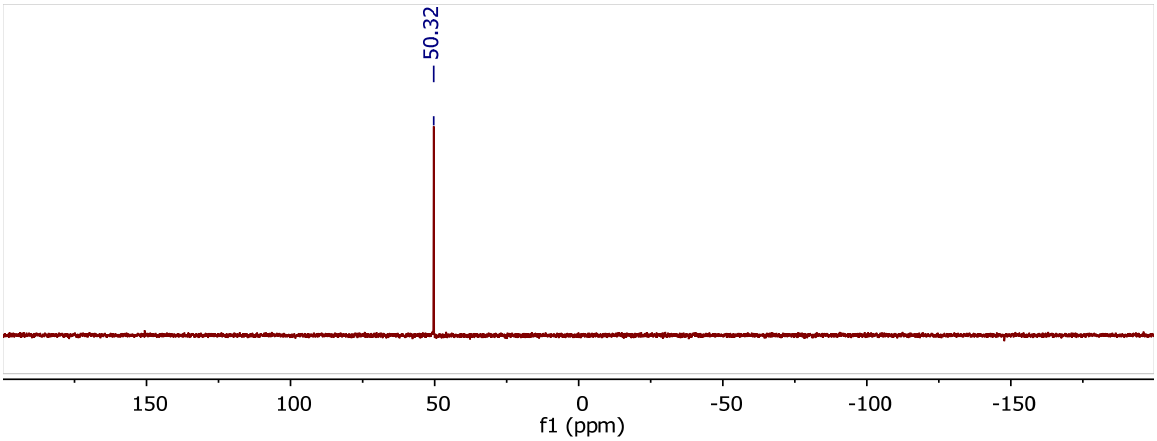

Figure 41. ^{31}P NMR (121 MHz, C_6D_6) spectrum of **13-CO**.

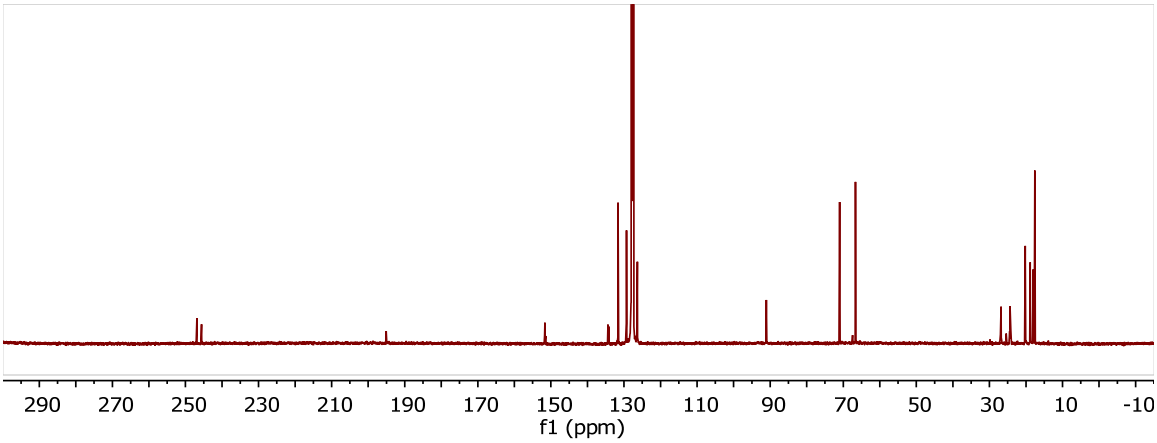

Figure 42. ^{13}C NMR (126 MHz, C_6D_6) spectrum of **13-CO**.

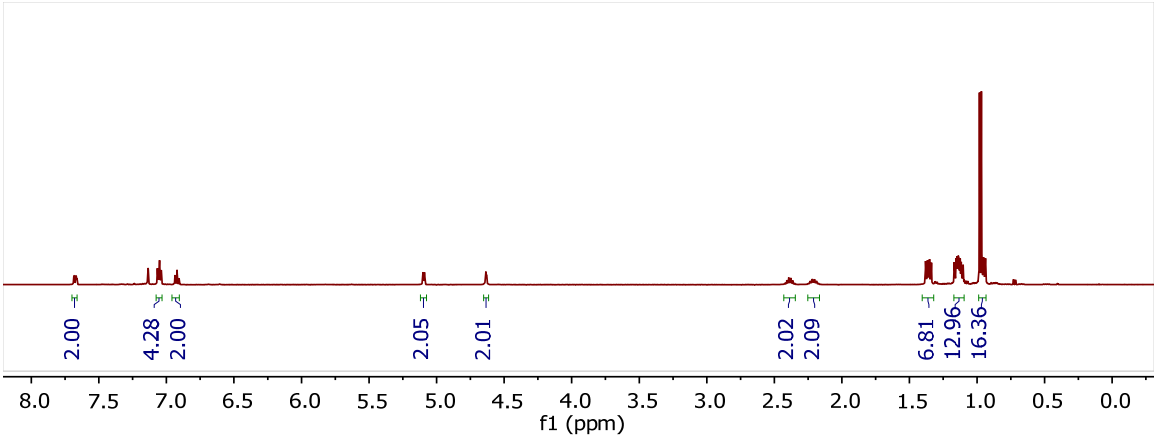

Figure 43. ^{1}H NMR (300 MHz, C_6D_6) spectrum of **13-PMe$_3$**.

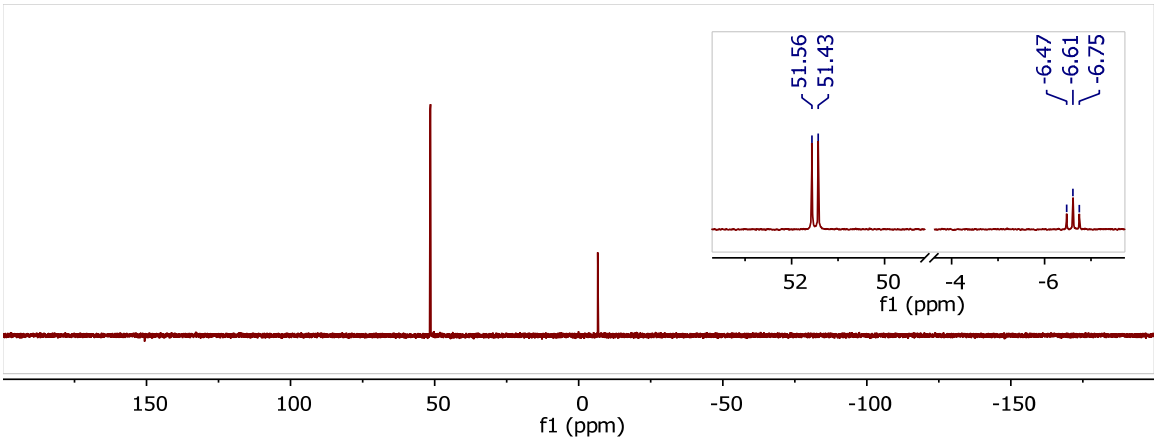

Figure 44. ^{31}P NMR (121 MHz, C_6D_6) spectrum of **13-PMe$_3$**.

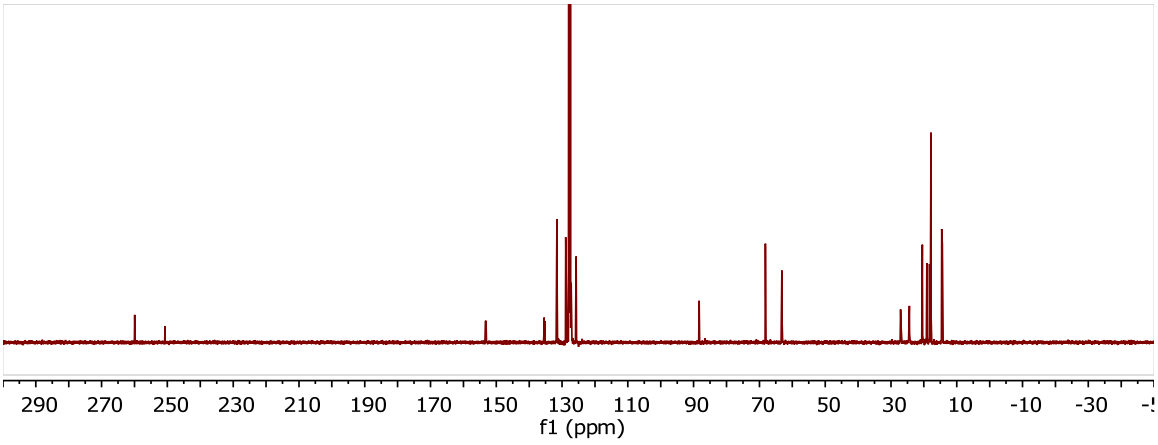

Figure 45. ^{13}C NMR (126 MHz, C_6D_6) spectrum of **13-PMe$_3$**.

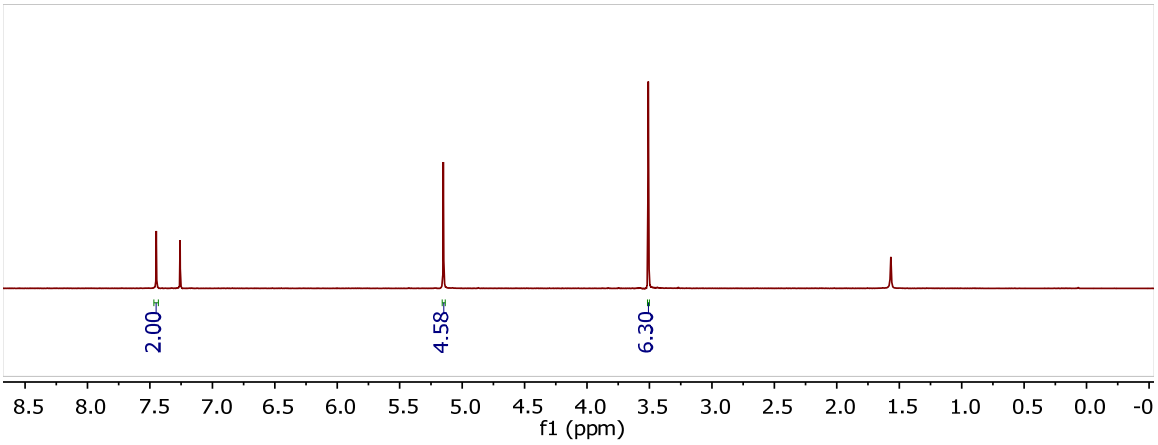

Figure 46. ^{1}H-NMR (500 MHz, $CDCl_3$) spectrum of **A**.

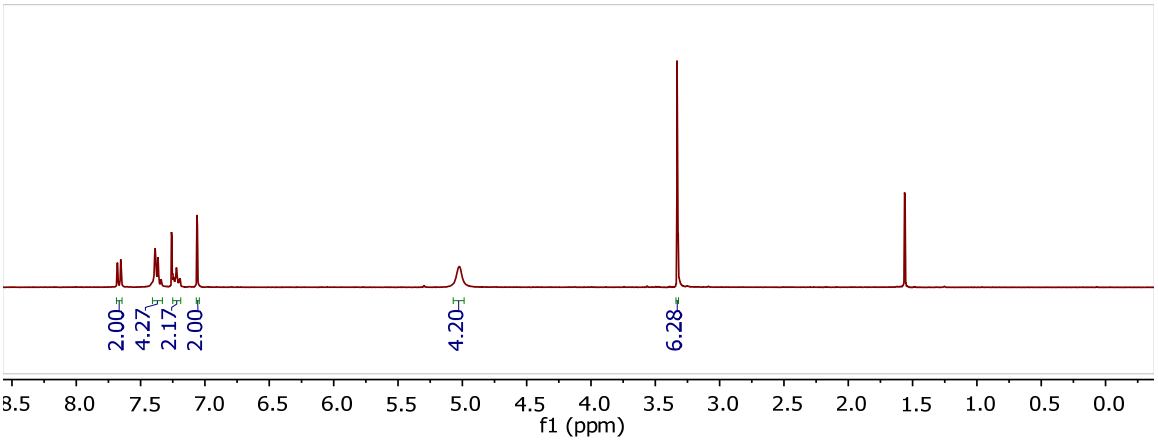

Figure 47. ^{1}H-NMR (500 MHz, $CDCl_3$) spectrum of **B**.

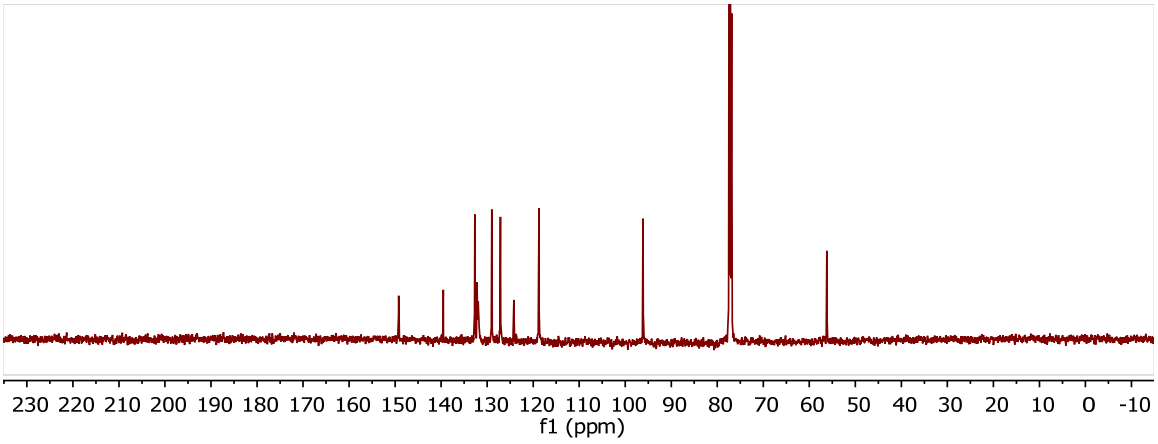

Figure 48. ^{13}C-NMR (126 MHz, $CDCl_3$) spectrum of **B**.

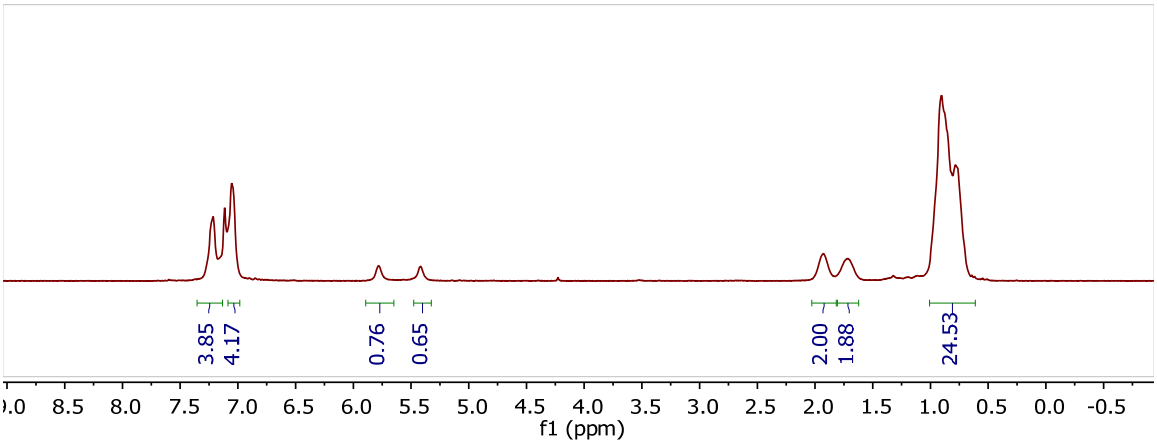

Figure 49. ^{1}H-NMR (300 MHz, C_6D_6) spectrum of **1-H**.

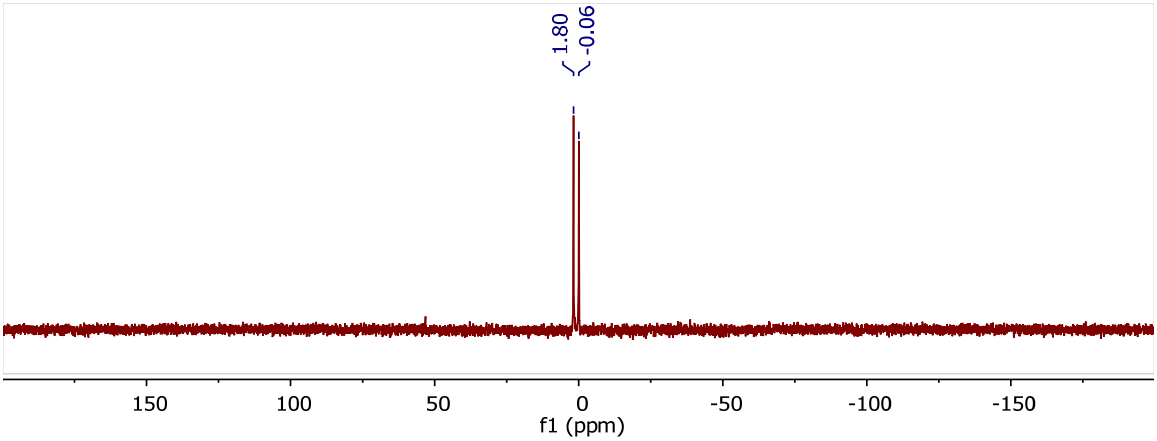

Figure 50. ^{31}P-NMR (121 MHz, C_6D_6) spectrum of **1-H**.

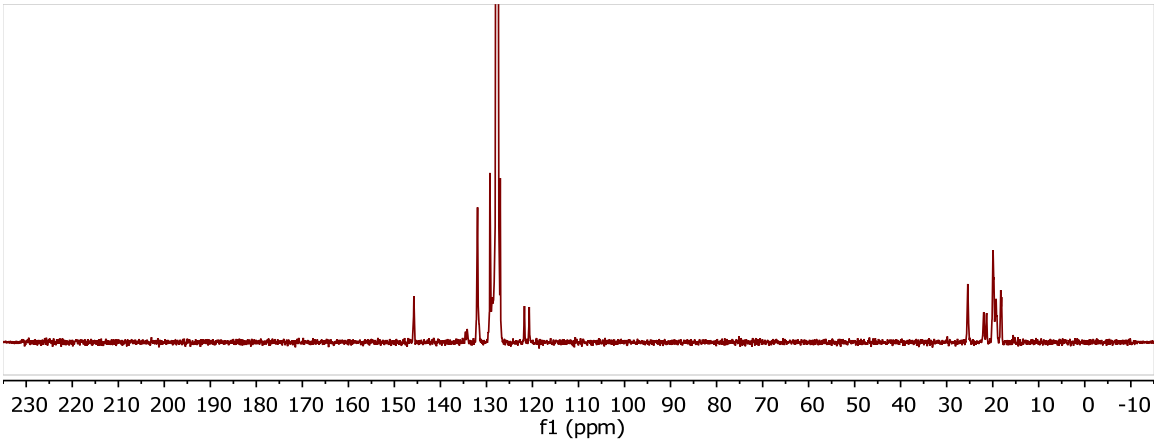

Figure 51. ^{13}C-NMR (126 MHz, C_6D_6) spectrum of **1-H**.

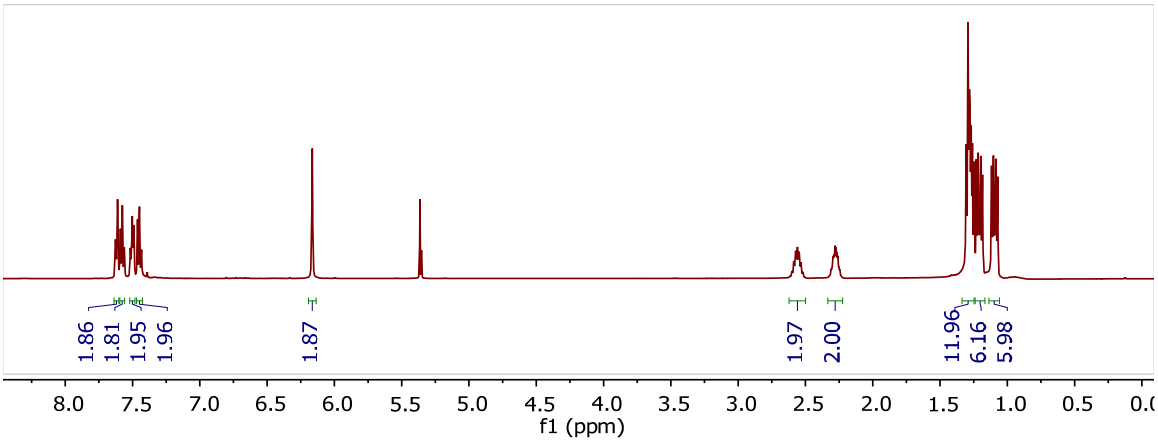

Figure 52. ^{1}H-NMR (500 MHz, CD_2Cl_2) spectrum of **2**.

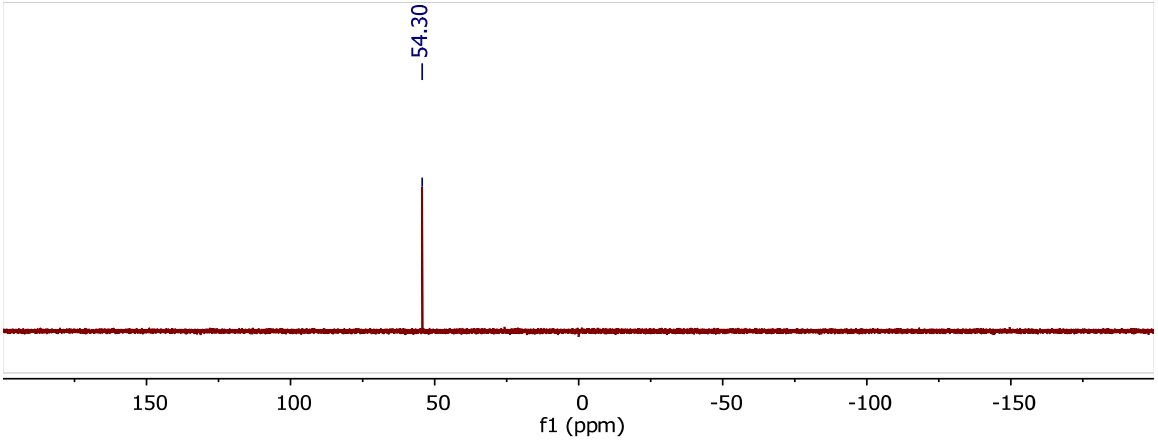

Figure 53. ^{31}P-NMR (121 MHz, CD_2Cl_2) spectrum of **2**.

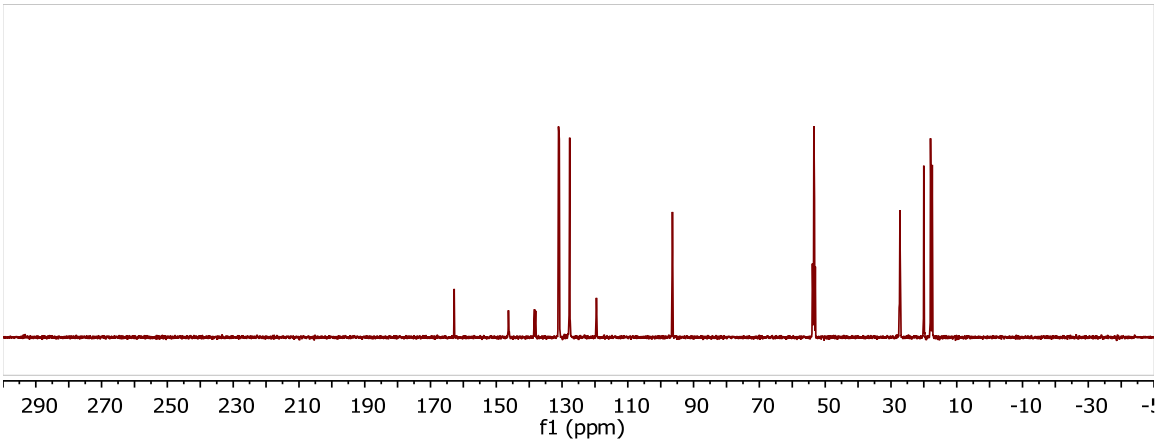

Figure 54. ^{13}C-NMR (126 MHz, CD_2Cl_2) spectrum of **2**.

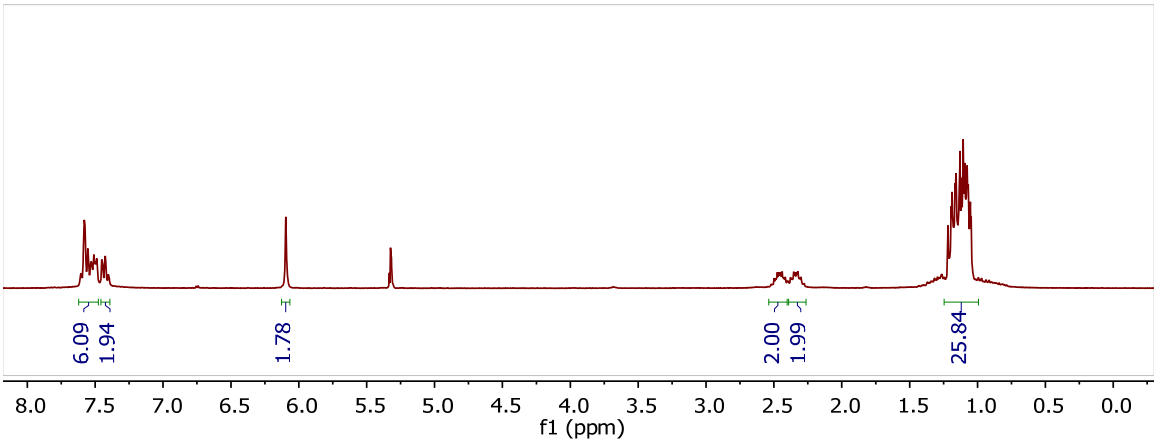

Figure 55. ^{1}H-NMR (500 MHz, CD_2Cl_2) spectrum of **3**.

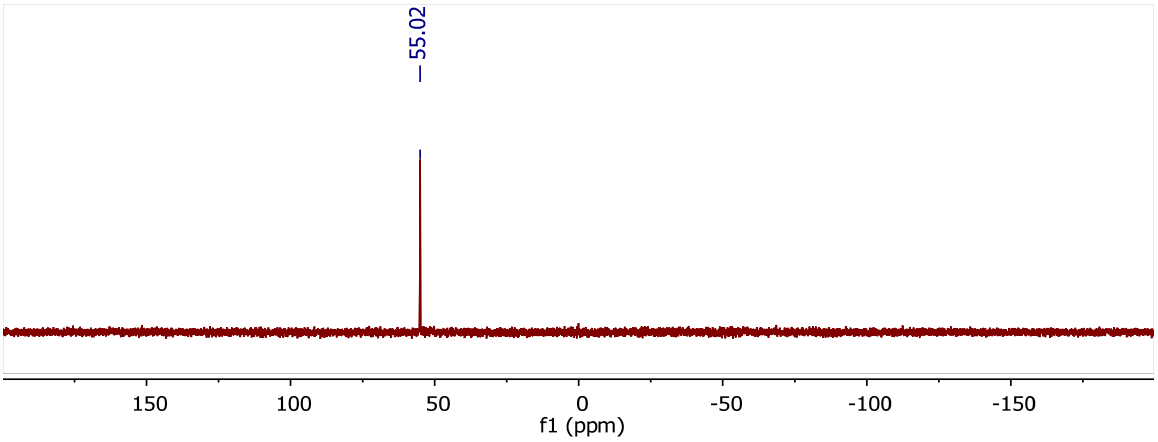

Figure 56. ^{31}P-NMR (121 MHz, CD_2Cl_2) spectrum of **3**.

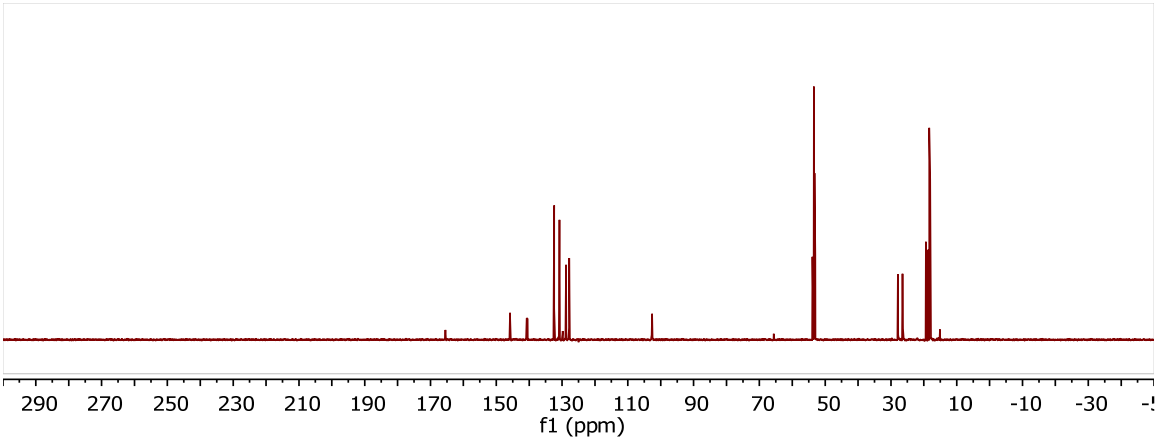

Figure 57. ^{13}C-NMR (126 MHz, CD_2Cl_2) spectrum of **3**.

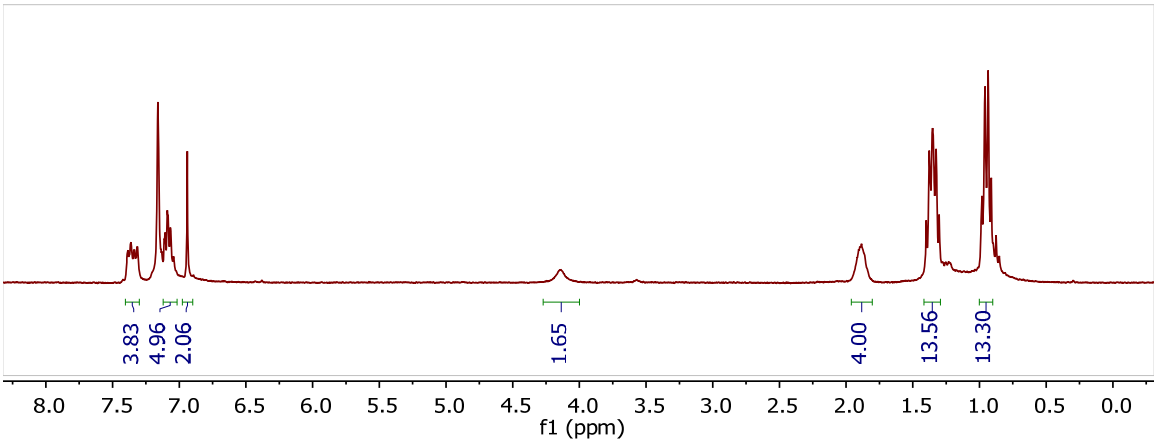

Figure 58. ^{1}H-NMR (500 MHz, C_6D_6) spectrum of **4-H**.

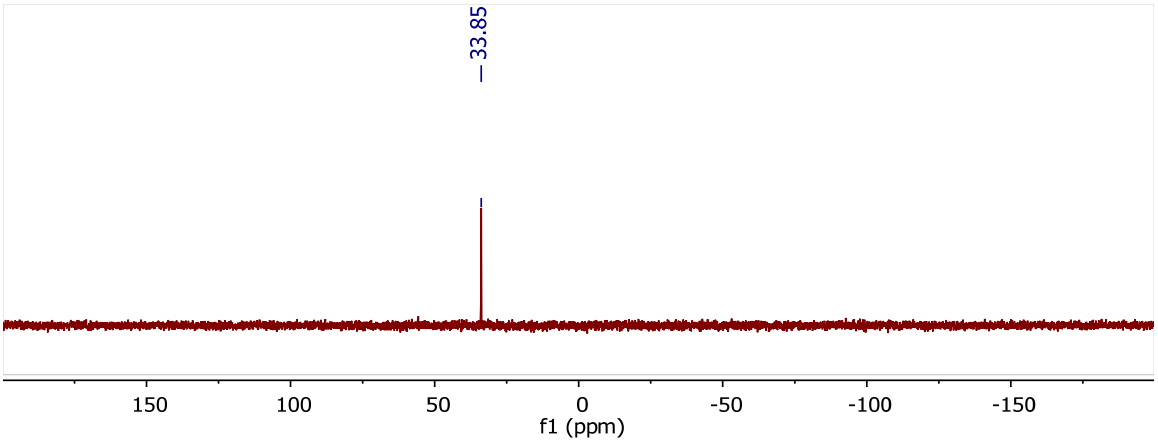

Figure 59. ^{31}P-NMR (121 MHz, C_6D_6) spectrum of **4-H**.

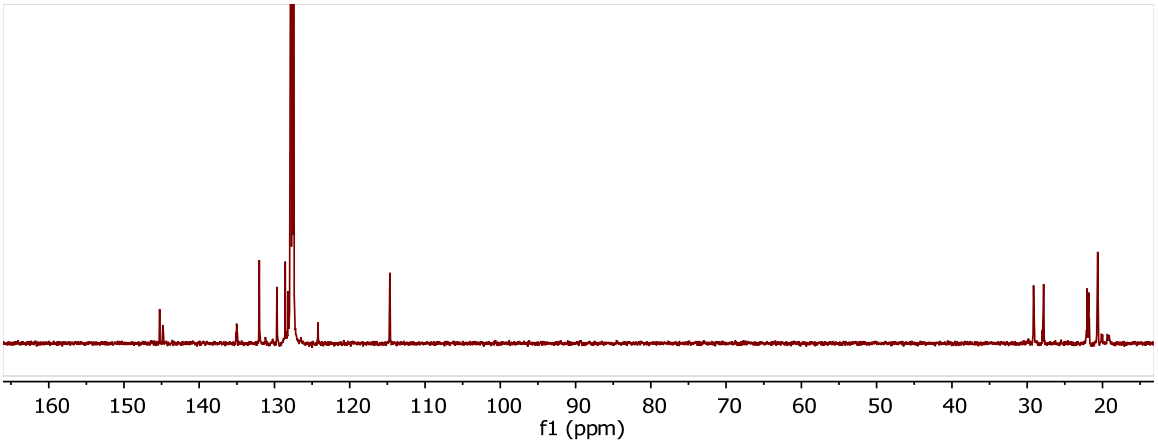

Figure 60. ^{13}C-NMR (126 MHz, C_6D_6) spectrum of **4-H**.

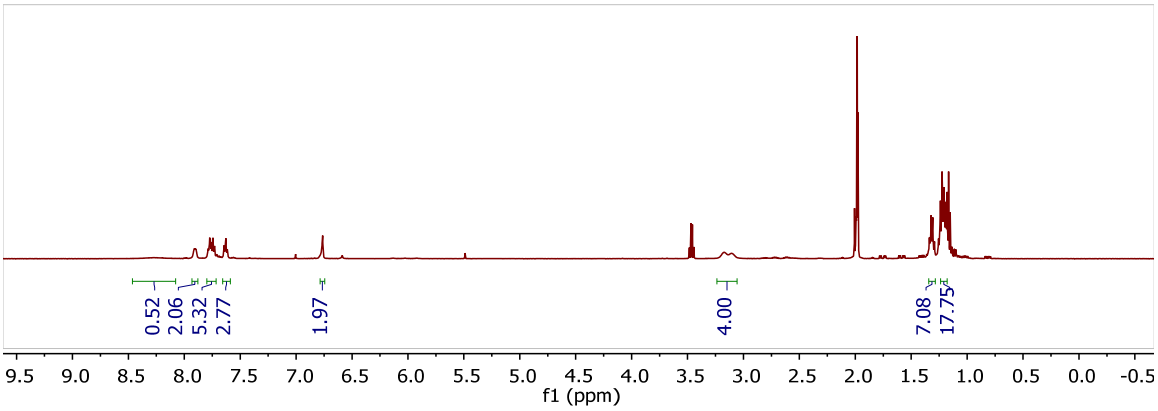

Figure 61. ^{1}H-NMR (500 MHz, CD_3CN) spectrum of **5-H**.

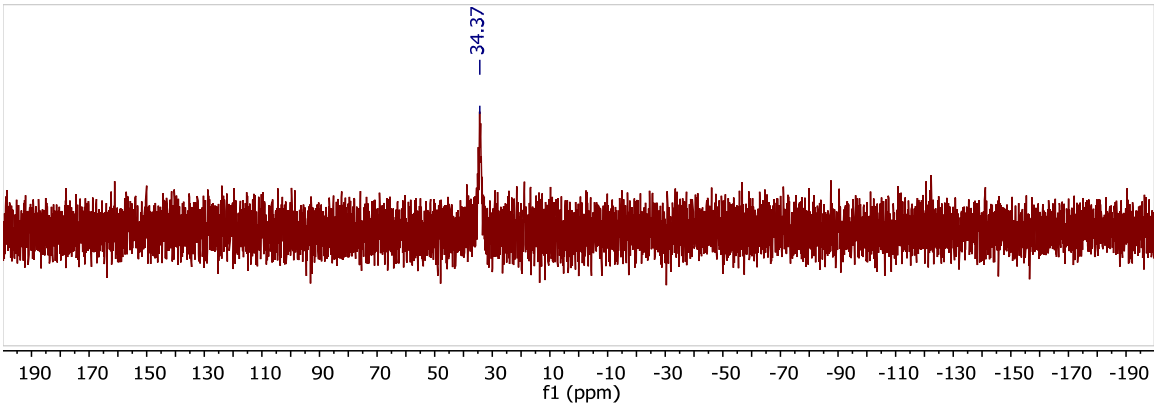

Figure 62. ^{31}P-NMR (121 MHz, CD_3CN) spectrum of **5-H**.

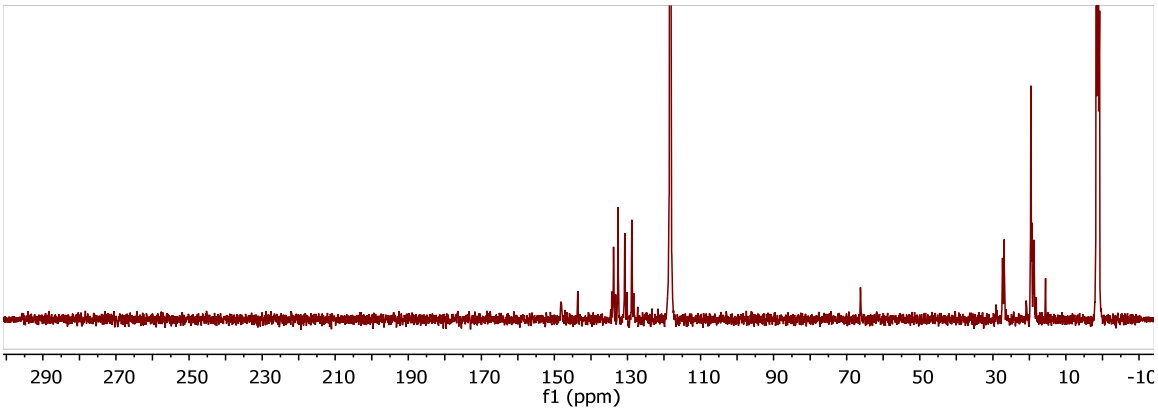

Figure 63. ^{13}C-NMR (126 MHz, CD_3CN) spectrum of **5-H**.

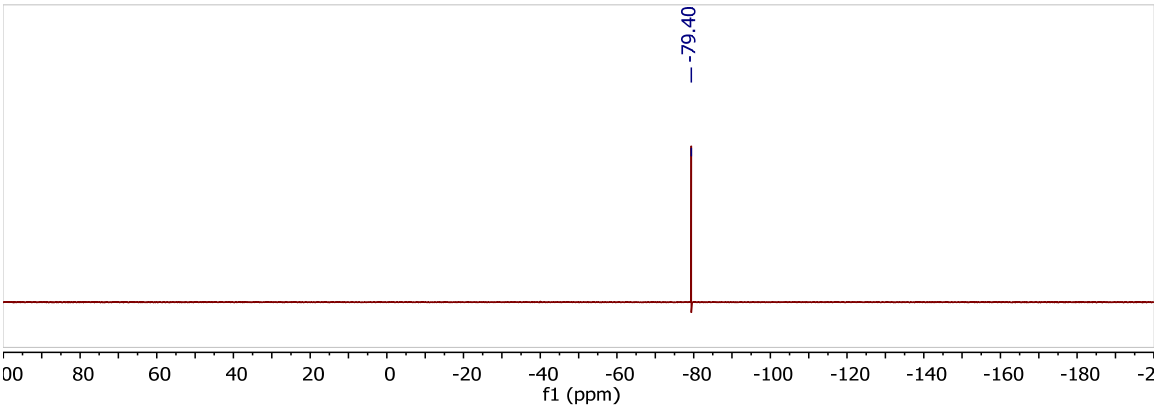

Figure 64. ^{19}F-NMR (282 MHz, CD_3CN) spectrum of **5-H**.

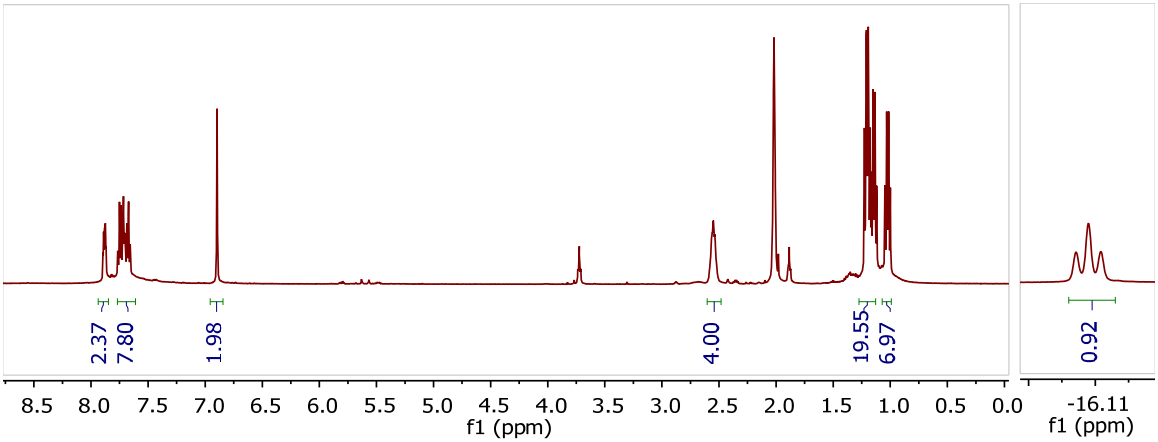

Figure 65. ^{1}H-NMR (500 MHz, CD_3CN) spectrum of **6-H**.

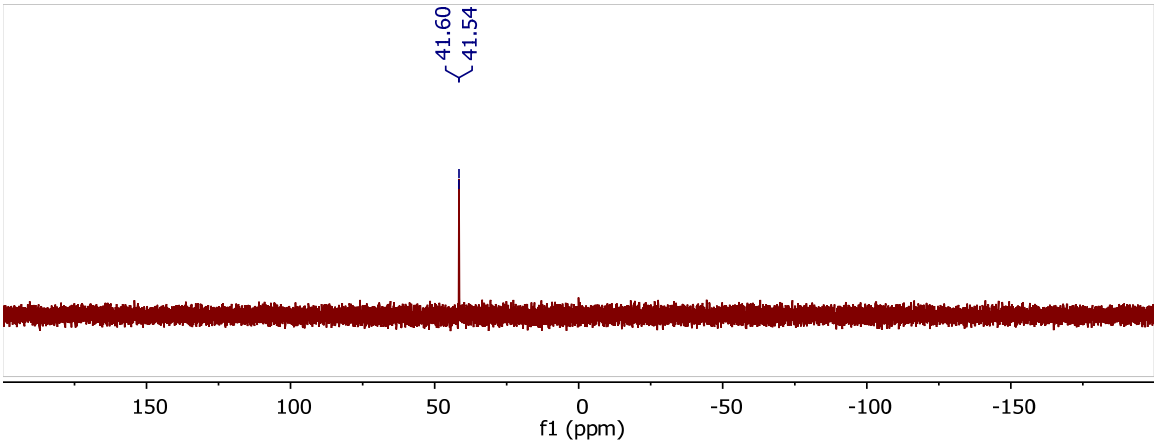

Figure 66. ^{31}P-NMR (121 MHz, CD_3CN) spectrum of **6-H**.

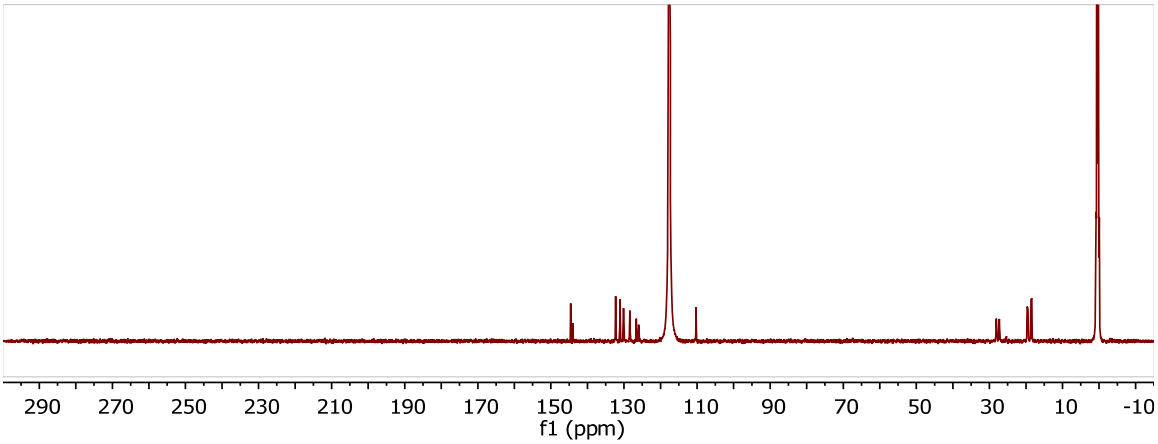

Figure 67. ^{13}C-NMR (126 MHz, CD_3CN) spectrum of **6-H**.

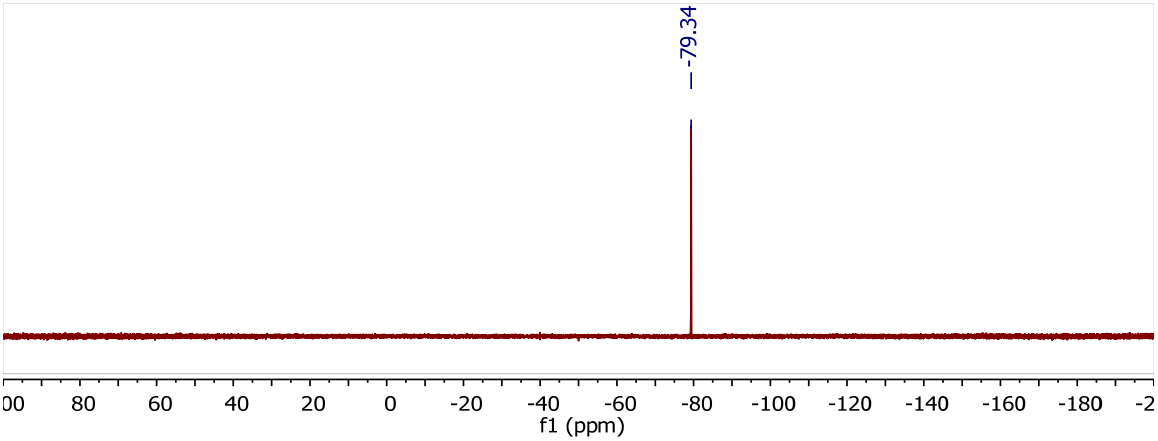

Figure 68. ^{19}F-NMR (282 MHz, CD_3CN) spectrum of **6-H**.

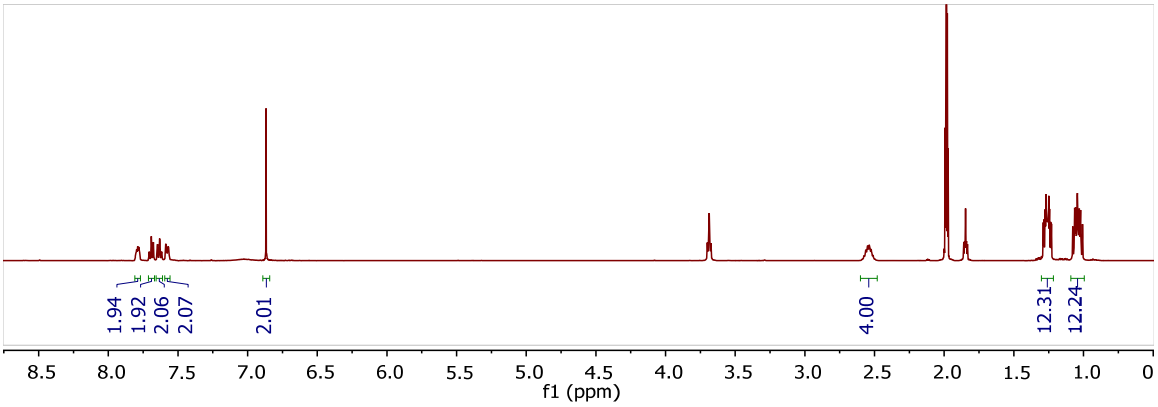

Figure 69. ^{1}H-NMR (500 MHz, CD_3CN) spectrum of **7-H**.

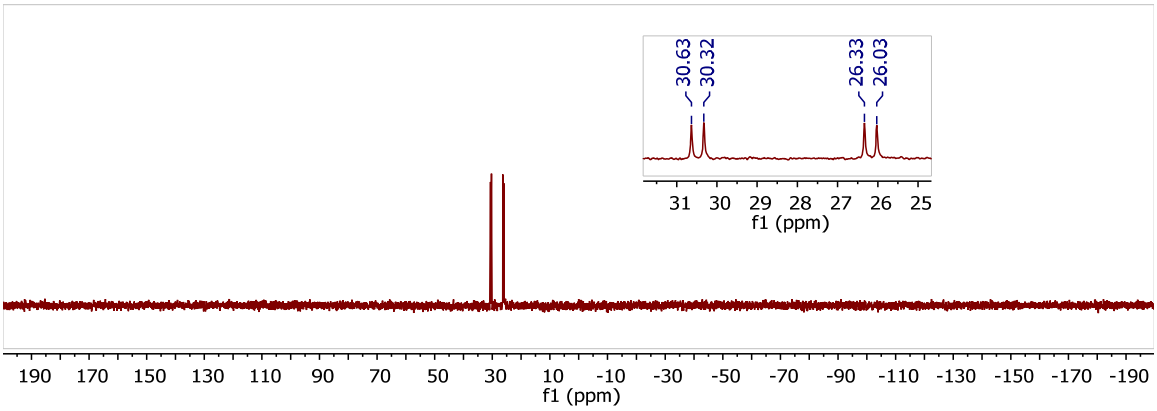

Figure 70. ^{31}P-NMR (121 MHz, CD_3CN) spectrum of **7-H**.

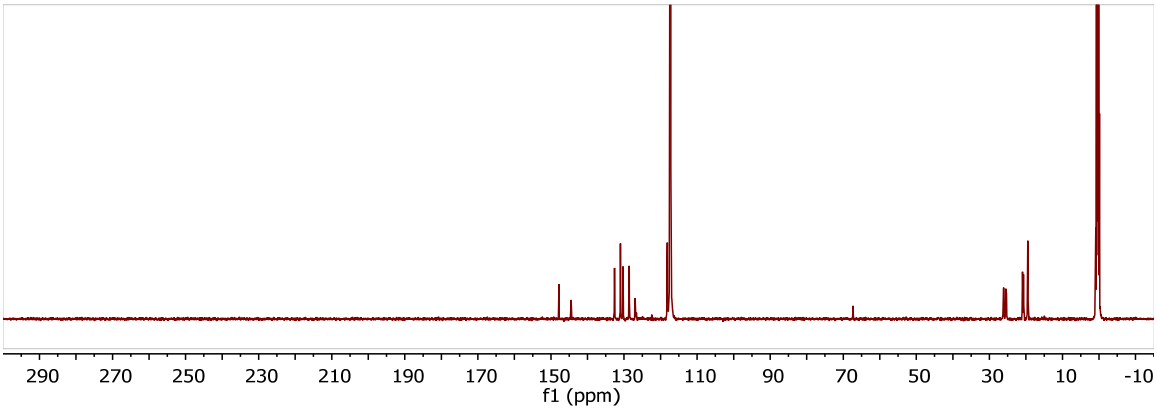

Figure 71. ^{13}C-NMR (126 MHz, CD_3CN) spectrum of **7-H**.

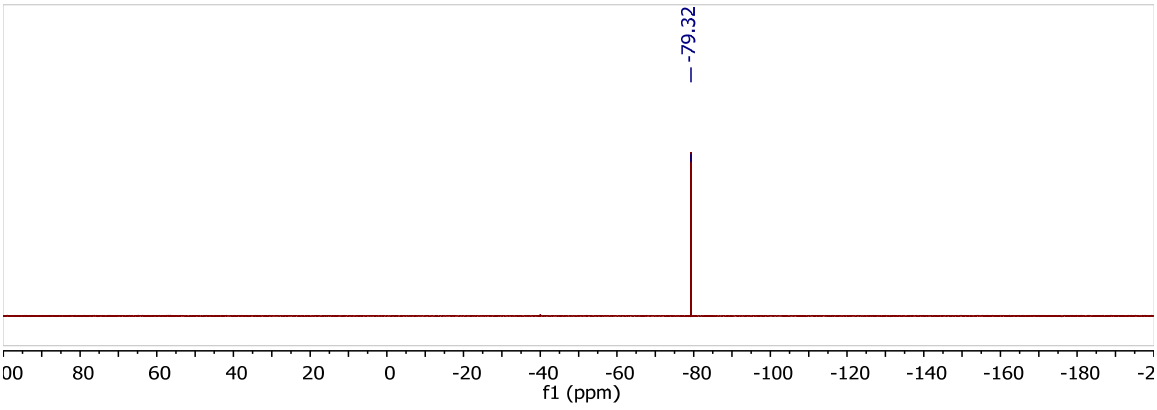

Figure 72. ^{19}F-NMR (282 MHz, CD_3CN) spectrum of **7-H**.

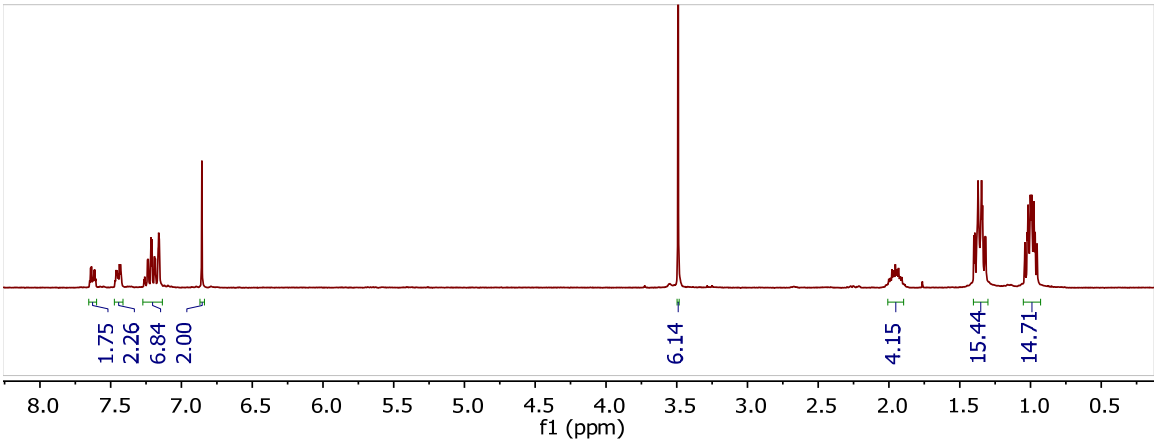

Figure 73. ^{1}H-NMR (500 MHz, C_6D_6) spectrum of **4-Me**.

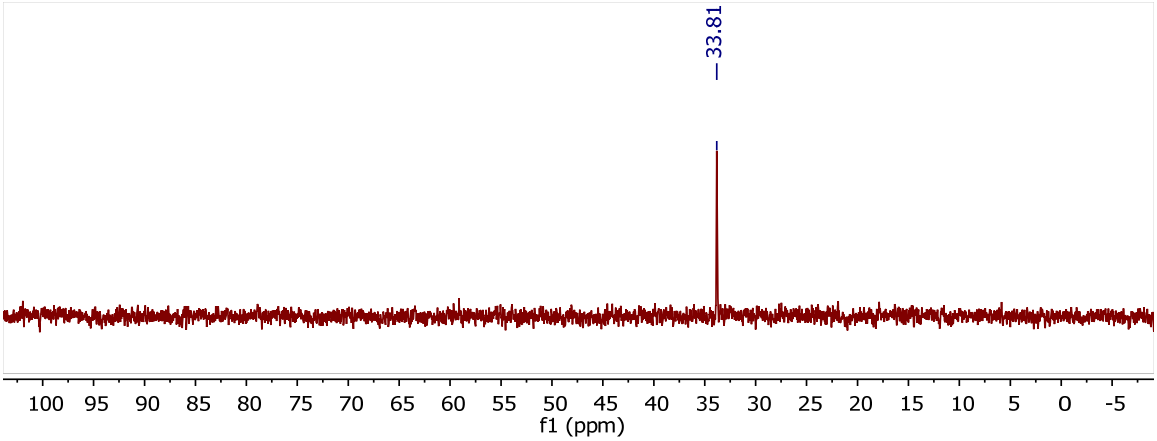

Figure 74. ^{31}P-NMR (121 MHz, C_6D_6) spectrum of **4-Me**.

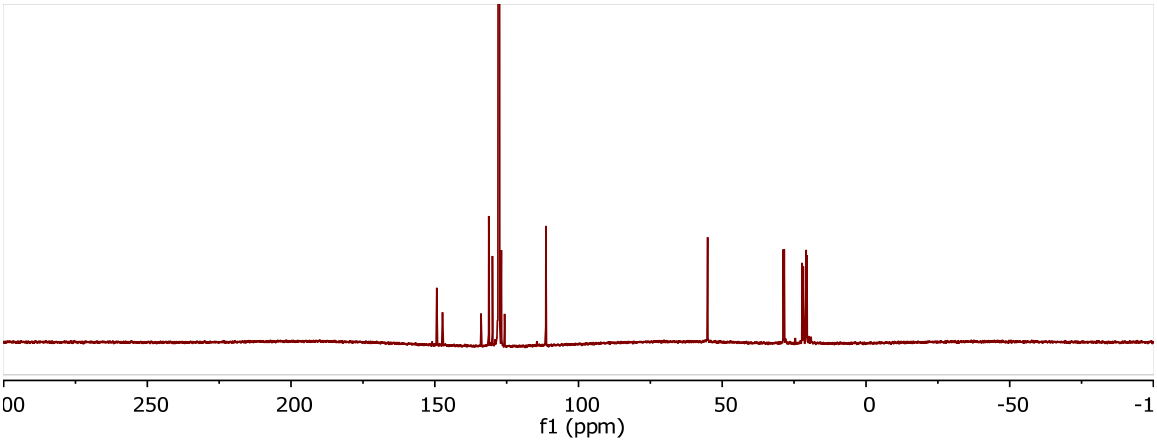

Figure 75. ^{13}C-NMR (126 MHz, C_6D_6) spectrum of **4-Me**.

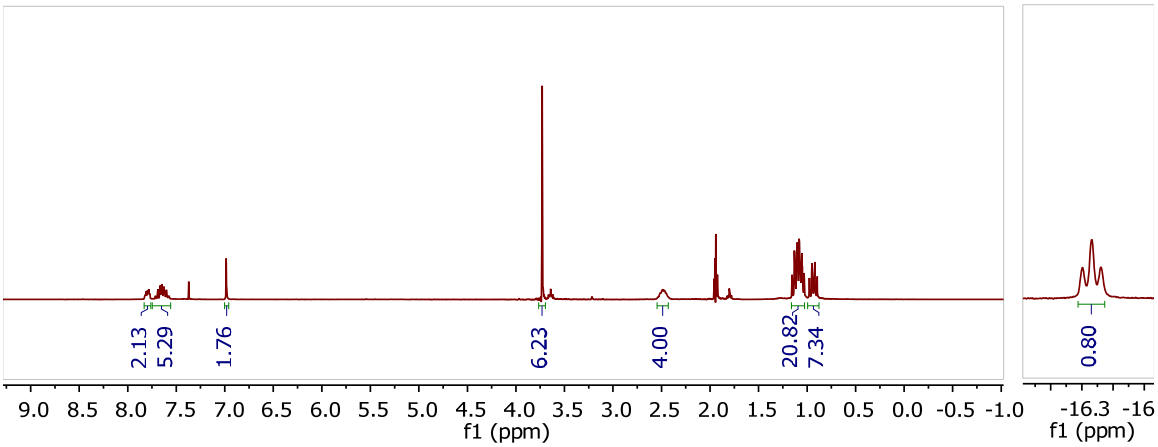

Figure 76. ^{1}H-NMR (500 MHz, CD_3CN) spectrum of **6-Me**.

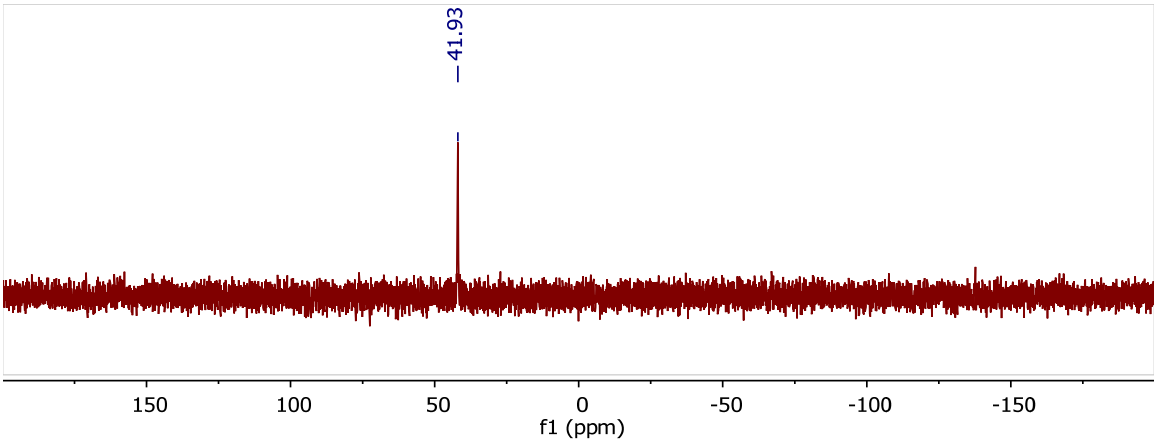

Figure 77. ^{31}P-NMR (121 MHz, CD_3CN) spectrum of **6-Me**.

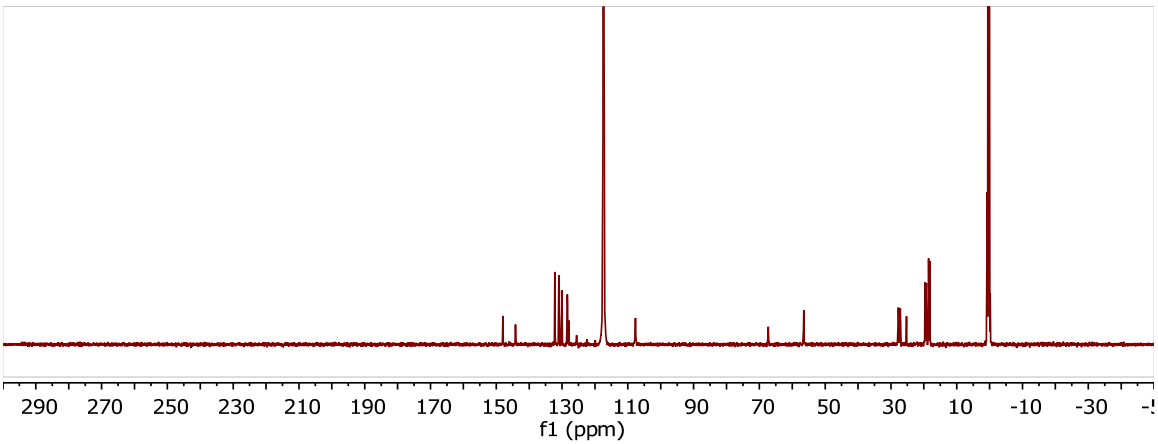

Figure 78. ^{13}C-NMR (126 MHz, CD_3CN) spectrum of **6-Me**.

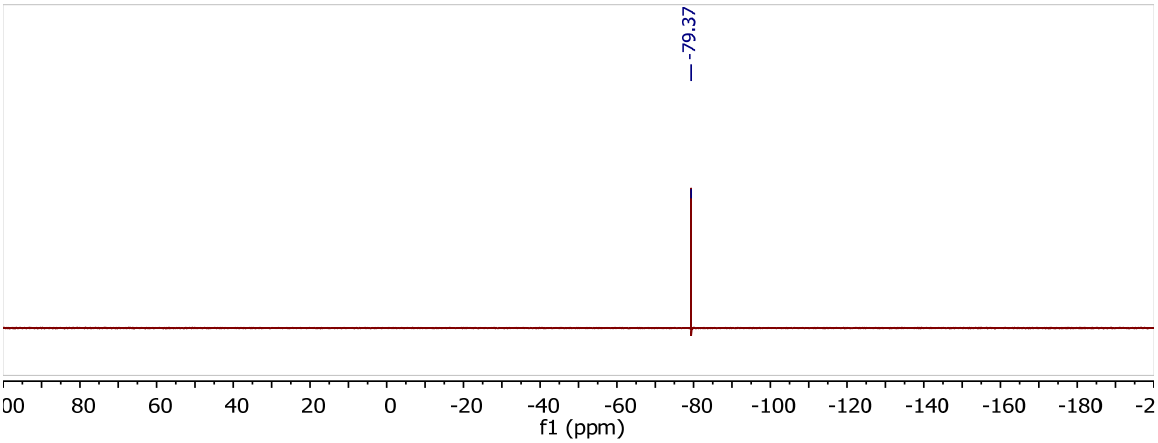

Figure 79. ^{19}F-NMR (282 MHz, CD_3CN) spectrum of **6-Me**.

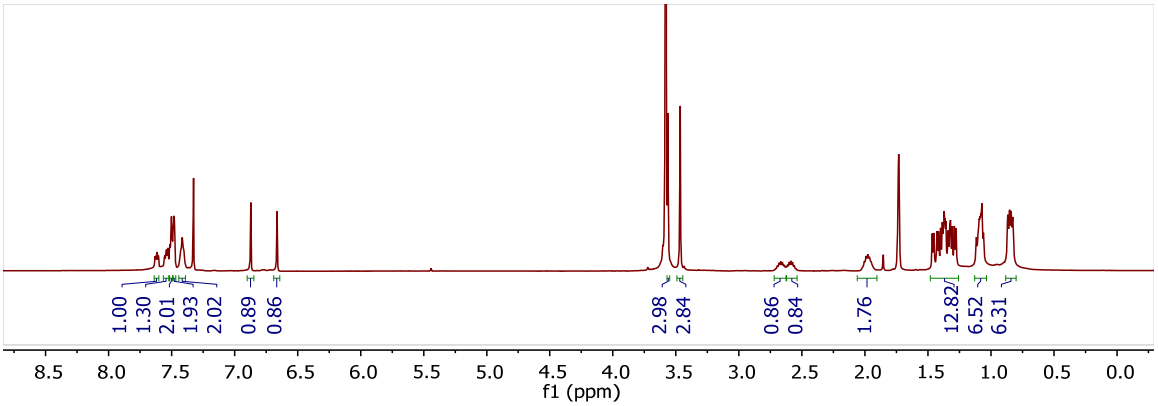

Figure 80. ^{1}H-NMR (500 MHz, d_8-THF) spectrum of **8-Me**.

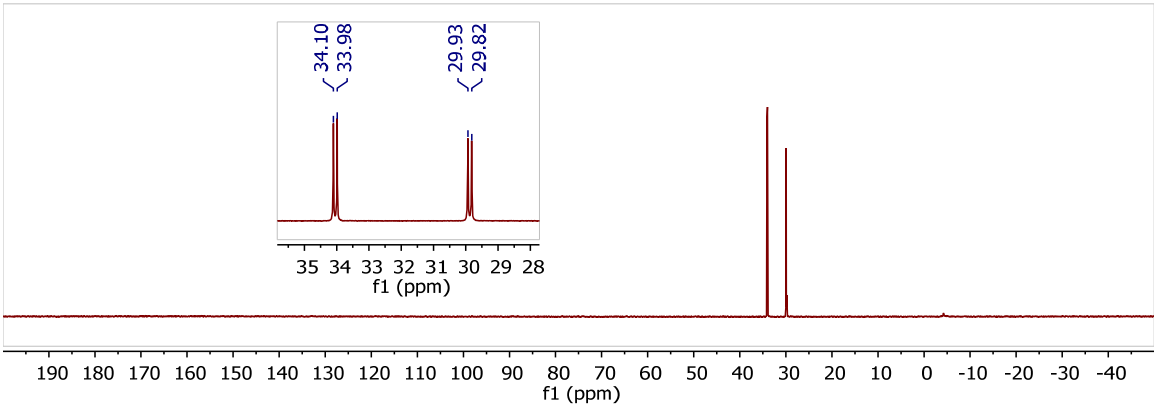

Figure 81. ^{31}P-NMR (202 MHz, d_8-THF) spectrum of **8-Me**.

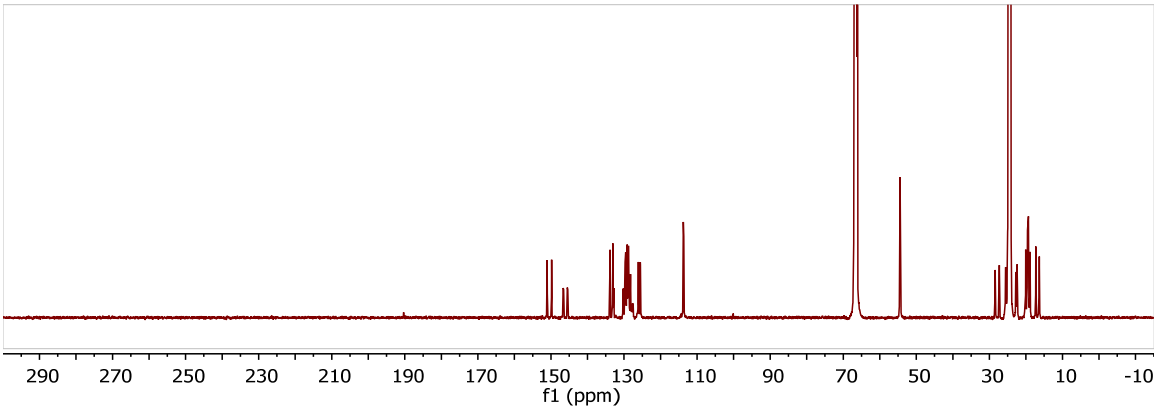

Figure 82. ^{13}C-NMR (126 MHz, d_8-THF) spectrum of **8-Me**.

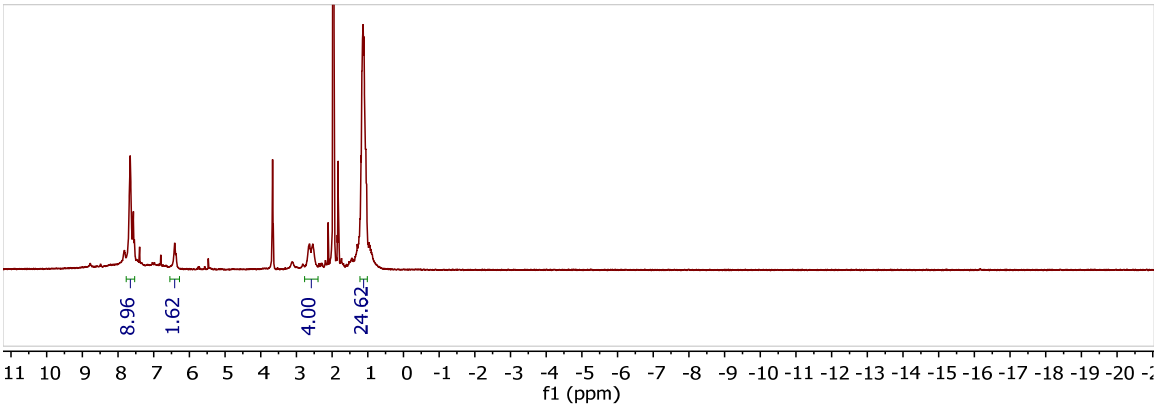

Figure 83. ^{1}H-NMR (300 MHz, d_8-THF) spectrum of **(3)H$^+$**.

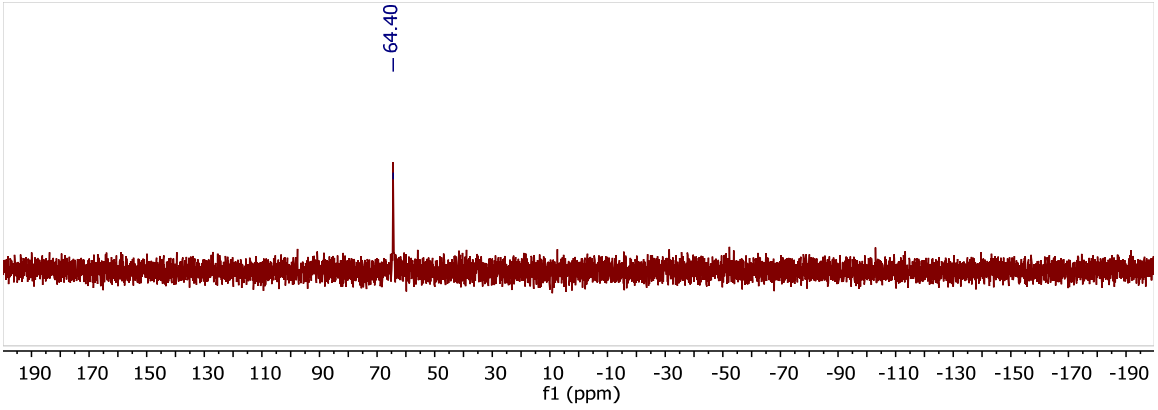

Figure 84. ^{31}P-NMR (202 MHz, d_8-THF) spectrum of **(3)H$^+$**.

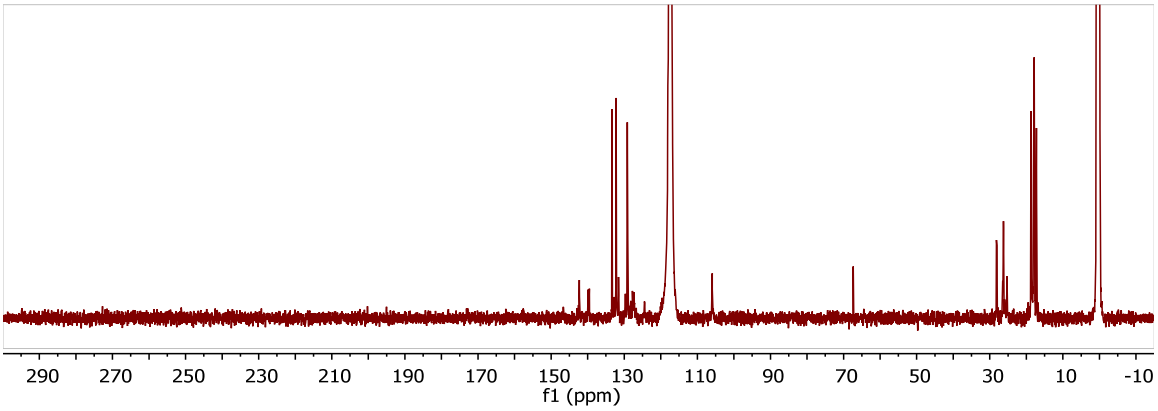

Figure 85. ^{13}C-NMR (126 MHz, d_8-THF) spectrum of **(3)H$^+$**.

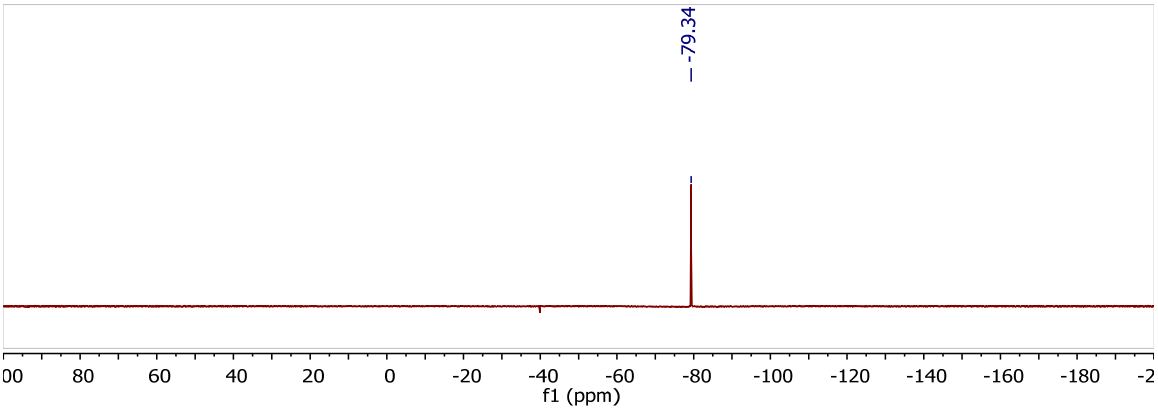

Figure 86. ^{19}F-NMR (282 MHz, CD_3CN) spectrum of **(3)H$^+$**.

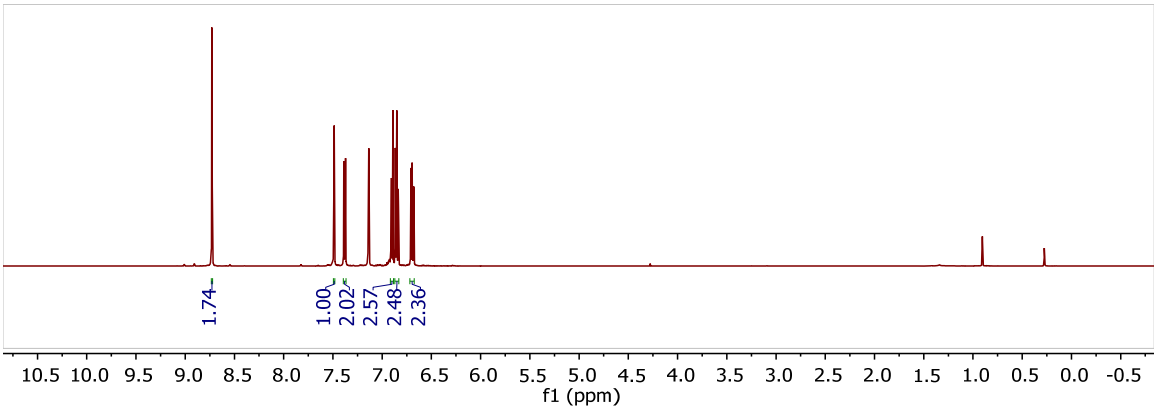

Figure 87. ^{1}H NMR (500 MHz, C_6D_6) spectrum of **mBr$_2$N**.

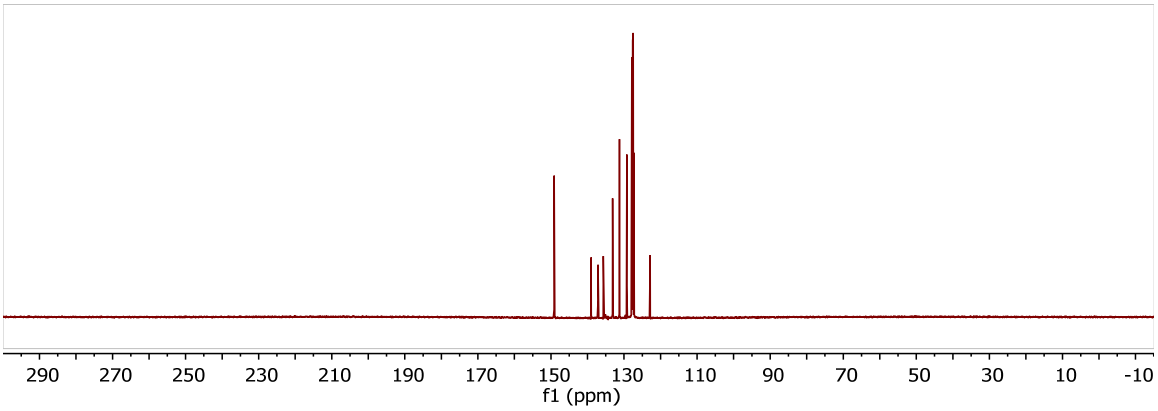

Figure 88. ^{13}C{^{1}H} NMR (126 MHz, C_6D_6) spectrum of **mBr$_2$N**.

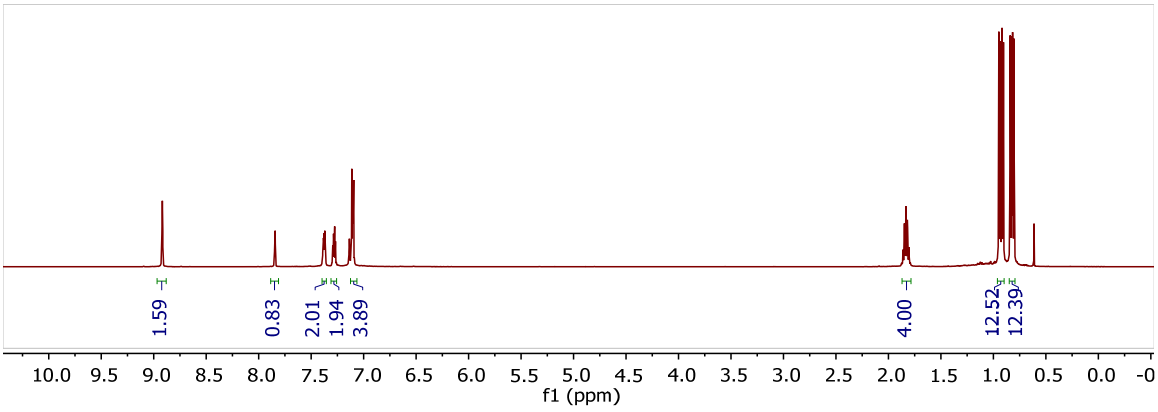

Figure 89. ^{1}H NMR (500 MHz, C_6D_6) spectrum of **1**.

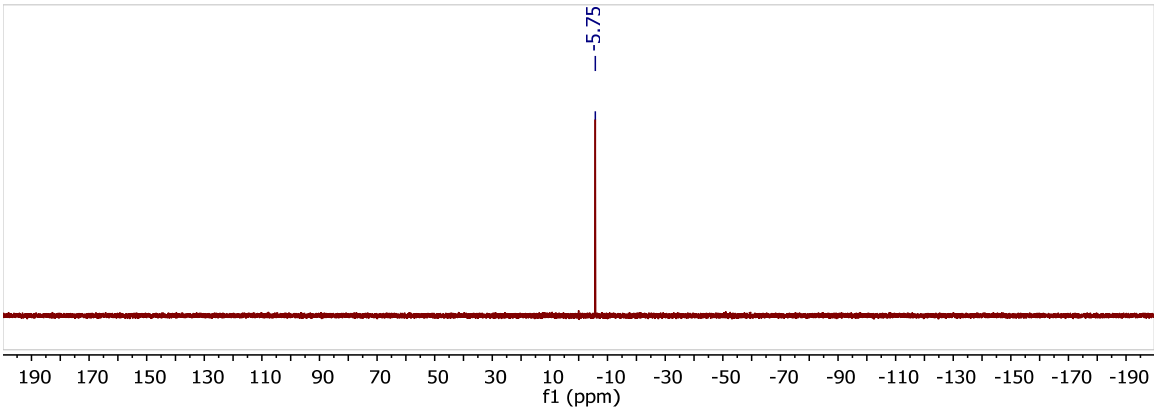

Figure 90. $^{31}P\{^{1}H\}$ NMR (121 MHz, C_6D_6) spectrum of **1**.

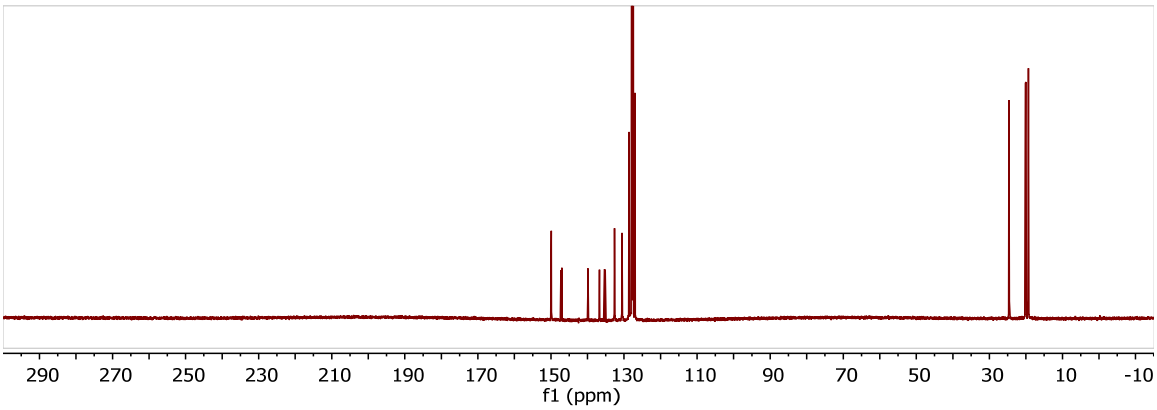

Figure 91. $^{13}C\{^{1}H\}$ NMR (126 MHz, C_6D_6) spectrum of **1**.

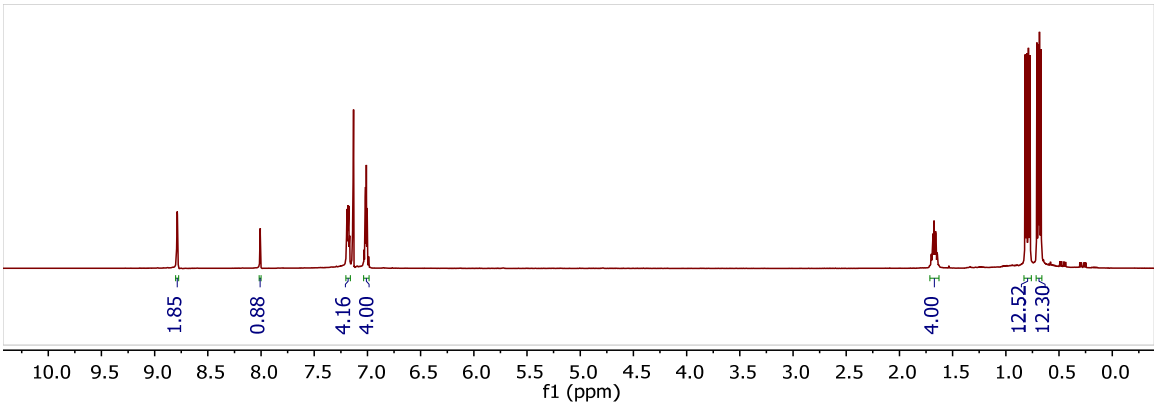

Figure 92. ^{1}H NMR (500 MHz, C_6D_6) spectrum of **1-B(C_6F_5)$_3$**.

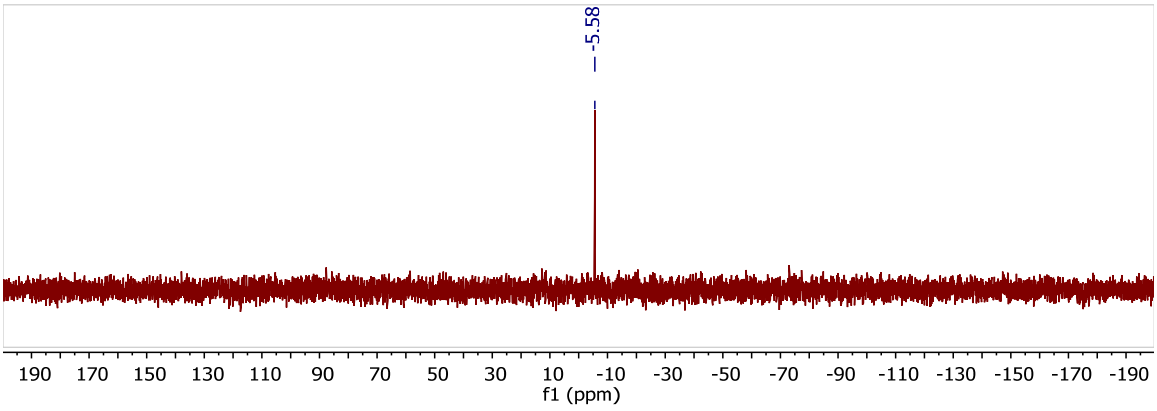

Figure 93. $^{31}P\{^{1}H\}$ NMR (121 MHz, C_6D_6) spectrum of **1-B(C_6F_5)$_3$**.

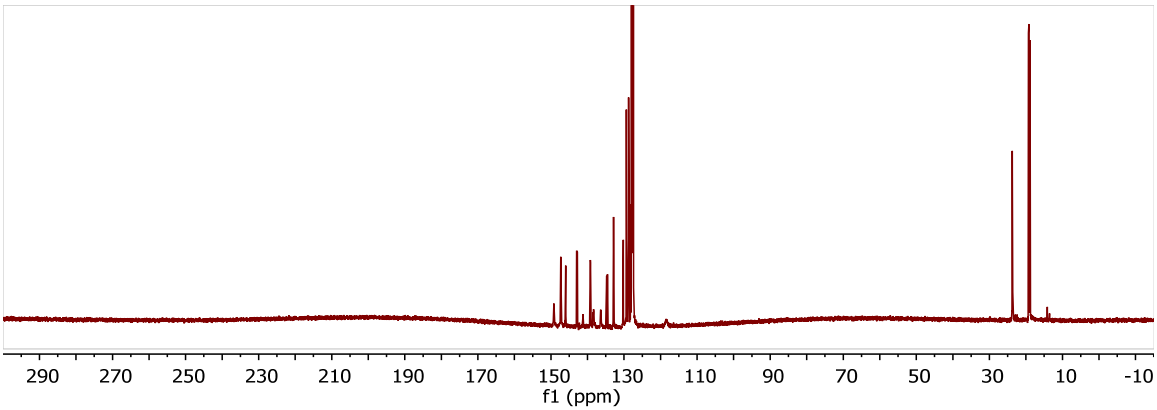

Figure 94. $^{13}C\{^{1}H\}$ NMR (126 MHz, C_6D_6) spectrum of **1-B(C_6F_5)$_3$**.

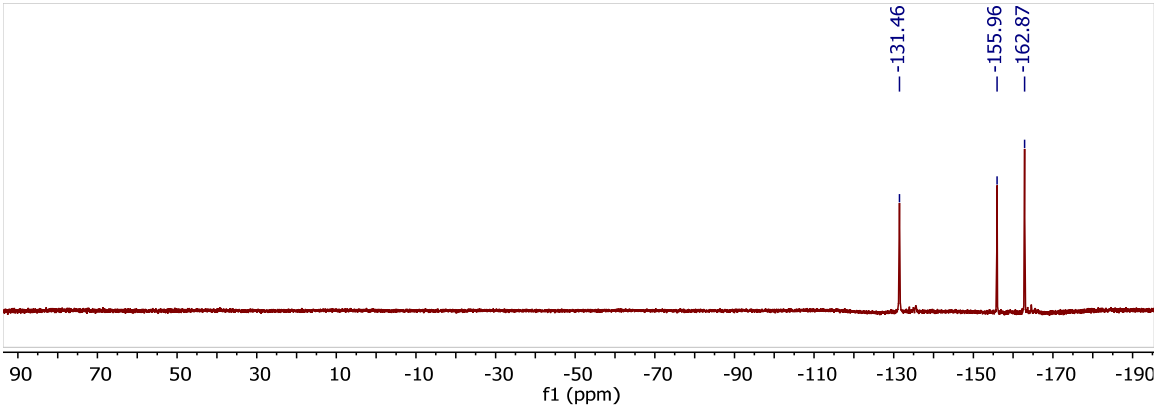

Figure 95. ^{19}F NMR (282 MHz, C_6D_6) spectrum of **1-B(C_6F_5)$_3$**.

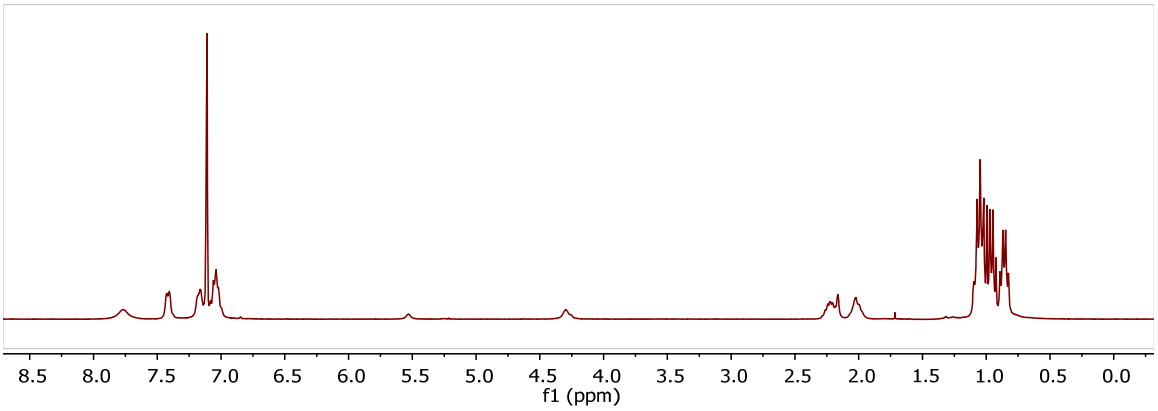

Figure 96. ^{1}H NMR (300 MHz, C_6D_6) spectrum of **2Ni**.

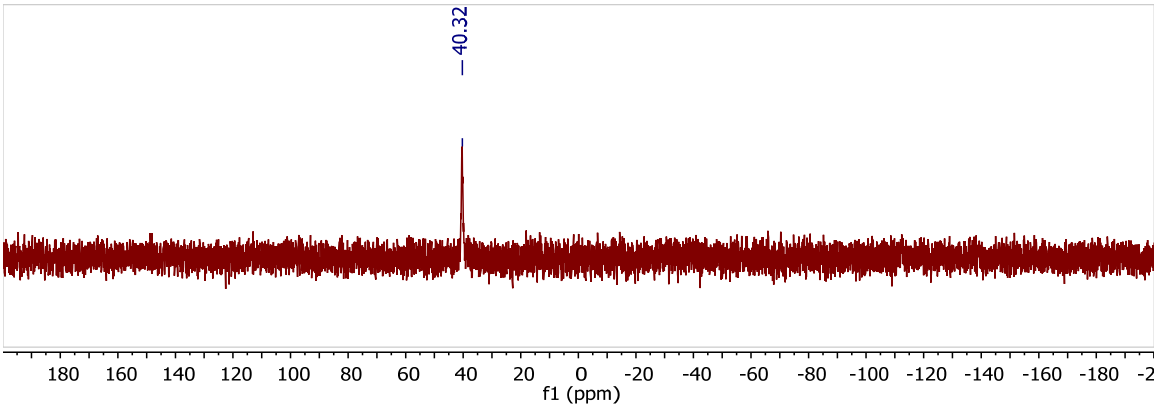

Figure S97. ^{31}P{^{1}H} NMR (121 MHz, C_6D_6) spectrum of **2Ni**.

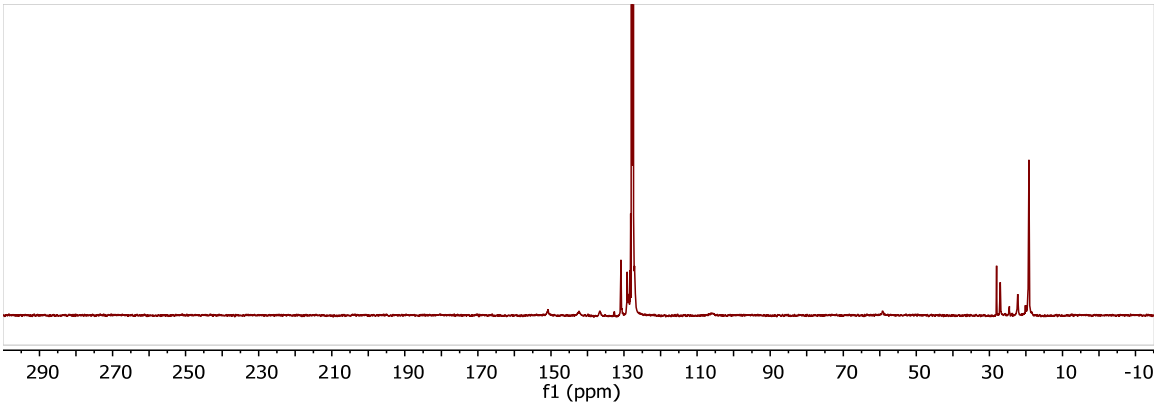

Figure 98. ^{13}C{^{1}H} NMR (126 MHz, C_6D_6) spectrum of **2Ni**.

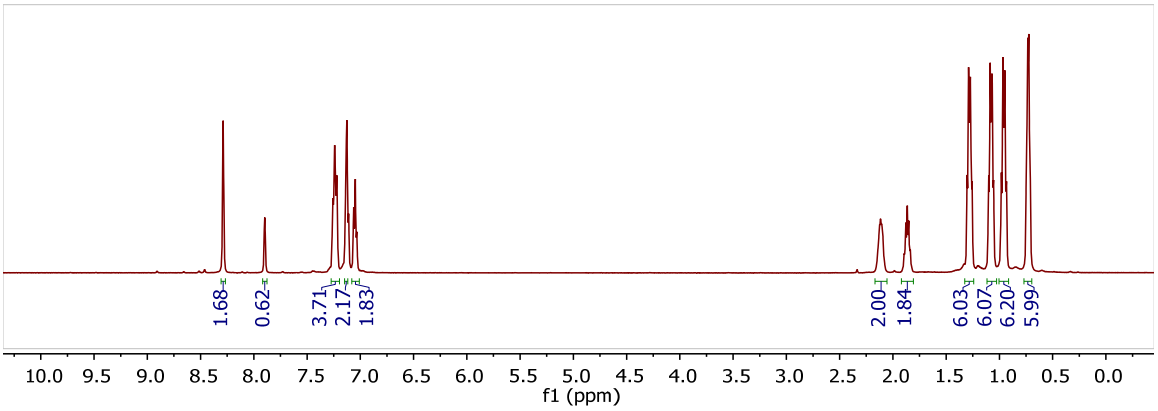

Figure 99. ^{1}H NMR (500 MHz, C_6D_6) spectrum of **2Pd**.

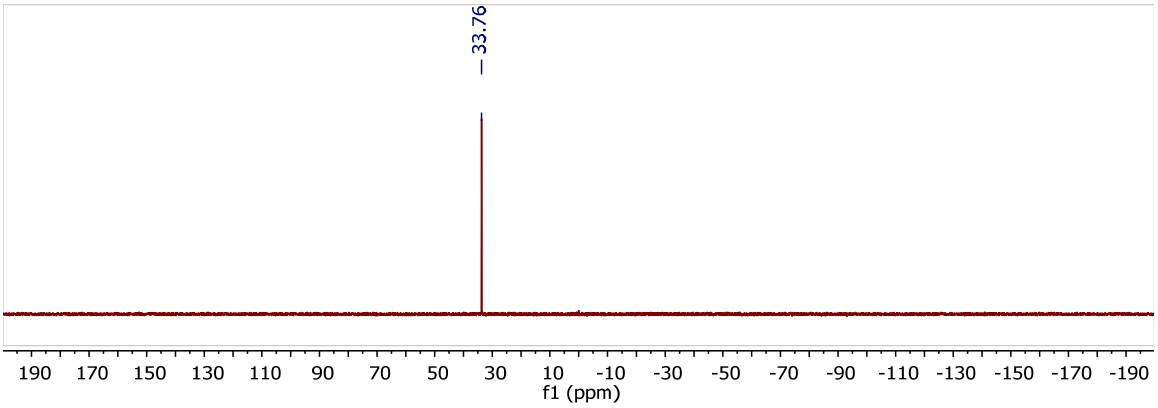

Figure 100. ^{31}P{^{1}H} NMR (121 MHz, C_6D_6) spectrum of **2Pd**.

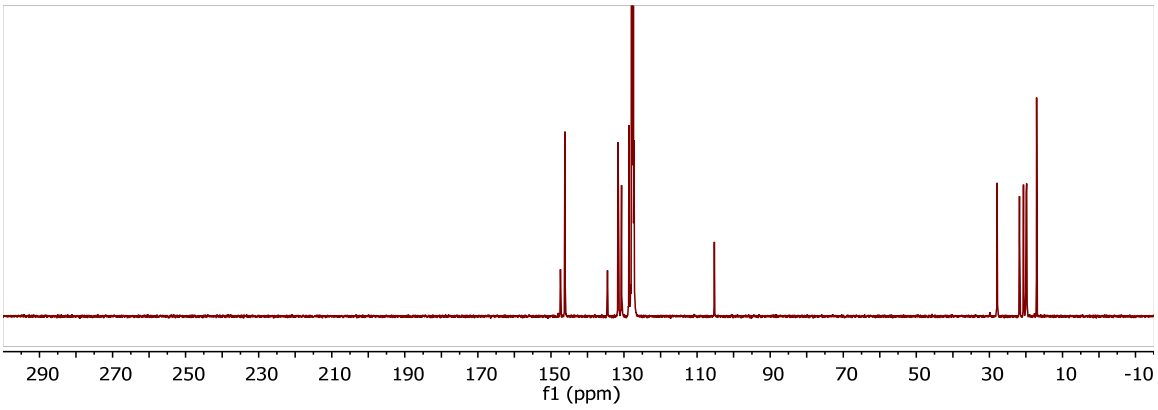

Figure 101. ^{13}C{^{1}H} NMR (126 MHz, C_6D_6) spectrum of **2Pd**.

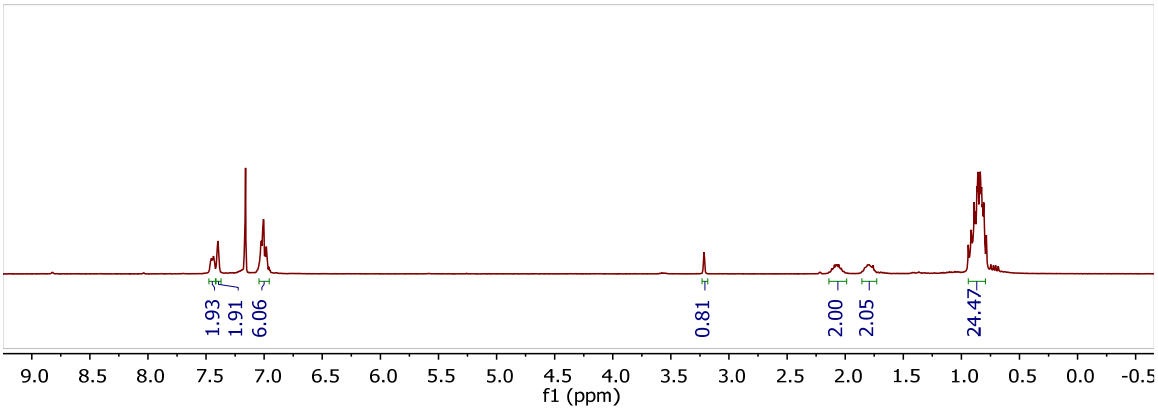

Figure 102. ^{1}H NMR (300 MHz, C_6D_6) spectrum of **2Ni-B(C_6F_5)$_3$**.

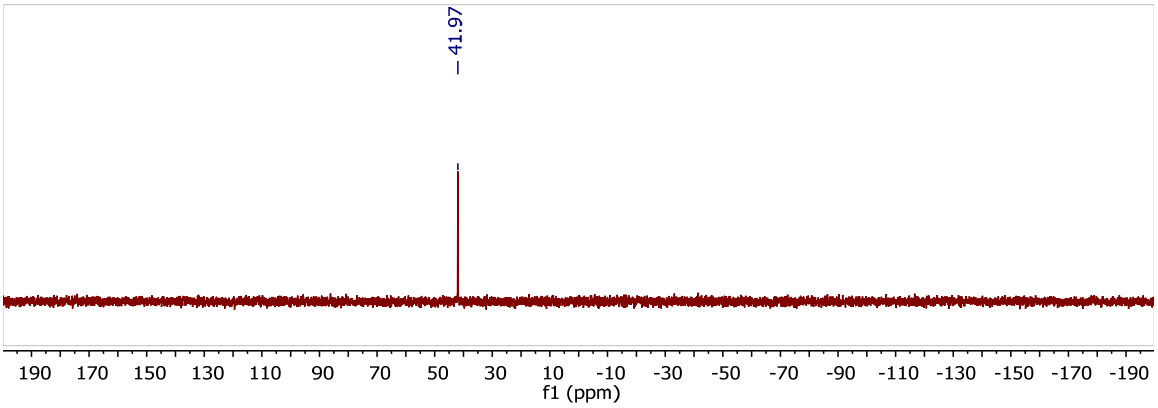

Figure 103. ^{31}P{^{1}H} NMR (121 MHz, C_6D_6) spectrum of **2Ni-B(C_6F_5)$_3$**.

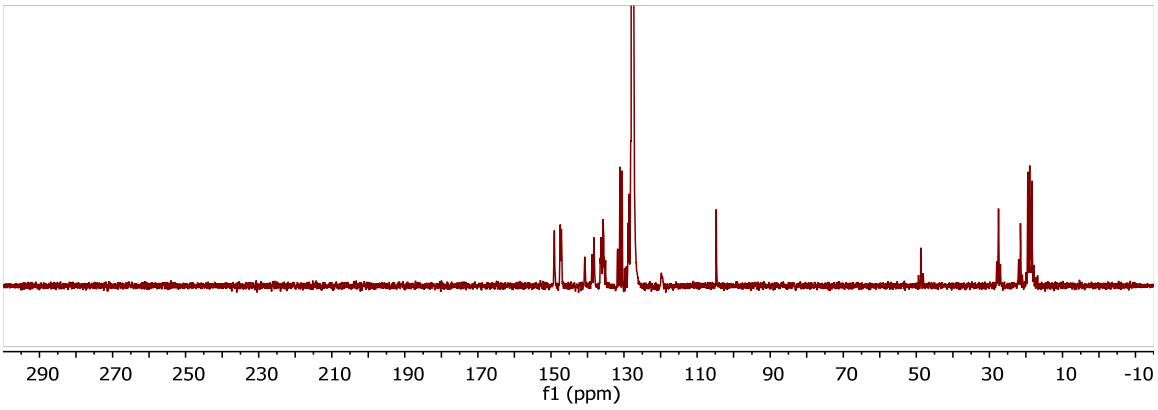

Figure 104. ^{13}C{^{1}H} NMR (126 MHz, C_6D_6) spectrum of **2Ni-B(C_6F_5)$_3$**.

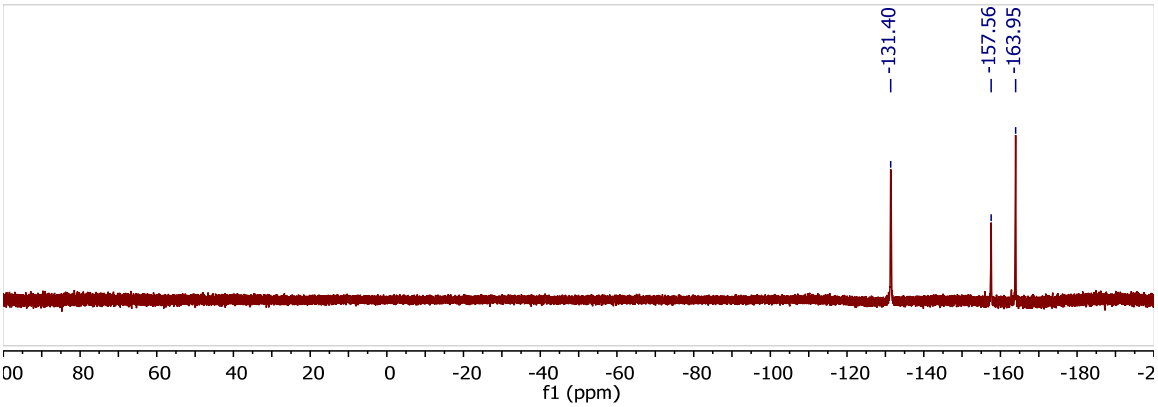

Figure 105. $^{19}F\{^{1}H\}$ NMR (282 MHz, C_6D_6) spectrum of **2Ni-B(C_6F_5)$_3$**.

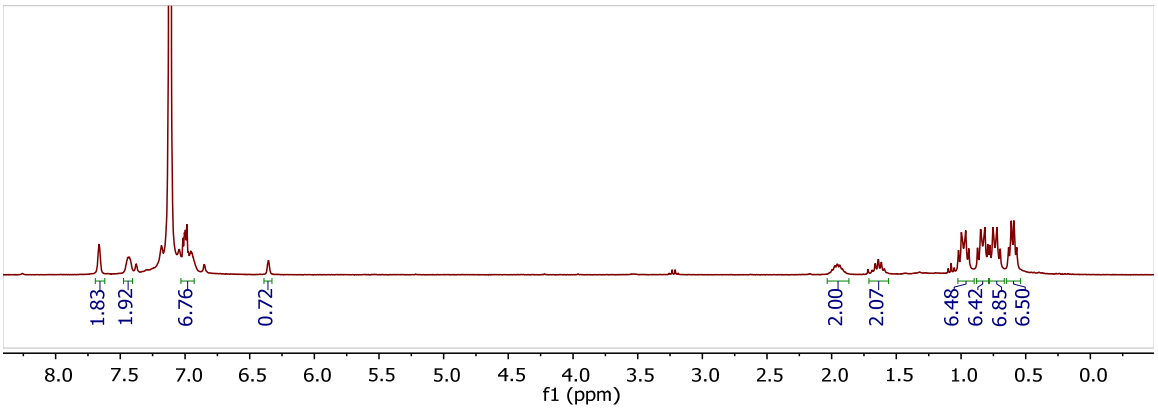

Figure 106. ^{1}H NMR (500 MHz, C_6D_6) spectrum of **2Pd-B(C_6F_5)$_3$**.

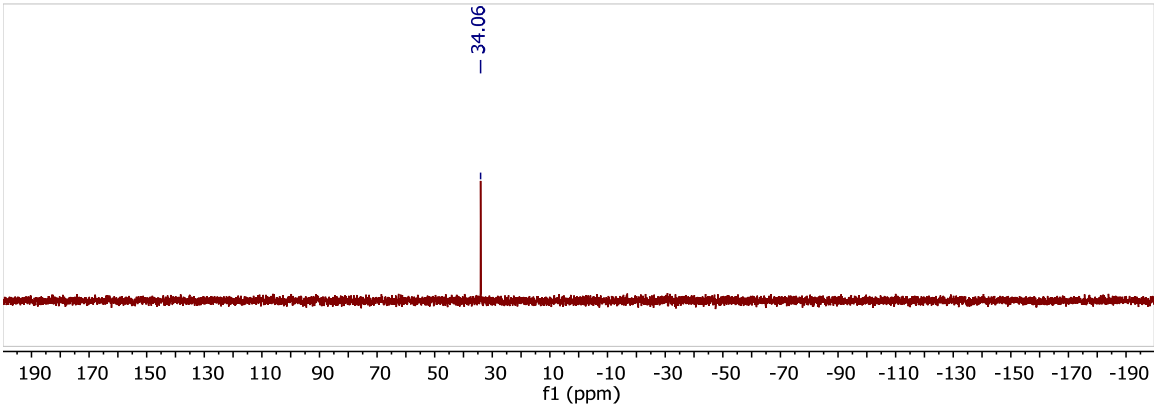

Figure 107. $^{31}P\{^{1}H\}$ NMR (121 MHz, C_6D_6) spectrum of **2Pd-B(C_6F_5)$_3$**.

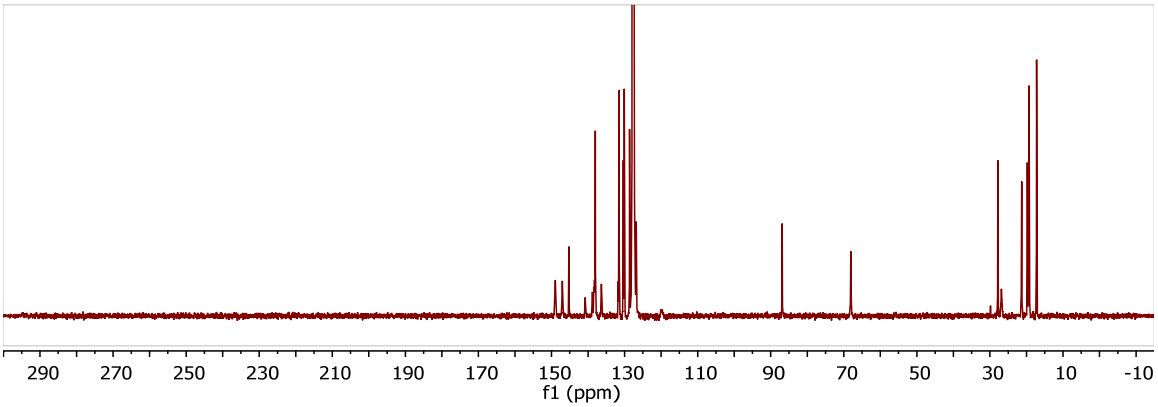

Figure 108. $^{13}C\{^{1}H\}$ NMR (126 MHz, C_6D_6) spectrum of **2Pd-B(C_6F_5)$_3$**.

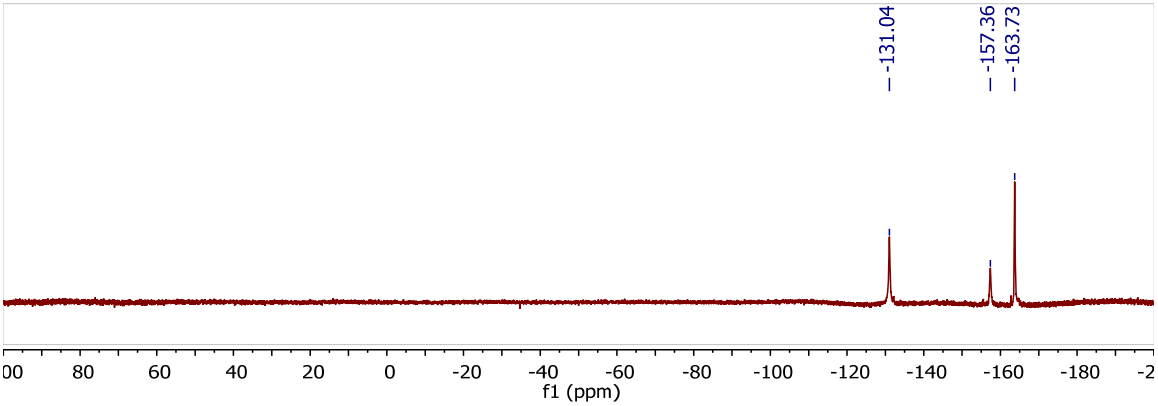

Figure 109. ^{19}F NMR (282 MHz, C_6D_6) spectrum of **2Pd-B(C_6F_5)$_3$**.

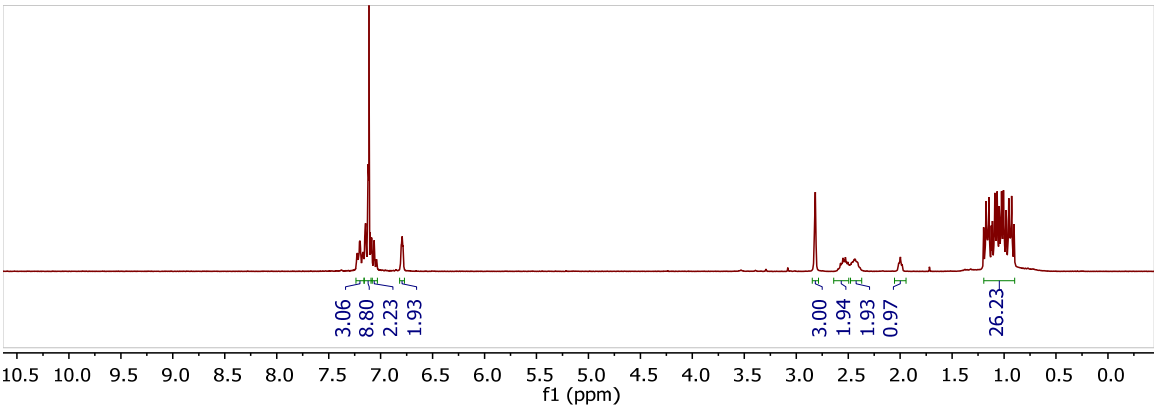

Figure 110. ^{1}H NMR (300 MHz, C_6D_6) spectrum of **2Ni-Me**.

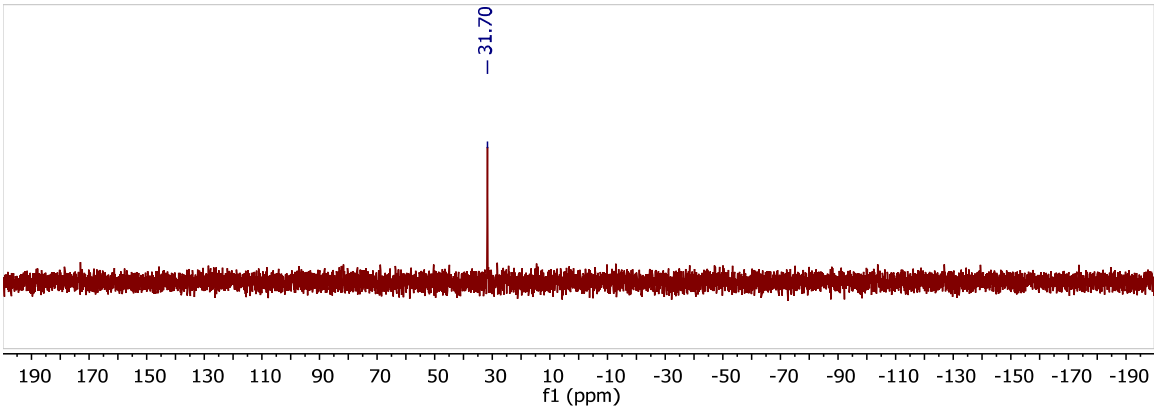

Figure 111. $^{31}P\{^{1}H\}$ NMR (121 MHz, C_6D_6) spectrum of **2Ni-Me**.

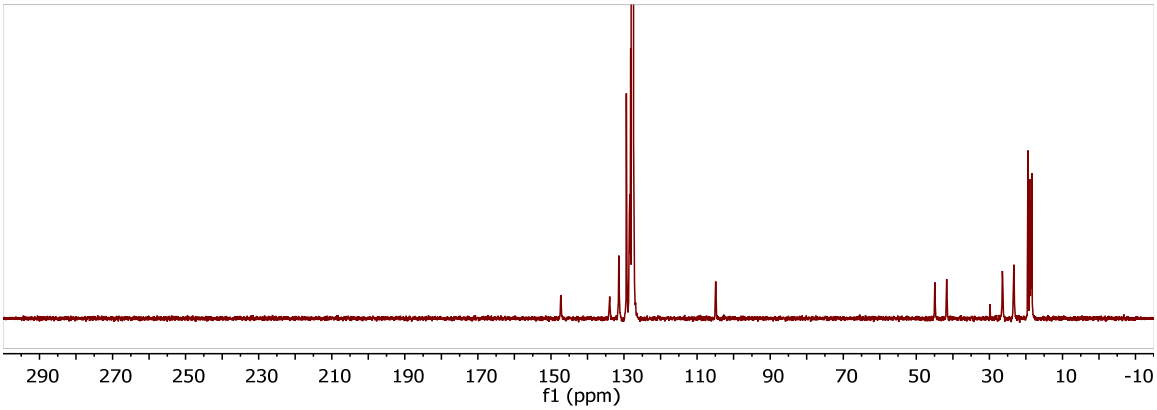

Figure 112. $^{13}C\{^{1}H\}$ NMR (126 MHz, C_6D_6) spectrum of **2Ni-Me**.

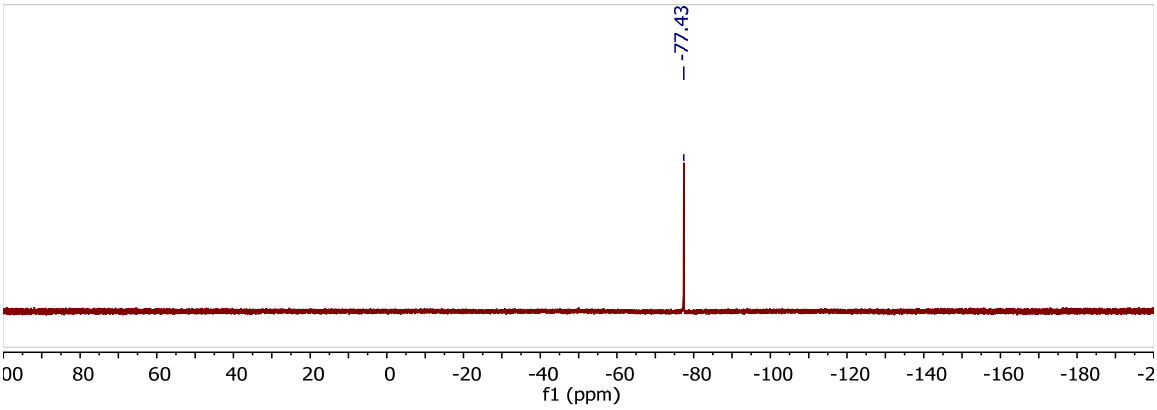

Figure 113. ^{19}F NMR (282 MHz, C_6D_6) spectrum of **2Ni-Me**.

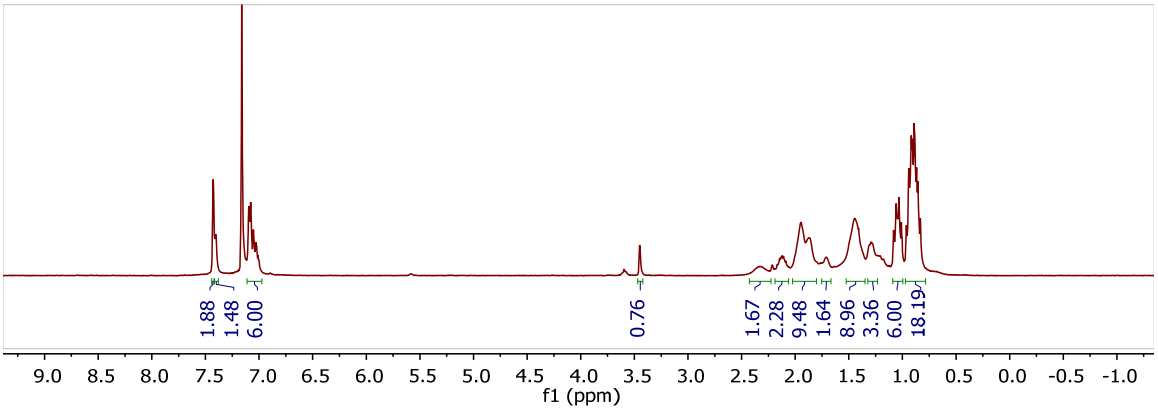

Figure 114 ^{1}H NMR (300 MHz, C_6D_6) spectrum of **2Ni-BCy$_2$OTf**.

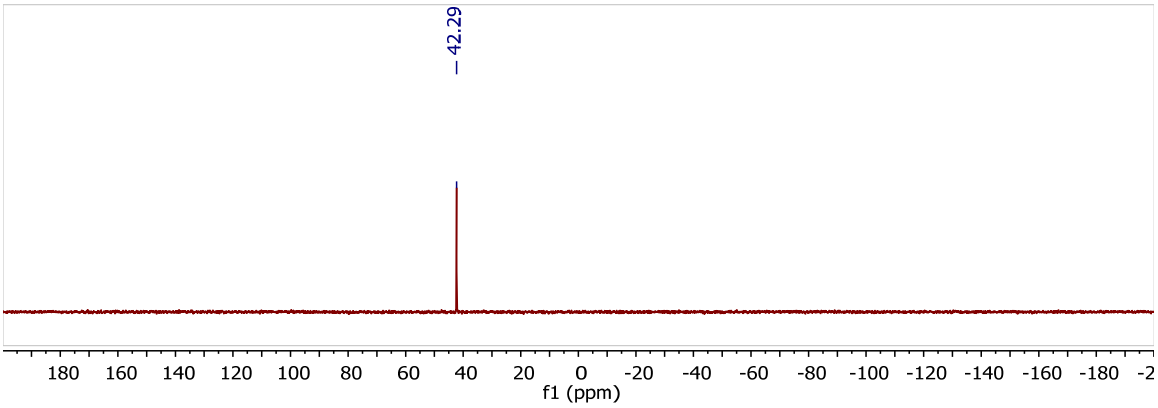

Figure 115. ^{31}P{^{1}H} NMR (121 MHz, C_6D_6) spectrum of **2Ni-BCy$_2$OTf**.

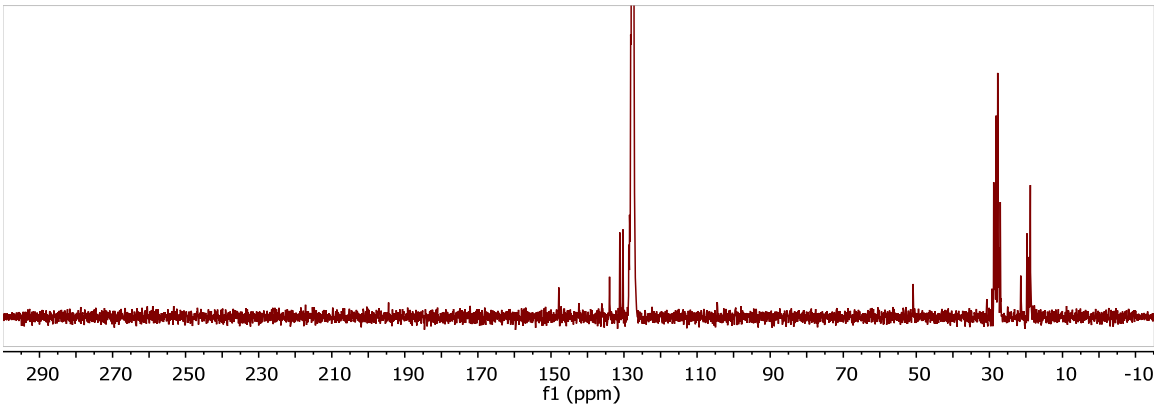

Figure 116. ^{13}C{^{1}H} NMR (126 MHz, C_6D_6) spectrum of **2Ni-BCy$_2$OTf**.

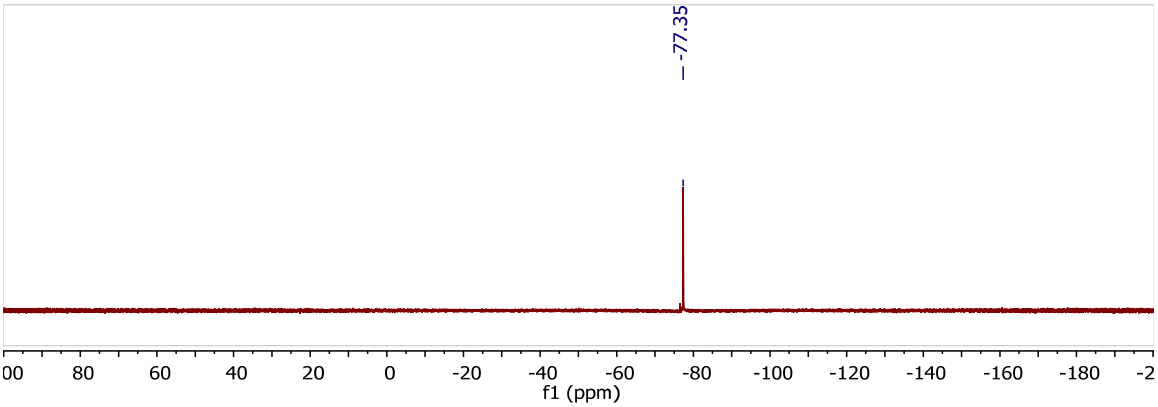

Figure 117. ^{19}F NMR (282 MHz, C_6D_6) spectrum of **2Ni-BCy$_2$OTf**.

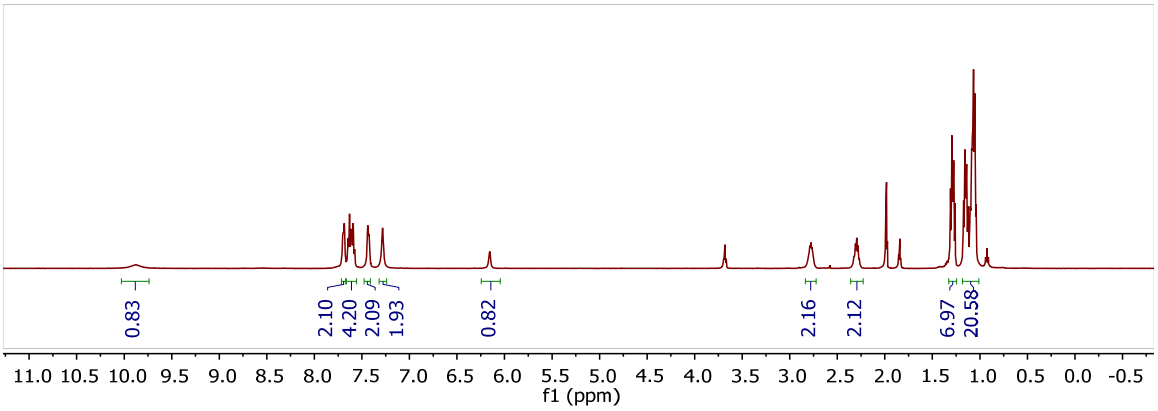

Figure 118. ^{1}H NMR (500 MHz, CD_3CN) spectrum of **2Pd-H**.

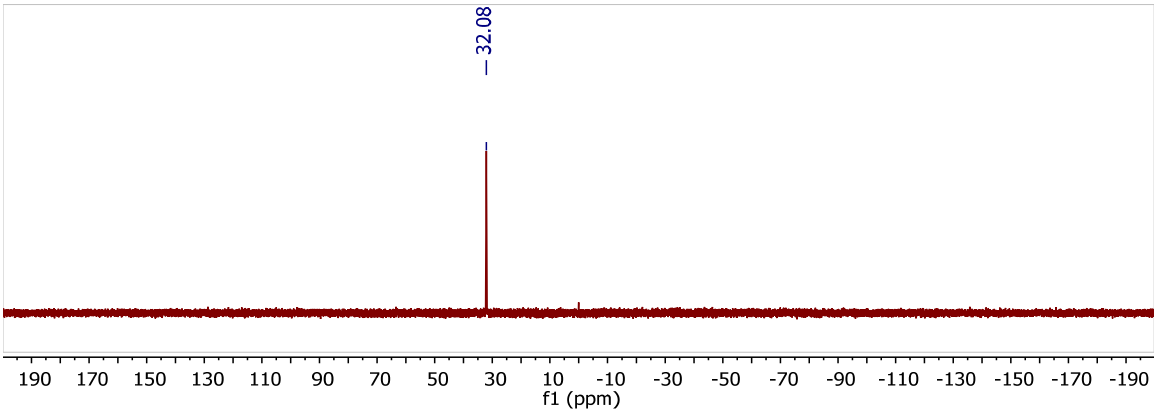

Figure 119. $^{31}P\{^{1}H\}$ NMR (121 MHz, CD_3CN) spectrum of **2Pd-H**.

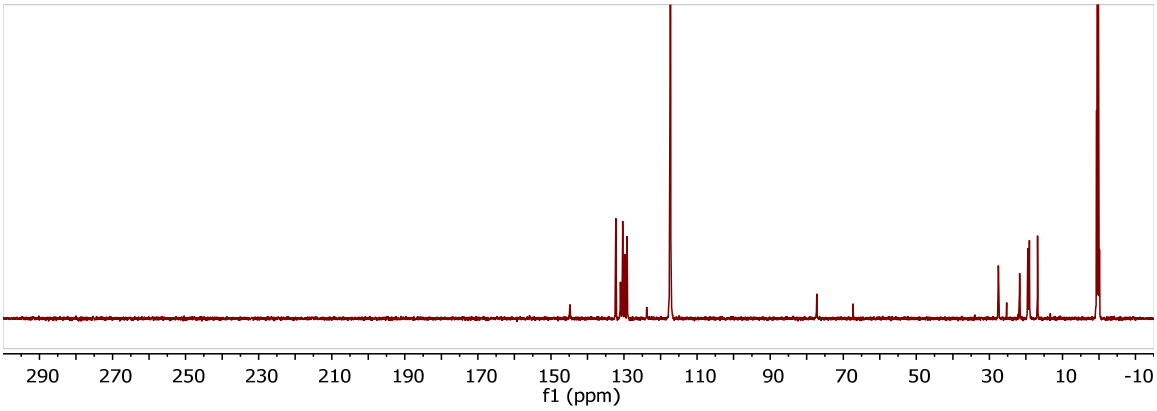

Figure 120. $^{13}C\{^{1}H\}$ NMR (126 MHz, CD_3CN) spectrum of **2Pd-H**.

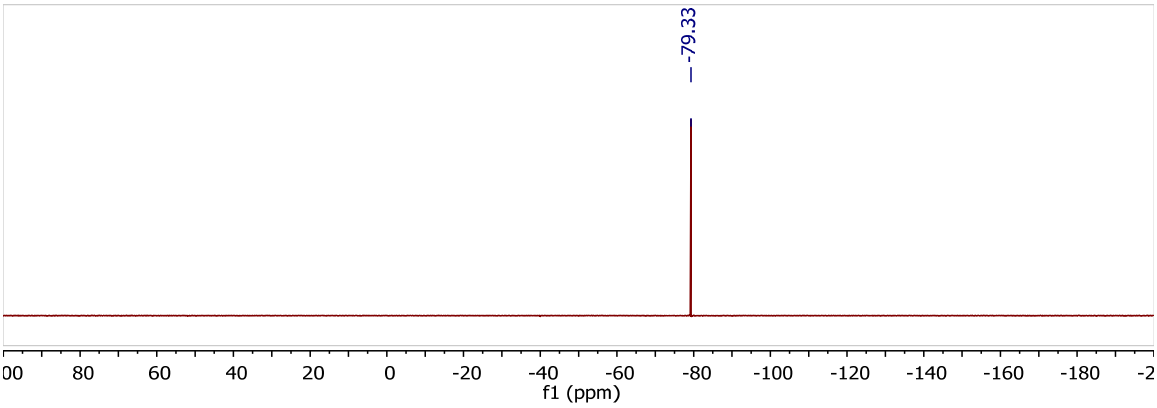

Figure 121. ^{19}F NMR (282 MHz, CD_3CN) spectrum of **2Pd-H**.

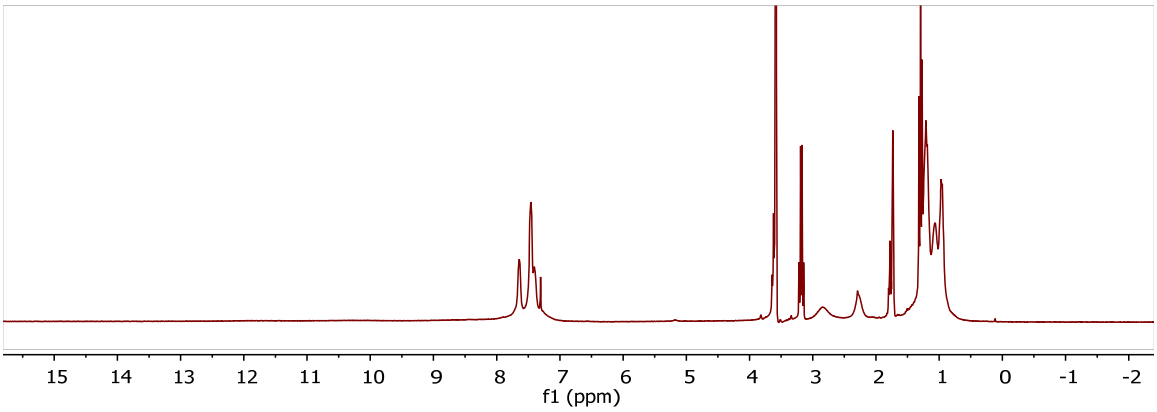

Figure 122. ^{1}H NMR (300 MHz, d_8-THF) spectrum of **3Ni**.

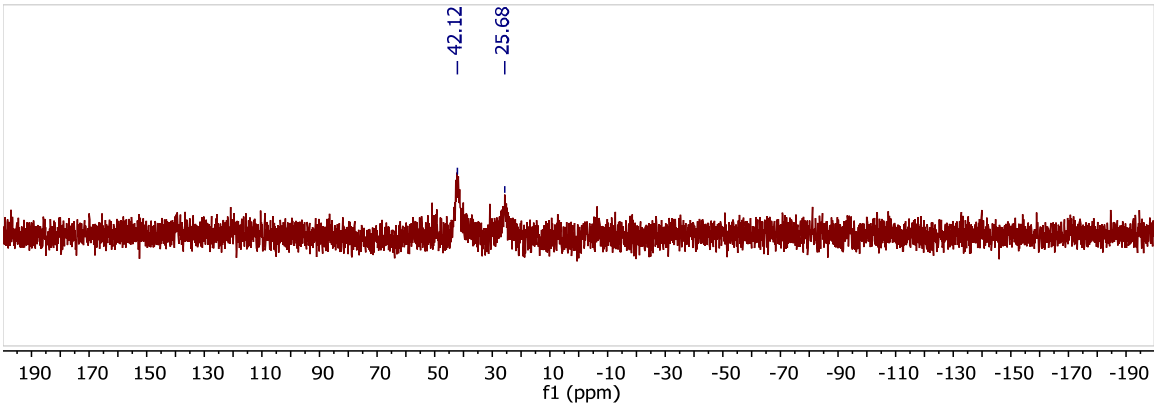

Figure 123. $^{31}P\{^{1}H\}$ NMR (121 MHz, d_8-THF) spectrum of **3Ni**.

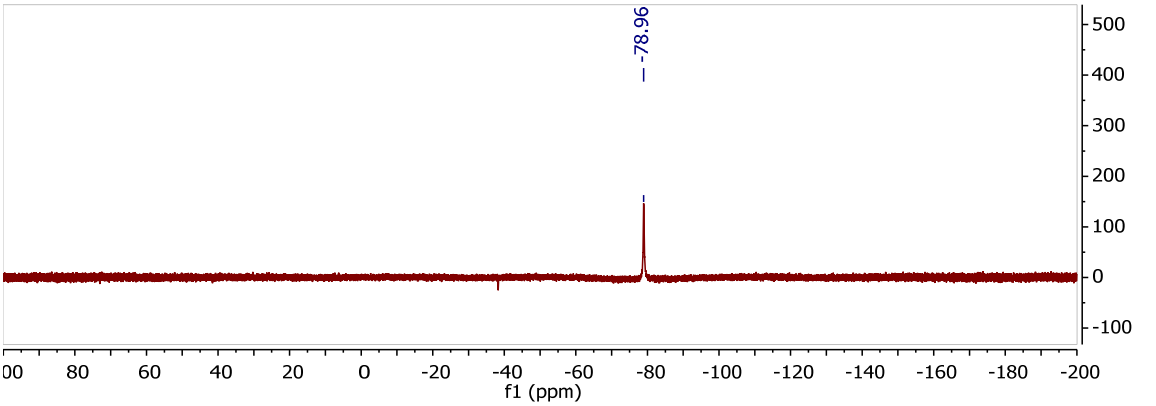

Figure 124. ^{19}F NMR (282 MHz, d_8-THF) spectrum of **3Ni**.

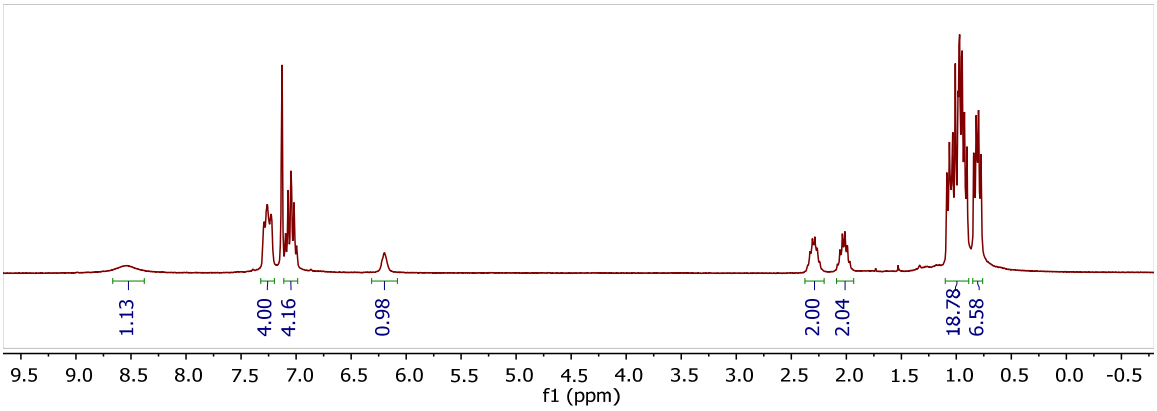

Figure 125. ^{1}H NMR (500 MHz, C_6D_6) spectrum of **4Ni**.

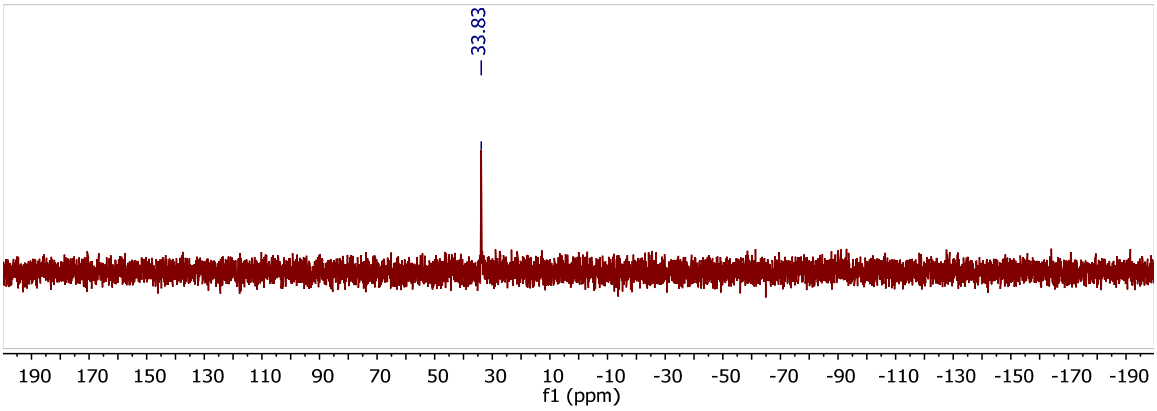

Figure 126. $^{31}P\{^{1}H\}$ NMR (121 MHz, C_6D_6) spectrum of **4Ni**.

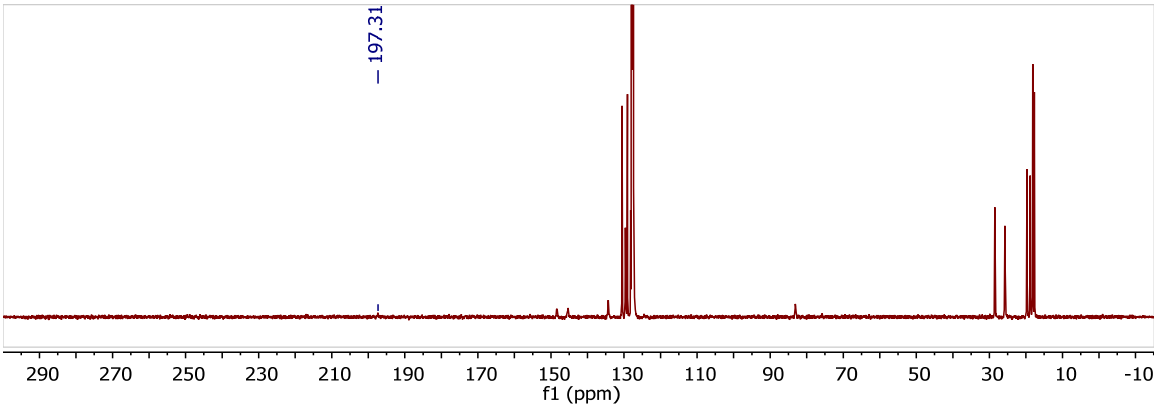

Figure 127. $^{13}C\{^{1}H\}$ NMR (126 MHz, C_6D_6) spectrum of **4Ni**.

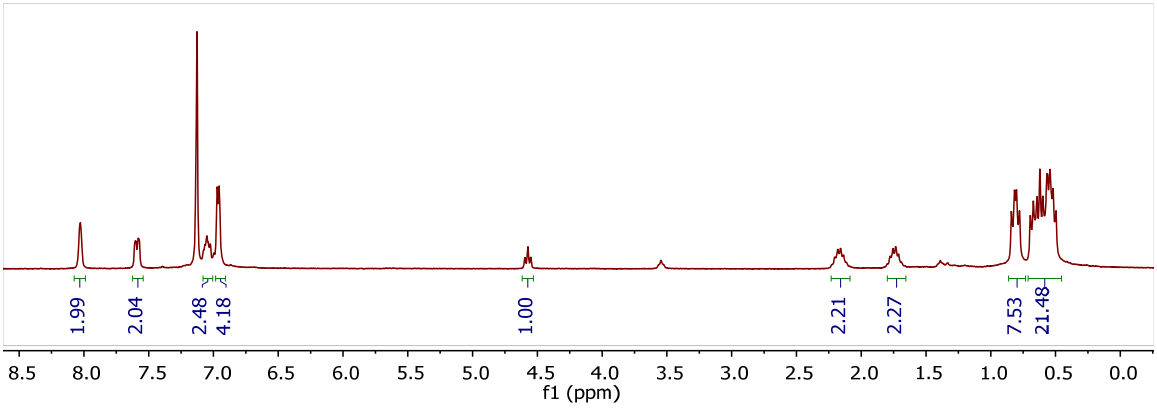

Figure 128. ^{1}H NMR (300 MHz, C_6D_6) spectrum of **4Ni-B(C_6F_5)$_3$**.

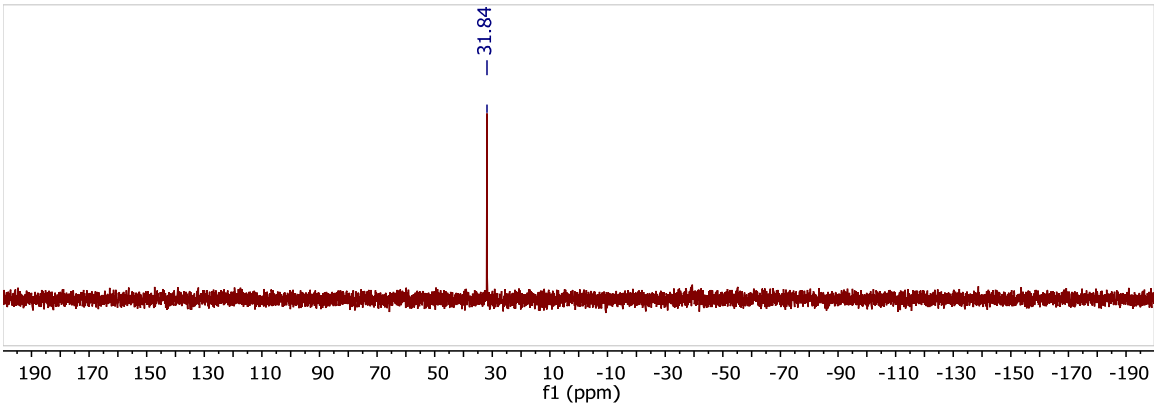

Figure 129. $^{31}P\{^{1}H\}$ NMR (121 MHz, C_6D_6) spectrum of **4Ni-B(C_6F_5)$_3$**.

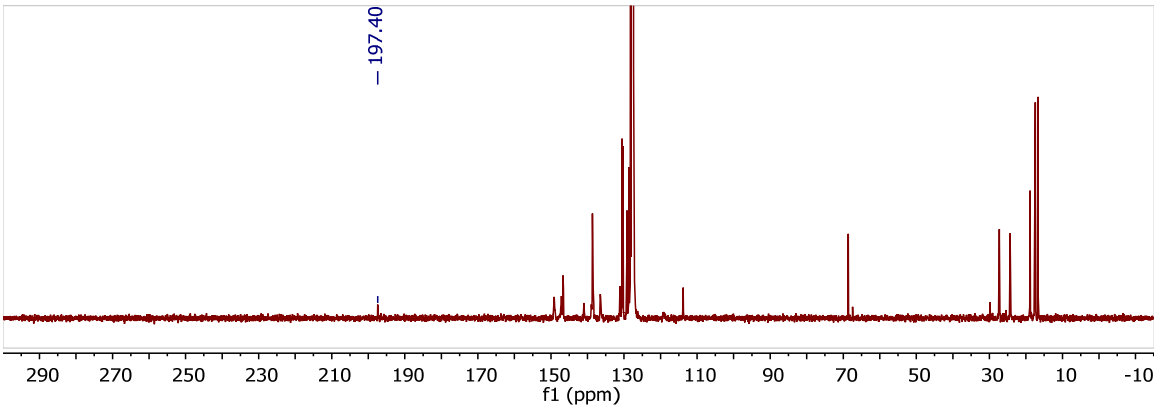

Figure 130. $^{13}C\{^{1}H\}$ NMR (126 MHz, C_6D_6) spectrum of **4Ni-B(C_6F_5)$_3$**.

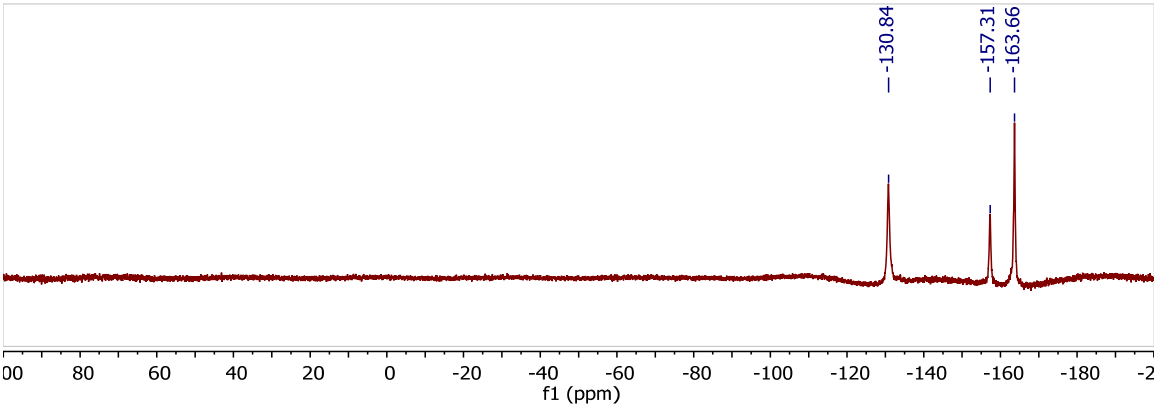

Figure 131. ^{19}F NMR (282 MHz, C_6D_6) spectrum of **4Ni-B(C_6F_5)$_3$**.

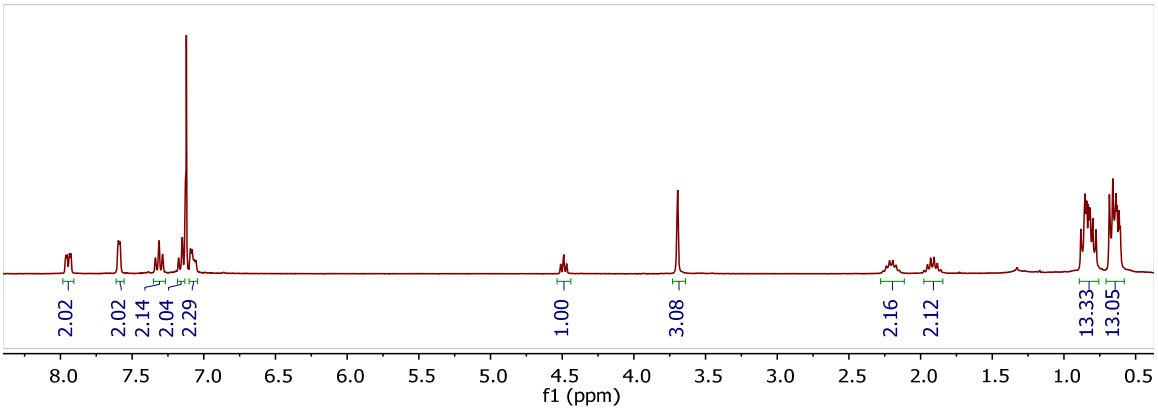

Figure 132. ^{1}H NMR (500 MHz, C_6D_6) spectrum of **4Ni-Me**.

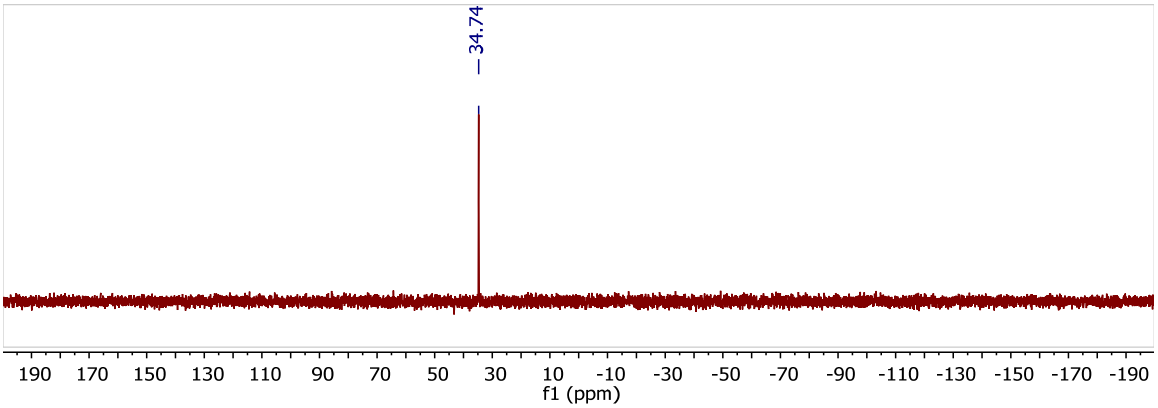

Figure 133. ^{31}P{^{1}H} NMR (121 MHz, C_6D_6) spectrum of **4Ni-Me**.

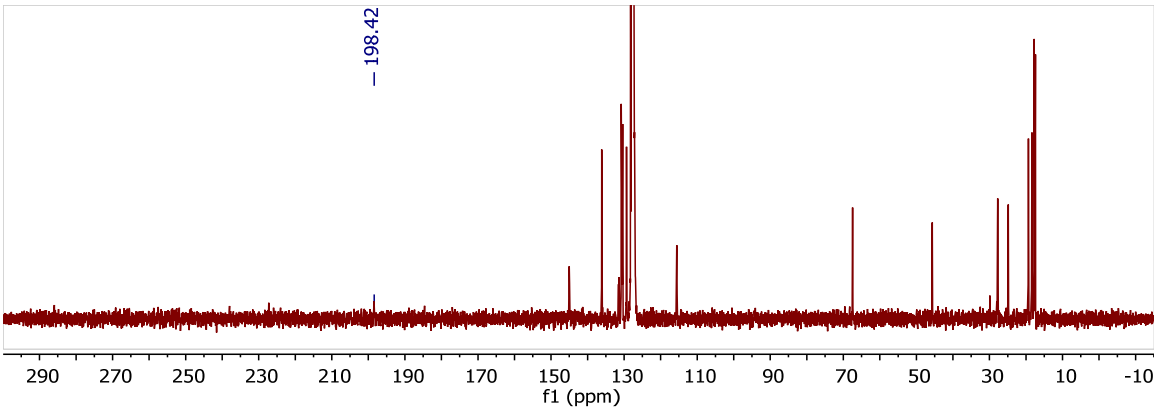

Figure 134. ^{13}C{^{1}H} NMR (126 MHz, C_6D_6) spectrum of **4Ni-Me**.

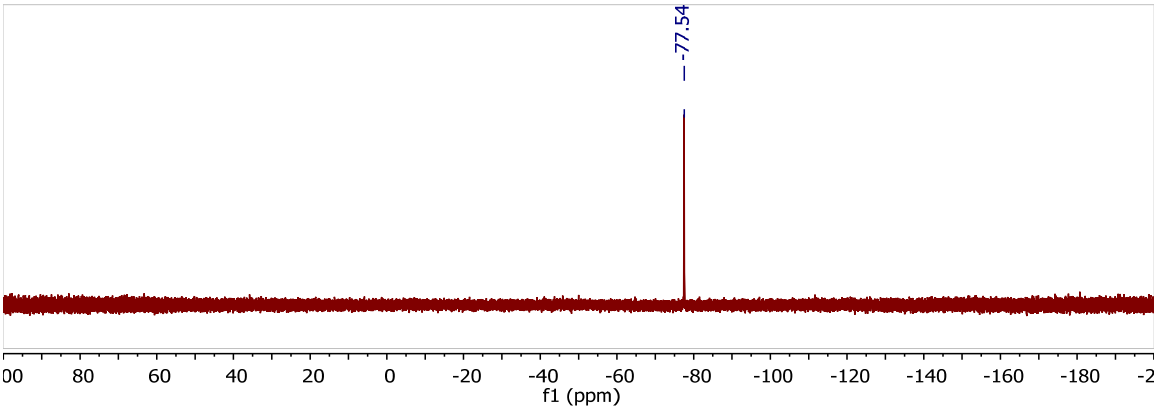

Figure 135. ^{19}F NMR (282 MHz, C_6D_6) spectrum of **4Ni-Me**.

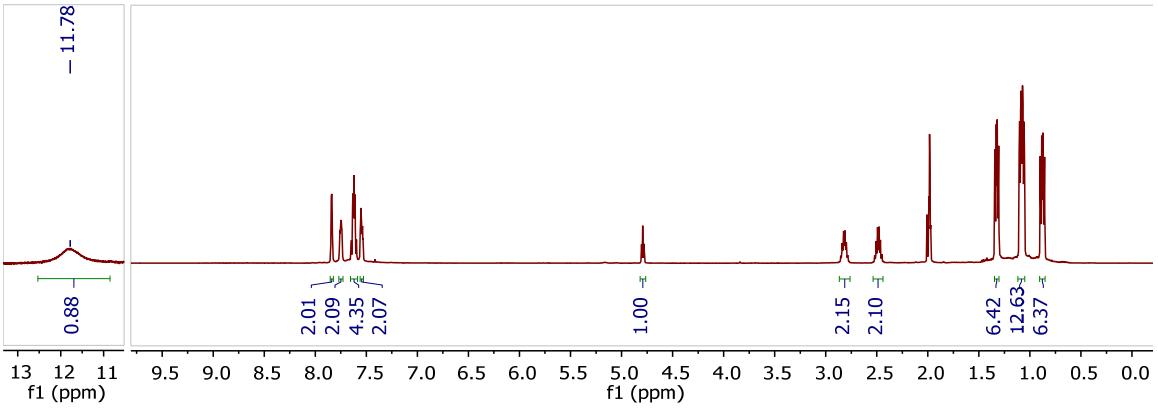

Figure 136. ^{1}H NMR (500 MHz, CD_3CN) spectrum of **4Ni-H**.

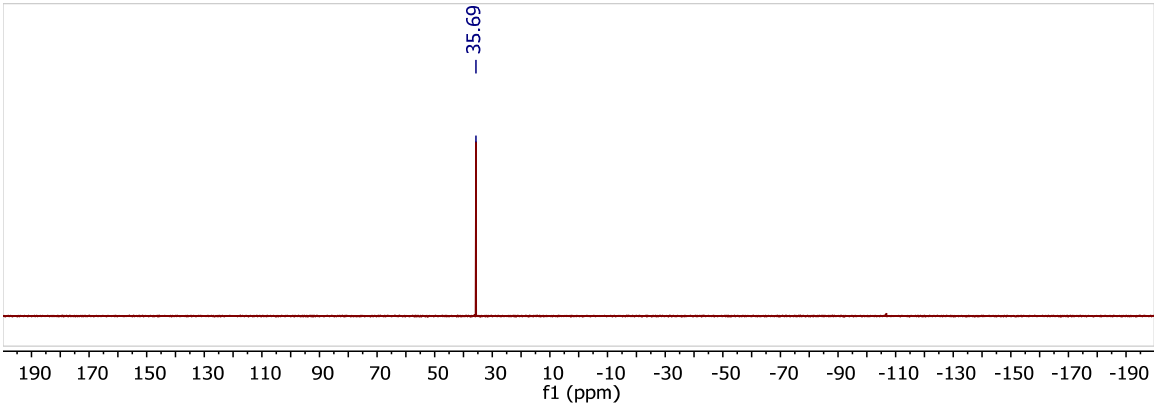

Figure 137. $^{31}P\{^{1}H\}$ NMR (121 MHz, CD_3CN) spectrum of **4Ni-H**.

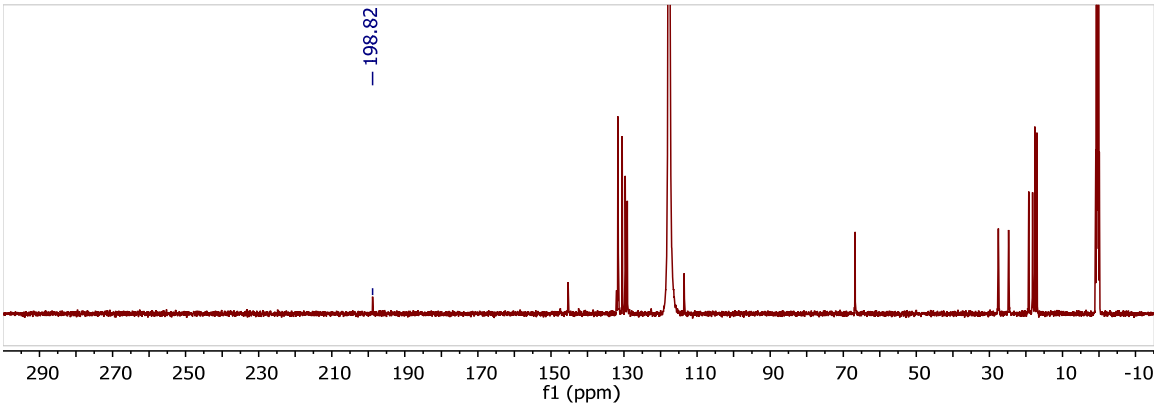

Figure 138. $^{13}C\{^{1}H\}$ NMR (126 MHz, CD_3CN) spectrum of **4Ni-H**.

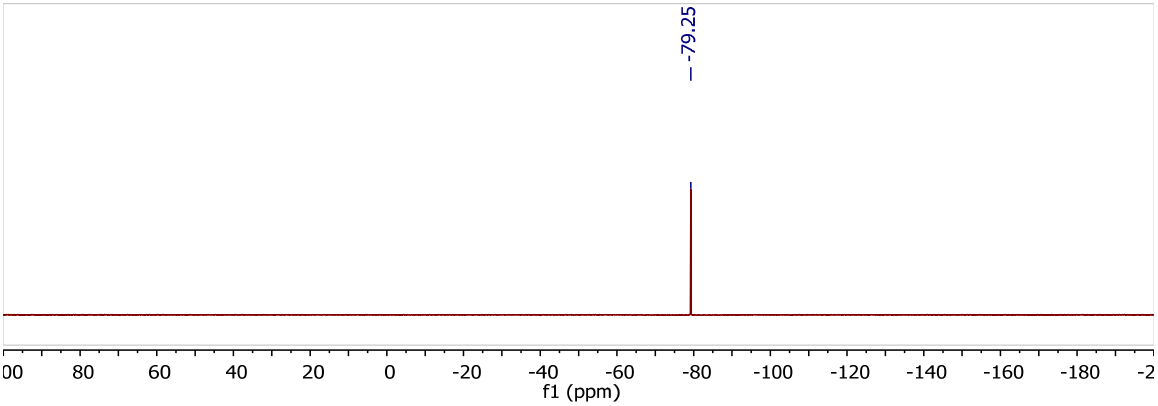

Figure 139. ^{19}F NMR (282 MHz, CD_3CN) spectrum of **4Ni-H**.

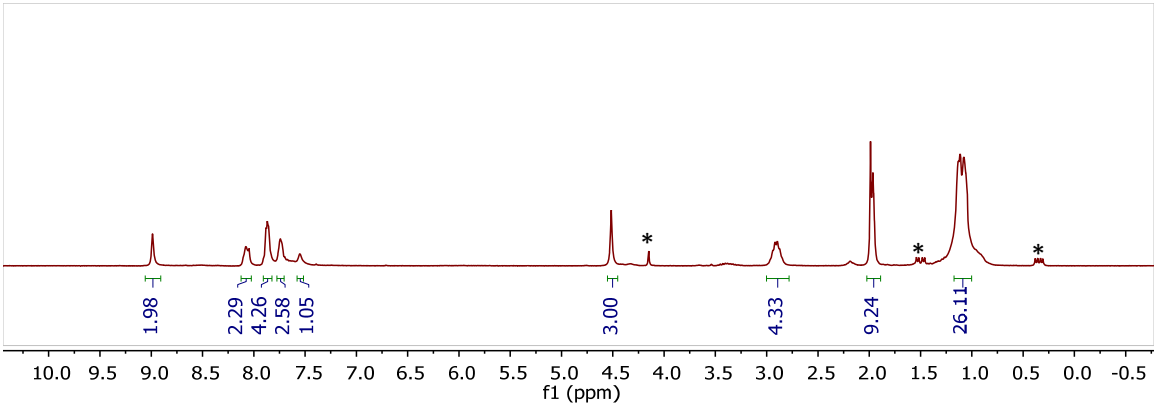

Figure 140. ^{1}H NMR (500 MHz, C_6D_6) spectrum of **5Ni**. Peaks marked with an asterisk are from the gradual decomposition of **5Ni** in solution.

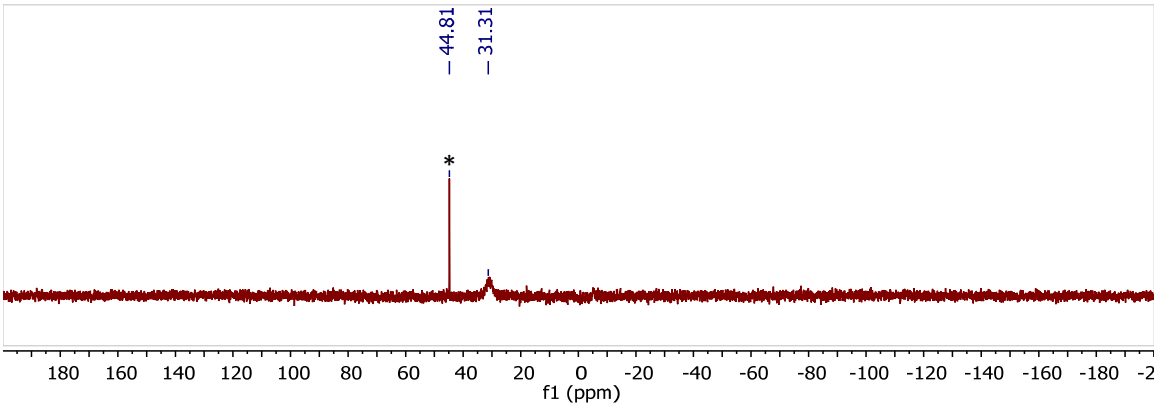

Figure 141. $^{31}P\{^{1}H\}$ NMR (121 MHz, C_6D_6) spectrum of **5Ni**. Peaks marked with an asterisk are from the gradual decomposition of **5Ni** in solution.

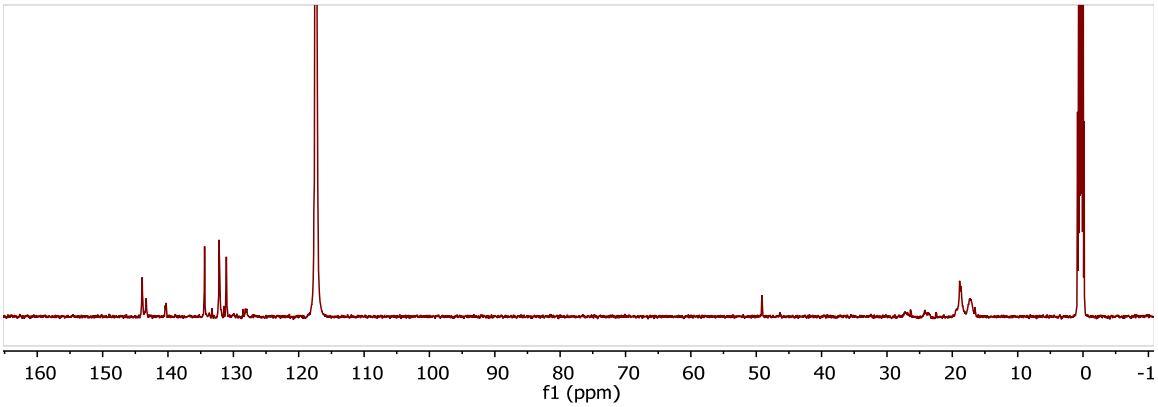

Figure 142. $^{13}C\{^{1}H\}$ NMR (126 MHz, C_6D_6) spectrum of **5Ni**.

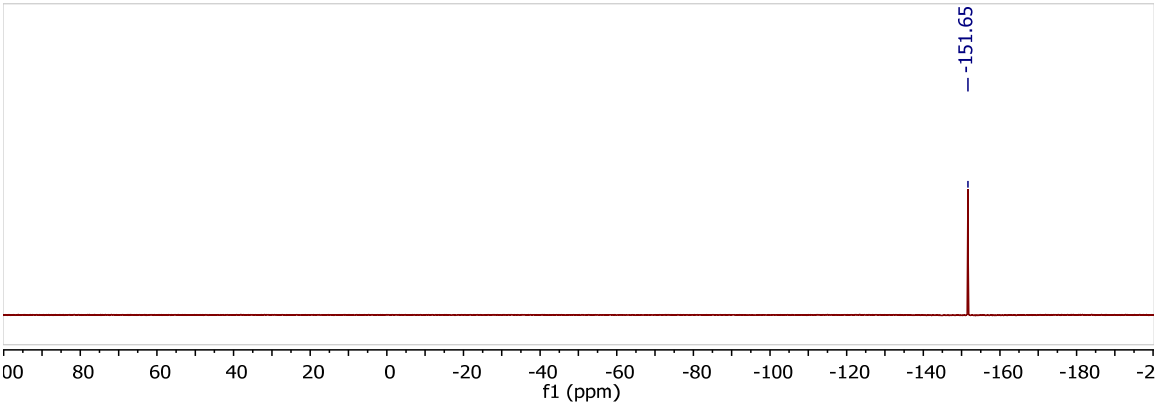

Figure 143. ^{19}F NMR (282 MHz, C_6D_6) spectrum of **5Ni**.

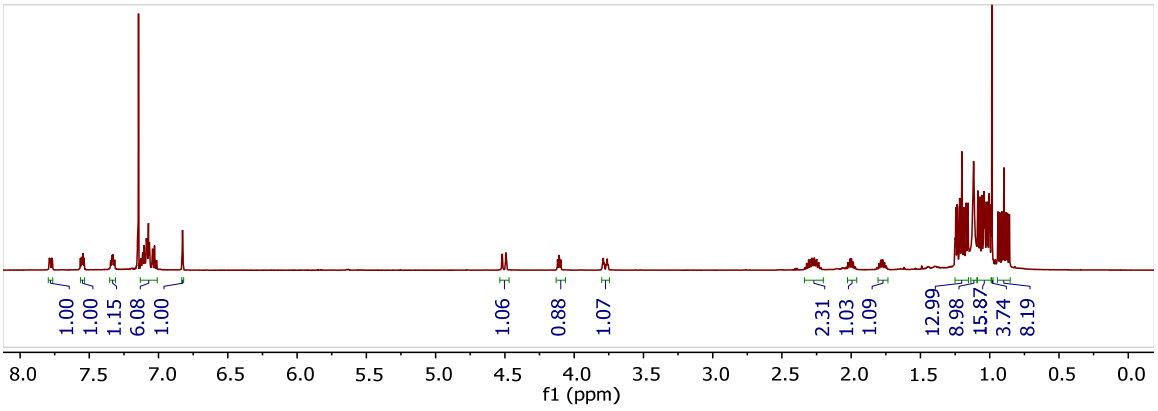

Figure 144. ^{1}H NMR (500 MHz, C_6D_6) spectrum of **6Ni**.

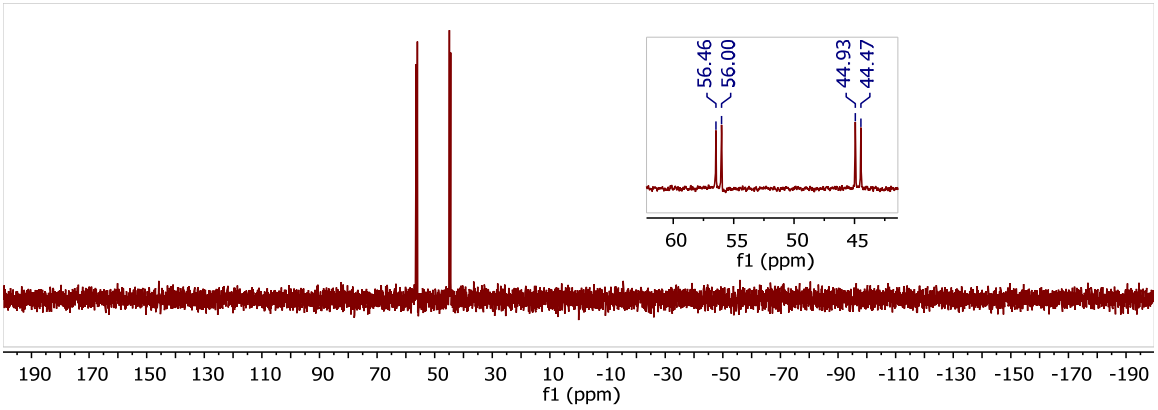

Figure 145. ^{31}P{^{1}H} NMR (121 MHz, C_6D_6) spectrum of **6Ni**.

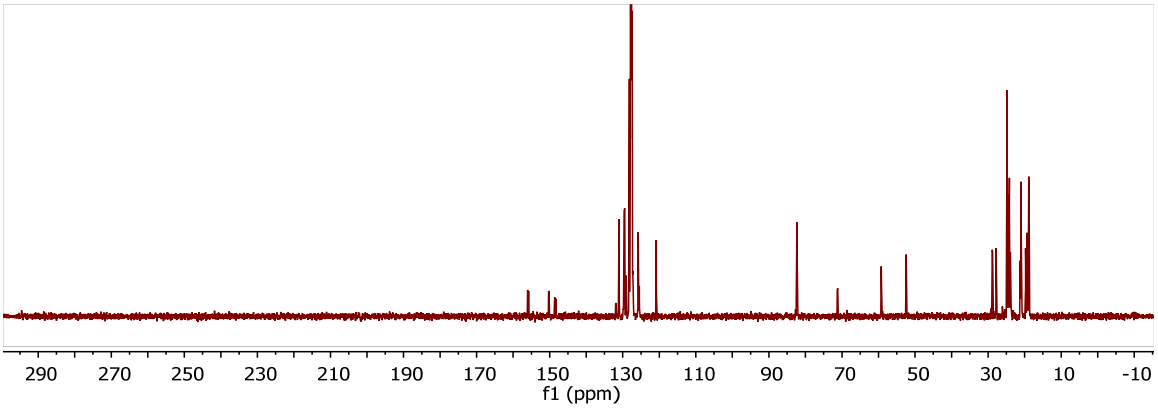

Figure 146. ^{13}C{^{1}H} NMR (126 MHz, C_6D_6) spectrum of **6Ni**.

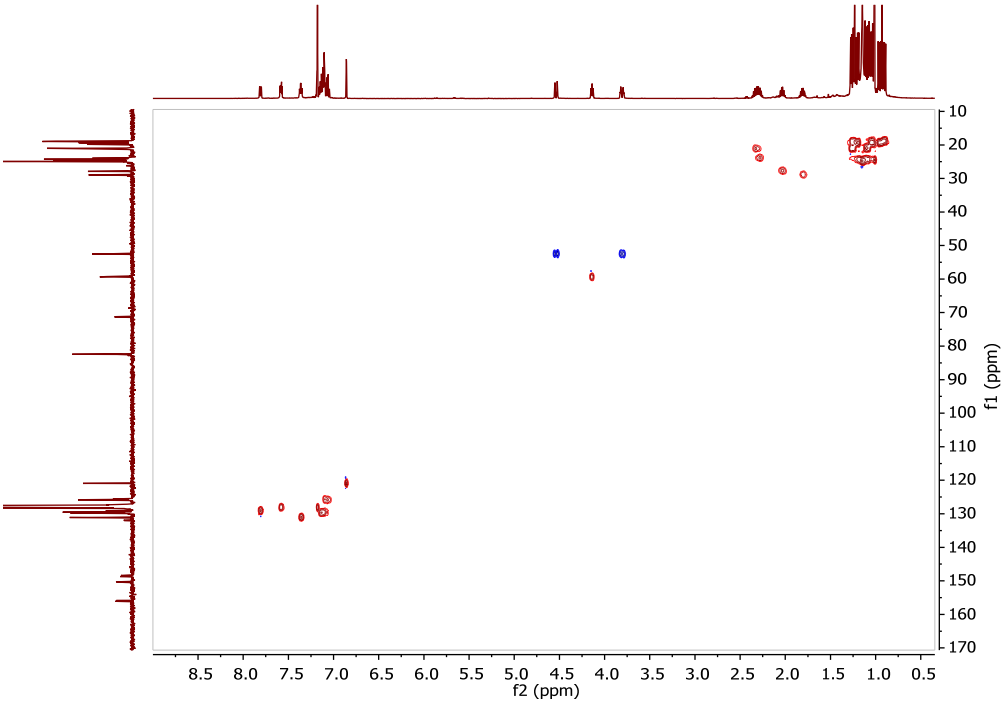

Figure 147. gHSQCAD NMR (500 MHz ^{1}H, C_6D_6) spectrum of **6Ni**.

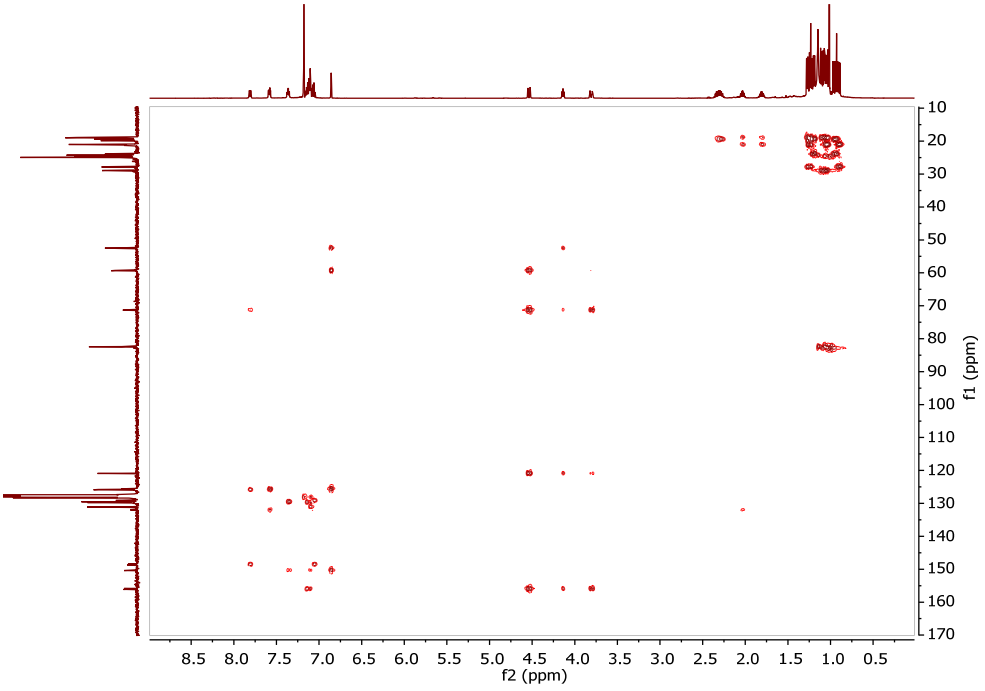

Figure 148. gHMBCAD NMR (500 MHz ^{1}H, C_6D_6) spectrum of **6Ni**.

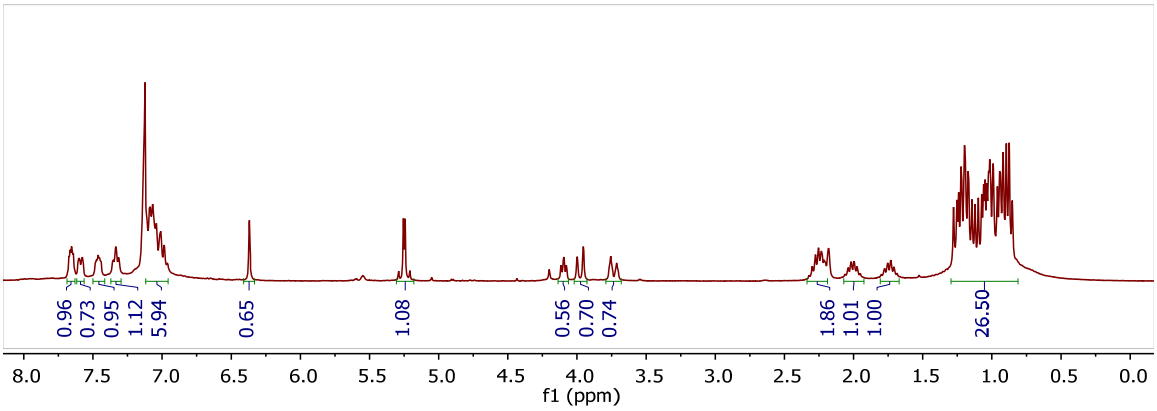

Figure 149. ^{1}H NMR (500 MHz, C_6D_6) spectrum of **7Ni**.

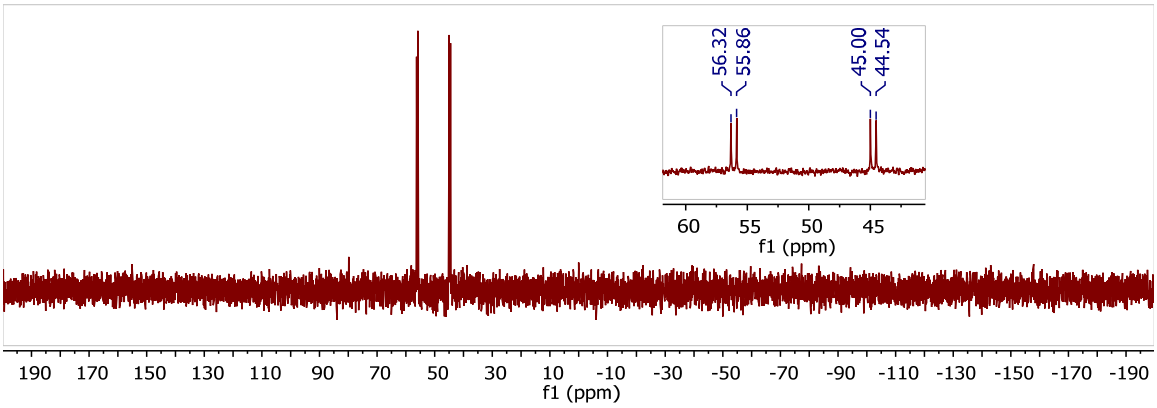

Figure 150. ^{31}P{^{1}H} NMR (121 MHz, C_6D_6) spectrum of **7Ni**.

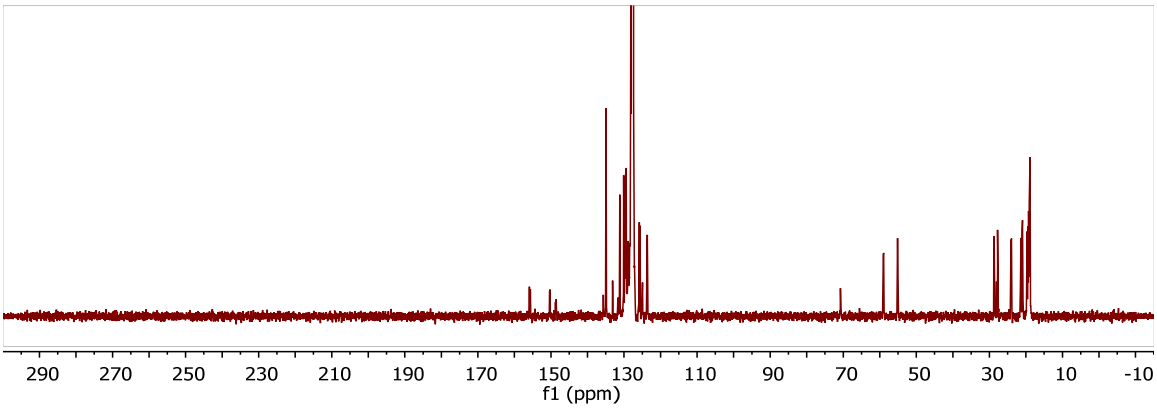

Figure 151. ^{13}C{^{1}H} NMR (126 MHz, C_6D_6) spectrum of **7Ni**.

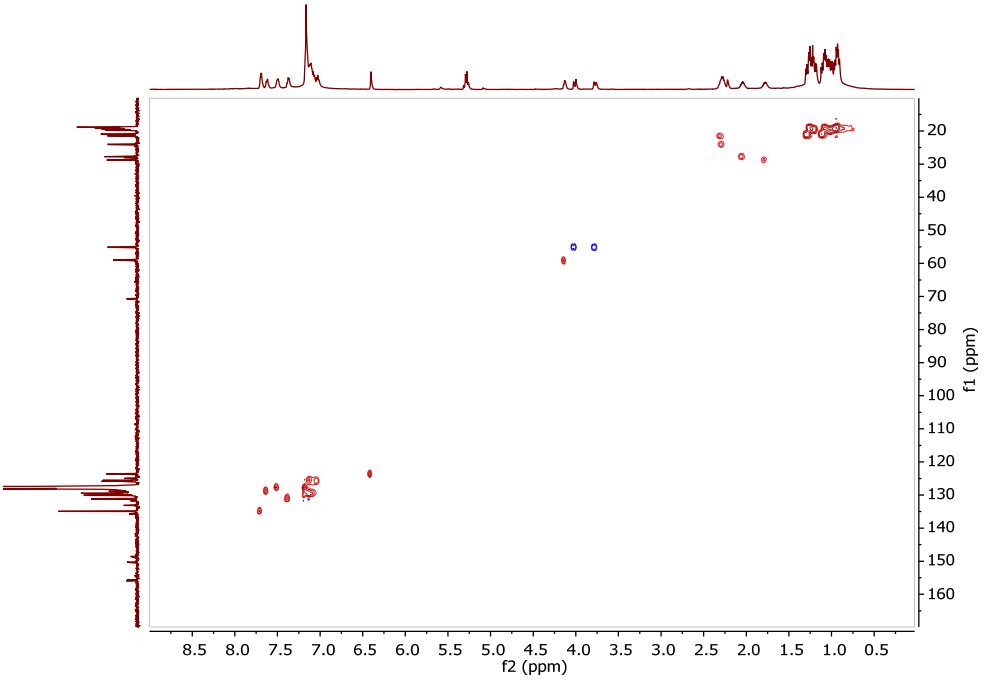

Figure 152. gHSQCAD NMR (500 MHz ^{1}H, C_6D_6) spectrum of **7Ni**.

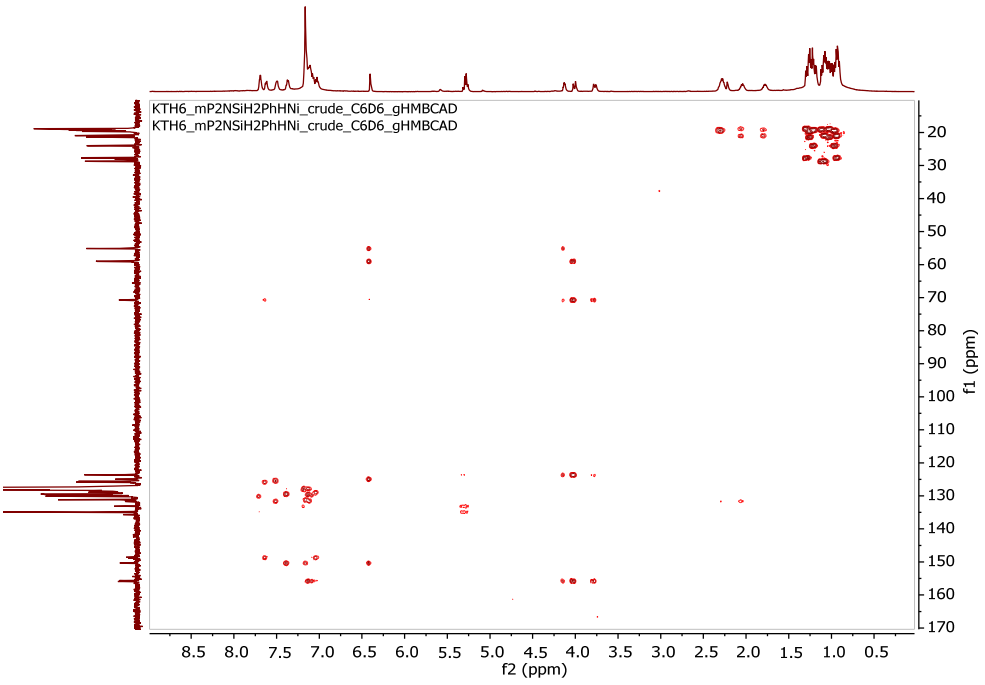

Figure 153. gHMCAD NMR (500 MHz ^{1}H, C_6D_6) spectrum of **7Ni**.

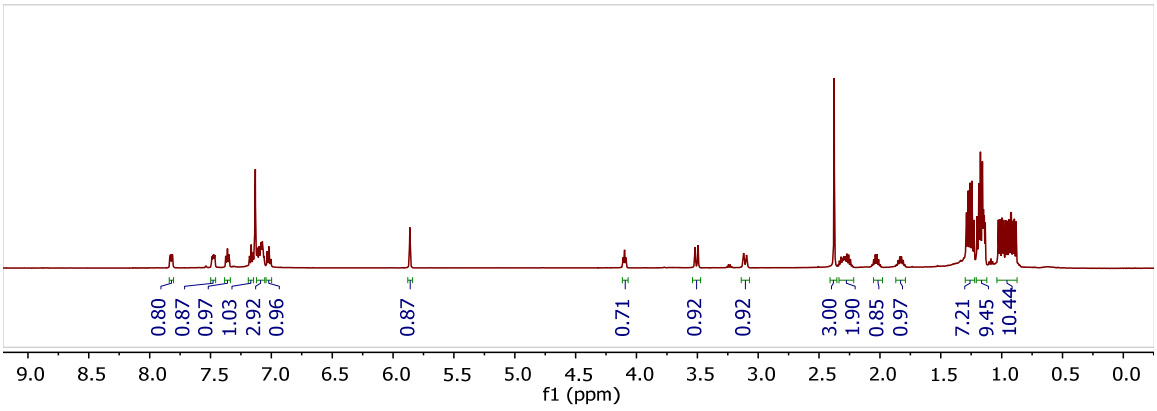

Figure 154. ^{1}H NMR (500 MHz, C_6D_6) spectrum of **8Ni**.

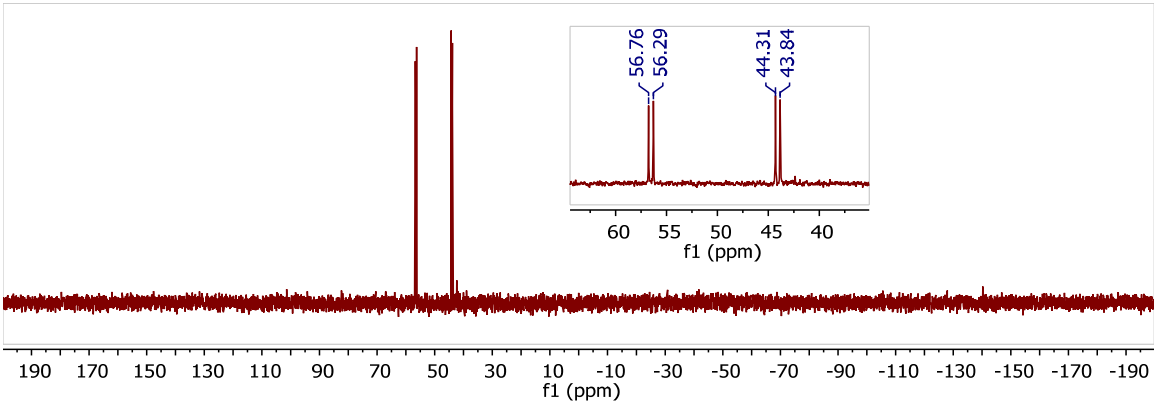

Figure 155. ^{31}P{^{1}H} NMR (121 MHz, C_6D_6) spectrum of **8Ni**.

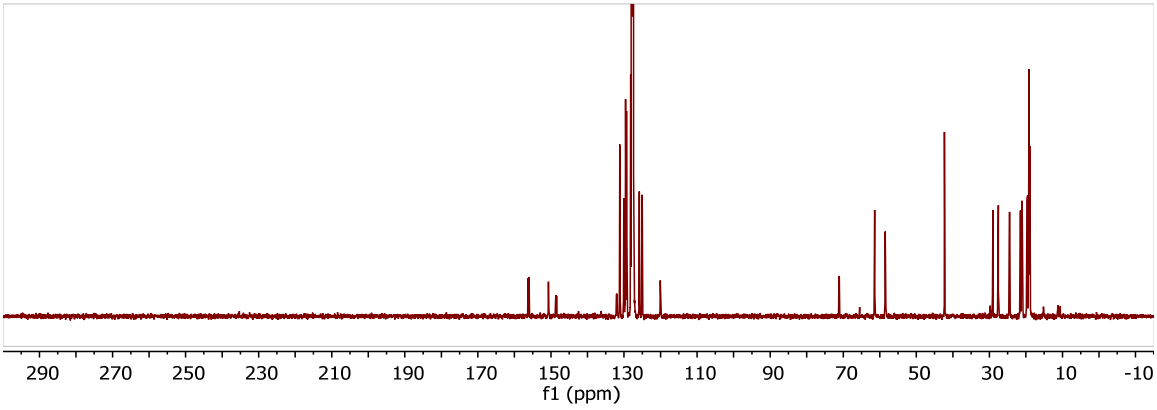

Figure 156. ^{13}C{^{1}H} NMR (126 MHz, C_6D_6) spectrum of **8Ni**.

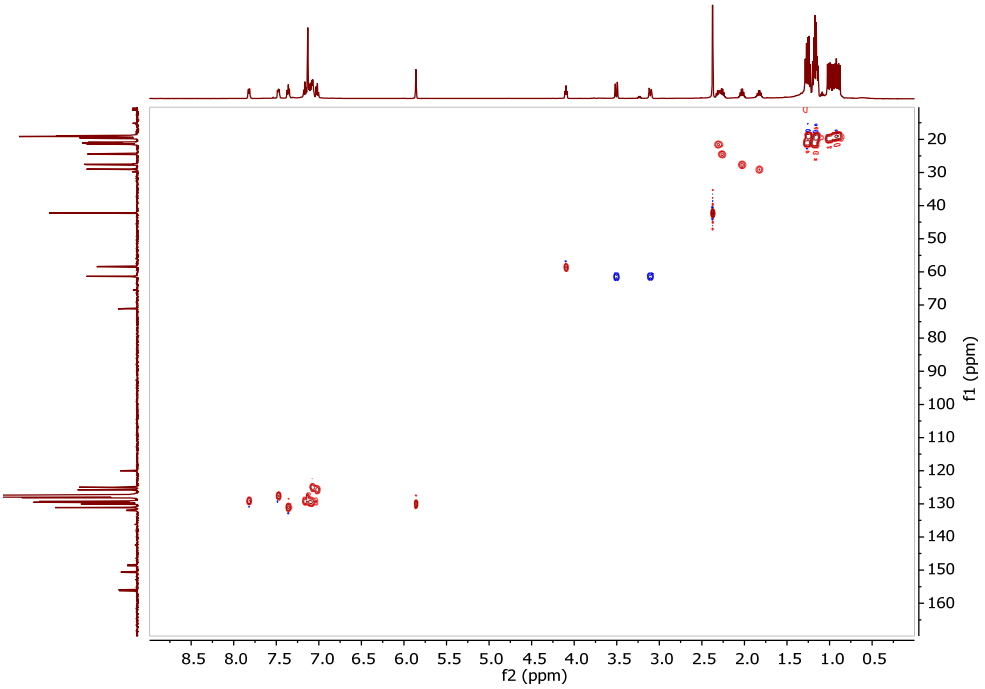

Figure 157. gHSQCAD NMR (500 MHz ^{1}H, C_6D_6) spectrum of **8Ni**.

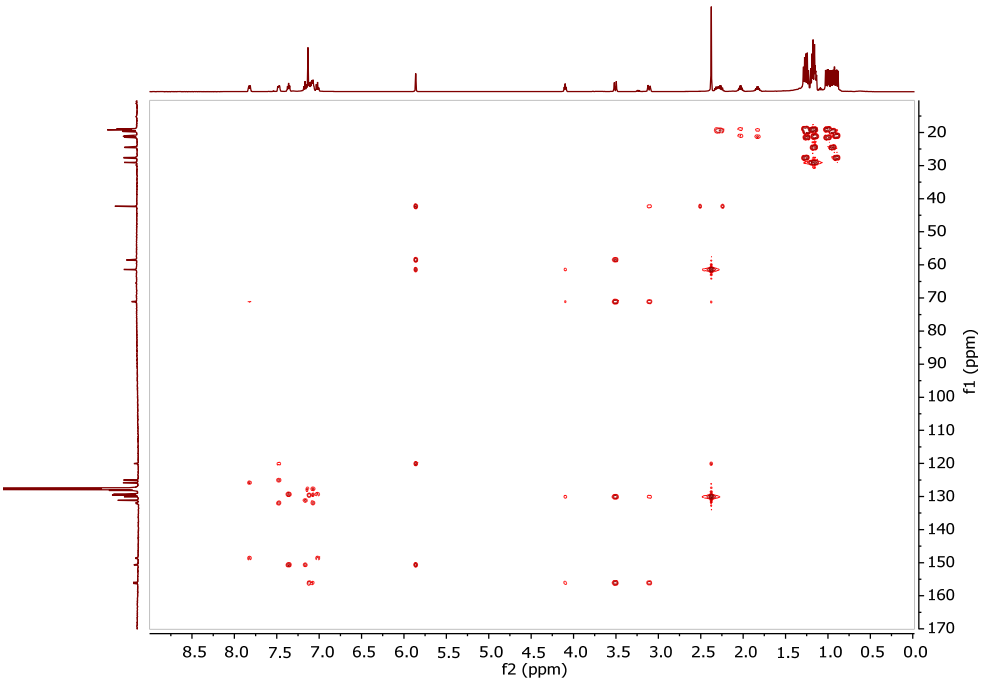

Figure 158. gHMCAD NMR (500 MHz ^{1}H, C_6D_6) spectrum of **8Ni**.

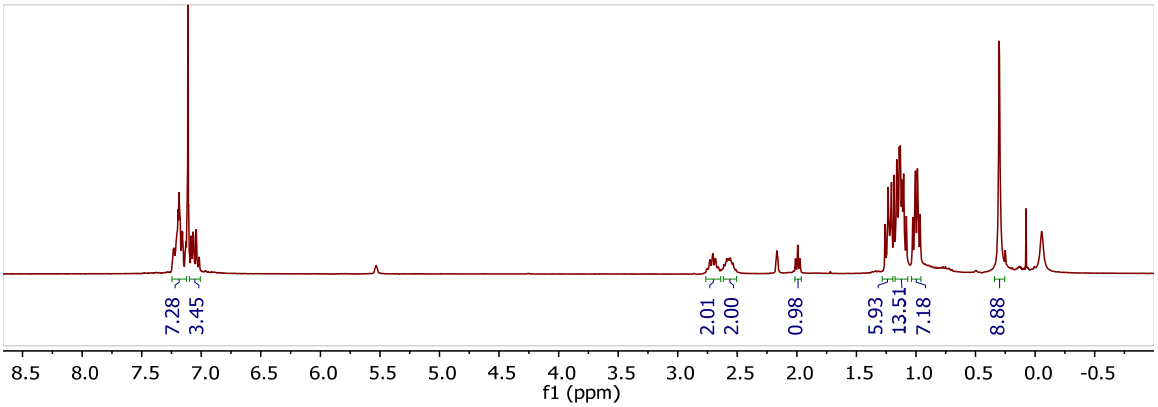

Figure 149. ^{1}H NMR (300 MHz, C_6D_6) spectrum of **2Ni-SiMe$_3$**.

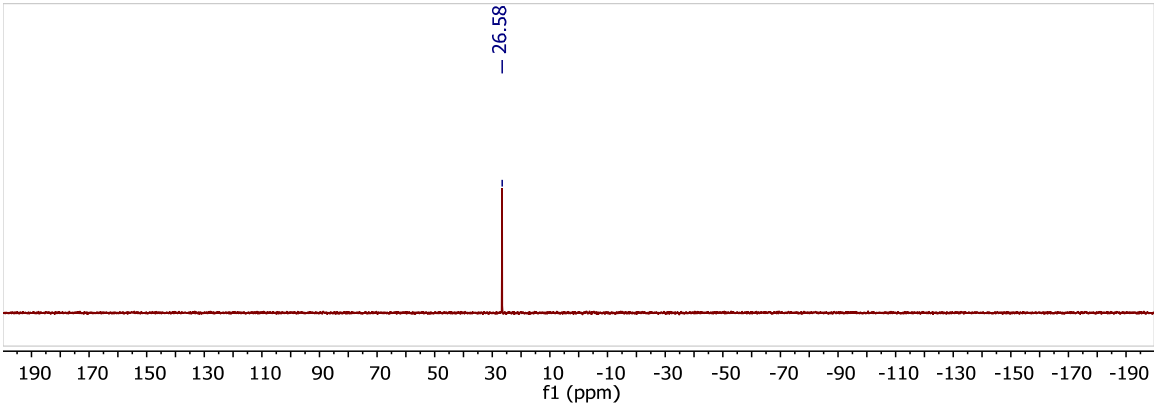

Figure 150. ^{31}P{^{1}H} NMR (121 MHz, C_6D_6) spectrum of **2Ni-SiMe$_3$**.

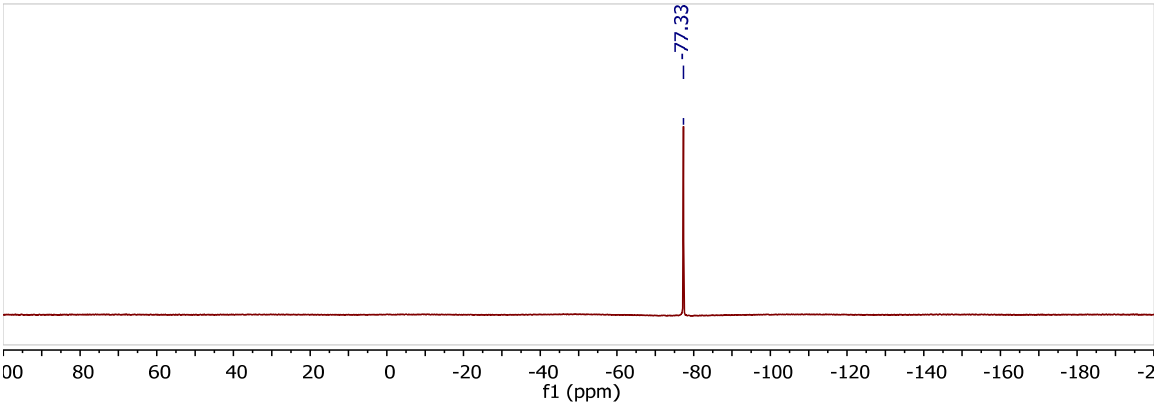

Figure 151. ^{19}F NMR (282 MHz, C_6D_6) spectrum of **2Ni-SiMe$_3$**.

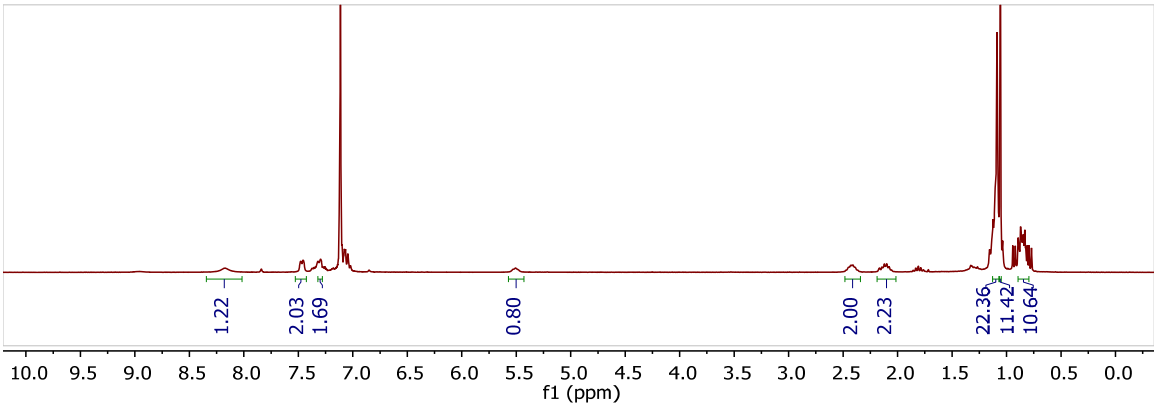

Figure 152. ^{1}H NMR (300 MHz, C_6D_6) spectrum of **4Ni(CN*t*Bu)**.

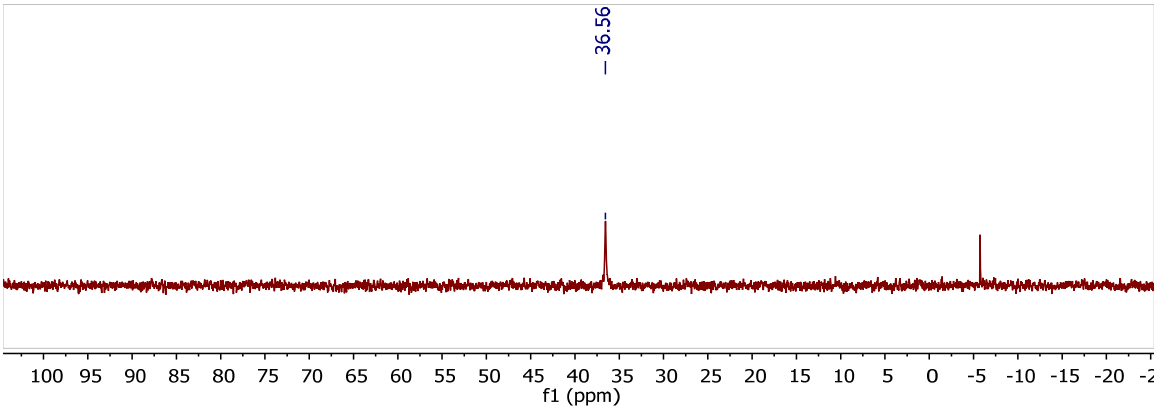

Figure 153. ^{31}P{^{1}H} NMR (121 MHz, C_6D_6) spectrum of **4Ni(CN*t*Bu)**.

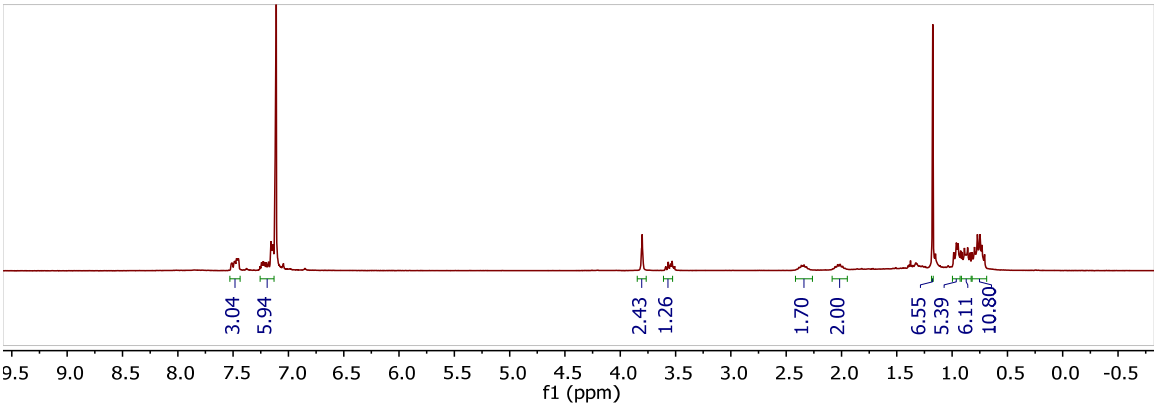

Figure 154. ^{1}H NMR (300 MHz, C_6D_6) spectrum of **4Ni(CN*t*Bu)-Me**.

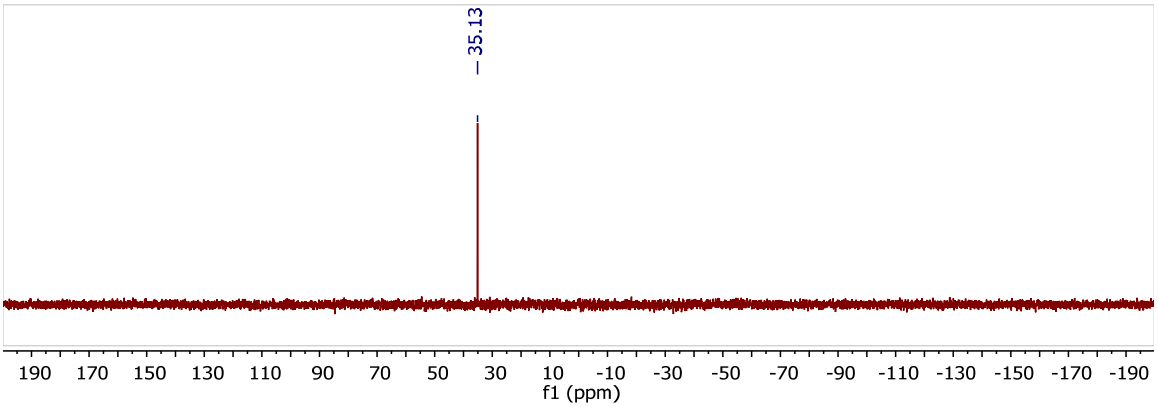

Figure 155. $^{31}P\{^{1}H\}$ NMR (121 MHz, C_6D_6) spectrum of **4Ni(CN*t*Bu)-Me**.

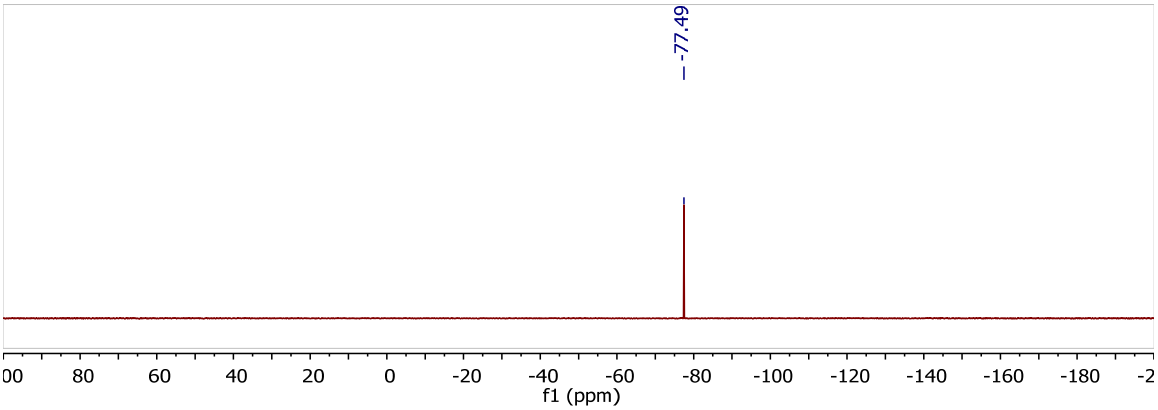

Figure 156. ^{19}F NMR (282 MHz, C_6D_6) spectrum of **4Ni(CN*t*Bu)-Me**.

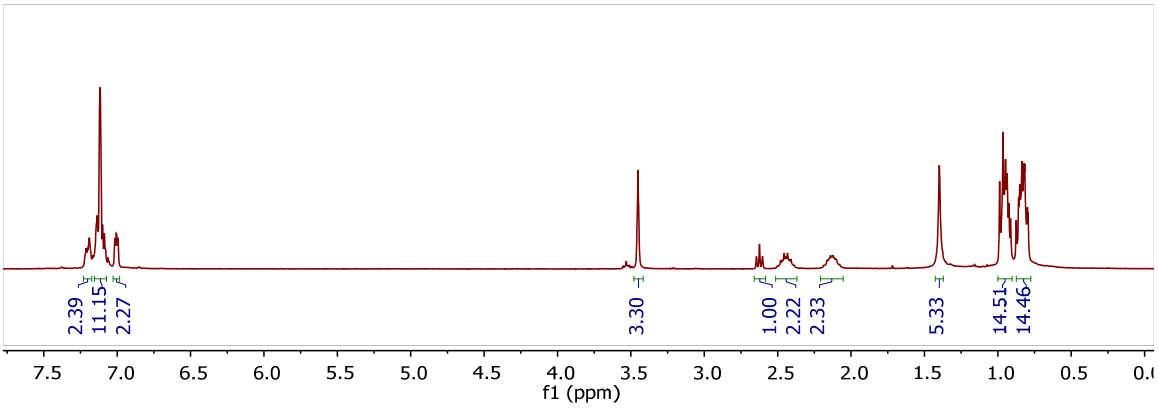

Figure 157. ^{1}H NMR (300 MHz, C_6D_6) spectrum of **4Ni(MeCN)-Me**.

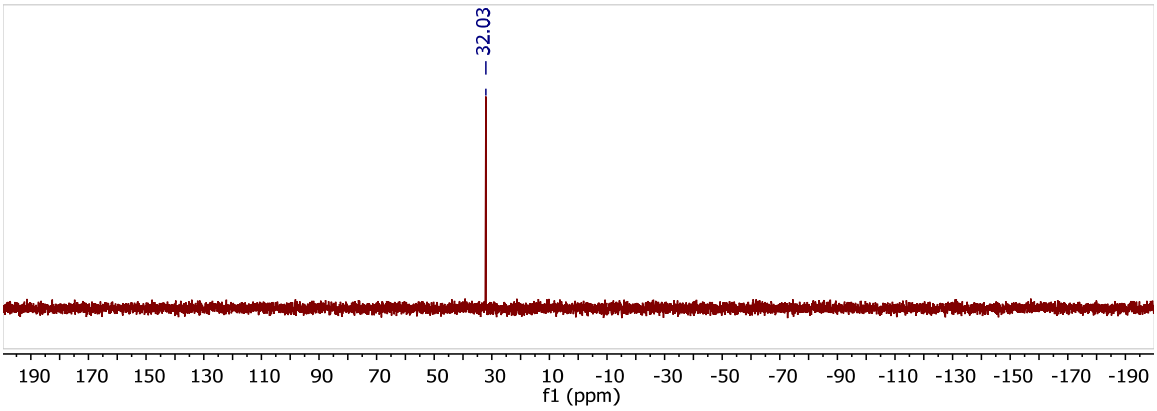

Figure 158. $^{31}P\{^{1}H\}$ NMR (121 MHz, C_6D_6) spectrum of **4Ni(MeCN)-Me**.

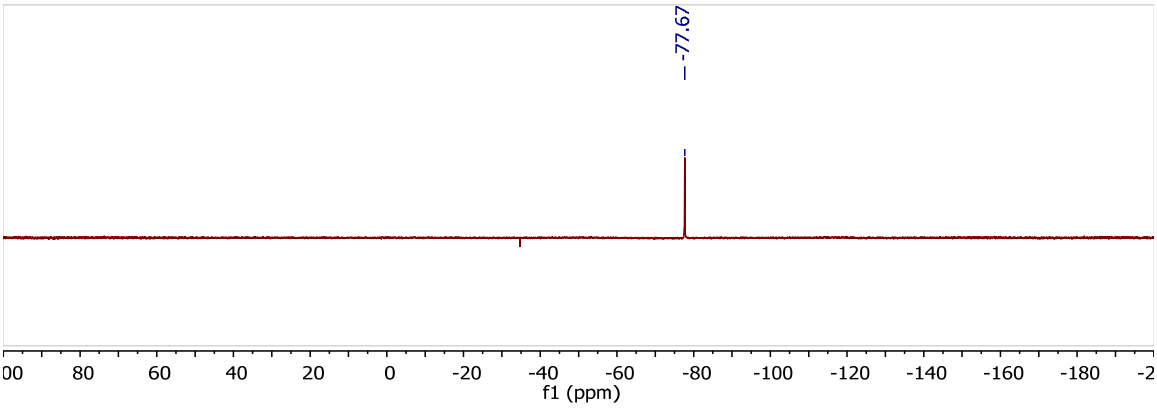

Figure 159. ^{19}F NMR (282 MHz, C_6D_6) spectrum of **4Ni(MeCN)-Me**.

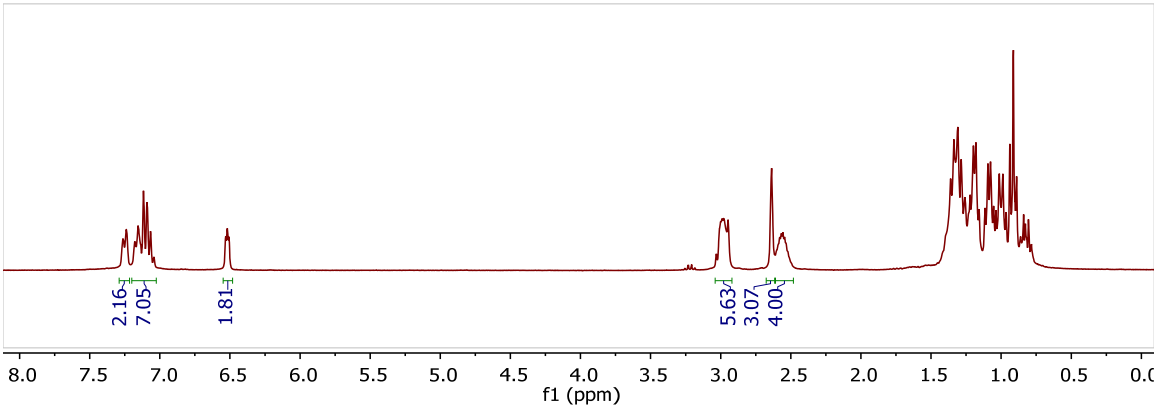

Figure 160. ^{1}H NMR (300 MHz, C_6D_6) spectrum of **4Ni(CN)-Me**.

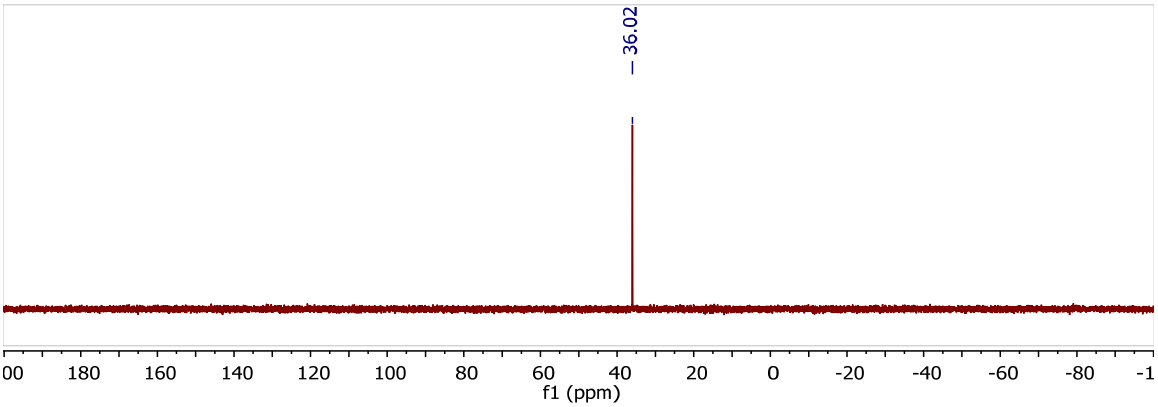

Figure 161. $^{31}P\{^{1}H\}$ NMR (121 MHz, C_6D_6) spectrum of **4Ni(CN)-Me**.

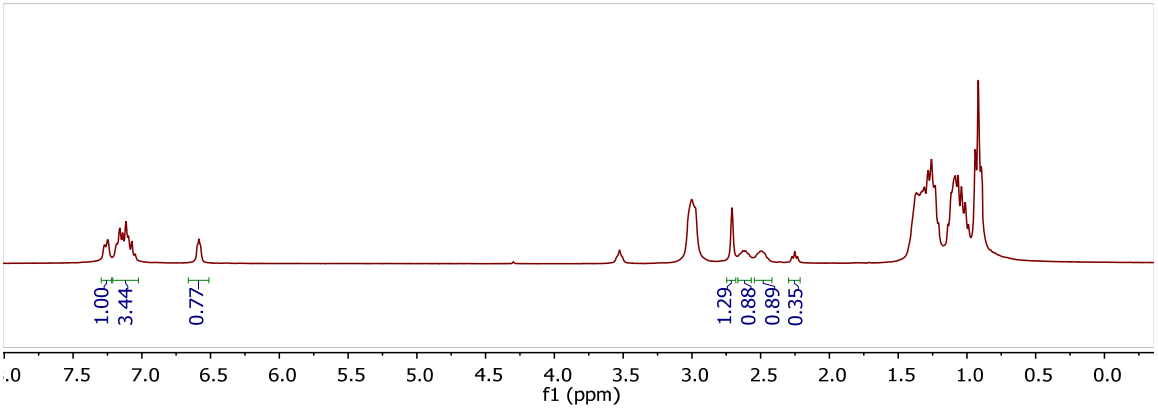

Figure 162. ^{1}H NMR (300 MHz, C_6D_6) spectrum of **4Ni(N_3)-Me**.

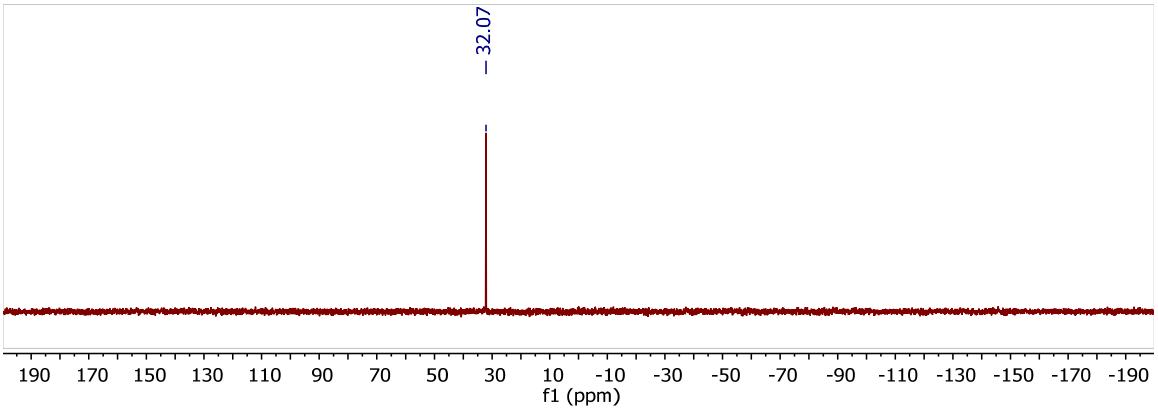

Figure 163. $^{31}P\{^{1}H\}$ NMR (121 MHz, C_6D_6) spectrum of **4Ni(N_3)-Me**.

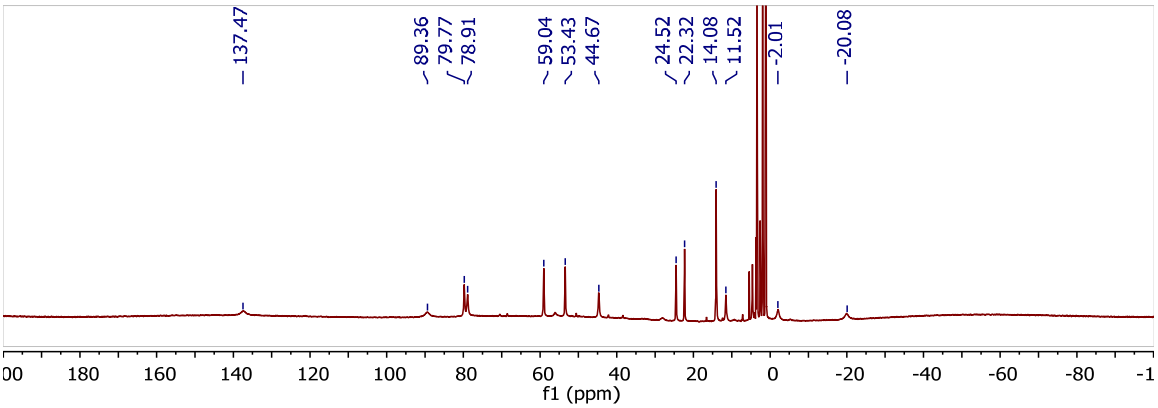

Figure 164. ^{1}H NMR (300 MHz, CD_3CN) spectrum of **3-Cl**.

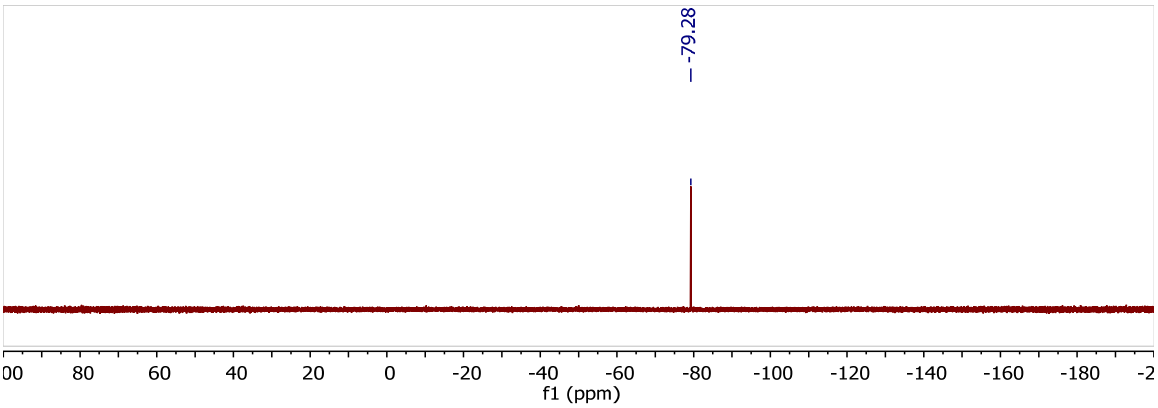

Figure 165. ^{19}F NMR (282 MHz, CD_3CN) spectrum of **3-Cl**.

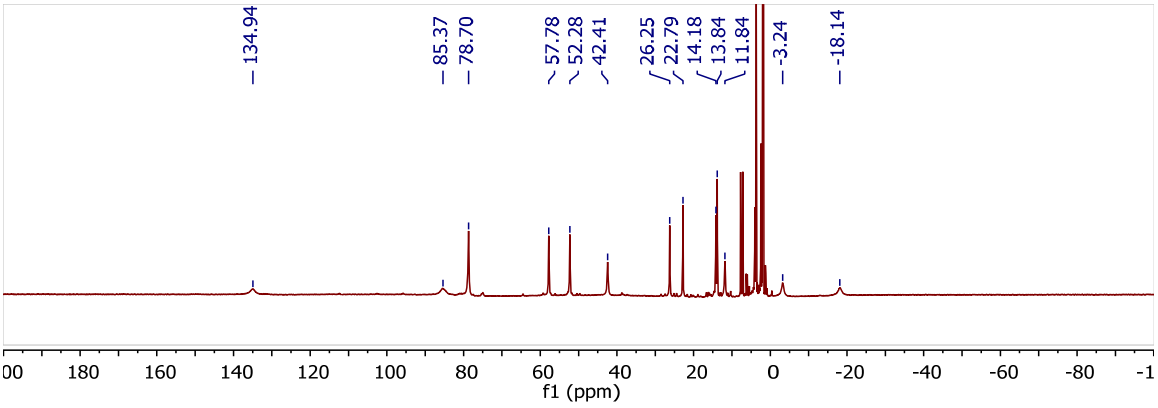

Figure 166. ^{1}H NMR (300 MHz, CD_3CN) spectrum of **3-N_3**.

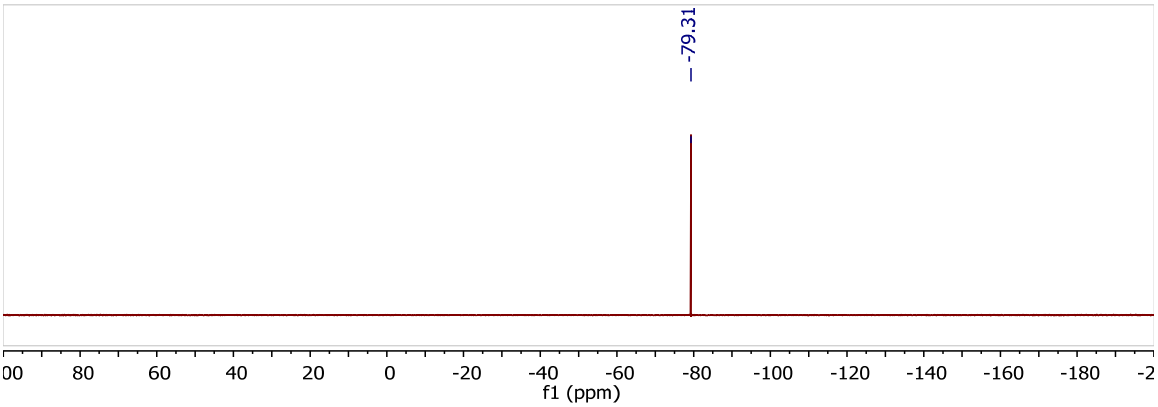

Figure 167. ^{19}F NMR (282 MHz, CD_3CN) spectrum of **3-N_3**.

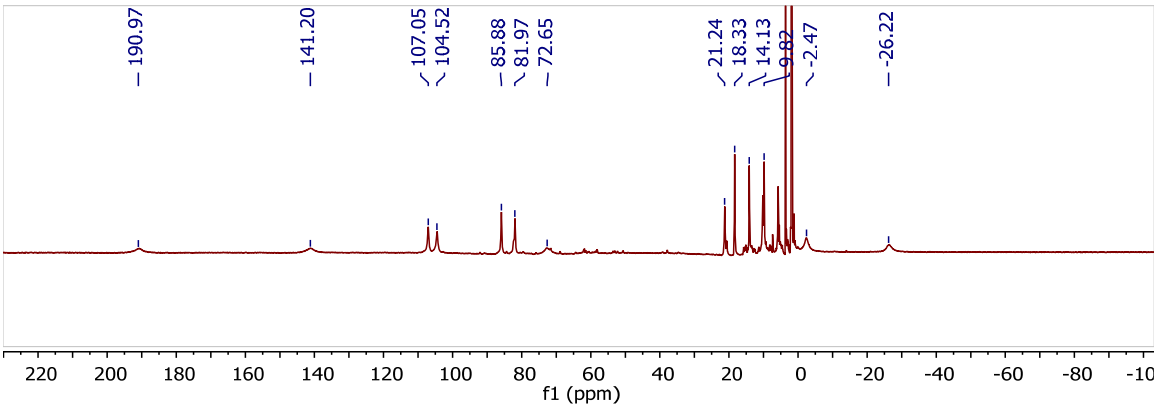

Figure 168. ^{1}H NMR (300 MHz, CD_3CN) spectrum of **3-Cl** after $AgNO_2$ addition.

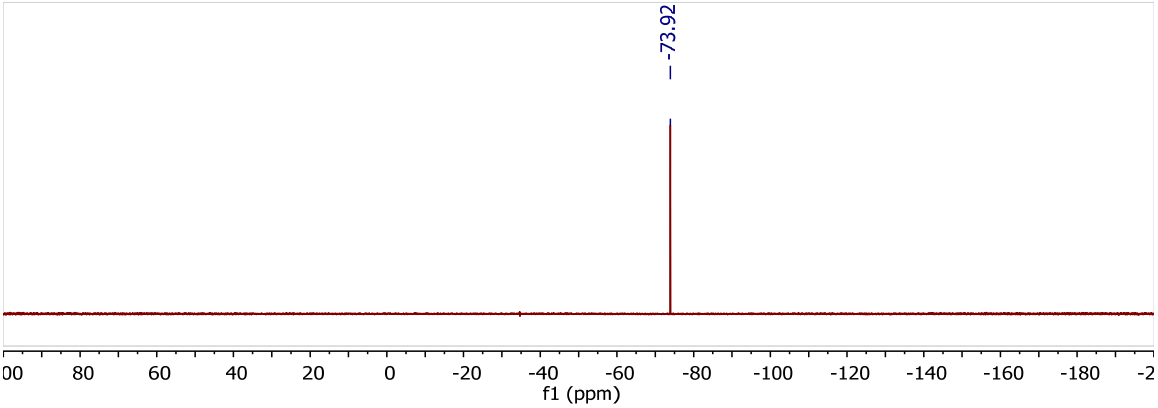

Figure 169. ^{19}F NMR (282 MHz, CD_3CN) spectrum of **3-Cl** after $AgNO_2$ addition.

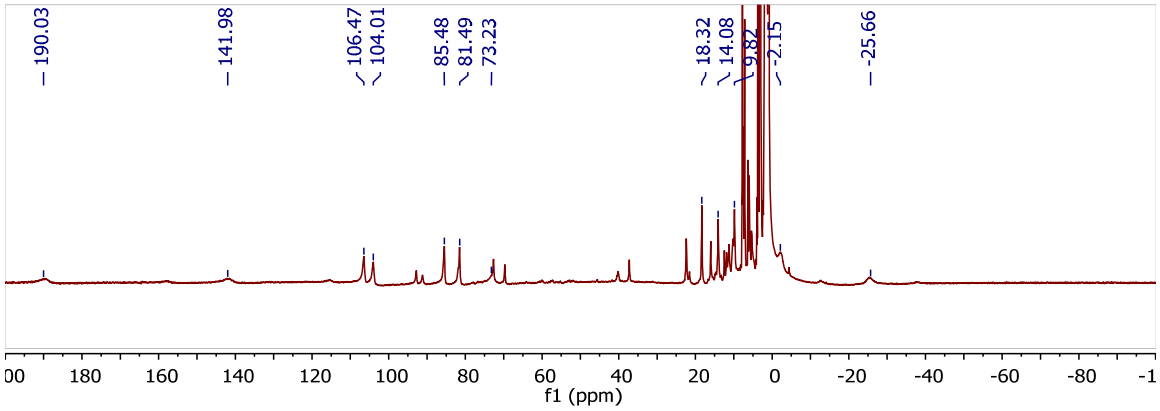

Figure 170. ^{1}H NMR (300 MHz, CD_3CN) spectrum of **3-Cl** after [TBA][IO_4] addition.

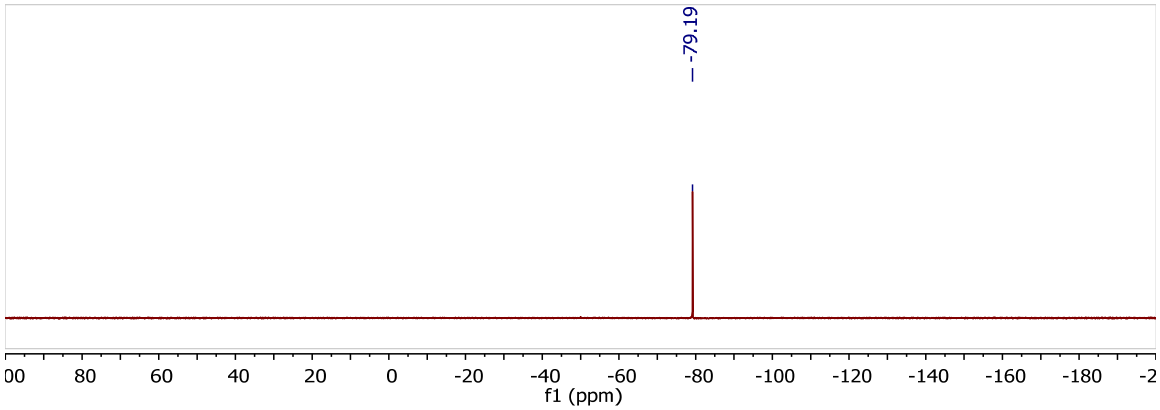

Figure 171. ^{19}F NMR (282 MHz, CD_3CN) spectrum of **3-Cl** after [TBA][IO_4] addition.

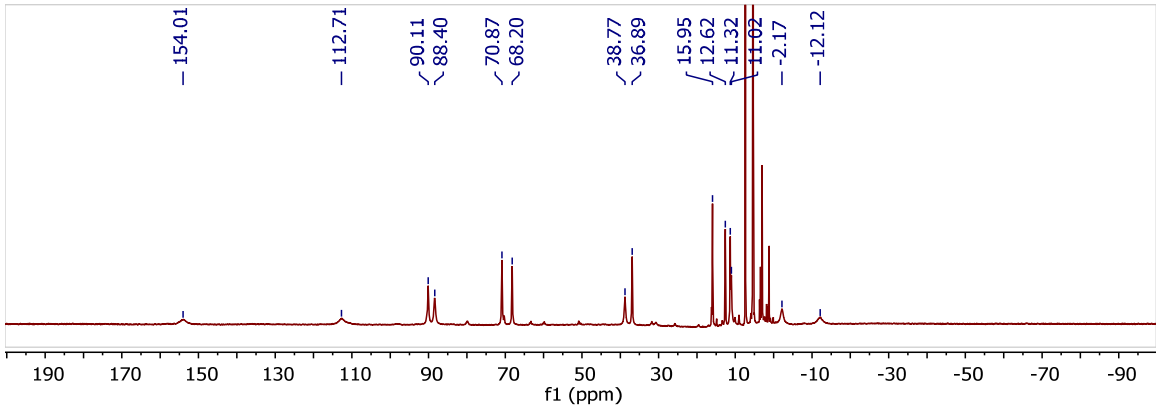

Figure 172. ^{1}H NMR (300 MHz, CD_2Cl_2) spectrum of **4-Cl**.

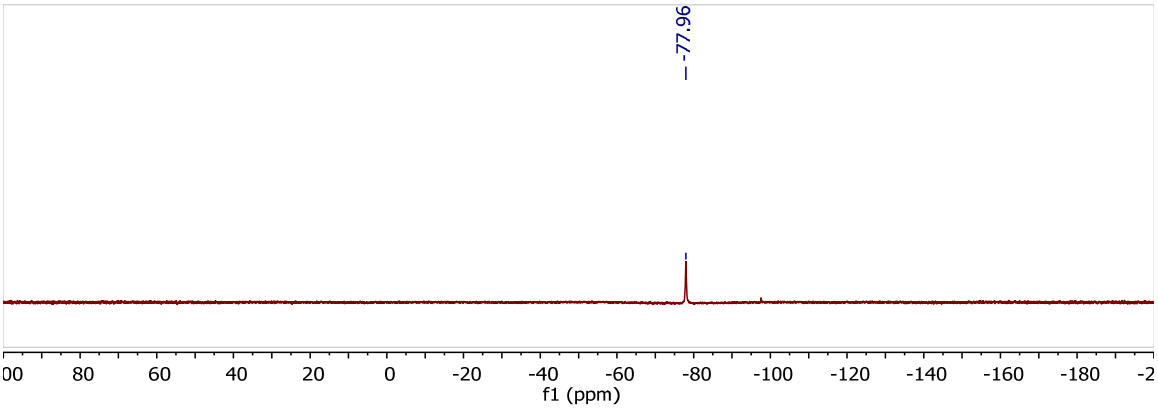

Figure 173. ^{19}F NMR (282 MHz, CD_2Cl_2 spectrum of **4-Cl**.

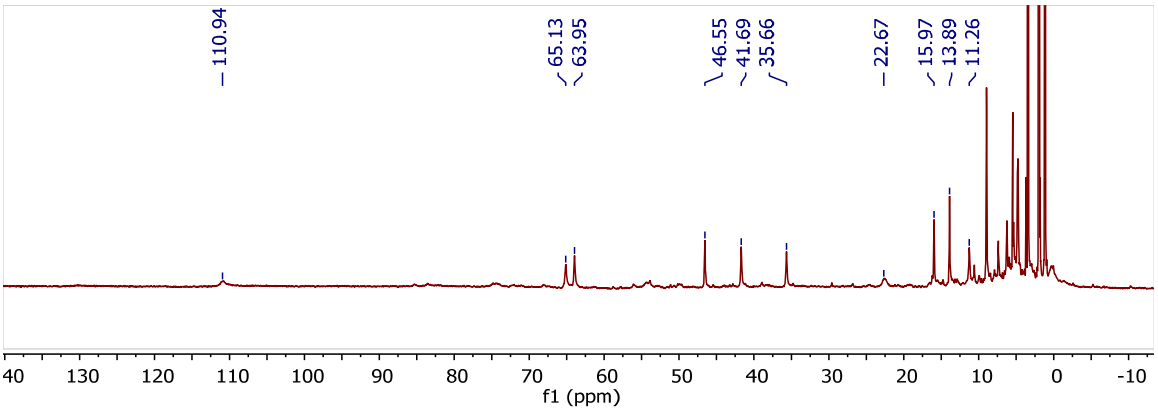

Figure 174. ^{1}H NMR (300 MHz, CD_3CN) spectrum of **6-Cl**.

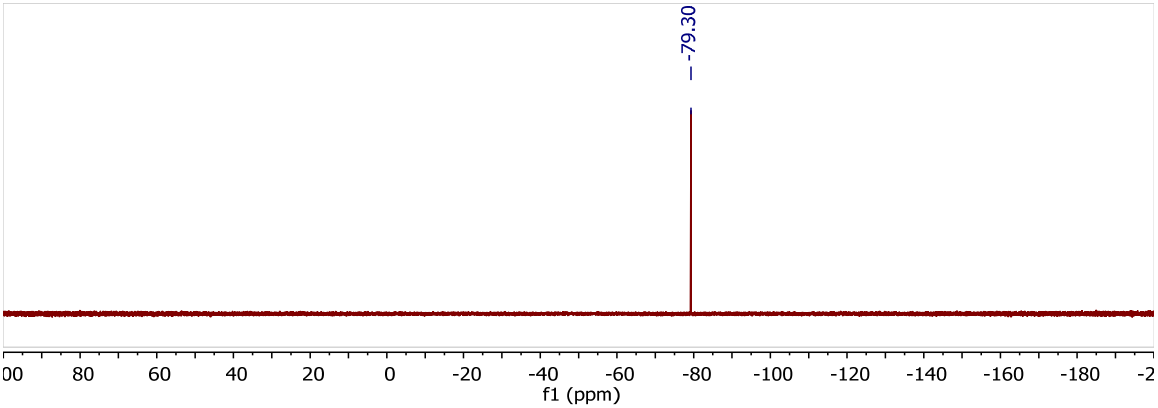

Figure 175. ^{19}F NMR (282 MHz, CD_2Cl_2) spectrum of **6-Cl**.

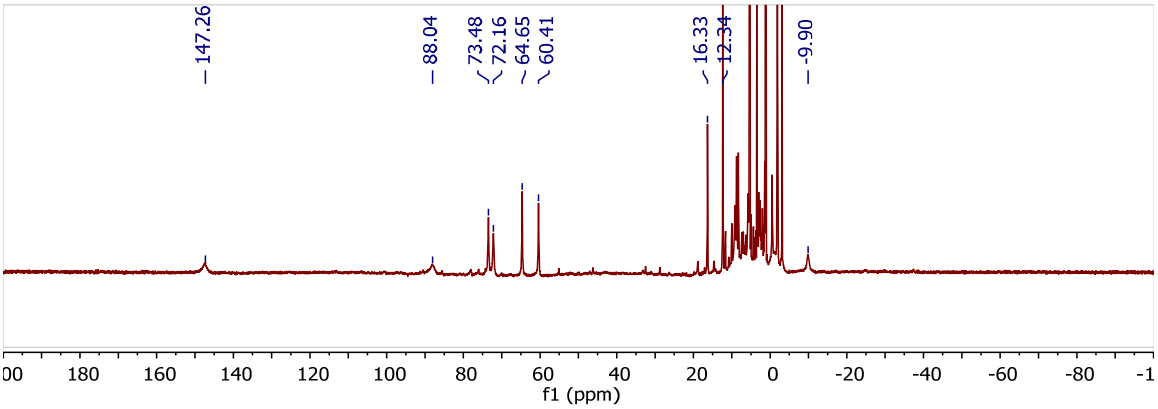

Figure 176. ^{1}H NMR (300 MHz, CD_2Cl_2) spectrum of **7-Cl**.

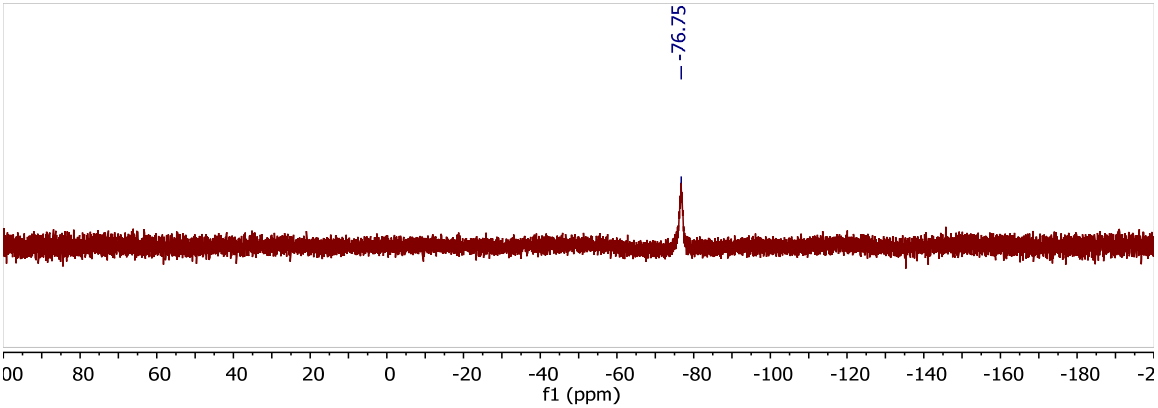

Figure 177. ^{19}F NMR (282 MHz, CD_3CN) spectrum of **7-Cl**.

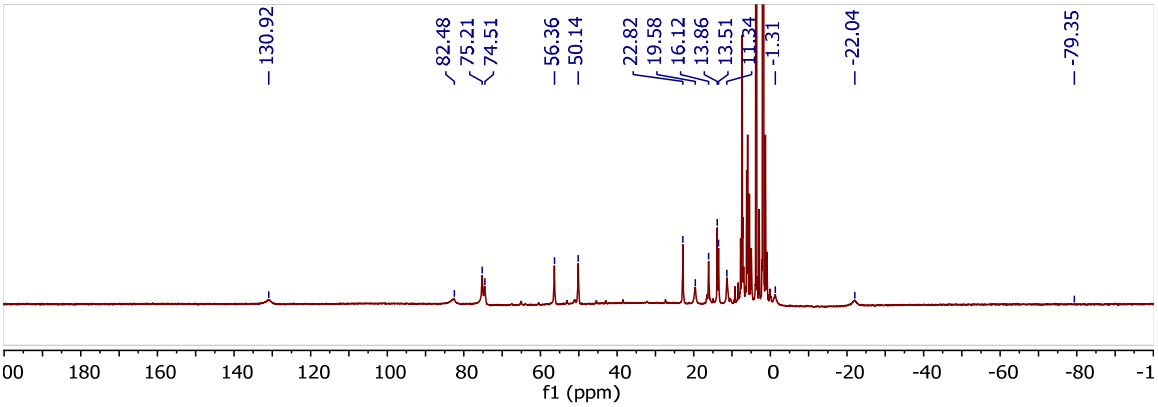

Figure 178. ^{1}H NMR (300 MHz, CD_3CN) spectrum of **6-OH**.

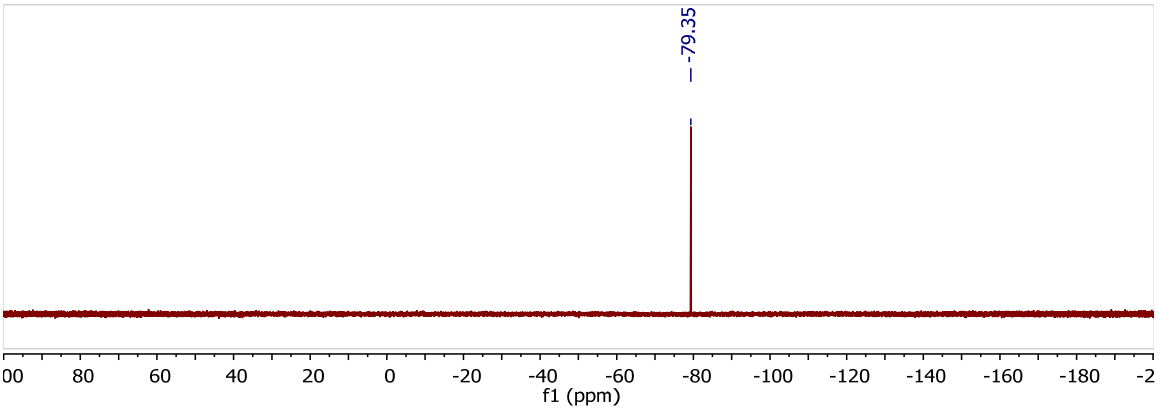

Figure 179. ^{19}F NMR (282 MHz, CD_3CN) spectrum of **6-OH**.

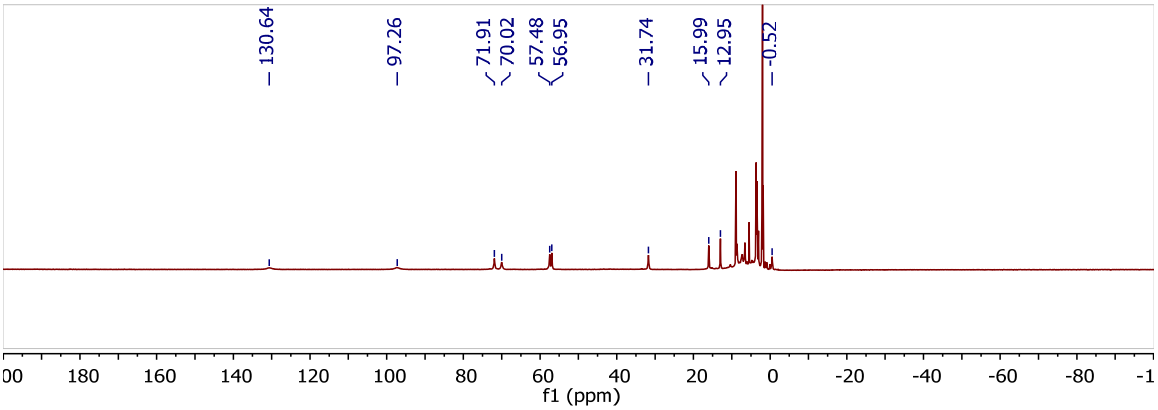

Figure 180. ^{1}H NMR (300 MHz, CD_3CN) spectrum of **9**.

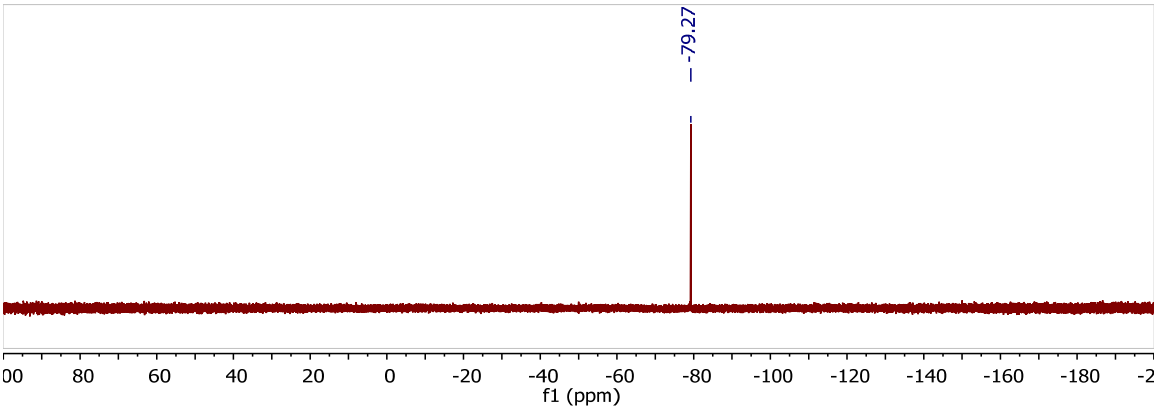

Figure 181. ^{19}F NMR (282 MHz, CD_3CN) spectrum of **9**.

Appendix A

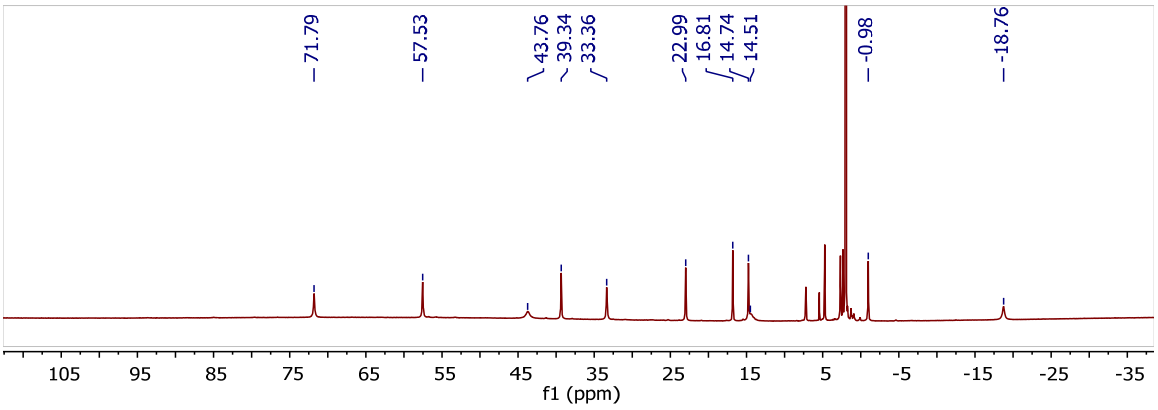

Figure 182. ^{1}H NMR (300 MHz, CD_3CN) spectrum of **3**.

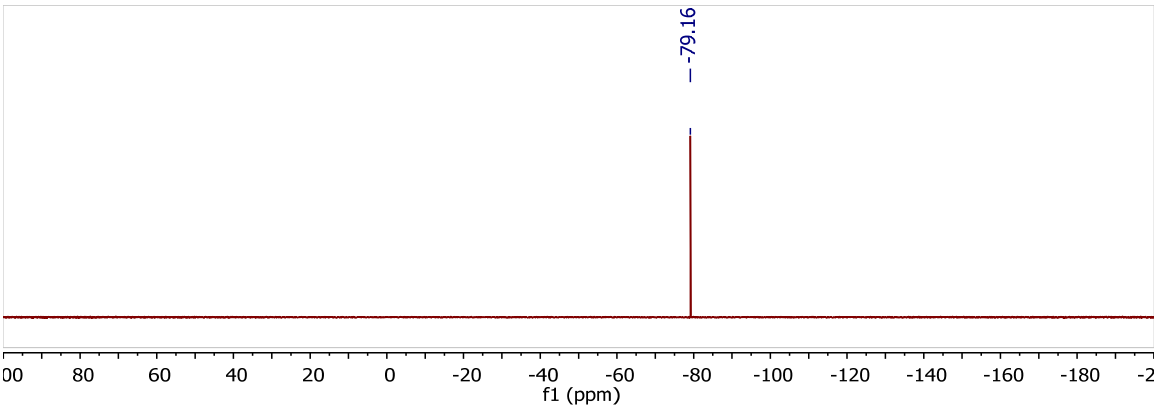

Figure 183. ^{19}F NMR (282 MHz, CD_3CN) spectrum of **3**.

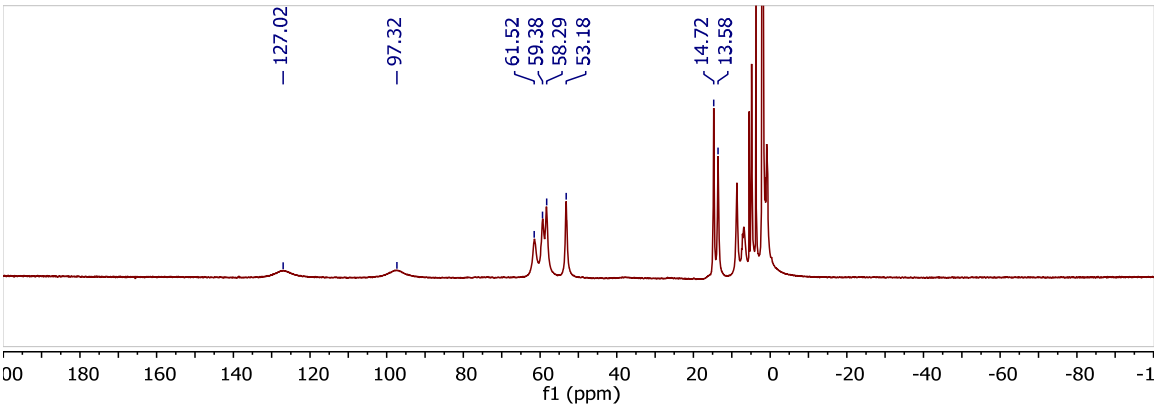

Figure 184. ^{1}H NMR (300 MHz, CD_3CN) spectrum of **5**.

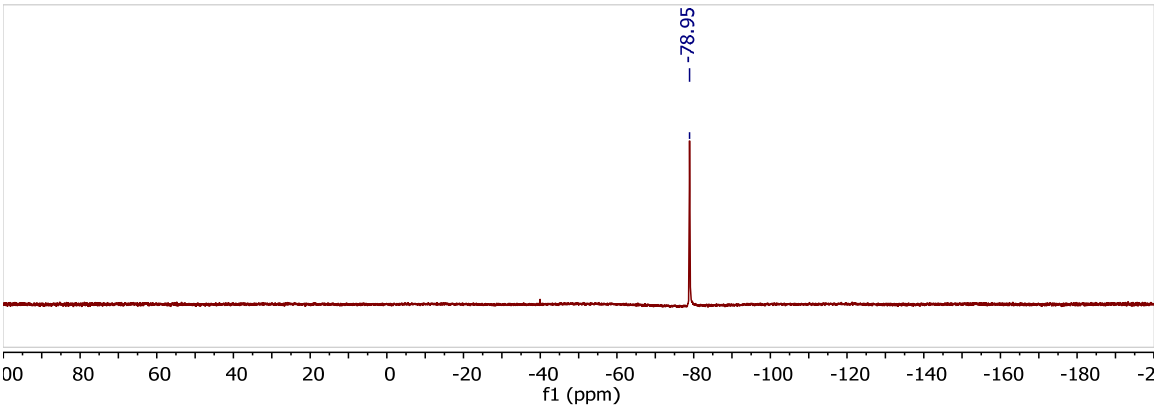

Figure 185. ^{19}F NMR (282 MHz, CD_3CN) spectrum of **5**.

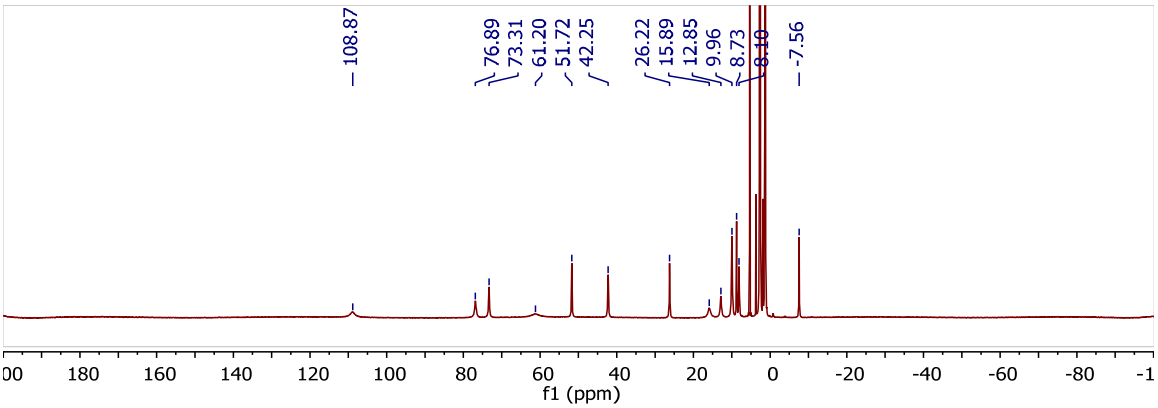

Figure 186. ^{1}H NMR (300 MHz, CD_2Cl_2) spectrum of **6**.

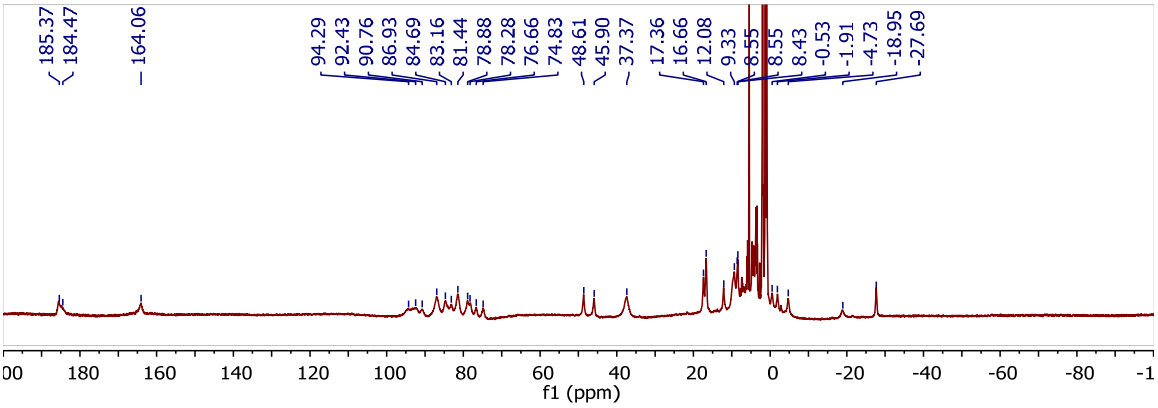

Figure 187. ^{1}H NMR (300 MHz, CD_3CN) spectrum of **8**.

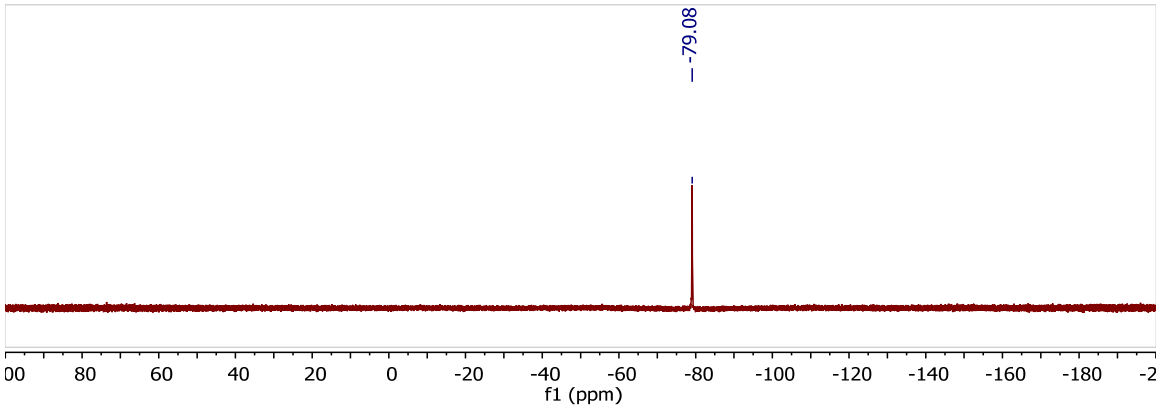

Figure 188. ^{19}F NMR (282 MHz, CD_3CN) spectrum of **8**.

ABOUT THE AUTHOR

Kyle Tadashi Horak was born in Burlington, VT on August 8th, 1988. He and his younger brother, Erik Hiroshi Horak, were raised nearby in Essex Junction, VT, by his parents David Vaclav Horak and Lois May Shiozawa. He attended Essex Junction High School, finishing in 2006, and went on to graduate from Cornell University with a B. A. in Chemical Biology in 2010. During his undergraduate studies, he completed two summer internships in the laboratories of Dr. Karel Pacak at the Eunice Kennedy Shriver National Institute of Child Health and Human Development, and then went on to work in the laboratories of Prof. Hening Lin. He completed his Ph. D. studies in the laboratories of Prof. Theodor Agapie at the California Institute of Technology in 2016. He is currently planning to begin work as a process engineer with Intel in March 2016 at the research and development facility in Hillsboro, OR. Kyle's interest in the sciences was the product of many mentors; however a substantial source of inspiration was his grandfather, Prof. Vaclav Horak, whose love of chemistry most certainly led his son David and grandsons Kyle and Erik to all pursue advanced degrees in chemistry. Other hobbies of Kyle's include alpine skiing, hiking, and pen/pencil illustrations.

"Ad astra."

-Mom and Dad, *Senior High School Yearbook Quote for Me*